THE JOURNAL
OF
CHEMICAL PHYSICS

VOLUME 21, NUMBER 5 MAY, 1953

A Semi-Empirical Theory of the Electronic Spectra and Electronic Structure of Complex Unsaturated Molecules. II*

RUDOLPH PARISER,
Jackson Laboratory, E. I. du Pont de Nemours and Company, Wilmington, Delaware

AND

ROBERT G. PARR,
Department of Chemistry, Carnegie Institute of Technology, Pittsburgh, Pennsylvania

(Received December 11, 1952)

The theory of electronic spectra and electronic structure, the elucidation of which was begun in the first paper of this series, is further developed and applied to ethylene, butadiene, benzene, pyridine, pyrimidine, pyrazine, and *s*-triazine.

A realistic and consistent LCAO-MO π-electron theory should allow the σ-electrons to adjust themselves to the instantaneous positions of the mobile π-electrons. This is accomplished in the theory by assignment of empirical values to the Coulomb electronic repulsion integrals and Coulomb penetration integrals which enter the formulas, these values being obtained in a prescribed way from valence state ionization potentials and electron affinities of atoms. Use of the empirical values in the molecular orbital theory reduces the magnitude of computed singlet-triplet splittings and the effects of configuration interaction without complicating the mathematics. From the valence-bond point of view, ionic structures may be said to be enhanced.

The applications to hydrocarbons and heteromolecules which are considered show that the theory can correlate known π-electron spectral wavelengths and intensities very successfully, which, together with the simple structure of the theory, signals that manifold applications of the theory are in order elsewhere.

1. INTRODUCTION

IN the first paper of this series,[1] hereafter denoted by I, the elements of a theory were presented for the determination of the electronic spectra and electronic structure of complex unsaturated molecules. In the present paper the theory is further expanded and applied to the calculation of some of the spectral properties of ethylene, benzene, butadiene, pyridine, pyrimidine, pyrazine, and *s*-triazine.

In I, results identical in effect with those of purely theoretical LCAO-MO π-electron calculations[2] on ethylene[3] and benzene[4] were obtained from the new theory with relatively little labor, indicating that the new theory can duplicate the results of the old while using a much simpler computational scheme. The present paper shifts the emphasis, duplication of *experimental* results now being taken as the primary desideratum. The guiding principle in molding the theory to give agreement with experiment has been that, to achieve this end, quantities conventionally regarded as purely theoretical may rightly be regarded as semi-empirical. As the shape of the mold emerged, it became apparent that no loss in rigor had actually been entailed, however. For, a re-examination of the assumptions of the purely theoretical LCAO-MO method (see below) shows that precisely such a semi-empirical evaluation of the basic quantities is what is called for by realistic consideration of the structure of the core which underlies the π-electrons in an unsaturated

* Presented at the Symposium on Molecular Structure and Spectroscopy, Ohio State University, June 9, 1952.

[1] R. Pariser and R. G. Parr, J. Chem. Phys. **21**, 466 (1953).

[2] The "purely theoretical LCAO-MO method" is the method of antisymmetrized products of molecular orbitals, in LCAO approximation, including configuration interaction, as developed by Goeppert-Mayer and Sklar, Craig and Roothaan. In this method all quantities which enter the formulas are computed theoretically in terms of a single parameter, the effective nuclear charge of an atom for a π-electron, taken as 3.18 for carbon. For detailed references, see reference 1.

[3] R. G. Parr and B. L. Crawford, Jr., J. Chem. Phys. **16**, 526 (1948).

[4] Parr, Craig, and Ross, J. Chem. Phys. **18**, 1561 (1950).

TABLE I. Theoretical and experimental electronic energy levels of ethylene and benzene (ev).

Molecule	State[a]	Theoretical LCAO MO energy[b]	Experimental energy
Ethylene	$N(^1A_{1g})$	0.0	0.0
	$T(^3B_{1u})$	3.1	3.1—5.6[c]
	$V(^1B_{1u})$	13.5	7.6[d]
Benzene	$^1A_{1g}$	0.0	0.0
	$^1B_{2u}$	5.9	4.9[e]
	$^1B_{1u}$	7.3	6.2[e]
	$^1E_{1u}$	9.8	7.0[e]
	$^3B_{2u}$	5.8	···
	$^3B_{1u}$	3.1	3.8[e]
	$^3E_{1u}$	4.4	···

[a] For notation, see references 3 and 4.
[b] Reference 3 and 4. Values given are for Slater $2p\pi$ AO's with effective charge 3.18. For benzene the values are those obtained with no consideration of configuration interaction beyond that dictated by the molecular symmetry. Values including more configuration interaction are somewhat different; see reference 4.
[c] The lowest triplet state of ethylene has not been unambiguously located, and its symmetry has not been definitely established. Several authors have assigned its location in the indicated range, and the symmetry $^3B_{1u}$ seems most reasonable.
[d] The strong ethylene absorption at 7.6 ev is undoubtedly due to a singlet excited state. The symmetry of this state is less sure.
[e] The locations and symmetries of the benzene excited states are still being debated. The absorption at 4.9 ev corresponds to a forbidden transition from the ground state and has most probably the symmetry $^1B_{2u}$. The triplet at 3.8 ev may be either a $^3B_{1u}$ or $^3B_{2u}$ state and is probably the lowest triplet state of the molecule. The excited state at 7.0 ev corresponds to an allowed transition; the one at 6.2 ev could be either allowed or symmetry forbidden.

molecule and the mutual shielding effects of the electrons on one another. That is to say, the semi-empirical method appears to be more correct than the purely theoretical method as a derangement of which it has been developed.

The methods employed in the present paper are to a certain extent arbitrary and tentative. The flexibility of the theory presents a welcome challenge, but it does mean that results obtained now may require revision later as the base of experience becomes more broad.

2. EXPERIMENT AND THEORY IN ETHYLENE AND BENZENE

The first question then is: To what extent do the results of the purely theoretical method (or alternatively the simplified method described in I which is numerically equivalent) agree with experiment? Unfortunately, even for the simple unsaturated molecules ethylene and benzene the experimental spectra are not completely understood, but enough is known to effect the desired comparison. Table I gives theoretical *versus* experimental electronic levels for these molecules.

There appear to be two major points of disagreement between theory and experiment. First, the quantitative agreement is rather poor, the theoretical energies of the lowest excited singlets being too high by several ev. Second, the splitting between corresponding singlets and triplets computed theoretically is much too large.

Before abandoning the purely theoretical method, one might try to extend it by including more configuration interaction or test it further by varying the effective charge parameter which enters the calculations. Both of these possibilities have been explored, however, and the modified results are not particularly encouraging.[5]

Thus, the purely theoretical LCAO-MO method is not entirely adequate for quantitative purposes, and a detailed and realistic re-examination of the basic quantities which enter the theory is in order. For this the theory outlined in I, being relatively simple, seems admirably suited.

3. BASIC QUANTITIES OF THE THEORY

As was pointed out in the last section of I, four basic types of quantities, W_p, β_{pq}, $(pp|qq)$, and $(q:pp)$, are sufficient to express the electronic energy of a molecule. Of these only the resonance integrals β_{pq} and the Coulomb repulsion integrals $(pp|qq)$ are required in the computation of the electronic excitation energies for ethylene and benzene.

One might try varying only β_{pq} empirically in order to fit the lowest excited singlet states of ethylene and benzene, the states $^1B_{1u}$ and $^1B_{2u}$, respectively, to the observed 7.6 and 4.9 ev. One then finds, setting nonneighbor β's equal to zero and calling $\beta=\beta_{12}$, $\beta=-1.5$ ev for ethylene and $\beta=-2.2$ ev for benzene.

Now the theoretical expression for β_{pq}, when p and q are alike, namely,[6]

$$\beta_{pq}=\sum_{l,\neq q}[S_{pq}(l:qq)+S_{pq}(ll:qq)-(l:pq)-(ll|pq)]+\sum_{r}[S_{pq}(r:qq)-(r:pq)], \quad (1)$$

implies that β_{pq} is zero for infinite separation of atoms p and q. This and other theoretical considerations, plus semi-empirical correlations of bond properties such as force constants and bond dissociation energies as functions of distance with resonance integrals as functions of distance,[7] all indicate strongly that the absolute value of β_{pq} should increase with decreasing distance. This behavior is clearly not followed by the above values of β for a carbon-carbon bond. Moreover, neither inclusion of nonneighbor resonance integrals nor inclusion of more configuration interaction[4] improves the situation. And a final, somewhat unsatisfactory, result of the adjustment of β in ethylene to give the correct singlet-singlet excitation energy is that the triplet $^3B_{1u}$ state becomes the theoretically predicted ground state!

One is thus led to re-examine the values, through the meanings, of the Coulomb repulsion integrals $(pp|qq)$.[8]

Consider two neutral infinitely separated carbon

[5] For the effect of configuration interaction in ethylene and benzene, see references 3 and 4, respectively. For the effect of variation of the effective charge in ethylene, see reference 3; in benzene, see H. Shull and F. Ellison. J. Chem. Phys. **19**, 1215 (1951).
[6] For notation and definitions of the various terms, see reference 1. Equation 1 is obtained from the definition of β_{pq} as in footnote 11 of reference 1.
[7] See, for example, R. S. Mulliken, J. chim. phys. **46**, 497, 695 (1949). The quantities called β in the present papers are called β^{core} by Mulliken.
[8] R. Pariser, J. Chem. Phys. **21**, 568 (1953).

atoms in their sp^2 valence states. By the usual π-electron theory their combined energy would be given by $2W_p$, where W_p is the orbital energy or ionization potential of the $2p\pi$-electron. Now consider the ions C^+ and C^- which are formed by ionization of one of the π-electrons and placement of it in the $2p\pi$-orbital of the other atom. The energy of the ion pair is by the same theory $2W_p+(11|11)$, so that the difference of energy between the ion pair and the neutral pair is simply $(11|11)$. But experimentally this difference is the ionization potential I of a neutral carbon atom in its valence state minus the electron affinity A of such a neutral carbon atom. Thus, formally,

$$(11|11)=I-A. \tag{2}$$

According to Mulliken,[9] $I=11.22$ ev and $A=0.69$ ev for carbon, so that Eq. (2) gives $(11|11)=10.53$ ev for carbon.

But theory, using Slater orbitals with $Z=3.18$ for carbon, gives $(11|11)=16.93$ ev! In view of Eq. (2), this imples either a high ionization potential of about 16 ev or a high negative electron affinity of about -6 ev, which values are inconsistent with the basic assumption that a carbon atom in a molecule behaves essentially as a free carbon atom in the appropriate valence state. The discrepancy is due, in the main, to the failure to consider in the derivation given above the change in σ-electron energy in passing from 2C to $C^+ + C^-$.

Further illustrations of the inadequacy of nonempirical values for the integral $(11|11)$ at large interatomic distances may be found in various relationships involving heteroatoms. Thus, one may compare the process

$$C(sp^3, V_4)+e \rightarrow C^-(sp^4, V_3), \Delta E_a$$

with the process

$$N(sp^4, V_3)+e \rightarrow N^-(sp^5, V_2), \Delta E_b.$$

According to the conventional theory,

$$\Delta E_a-\Delta E_b=W_C-W_N+(11|11)_C-(11|11)_N. \tag{3}$$

Using Mulliken's valence state ionization potentials for W_C and W_N,[9] and theoretically computed values for $(11|11)_C$ and $(11|11)_N$ with $Z_N-Z_C=0.65$,[10] this energy difference is computed to be -0.05 ev. From valence state electron affinities the same difference may be computed to be $+1.67$ ev;[9] the nonempirical calculation predicts that it takes more energy to form N^- than C^-, whereas the reverse is unquestionally true.

If the usual interpretation of the π-electron approximation were taken literally, the self-penetration integral (1:11) would be equal to the valence state electron affinity of the atom 1. For carbon, with $Z=3.25$, the computed value is 25.90 ev,[10] which is somewhat in excess of the carbon electron affinity of 0.69 ev.[9]

It would appear evident from these results that when theoretically computed values for Coulomb repulsion and Coulomb penetration integrals are used within the framework of the π-electron approximation, the results are neither realistic nor trustworthy. To retain the mathematical scheme of the π-electron approximation, one must alter the values of the integrals, especially $(11|11)$. The LCAO-MO method with all possible configuration interaction is equivalent to the valence-bond method including all ionic structures. Thus, an electronic wave function expressed in terms of LCAO-MO's can always be written out as a series of non-ionic and ionic resonance structures, and the appearance of the integral $(11|11)$ in the expression for the energy of some electronic state implies two electrons on the same atom and consequently some other atom devoid of its π-electron. In other words, an ion pair is formed, and to a first approximation the change in both π- and σ-electronic energy accompanying this change may be included in the integral $(11|11)$ by the use of Eq. (2) above.

These considerations provide justification for evaluation of one-center repulsion and penetration integrals from atomic ionization potentials and electron affinities. In the next section this evaluation is carried out for the integrals of this type required in the present calculations. There the corresponding two-center integrals are also evaluated by a method which is also partly semi-empirical. Justification for this is somewhat hard to make precise, but some lowering of $(pp|qq)$ and $(q:pp)$ values from those computed from Slater orbitals with $Z=3.18$ for carbon appears reasonable for reasons analogous to those given above for lowering of $(pp|pp)$ and $(p:pp)$ values and, at any rate, appears desirable from a semi-empirical point of view.

4. SEMI-EMPIRICAL EVALUATION OF THE BASIC QUANTITIES

The method now to be prescribed for evaluating the basic quantities represents an attempt to obtain a correct energy relationship between the ionic and non-ionic resonance structures of a π-bond by taking advantage of empirical ionization potentials and electron affinities of atoms.

A two-electron π-bond between atoms p and q may be described, in the usual approximation, as a superposition of four wave functions, the first two non-ionic, the second two ionic, namely,

$$\left.\begin{aligned}
\Phi_a&=\frac{1}{\sqrt{2}}\begin{vmatrix}(\chi_p\alpha)^1(\chi_q\beta)^1\\(\chi_p\alpha)^2(\chi_q\beta)^2\end{vmatrix}\\
\Phi_b&=\frac{1}{\sqrt{2}}\begin{vmatrix}(\chi_p\beta)^1(\chi_q\alpha)^1\\(\chi_p\beta)^2(\chi_q\alpha)^2\end{vmatrix}\\
\Phi_c&=\frac{1}{\sqrt{2}}\begin{vmatrix}(\chi_p\alpha)^1(\chi_p\beta)^1\\(\chi_p\alpha)^2(\chi_p\beta)^2\end{vmatrix}\\
\Phi_d&=\frac{1}{\sqrt{2}}\begin{vmatrix}(\chi_q\alpha)^1(\chi_q\beta)^1\\(\chi_q\alpha)^2(\chi_q\beta)^2\end{vmatrix}
\end{aligned}\right\}. \tag{4}$$

[9] R. S. Mulliken, J. Chem. Phys. **2**, 782 (1934).
[10] R. G. Parr and B. L. Crawford, Jr., J. Chem. Phys. **16**, 1049 (1948).

TABLE II. Integrals over atomic orbitals (ev).

Integral[a]	R (in A)	Value[b]	Molecule[d]
$(11\|11)_{CC}$	0.00	10.53	all
$(11\|22)_{CC}$	1.35	7.38	ethylene
	1.39	7.30	Bz, Py, Pz, Pm
	1.46	7.16	cB, tB
	2.41	5.46	Bz, Py, Pz, Pm, T
	2.48	5.35	cB, tB
	2.78	4.90	Bz, Py, Pz, Pm
	2.97	4.65	cB
	3.72	3.75	tB
$(11\|11)_{NN}$	0.00	12.27	Py, Pz, Pm, T
$(11\|22)_{NN}$	1.36	8.00	none
	2.36	5.72	Pm, T
	2.75	5.03	Pz
$(11\|22)_{CN}$	1.36	7.68	Py, Pz, Pm, T
	2.38	5.60	Py, Pz, Pm
	2.76	4.97	Py, Pm, T
(N:CC)−(C:NN)	1.36	0.82[c]	Py, Pz, Pm, T
	2.37	0.14[c]	Py, Pz, Pm, T
	2.75	0.01[c]	Py, Pz, Pm, T

[a] Letters indicate the centers, C for carbon, N for nitrogen.
[b] See text for methods used for obtaining values, especially Sec. 4. $(11|11)_C=11.22-0.69$, $(11|11)_N=14.63-2.36$. For $r\geq 2.8$A one uses Eq. (11), with $Z_C=3.25$, $Z_N=3.90$. For $r\leq 2.8$A, one obtains $(11|22)_{CC}=0.2157r^2-2.625r+10.53$, $(11|22)_{NN}=0.3636r^2-3.634r+12.27$, $(11|22)_{CN}=0.2875r^2-3.123r+11.40$. Also, from the average of Eqs. (14), $(N:CC)-(C:NN)=0.2439r^2-1.585r+2.525$.
[c] From Eq. (14). The values obtained by considering C^+-N^- are 0.818, 0.136, 0.015; by considering C^-N^+ are 0.824, 0.143, 0.008. The average is listed in the table and gives the formula in note *b*.
[d] The symbols refer to the molecule for which the integrals are employed in the present paper: cB = *cis*- butadiene, tB = *trans*-butadiene, Bz = benzene, Py = pyridine, Pz = pyrazine, Pm = pyrimidine, T = *s*-triazine.

The matrix elements for the determination of the energy then are, in the notation of I, since $\mathbf{H}=\mathbf{H}_{\text{core}}^{(1)}+\mathbf{H}_{\text{core}}^{(2)}+(e^2/r_{12})$,

$$\left.\begin{aligned} H_{aa}&=H_{bb}=\alpha_p+\alpha_q+(pp|qq)\\ H_{cc}&=2\alpha_p+(pp|pp)\\ H_{dd}&=2\alpha_q+(qq|qq)\end{aligned}\right\}. \tag{5}$$

Making use of Eq. (25) of I (that is, the conventional theory), one thus obtains

$$H_{cc}-H_{aa}=W_p-W_q+(p:qq)-(q:pp)+(pp|pp)-(pp|qq), \tag{6}$$

$$H_{dd}-H_{aa}=W_q-W_p+(q:pp)-(p:qq)+(qq|qq)-(pp|qq), \tag{7}$$

$$(1/2)(H_{cc}+H_{dd})-H_{aa}=(1/2)[(pp|pp)+(qq|qq)]-(pp|qq). \tag{8}$$

For the case atoms p and q alike, these equations reduce to

$$H_{cc}-H_{aa}=(pp|pp)-(pp|qq)\quad[p\text{ and }q\text{ identical}]. \tag{9}$$

Equations (6) through (8) given energy differences between the hypothetical nonresonating structures described by Φ_a, Φ_b, Φ_c, Φ_d. Under the assumption of zero differential overlap, Eqs. (6) and (7) give the energy differences between the ionic forms p^-q^+ and p^+q^- and the purely covalent form $p=q$, respectively.

Equations (6) through (8) may serve as a basis for estimating Coulomb repulsion and penetration integrals as functions of the interatomic distance r, as follows. First, the atomic integrals $(pp|pp)$ are obtained from free atom valence state ionization potentials, $-W_p$, and electron affinities, A_p, through the relations

$$(pp|pp)=-W_p-A_p, \tag{10}$$

and are assumed constant. Secondly, the two-center electronic repulsion integrals $(pp|qq)$ are determined for $r\geq 2.80$A from the uniformly charged sphere model formula.[11]

$$(pp|qq)=(7.1975/r)\{[1+(1/2r)^2(R_p-R_q)^2]^{-1}+[1+(1/2r)^2(R_p+R_q)^2]^{-1}\}\text{ev}, \tag{11}$$

in which

$$R_p=(4.597/Z_p)\times 10^{-8}\text{ cm}, \tag{12}$$

where Z_p is Slater's effective nuclear charge; for $r\leq 2.80$A, the integrals $(pp|qq)$ are determined by extrapolations of Eq. (8) down to $r=0$ by use of an equation of the form

$$ar+br^2=(1/2)[(pp|pp)+(qq|qq)]-(pp|qq), \tag{13}$$

in which the constants a and b are obtained by fitting values calculated from Eq. (11) for $r=2.80$A and $r=3.70$A. Thirdly, the two-center penetration integrals $(p:qq)$ are assumed equal to zero for $r\geq 2.80$A; for $r\leq 2.80$A, the differences $(q:pp)-(p:qq)$ are obtained by averaging extrapolations of Eqs. (6) and (7) down to $r=0$ by use of equations of the form

$$\left.\begin{aligned} a'r+b'r^2&=W_p-W_q+(p:qq)-(q:pp)+(pp|pp)-(pp|qq)\\ a''r+b''r^2&=W_q-W_p+(q:pp)-(p:qq)+(qq|qq)-(pp|qq)\end{aligned}\right\}, \tag{14}$$

in which the constants a', a'', b', and b'' are again obtained by fitting values calculated for $r=2.80$A and $r=3.70$A. In many cases, only differences of penetration integrals are needed in calculations of spectroscopic intervals and intensities.

Table II gives values obtained in this way of integrals used in the calculations on hydrocarbons and heteromolecules to be described below. This method for obtaining the values is admittedly rough; a multitude of approximations is implied. Nevertheless, the theory gives the correct values to integrals of the type $(pp|pp)$ at $r=\infty$, and the behavior of the σ-electrons has been approximately taken into account without complicating the mathematics of the π-electron approximation. Furthermore, the values of the several quantities entering the formulas are now all consistent with the notion that the atoms in molecules behave like free atoms in their appropriate valence states.

As has already been indicated, the resonance integrals β will be evaluated empirically, from experimental results on molecules. With the other integrals adjusted semi-empirically, β turns out to have a dependence on

[11] R. G. Parr, J. Chem. Phys. **20**, 1499 (1952).

distance of the sort required by the considerations of Sec. 3 above.

5. APPLICATION TO HYDROCARBONS

For the ground and excited states of ethylene and benzene the method of computation has already been outlined in I. Values for the MO repulsion integrals are obtained using Eqs. (33) and (35) of I and the AO repulsion integrals listed in Table II. Values of β are used which give the experimental value for the lowest singlet excited state in each case. The results thus obtained are summarized and compared with experiment in Tables III and IV. The agreement is good, especially with regard to the magnitude of the singlet-triplet splittings. And of the values of the resonance integrals,

$$\beta(\text{benzene}) = -2.39 \text{ ev},$$
$$\beta(\text{ethylene}) = -2.92 \text{ ev},$$

are satisfactory from the semi-empirical point of view.[12]

The treatment of butadiene differs from that of ethylene and benzene because the MO's in this case are not determined completely by symmetry. To avoid launching a complicated self-consistent field calculation, use will be made of the idea advanced in Sec. 3 of I, that any starting MO's will do, if configuration interaction is invoked. As starting MO's one may take, in order of increasing energy, the orthonormal (in zero differential overlap approximation) set

$$\left.\begin{aligned}\phi_1&=\tfrac{1}{2}(\chi_1+\chi_2+\chi_3+\chi_4)\\ \phi_2&=\tfrac{1}{2}(\chi_1+\chi_2-\chi_3-\chi_4)\\ \phi_3&=\tfrac{1}{2}(\chi_1-\chi_2-\chi_3+\chi_4)\\ \phi_4&=\tfrac{1}{2}(\chi_1-\chi_2+\chi_3-\chi_4)\end{aligned}\right\}, \tag{15}$$

where χ_p is a $2p\pi$ AO on carbon p, with carbons numbered consecutively along the (planar) chain. These orbitals are simple and convenient of manipulation; they have the requisite symmetries and are, in fact, fairly close to the best self-consistent field orbitals for the molecule.[13] Corrections to the energies of states described by various prescribed electron assignments of the MO's of Eq. (15) are obtainable through configuration interaction. Lower excited states will result from excitations of one electron from a lower to a higher MO; even when all the corresponding configurations are mixed the resultant corrections to the calculated energy spectrum are small.

The lowest configurational singlet state, of energy E_0 with wave function V_0, has two electrons in each of ϕ_1 and ϕ_2. A singlet excited state arises when an electron has been raised from ϕ_i to ϕ_j; let this be denoted by V_{ij}, with T_{ij} for the corresponding triplet. Computation of the energies then yields [Eq. (6) of I, but note that additional terms enter in cases such as V_{ij} in which the wave function is a combination of two or more determinants]

$$\left.\begin{aligned}E\left\{\begin{matrix}V_{23}\\T_{23}\end{matrix}\right\}-E_0&=I_3-I_2\pm K_{23}+K_{12}-K_{13}\\ E\left\{\begin{matrix}V_{14}\\T_{14}\end{matrix}\right\}-E_0&=I_4-I_1\pm K_{14}+K_{12}-K_{24}\\ E\left\{\begin{matrix}V_{24}\\T_{24}\end{matrix}\right\}-E_0&=I_4-I_2\pm K_{24}+K_{12}-K_{14}\\ E\left\{\begin{matrix}V_{13}\\T_{13}\end{matrix}\right\}-E_0&=I_3-I_1\pm K_{13}+K_{12}-K_{23}\end{aligned}\right\}, \tag{16}$$

where the upper and lower signs refer, respectively, to the singlet and triplet states indicated, the integrals

TABLE III. Electronic states of ethylene (ev).[a]

State	Calculated energy[b]	Observed energy
$N(^1A_{1g})$	0	0
$T(^3B_{1u})$	4.5	3.1—5.6
$V(^1B_{1u})$	7.6	7.6
$1(^1A_{1g})$	0.2	...[c]

[a] See explanatory notes to Table I.
[b] Calculated by the semi-empirical LCAO-MO theory of the present paper, using $\beta = -2.92$ ev and values of electronic repulsion integrals from Table II.
[c] "State 1" does not correspond to any actual molecular state.

TABLE IV. Electronic states of benzene (ev).[a]

State	Calculated energy[b]	Observed energy
$^1A_{1g}$	0	0
$^1B_{2u}$	4.9	4.9
$^1B_{1u}$	5.3	6.0
$^1E_{1u}$	7.0	7.0
$^3B_{2u}$	4.9	...
$^3B_{1u}$	4.0	3.8
$^3E_{1u}$	4.45	...

[a] See explanatory notes to Table I.
[b] Calculated by the semi-empirical LCAO-MO theory of the present paper, using $\beta = -2.39$ ev and values of electronic repulsion integrals from Table II.

[12] An interesting result of the use of the new semi-empirical values for Coulomb repulsion integrals is a marked reduction of the effects of configuration interaction. The lower value for integrals of the type $(pp|p\phi)$ decreases the energy of ionic forms and increases their contribution to the resonance hybrid. The MO method, without configuration interaction, postulates 50 percent ionic and 50 percent covalent character in the π-bond in ethylene. The wave functions for the ground state of ethylene, obtained with the inclusion of configuration interaction are

(a) $\Psi_N = 0.3185[\chi_1(1)\chi_1(2)+\chi_2(1)\chi_2(2)] + 0.6295[\chi_1(1)\chi_2(2)+\chi_2(1)\chi_1(2)]$,

corresponding to the use of integrals obtained by means of uniformly charged spheres (which are analogous to theoretical integrals), or

(b) $\Psi_N = 0.4300[\chi_1(1)\chi_1(2)+\chi_2(1)\chi_2(2)] + 0.5615[\chi_1(1)\chi_2(2)+\chi_2(1)\chi_1(2)]$,

corresponding to the use of the semi-empirical integrals of this paper. (a) Implies 21 percent ionic and 79 percent covalent character, whereas (b) gives 37 percent ionic and 63 percent covalent character. Thus the state expressed by (b) corresponds quite closely to the ground state configuration given by the MO method without configuration interaction.

[13] R. G. Parr and R. S. Mulliken, J. Chem. Phys. 18, 1338 (1950).

TABLE V. Butadiene matrix elements (ev).

Matrix element[a]	*trans*-butadiene	*cis*-butadiene
$E(V_{23})-E_0$	5.88	5.54
$E(V_{14})-E_0$	9.14	8.91
$E(V_{13})-E_0$	7.67	7.78
$E(V_{24})-E_0$	7.67	7.78
$E(T_{23})-E_0$	4.36	4.24
$E(T_{14})-E_0$	7.61	7.61
$E(T_{13})-E_0$	6.04	5.93
$E(T_{24})-E_0$	6.04	5.93
$(V_0 \mid V_{13})$	1.19	1.19
$(V_0 \mid V_{24})$	−1.19	−1.19
$(V_{13} \mid V_{24})$	−0.15	0.19
$(V_{23} \mid V_{14})$	−0.25	−0.37
$(T_{13} \mid T_{24})$	−1.78	−1.66
$(T_{23} \mid T_{14})$	−1.78	−1.66

[a] See text for definition of matrix elements.

are over the *molecular orbitals* of Eq. (15), and all integrals of the type J_{ij} cancel because of the simple form of these MO's.

The quantities appearing in Eqs. (16) may now be expressed in terms of integrals over *atomic orbitals*. The core energy terms, by Eqs. (17), (19), and (20) of I, are given by the formulas

$$\left.\begin{aligned} I_3-I_2&=-2\beta_{12}+\beta_{23}\\ I_4-I_1&=-2\beta_{12}-\beta_{23}\\ I_4-I_2&=I_3-I_1=-2\beta_{12}\end{aligned}\right\}, \tag{17}$$

provided nonneighbor resonance integrals are neglected. The electronic repulsion terms, by Eq. (30) of I, are given by the formulas

$$\left.\begin{aligned} K_{12}=K_{34}&=\tfrac{1}{8}[2(11\mid 11)+2(11\mid 22)\\ &\quad -(22\mid 33)-2(11\mid 33)-(11\mid 44)]\\ K_{13}=K_{24}&=\tfrac{1}{8}[2(11\mid 11)-2(11\mid 22)\\ &\quad +(22\mid 33)-2(11\mid 33)+(11\mid 44)]\\ K_{14}=K_{23}&=\tfrac{1}{8}[2(11\mid 11)-2(11\mid 22)\\ &\quad -(22\mid 33)+2(11\mid 33)-(11\mid 44)]\end{aligned}\right\}. \tag{18}$$

Here the integrals $(pp\mid qq)$ over AO's are the quantities listed in Table II.[14] The quantities β_{12} and β_{23} are merely the carbon-carbon resonance integral at distances 1.35A and 1.46A, respectively. The first of these may be taken as the already determined ethylene resonance integral

$$\beta_{12}=-2.92 \text{ ev}.$$

The second may be found by a suitable extrapolation based on the already determined ethylene ($r=1.35$A) and benzene ($r=1.39$A) resonance integrals. Thus the equation (r in A)

$$\beta(r)=-6442\exp(-5.6864r) \text{ ev}, \tag{19}$$

which fits the ethylene and benzene values, gives, for $r=1.46$A,

$$\beta_{23}=-1.68 \text{ ev}.$$

This value has been assumed for the present calculations.

To complete the calculation, one needs values for the appropriate interaction elements between the several configurations. The wave functions V_0, V_{24}, and V_{13}, all being of symmetry ^1A, must be mixed, as must the functions V_{23} and V_{14} of symmetry ^1B, the functions T_{23} and T_{14} of symmetry ^3B, and the functions T_{13} and T_{24} of symmetry ^3A. Letting

$$\int V_{ij}^*\mathbf{H}V_{kl}d\tau=(V_{ij}\mid V_{kl}), \tag{20}$$

one finds the following expressions for the required matrix elements in terms of integrals over *molecular orbitals:*

$$\left.\begin{aligned} (V_0\mid V_{13})&=2^{\frac{1}{2}}[I_{13}+(11\mid 13)\\ &\quad +2(22\mid 13)-(12\mid 23)]\\ (V_0\mid V_{24})&=2^{\frac{1}{2}}[I_{24}+(22\mid 24)\\ &\quad +2(11\mid 24)-(12\mid 14)]\\ (V_{13}\mid V_{24})&=2(13\mid 24)-(12\mid 34),\\ (T_{13}\mid T_{24})&=-(12\mid 34)\\ (V_{23}\mid V_{14})&=2(23\mid 14)-(12\mid 34),\\ (T_{23}\mid T_{14})&=-(12\mid 34)\end{aligned}\right\}. \tag{21}$$

The quantities appearing in these formulas may now be expressed in terms of integrals over *atomic orbitals*. The core energy terms, by Eqs. (17), (19), (20), and (25) of I, are given by the expressions

$$\left.\begin{aligned} I_{13}&=\tfrac{1}{2}[\alpha_1-\alpha_2-\beta_{23}]\approx\tfrac{1}{2}[(22\mid 33)-(11\mid 44)-\beta_{23}]\\ I_{24}&=\tfrac{1}{2}[\alpha_1-\alpha_2+\beta_{23}]\approx\tfrac{1}{2}[(22\mid 33)-(11\mid 44)+\beta_{23}]\end{aligned}\right\}, \tag{22}$$

where, in calculating $\alpha_1-\alpha_2$ by Eq. (25) of I, penetration integrals, since they are comparatively small and cancel each other to a large extent, have been neglected. Expansion of $(V_0\mid V_{13})$ and $(V_0\mid V_{24})$ in terms of β_{23} and AO repulsion integrals now results in complete

TABLE VI. Electronic states of butadiene (ev).

State *trans*	State *cis*	Calculated energy *trans*	Calculated energy *cis*	Observed energy[a]
^1A_g	$^1A_1$	0	0	0
^1B_u	$^1B_1$	6.21	5.91	6.0
^1A_g	$^1A_1$	7.87	8.29	7.2(?)
^1A_g	$^1A_1$	8.51	8.34	···
^1B_u	$^1B_1$	9.50	9.25	···
^3B_u	$^3B_1$	3.92	3.96	···
^3A_g	$^3A_1$	4.61	4.62	···
^3A_g	$^3A_1$	8.16	7.95	···
^3B_u	$^3B_1$	8.74	8.61	···

[a] The observed energies are probably for *trans*-butadiene, and are taken from R. S. Mulliken, Revs. Modern Phys. **14**, 265 (1942), corrected for new values of fundamental constants.

[14] The geometries assumed for *cis*- and *trans*-butadiene are planar carbon skeletons, $C_1-C_2-C_3-C_4$, with $r_{12}=1.35$A, $r_{23}=1.46$A, and 1–2–3 and 2–3–4 angles $=124°$. See V. Schomaker and L. Pauling, J. Am. Chem. Soc. **61**, 1769 (1939).

cancellation of the latter, giving

$$(V_0|V_{13})=-(V_0|V_{24})=-2^{-\frac{1}{2}}\beta_{23}. \tag{23}$$

There remain the electronic repulsion integrals in the last four of Eqs. (21); these are given by the formulas

$$\left.\begin{aligned}(12|34)^{\mathrm{MO}}&=K_{12}\\(13|24)^{\mathrm{MO}}&=K_{13}\\(23|14)^{\mathrm{MO}}&=K_{23}\end{aligned}\right\}, \tag{24}$$

where the superscripts have been added to indicate that MO's are involved in the various integrals.

Computation of the diagonal matrix elements of Eq. (16) and the off-diagonal matrix elements of Eq. (21), using the above formulas and the integral values given in Table II, yields the numerical results listed in Table V. Solutions of the secular equations for configuration interaction (of these there are one third-order and three second-order equations) then gives the final electronic states listed in Table VI. Agreement with the observed excitation energies, also given in the table, is good, although in this case the agreement, before configuration interaction is considered (Table V), is almost as good.

Any other unsaturated hydrocarbon containing no triple bonds could now be treated with the introduction of no further empirical data; the formulas for electronic repulsion integrals given in Table II and the formula for β, Eq. (19) being all that is required in the most general such case.

6. APPLICATION TO HETEROMOLECULES

As a test of the applicability of the theory to molecules containing other atoms than carbon in the conjugated system, the nitrogen-containing heterocyclic molecules, pyridine, pyrazine, pyrimidine, and *s*-triazine will now be treated. These molecules may be considered as derived from benzene by replacement of one or more CH groups by an N atom. Each N, like each CH, furnishes one π-electron to the conjugated system, so in the π-electron approximation each of these molecules presents a six-electron problem just as does benzene.

TABLE VII. Wave-function symmetries for benzene, pyridine, pyramidine, pyrazine, and *s*-triazine.[a]

Configuration	Combination[b]	Benzene	Pyridine	Pyrimidine	Pyrazine	*s*-Triazine
V_0		$^1A_{1g}$	$^1A_1$	$^1A_1$	$^1A_{1g}$	$^1A_1'$
V_{23}, V_{14}	−	$^1B_{2u}$	$^1B_1$	$^1B_1$	$^1B_{3u}$	$^1A_2'$
	+	$^1E_{1u}$	$^1B_1$	$^1B_1$	$^1B_{3u}$	$^1E'$
V_{13}, V_{24}	+	$^1B_{1u}$	$^1A_1$	$^1A_1$	$^1B_{2u}$	$^1A_1'$
	−	$^1E_{1u}$	$^1A_1$	$^1A_1$	$^1B_{2u}$	$^1E'$

[a] The table lists only singlet states. Symmetries of triplet wave functions are identical with symmetries of corresponding singlets.
[b] Combination + denotes a wave function of the type $\Psi=\sin\theta V_{ij}+\cos\theta V_{kl}$, − denotes one of the type $\Psi=\sin\theta V_{ij}-\cos\theta V_{kl}$, where $0\leqslant\theta\leqslant\pi/2$.

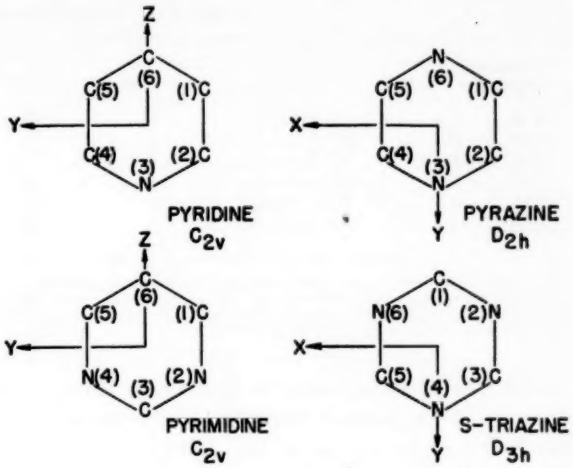

FIG. 1. Heterocyclic molecules.

The symmetries of these molecules (all planar) and the numbering employed for the atoms are shown in Fig. 1. For simplicity and the lack of more precise information, interatomic distances in all molecules will be taken as follows: nearest C−C distance, 1.39A (the benzene value); nearest C−N distance, 1.36A; nonneighbor C−C distances, 2.41 and 2.78A; nonneighbor C−N distances, 2.38 and 2.76A; nonneighbor N−N distances, 2.36 and 2.75A.[15]

The similarity of these molecules to benzene makes benzene MO's natural and convenient starting MO's. Real LCAO coefficients are preferable, so one takes the orthonormal (in zero differential overlap approximation) set, in order of increasing energy,

$$\left.\begin{aligned}\phi_0&=\frac{1}{6^{\frac{1}{2}}}(\chi_1+\chi_2+\chi_3+\chi_4+\chi_5+\chi_6)\\\phi_1&=\frac{1}{12^{\frac{1}{2}}}(\chi_1-\chi_2-2\chi_3-\chi_4+\chi_5+2\chi_6)\\\phi_2&=\frac{1}{4^{\frac{1}{2}}}(\chi_1+\chi_2-\chi_4-\chi_5)\\\phi_3&=\frac{1}{12^{\frac{1}{2}}}(\chi_1+\chi_2-2\chi_3+\chi_4+\chi_5-2\chi_6)\\\phi_4&=\frac{1}{4^{\frac{1}{2}}}(\chi_1-\chi_2+\chi_4-\chi_5)\\\phi_5&=\frac{1}{6^{\frac{1}{2}}}(\chi_1-\chi_2+\chi_3-\chi_4+\chi_5-\chi_6)\end{aligned}\right\}, \tag{25}$$

where the numbering of the AO's follow the numbering of the atoms in Fig. 1.

[15] Nearest neighbor distances are average distances obtained by V. Schomaker and L. Pauling, reference 14. Nonneighbor distances are estimated as follows: for N−N: $\sqrt{3}(1.36)A$, and $(1.36+1.39)A$; for C−N: $\frac{1}{2}\sqrt{3}(1.36+1.39)A$, and $(\frac{1}{2}\times1.36+\frac{3}{2}\times1.39)A$.

TABLE VIII. Energy formulas for benzene and *s*-triazine.[a,b]

Benzene quantity	*s*-Triazine quantity	$-2\beta_{12}$	$\frac{1}{2}(11\|11)$	$\frac{1}{2}(22\|22)$	$\frac{1}{2}(11\|22)$	$\frac{1}{2}(11\|33)$	$\frac{1}{2}(22\|44)$	$\frac{1}{2}(11\|44)$
$E(^1B_{2u})-E_N$	$E(^1A_2')-E_N$	1	0	0	1	−3/2	−3/2	2
$E(^1B_{1u})-E_N$	$E(^1A_1')-E_N$	1	1	1	−5	7/2	7/2	−4
$E(^1E_{1u})-E_N$	$E(^1E_1')-E_N$	1	1/2	1/2	4	−2	−2	−1
$E(^3B_{2u})-E_N$	$E(^3A_2')-E_N$	1	0	0	1	−3/2	−3/2	2
$E(^3B_{1u})-E_N$	$E(^3A_1')-E_N$	1	−1	−1	3	−1/2	−1/2	0
$E(^3E_{1u})-E_N$	$E(^3E_1')-E_N$	1	−1/2	−1/2	2	−1	−1	1

[a] The numbers in a given row of the table give the coefficients of the indicated atomic orbital integrals in the formula for the energy quantity listed in the first column. E_N is the ground-state energy. See text for notation for other energy states and atomic orbital integrals; see Fig. 1 for the numbering of atoms. Note that, in deriving the table, nonneighbor resonance integrals have been neglected and the zero differential overlap approximation employed.
[b] For benzene, $(11|11)=(22|22)$, $(11|33)=(22|44)$.

In benzene, the lower excited states arise through the promotion of an electron from one of the ground-state filled MO's ϕ_1 or ϕ_2 (ϕ_0 is also filled) to one of the excited MO's ϕ_3 or ϕ_4. The core energies of the resultant eight states, four singlets and four triplets, are the same. Their total π-electron energies are, however, split by (a) electronic interaction and (b) configuration interaction among themselves. The situation in the present heterocyclic molecules may be regarded as essentially equivalent. The core energies of the eight excited states are no longer necessarily the same, but the splittings (a) and (b) are formally just as before.

The symmetry properties for the ground and the eight excited states for the several molecules are summarized in Table VII. These symmetries are such that the configurational interaction among the eight excited states (interaction with the ground state, which is possible in three cases, is neglected) reduces to interaction within four pairs: V_{23}, V_{14}; V_{13}, V_{24}; T_{23}, T_{14}; T_{13}, T_{24}. The interactions in the cases of benzene and *s*-triazine can be handled by group theory and the final wave functions written down; computation of the energies of the states by the methods already described is then straightforward. The final energy formulas in terms of integrals over atomic orbitals are given in Table VIII. For the other three molecules four quadratic secular equations must be solved numerically; formulas for the necessary matrix elements are given in Tables IX, X, and XI.

The intensities of transitions from ground to excited states may be calculated by the methods summarized by Mulliken and Rieke,[16] simplified by the neglect of differential overlap. For transitions between nondegenerate states described by wave functions Ψ_k and Ψ_l, the formula for the oscillator strength f is

$$f=1.085\times10^{11}\omega\sum_{i=x,y,z}Q_i^2, \tag{26}$$

where ω is the frequency of the transition in cm^{-1} and

$$Q_i=\int\Psi_k^*\bar{\imath}\Psi_l dv(i=x,y,z), \tag{27}$$

where $\bar{\imath}$ is the algebraic sum of the i's for the several electrons. Now, the wave function for the lowest excited singlet state of each of the molecules here being considered has the form

$$\Psi_l=(\sin\theta)V_{23}-(\cos\theta)V_{14},\quad 0\leqslant\theta\leqslant\pi/2. \tag{28}$$

Accordingly, for the transition from the ground state V_0, which has the configuration $\phi_0^2\phi_1^2\phi_2^2$, to the lowest

TABLE IX. Energy formulas for pyridine.[a]

Quantity[b,c]	(1/72)(11|11)	(1/72)(33|33)	(1/72)(11|22)	(1/72)(22|33)	(1/72)(11|55)	(1/72)(11|33)	(1/72)(11|44)	(1/72)(33|66)
$E(V_{14})-E_N-\Delta I_{1,4}$	18	−12	50	−20	−6	−36	46	−40
$E(V_{23})-E_N-\Delta I_{2,3}$	−6	12	2	28	−54	12	−50	56
$E(V_{13})-E_N-\Delta I_{1,3}$	10	8	−14	8	10	8	2	−32
$E(V_{24})-E_N-\Delta I_{2,4}$	18	0	−6	0	18	0	−30	0
$E(T_{14})-E_N-\Delta I_{1,4}$	6	−12	38	−20	6	−36	58	−40
$E(T_{23})-E_N-\Delta I_{2,3}$	−18	12	−10	28	−42	12	−38	56
$E(T_{13})-E_N-\Delta I_{1,3}$	−10	−8	6	24	−10	−8	6	0
$E(T_{24})-E_N-\Delta I_{2,4}$	−18	0	30	0	−18	0	6	0
$(V_{14}\|V_{23})$	6	0	18	0	−6	0	−18	0
$(V_{13}\|V_{24})$	6	0	−30	−24	42	24	−18	0
$(T_{14}\|T_{23})$, $(T_{13}\|T_{24})$	−6	0	6	0	6	0	−6	0

[a] See Table VIII, note a.
[b] Here $\Delta I_{1,4}\equiv I_4-I_3=\frac{1}{2}(\alpha_1+\alpha_2-\alpha_3-\alpha_6)-(4/3)\beta_{12}-\frac{2}{3}\beta_{23}$
$\Delta I_{2,3}\equiv I_3-I_2=-\frac{1}{2}(\alpha_1+\alpha_2-\alpha_3-\alpha_6)-(4/3)\beta_{12}-\frac{2}{3}\beta_{23}$
$\Delta I_{1,3}\equiv I_3-I_1=-\frac{2}{3}\beta_{12}-(4/3)\beta_{23}$
$\Delta I_{2,4}\equiv I_4-I_2=-2\beta_{12}$
$(\alpha_1+\alpha_2-\alpha_3-\alpha_6)=(W_1-W_2)-[(11|22)-(22|33)]-[(11/55)-(11|33)]-2[(11|44)-(33|66)]-[(3:22)-(2:33)]-[(3:11)-(1:33)]-[(6:33)-(3:66)]$.
[c] In computing the terms ΔI (note b), use has been made of approximations of the type: $(2:33)\approx(2:11)$.

[16] R. S. Mulliken and C. A. Rieke, Repts. Prog. Phys. 8, 231 (1941).

TABLE X. Energy formulas for pyrazine.[a]

Quantity[b,c]	(1/36)(11|11)	(1/36)(33|33)	(1/36)(11|22)	(1/36)(22|33)	(1/36)(11|55)	(1/36)(11|33)	(1/36)(11|44)	(1/36)(33|66)
$E(V_{14})-E_N-\Delta I_{1,4}$	15	−12	35	−20	15	−36	23	−20
$E(V_{23})-E_N-\Delta I_{2,3}$	−9	12	−13	28	−33	12	−25	28
$E(V_{13})-E_N-\Delta I_{1,3}$	1	8	−11	8	1	8	1	−16
$E(V_{24})-E_N-\Delta I_{2,4}$	9	0	−3	0	9	0	−15	0
$E(T_{14})-E_N-\Delta I_{1,4}$	9	−12	29	−20	21	−36	29	−20
$E(T_{23})-E_N-\Delta I_{2,3}$	−15	12	−19	28	−27	12	−19	28
$E(T_{13})-E_N-\Delta I_{1,3}$	−1	−8	−9	24	−1	−8	3	0
$E(T_{24})-E_N-\Delta I_{2,4}$	−9	0	15	0	−9	0	3	0
$(V_{14}\|V_{23})$	3	0	9	0	−3	0	−9	0
$(V_{13}\|V_{24})$	3	0	−3	−24	9	24	−9	0
$(T_{14}\|T_{23}),(T_{13}\|T_{24})$	−3	0	3	0	3	0	−3	0

[a] See Table VIII, note a.
[b] Here $\Delta I_{1,4}=\frac{1}{3}(\alpha_1-\alpha_3)-\frac{1}{3}\beta_{12}-(4/3)\beta_{23}$
$\Delta I_{2,3}=-\frac{1}{3}(\alpha_1-\alpha_3)-\frac{1}{3}\beta_{12}-(4/3)\beta_{23}$
$\Delta I_{1,3}=\frac{1}{3}\beta_{12}-(8/3)\beta_{23}$
$\Delta I_{2,4}=-2\beta_{12}$
$(\alpha_1-\alpha_3)=(W_1-W_3)-[(11|22)-(22|33)]-[(11|55)-(11|33)]-[(11|44)-(33|66)]-[(3:22)-(2:33)]-[(3:11)-(1:33)]-[(1:44)-(3:66)]$.
[c] In computing the terms ΔI (note b), use has been made of approximations of the type: $(2:33)\approx(2:11)$.

singlet excited state one has

$$Q_i=\sqrt{2}\left[\sin\theta\int\phi_3 i\phi_2 dv-\cos\theta\int\phi_4 i\phi_1 dv\right], \quad (29)$$

where i refers to, and the integrations are over the coordinates of, a single electron. But, assuming for all of the molecules the same distance between next nearest neighbors 2.4A, and invoking the assumption of zero differential overlap,[16]

$$\left.\begin{aligned}&\int\phi_3 i\phi_2 dv=\int\phi_4 i\phi_1 dv=0,\\ &\text{except}\\ &\int\phi_3 y\phi_2 dv=\int\phi_4 y\phi_1 dv=\frac{2.4}{2\sqrt{3}}A=0.693\times10^{-8}\text{ cm}\\ &\text{for pyridine and pyrimidine and}\\ &\int\phi_3 x\phi_2 dv=\int\phi_4 x\phi_1 dv=0.693\times10^{-8}\text{ cm}\\ &\text{for pyrazine.}\end{aligned}\right\} \quad (30)$$

Hence

$$Q_i=0, \quad (31)$$

except

$$Q_y^{\text{pryidine}}=Q_x^{\text{pyrazine}}=Q_y^{\text{pyrimidine}}=0.980\times10^{-8}[\sin\theta-\cos\theta]\text{ cm}.$$

These results upon insertion in Eq. (26) will give final expressions for the oscillator strengths.

Table XII presents the results of calculations on these molecules using the integral values of Table II, the formulas of Tables VIII–XI and this section, the $\beta_{CC}=-2.390$ ev value obtained in the previous section, and $\beta_{CN}=-2.576$ ev. The latter value has been chosen to give agreement with Halverson and Hirt's estimated value for the lowest singlet transition of the experimentally unknown *s*-triazine.[17] Given in the table are computed and experimental[17–19] values for the positions and oscillator strengths of the lowest-lying singlet and triplet states of these molecules. The agreement between calculated and observed values is very good and could be improved still further by adjustment of the β_{CN} value employed.

TABLE XI. Energy formulas for pyrimidine.[a]

Quantity[b,c]	(1/72)(11|11)	(1/72)(22|22)	(1/72)(11|66)	(1/72)(22|33)	(1/72)(11|33)	(1/72)(22|66)	(1/72)(22|44)	(1/72)(33|66)	(1/72)(11|44)
$E(V_{14})-E_N-\Delta I_{1,4}$	−9	15	−20	50	−21	−36	15	−40	46
$E(V_{23})-E_N-\Delta I_{2,3}$	15	−9	28	2	−21	12	−33	56	−50
$E(V_{13})-E_N-\Delta I_{1,3}$	17	1	8	−14	9	8	1	−32	2
$E(V_{24})-E_N-\Delta I_{2,4}$	9	9	0	−6	9	0	9	0	−30
$E(T_{14})-E_N-\Delta I_{1,4}$	−15	9	−20	38	−15	−36	21	−40	58
$E(T_{23})-E_N-\Delta I_{2,3}$	9	−15	28	−10	−15	12	−27	56	−38
$E(T_{13})-E_N-\Delta I_{1,3}$	−17	−1	24	6	−9	−8	−1	0	6
$E(T_{24})-E_N-\Delta I_{2,4}$	−9	−9	0	30	−9	0	−9	0	6
$(V_{14}\|V_{23})$	3	3	0	18	−3	0	−3	0	−18
$(V_{13}\|V_{24})$	3	3	−24	−30	33	24	9	0	−18
$(T_{14}\|T_{23}),(T_{13}\|T_{24})$	−3	−3	0	6	3	0	3	0	−6

[a] See Table VIII, note a.
[b] Here $\Delta I_{1,4}=\frac{1}{3}(\alpha_1+\alpha_2-\alpha_3-\alpha_6)-(4/3)\beta_{23}-\frac{1}{3}\beta_{16}$
$\Delta I_{2,3}=-\frac{1}{3}(\alpha_1+\alpha_2-\alpha_3-\alpha_6)-(4/3)\beta_{23}-\frac{1}{3}\beta_{16}$
$\Delta I_{1,3}=-\frac{1}{3}\beta_{23}-(4/3)\beta_{16}$
$\Delta I_{2,4}=-2\beta_{23}$
$(\alpha_2+\alpha_6-\alpha_1-\alpha_3)=(W_1-W_2)-[(11|66)-(11|22)]-[(22|66)-(22|44)]-2[(33|66)-(11|44)]-[(2:11)-(1:22)]-[(1:44)-(4:11)]-[(3:66)-(4:11)]$.
[c] In computing the terms ΔI (note b), use has been made of approximations of the type: $(1:22)\approx(1:66)$.

[17] F. Halverson and R. C. Hirt, J. Chem. Phys. **19**, 711 (1951).
[18] H. Shull, J. Chem. Phys. **17**, 295 (1949).
[19] Barany, Braude, and Pianka, J. Chem. Soc. **1949**, 1898.

TABLE XII. Lowest singlet and triplet excited electronic states of benzene, pyridine, pyrazine, pyrimidine, and *s*-triazine.

Molecule	State	Calculated energy (ev)	Observed energy (ev)	Calculated f	Observed f
pyrazine	$^1B_{3u}$	4.71	4.77[a]	0.121	0.130[d]
benzene	$^1B_{2u}$	4.90	4.90[a]	0	~0[a]
pyridine	$^1B_1$	4.90	4.95[a]	0.046	0.041[e]
pyrimidine	$^1B_1$	5.05	5.15[a]	0.038	...
s-triazine	$^1A_2'$	5.29	5.29[a]	0	(~0)[a]
pyrazine	$^3B_{3u}$	3.85	3.35[b]	0	~0[b]
benzene	$^3B_{1u}$	4.01	3.65[c]	0	~0[c]
pyridine	$^3A_1$	4.08	...	0	...
pyrimidine	$^3A_1$	4.16	...	0	...
s-triazine	$^3A_1'$	4.26	...	0	...

[a] See reference 17, and references cited there. The various references differ as to the precise location of absorption maxima.
[b] Estimated, from a privately communicated pyrazine absorption spectrum by R. C. Hirt.
[c] Reference 18.
[d] f is estimated by assuming it proportional to the maximum extinction coefficient in hexane and determining the proportionality constant from pyridine data. $\epsilon_{max}=6350$ for pyrazine (reference 17), and $\epsilon_{max}=2000$ for pyridine (reference 19), both in hexane.
[e] H. P. Stephenson, presented at the Symposium on Molecular Structure and Spectroscopy, Ohio State University, June 9, 1952.

As indicated by the notes to Table XII, too much reliance should not be placed on the experimental values which are quoted for positions of absorption bands. There seems little doubt that the molecules absorb at increasing wavelengths in the order, *s*-triazine, pyrimidine, pyridine, benzene, and pyrazine, however. This is the order the theory predicts. The theory also indicates that the lowest triplets of these molecules should fall in the same order as the singlets; the observed triplets in benzene and pyrazine follow this rule. Calculated transition probabilities appear to be in excellent agreement with experimental values (here one should note that the calculation is absolute; no empirical correction factor has been employed). The theory thus fits thirteen experimental results or estimates with the use of only two empirical parameters (the CC and CN resonance integrals).

7. DISCUSSION

The flexibility of the theory that has been outlined and tested in these two papers is such that more experience must be acquired before a completely definitive recipe can be given for its application. In this very flexibility there appears to lie much power, however.

Among the fundamental questions that still should be asked, the following may be mentioned: How much configuration interaction should be included? Can resonance integrals be computed theoretically? Can nonneighbor resonance integrals be neglected? Can resonance integrals be carried from molecule to molecule? Can the theory be applied to molecules containing triple bonds? Can the theory be adapted to σ-bonds? Can a rationalization of the empirical $(pp|qq)$ and $(p:qq)$ *versus* distance curves be made in terms of Slater effective charges which vary with distance? Tentatively, the authors would answer: Some, but not very much, configuration interaction should be included. Resonance integrals can be estimated, sometimes computed, theoretically (a theoretical calculation of the resonance integrals for ethylene and benzene gives -2.80 and -2.48 ev, which compare favorably with the empirical values of -2.92 and -2.39 ev). Nonneighbor resonance integrals, even though perhaps in principle important, may usually be neglected, because what small effects they have can be taken into account elsewhere. Resonance integrals can be carried over from molecule to molecule as a first approximation, but small adjustments should be expected. Application of the theory to molecules containing triple bonds will be straightforward. Adaptation to σ-bonds is also feasible (calculations on the hydrogen molecule using the zero differential overlap approximation give quite startling results). And finally, rationalizations of the electronic repulsion integral and penetration integral curves are possible in terms of varying effective charges, but such rationalizations may be dangerous.

The authors are pleased to thank Professor R. S. Mulliken, Professor C. C. J. Roothaan, Dr. K. Rüdenberg, and Dr. F. G. Fumi for helpful discussions.

Precision Measurements of the Enthalpy of KBr and KI at High Temperatures*

CHARLES B. COOPER
Physics Department, University of Maryland, College Park, Maryland
(Received December 15, 1952)

By use of an ice calorimeter precision measurements of the enthalpies of pure samples of KBr and KI between 300°C and their melting points were made. Values for the specific heats at constant pressure of these substances through the same temperature range were calculated and tabulated.

INTRODUCTION

A LARGE amount of theoretical work on the structure and properties of the alkali halides has been done. The existing experimental data on their enthalpies and specific heats, however, are meager, especially at high temperatures. The present measurements were undertaken with the object of obtaining results on the enthalpy and specific heat at constant pressure of pure samples of KBr and KI with high precision over a temperature range from 300°C to their melting points. Work is under way in this laboratory to measure the compressibility and thermal expansion of these substances, which results can be used with the present data to obtain the specific heat at constant volume. This quantity is of interest, in addition to its use in thermodynamic tables, in that it offers a direct experimental check on the theories of the internal energies of substances, and in particular, for example, will determine whether the Dulong and Petit law will hold at high temperatures, a question raised in the literature.

EXPERIMENTAL METHOD

The experimental method used to measure the heat content was a drop method. In this technique a sample of KBr or KI enclosed in a sealed capsule was suspended in a furnace and heated to the desired temperature. After the sample had reached thermal equilibrium it was dropped into an ice calorimeter where the enthalpy change of the sample between the furnace temperature and 0°C could be measured.

Ginnings and Corruccini[1] at the National Bureau of Standards describe a modern ice calorimeter of their design and have made a thorough study of the reproducibility of the measurements of the density of ice, of the calibration factor of the calorimeter, of the many corrections which must be made to the data for accurate work, and of the accuracy which can be expected with the instrument.

The calorimeter used in these experiments was similar to that designed by Ginnings, Douglas, and Ball.[2] The furnace used was wound with platinum-rhodium windings on a cylindrical core 18 inches long and 1½ inches in inside diameter. This core had a favorable ratio of length to diameter, and to further facilitate maintaining a low temperature gradient in the central part of the furnace two separate end windings were also used. The temperature inside the furnace was read with three platinum-rhodium thermocouples which had been calibrated at the National Bureau of Standards. These were mounted at two-inch intervals on an inconel tube mounted snugly inside the furnace core. A Leeds and Northrup Wenner precision potentiometer was used to measure the voltage of the thermocouples.

The capsule was suspended in the furnace and allowed to fall into the calorimeter, its fall being checked near the end by an air brake similar in design to that of Southard.[3] The capsules for containing the samples were fabricated of Nichrome and Nichrome V. They were about 1½ inches long and 0.6 inch in diameter, weighing about 15 grams, and were threaded on top to be used with a threaded cap which could be screwed on or removed easily. Care was taken to fill the capsule with a sample in a moisture free atmosphere,

TABLE I.

KBr		KI	
Temperature (deg C)	Enthalpy (cal/g)	Temperature (deg C)	Enthalpy (cal/g)
297	32.06	297	23.47
334	36.17	346.5	27.44
396	43.31	396	31.53
530.3	59.30	495	40.09
594	67.06	600	49.37
693	79.35	650	53.85
720	82.85	700	58.32

TABLE II.

Temperature (deg C)	Enthalpy KBr (cal/g)	Enthalpy KI (cal/g)
300	32.38	23.71
350	38.04	27.73
400	43.84	31.87
450	49.74	36.14
500	55.71	40.50
550	61.74	44.92
600	67.86	49.38
650	74.03	53.85
700	80.29	58.32
730	84.07	

* Contract supported by U. S. Office of Naval Research.
[1] D. C. Ginnings and R. J. Corruccini, J. Research Natl. Bur. Standards **38**, 583 (1947).
[2] Ginnings, Douglas, and Ball, J. Research Natl. Bur. Standards **45**, 23 (1950).
[3] J. C. Southard, J. Am. Chem. Soc. **63**, 3142 (1941).

TABLE III.

Temperature (deg C)	C_p KBr cal/g/deg	C_p KI cal/g/deg
300	0.1126	0.07918
350	0.1147	0.08157
400	0.1168	0.08360
450	0.1185	0.08545
500	0.1201	0.08675
550	0.1216	0.08770
600	0.1230	0.08845
650	0.1244	0.08910
700	0.1258	0.08960
730	0.1265	

and the capsule was filled with dry helium gas and sealed using a gold gasket before measurements were taken. The weight of the samples of KBr and KI used in each test was about 10 grams. These samples were obtained from the Harshaw Chemical Company.

A series of heat content measurements was made with the capsule empty, and this followed by a series with the capsule containing a sample. The drop method is a convenient one in that when the data for the empty capsule is subtracted from that for the loaded capsule any heat losses occurring during the capsule drop will be nearly equal in both cases and will thus cancel out. A series of runs with an empty capsule, and a capsule filled with pure Al_2O_3, obtained from the Linde Air Products Company, was also made for the purpose of calibrating the calorimeter. The enthalpy of this substance has been very accurately measured by Ginnings and Corruccini.[4] To check the accuracy of the temperature measurements in the furnace, various crystalline substances were sealed inside a capsule and their melting points noted.

RESULTS

In Table I are listed the values for the enthalpy of KBr and KI, between 0°C and the temperature listed. These values were calculated directly from the data taken, after a number of corrections had been made. All weight readings were corrected for buoyancy, and the difference in heat content of the helium gas in a full and empty capsule was taken into account. From the results of Table I values of the enthalpies of KBr and KI were calculated for even temperature intervals. These are given in Table II.

Once the smoothed values of the enthalpies were found, the specific heats at constant pressure were calculated. These are listed in Table III. These data are plotted in Fig. 1.

DISCUSSION

An idea as to the reproducibility of the results for the enthalpy is given by the deviations from the mean of the mass, corrected for buoyancy, of the mercury readings obtained from the calorimeter at a given temperature. The average deviation of these readings is in the neighborhood of 0.1 or 0.2 percent. The calorimeter was calibrated by making measurements on Al_2O_3. In the calibration of this substance at the National Bureau of Standards an accuracy of 0.2 percent is claimed. This percentage includes uncertainties due to such factors as the difference in heat loss during the fall of an empty and full capsule, conduction up the calorimeter well, elasticity of the calorimeter, etc. In addition, in the present measurements the heat leak of the calorimeter, which was very small, was noted at each run and corrected for; the gate (which prevents radiation from entering the calorimeter from the furnace) was kept open the same length of time for all drops; and two platinum shields were fastened to the drop wire directly above the capsule, a precaution which prevents nearly all heat from being lost by radiation from the hot capsule up the calorimeter well. Thus the present values for the enthalpy of KBr and KI are presumed accurate to within about one percent.

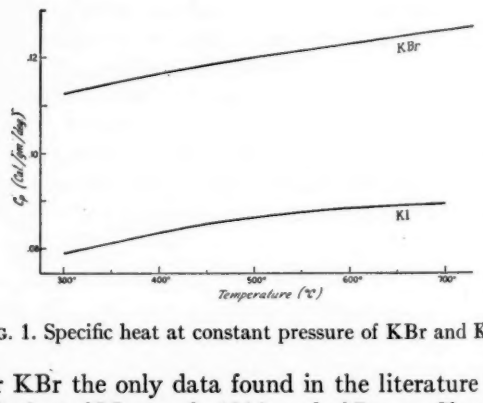

FIG. 1. Specific heat at constant pressure of KBr and KI.

For KBr the only data found in the literature since 1900 is that of Magnus in 1913, and of Popov, Skuratov, and Nikonova[6] in 1940, the latter enthalpies having an accuracy of about two percent. The present results agree within about one percent with the results of these investigators.

In the case of KI the only data found in the literature was that of Nernst, Koref, and Lindemann[7] taken in 1910. The results of the present data differ from these, ranging from about a one percent higher value at lower temperatures, to about three percent higher value at higher temperatures.

The author wishes to express his thanks to Professor Raymond Morgan and Professor R. D. Myers for their help and encouragement on this problem.

[4] D. C. Ginnings and R. J. Corruccini, J. Research Natl. Bur. Standards **38**, 593 (1947).

[6] A. Magnus, Physik. Z. **14**, 5 (1913).

[6] Popov, Skuratov, and Nikonova, J. Gen. Chem. (U.R.S.S.) **10**, 2017 (1940).

[7] Nernst, Koref, and Lindemann, Sitzb. Berlin Akad. **12**, 247 (1910).

The Limiting Thickness of an Electrolyzed Gas Film Capable of Sustaining a Given Negative Pressure

LYMAN J. BRIGGS
National Bureau of Standards, Washington, D. C.
(Received September 22, 1952)

The critical thickness of a gas film that is just capable of withstanding a given negative pressure P_N in a liquid column has been studied. The film was generated electrolytically on the surface of a spherical platinum electrode of known area. The number of gas molecules corresponding to the measured charge required to release the negative column was then computed from the relation between the Faraday constant and Avogadro's number. The number of gas molecules required to form a monolayer on the electrode was next computed from the molecular diameter, based on van der Waals' equation. The ratio of these numbers gives the "thickness" t of the film in fractions of a monolayer.

Both O_2 and H_2 gas films were measured under conditions such that the same number of gas molecules were deposited on the same electrode and the corresponding critical negative pressures observed. Assuming the effectiveness of the film to be proportional to the area covered, the ratio of the diameters of the O_2 and H_2 molecules is inversely proportional to the square root of the ratio of their critical negative pressures. This gave $O_2/H_2=1.11$ as compared with 1.06 from measurements based on van der Waals' equation.

Measurements of oxygen films were made at various negative pressures, ranging from $P_N=90$ cm of water, $t=0.55$ monolayer, to $P_N=4$ cm, $t=0.87$ monolayer. The results lie on a smooth curve down to $P_N=10$ cm, t increasing steadily as P_N is reduced. Below $P_N=10$ cm, the thickness of the film no longer increases, indicating that the zone of influence of the gas molecule extends beyond its projected area.

THE maximum negative pressure that can be developed in a liquid depends upon (1) the cohesive force of the molecules in the body of the liquid; or (2) the adhesive force between the molecules of the liquid and the walls of the container. The adhesion is greatly reduced by the presence of undissolved gas on the surfaces in contact with the liquid. The rupture of a liquid column under negative pressure thus provides a very sensitive way of determining when an electrolyzed layer of gas on an electrode in contact with the liquid has reached its critical thickness. This technique is utilized in the present investigation, which deals with the relationship between the thickness of a gas film developed by electrolysis on a spherical platinum electrode and the negative pressure P_N which the film is just able to withstand.

APPARATUS

The apparatus used is shown in Fig. 1. The vertical glass tube in which a negative pressure is developed is provided at its top with two spherical electrodes made by fusing the ends of the platinum lead-in wires. The shank of each electrode is coated with a thin layer of glass, so as to confine the exposed area to the spherical surface. This area is computed from the diameter, with the assumption that the fused surface is ideally smooth and free from pits.

The vertical tube with its attached reservoir is filled with electrolyte to the extent indicated and then evacuated and sealed off. When the apparatus is rotated in the plane of the paper until the electrodes are below the level of the reservoir, the tube fills. It may now be brought to a vertical position with the liquid hanging from the top of the tube under negative pressure. With the discharge of the critical quantity of electricity across the electrodes, the gas layer formed breaks down the adhesion and the column falls.

The apparatus, when sealed off, still contained some air. Consequently, when the column collapsed and the tube was again inverted, a bubble appeared. This was transferred to the reservoir, sweeping the column free from minute bubbles formed by the collapse.

The electrical circuit used is shown in Fig. 2. The charging potential V (46 volts), is obtained from heavy-duty B batteries. C is a high-quality mica capacitor, adjustable in steps of 0.001 μf. The number of microcoulombs Q discharged between the electrodes is $Q=(V-a)C$, where C is expressed in microfarads, and a is the back emf of the polarized electrode. The value of a has been assumed equal to a decomposition potential of 1.7 volts, which may be a little high, since the electrode is not fully polarized.

In contrast with an adsorbed film, the electrolyzed film is a transient film. It soon leaves the electrode and dissolves in the electrolyte. However, when the discharge of a quantity Q slightly less than the critical value is followed quickly by the discharge of a second quantity Q, the column drops, showing that a residuum of gas remained on the electrode.

EXPERIMENTAL RESULTS

Measurements were made with normal solutions of $CuSO_4$ and H_2SO_4 as electrolytes. With $CuSO_4$, the gas appearing on the critical electrode during the discharge of the capacitor is oxygen; with H_2SO_4, hydrogen, since the amount of H_2 generated is twice that of O_2.

For oxygen, the critical charge Q_0 required to release the column was found to be $Q_0=9.90\pm0.006\mu$-coulombs, under a negative pressure of 52 cm of water. This is the mean of 8 sets of observations, taken during a period

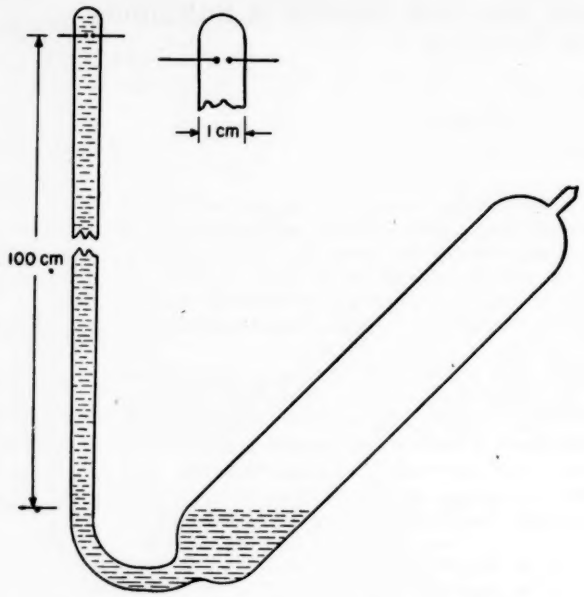

FIG. 1. Negative pressure apparatus with spherical platinum electrodes; filled with electrolyte and evacuated.

of one week. The critical charge was remarkably constant and definite, as shown by the probable error. The charge required to drop the column was usually not more than 0.5 percent greater than the charge which the column would withstand.

For hydrogen, the observations varied more from day to day. The critical charge Q_H was found to be $Q_H = 4.96 \pm 0.014\mu$-coulombs under a negative pressure of 64 cm of water. This is the mean of 11 sets of observations, extending over one week.

Since oxygen is bivalent, one molecule of oxygen set free on the surface of an electrode represents the transport of 4 electrons, compared with 2 electrons for a molecule of hydrogen. The ratio of the critical charges Q_0 and Q_H for oxygen and hydrogen required to release the column is

$$\frac{Q_0}{Q_H} = \frac{9.90 \pm 0.006}{4.96 \pm 0.014} = 1.996 \pm 0.006,$$

which corresponds closely to the ratio of the valencies.

These measurements show that the number of O_2 and H_2 molecules required to release the negative column was the same, since the same electrode was used for both gases. But the negative pressure at the moment of release was different: 52 cm for O_2 and 64 cm for H_2. If we assume that the effectiveness of the film in sustaining a negative pressure is inversely proportional to the area covered by the molecules, then the oxygen area is $64/52 = 1.23$ that of the hydrogen area. From this it follows that the diameter of the O_2 molecule is $\sqrt{1.23} = 1.11$ that of the H_2 molecule. This is a preliminary value of the *relative* diameters of O_2 and H_2 by a new method.

THICKNESS OF THE GAS FILM REQUIRED TO RELEASE THE COLUMN

The "thickness" of the gas film required to release a column under negative pressure is here defined as the ratio of the critical number of gas molecules on the electrode divided by the number required to form one complete monolayer (cubic array). It is thus necessary to know the diameter of the molecule in order to compute the thickness. Dushman[1] gives the values for H_2 and O_2 obtained by various methods, which range from 2.45 to 4.68 cm$\times 10^{-8}$ for H_2; and from 2.50 to 3.73 cm $\times 10^{-8}$ for O_2. I have chosen the values obtained by the application of the van der Waals' equation: $H_2 = 2.76$; $O_2 = 2.93$ cm$\times 10^{-8}$. The ratio of the diameters is $O_2/H_2 = 1.06$, as compared with the ratio 1.11 obtained by the negative pressure method just described.

NEGATIVE PRESSURE *VS* THICKNESS OF LIMITING GAS FILM

In a liquid column under negative pressure, the force of attraction across the boundary between the liquid and the containing solid is opposed by the hydrostatic head minus the vapor pressure in the reservoir. The introduction of a gas film in effect pushes the liquid surface away from contact with the solid surface. The attractive force diminishes as the distance between the two surfaces, i.e., the thickness t of the gas film, is increased. When t increases to the point where the attractive force per unit area is no longer greater than the opposing negative pressure, the column drops.

To investigate this relationship, a new apparatus, similar to that shown in Fig. 1, was constructed of soft glass. It was filled as shown with a normal solution of $CuSO_4$ and evacuated. The residual air pressure in the reservoir after sealing off was about 1 mm of water. The negative pressure when the tube was vertical was equivalent to 90 cm of water, which is the hydrostatic head less the vapor pressure of the solution in the reservoir at 17°C. The diameter of the spherical platinum electrode used was 0.90 mm.

The maximum charge on the electrode which the column could withstand under a negative pressure of 90 cm of water was 9.14μ coulomb. The deposition of one bivalent oxygen molecule represents the transfer of

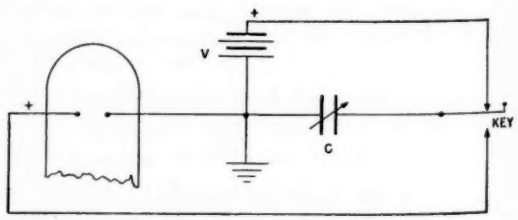

FIG. 2. Electrical circuit with quick-acting double-throw switch. Key shown in charging position.

[1] *Scientific Foundations of Vacuum Technique* (John Wiley and Sons, Inc., New York, 1949), p. 43.

4 electrons. The number of oxygen molecules on the electrode is now calculated from the relationship between the Faraday constant and Avogadro's number, as follows:

$$96\,500 \text{ coulombs} \times 4 \rightarrow 6.02 \times 10^{23} \text{ } O_2 \text{ molecules}$$
$$1 \text{ microcoulomb} \rightarrow 1.556 \times 10^{12} \text{ } O_2 \text{ molecules}$$
$$9.14 \text{ microcoulomb} \rightarrow 1.42 \times 10^{13} \text{ } O_2 \text{ molecules.}$$

The number of oxygen molecules required to form a complete monolayer on the electrode is next computed:

Diameter spherical electrode = 0.90 mm
Area spherical electrode = 2.54 sq mm
Diameter O_2 molecule = 2.93×10^{-8} cm
Projected area (cubic array) = 8.58×10^{-14} sq mm

$$2.54 \div (8.58 \times 10^{-14}) = 2.96 \times 10^{13} \text{ } O_2 \text{ molecules.}$$

The "thickness" of the gas film is then

$$\frac{1.42 \times 10^{13}}{2.96 \times 10^{13}} = 0.48 \text{ monolayer } O_2.$$

The above computation is based on the assumption that the charge Q is distributed uniformly over the surface of the electrode. But owing to the proximity of the electrodes, the density is not uniform, and is greatest at the point where the distance between the electrode surfaces is a minimum. Dr. Chester Snow kindly developed for me an equation giving the ratio of the density of the charge at this point to the average density. This ratio is 1.14 for the apparatus used. We have then to increase the computed thickness of the fractional monolayer by this factor, giving

$$O_2 = 0.48 \times 1.14 = 0.55 \text{ monolayer for } P_N = 90 \text{ cm.}$$

The above value provides the basic entry in Fig. 3, represented by the open circle. The tube was next inclined in different positions and the critical charge Q required to drop the column was measured. The ratios Q/Q_0, where Q_0 is the charge with the tube vertical, are plotted as abscissas in Fig. 3 (lower line). The corresponding negative pressures were determined by measuring the height of the column with a cathetometer and then correcting for density and for the vapor pressure in the reservoir at 17°C. Finally, the critical thickness of the film for each value of the negative pressure was found by multiplying Q/Q_0 by 0.55, the computed thickness for $P_N = 90$ cm.

It will be seen from Fig. 3 that the critical thickness of the gas film increases as the negative pressure is

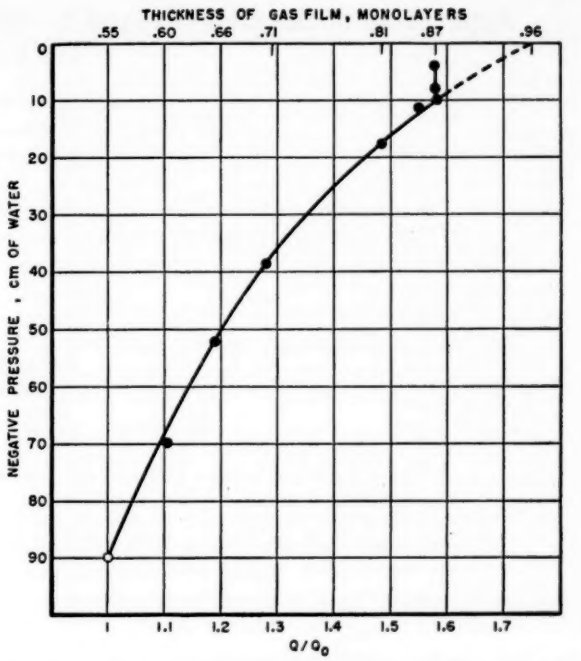

FIG. 3. Limiting negative pressure *vs* thickness of electrolyzed gas film on spherical electrode. Upper scale shows thickness of film in fractions of a monolayer, based on absolute measurement $t = 0.55$ at $P_N = 90$-cm water (open circle). Lower scale shows relative thickness of gas film with changing P_N.

decreased and approaches (but does not reach) one complete monolayer as the negative pressure approaches zero. The dotted line is an extrapolation of the curve to zero pressure, corresponding to a "thickness" of 0.96 monolayer. But actually the curve abruptly changes its direction when $P_N = 10$ cm of water. The charge required to drop the column remains constant as the negative pressure is further reduced, even though the computed area covered by the molecules of the gas film is only 0.87 of a complete monolayer. In effect the system acts as if the electrode were covered with a complete monolayer of gas. This effect is in accord with Langmuir's conclusion that the zone of influence of an *adsorbed* molecule extends beyond its projected area.

The conclusion that a liquid column can no longer sustain a negative pressure when an immersed platinum electrode carries an oxygen film equivalent to 0.87 of a complete monolayer is of course subject to the experimental uncertainty in the values chosen for the diameter of the oxygen molecule and for the area of the electrode. The experimental evidence clearly indicates that no appreciable negative pressure can be developed in the presence of a complete monolayer of gas at any point on the containing wall.

Application of the Cell Method to the Statistical Thermodynamics of Solutions. II. Experimental

V. MATHOT * AND A. DESMYTER †
Faculté des Sciences de l'Université Libre de Bruxelles, Brussels, Belgium
(Received August 13, 1952)

In connection with the theory of solutions proposed by Prigogine and Mathot [J. Chem. Phys. **20**, 49 (1952)], total vapor pressures and volume changes on mixing have been measured for the systems:

$CCl_4-C(Me)_4$ I
$C_6H_{12}-C(Me)_4$ II
$C_6H_6-C(Me)_4$ III.

Volume changes only for the systems:

$CCl(Me)_3-CCl_4$ IV
$CCl_2(Me)_2-CCl_4$ V
$CCl_3(Me)-CCl_4$ VI
$C(Me)_3OH-CCl_4$ VII.

For the first three systems I, II, and III, one observes a *positive* excess free energy (positive deviations to the Raoult law) together with a *negative* excess volume (contraction on mixing), whereas for the last four IV, V, VI, and VII there is a gradual passage from negative (IV) to positive (VII) excess volume. These results are discussed in terms of the molecular interactions AA, BB, and AB. Reasonable agreement is observed between Prigogine and Mathot's theory and experiment.

1. INTRODUCTION

APPLYING the cell method to liquid mixtures Prigogine and Mathot[1] have developed a new theory of solutions relating all thermodynamic properties to molecular interactions. The purpose of this work is to compare the preceding theoretical predictions with experiment.

The essential assumptions underlying the treatment are:

1. The molecules of the constituents A and B are spherical in shape with isotropic field of forces.
2. The distance of maximum interaction for AA, BB, and AB pairs is about the same.
3. There is random mixing.
4. The mean potential field in the "cage" is of the smoothed potential type (vertical walls and flat bottom) with both depth and width depending on concentration.

With these assumptions it is possible to calculate the excess free energy F^e, and any derived thermodynamic property in terms of the parameters δ and θ defined as

$$\delta=\frac{\Lambda_{BB}-\Lambda_{AA}}{\Lambda_{AA}}, \tag{1-1}$$

$$\theta=\left(\Lambda_{AB}-\frac{\Lambda_{AA}+\Lambda_{BB}}{2}\right)\Big/\Lambda_{AA}, \tag{1-2}$$

where $\Lambda_{ij}=-z\epsilon_{ij}^*$, z is the constant number of nearest neighbors, and ϵ_{ij}^* is the minimum potential energy of the pair $i-j$. Thus, the excess free energy F^e and the excess volume $v^e=v-v_Ax_A-v_Bx_B$ are given by [see reference 1, formulas (6–9) and (6–12)]

$$\frac{F^e}{NkT}=x_Ax_B\left(-1.439\frac{\Lambda_{AA}}{kT}\theta-12.16\frac{kT}{\Lambda_{AA}}[-\delta^2-2\theta+4x_B\delta\theta+4x_Ax_B\theta^2]\right), \tag{1-3}$$

$$\frac{v^e}{v^*}=1.64\frac{kT}{\Lambda_{AA}}(-\delta^2-2\theta+4x_B\delta\theta+4x_Ax_B\theta^2)x_Ax_B. \tag{1-4}$$

Let us consider two limiting cases of interest in connection with the experiments described later:

(a) When the interactions are due to dispersion forces

$$\Lambda_{AB}=(\Lambda_{AA}\cdot\Lambda_{BB})^{\frac{1}{2}}$$

and

$$\theta=-\frac{\delta^2}{8}$$

formulas (1–3) and (1–4) then become, neglecting third and higher order terms

$$\frac{F^e}{NkT}=x_Ax_B\left(\frac{1.439}{8}\frac{\Lambda_{AA}}{kT}+12.16\cdot\frac{3}{4}\frac{kT}{\Lambda_{AA}}\right)\delta^2>0 \tag{1-5}$$

$$\frac{v^e}{v^*}=-1.64\cdot\frac{3}{4}\frac{kT}{\Lambda_{AA}}\delta^2<0. \tag{1-6}$$

The excess volume is *negative* and proportional to the positive excess free energy.

* Chargé de Recherches du Fonds National de la Recherche Scientifique Belge.
† Titulaire d'une Bourse de Recherches de l'Institut pour la Recherche Scientifique dans l'Industrie et l'Agriculture
[1] I. Prigogine and V. Mathot, J. Chem. Phys. **20**, 49 (1952). I. Prigogine and G. Garikian, Physica **16**, 239 (1950).

TABLE I

	Boiling point under atmospheric pressure in °C	Slope of experimental $\ln_{10} p_{atmos}$ *versus* $1/T$ plot	Λ/kT values at 0°C (for $HOC(CH_3)_3$ at 25°C)	$(v^*/v)^2$ values from equation of state (1–10)	Experimental molar volume v at 0°C (for $HOC(CH_3)_3$ at 25°C)	v^* values from 2, 3, 4, 5	References
$C(CH_3)_4$	9.5	1264.14	15.68	0.9097	117.91	112.46	a
CCl_4	76.7	1741.10	21.6	0.9827	94.23	93.40	b
C_6H_{12}	81.4	1693.33	21.01	0.9773	105.57	104.36	c
C_6H_6	80.1	1789.00	22.20	0.9879	86.78	86.26	d
$ClC(CH_3)_3$	50.8				106.82		
$Cl_2C(CH_3)_2$	70.5				100.97		
Cl_3CCH_3	74.0	1729.00	21.45	0.9814	97.31	96.40	e
$HOC(CH_3)_3$	82.8	2381.00	27.07	1.0219	94.85	95.89	f

[a] "Selected Values of Properties of Hydrocarbons." Circular of the National Bureau of Standards C461 (1947).
[b] S. Young, Sci. Proc. Soc. Dublin NS **XII**, 374 (1909–10), as selected by J. Timmermans. See reference 6.
[c] Aston, Szasz, and Fink, J. Am. Chem. Soc. **65**, 1035 (1943).
[d] Willingham, Taylor, Pignocco, and Rossini, J. Research Natl. Bur. Standards **35**, 219 (1945).
[e] Rubin, Leven, and Yost, J. Am. Chem. Soc. **66**, 279 (1944).
[f] G. S. Parks and B. Barton, J. Am. Chem. Soc. **50**, 24 (1928).

(b) If the AB interaction is of the order of the AA interaction but the BB interaction is much larger, one may write

$$\Lambda_{AB} \simeq \Lambda_{AA} \quad \text{or} \quad \theta \simeq -\frac{\delta}{2},$$

$$\frac{F^e}{NkT} = x_A x_B \left[\delta \left(0.719 \frac{\Lambda_{AA}}{kT} - 12.16 \frac{kT}{\Lambda_{AA}} \right) + \delta^2 \left(12.16 \frac{kT}{\Lambda_{AA}} \right) (1 + x_B + x_B^2) \right] > 0, \quad (1\text{–}7)$$

$$\frac{v^e}{v^*} = 1.64 \frac{kT}{\Lambda_{AA}} x_A x_B [\delta - \delta^2 (1 + x_B + x_B^2)] > 0. \quad (1\text{–}8)$$

This time the excess volume becomes positive‡ and no longer remains symmetrical. The excess free energy is positive and much larger than it was in the dispersion forces case.

The major difficulty involved in the comparison of these predictions with experiment lies in the severe restrictions imposed by the theoretical requirements 1 to 4 on the choice of possible systems; condition 2 especially is very restrictive. Among the most immediate possibilities, we have studied the following seven systems:

I. 2,2-dimethylpropane–carbon tetrachloride (tetramethylmethane or neopentane)
II. 2,2-dimethylpropane–cyclohexane
III. 2,2-dimethylpropane–benzene
IV. 2-chlor-2-methylpropane–carbon tetrachloride
V. 2,2-dichlorpropane–carbon tetrachloride
VI. 1,1,1-trichlorethane–carbon tetrachloride
VII. 2-methyl-2-propanol–carbon tetrachloride.

The first three systems are thought to provide examples in which dispersion forces are predominant, especially system I. System VII is a good example of association in an inert solvent briefly discussed before ($\theta = \delta/2$). Systems IV, V, and VI are intermediate between I and VII, the polarity of one constituent gradually increasing from IV to VI. It should be kept in mind that when dealing with polar molecules, we "smear out" the anisotropic character of their interactions into the isotropic interaction parameter Λ, i.e., we only consider the case of central forces [according to assumption (1)]. This is why we have chosen molecules with spherical structure as demonstrated by their globular character (low entropy of fusion).

We have determined the excess free energy and excess volume for I, II, and III from vapor pressure and density measurements (see Sec. 4) and the excess volume only for IV, V, VI, and VII. Vapor pressure and heat of mixing experiments are now in progress in this laboratory in order to complete the measurements of the thermodynamic properties of these systems.

The constants Λ and v^* for the pure constituents have been calculated from informations on the liquid state itself,§ i.e., from the enthalpy of vaporization using formula[2]

$$\ln_{10} p_{atmos} = -0.295 \frac{\Lambda}{kT} - 5.15 + \ln_{10} \frac{\Lambda}{v^*} \quad (1\text{–}9)$$

and experimental values of $\ln_{10} p_{atmos}$ *versus* $1/T$.

The volume v^*, related to the distance of minimum interaction by

$$v^* = \gamma r^{*3},$$

is deduced from the Λ-value obtained as indicated, using the equation of state corresponding to the smoothed potential model[1]

$$\left(\frac{v^*}{v} \right)^2 = 1.1764 - 4.1833 \frac{kT}{\Lambda} \quad (1\text{–}10)$$

‡ For δ small compared to unity. For large δ, the exact expressions should be used instead of the series expansions (1–3) and (1–4) (see reference 1) and the discussion would remain the same.

§ Λ and v^* calculated from other experimental sources are not necessarily in agreement with these, a situation due to the limitations inherent in the cell model itself. See reference 2.

[2] I. Prigogine and G. Garikian, J. chim. phys. **45**, 273 (1948).

FIG. 1. Excess free energy of the systems I (○), II (□), and III (△).

and the experimental value of the molecular volume v.

Table I collects all data on the pure constituents with full references.

It should be noted that even for such similar molecules as those quoted, there is on the average 20 percent difference between the v^* values or 7 percent between the r^* values.

2. SYSTEMS I, II, AND III

The measured excess volume and excess free energy of the systems I, II, and III have been plotted in Figs. 1 and 2. The experimental points have been drawn with a vertical stripe indicating the magnitude of the experimental uncertainty. For the excess free energy a smoothed curve obtained as described in the experimental part has been drawn on the figure.

The excess free energy is *positive* and relatively large for systems of such similar constituents (especially I). The excess volume is *negative*: there is a definite contraction on mixing which, however small, definitely exceeds the experimental uncertainty.

Qualitatively the largest excess free energy (III) corresponds to the smallest excess volume (in absolute value) and vice versa. This situation is to be expected from a comparison of formulas (1–3) and (1–4) for systems having approximately the same δ-value. The obvious test for the theory is to see whether the interaction parameters θ calculated from the excess free energy measurements are consistent with those derived from volume changes on mixing. We have calculated the θ-parameters from expressions (1–3) and (1–4). θ is very close to zero so that the θ^2 term can be dropped in the calculation. The slightly unsymmetrical remaining expressions can be compared with the experimental smoothed values for equimolal mixtures.

Formulas (1–3) and (1–4) can then be transformed into

$$\theta(g^e)=\frac{\frac{4}{RT}(g^e)_{x=0.5}-12.16\frac{kT}{\Lambda_{AA}}\delta^2}{-1.439\frac{\Lambda_{AA}}{kT}+24.32\frac{kT}{\Lambda_{AA}}(1-\delta)}, \tag{2-1}$$

$$\theta(v^e)=\frac{\left(\frac{v^e}{v^*}\right)_{x=0.5}+\frac{1.64}{4}\frac{kT}{\Lambda_{AA}}\delta^2}{-\frac{1.64}{2}\frac{kT}{\Lambda_{AA}}(1-\delta)}. \tag{2-2}$$

For the v^* value of the mixture, the arithmetic mean of the "pure" v^* values has been used.

The results of these θ-calculations are collected in Table II. Incidentally, formula (1–4), quite apart from the approximate equation of state (1–10) also used in (1–3), involves a series expansion which does not converge very rapidly [see reference 1: passage from (5-6) to (5-7)]. Consequently, θ has also been calculated from the following more exact expression avoiding the use of any series expansion:

$$\theta(v^e)=\frac{4.1833\frac{kT}{\Lambda_{AA}}}{1.1764-\left[\left(\frac{v^e}{v^*}\right)_{x=0.5}+\frac{1}{2}\left(\frac{v_A}{v^*}+\frac{v_B}{v^*}\right)\right]^{-2}}-2-\delta. \tag{2-3}$$

In (2–3) v^e is the experimental smoothed value whereas v_A/v^* and v_B/v^* are calculated by (1–10). A comparison of line 6 and 7, Table II, gives an idea of the error introduced in (2–1) and consequently (1–3) by the use of this series expansion. For reference the θ-value for the dispersion forces case has also been tabulated on line 4.

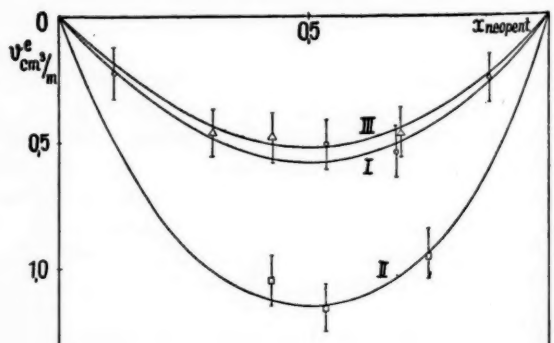

FIG. 2. Excess volume of the systems I (○), II (□), and III (△).

The scatter of the θ-value around zero is not very significant in view of the absolute error introduced in $\theta(g^e)$ and mainly in $\theta(v^e)$. Actually, a simple examination on the structure of formulas (2–2) and (2–3) shows that the uncertainty on the $\theta(v^e)$ value is so large that it is hardly possible to ascertain even the sign of the interaction parameter by this method. Therefore we have calculated backward the excess volume from $\theta(g^e)$ values (line 9) and compared it with the measured excess volume (line 8): the order of magnitude and the sign of the excess volume is correctly predicted by the theory. In view of the various approximations involved in the theoretical treatment, of the severe restrictions on the choice of the systems and of the inherent difficulty in measuring small differences between large quantities the agreement between experiment and theory could hardly be better than observed.

Incidentally, it is interesting to note that the behavior observed here experimentally (positive excess free energy and negative excess volume) cannot even qualitatively be accounted for by Longuet-Higgins theory of conformal solutions retaining only first-order terms.[3] His formula (9–7) (reference 9) gives

$$\Delta G/\Delta V=(RT-Q_0)/V(p\beta_0-T\alpha_0)>0$$

which is essentially positive. Thus, with a positive ΔG one should observe here a positive ΔV, which is obviously not the case.

The same theoretical predictions (excess free energy and excess volume of the same sign) have been attained earlier by Scatchard,[4] though starting from rather empirical assumptions, and apparently there is a large number of systems exhibiting this behavior.[5] A careful examination of these systems, however, reveals that none of them fulfils the theoretical requirements underlying the present treatment. This situation further emphasizes the importance of a proper choice of the systems.

TABLE II

	CCl_4–CMe_4	C_6H_{12}–CMe_4	C_6H_6–CMe_4
v^*	93.4 112.46	104.36 112.46	86.25 112.46
$\bar{v}^*$	102.93	180.41	99.35
δ	0.3775	0.3999	0.4158
$\theta=-\frac{\delta^2}{8}$	−0.0178	−0.0144	−0.0216
$\theta(g^e)$	−0.0245	−0.0079	−0.0510
$\theta(v^e)$ from 2–2 approx.	+0.0490	+0.2211	+0.0240
$\theta(v^e)$ from 2–3 exact	+0.0310	+0.1516	+0.0190
$\frac{v^e}{v^*}$ experimental	−0.00535	−0.0106	−0.00525
$\frac{v^e}{v^*}$ from $\theta(g^e)$ exact equat.	−0.0024	−0.0030	−0.0017
$\frac{v^e}{v^*}$ from $\theta(g^e)$ approx. equat.	−0.0032	−0.0029	−0.0031

TABLE III. Vapor pressure measurements at 0°C.[a]

System I. Tetramethylmethane–carbon tetrachloride			
x	p	g^e	
0	33.7	0	
0.059	84.8	24	
0.141	141.7	45	
0.249	201.4	60	
0.438	296.5	77	$\bar{\beta}=0.600$
0.649	383.6	69	
0.768	436.0	68	
0.815	451.8	51	
1	535.4	0	
System II. Tetramethylmethane–cyclohexane			
x	p	g^e	
0	29.2	0	
0.124	104.7	13	
0.417	261.4	35	
0.545	322.6	37	$\bar{\beta}=0.26$
0.821	449.3	19	
1	535.4	0	
System III. Tetramethylmethane–benzene			
x	p	g^e	
0	26.5	0	
0.114	160.3	86	
0.201	225.8	122	
0.295	275.8	140	
0.376	304.0	136	$\bar{\beta}=1.18$
0.448	337.5	146	
0.613	398.7	145	
1	535.4	0	

[a] x, mole fraction of neopentane. p, total vapor pressure in mm of mercury at 0°C. g^e, excess free energy in calorie per mole of mixture.

3. SYSTEMS IV, V, VI, AND VII

The measured excess volume of these four systems has been represented in Fig. 3.[11] There are unfortunately little data available on the Λ of the pure constituents. Therefore we intend to discuss the preceding results from a more qualitative point of view. This series of systems provides a very striking example of the influence of both δ and θ parameters on the excess volume. Systems I and VII typify, respectively, the case of dispersion forces and association in an inert solvent. Systems IV, V, and VI are intermediate cases where the interaction BB gradually increases whereas Λ_{AB} tends towards the Λ_{AA} value. Indeed the boiling point of the second constituent (Table I) increases in the order

$$bp_{ClCMe_3}<bp_{Cl_2CMe_2}<bp_{Cl_3CMe}.$$

Any further discussion must be postponed until more information is available.

[3] Longuet-Higgins, Proc. Roy. Soc. (London) **A205**, 247 (1951); **A209**, 28 (1951); **A209**, 416 (1951).

[4] G. Scatchard, Trans. Faraday Soc. **33**, 160 (1937).

[5] See, for example, J. H. Hildebrand and R. L. Scott, *Solubility of Non Electrolytes* (Reinhold Publishing Corporation, New York, 1949), p. 142.

[11] The measurements on systems IV, V, and VI have been performed by M. Lebrun, Mémoire de Licence, Université de Bruxelles, 1951.

TABLE IV. Volume measurements.[a]

System I. Tetramethylmethane–carbon tetrachloride at 0°C

$x_{C(Me)_4}$	d	v^e
0	1.6327	0
0.1094	1.5002	−0.23
0.5356	1.0346	−0.51
0.6765	0.8984	−0.54
0.8610	0.7301	−0.25
1	0.6113	0

System II. Tetramethylmethane–cyclohexane at 0°C

$x_{C(Me)_4}$	d	v^e
0	0.7972 (extrapolated)	
0.4242	0.7204	−1.05
0.5333	0.7005	−1.16
0.7387	0.6619	−0.95
1	0.6113	0

System III. Tetramethylmethane–benzene at 0°C

$x_{C(Me)_4}$	d	v^e
0	0.9000 (extrapolated)	
0.3071	0.7956	−0.46
0.4272	0.7587	−0.48
0.6835	0.6881	−0.46
1	0.6113	0

System IV. Chlor-2-methyl-2-propane–carbon tetrachloride at 0°C

x_{CCl_4}	d	v^e
0	0.8666	0
0.141	0.9647	−0.13
0.261	1.0506	−0.20
0.508	1.2349	−0.257
0.552	1.2687	−0.249
0.725	1.4052	−0.208
0.914	1.5621	−0.144
1	1.6325	0

System V. Dichlor-2,2-propane–carbon tetrachloride at 0°C

x_{CCl_4}	d	v^e
0	1.1191	0
0.102	1.1690	−0.062
0.262	1.2478	−0.08
0.438	1.3373	−0.152
0.575	1.4077	−0.145
0.726	1.4865	−0.118
1	1.6325	0

System VI. Trichlor-1,1,1-ethane–carbon tetrachloride at 0°C

x_{CCl_4}	d	v^e
0	1.3711	0
0.220	1.4250	+0.147
0.473	1.4889	+0.238
0.511	1.4986	+0.252
0.687	1.5453	+0.221
0.834	1.5863	+0.097
1	1.6325	0

System VII. Methyl-2-propanol-2–carbon tetrachloride at 25°C

x_{CCl_4}	d	v^e
0	0.7814	0
0.2190	0.9572	+0.32
0.5698	1.0773	+0.48
0.6781	1.3319	+0.54
0.7049	1.3440	+0.52
0.8083	1.4275	+0.39
1	1.5845	0

[a] x, mole fraction. d, density. v^e, excess volume in cm³ per mole of solution.

4. EXPERIMENTAL

a. Pure Materials

The carbon tetrachloride, cyclohexane, tert. butyl chloride, 2,2-dichlorpropane, methylchloroform samples have been provided by the Bureau International des Etalons Physico-chimiques. Their physical constants and purification methods have been fully described.[6]

The neopentane sample used was a product of the Phillips Petroleum Company research grade (indicated purity 99.83 mole percent). It was used without any further purification. The tert. butyl alcohol has been provided by the Shell Company. It was purified by several fractional fusions. Melting point of the initial material: 24°C. Melting point of the purified sample used: 25.50°C.

b. Vapor Pressure Measurements

The total vapor pressure was measured by the static method already described elsewhere.[7] The liquids were degassed by boiling under vacuum, distilled into small glass bulbs and sealed off for weighing. These bulbs again were broken under vacuum by a magnetic hammer and distilled into the tensiometer consisting of a U-type mercury manometer connected to a 1–2 cm³ bulb. The tensiometer was then sealed off and completely immersed in an ice thermostat.

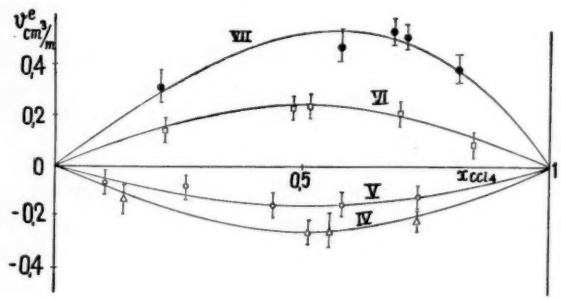

FIG. 3. Excess volume of the systems IV (△), V (○), VI (□), and VII (●).

When the departure from ideality is not too large one can obtain the excess free energy directly from the total vapor pressure by using, for the activity coefficients, the Duhem-Margulès series expansion limited to the first term[8]

$$\ln \gamma_A = \beta x_B^2, \qquad \ln \gamma_B = \beta x_A^2, \tag{4-1}$$

where β is independent of x and p in the pressure range considered. Then it can be shown that

$$g_e = \beta RT x_A x_B \tag{4-2}$$

with[8]

$$\beta = \frac{p - p^*}{x_A x_B (p_A^0 + p_B^0) - p^*}. \tag{4-3}$$

p = total vapor pressure of the mixture, p^* = total ideal vapor pressure of the mixture, and p_A^0, p_B^0 = vapor pres-

[6] J. Timmermans, *Physico-Chemical Constants of Pure Organic Compounds* (Elsevier Publishing Company, Inc., Houston, 1950).
[7] V. Mathot, Bull. soc. chim. Belges **59**, 111 (1950).
[8] N. I. Joukowski, Bull. soc. chim. Belges **43**, 299 (1934).

sure of pure A or B. From (4–2) and (4–3) every measurement of the total pressure gives a value of g^e, so long as (4–1) is obeyed. The results of the measurements are given in Table III. The mole fractions have been corrected for vaporization of the solution into the gas phase of different composition contained in the dead space of the tensiometer.

The plain curves in Fig. 1 represent Eq. (4–2) with $\tilde{\beta}$ equal to the arithmetic mean of the β's calculated from each measured vapor pressure. The points in Fig. 1 correspond to the actual measurements.

The experimental error in the pressure is about 0.1 mm of mercury. The mole fraction is known to about 2 percent because of the volatility of the neopentane. Still the difference $p-p^*$ being relatively large, β is determined to ± 5 percent approximately which corresponds altogether to an average error of ± 10 percent on the excess free energy.

c. Density Measurements

The excess volume has been calculated from density measurements. Table IV and Figs. 2 and 3 give the numerical results, corrected for the effect of buoyancy in air and for the weight of the vapor in the pycnometer tubes.

For the systems I, II, and III in which one constituent is very volatile (neopentane), a special pycnometer has been used (Fig. 4). A cylindrical bulb of approximately ten cc is provided with two parallel graduated capillary tubes (10 cm in length and 0.015 cm² in cross section) both fitted with a ground cap. A suitable small hole has been bored in both cones and sockets to equalize the pressure on each side by turning the caps. To prepare the solution, a certain amount of the less volatile component is first weighed in the pycnometer. The pycnometer is then cooled to a temperature slightly below 0°C and nearly filled with pure neopentane by condensation from a storage cylinder, with constant stirring in order to mix thoroughly the solution. It is then put into melting ice. When thermal equilibrium has been reached and pressure equalized in the capillaries the position of the liquid menisci is observed and the pycnometer is weighed. These filling and weighing operations are carried out in a refrigerated room, thermostated at 0°C, (although, even at 15°C the vapor pressure of the solution is below one atmosphere up to a mole fraction of 0.7–0.8).

5. CONCLUSION

This work provides some experimental evidence in favor of the theory of solutions developed by Prigogine and Mathot.[1] The main interest of this theory is to relate the sign of the excess functions to the available information on the intermolecular forces ϵ_{AA}^*, ϵ_{BB}^*, ϵ_{AB}^*. Within the limits of experimental errors, the predicted relationship between vapor pressure and volume measurements is obeyed for the systems I, II, and III, whereas the remarkable sequence of excess volume observed for systems IV, V, VI, and VII can be

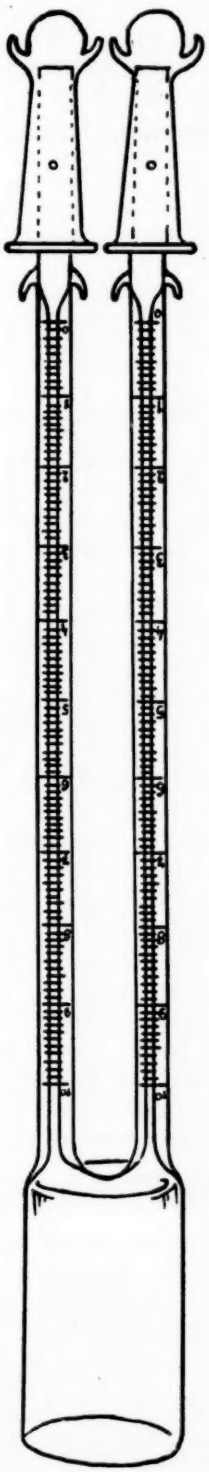

FIG. 4. The pycnometer.

reasonably explained in terms of molecular interactions.

By far the best test of the theory is to compare heat of mixing and vapor pressure data, which are both very sensitive to molecular interaction. It should even be possible to calculate the properties of the liquid solution from virial coefficient measurements on pure and mixed gases.

ACKNOWLEDGMENTS

We are much indebted to Professor Prigogine for constant advice and interest, to Professor Timmermans in whose laboratory the measurements have been made, to the Bureau International des Etalons Physico-chimiques who has provided many pure chemicals, and to the Centre de Physique Moléculaire for financial aid.

THE JOURNAL OF CHEMICAL PHYSICS VOLUME 21, NUMBER 5 MAY, 1953

On the Emission Bands of the NO Molecule in the Vacuum Ultraviolet Region*

YOSHIO TANAKA †
Department of Physics, The University of Chicago, Chicago 37, Illinois
(Received September 3, 1952)

With 85-cm and 21-foot normal-incidence vacuum spectrographs the NO emission spectrum in the far-ultraviolet region was investigated. The existence of the ϵ-system is confirmed. The β' bands are reinvestigated, and a curious appearance was observed in the (4,0) band. New bands which have an appearance similar to the β' bands are observed in the region of 1500A, and tentative analysis is made.

INTRODUCTION

RECENTLY, many authors have been interested in studying the emission and the absorption spectra of NO throughout the region from the infrared to the far ultraviolet. Leifson's[1] pioneer work on the absorption bands of NO in the far-ultraviolet region confirmed the β- and the γ-bands which were well known in the emission work. He found a new group of bands in the same region, and Birge[2] later called it the "ϵ-bands." As regards the existence of the ϵ-bands, Herzberg and Mundie[3] have presented the explanation that the ϵ-bands in Leifson's spectrogram are merely the extension of the γ-progression. They further proposed the existence of predissociation at around $v'=4$ of the upper state of the γ-bands to explain the intensity anomaly existing in between the (3,0) and the (4,0) bands in that progression. Gaydon[4] and Ogawa[5] independently studied these bands in emission and, after making a rotational analysis, both of them confirmed the existence of the ϵ-bands. Tanaka[6] has studied the absorption bands of NO in the far-ultraviolet region, and, observing the diffuse appearance of the (4,0) γ-band, he thought that there was a predissociation around $v'=4$ in the γ-bands. However, the (4,0) band of the γ-system and the (0,0) band of the ϵ-system appear at almost the same position, making it quite difficult to separate them without using equipment with large dispersion.

On the other hand, Flory and Johnston[7] made a precise measurement of the photochemical decomposition of the NO molecule due to the radiations which correspond energetically to the (1,0), (2,0) δ-bands, and they proposed a predissociation at around $v'=1$ and $v'=2$ in the upper state of the δ-bands. Tanaka[6] confirmed their idea by observing a diffuse and enormously strong appearance of these bands in absorption. The δ-bands, which had been discovered by Knaus[8] in emission, have a peculiar appearance—namely, in emission, only the $(0,v'')$ progression is observed, and it is in the afterglow of nitrogen, rather than in the ordinary discharge, that the bands are highly excited. This progression is especially well developed in the air afterglow in its blue stage.[9] After considering the above evidence, one is quite certain to conclude that there is predissociation around $v'=1$ in the upper state of the δ-bands.

As regards new electronic bands of the NO molecule, Feast[10] recently studied the 6000A bands which had been previously observed and ascribed to NO^+ molecules by Duffieux and Grillet.[11] Feast made a rotational analysis of these bands and concluded that these bands are due to the transition from the upper new $^2\Sigma$ state (E) to the upper state of the γ-bands ($^2\Sigma^+$) of the NO neutral molecule. Recently, Tanaka and his co-workers[12] found the absorption bands which correspond to the

* This work was assisted by the U. S. Office of Naval Research under Task Order IX of Contract N6ori-20 with the University of Chicago.

† On leave from the Department of Physics, the Tokyo University of Education, 24 Otsuka-Kubomachi, Bunkyo-ku, Tokyo, Japan. Address after September 15, 1952: Cambridge Air Force Research Center, Cambridge, Massachusetts.

[1] S. W. Leifson, Astrophys. J. **63**, 73 (1926).
[2] R. T. Birge, Trans. Faraday Soc. **25**, 707 (1929).
[3] G. Herzberg and L. G. Mundie, J. Chem. Phys. **8**, 263 (1940).
[4] A. C. Gaydon, Proc. Phys. Soc. (London) **95**, 56 (1944); **96**, 160 (1944); Nature (London), **153**, 407 (1944).
[5] M. Ogawa, Science of Light **1**, 19 (1951).
[6] Y. Tanaka, J. Sci. Research Inst. Tokyo **43**, 160 (1949).
[7] P. J. Flory and H. L. Johnston, J. Am. Chem. Soc. **57**, 2641 (1935).
[8] H. P. Knauss, Phys. Rev. **32**, 417 (1928).
[9] Y. Tanaka and M. Shimazu, J. Sci. Research Inst. Tokyo **43**, 9 (1949).
[10] M. W. Feast, Can. J. Research, **A28**, 488 (1950).
[11] M. Duffieux and L. Grillet, Compt. rend. (Paris) **202**, 957 (1936).
[12] Tanaka, Seya, and Mori, J. Chem. Phys. **19**, 979 (1951).

transition between the upper state of Feast's bands and the ground state ($^2\Pi$) of NO.

There is another new group of bands which has been observed very recently by Miescher and Baer[13] in emission in the region between 1570A and 2000A. These bands are double-headed and degraded towards the red. The explanation given by Miescher and Baer is that this corresponds to the transition between the new upper state and the ground state ($^2\Pi$). They named it the β' system, which has the upper $B'\,^2\Pi$ state, because of the similarities between these bands and the β-bands with respect to their appearance and molecular constants. At almost the same time, Tanaka and his coworkers[14] found these bands in absorption as well as in emission.

The main purpose of the present work is to reinvestigate the NO bands in emission in the far-ultraviolet region because, in the former work, not only did there appear some impurity bands (mostly CO bands), but also the NO bands were so poor the measurements could not be accurately carried out. Another purpose is to find some new band systems which can be expected from the results obtained in the absorption work.

EXPERIMENTAL PROCEDURES

Two vacuum spectrographs (both of them normal-incidence type) one with a 85-cm grating and the other with a 21-foot grating, were used. The small one has a dispersion of 15A/mm, and the plate covers from zero to about 3000A in the first order. The larger one was made by Harrison[15] a long time ago, and recently it has been reconstructed in the University of Chicago. The ruled area of the grating used is about 2×6 inches and has 15 000 lines/inch. The dispersion is about 2.7 A/mm, and a 4×16 inch plate is used enabling about a 1000A region to be covered on one plate.

Tank nitrous oxide (N_2O) gas, which was dried by passing it through $CaCl_2$, was used most of the time. To check the appearance of the N_2O spectrum, sometimes N_2+O_2 mixtures, in various proportions, were also tried. In the latter case, the tank nitrogen was purified by passing it through hot copper and then a trap cooled with liquid nitrogen. It was finally stored in a flask 3 liters in capacity. This nitrogen was then mixed in the discharge tube with tank oxygen which was dried by passing it through a trap cooled with liquid nitrogen. No differences were observed in the spectrum in the two cases. There were no troubles due to the presence of the CO fourth positive bands, but the Lyman-Birge-Hopfield bands of the nitrogen molecule appeared with strong intensity. No window was used between the spectrograph and the discharge tube so the gas went to the spectrograph through the slit and was pumped out by an oil diffusion pump (for the small spectrograph, an ordinary oil diffusion pump made of glass is used, but for the big spectrograph a big oil diffusion pump made of metal is used) backed by a Megavac pump. The pressure in the discharge tube was varied from a few tenths mm to a few mm Hg.

It is already known that the N_2O molecule has continuous absorptions below 2000A at around 1900A, 1466A, 1284A, 1176A, and 1096A, but in the present work these continua presented no serious problems. The main reason why we did not use NO gas was to get away from the self-absorption of the molecule. The intensity of the absorption bands of NO below 1850A is strong; therefore, if we had used NO gas, there was a possibility of missing the $(v',0)$ band progression in the emission work unless we used the gas at very low pressures (in this case, there is a great possibility of contamination by impurity bands), or diluted with a noble gas like helium as was done by Miescher and Baer.

With N_2O gas, there appears a strong air afterglow, greenish-yellow in color, outside the main discharge, and sometimes it goes into the spectrograph through the slit and causes unfavorable fogging of the plate, especially in the case of the small spectrograph.

An ordinary II-shaped discharge tube, which was made of Pyrex glass 5 mm in diameter and 40 cm in length, was used. The outside of the main part was cooled with running water. A transformer 2KV, 4KVA was used with the primary current of 15A. In the case of the big spectrograph, exposure time was varied from 3 to 8 hours. In the small spectrograph, 5 minutes was sufficient for the strong bands, but for the weak ones one hour was necessary. In the present case, the current density was quite high so that the rotational structure is well developed up to high J values, especially in the strong γ-bands. As pointed out by Gaydon, such a condition is not desirable in searching for new weak bands because of possible masking of the weak bands by strong, well-developed, known bands. We tried also a low current density discharge in parallel.

Ilford QI and Kodak SWR[16] plates were used. In this author's opinion, the QI plate has a finer grain emulsion than the SWR plate so that, for the fine structure measurement, QI is preferable. But, as regards sensitivity, the SWR is much superior to the QI plate. For the small spectrograph, mostly QI extra-thin plates were used because the SWR film is so thin that it was difficult to fix it in the right position on the focal plane.

RESULTS AND DISCUSSION

As stated above, the spectrograms were taken using two vacuum spectrographs, employing the small spectrograph for the preliminary vibrational analysis and the big one for the fine-structure analysis. The latter work is still going on; at present the results obtained by the former work are reported.

Figure 1 is a reproduction of one of the plates taken with

[13] P. Baer and E. Meischer, Helv. Phys. Acta **24**, 331 (1951).
[14] Tanaka, Seya, and Mori, Science of Light **1**, 80 (1951); Y. Tanaka and T. Sai, Science of Light **1**, 85 (1951).
[15] G. R. Harrison, Rev. Sci. Instr. **4**, 651 (1933).
[16] A. L. Schoen and E. S. Hodge, J. Opt. Soc. Am. **40**, 23 (1950).

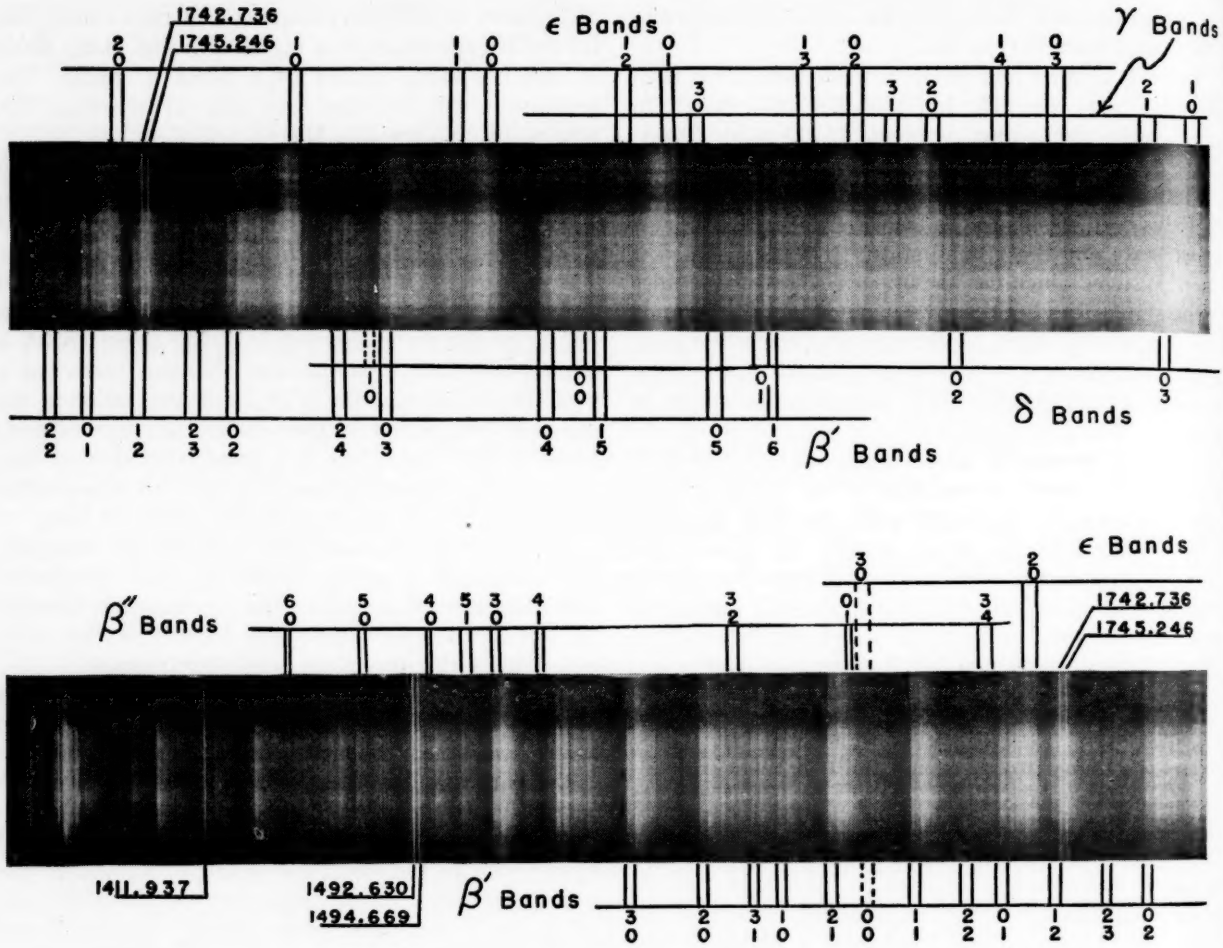

FIG. 1. NO emission bands.

the 85-cm vacuum spectrograph using N_2O gas as an emitter. With a gross survey, the NO bands appear very strong, in addition to N_2 L-B-H bands which appear mostly in the region below about 1500A. There are almost no contaminations by the CO fourth positive bands; but in the long wavelength end of the plate OH bands appear weakly.

The γ-bands are strongest of all the NO bands, and we can follow them up to the (3,0) band on the shorter wavelength side. In the sequence $\Delta v=+2$, the (4,2) γ-band comes close to the (0,2) ϵ-band, and in the sequence $\Delta v=+3$, the (4,1) γ-band also comes close to the (0,1) ϵ-band. Strong bands are actually observed in both positions. If we consider these two bands as belonging to the γ-system, then there appear intensity anomalies at the position of each of these bands in the corresponding sequences. If, however, we consider them as belonging to the ϵ-system, then the intensity relation in the $(0,v'')$ progression looks normal. A similar anomaly of the band intensity was observed in the sequence $\Delta v=+1$ in the γ-bands, but this is not as conspicuous as in the cases mentioned above. The clearest discrimination of the existence of the ϵ-bands is the strong appearance of the (0,0) band. Unfortunately, in Gaydon's plate it appeared very weak because he investigated with a quartz spectrograph. Tanaka and Sai worked with a vacuum spectrograph in this region,

TABLE I. ϵ-system (below 2000A).[a]

v' \ v''	0	1	2
0	53 145.4(4)	51 273.1(4)	
	169.7(5)	293.6(5)	
	269.1(5)	395.1(4)	
	287.9(5)	414.9(5)	
1	55 421.9(4)	...	51 731.2(2)
	447.4(5)	53 559.3(3)	750.7(2)
	547.5(4)	...	...
	568.5(4)	53 672.5(3)	...
2	57 658.2(4)	...	...
	680.8(5)	...	53 939.8(2)
	778.8(5)	55 892.8(2)	54 067.5(2)
	800.5(6)	...	...
3	...	...	
	59 888.1(1)	57 981.8(3)	
	...	...	
	59 997.4(3)	58 113.2(2)	

[a] Vibrational constants for the upper state: $\omega_e=2325$ cm^{-1}, $\omega_e x_e=23$ cm^{-1}.

TABLE II. β' system.[a,b]

v' \ v''	0	1	2	3	4	5	6
0		[c]58 022.5(2)	56 170.3(4)	54 354.9(4)	52 562.7(4)	50 799.6(3)	
		[c]...	192.7(3)	370.3(4)	577.6(3)	810.4(3)	
		143.6(3)	296.8(3)	457.0(4)	683.4(3)	...	
		158.8(3)	311.4(3)	491.8(4)	699.5(3)	936.7(4)	
1	61 078.4(4)	59 186.7(5)	57 360.8(3)	strong		52 000.5(2)	50 246.7(3)
	...	203.8(5)	[c]379.6(3)	ϵ(1.0)		...	275.8(1)
	214.5(4)	327.1(5)	494.4(4)			125.4(2)	369.2(3)
	...	340.5(5)	...			...	383.2(4)
2	62 237.8(6)	60 355.1(5)	58 525.1(1)	56 692.9(1)	54 901.0(3)		
	...	...	...	714.4(1)	...		
	369.0(6)	495.0(5)	655.2(1)	808.5(1)	55 032.7(3)		
	...	...	...	827.6(1)	...		
3	63 348.9(5)	61 482.1(4)					
	363.3(5)	494.6(3)					
	486.8(5)	613.2(4)					
	...	...					

[a] Vibrational constants for the upper-state: $\omega_e' = 1211$ cm^{-1}. $\omega_e'x_e' = 12.5$ cm^{-1}.
[b] Figures in parentheses: intensity.
[c] Superposed with other band or line.

TABLE III. β''-system[a,b]

v' \ v''	0	1	2	3	4	5	6	7
0	62 014.7(2)	...						
	...	60 231.5(2)						
1	[c] Tail of $\beta'(3,0)$							
2	64 361.3(3)	62 482.8(1)		...	57 037.3(1)			
	483.7(4)	612.3(1)		58 930.3(1)	...			
3	65 521.4(6)		61 778.4(3)	...	...	56 418.1(1)	...	52 965.5(1)
	635.8(6)		912.6(3)	60 086.8(2)	58 304.3(1)	538.4(1)	54 801.4(3)	53 094.4(1)
4	66 633.8(4)	64 743.4(1)		[c]61 078.4(3)	[c]59 263.1(3)			
	738.7(3)	...		214.5(3)	...			
5	67 688.8(3)	...					56 876.4(2)	
	...	65 947.8(2)					...	
6	68 617.7(2)	66 738.7(2)						
	741.3(2)	...						

[a] Vibrational constants for the upper-state: $\omega_e' = 1207$ cm^{-1}, $\omega_e'x_e' = 9$ cm^{-1}.
[b] Figures in parentheses: intensity.
[c] Superposed with other band or line.

but in their plate also this band appeared weak. This was due to the fact that they used NO gas as the emitter and thus the intensity of this band was reduced somewhat because of self-absorption.

In the present work, as shown in Fig. 1, the (0,0) band appeared very strong. Simple calculation shows that the heads of the (4,0) γ-bands come close to the heads of the (0,0) ϵ-band. Even if there is no predissociation at $v'=4$ of the upper state of the γ-band, the (4,0) band should be quite weak because, in the (v',0) progression of the γ-bands, the (0,0) band is the strongest and the intensity is gradually reduced as the v' value increases. Furthermore, the (3,0) band appears quite weak. If there is predissociation at $v'=4$, as proposed by Herzberg and Mundie,[5] the actual intensity of the (4,0) γ-band should be much weaker than that of the (3,0) band. However, in the plate there appeared a very strong double double-headed band. It is safe, therefore, to conclude that this band is the (0,0) ϵ-band. The (1,1) ϵ-band appeared with a medium intensity, but the (2,2) band was very weak.

It seems worth while to note that the distribution of rotational fine structures is homogeneous near the head of the (0,1) and the (0,2) band, but in the region between the heads of the (0,0) and (1,1) bands it looks inhomogeneous. We offer no explanation as to whether this is due to perturbations or to superpositions of some other bands.

The (v',0) progression of the ϵ-bands can be extended clearly up to the (2,0) band. The (3,0) band was very weak, and, moreover, in this position there is present the (0,0) β' band and the (0,4) band of the N_2 L-B-H bands. It is thus difficult to identify the (3,0) band without doubt. The intensity of the (1,0) band is slightly stronger than that of the (0,0) band. The (2,0) band appears with medium intensity. The (3,1) band is also observed. In Table I, the results of the measurements for the ϵ-bands are shown.

It is well known that the β- and δ-bands of NO appear stronger in nitrogen afterglow than in the ordinary discharge. As in the usual case, in the present work the β-bands were very weak and the δ-bands also appeared

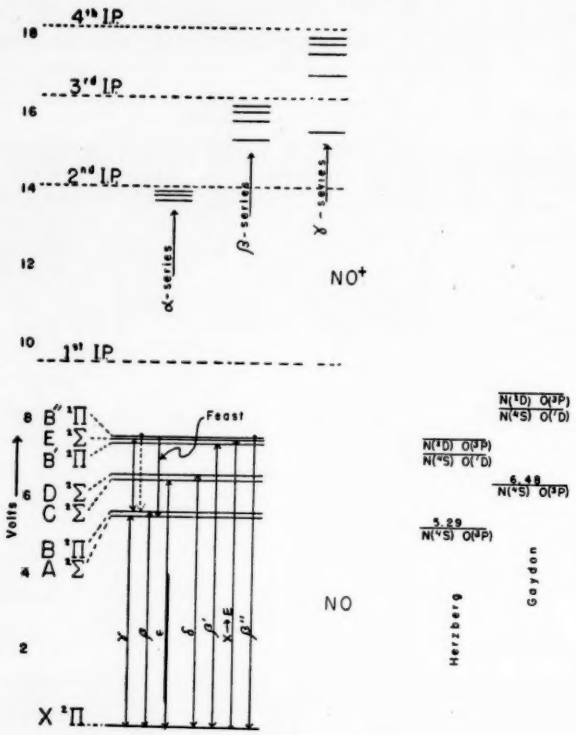

FIG. 2. Energy level diagram of NO molecule.

weak. As mentioned before, the δ-bands had first been observed by Knaus[8] in emission, and he obtained a single progression of $(0,v'')$ in the nitrogen afterglow. Flory and Johnston[7] have proposed a predissociation at $v'=1$, and $v'=2$ in the upper state. Afterwards, Tanaka confirmed their proposal by observing the strong and diffuse appearance of the (1,0) and (2,0) bands in absorption.

In Fig. 1, as mentioned above, the rotational lines of the γ- and ϵ-bands are well developed in their high J values. It was therefore difficult to pick up the δ-bands isolated from them; still, some of the δ-bands were identified. As in the case of Knaus, there is observed only a single $(0,v'')$ progression. It was also observed that these bands have an appearance different from that of the γ- and ϵ-bands—namely, several rotational lines near the heads are observable. Schmid[17] has made the rotational analysis for some of the δ-bands but he has not remarked on such a curious feature. It seems likely to consider that there might be a predissociation even in $v'=0$ of the upper state of the δ-bands.

Very recently, Miescher and Baer[13] found a new band system of NO in emission in the region 1500–2000A. Tanaka and Sai[14] found the same bands independently in emission, and Tanaka, Seya, and Mori[14] also found these bands in absorption together with other new bands. Tanaka and Sai used NO gas at the various pressures, but, as mentioned above, no window is used to separate the spectrograph and discharge tube, so that the $(v',0)$ progression was not conspicuous due mainly to self-absorption. In the present case, as shown in Fig. 1, they appeared very clearly. Meischer and Baer, however, obtained this system using helium containing a small amount of NO. They suggested that the strong appearance of these bands was due to the energy transfer from helium atoms to NO molecules to excite them into the upper state of the bands. In the present case, N_2O and N_2+O_2 mixtures were used, and, in both instances, these bands nevertheless appeared strong.

All the bands belonging to this system degrade towards the red and have double heads, but close inspection shows that some of them have double double-heads—we can see them clearly in the (1,1), (0,2), and (0,3) bands. According to Jenkins, Barton and Mulliken's[18] work on NO β-bands ($B\,^2\Pi\rightarrow X_A\,^2\Pi$), the Q branches of each of the sub-bands are very weak and thus each band has two heads, because both the upper and lower states can be considered as Hund's case (a). As observed by Miescher and Baer, and in the present work, the doublet separation of the bands is almost equal to the doublet separation of the ground state. Therefore, if the upper state of these bands, as suggested by Miescher and Baer, is $^2\Pi$, then the spin separation of this state is very small and we can assume that this state will be Hund's case (b). If this is true, then, as in the case of SiF α-bands ($^2\Pi(b)\rightarrow{}^2\Pi(a)$), there is a possibility of the appearance of $^SR_{21}$ and $^QR_{12}$ branches forming weak heads, thus giving the whole band four heads.

Most of the bands belonging to the $\Delta v<0$ sequences appear in the region where strong ϵ-bands are present, but still we can observe the $(0,v'')$ progression up to the (0,5) band. The (0,0) band is very weak, and it also comes almost in the same position as the (3,0) ϵ-band and the (0,4) L-B-H N_2 band. In the $(v',0)$ progression, the intensity of the bands goes up smoothly up to the (3,0) band, but in the expected position of the (4,0) band there appears a band which is double-headed, and each of the heads is cut off sharply at about 1.5A on the longer wavelength side. If we suppose these to belong to the (4,0) β'-band, its separation of the heads comes out to be 117.5 cm^{-1}, and it is almost equal to the separation in the other bands belonging to β'-system. However, if we make a $\Delta G:v$ curve for the upper state of this system including this band, there comes an irregularity on the curve between $v=3$ and $v=4$—namely, $\Delta G_{v+\frac{1}{2}}$ is abnormally big compared with $\Delta G_{v\frac{1}{2}}$. Considering the curious appearance of this band (abruptly cut off), together with this irregularity of the $\Delta G:v$ curve, it seems probable that there is a perturbation or a predissociation in the $v'=4$ level. The results of the measurement of this system are shown in Table II.

Near the calculated positions of the (5,0) and (6,0) bands there appear similar types of bands—i.e., double-headed and degraded towards red. The former

[17] R. Schmid, Z. Physik **64**, 279 (1930).

[18] Jenkins, Barton, and Mulliken, Phys. Rev. **30**, 150 (1927).

has strong intensity, comparable to the (3,0) band, but the latter is weak. If we assume these as the (5,0) and (6,0) bands of the β' system, then the $\Delta G:v$ curve shows strong irregularities at $v=4$, 5, and 6. Moreover, the intensity distribution in the $(v',0)$ progression also, shows an irregularity at the same position; therefore it seems more likely that these bands belong to another new system including the other weak bands which appear below 1500A.

A preliminary vibrational analysis was attempted, and the results obtained are shown in Table III. Unfortunately, except for a few, most of the bands are very weak so that the measurement did not carry out accurately. Considering the similarities of the molecular constants and of the appearance between this system and the β' system, the upper state of this system will also be $^2\Pi$, and the separation of two heads of each band is nearly equal to the spin separation of the ground state $^2\Pi$, so that, as mentioned above, the upper state of the system will be Hund's case (*b*). Of all the bands belonging to this transition, the (3,0) band is abnormally strong.

Recently, Ogawa[19] found that a part of the bands which he found in the high pressure NO discharge in the visible region are attributable to the transition between the upper state of the β' bands and the upper state of the β-bands. He also found there still remain some bands which cannot be explained by this transition. But, if we assume a new electronic state, then they are explainable as a single progression from a certain vibrational level of the supposed electronic state to the various vibrational levels ($v''=0$, 1, 2, $\cdots$, 5) of the upper state of the β-bands ($v'=$constant and v'' progression).

Incidentally, the (3,0) band of the new system found in the present work agrees well with the expected band which comes from the transition from the upper level assumed by Ogawa to the $v''=0$ of the ground state $^2\Pi$. The latter also said that he could find an absorptoin band exactly in the same position (1526.5, 1523.7A) of the (3,0) band in the plates which are taken by Seya.

There remain some bands unclassified below 1500A (1464.3, 1461.1, 1460.2, and 1450.2A). Though strong N_2 bands appear in this region, these four bands are easy to distinguish from them and seem to belong to another system of the NO molecule.

It can be expected that the $E\rightarrow X$ band should be appearing in the region now investigated. These bands were examined in the plates, but could not be distinguished with certainty.

In absorption, there appear many other bands below 1500A and most of them are diffuse, but some others are sharp. It can be expected that there should appear some new bands corresponding to the sharp bands in emission below 1500A. The electronic energy levels of NO which are known up to present are shown in Fig. 2. This work is still in continuation.

In conclusion, the author wishes to express his hearty thanks to Professor R. S. Mulliken and Professor J. R. Platt for their valuable suggestions and discussions. He also wishes to express this thanks to Dr. D. Leenov for his great help in the construction of the big vacuum spectrograph.

[19] M. Ogawa (private communication).

Absorption Bands and Lines in Irradiated LiF

CHARLES J. DELBECQ AND PETER PRINGSHEIM
Chemistry Division, Argonne National Laboratory, Lemont, Illinois
(Received December 8, 1952)

The paper deals with a number of phenomena observed in lithium fluoride after formation of color centers by exposure to x-rays, Van de Graaff electrons, or neutrons and not observed in other alkali halides under similar conditions. The most important of these phenomena are: (1) The appearance of a new band at 222 mμ, when the crystal is bleached with light of wavelength 254 mμ absorbed in the *F* band, and the inverse effect by subsequent irradiation with light of shorter wavelengths. (2) The production of *F* centers in a crystal heated to temperatures up to at least 450°C. The higher the temperature at which the *F* centers were produced, the greater is the intensity of the band at 222 mμ obtained by subsequent optical bleaching of the *F* band at room temperature. (3) The appearance of fine structure in a relatively weak band with peak at 380 mμ and of a very weak line at 523 mμ when the spectrum is recorded at the temperature of liquid nitrogen. (4) The very strong increase in the intensity of the band at 380 mμ and the line at 523 mμ by irradiation with short wavelength ultraviolet. (5) The sharpness at low temperatures of the first line of the band at 380 mμ and the line at 523mμ. At the temperature of liquid helium their half-widths are of the order of 1A.

I. INTRODUCTION

THE analogy between the absorption spectra produced in various alkali chlorides and bromides by x-ray irradiation and similar methods is fairly clear so that corresponding bands in each of them can be classified as *F*, *F'*, *M*, *R*, *V*, etc. The correspondence is not so clear in the case of lithium fluoride. This may be due, in part, to two facts: (1) The band which almost certainly must be designated as the *F* band of lithium fluoride, with peak at 250 mμ, lies so far in the ultraviolet that, with quartz optics in air, only a very small range beyond the *F* band can be investigated, while a much greater range is accessible in the region of longer wavelengths. Moreover, the fact that the first fundamental absorption band lies below 1200A renders the search for bands of the α-β type quite hopeless without the use of vacuum spectrophotometry.[1] (2) Most of the bands of lithium fluoride are much more stable at room temperature and at higher temperatures than those of other alkali halides, and thus certain bands of an intermediate stability can be observed which in other halides may be too short-lived to be noticed.

In order to avoid ambiguity the various bands occurring in the spectrum of lithium fluoride under various conditions are designated in the following, with the exception of the *F* band, by their approximate peak wavelength in mμ, such as the 450 band, 313 band, 222 band, etc. Penneman and Powers[2] proposed the classification of lithium fluoride bands listed in Table I. Some of the characteristic properties of the bands seem to fit these designations, but in other respects there are striking differences.

TABLE I.

Approximate peak wavelength (mμ)	222	250	313	340[a]	380	450	518	620
Penneman and Powers	—	*F*	R_1	—	R_2	*M*	—	*F'*

[a] In the same spectral region a weak band with peak at 348 mμ appears immediately after a crystal has been exposed to x-rays at room temperature. This band also is unstable and vanishes at room temperature within a day, while the intensities of the adjacent "*R* bands" remain practically unaltered. It may be mentioned that the bands which we observed in the absorption spectra of lithium fluoride between 450 and 250 mμ do not correspond in their wavelengths and even less in their relative intensities to the numerous bands reproduced by Ushida and Yagi in Fig. 1 of their paper [J. Phys. Soc. Japan **7**, 109 (1952)].

While, for instance, the "normal" *M* bands of other alkali halides are mainly produced by light absorption in the *F* band, this is not the case with the 450 band of lithium fluoride. If a lithium fluoride crystal is exposed at −190°C to x-rays and its absorption spectrum is recorded at this temperature, none of the visible bands appear, while the *F* band and the broad band with peak at 340 mμ are present. The latter reaches with its long wavelength tail well into the blue and thus gives the crystal a light yellow color in transmitted light. By heating the sample to −135°C the *F* band loses little of its intensity, but the 340 band vanishes completely, and the crystal becomes colorless. When the crystal is warmed up to room temperature, the intensity of the *F* band drops by about 50 percent of its initial value and the 620 band is formed, producing a deep blue color in the crystal. This latter band, which is stable at temperatures below 0°C, disappears at room temperature within a few hours and gives way to the 450 band.[3] If the primary exposure to x-rays takes place at room temperature, a relatively strong 620 band and a weaker 450 band are produced simultaneously with the *F* band. It cannot be decided whether, under these conditions, the two bands in the visible are formed directly or if the primary effect is the formation of *F* centers only, from which 620 centers and subsequently 450 centers are derived. Also in this case the 620 band disappears after a few hours, while the intensity of the 450 band is greatly enhanced.

[1] Delbecq, Pringsheim, and Yuster, J. Chem. Phys. **19**, 574 (1951).

[2] R. A. Penneman, Atomic Energy Commission Report No. AECD-1859 (March, 1945); J. A. Powers, dissertation, University of Notre Dame, 1950.

[3] P. Pringsheim and P. H. Yuster, Phys. Rev. **78**, 293 (1950).

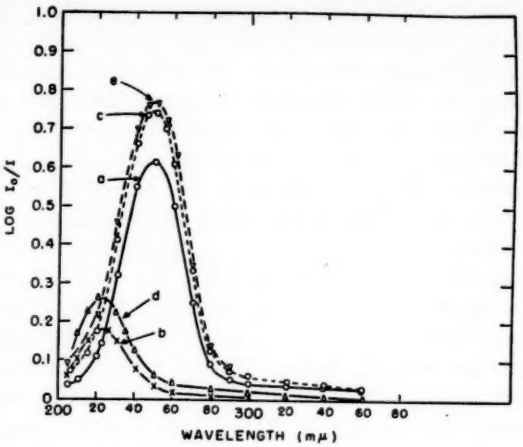

FIG. 1. Lithium fluoride alternately exposed at room temperature to x-rays and to ultraviolet light (2537A), measured at room temperature. (a) Three minute x-rays. (b) 25 hours ultraviolet. (c) Three minute x-rays. (d) 40 hours ultraviolet. (e) Three minute x-rays.

The intensity of the 450 band, after having reached this state, is in general about ten times weaker than the *F* band; the 380 and 313 bands appear with still much lower intensities after prolonged exposure of lithium fluoride to x-rays, electron bombardment, etc. Once the conversion of the 620 band to the 450 band has been completed, the 450 band is very stable at room temperature and is not bleached by blue light or even continuous exposure to daylight, while in other alkali halides *M* bands are bleached by *M* light and give way to *R* bands.

II. EXPERIMENTAL PROCEDURES

The lithium fluoride plates used in this investigation were between 0.5 and 1 mm thick and were cleaved from crystals obtained from the Harshaw Chemical Company.

Some samples were colored by neutron bombardment, but in most instances the plates were exposed to x-rays from a 50-kv Machlett tube at a distance of about 3 cm from the beryllium window. Under these conditions, the plates were fairly uniformly colored throughout their thickness. The exposure times varied from a few minutes to many hours and even several days depending on the features of the absorption spectrum under investigation. Only when color centers were to be produced at high temperatures (up to 450°C) were the samples exposed to 1-Mev electrons from a Van de Graaff machine which allowed relatively short exposure times even at high temperatures.

The spectral absorption curves on which individual measuring points are marked (Figs. 1, 2, 4, 5, 6, and 7) were obtained with a Beckman spectrophotometer; the solid line curves are traced from recordings made with a Cary spectrophotometer.

III. THE 222 BAND IN CRYSTALS IRRADIATED AT ROOM TEMPERATURE

When a lithium fluoride crystal in which *F* centers have been produced at room temperature, or lower temperatures, is exposed to light of wavelength 2537A, for instance, to the radiation from a so-called Mineralight filtered through a red purple glass, the *F* band is bleached; when its intensity has reached a relatively low value, its peak shifts to shorter wavelengths, and finally the band is replaced by a much weaker band with peak at 222 mμ.[4] During this process the 450 band is slightly bleached. By re-exposing the crystal to x-rays or electron bombardment the 222 band disappears again, and a normal *F* band is reformed. If the x-ray doses given in the first and the second exposures are the same, the newly formed *F* band has an intensity only slightly greater than it had before the conversion from the *F* band to the 222 band. Thus it does not seem that the destruction of 222 centers in this process contributes essentially to the rebuilding of *F* centers (Fig. 1).

The spectrum of the Mineralight radiation contains, in addition to the 2537A line and some radiation of greater wavelengths reaching to the visible, also shorter wavelengths (including the mercury line at 1849A) of appreciable intensity, which are not transmitted by the red purple filter. If, after formation of the 222 band, the crystal is exposed to the full radiation from the Mineralight, the band is broadened, and its peak is shifted back to longer wavelengths, staying finally at 230 mμ (Fig. 2). This seems to correspond to a state of equilibrium, since the same shape and peak wavelength of the band is attained if the crystal containing *F* centers is directly exposed to the full radiation from the Mineralight or from a zinc or cadmium arc, which emit their strong resonance lines at 2114A and 2288A, respectively. The mercury line 2537A which alone is transmitted through the red

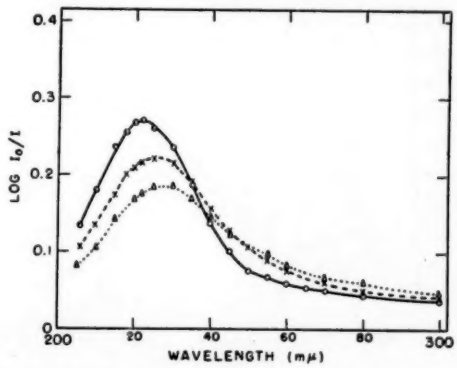

FIG. 2. Lithium fluoride after three-minute irradiation with x-rays at room temperature (peak height of initial *F* band was 1.12), bleached with various ultraviolet light sources, measured at room temperature. o-o-o, 30-minute Mineralight with filter at room temperature. x-x-x, three hours cadmium arc at room temperature. Δ-Δ-Δ, two hours zinc arc at room temperature.

[4] Argonne National Laboratory Report No. ANL-4232, Sec. 2.8 (Februrary 10, 1949); R. S. Alger, J. Appl. Phys. **21**, 30 (1950).

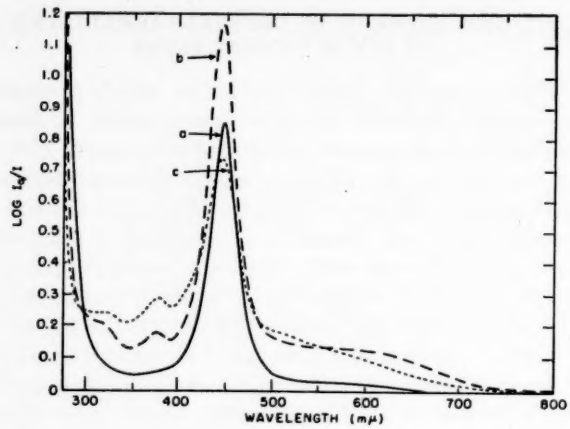

FIG. 3. Change in intensity of 450 band of lithium fluoride by irradiation with short wavelength ultraviolet, measured at room temperature. (a) Five-minute neutron bombardment at room temperature. (b) One hour Mineralight, no filter, at room temperature. (c) Three hours Mineralight, no filter, at room temperature.

purple filter is absorbed by the F centers only and bleaches them or transforms them into 222 centers. Radiation of shorter wavelengths (nonfiltered Mineralight, zinc, and cadmium arcs) is absorbed by the 222 band and also in the tail of the 250 band and thus converts F centers into 222 centers and vice versa, establishing an equilibrium. By using various filter glasses, it was shown that it is not the light of greater wavelengths which causes the difference in the effects produced by the Mineralight radiation with and without red purple filter.[5]

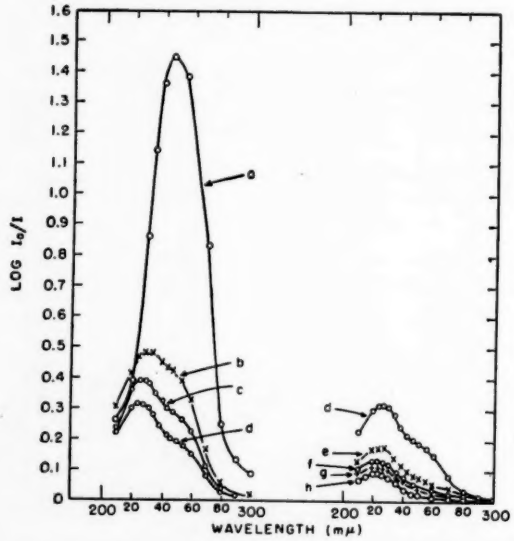

FIG. 4. Heat bleaching of F band produced in lithium fluoride at room temperature, measured at room temperature. (a) Six-minute x-rays at room temperature. (b) Heated ten minutes at 250°C. (c) Thirty minutes at 250°C. (d) One hour at 250°C. (e) Ten minutes at 300°C. (f) Thirty minutes at 300°C. (g) One hour at 300°C. (h) Three hours at 300°C.

[5] Argonne National Laboratory Report No. ANL-4833, Sec. 1.5 (October 15, 1952).

It has been mentioned already that the Mineralight radiation filtered through the red purple glass causes a slight intensity decrease in the 450 band. Irradiation without the filter, however, enhances this band very appreciably, the maximum intensity exceeds the initial intensity in general by about 50 percent. Simultaneously, the weak bands at 380 and 313 mμ gain in intensity. The same effect is produced by irradiation with the zinc and cadmium arc light. It is reasonable to assume that 450 centers, even if they are not "normal M centers," are some sort of electron surplus centers and that, by irradiating 222 centers with light absorbed in them, electrons are transferred to lattice points, where either they reform F centers or increase the number of 450 centers. It is noteworthy that this is a second indirect process by which 450 centers can be produced. By prolonged irradiation with

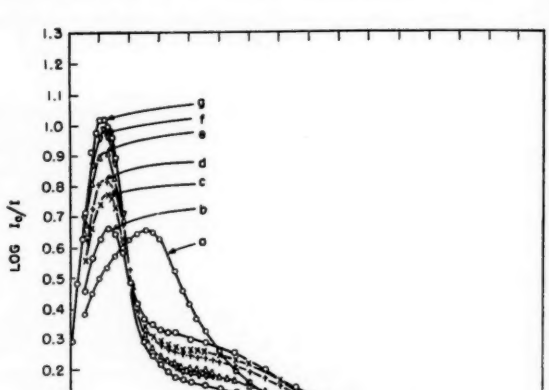

FIG. 5. Bleaching at room temperature by F light of F band produced in lithium fluoride at 350°C, measured at room temperature. (a) Two minute bombardment with 1-Mev electrons at 350°C. (b) Bleached three hours. (c) Bleached five hours. (d) Bleached nine hours. (e) Bleached 27 hours. (f) Bleached 48 hours. (g) Bleached 88 hours and kept in dark for eight days.

short wavelength ultraviolet the intensity of the 450 band is decreased again and is slowly bleached out (Fig. 3).

When a lithium fluoride crystal which contains F centers formed at room temperature is heated to 100°C, the F band is slowly bleached out, without an appreciable change in its shape.[6] If the temperature is raised to 200°C and higher, the bleaching rate is greatly increased, and after some time the new band with peak at 222 mμ is left over almost alone. This band was not hidden under the F band initially, since points on its short wavelength branch lie above the corresponding points of the original F band (Fig. 4).[7]

[6] Casler, Yuster, and Pringsheim, J. Chem. Phys. 18, 887 (1950), Figs. 1 and 5.

[7] Argonne National Laboratory Report No. ANL-4427, Sec. 1.8 (July 28, 1950).

IV. THE 222 BAND IN CRYSTALS IRRADIATED AT HIGH TEMPERATURE

It is not possible in alkali halides such as potassium chloride and potassium bromide to produce stable F centers by exposing the crystal to x-rays or electron bombardment at temperatures above 100°C, and F centers formed at room temperature in these crystals are easily bleached out at 200°C. In lithium fluoride F centers are produced by electron bombardment at temperatures at least up to 450°C. The time needed to produce a certain optical density D in a sample is longer at higher temperatures, and, while the peak lies as usual at about 250 mμ, the band is broader with about twice the normal half-width of 0.78 ev at room temperature. Frequently it shows a bulge on the short wavelength side and a flat tail on the side of longer wavelengths, both indicating the presence of additional bands hidden under the F band.

The effect of irradiating with F light a lithium fluoride crystal containing F centers produced at 350°C is shown in Fig. 5, which differs in a very characteristic way from Fig. 1.[7] In the latter, the F band is at first strongly bleached by the F light and the remaining intensity of the 222 band is low; in the former the F band is converted into the 222 band without any loss of peak intensity, and at the end of the process the 222 band is much sharper and appreciably higher than the F band complex from which it originated.

Figure 6 shows how crystals with F bands produced at intermediate temperatures exhibit an intermediate behavior with a continuous transition from the predominance of the 222 band formation to the bleaching by other competing processes.[8] The formation of a new band may be due either to the capture of a free electron by some lattice irregularity or by the addition of some new units (positive or negative ion vacancies, etc.) to an F center which disappears as such. Since bleaching of the F band and production of the 222 band are both effected by the absorption of F light, it is more probable that both processes are initiated by the ejection of an electron from an F center.

Although nothing is known concerning V centers in lithium fluoride, the simplest way of interpreting our results is to assume that the V centers formed in lithium fluoride at high temperatures are very stable and have a very low electron capturing cross section, while the unknown lattice configurations which, by capture of electrons, become 222 centers are more numerous if the temperature at which the F centers are produced is increased. The increase in thermal stability of F centers with increasing temperature at which they are formed is a phenomenon common to all alkali halides.[6] A comparison of Figs. 4 and 7 shows the difference in the heat bleaching of lithium fluoride samples with F centers produced at 25° and 300°C, respectively. The great stability of centers produced in lithium fluoride at high temperatures is also illustrated by Fig. 8. The partial reconversion of the 222 band into the 250 band (shift of the peak from 222 to 230) and the inverse effect are accomplished with almost no loss in the total absorption, while in Fig. 2 an analogous shift was accompanied by a very appreciable loss in total absorption.

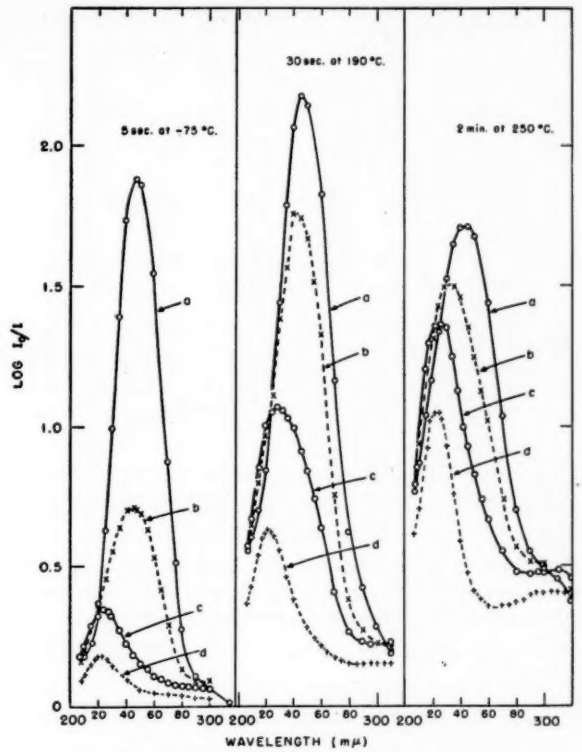

FIG. 6. Bleaching at room temperature by F light of F bands produced in lithium fluoride at various temperatures, measured at room temperature. (a) After electron bombardment as indicated. (b) Bleached 1.5 hours. (c) Bleached six hours. (d) Bleached 30 hours.

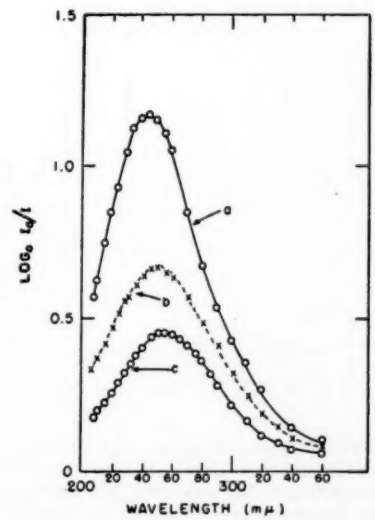

FIG. 7. Heat bleaching of F centers produced in lithium fluoride by electron bombardment at 300°C, measured at room temperature. (a) After two minutes electron bombardment. (b) After one hour at 350°C. (c) After two additional hours at 350°C.

[8] Argonne National Laboratory Report No. ANL-4449, Sec. 1.7 (October 19, 1950).

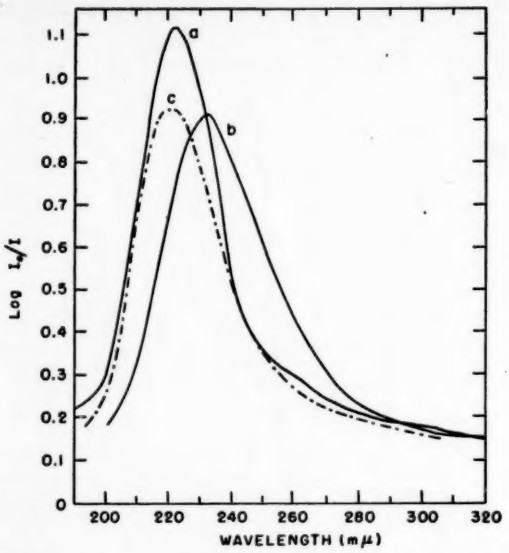

FIG. 8. Effect of ultraviolet irradiation at room temperature on short wavelength bands of lithium fluoride after electron bombardment at 250°C, measured at room temperature.

Light source	Area covered by curve (arbitrary units)
(a) 25 hours Mineralight through filter (2537A)	509
(b) 40 hours zinc arc	485
(c) 21 hours Mineralight through filter	475

V. THE 523 LINE AND THE STRUCTURE OF THE 380 BAND

If a lithium fluoride crystal has been colored so deeply by exposure to x-rays or neutron bombardment that the optical densities, not only in the F band but also in the 450 band, are too high to be measured ($D>3.4$), a very weak line can just be recognized at 523.5 mμ in the spectrum recorded at −190°C. This means that the intensity of the line is at least 1000 times lower than that of the 250 band. The line is accompanied by an even weaker band with peak at 517 mμ.

If, by prolonged exposure to the radiation from a Mineralight, the intensity of the 450 band is greatly reduced (Fig. 3, Curve c; in the case of the lithium fluoride sample represented in Fig. 9 from $D=3.4$ to 1.37), the line is greatly enhanced (namely, from 0.02 to 0.55). Again nonfiltered radiation from the source is more effective than when the light is passed through the red purple filter. It seems, therefore, that again absorption in the 222 band plays an important part in the process. At liquid nitrogen temperature the 523 line is very sharp, and cooling the crystal to liquid helium temperature does not alter the shape of the line on the spectrophotometer curve any further. The apparent half-width of about 6A shown in Figs. 9 and 10 is caused, however, by the low resolving power of the spectrophotometer in the spectral range above 500 mμ.

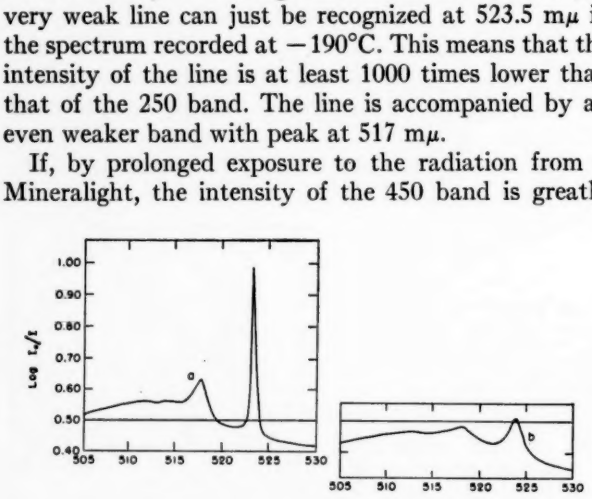

FIG. 9. The 523 line and adjacent band of lithium fluoride after five hours x-rays and 15 hours Mineralight (no filter) at room temperature. (a) Measured at −190°C. (b) Measured at −120°C. (c) Measured at −75°C. (d) Measured at +25°C.

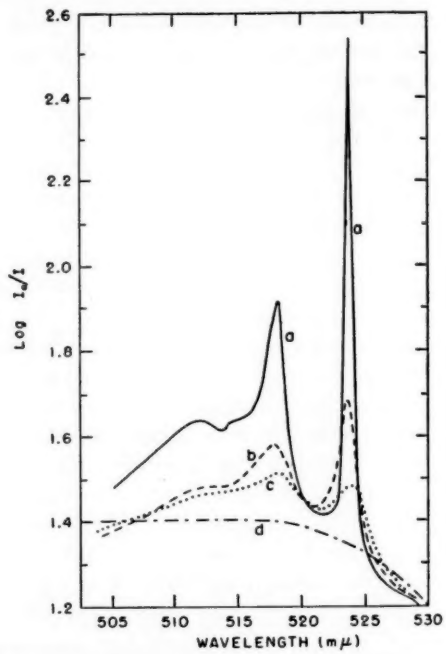

FIG. 10. The 523 line and adjacent band of lithium fluoride after ten minute neutron bombardment and nine hours Mineralight (no filter) at room temperature. (a) Measured at −190°C. (b) Measured at −120°C. (c) Measured at −75°C. (d) Measured at +25°C.

Absorption spectra obtained with a 3.4-meter Jarrell-Ash Wadsworth mounting spectrograph prove that the half-width of the line at liquid nitrogen temperature does not exceed 2A and is appreciably smaller at liquid helium temperature.*

In the spectrum of the crystal represented by Fig. 10 the optical density at the peak of the 450 band was greater than 3.5. The crystal had been exposed to neutron bombardment and subsequently for nine hours to the nonfiltered radiation of the Mineralight. Not a trace of the line remains in the spectrum taken at room temperature. This is due only partly to the broadening of the 450 band; to a greater extent it is caused by the

* We want to thank Dr. Mark Fred for taking these spectrograms.

broadening of the line itself, as shown in Curves b, c, and d of Figs. 9 and 10. Even at −120°C the line is quite diffuse.

The 523 line was observed first in crystals of lithium fluoride colored by neutron bombardment, and this suggested that the line might originate from atoms dislodged from their normal position in the lattice by the slow neutron Li^6 reaction. It was shown later, however, that in the spectra of crystals in which a sufficient number of F centers have been produced by exposure to x-rays, the 523 line appeared with low intensity, and a crystal which after 60 hours exposure to x-rays had become deep red in transmitted light showed the 523 line with the very appreciable optical density of $D=1.3$ above a strong continuous background. It is improbable that interstitial atoms are produced in appreciable number under these conditions. However, it must be kept in mind that, even in the extreme case when the optical density at the line center is comparable with that of the 450-band peak (in the case represented by Fig. 9

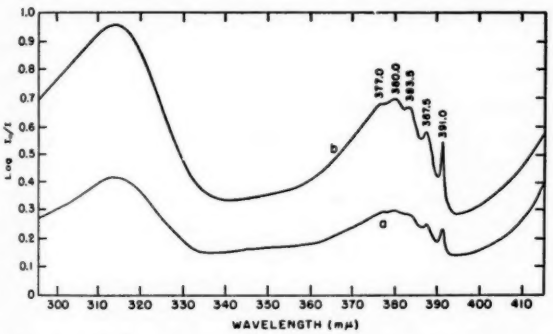

FIG. 11. The 380 and 313 bands of lithium fluoride. (a) After five hours x-rays at room temperature, measured at −190°C. (b) After two hours Mineralight (no filter) at room temperature, measured at −190°C.

the ratio is 1:2.5), the area covered by the line, because of its sharpness, is still much smaller than the area covered by the 450 band. Thus, assuming an oscillator strength which is not too small, the number of "line centers" is by several orders of magnitude lower than that of the F centers, the latter being about 10^{17}/cc. The only properties of the carriers of the line absorption which seem to be fairly well established are their origin, namely, the capture by some lattice singularity of an electron ejected from an F or a 222 center, and their good protection against perturbations caused by interactions with the crystal lattice. The appearance in Figs. 9 and 10 of a band at the short wavelength side of the line, which will be discussed later, indicates, however, that some coupling of the electronic transition with certain interionic vibrations must exist. Three peaks can be observed in the band associated with the 523 line; the spacing between adjacent peaks is 221 cm^{-1} and 227 cm^{-1}.

The 380 band also exhibits a very pronounced line structure when the spectrum of a lithium fluoride

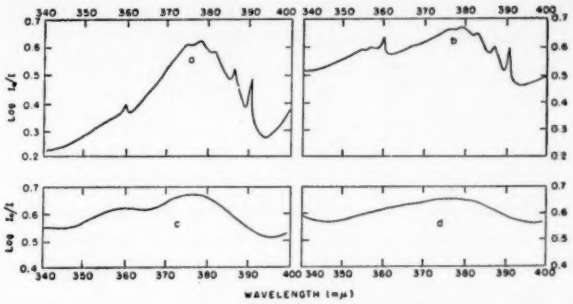

FIG. 12. The 380 band of lithium fluoride after five hours x-rays at room temperature. (a) After four hours Mineralight, measured at −190°C. (b) After nine hours Mineralight, measured at −190°C. (c) After nine hours Mineralight, measured at −75°C. (d) After nine hours Mineralight, measured at +25°C.

crystal with F centers is recorded at −190C. The structure consists of a narrow line, with a half-width of not more than 2A, at 391 mμ and a sequence of more diffuse peaks towards shorter wavelengths (Figs. 11, 12, and 13). The wavelengths of these peaks, derived from spectrophotometer curves, are listed in the first line of Table II. The second line gives the value calculated under the assumption of a constant wave number spacing of 237.5 cm^{-1} between adjacent peaks. The discrepancies between the two sets of data do not exceed the probable errors of the measurements.

After exposure to x-rays, the 380 band (the so-called R_2 band) has an appreciably greater intensity than the 523 line and, whenever its intensity is sufficient for spectrophotometric recording, it exhibits at −190°C the fine structure quite clearly (Fig. 11, Curve a). By bleaching with Mineralight radiation the 380 band with its line structure and the 313 band as well (so-called R_1) are greatly enhanced. More prolonged exposure to the Mineralight reduces their intensities again and begins to submerge the selective peaks of the 380 band under an increasing continuous absorption (Fig. 12, Curves a and b).

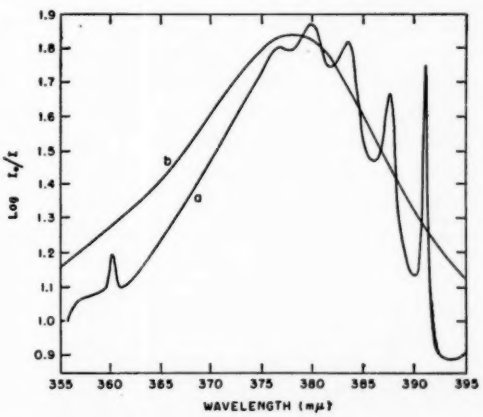

FIG. 13. The 380 band of lithium fluoride after neutron bombardment and fifty hours exposure to Mineralight (no filter) at room temperature. (a) Measured at liquid helium temperature. (b) Measured at −120°C.

TABLE II. Wavelengths of the peaks in the 380 bands in mμ.

Observed	391.0	387.5	383.5	379.5	377.0
Calculated	391.0	387.4	383.9	380.4	377.0

Another feature caused by the long-lasting exposure to Mineralight radiation can be seen in its beginning in Fig. 12, Curve a, which is the continuation of Curve b of Fig. 11. This feature is the appearance of a new peak at 360 mμ which, in Fig. 12, Curve b, has greatly gained in intensity and seems now to form the origin of a new band system with still very weak secondary peaks at 357.5 and 355 mμ. The new peak at 360 mμ shows up even more clearly in Fig. 13 representing the 380 band of another lithium fluoride plate recorded at liquid helium temperature.

In contradistinction to the behavior of the 523 line, the sharpening up of the peaks in the 380 band at very low temperatures, especially in its first line at 391 mμ, is quite obvious when Curve a in Fig. 13 is compared with Fig. 11, Curve b. This is due to the better resolving power of the spectrophotometer below 400 mμ. The structure of the 380 band becomes more diffuse as the temperature is raised above that of liquid nitrogen and vanishes at temperatures lower than −100°C (Curves c and d in Fig. 12, Curve b in Fig. 13). Apparently the electronic transition corresponding to the line at 391 mμ is coupled more closely with some lattice vibrations than is the case for the 523 band, and therefore the structure of the band is more dependent on temperature. The 313 band, which is supposed to correspond to an R_1 band, shows no trace of structure even at liquid helium temperature.

The lines at 523 and 391 mμ do not seem to belong to the same centers. Their relative intensities vary greatly under various conditions. Nonetheless the same vibrational frequency, or a vibrational frequency of nearly the same order, seems to be superimposed upon the electronic transition in the two centers.

The appearance and regular spacing (*ca* 240 cm^{-1}) of the peaks in the 380 band (when observed at low temperature) suggest that the absorption band is due to an electronic transition to several vibrational levels of the upper electronic state. It seems reasonable to expect that the observed vibrational frequency of the absorbing center should be close to one of the vibrational frequencies characteristic of a lithium fluoride crystal. The principle infrared absorption band of lithium fluoride has a frequency of $\nu_0 = 307$ cm^{-1} which is of the same order of magnitude as the observed spacing for the 380 band.[9] Born and Blackman[10] have given a theoretical interpretation of the infrared absorption spectra of the alkali halides, using a one-dimensional lattice as a model. They determine one of the characteristic frequencies of lithium fluoride to be $\nu_1 = 260$ cm^{-1}, which is very close to the spacing observed for the 380 band. The spacing of the peaks associated with the 523 line is approximately 225 cm^{-1}. It can be expected that the lattice frequencies are somewhat altered in the neighborhood of a lattice singularity, and that, on the other hand, the vibrational frequencies in the ground and excited states do not differ greatly. Thus, the structure associated with the 380 band and the 523 line may be due to vibrations in the immediate neighborhood of the absorbing center which correspond to either of the two characteristic frequencies ν_0 or ν_1.

It might be suggested that the electronic transitions causing the sharp lines in the absorption spectra occur in certain impurities, such as rare earth ions, which may be present in the lithium fluoride lattice. Such impurities have not been found in our crystals to date; however, our analyses were not sufficiently sensitive to detect concentrations of 10^{-7} or 10^{-8} which could perhaps suffice to produce the lines. On the other hand, for the line at 391 mμ and the accompanying 380 band, at least, this interpretation seems to be improbable, because this complex band is always formed together with the 313 band, which does not show any fine structure; both bands appear definitely to belong to the system of bands which are successively produced by x-ray irradiation in the lattice of the lithium fluoride crystal itself.

If the 380 band is an *R* band, one might expect that also in other alkali halides the *R* bands should exhibit some fine structure at low temperatures. The *R* bands of potassium chloride and of natural rocksalt are easily obtained by exposing an x-rayed crystal of potassium chloride or rocksalt for some time to *F* light. For both crystals the *R* bands are well separated from each other and from the adjacent *F* band at −190°C. In none of the bands can a trace of structure be observed even at the temperature of liquid helium.

[9] R. B. Barnes, Z. Physik **75**, 723 (1932); K. Korth, Nachr. Akad. Wiss. Göttingen, Math.-physik. Kl. II **1**, 187 (1933).
[10] M. Born and M. Blackman, Z. Physik **82**, 551 (1933).

On the Electrical Conductivity of Some Alkaline Earth Titanates*

E. K. WEISE AND I. A. LESK†
Department of Electrical Engineering, University of Illinois, Urbana, Illinois
(Received October 20, 1952)

The compounds Mg_2TiO_4, $MgTiO_3$, $MgTi_2O_5$, $CaTiO_3$, $SrTiO_3$, and $BaTiO_3$ were prepared in crystalline form by reactions in the solid state. The rod-shaped samples were sintered in oxygen at 1450°C and reduced in hydrogen at temperatures from 560°C to 1400°C producing *n* type semiconductors. Resistivity values from 10^{-1} to $10^{8}\Omega\cdot$cm at 25°C were obtained. Reductions of about 3 percent by weight could be given the most reduced magnesium titanates while the largest reduction obtainable in $CaTiO_3$, $SrTiO_3$, or $BaTiO_3$ was less than 0.25 percent.

The logarithm of resistivity was plotted *versus* reciprocal absolute temperature and showed a linear dependence in most cases over a wide range of temperature and resistivity. The curves for $BaTiO_3$ changed the slope abruptly at approximately 115°C, probably attributable to the crystal structure change at the Curie temperature, about 120°C.

The dependences of impurity activation energy and Fermi level on percent reduction were determined for the case of Mg_2TiO_4. The Biltz-Meyer rule, stating a linear relationship of impurity activation energy with resistivity at a reference temperature, was not obeyed over the large range of reductions obtained.

INTRODUCTION

THE use of magnesium titanate as the constituent of commercial "Urdox" thermistors was proposed in 1932 by W. Meyer of the Osram Company, Germany. This material replaced the previously used uranium dioxide, which is unstable even at the lower operating temperatures. It has since been found that there exist three magnesium titanates, each of which is a proper compound. However, no detailed information on the electrical conductivities of the magnesium titanates over wide ranges of temperature and composition has been published. The purpose of this investigation was to supply resistivity data for as many of the alkaline earth titanates as was practical. Beryllium and radium were omitted from the standpoint of safety, so only the following were investigated: Mg_2TiO_4, $MgTi_2O_5$, $SrTiO_3$, $MgTiO_3$, $CaTiO_3$, and $BaTiO_3$.

CRYSTAL STRUCTURES

(A) The System $MgO:TiO_2$

Three compounds have been found[1–3] to exist in this system. They are $2MgO\cdot TiO_2$ or Mg_2TiO_4, $MgO\cdot TiO_2$ or $MgTiO_3$, $MgO\cdot 2TiO_2$ or $MgTi_2O_5$.

Mg_2TiO_4 has the spinel crystal structure,[2] and $MgTiO_3$ is of the ilmenite[2,4] (or corundum-ilmenite[5]) type. The structure of $MgTi_2O_5$ does not seem to be certain.[2,3]

(B) The System $CaO:TiO_2$

Although earlier workers[6–8] reported several compounds in this system, a recent thorough investigation[9] revealed only one. It is $CaO\cdot TiO_2$ or $CaTiO_3$.

What were thought to have been other compounds may have been solid solutions of CaO in $CaTiO_3$, which exist[9,10] up to the composition $3CaO\cdot 2TiO_2$.

Although $CaTiO_3$ is the mineral perowskite,[11,12] its crystal structure is not of the ideal perowskite type. It exhibits a doubling of the perowskite unit cell, a phenomenon which has been interpreted in two different ways.[13,14]

(C) The System $SrO:TiO_2$

Only one compound in this system has been found.[15] It is $SrO\cdot TiO_2$ or $SrTiO_3$. $SrTiO_3$ has the ideal perowskite structure.[14,16]

(D) The System $BaO:TiO_2$

Although many compounds in this system have been reported,[17–21] the existence of only one was felt to be

* Research partially supported by the Air Materiel Command, Air Research and Development Center.

† In partial fulfillment of the requirements for the Degree of Doctor of Philosophy, Department of Electrical Engineering, University of Illinois, September, 1951.

[1] H. v. Wartenberg and E. Prophet, Z. anorg. u. allgem. Chem. **208**, 269 (1932).

[2] Büssem, Schusterius, and Ungewisz, Ber. deut. keram. Ges. **18**, 433 (1937).

[3] Y. Tanaka, Bull. Chem. Soc. Japan **16**, 428 (1941).

[4] E. Posnjak, Z. Krist. **88**, 271 (1934).

[5] T. F. W. Barth and E. Posnjak, Z. Krist. **88**, 265 (1934).

[6] Wartenberg, Reusch, and Saran, Z. anorg. u. allgem. Chem. **230**, 257 (1937).

[7] I. Parga-Pondal and K. Bergt, Chem. Abstracts, p. 61 (1934).

[8] L. D. Ershov, Chem. Abstracts, p. 5273 (1941).

[9] Y. Tanaka, Bull. Chem. Soc. Japan **16**, 455 (1941).

[10] H. J. Goldschmidt and J. R. Rait, Nature **152**, 356 (1943).

[11] Electrical Engineering Research Laboratory, Engineering Experiment Station, University of Illinois. AF33-038-12644 Report No. 12644-3.

[12] *Strukturbericht* (1928–1932), Vol. 2, p. 49.

[13] I. Naray-Szabo, Naturwiss. **31**, 202 (1943); **31**, 466 (1943).

[14] H. D. Megaw, Proc. Phys. Soc. (London) **58**, 133 (1946).

[15] A. Hoffman, Z. Physik. Chem. **B28**, 65 (1935).

[16] H. P. Rooksby, Nature **155**, 484 (1945).

[17] H. T. Evans, Jr., and R. D. Burbank, J. Chem. Phys. **16**, 634 (1948).

[18] H. Blattner, W. Känzig, and W. Merz, Helv. Phys. Acta. **22**, 35 (1949).

[19] H. D. Megaw, Nature **155**, 484 (1945).

[20] J. W. Mellor, *A Comprehensive Treatise on Inorganic and Theoretical Chemistry* (Longmans Green and Company, London, 1927), Vol. 7, p. 52.

[21] W. O. Statton, J. Chem. Phys. **19**, 33 (1951).

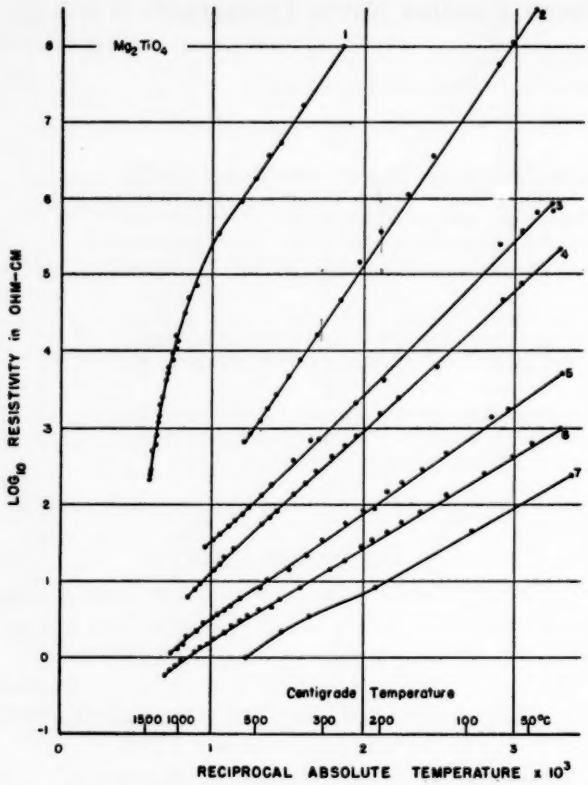

FIG. 1. Resistivity as a function of temperature for Mg_2TiO_4. Sample 1 unreduced; each succeeding sample more strongly reduced.

definite enough to warrant investigation of its conductivity. It is $BaO \cdot TiO_2$ or $BaTiO_3$.

Below 120°C, $BaTiO_3$ has been found to exhibit any of the tetragonal,[19,22] hexagonal,[23] or rhombohedral[14] crystal structures. Tetragonal and cubic forms coexist[23] between 122°C and 129°C. Above 129°C it has the ideal perowskite structure.[19,22]

PREPARATION OF COMPOUNDS AND SAMPLES

All compounds were prepared in polycrystalline form by reaction in the solid state between TiO_2 and the carbonate or oxide of the appropriate alkaline earth.

$CaTiO_3$ and $SrTiO_3$ were prepared directly by reaction in the solid state. The weight losses on ignition, due to traces of water and other volatile impurities, were found for the TiO_2 and for the carbonates in order to secure more exact mixing ratios. All weight losses were obtained at the formation temperature, 1300°C.

$BaTiO_3$ was made in the same way, except that the loss on ignition of $BaCO_3$ could not be found since it strongly corroded the platinum crucible. However, since consideration of the weight losses of the compounds used in the formation of $CaTiO_3$ and $SrTiO_3$ led to corrections in the theoretical weighing ratios of less than 0.3 percent, it was felt that neglect of the weight loss in this case would not result in a larger error. This was confirmed by x-ray analysis described later.

No consistent values for the weight losses on ignition of $MgCO_3$ or MgO could be obtained, probably due to volatilization of MgO at the temperatures used. Hence a method[3] of formation employing the chemical separation of the three magnesium titanates was used.

Free MgO may be dissolved out of a mixture of magnesium titanates by heating in 20 percent NH_4Cl solution for 20 minutes. Mg_2TiO_4, with a trace of $MgTiO_3$, is completely soluble in 4*N* HCl. $MgTiO_3$, with a trace of $MgTi_2O_5$, is completely soluble in 12*N* HCl. The major part of $MgTi_2O_5$ and free TiO_2 are insoluble even in concentrated HCl. It was found that solubilities in 4*N* and 12*N* HCl were not completed unless the mixtures were heated on a water bath for about 40 minutes. The order of these solubilities suggested a method for preparing pure samples of each of the magnesium titanates by dissolving away unwanted compounds.

In the mixture of MgO and TiO_2, approximately 20 percent more MgO was added than required for the desired stoichiometric magnesium titanate. This assured that, after suitable heating, all compounds formed would be on the MgO-rich side of the desired compound. For example, in the case of $MgTiO_3$, only $MgTiO_3$, Mg_2TiO_4, and MgO were present, with no $MgTi_2O_5$ or

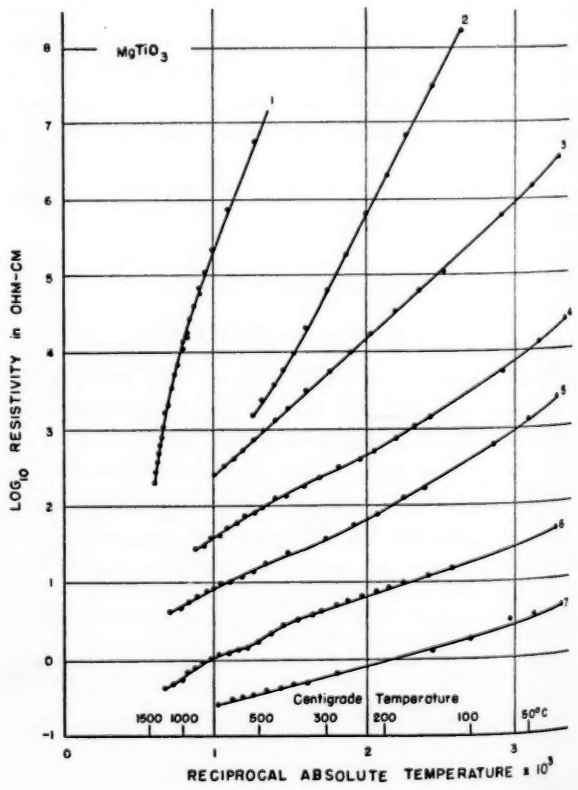

FIG. 2. Resistivity as a function of temperature for $MgTiO_3$. Sample 1 unreduced; each succeeding sample more strongly reduced.

[22] H. F. Kay and R. G. Rhodes, Nature **160**, 126 (1947).
[23] M. G. Harwood, P. Popper, and D. F. Rushman, Nature **160**, 58 (1947).

TiO_2. Then the mixture resulting after heating was treated with NH_4Cl and 4*N* HCl, leaving only the $MgTiO_3$. The other two magnesium titanates were prepared similarly.

Components were ball milled (wet) for 5 hours. A cooked starch and water solution was added as a binder, and the mixture formed into balls and heated to 1300°C in air in a globar furnace for 15 hours. The balls were then crushed by means of a mortar and pestle, ball milled (dry) for 8 hours, and the heating procedure repeated. The last milling and heating operations were repeated once again, so that total milling time was 21 hours, total heating time at 1300°C, 45 hours. Porcelain impurities added during ball milling were found by a control test to be insignificant.

Limitations on the purities of the completed compounds were found by means of x-ray powder patterns taken with copper K_α radiation at 40 kv, 15 ma, with a nickel filter. The patterns obtained were compared with published data.[2,24–26] Amounts of uncombined components were estimated by comparison with patterns of a set of standards prepared by systematically adding an excess of one component to the compound. Purity was better than 98 percent for the $CaTiO_3$ and Mg_2TiO_4 and better than 99 percent for the other four compounds.

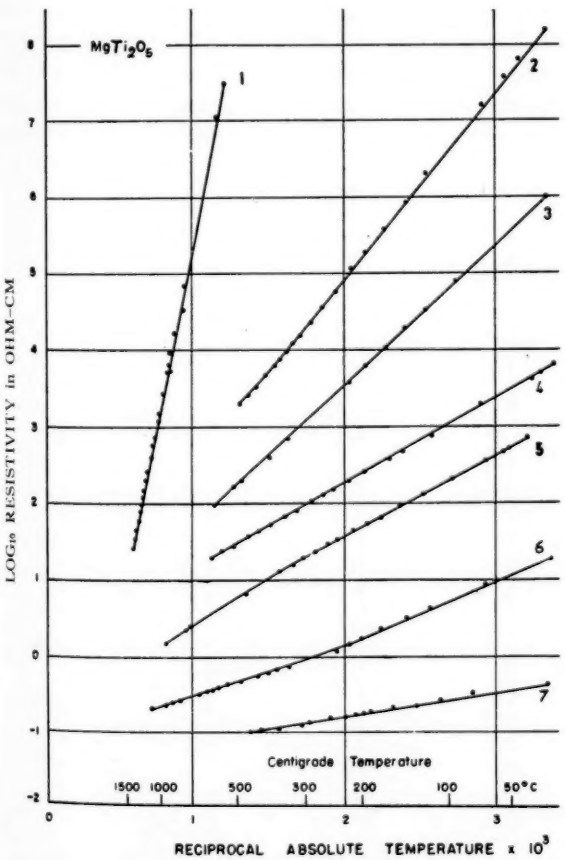

FIG. 3. Resistivity as a function of temperature for $MgTi_2O_5$. Sample 1 unreduced; each succeeding sample more strongly reduced.

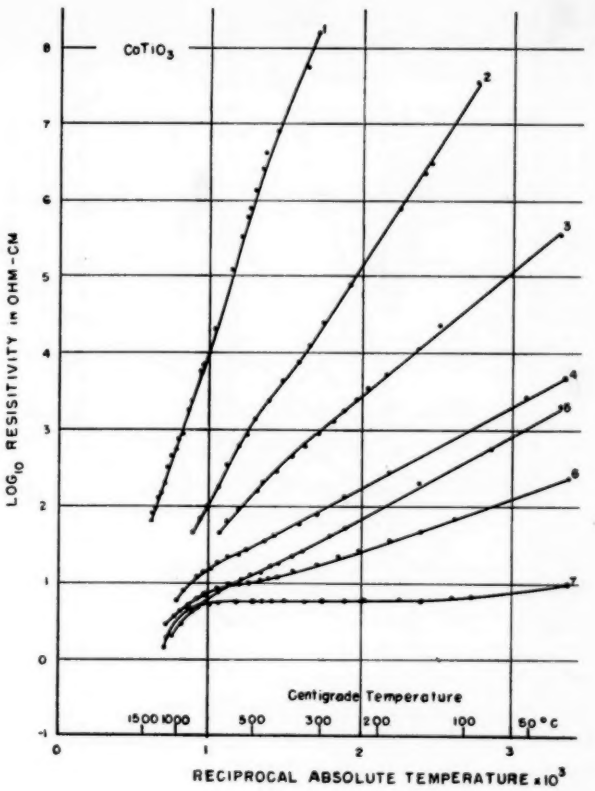

FIG. 4. Resistivity as a function of temperature for $CaTiO_3$. Sample 1 unreduced; each succeeding sample more strongly reduced.

After efforts at ordinary extrusion failed, the powders were obtained in convenient rod form by making a dry mixture with a cooked starch and water binder, packing into a glass tube of the desired inside diameter, and pushing out the rod so formed with a glass rod.

The titanate rods were next heated to 1300°C in air. This burnt out all the binder and sintered the rods slightly, making them quite hard and thus easy to work with.

FINAL TREATMENT OF COMPOUNDS

All rods were sintered in oxygen at a temperature of 1450°C, the highest temperature attainable in the platinum strip resistance furnace. No resistivity values were taken within 50°C of this temperature so that stable conditions would be maintained within the rods during measurements. All the compounds had densities, measured by means of a pycnometer, within 8 percent of their published x-ray values.[15,27,28] The density of $MgTi_2O_5$ was found to be 3.58.

[24] American Society for Testing Materials. X-ray Diffraction Data Cards.
[25] American Society for Testing Materials. X-ray Diffraction Data Cards. First Supplement, 1944.
[26] American Society for Testing Materials. X-ray Diffraction Data Cards. Second Supplement, 1950.

[27] *Strukturbericht*, 1928–1932, Vol. 2, p. 485.
[28] W. Biltz, Raumchemie der festen Stoffe. Leipzig, 1934.

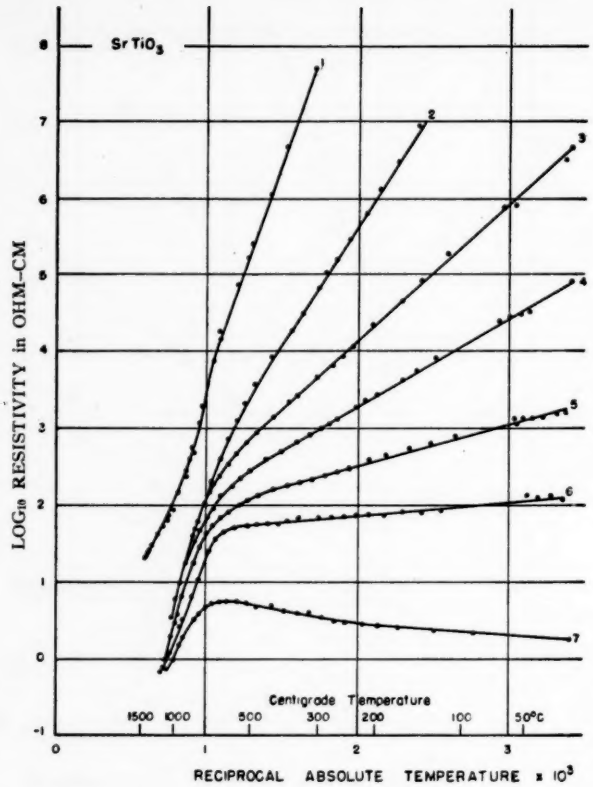

FIG. 5. Resistivity as a function of temperature for $SrTiO_3$. Sample 1 unreduced; each succeeding sample more strongly reduced.

All magnesium titanate rods were white. The $CaTiO_3$ rods were light brown, mottled somewhat with a little darker brown. $SrTiO_3$ rods were a light brownish yellow, and $BaTiO_3$ rods were a very light green.

All rods were cut to 15-mm lengths and their ends coated with platinum paste, the solvent of which was driven off by means of a nonreducing torch flame. This left metallic platinum end caps and gave good electrical contact to the rods.

MEASUREMENT PROCEDURE

A small resistance furnace[11,29,30] was used for conductivity measurements at temperatures from 1400°C down to 70°C. The rod to be measured was supported entirely by platinum spring leads and enclosed in an alumina shell (sample holder) to protect it from metal vaporizing from the neighboring heater elements. Electrical contacts were made to the end caps of the rod through the platinum spring leads, and thence, via platinum wires, outside the furnace.

Temperatures above 1100°C were measured with an optical pyrometer, below 1100°C with a Pt—Pt, Rh 13 percent thermocouple. Conductivity data from 70°C down to room temperature were obtained in a CCl_4 bath, temperatures being measured with a thermometer.

Resistances above 100 megohms were measured by the voltmeter-ammeter method. Below 100 megohms, a standard ohmmeter was used. Resistance *vs* temperature data were taken for the sample holder when empty. When the resistance of a titanate rod approached within 10 percent of that of the empty sample holder, further measurements were omitted.

Some workers have reported the existence of large potential drops in sintered bodies next to the metallic electric contacts. The bulk resistivity ρ of such a sample is obtained by using the potential gradient E at the center of the sample, where the contact effects are absent, and the current density J, by means of the formula

$$\rho = E/J.$$

Potential probe measurements at room temperature, down reduced rods of each of the six titanates, showed almost linear voltage distributions. The error involved in calculating the resistivity using the average potential gradient was found to be approximately 10 percent and remained the same over a test range of temperatures from −70°C to 70°C. Thus the use of potential probes for the measurement of resistivity was not considered

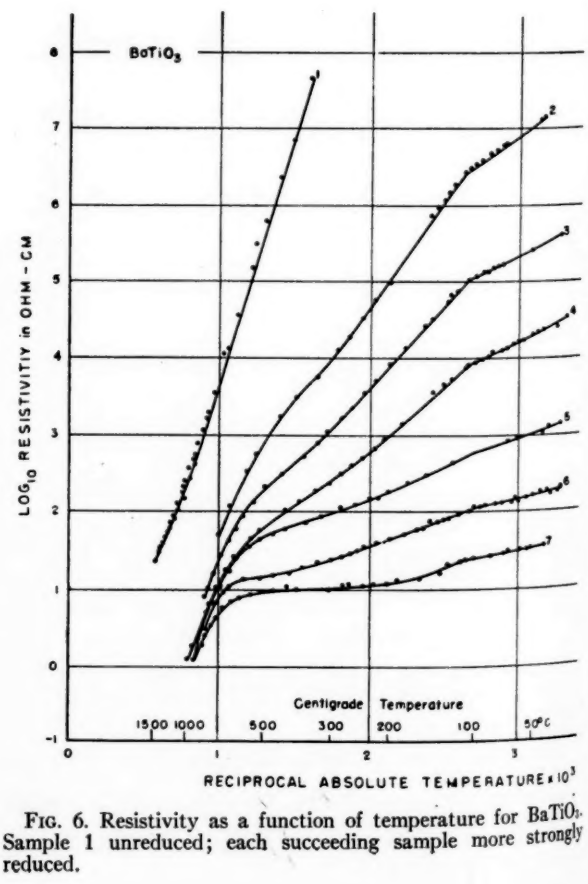

FIG. 6. Resistivity as a function of temperature for $BaTiO_3$. Sample 1 unreduced; each succeeding sample more strongly reduced.

[29] Electrical Engineering Research Laboratory, Engineering Experiment Station, University of Illinois. AF33-038-12644 Report No. 12644-2.

[30] Electrical Engineering Research Laboratory, Engineering Experiment Station, University of Illinois. AF33-038-12644 Report No. 12644-4.

necessary, and results obtained were accurate to about 10 percent.

The titanate rods of stoichiometric composition were measured in an oxygen atmosphere. However, all attempts to obtain a truly neutral atmosphere, so that reduced rods could be measured at high temperatures without change in composition, failed. To circumvent this difficulty, a dynamic method was used.

A sample rod was heated in an atmosphere of helium to the temperature at which reduction was desired. The helium was turned off and hydrogen substituted. After 15 minutes, power to the furnace heater was cut off and resistance readings taken simultaneously with temperature readings at temperature intervals of about 50°C as the furnace cooled. During the 15-minute period at constant temperature the reduction rate decreased with time in an almost exponential manner, so that near the end of the 15 minutes it remained very small. Since the amount of reduction per unit of time increased with increasing reduction temperature, it may be concluded that at lower temperatures further reduction was negligible. Also, the time constant of the curve of resistance of a rod *vs* time after a sudden temperature drop was found to be very much less than the time constant of the curve of furnace temperature *vs* time after the heater power was cut off. Thus the temperature of the rod could not have lagged appreciably behind the temperature of the furnace. The accuracy of a curve was checked by reheating a rod in hydrogen and measuring the resistance values as the temperature was increased. Up to temperatures not far from the reduction temperature, correlation was excellent. Thus the error involved in resistivity measurements taken in this way was small.

The reduced titanate rods were stable up to about 200°C, so that measurements in CCl_4 from room temperature to 70°C presented no difficulty.

All titanates turned black with reduction, the degree of darkness increasing with the amount of reduction. The uniformity of reduction throughout the body of a rod was judged by eye, comparing the colors of different sections. All rods had very uniformly colored interiors, with very thin, somewhat darker, outside layers. However, the resistance of a rod was not noticeably affected when its outside layer was scraped off. Hence resistivity values obtained were true bulk resistivities.

TABLE I. Band gaps, activation energies, percents of reduction (where obtainable), and *y* axis intercepts for alkaline earth titanates.

Compound	Curve number	Reduction weight percent	Act. energy electron volts	*Y* axis intercept straight line section in Ω·cm
Mg_2TiO_4	1	0	4.22 (Gap)	
	2	...	1.18	0.14
	3	0.13	0.832	0.17
	4	0.15	0.732	0.16
	5	0.73	0.558	0.12
	6	1.07	0.482	0.093
	7	1.25	0.463	0.027
$MgTiO_3$	1	0	2.42 (Gap)	
	2	...	1.53	0.017
	3	...	0.707	4.3
	4	0.03	0.500	1.2
	5	0.11	0.475	0.25
	6	0.98	0.251	0.34
	7	2.11	0.195	0.08
$MgTi_2O_5$	1	0	4.46 (Gap)	
	2	...	0.97	1.4
	3	...	0.734	0.76
	4	...	0.446	1.0
	5	0.16	0.434	0.23
	6	0.94	0.330	0.030
	7	2.88	0.118	0.039
$CaTiO_3$	1	0	2.61 (Gap)	
	2	...	1.19	0.22
	3	...	0.651	1.3
	4	...	0.426	1.2
	5	...	0.433	0.44
	6	...	0.286	0.81
	7	0.06	0.086	1.6
$SrTiO_3$	1	0	3.27 (Gap)	
	2	...	1.24	0.33
	3	...	0.716	4.1
	4	...	0.467	8.8
	5	...	0.221	24
	6	...	0.087	21
	7	0.23	...	...
$BaTiO_3$ above Curie temp.	1	0	2.47 (Gap)	
	2	...	1.12	0.13
	3	...	0.858	0.23
	4	...	0.765	0.074
	5	...	0.389	1.7
	6	...	0.337	0.56
	7	<0.1	0.298	0.42
$BaTiO_3$ below Curie temp.	1	0	...	...
	2	...	0.516	1100
	3	...	0.387	520
	4	...	0.349	38
	5	...	0.214	24
	6	...	0.151	10
	7	<0.1	0.119	3.5

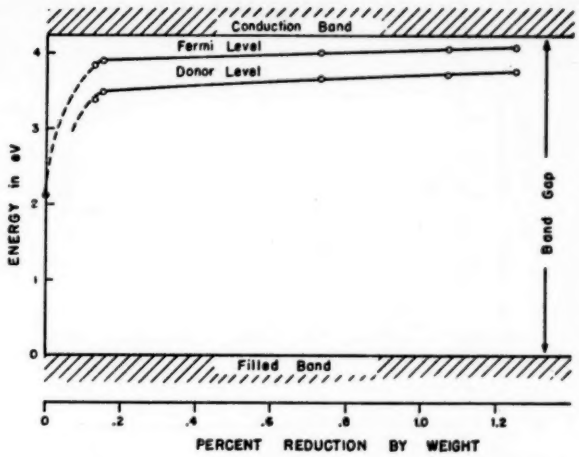

FIG. 7. Variation of Fermi level and donor level of Mg_2TiO_4 with reduction.

RESISTIVITY VARIATION WITH TEMPERATURE

Figures 1 to 6 show families of curves for each of the alkaline earth titanates made. Logarithm of resistivity

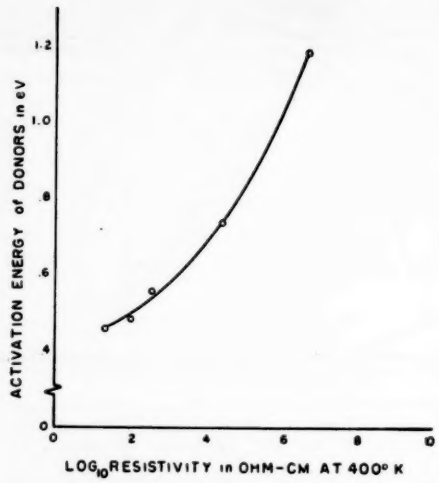

FIG. 8. Impurity activation energy as a function of resistivity at 400°K for Mg_2TiO_4.

was plotted *versus* reciprocal absolute temperature because this type of plot usually gives straight lines over considerable portions of the temperature range, making a comparison with theory easier.[31,32]

Curves for the unreduced compounds (intrinsic curves) should be straight lines, the slopes of which yield the energy gaps. Large deviations from straight lines in the cases of Mg_2TiO_4, $MgTiO_3$, and $SrTiO_3$ are probably due to impurities in the compounds.

The reduced samples of each compound, in the lower temperature range, formed a family of straight lines, the slopes of which give the impurity activation energies, according to theory. Discontinuities in slopes for the reduced $BaTiO_3$ samples took place in the neighborhood of 115°C. These may be attributable to the change in crystal structure of $BaTiO_3$ that takes place at its Curie temperature, about 120°C.

At higher temperatures, the curves for the reduced samples of each family should join up with the intrinsic curve. Temperatures high enough to check this were not reached in the cases of the magnesium titanates. The curves for reduced samples of $CaTiO_3$, $SrTiO_3$, and $BaTiO_3$ all approach or join one another but do not join the intrinsic curve. The reason for this is not certain.‡

In order to determine the percent reduction of each reduced rod, a small piece of it was weighed, heated in oxygen to 1200°C, and reweighed. The difference gave the reduction by weight. The alkaline earth titanates are considered not to accept more oxygen than the stoichiometric composition calls for. This was demonstrated, to the accuracy of weighing, by the fact that no weighable difference was detected between slightly reduced samples before and after oxidation.

Experimental attempts were made to correlate volume magnetic susceptibility with percent reduction, as has been done[33] in the case of TiO_2. It was thought that the greater sensitivity to measurement of magnetic susceptibility would permit evaluation of reductions that were too small to be weighed. Experiments showed, however, that the relation of susceptibility to degree of reduction is far from simple, so further investigations were dropped.

ANALYSIS OF RESULTS

Curve parameters of interest are the slopes of the straight line sections and their y axis intercepts. These values are all compared in Table I. The slope given for each curve of an unreduced compound is the steepest one existing on that curve. The curve numbers coincide with those of Figs. 1 to 6.

On the assumption that each missing oxygen atom leaves two donor centers, the position of the Fermi level as a function of percent reduction was calculated for the case of Mg_2TiO_4, where the largest number of weighable reductions was available. The resulting formula was, at a temperature of 400°K,

$$3.87\times10^{19}\epsilon^{-S/87.0}=\frac{N_d\epsilon^{2\times29(V_d-V_F)}}{1+\epsilon^{29(V_d-V_F)}},$$

where S=slope of curve in low temperature region, (Fig. 1), N_d=number of donors/cm^3, and V_d-V_F =energy separation (in volts) between the donor level and the Fermi level.

Fermi level and impurity activation energy are plotted as a function of percent reduction for Mg_2TiO_4 in Fig. 7. The band gap is also shown in the figure.

As early as 1924, Biltz[34] found a linear dependence of the temperature coefficient of resistance of electrolytes, metals, and semiconductors on their resistances at a reference temperature. In 1933, Meyer[35] investigated this relation as applied to semiconductors and found that the logarithm of the electrical conductivity at a reference temperature was a linear function of the impurity activation energy, which determines the temperature coefficient of resistivity. This is known as Meyer's rule, or the Biltz-Meyer rule.

To check the Biltz-Meyer rule, impurity activation energy was plotted against logarithm of resistivity at 400°K for the titanates investigated, as shown in Fig. 8 for Mg_2TiO_4. The relation is here, and also for the other compounds, a curve rather than a straight line over the large range of reductions used.

[31] F. Seitz, *The Modern Theory of Solids* (McGraw-Hill Book Company, Inc., New York, 1940).

[32] J. A. Becker and J. N. Shive, *Theory of Semiconductor Devices* (Bell Telephone Laboratories, Inc., Murray Hill, New Jersey, 1950).

‡ More accurate investigations in the high temperature range are under way and will be published at a later date.

[33] P. Ehrlich, Z. Electrochem. **45**, 362 (1939).

[34] W. Biltz, Z. anorg. u. allgem. chem. **133**, 306 (1924).

[35] W. Meyer, Z. Phys. **85**, 278 (1933).

Intermolecular Force Constants from Thermal Diffusion and Other Properties of Gases

B. N. SRIVASTAVA AND M. P. MADAN
Department of Physics, University of Lucknow, India

(Received September 25, 1952)

The thermal diffusion data on argon have been examined on the basis of the Lennard-Jones 12:6 model by reducing the experimental data through a more appropriate variation of R_T with temperature than has been done hitherto. The value of the force constant ϵ, thus determined from the observed variation of R_T with temperature, is found to increase slightly with temperature. This variation of ϵ shows the inadequacy of the model in the entire range of temperatures but gives a good idea of its effective range of usefulness. These values of ϵ have been utilized to give r_0 from the viscosity and self-diffusion data. From these the force constants μ and λ have also been evaluated and are likewise found to vary with temperature. These variations of ϵ, r_0, μ, and λ have been explained theoretically and are shown to be in accord with experimental data on the second virial coefficients of argon. The force constants for O_2, N_2, CH_4, and CO have also been similarly determined and are found to agree with other determinations.

1. INTRODUCTION

THE Chapman-Enskog theory of nonuniform gases expresses the transport properties in terms of a set of collision integrals, which depend on the law of interaction between the colliding molecules. These integrals have been evaluated for various molecular models, and the computed values of the transport coefficients have been compared with the experimentally observed values by Chapman and Cowling.[1] They summarize the work which had been done by 1938 upon the inverse power and the Sutherland models and the various models of Lennard-Jones as well as the simple case of rigid, smooth, elastic spheres. More recently Jones,[2] Jones and Furry,[3] and Grew[4] have discussed certain of these models. Hirschfelder, Bird, and Spotz,[5,6] Winter,[7] and others have shown that the Lennard-Jones 12:6 model is more in accord with the observed properties of gases than any other model. We shall therefore in this paper start with Lennard-Jones 12:6 potential energy function

$$E(r)=\lambda/r^{12}-\mu/r^{6}, \tag{1}$$

which gives the interaction energy of two molecules separated by the distance r and can be shown to yield

$$E(r)=4\epsilon[(r_0/r)^{12}-(r_0/r)^{6}], \tag{2}$$

where λ and μ are constants, and ϵ is the minimum potential energy taken as positive, and r_0 the separation for zero interaction energy. We shall use Eq. (2) to evaluate ϵ and r_0 from the observed transport coefficients. The experimental determination of these force constants is of great importance as it enables us to predict the various properties of actual gases, for which, at present, the theory alone is inadequate.

Until now the values of ϵ and r_0 have been determined only from viscosity and virial coefficient measurements,[5,6] the former method yielding a more accurate value. We have, however, shown[8] that the temperature dependence of viscosity cannot yield a very accurate value, partly on account of the not too great sensitivity of viscosity to the law of force and partly because of the slight dependence of ϵ and r_0 on temperature. The coefficient of self-diffusion has also been utilized by us[9] to calculate the force constants ϵ and r_0, but this method too suffers from the same defect as the coefficient of viscosity and is, in addition, somewhat less accurate on account of the greater probable errors in the measurement of self-diffusion. Fortunately thermal diffusion provides a very sensitive method of determining the force constants and the force index, since the thermal diffusion constant α is positive for the inverse power index $\nu>5$, but is negative for $\nu<5$. It follows from this critical dependence of the thermal diffusion constant on the nature of intermolecular force that it should be possible to determine the correct law of intermolecular interaction from a detailed study of the observed thermal diffusion. The purpose of the present paper is to assess correctly the existing experimental data on the thermal diffusion of isotopes of argon and other gases and to determine the law of force from the observed temperature dependence of the thermal diffusion constant.

2. FORMULAS FOR TRANSPORT COEFFICIENTS

In the discussion of thermal diffusion experiments, usually a quantity R_T called the thermal separation ratio is introduced, defined by

$$R_T=\alpha/[\alpha_\infty]_1, \tag{3}$$

[1] S. Chapman and T. G. Cowling, *The Mathematical Theory of Non-Uniform Gases* (Cambridge University Press, Cambridge, 1939).
[2] R. C. Jones, Phys. Rev. **59**, 1019 (1941).
[3] R. C. Jones and W. H. Furry, Revs. Modern Phys. **18**, 151 (1946).
[4] K. E. Grew, Proc. Roy. Soc. (London) **A189**, 402 (1947).
[5] Hirschfelder, Bird, and Spotz, J. Chem. Phys. **16**, 968 (1948).
[6] Hirschfelder, Bird, and Spotz, Chem. Rev. **44**, 205 (1949).
[7] E. R. S. Winter, Trans. Faraday Soc. **46**, 81 (1950).
[8] B. N. Srivastava and M. P. Madan, Proc. Nat. Acad. Sci. India (to be published).
[9] B. N. Srivastava and M. P. Madan, Phil. Mag. **43**, 968 (1952).

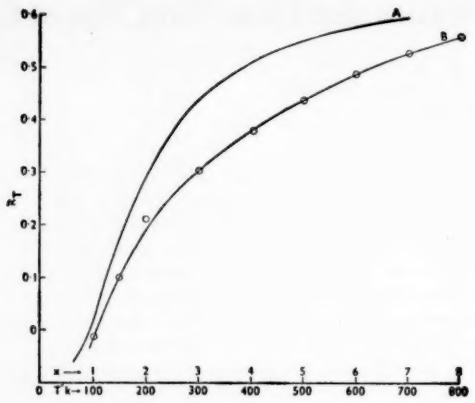

FIG. 1. Values of R_T for different values of x.

where α is the thermal diffusion constant and $[\alpha_\infty]_1$ the value of α, in first approximation, for molecules of the same mass and size as the actual ones, but interacting as rigid elastic spheres ($\nu=\infty$).

From the Chapman-Enskog theory, it has been shown by Jones[10] and Winter[7] that, for a gas consisting of two isotopic components with only a small mass difference, R_T, to the first approximation, is given by

$$[R_T]_1=\frac{16.9(C-1)(1+A)}{A(11-4B+8A)}, \tag{4}$$

where A, B, C are defined to be

$$A=\frac{W_2^2}{5W_1^1};\quad B=\frac{5W_2^1-W_3^1}{5W_1^1};\quad C=\frac{2W_2^1}{5W_1^1}. \tag{5}$$

The various W_n^l in (5) are the collision integrals for the interaction of a molecule of component 1 with one of component 2 and are functions of kT/ϵ_{12}.

As shown by Winter, Eq. (4) is a good first approximation for isotopes, provided $(m_1-m_2)/(m_1+m_2)$ is less than 10 percent. The second approximation involves very complicated algebra, and no expression for it has been given, so that the error in putting $R_T=[R_T]_1$ cannot be definitely stated, but certain considerations show that the error involved in assuming the theoretical value of R_T to be given by $[R_T]_1$ is considerably less than 23 percent for the case of isotopes.

The coefficient of viscosity is shown[5] to be given by

$$\eta=266.93(MT)^{\frac{1}{2}}[r_0(A)]^{-2}V/W_2^2\times10^{-7}\ \text{g/cm sec}, \tag{6}$$

where M represents the molecular mass and V/W_2^2 is a function of kT/ϵ. The coefficient of self-diffusion D_{12} is likewise given by

$$D_{12}=\frac{0.00092916T^{\frac{1}{2}}[(M_1+M_2)/M_1M_2]^{\frac{1}{2}}}{p(r_{12})^2W_1^1}\ \text{cm}^2\ \text{sec}^{-1}, \tag{7}$$

[10] R. C. Jones, Phys. Rev. **58**, 111 (1940).

where p is the pressure in atmospheres, M_1, M_2 are the molecular masses of the two isotopes, and W_1^1 is a function of kT/ϵ.

Winter[7] has tried to calculate R_T at different temperatures for argon and some other gases by assuming the value of ϵ obtained from viscosity data. The agreement with experimental results is not quite satisfactory. Since thermal diffusion is much more sensitive than viscosity to the law of force, it is preferable to calculate ϵ by using Eq. (4). It will be seen from Eq. (4) that R_T does not involve r_0 but depends only on ϵ and T. It is therefore possible to calculate ϵ from Eq. (4) by using values of R_T at different temperatures, without a knowledge of the value of r_0. This we proceed to do, but before doing so it is necessary to assign correct values of R_T to different temperatures as determined experimentally.

3. COMPARISON WITH EXPERIMENTAL DATA ON ARGON

The only extensive data on the experimental determination of R_T for isotopes at different temperatures are those of Stier[11] for argon (A^{36}, A^{40}) and neon. The difficulty in the accurate measurement of R_T arises from the fact that the separation obtained in the usual two-bulb experiment is small, unless the temperature difference is quite large. Since R_T itself varies with temperature, it becomes difficult to find the correct value of R_T corresponding to a particular temperature, unless the law of variation is definitely known. In the column method of measuring R_T where separations can be obtained even for small temperature differences, the uncertainty in the hydrodynamics of the column brought about by various assymmetries makes the exact evaluation of R_T extremely difficult.

From the two-bulb experiment, in the steady state, we have from the theory of thermal diffusion

$$\frac{1}{\alpha_\infty}\int\frac{dc}{cc'}=\int_{T_1}^{T_2}R_T\frac{dT}{T}=R_T^*\ln\frac{T_2}{T_1}, \tag{8}$$

TABLE I. Experimental data for thermal separation ratio R_T, along with the values of the corresponding effective temperature T' as calculated from different formulas.

No.	Temp. range °K	R_T	T_r °K Eq. I[a]	Eq. II[b]	Eq. III[c]
1	90–195	0.0673±10%	136	132	129
2	90–296	0.151 ±5%	173	163	154
3	195–296	0.248 ±5%	240	240	238
4	195–495	0.312 ±5%	305	311	300
5	273–623	0.389 ±5%	419	412	400
6	455–685	0.466 ±5%	558	558	555
7	638–833	0.534 ±5%	728	729	720

[a] I. $R_T=A-B/T+C/T^3$, and $R_T=A+BT$ at very low temperatures.
[b] II. $R_T=a\ln(T/b)$ Stier.
[c] III. $R_T=A-B/T$ (Brown).

[11] L. Stier, Phys. Rev. **62**, 548 (1942).

where c is the concentration of the lighter component and c' of the heavier component. The values of R_T^* have been tabulated by Stier, and the problem is therefore to find out to what actual temperature this R_T^* corresponds for the case when R_T varies with temperature. Assuming that

$$R_T = R_\infty - B/T, \tag{9}$$

Brown[12] showed that this R_T^* corresponds to T_r, such that

$$T_r = \frac{T_1 T_2}{T_2 - T_1} \ln \frac{T_2}{T_1}, \tag{10}$$

and Stier has given the corresponding T_r values. (See Table I, column 6.) Stier however finds that his experimental results for argon are given by the equation

$$R_T = 0.25 \ln(T_r/86.9), \tag{11}$$

which becomes inconsistent with the variation of R_T assumed by him in reducing the experimental data. Evidently the procedure is quite unsatisfactory, even for reducing the experimental data, and we have to conclude that the R_T values are not correctly assigned by Stier to the appropriate T_r values. The most satisfactory procedure would be to assume a functional dependence of R_T on temperature in Eq. (8) and write out a number of integral equations based on the experimental data and solve to give the temperature dependence of R_T. This is however mathematically not feasible. We have therefore either to proceed by trial and error by assuming various possible relationships of R_T with T and assume that particular relationship as correct, which reproduces itself in the results thereby obtained from the experimental data. The procedure however is too laborious. We have therefore adopted the alternative procedure of assuming the theoretically predicted variation of R_T with T to be correct and used it to interpret the experimental data and see if the theoretically assumed variation is confirmed experimentally. For this purpose it was necessary to determine the theoretically expected variation of R_T with T in accordance with Eq. (4).

The values of A, B, C occurring in (4) have been given by Hirschfelder *et al.*[5] for the 12:6 model for different values of x, where $x = kT/\epsilon$. Substituting these in Eq. (4), R_T is calculated for different values of x and the results given in Table II and plotted in Fig. 1 (curve A). The shape of the curve was compared with the plots of the more common types of equations with a view to discover similarities, and a few empirical equations were chosen and the tabular suitability test applied to see if they represented the data given in Table II. In particular the equations $R_T = A + B/x$, $R_T = A + B/x + C/x^2$, $R_T = A + Bx + Cx^2$ and $R_T = A + B \log x$ were tested, the first two with the help of Fig. 2.

TABLE II. Theoretical R_T values for different values of x.

x	R_T	x	R_T	x	R_T
0.6	−0.0631	1.6	0.198	3.0	0.435
0.7	−0.0574	1.7	0.221	3.5	0.476
0.8	−0.039	1.8	0.245	4.0	0.508
0.9	−0.0104	1.9	0.263	4.5	0.531
1.0	+0.0189	2.0	0.287	5	0.548
1.1	0.0472	2.1	0.305	6	0.579
1.2	0.0802	2.2	0.324	7	0.592
1.3	0.109	2.3	0.338	8	0.606
1.4	0.142	2.4	0.357	9	0.609
1.5	0.17	2.5	0.370	10	0.618

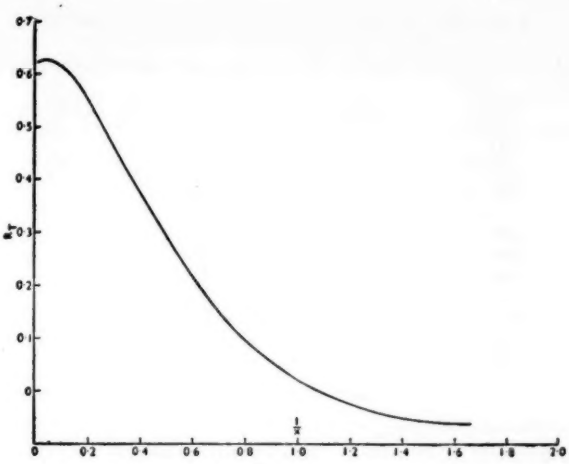

FIG. 2. Values of R_T *versus* $1/x$.

These tests revealed the inadequacy of any of the equations in the entire region but showed that $R_T = A + B/x + C/x^2$ satisfies the data from $x=4$ to $x=10$ with one set of values of A, B, and C and from $x=0.8$ to $x=4$ with another set of values, while from $x=0.7$ to $x=2$ the equation $R_T = A + Bx$ could as well serve the purpose. The relation $R_T = A + B/x$ as assumed by Brown[12] is, however, never truly valid over any extended region as seen in Fig. 2. Hence on theoretical grounds, since x is proportional to T, if ϵ is assumed to be constant over that small range of T, we can write

$$R_T = A - B/T + C/T^2, \tag{12}$$

and then Eq. (8) yields

$$R_T^* \ln \frac{T_2}{T_1} = A \ln \frac{T_2}{T_1} + B\left(\frac{1}{T_2} - \frac{1}{T_1}\right) - \frac{C}{2}\left(\frac{1}{T_2^2} - \frac{1}{T_1^2}\right) \tag{13}$$

or

$$R_T^* = A + \beta B + \gamma C,$$

where

$$\beta = \left(\frac{1}{T_2} - \frac{1}{T_1}\right)\left(\ln \frac{T_2}{T_1}\right)^{-1},$$
$$\gamma = -\frac{1}{2}\left(\frac{1}{T_2^2} - \frac{1}{T_1^2}\right)\left(\ln \frac{T_2}{T_1}\right)^{-1}. \tag{14}$$

The values of R_T^*, β, and γ are known from the experiment. At least three such equations are necessary to

[12] H. Brown, Phys. Rev. **58**, 661 (1940).

TABLE III. Comparison of experimentally determined values of R_T with theoretical values.

Temp. °K	R_T (experimental)	R_T from Eq. (8) with appropriate ϵ	
100	−0.0132	−0.022	$\epsilon/k=117.9$
150	+0.0993	+0.102	
200	+0.212	+0.222	
300	0.308	0.280	$\epsilon/k=154.7$
400	0.375	0.393	
500	0.437	0.455	
600	0.485	0.500	
700	0.525	0.530	
800	0.556	0.556	

determine A, B, and C, and by substitution in Eq. (12) the true value of R_T for any temperature T can be calculated from the experimental data.

Stier's last three data (5, 6, 7 in Table I) yield in this manner $A=0.837$, $B=265.1$, $C=32450$, while data 2, 3, 4 yield $A=0.625$, $B=114.0$, $C=5662$. The values of R_T calculated in this way from Eq. (12) have been given in Table III, column 2, and plotted against T in Fig. 1, curve B. However, when transposed for very low temperatures, data 1 and 2 have been utilized in conjunction with the relation $R_T=A+BT$ to give R_T at different temperatures, with the help of two equations of the type

$$R_T^*=A+B(T_2-T_1)\,(\ln T_2/T_1)^{-1},$$

the values of the constants thus determined being $A=-0.238$ and $B=0.00225$. This is done in the range $T=100°$K to $T=200°$K. The two curves R_T *vs* T (experimental curve B) and R_T *vs* x (theoretical curve A) plotted in Fig. 1 with arbitrarily different T, x scales, show a good parallelism, which implies that the assumed 12:6 law is almost correctly obeyed. Drawing the abscissa for different R_T values, we get the corresponding x and T values from which $\epsilon/k=T/x$ is easily determined. The values of ϵ/k thus determined are given in Table IV.

The results show a slow decrease in the value of ϵ with decrease in temperature, though it must be remarked that the experimental values of R_T have the most probable error of ±5 percent which is likely to produce an error of ±15 percent in the value of ϵ at high temperatures and of about ±5 percent at very low temperatures. Nevertheless the decrease in the value of ϵ is definite and unmistakable showing the inadequacy of the 12:6 model with constant ϵ over a long range of temperatures. We may however select two mean values of ϵ/k, one for the high temperature range 300–800°K and the other for the low temperature range 100–200°K. These are, respectively, 154.7 and 117.9. On the basis of these two values of ϵ/k for the relevant ranges, values of R_T are calculated from Eq. (4) and given in column 3 of Table III. This shows a striking agreement with the experimental values proving thereby that the 12:6 law is valid over small ranges only. The method gives us the appropriate value of ϵ for the relevant range. The experimental observations show clearly that R_T changes sign at $T=108°$K while theory gives for this point $T=111°$K, using the appropriate value of $\epsilon/k=117.9$ for the low temperature range.

It is of interest to find an empirical equation which will fit the experimental data on R_T as given in column 2 of Table III. We have found that a relation of the form $R_T=A-B/T+C/T^2$ with the constants $A=0.737$, $B=166.7$, and $C=10650$ determined by the method of least squares, fits the experimental data within the limits of experimental error. It is however seen from Fig. 3, curve B (experimental R_T *vs* log$T$) that the high temperature observations are well represented by the equation

$$R_T=0.25\,\ln(T/93.3), \tag{15}$$

which is in approximate agreement with Stier's formula (11).

Some research workers have remarked that this linear dependence on the logarithm of temperature is not predicted by theory. This is quite so as Fig. 3, curves A (theoretical R_T *vs* log$x$) and B show, but is nevertheless true as shown above for the limited high temperature range. The cause of this divergence is the variation of ϵ with temperature.

For the sake of comparison we have given in Table I, column 4, the T_r values, derived from our assumed dependence of R_T on temperature. These are calculated from the equation

$$T_r=(1/2F)\{-B-(B^2+4FC)^{\frac{1}{2}}\}, \tag{16}$$

where

$$F=B\left(\frac{1}{T_2}-\frac{1}{T_1}\right)\left(\ln\frac{T_2}{T_1}\right)^{-1}-\frac{C}{2}\left(\frac{1}{T_2^2}-\frac{1}{T_1^2}\right)\left(\ln\frac{T_2}{T_1}\right)^{-1}$$

in the case of data 3 to 7, and from the equation

$$T_r=(T_2-T_1)\,(\ln T_2/T_1)^{-1} \tag{17}$$

for data 1 and 2.

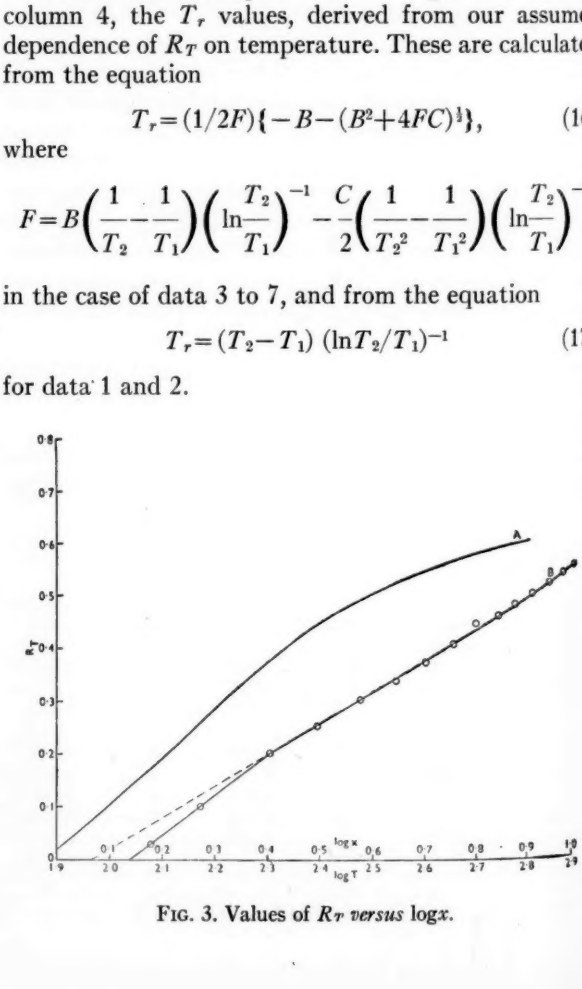

FIG. 3. Values of R_T *versus* log$x$.

4. DETERMINATION OF r_0

The values of ϵ calculated above from the thermal diffusion data can now be used to calculate r_0 from viscosity or self-diffusion data. Equations (6) and (7) show that the determination of r_0 at any particular temperature requires a knowledge of η, D_{12}, V/W_2^2, and W_1^1. η and D_{12} at the desired temperatures were read from the plots of these coefficients against temperatures.[8,9] Using the value of ϵ/k at the proper temperature from thermal diffusion, as given in Table IV, column 2, the value of kT/ϵ was found and the corresponding values of V/W_2^2 and W_1^1 were read from the tables given by Hirschfelder *et al.*[5] Substituting these values of V/W_2^2 and W_1^1 in Eqs. (6) and (7), respectively, the value of r_0 at any particular temperature was calculated from viscosity and self-diffusion. These are given in Table IV, columns 3 and 4 and are seen to be in good agreement with each other and well within the limits of experimental error in the measurement of self-diffusion. The correctness of the various formulas employed herein previously is thus established.

It may be remarked that the calculation of ϵ from thermal diffusion and the subsequent evaluation of r_0 from viscosity and self-diffusion is much more accurate than the practice hitherto of evaluating ϵ and r_0 both from viscosity. This is attributable to the fact that Eq. (4) does not involve r_0 and gives ϵ correctly for any temperature, while Eqs. (6) and (7) involve both ϵ and r_0 and can therefore be made to give ϵ only when r_0 does not vary. As we have seen above, both ϵ and r_0 vary to some extent, and therefore we cannot determine one unless we know the variation of the other by some different method. It is therefore impossible to determine ϵ and r_0, if both vary with temperature, from either viscosity alone or from self-diffusion alone. It is, of course, theoretically possible to combine viscosity and self-diffusion data at the same temperature, and by eliminating r_0 to determine ϵ from the observed temperature dependence of the ratio $\eta T/D_{12}$. Practically, however, on account of the errors in the experimental values of η and D_{12} and the very slight dependence of $\eta T/D_{12}$ upon temperature, the method was found to be useless.

5. VARIATION OF ϵ AND r_0 WITH TEMPERATURE

Table IV shows unmistakably that, with rise of temperature, ϵ increases while r_0 decreases. However, when transposed the observed magnitude of variation is subject to uncertainties on account of the possible errors in the experimental data. All the previous workers who have calculated the transport coefficients from the Lennard-Jones model and compared them with experiment, have so far treated ϵ to be absolutely constant, but we have shown that ϵ varies slightly with temperature, if the 12:6 power law is assumed to hold. This is seen clearly from Fig. 3, in which the two curves A and B should have been parallel if ϵ were quite independent of T. Our calculations given above merely assume the constancy of ϵ over a short range of temperatures and the validity of Eq. (4) over this limited range only. Hence, our method would give an average value of ϵ over that small temperature interval. Exact calculations by us from viscosity data[8] also show an unmistakable tendency for ϵ to increase with temperature, though it is not so noticeable there, as in the present case of thermal diffusion on account of the comparative insensitivity of viscosity to the value of ϵ. The question arises: What is the cause of this variation?

TABLE IV. Force constants ϵ and r_0 for argon.

Temp. °K	ϵ/k	r_0 in A from viscosity	r_0 in A from self-diffusion
130	115.0	3.473	3.473
140	116.6	3.468	3.447
160	120.3	3.443	3.432
180	120.0	3.449	3.424
250	135.1	3.370	3.337
300	142.9	3.344	3.319
350	152.2	3.321	3.295
400	158.1	3.309	
480	165.5	3.300	
530	168.3	3.293	

For finding this we have naturally to look closely into the Lennard-Jones potential energy function. It is well known that according to quantum mechanics[13] the dispersion energy leading to the Van der Waals' attraction is of the form[14]

$$-(cr^{-6}+dr^{-8}+gr^{-10}+\cdots), \tag{18}$$

which reduces to the Lennard-Jones term $-\mu r^{-6}$ for large intermolecular distances. It is evident that, at different temperatures, different parts of the molecular field are the most effective in contributing to the transport properties of a gas, the critical distance being smaller at higher temperatures on account of the increased molecular kinetic energies. Equation (18) shows that if, for smaller molecular distances also, the expression $-\mu r^{-6}$ is to represent the attraction energy, μ must be increased, as the critical distance decreases with rise of temperature, over the value which it has at large distances. Thus, by treating μ as a slowly varying function of T, increasing with increase of T, the attraction energy term $-\mu r^{-6}$ becomes sufficiently flexible to represent the true interaction accurately over the whole range of values of T.

Again, at great distances, the energy of molecular repulsion $P(r)\exp(-r/\rho)$ can be put equal to $b\exp(-r/\rho)$ approx. over a small range of r, as shown by Slater,[15] Bleick and Mayer,[16] Born and Mayer,[17] and Huggins,[18]

[13] H. Margenau, Revs. Modern Phys. **11**, 1 (1939).
[14] F. London, Z. Physik **63**, 245 (1930).
[15] J. C. Slater, Phys. Rev. **32**, 349 (1928).
[16] W. E. Bleick and J. E. Mayer, J. Chem. Phys. **2**, 252 (1934).
[17] M. Born and J. E. Mayer, Z. Physik **75**, 1 (1932).
[18] M. L. Huggins, J. Chem. Phys. **5**, 143 (1937).

b and ρ being constants. Buckingham[19] shows that the term $b\exp(-r/\rho)$ represents quite adequately the data on the second virial coefficient of neon and argon, though in the argument he assumes μ to remain constant. In the Lennard-Jones formula this exponential term is put equal to λr^{-12}. Since λr^{-12} does not fall off as rapidly as the term $b\exp(-r/\rho)$, we can increase the flexibility of the inverse power function by allowing λ to vary slowly with r. It will be shown in the next section that, for the temperatures with which we are concerned in the case of argon, this requires a decrease of λ with decrease of r, i.e., with increase of temperature. For the Lennard-Jones 12:6 model it can be shown that the minimum energy is

$$-\epsilon=-\tfrac{1}{4}(\mu^2/\lambda). \tag{19}$$

Hence, ϵ will increase with rise of temperature due both to the increase of μ and the decrease of λ with rise of temperature. However, the magnitude of variation cannot be theoretically calculated with any exactness.

We have now to explain the observed decrease of r_0 with rise of temperature. The Lennard-Jones potential energy function (1) can be written in the alternative form

$$E(r)=\epsilon_0[2(d_0/r)^6-(d_0/r)^{12}], \tag{20}$$

where d_0 is the distance between the molecules for which the energy is minimum and is equal to $(2\lambda/\mu)^{1/6}$, and ϵ_0 is the minimum negative energy given by $-\frac{1}{4}\mu^2/\lambda$. From Eq. (20), r_0, the separation for which the potential energy is zero, is given by

$$r_0=(1/2)^{1/6}d_0=(\lambda/\mu)^{1/6}. \tag{21}$$

As shown above, μ increases with increase of temperature while λ decreases; hence, r_0 ought to decrease with rise of temperature as is actually observed.

6. CALCULATION OF THE FORCE CONSTANTS μ AND λ

From Eqs. (19) and (21) it follows that, if we know ϵ and r_0 at a particular temperature, as in Table IV, we can calculate the values of μ and λ *at the temperature*. It is evident that at different temperatures different parts of the molecular field are most effective in producing the transport properties of the gas, and when we consider a particular temperature, as was just mentioned, the values of μ and λ deduced are those which give a good representation of the potential field over the range of r, in which the transport property is most sensitive to changes in the field. This critical range depends upon the temperature moving inwards as the temperature rises and, since μ and λ must be made to vary with r, in order to give respectively the correct dispersion and overlap energies as shown in the preceding section; it follows that μ and λ must be functions of temperature giving a good representation of the potential field over the corresponding critical range of values of r for the temperature in question. These values may be called the effective values of μ and λ for that temperature. These effective μ- and effective λ-values for argon at different temperatures are given in Table V. The experimental errors in the value of R_T are likely to produce an error of about ± 2 percent in μ and ± 1 percent in λ at low temperatures and approximately double the amount at high temperatures.

TABLE V. Force constants μ and λ for Argon.

Temp. °K	Effective $\mu\times10^{60}$ erg cm^6	Effective $\lambda\times10^{104}$ erg cm^{12}	Author
180	110.8	18.65	Present work
250	108.5	15.88	Present work
300	109.5	15.30	Present work
350	111.9	14.99	Present work
400	113.9	14.95	Present work
480	117.1	15.13	Present work
530	117.7	15.01	Present work
	103.0	16.20	Buckingham (reference 19)
	108.3	17.7	Lennard-Jones (reference 20)

[19] R. A. Buckingham, Proc. Roy. Soc. (London) **A168**, 264 (1938).
[20] J. E. Lennard-Jones, Proc. Phys. Soc. (London) **43**, 461 (1931).

7. VARIATION OF EFFECTIVE μ AND λ WITH TEMPERATURE

It is seen from Table V that effective μ increases with increase of temperature while λ decreases. This is in agreement with our theoretical conclusions in Sec. 5. It may be remarked that Buckingham[19] from a study of the data on the second virial coefficients comes to the exactly opposite conclusion that effective λ tends to increase in most cases with temperature. His conclusion is however based on the assumption that μ is constant, while, as we have shown previously, μ decreases with increase of r or with decrease of T. As a matter of fact, it can be shown that the virial coefficient data also, if properly interpreted, yield a decrease of effective λ with rise of temperature. This is done in the next section.

Putting the exponential in the inverse power form for two adjacent values of r, we have

$$be^{-r/\rho}=\lambda r^{-12}, \quad \text{and} \quad be^{-r'/\rho}=\lambda' r'^{-12}, \tag{22}$$

whence

$$e^{-(r-r')/\rho}=\frac{\lambda}{\lambda'}\left(\frac{r}{r'}\right)^{-12}. \tag{23}$$

For $(r-r')/\rho\ll 1$, we have

$$1-\frac{r-r'}{\rho}=\frac{\lambda}{\lambda'}\left[1-\frac{12}{r}(r-r')\right]$$

or

$$\frac{\lambda}{\lambda'}=\frac{1-(r-r')/\rho}{1-12(r-r')/r}, \tag{24}$$

TABLE VI. Values of $\log|F(y)|$ for various values of y.

$y=1.1$	1.2	1.3	1.4	1.5	1.6	1.7	1.8
$\log\|F(y)\|=\bar{2}.4200$	$\bar{1}.2853$	$\bar{1}.5796$	$\bar{1}.7746$	$\bar{1}.9151$	0.0434	0.1473	0.2413

which shows that for $r/12<\rho$, $\lambda'<\lambda$ for $r'<r$, i.e., $T'>T$; while for $r/12>\rho$, $\lambda'>\lambda$ for $r'<r$. Thus with increase of temperature, i.e., decrease of r, λ will increase if the effective $r>12\rho$ while it will decrease if the effective $r<12\rho$. Taking r_0 to denote the effective r at the Boyle point, it follows that in this region λ will decrease with increase of temperature if $\rho>r_0/12$, or putting down the value $r_0=3.3$ from Table IV, if $\rho>0.275$. This is actually so, as has been shown by Buckingham[19] in his Table VI, calculated from the crystal properties of argon. He finds that for $\mu=117\times10^{-60}$ erg cm^6 (which is the value of μ we have found at about the Boyle point) $\rho=0.32$ approx, which is greater than 0.275. Hence, λ at the Boyle point will decrease with increase of temperature. For lower temperatures also, the condition of effective $r/12<\rho$ will evidently be satisfied, as ρ is so much greater, and λ will show a decrease with increase of temperature. Thus the variation of μ and λ observed in Table V have been theoretically accounted for.

8. CALCULATION OF THE CONSTANT λ FROM THE SECOND VIRIAL COEFFICIENT

Attempts have been made by Lennard-Jones[21] and others to calculate μ and λ from the observed second virial coefficient at various temperatures, but the conclusions arrived at are not sufficiently precise in view of the three unknowns μ, λ, and the repulsive force index. Even with the force index fixed at 13, various sets of values of μ and λ have been obtained by them, from which the average values of μ and λ are calculated. Thus, no correct idea of their variation with temperature can be obtained from such investigations. Buckingham[19] assumed this average value of μ as fixed and tried to calculate the repulsive exponential term, and thereby purports to show that λ varies slowly with r. He even calculates the repulsive exponential term by assuming arbitrary fixed values of μ. These calculations lose their significance if μ is a variable, as we have shown above. We therefore proceed to calculate λ for different temperatures, assuming both μ and λ to be variable and using the values of μ obtained above by us, by combining the thermal diffusion and viscosity data of argon. The procedure adopted is analogous to that of Buckingham, except that μ is not taken to be constant, but the experimental values of μ at different temperatures are utilized.

[21] J. E. Lennard-Jones, Proc. Roy. Soc. (London) **A106**, 463 (1924).

The equation of states of a gas may be written as

$$pV=NkT\left\{1+\frac{B}{V}+O\left(\frac{1}{V^2}\right)\right\}, \tag{25}$$

where the classical formula for B for a spherically symmetrical field is

$$B=2\pi N\int_0^\infty r^2[1-\exp\{-E(r)/kT\}]. \tag{26}$$

With μ and λ as constants, Lennard-Jones[21] derived the closed formula for B in the form

$$B=\tfrac{2}{3}N\pi(\lambda/\mu)^{\frac{1}{4}}F(y), \tag{27}$$

where

$$F(y)=y^{\frac{1}{4}}\{\Gamma(3/4)-\sum_{n=1}^{\infty}C_n y^n\}, \tag{28}$$

and y is a function of temperature given by

$$y=(\mu/kT)(kT/\lambda)^{\frac{1}{2}}. \tag{29}$$

The coefficients C_n are given by

$$C_n=3\Gamma\left\{\frac{(6n-3)}{12}\right\}\Big/n!12. \tag{30}$$

Buckingham[19] has shown how this formula can still be used when μ and λ are treated as variables, in which case they may be called the effective values such that these effective values give a good representation of the potential field over the range in which B is most sensitive to changes in the field.

From Eqs. (27) and (29) we have

$$2\log y-2\log F(y)=\log\{(2\pi N/3B)^2\mu/kT\} \tag{31}$$

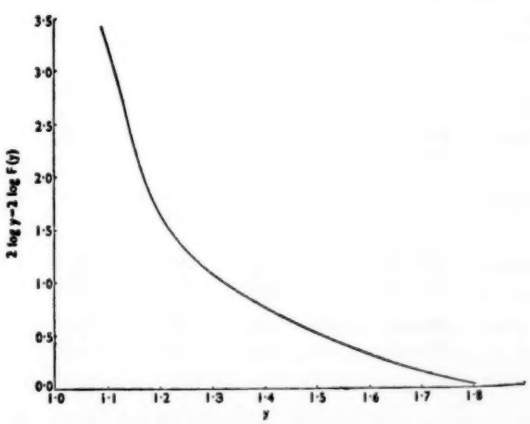

FIG. 4. Plot of $2\log y-2\log F(y)$ *versus* y.

TABLE VII. Force constant λ from virial coefficient by utilizing the values of μ from Table V for argon.

Temp. °K	$B\times10^3$	$\lambda\times10^{104}$ in erg cm^{12} (from virial coeff.)	$\lambda\times10^{104}$ in erg cm^{12} (Th. diffusion and viscosity)
180	−2.70	18.94	18.65
250	−1.30	17.78	15.88
300	−0.70	18.24	15.30
350	−0.30	18.99	14.99
400	−0.05	19.62	14.95
480	+0.25	15.28	15.13
530	+0.40	12.96	15.01

and

$$\log\lambda=2(\log\mu-\log y)-\log kT. \qquad (32)$$

The left-hand side of Eq. (31) is a function of y alone and can be plotted for arbitrary values of y. The right-hand side is known when the virial coefficient B at a particular temperature and the corresponding μ for that temperature, as given in Table V, are substituted. Using this numerical value of the right-hand side of (31), we can at once read from the plot of the left-hand side of (31), the corresponding value of y. This value of y is then substituted in (32), with the corresponding values of μ and T, to give λ at the temperature in question.

This method has been adopted for argon to estimate the value of λ at various temperatures. For arbitrary values of y between 1.1 and 1.8, the corresponding values of $\log|F(y)|$ were calculated and are given in Table VI. Then $2\log y-2\log F(y)$ was plotted against y as shown in Fig. 4. The values of B were taken from the data of Holborn and Otto[22] and plotted against T, so that the value of B corresponding to any desired temperature could be easily read. These are given in column 2 of Table VII. The values of λ thus obtained from the virial coefficient data are given in column 3, which may be compared with the values of λ in column 4 obtained previously by combining the thermal diffusion and viscosity data.

TABLE VIII. Force constants for O_2, N_2, CH_4, and CO from thermal diffusion.

Gas	Temp. range °K	T_r	R_T	ϵ/k	r_0 in A (viscosity)	r_0 in A (self-diffusion)
Oxygen	195–373	265	0.367	108.1	3.456	3.294
	295–528	389	0.475	111.4	3.394	
Nitrogen	195–427	281	0.47	82.73	3.721	3.624
	294–678	434	0.58	70.0	3.729	
Methane	195–435	284	0.25	155.2	3.718	3.588
	295–708	443	0.41	158.2	3.676	
CO	195–427	281	0.45	88.63	3.703	
	293–683	434	0.57	76.14	3.729	

[22] L. Holborn and J. Otto, Z. Physik **23**, 77 (1924); **38**, 359 (1926).

It will be seen that λ as calculated from the virial coefficient data also shows a decrease with increase of temperature, thereby confirming the similar trend of variation of λ obtained from the transport properties. The values of λ in the region from 300 to 400°K show some irregularity. This is obviously to be attributed to the extreme sensitivity of the second virial coefficient B to the law of force in this region close to the Boyle point, so that even small errors in the measurement of B will produce large errors in the value of λ.

9. FORCE CONSTANTS FOR OTHER ISOTOPIC GASES

The data on neon are sufficiently extensive, but the main difficulty in drawing any conclusion from them lies in the fact that the observed values of R_T for neon at high temperatures are much above that given by the 12:6 model. It is generally believed that a repulsive force index greater than 13 would be necessary to account for the large values of R_T, but nothing definite can be stated. The data on thermal diffusion of other gases are much less extensive. The only available data

TABLE IX. Comparison of the values of ϵ obtained from transport properties and virial coefficients.

Gas	Temp. range °K	Mean ϵ/k from thermal diffusion	Average r_0 from viscosity from col. 3	ϵ/k from viscosity (low temp.) reference 8	ϵ/k from viscosity (high temp.) reference 8	ϵ/k from self-diffusion reference 9	ϵ/k from virial coefficient reference 5
Oxygen	195–528	109.8	3.425	112.7	134.9	119.2	117.5
Nitrogen	195–678	76.4	3.725	89.8	117.1	102.4	95.9
Methane	195–708	156.7	3.697			154.1	142.7
CO	195–683	82.4	3.716				95.3

are those for oxygen, nitrogen, CH_4, and CO[23–25], and these are not sufficiently accurate and extensive to provide a satisfactory evaluation of the force constants at different temperatures. For these gases therefore Eq. (12) cannot be applied to yield the values of R_T at various temperatures as in the case of argon. We have therefore used Brown's formula [Eq. (9)], which, as shown previously, is only approximately valid over a small range. The effective value T_r, *viz.*, the temperature to which R_T values should be taken to apply, is given by Eq. (10) and will be correct to within a few percent. These temperature ranges along with their respective T_r values are given in Table VIII, columns 2 and 3. The corresponding values of ϵ were found from the graph R_T *vs* kT/ϵ (Fig. 1). These values are recorded in Table VIII, column 5, for different gases and the different ranges of temperature, and the corresponding values of r_0 are given in columns 6 and 7.

Since the data on R_T are not sufficiently extensive,

[23] A. N. Davenport and E. R. S. Winter, Trans. Faraday Soc. **47**, 1160 (1951).
[24] A. O. Nier, Phys. Rev. **56**, 1009 (1939).
[25] A. K. Mann, Phys. Rev. **73**, 412 (1948).

it is not possible to obtain the values of ϵ at a large number of temperatures with any certainty. No reliance can therefore be placed on the variation with temperature of the value of ϵ as recorded in column 5, of Table VIII. Hence the mean value of ϵ has been calculated and given in column 3 of Table IX, along with the other determinations of ϵ from viscosity, self-diffusion, and the second virial coefficient. The values are seen to be in agreement with other determinations. Further work on the thermal diffusion of these gases is desirable in order to determine the variation of ϵ and r_0 with temperature as in the case of argon.

The values of ϵ and r_0 given in Table IX were utilized to calculate μ and λ with the help of Eqs. (19) and (21).

TABLE X. Force constants μ and λ for various gases.

Gas	Average $\mu \times 10^{60}$ erg cm^6	Average $\lambda \times 10^{104}$ erg cm^{12}
Oxygen	97.12	15.66
Nitrogen	111.7	29.88
Methane	219.3	55.94
CO	119.1	31.34

These are given in Table X and may be taken to represent average values.

We record our thanks to the Government of Uttar Pradesh for the award of a research scholarship to one of us (M. P. M.).

THE JOURNAL OF CHEMICAL PHYSICS VOLUME 21, NUMBER 5 MAY, 1953

Rotational Isomerism in Chloroacetone

SAN-ICHIRO MIZUSHIMA, TAKEHIKO SHIMANOUCHI, TATSUO MIYAZAWA, ISAO ICHISHIMA, KENJI KURATANI, ICHIRO NAKAGAWA, AND NOBUHIKO SHIDO
Chemical Laboratory, Faculty of Science, Tokyo University, Hongo, Tokyo, Japan

(Received January 5, 1953)

Raman spectra of chloroacetone were measured in the liquid and solid states and in solutions. Infrared absorption spectra of this substance were measured in the gaseous, liquid, and solid states and in solutions. The temperature dependence of the intensity of the Raman lines and of the absorption bands were measured in the liquid state. From the experimental results together with the dipole data it was concluded that chloroacetone exists in two molecular forms in the liquid and gaseous states and in one form in the solid state. The less stable form in the liquid state becomes much more abundant than the other form in the gaseous state. Some considerations on the nature of hindering potential of internal rotation have been made.

IN our last report on rotational isomerism, we published our experimental results on the molecules of the type XH_2C-COY, in which X and Y denote halogen atoms.[1,2] It was shown that in the liquid and gaseous states there are two different molecular forms, of which only one form persists in the solid state. In order to obtain further information on the internal rotation of such a kind of molecule, we measured the Raman and infrared spectra of chloroacetone $ClH_2C-COCH_3$ which has a similar skeletal structure as XH_2C-COY. We are interested to see how the replacement of Y-atom by CH_3-group affects the internal rotation about the central C–C bond.

EXPERIMENTAL

Chloroacetone was prepared by passing chlorine gas through acetone in the presence of calcium carbonate. By changing the condition of this reaction in various ways we could succeed to obtain spectroscopically pure samples of chloroacetone. (The main by-product of this reaction is dichloroacetone. The spectra of the pure samples did not show any absorption peak of this substance.)

The Raman spectra of chloroacetone were measured in the solid and liquid states and in solutions. (See Fig. 1.) The solid spectrum was observed by cooling the sample with the mixture of dry ice and acetone and by using aqueous solution of $Pr(NO_3)_3$ as the filter. The Raman spectrum of chloroacetone at room temperature was already measured by H. Cheng.[3] There are some discrepancies between his result and ours, but we believe our spectrum was obtained with a purer sample.

Our infrared absorption measurements were made for the gas at about 140°C, for the liquid at different temperatures and for the solid at about −65°C. The spectrometer of our own construction and the Baird instrument were used in these measurements. The results of the measurements are shown in Table I together with those of the Raman measurements.

DISCUSSION

Let us discuss the experimental results shown in Table I, just as we did in the case of the type of molecules XH_2C-COY, since, as stated in the beginning of this paper, there is a close similarity in the skeletal structure between $ClH_2C-COCH_3$ and XH_2C-COY. For the latter molecule we could assign C=O, C–X,

[1] Nakagawa, Ichishima, Kuratani, Miyazawa, Shimanouchi, and Mizushima, J. Chem. Phys. **20**, 1720 (1952).
[2] For the summary of our works on internal rotation, see S. Mizushima, Reilly Lecture, University of Notre Dame (1951).
[3] H. Cheng, Z. physik. Chem. **B26**, 288 (1934).

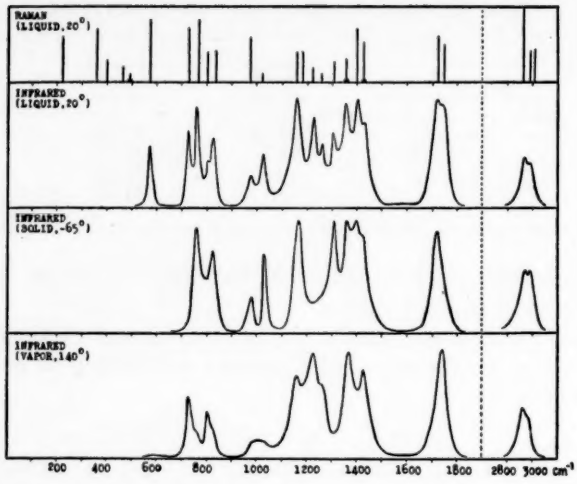
RAMAN (LIQUID, 20°)
INFRARED (LIQUID, 20°)
INFRARED (SOLID, -65°)
INFRARED (VAPOR, 140°)
200 400 600 800 1000 1200 1400 1600 1800 2800 3000 cm⁻¹

FIG. 1. Raman and infrared spectra of chloroacetone.

and C—Y stretching frequencies quite distinctly for each of the rotational isomers.[1]

The two Raman lines of almost the same intensity observed at 1722 and 1745 cm^{-1} are undoubtedly assigned to the C=O stretching frequencies. Of these only the former line persists in the solid spectrum. This can be explained by considering two stable molecular configurations in the liquid state and only one in the solid state, just as we have proved experimentally in many molecules with internal rotation axes.[2] If these two lines of almost the same intensity would arise from one molecular configuration, we cannot understand why only one of them disappears in the solid spectrum. This conclusion is confirmed by the observation of the C—Cl stretching frequencies which are expected to appear at about 750 cm^{-1} as one Raman line for one configuration. We observed two Raman lines of almost the same intensity at 728 and 764 cm^{-1} in the liquid state and of these only the latter persists in the solid state.

In the frequency region between 200 and 600 cm^{-1} we can expect four Raman lines for one configuration corresponding to the three skeletal deformation vibration and one π-vibration which is a vibration out of the

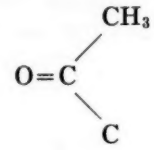

plane. Actually we observed six Raman lines in this region in the liquid state. This is also consistent with the view that we have two different molecular forms in the liquid state (see Table I). Below this frequency region we may observe Raman lines corresponding to the torsional motions about C—C single bonds. None of them has, however, been observed, presumably because of the weak intensity.

The change of relative intensity of the Raman lines with temperature provides another evidence for the existence of two isomers in the liquid state. Of the two C—Cl frequencies of the liquid spectrum stated above, the line at 764 cm^{-1}, which persists in the solid state, increased in intensity at lower temperatures, while the other line at 728 cm^{-1} became weaker as the temperature is lowered, and it disappeared completely

TABLE I. Raman and infrared frequencies of chloroacetone in the solid, liquid, and gaseous states.[a]

Molecular form	Assignment	Raman frequencies		Infrared frequencies		
		Liquid	Solid	Gas	Liquid	Solid
M, L	δ_1	220(6)				
M	δ_2	357(7)	358(1)			
L	δ_2	398(3)				
M	π	462(2)				
L	δ_3	490(1b)				
M	δ_3	571(8)	568(3)		572(m)	
L	ν(C—Cl)	728(7)		731(m)	728(m)	
M	ν(C—Cl)	764(8)	762(3)	760(vw)	763(s)	761(m)
L		802(4)		805(w)	805(w)	
M		833(4)		830(vw)	827(m)	829(m)
M		973(6)			972(w)	977(w)
M		1026(1)		1000(w, br)	1023(m)	1029(m)
M		1161(4)		1160(s)	1162(s)	1167(s)
		1184(4)				
L		1225(2)		1226(vs)	1227(s)	
L		1258(1)		1261(m)	1259(w)	
M		1304(3)			1304(m)	1305(m)
M, L		1356(3b)		1370(s)	1359(s)	1357(s)
M		1400(7)	1400(2b)		1402(s)	1401(s)
M, L		1428(5b)		1427(s)	1428(m)	1425(m)
M	ν(C=O)	1722(6)	1714(1)		1725(vs)	1718(vs)
L	ν(C=O)	1745(5)		1742(vs)	1745(vs)	
		2930(10)	2932(5)	2940(m)	2930(m)	2930(m)
		2977(4)	2980(2)	2980(w)	2975(m)	2975(m)
		3016(4)				

[a] M: more polar form, L: less polar form, ν: stretching vibration, δ: deformation vibration, π: out-of-plane vibration, vs: very strong, s: strong, m: medium, w: weak, vw: very weak, br: unusually broad.

in the solid spectrum. Accordingly, we can conclude that the more stable form in the liquid state persists in the solid state, just as we have observed for many substances showing rotational isomerism.[2]

Exactly the same conclusion was drawn from our measurements on the infrared spectra of chloroacetone in the liquid and solid states (see Table II). In this case we also measured the spectrum in the gaseous state in which the relative intensity of the 728 cm^{-1} band became much stronger than that in the liquid state. In other words the less stable form in the liquid state becomes much more abundant than the other form in the gaseous state.

We also measured the change of intensity of the Raman lines and absorption bands with solvent. As shown in Table II, the Raman line at 764 cm^{-1} increased in its relative intensity in a solvent of higher dielectric constant. This is also the case for the absorption bands, if we consider vacuum as a solvent of dielectric constant = 1. According to the result of our previous studies,[4,5] the energy of the more polar form, or the form with larger dipole moment, is generally decreased more conspicuously in a solvent of higher dielectric constant. In other words, the relative number of the more polar form will become larger as the dielectric constant of the solvent becomes larger. Accordingly, we can assign the Raman line and the absorption peak at 764 cm^{-1}, which increases in relative intensity in a more polar solvent, to a vibration of the more polar form and those at 728 cm^{-1} to that of the less polar form. This means that the more polar form corresponds to the more stable form and the less polar form to the less stable form in the liquid state. Now that the moment value calculated from the bond moment decreases with azimuthal angle of internal rotation (see Table III), we can conclude that the more polar form has an azimuthal angle smaller than that of the less polar form. Here the origin of the azimuthal angle is taken at the *trans*-position for Cl-atom and CH_3-group (Fig. 2). From the comparison of the calculated values with those observed in the gaseous state and in nonpolar solutions (see Table IV), we can consider that the Cl-atom and the CH_3 group are near the *trans*-position ($\theta = 0°$) with each other in the more polar form, and they are near the *cis*-position in the less polar form.

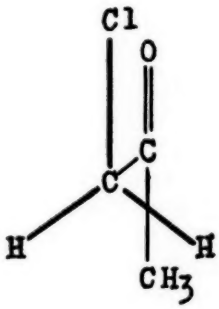

FIG. 2. The *trans*-configuration of chloroacetone ($\theta = 0°$).

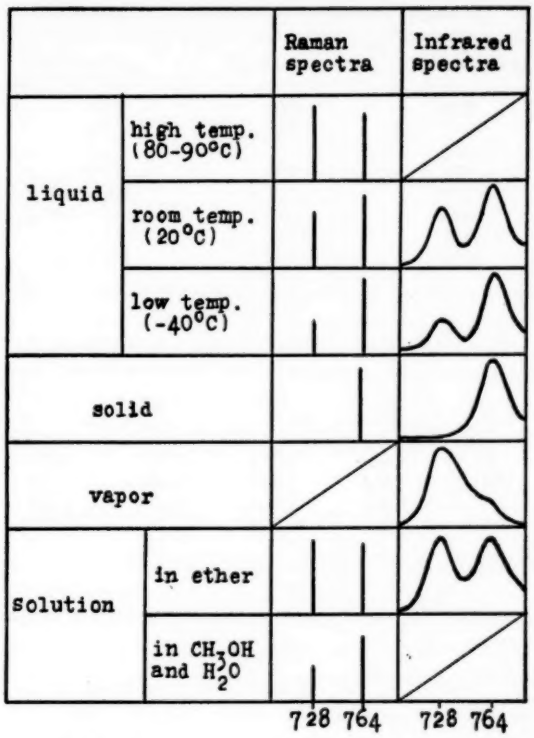

TABLE II. Behavior of two frequencies, 728 cm^{-1} and 764 cm^{-1}.

In order to estimate the azimuthal angle of these stable forms, we applied the product rule of rotational isomers derived in our previous papers:[6,7]

$$\left(\frac{\Pi\nu'}{\Pi\nu}\right)^2 = \frac{|G'|}{|G|}, \tag{1}$$

TABLE III. Calculated moments at different azimuthal angles.[a]

θ	0°	30°	60°	90°	120°	150°	180°
μ corrected	3.6	3.5	3.3	2.8	2.1	1.5	1.2
μ uncorrected	4.2	4.0	3.7	3.1	2.3	1.6	1.2

[a] The values in the second row have been corrected for induction effect.

TABLE IV. Observed moments of chloroacetone.

In CCl_4 solution	$2.38D$	Present experiment
In n-C_6H_{14} solution	$2.35D$	H. Mohler[a]
In the gaseous state	2.17–$2.24D(d\mu/dT>0)$	C. T. Zahn[b]

[a] H. Mohler, Helv. Chim. Acta **21**, 67 (1938).
[b] C. T. Zahn, Physik. Z. **33**, 686 (1932).

[4] Watanabe, Mizushima, and Masiko, Sci. Papers Inst. Phys. Chem. Research (Tokyo) **40**, 425 (1943). See also S. Mizushima and H. Okazaki, J. Am. Chem. Soc. **71**, 3411 (1949).
[5] Morino, Mizushima, Kuratani, and Katayama, J. Chem. Phys. **18**, 754 (1950).
[6] Mizushima, Morino, and Shimanouchi, Sci. Papers Inst. Phys. Chem. Research (Tokyo) **40**, 87 (1942): J. Chem. Phys. **17**, 663 (1949).
[7] Mizushima, Shimanouchi, Nakagawa, and Miyake, J. Chem. Phys. **21**, 215 (1953).

TABLE V. Assignment of skeletal frequencies.

More polar form	Less polar form	Assignment
220	220	δ_1
357	398	δ_2
462	...	π
571	490	δ_3
764	728	ν(C−Cl)
833	802	ν_1(C−C)
1161	1225	ν_2(C−C)
1722	1745	ν(C=O)

TABLE VI. $|G_{\theta'}|/|G_\theta|$ for various values of θ and θ'.

θ \ θ'	90°	120°	150°	180°
0°	3.648	2.913	0.922	0.895
30°	2.314	1.848	0.585	0.567
60°	1.262	1.008	0.319	0.309
90°	1.000	0.799	0.253	0.245

TABLE VII. The two stable molecular forms of chloroacetone.

Molecular form	Azimuthal angle	Solid	Liquid	Gas
more polar form	0°–30°	present	more stable	much less abundant
less polar form	*ca* 150°	absent	less stable	much more abundant

where ν and ν' are, respectively, the normal frequencies of the more polar and the less polar forms and **G** and **G′** are the kinetic energy matrices of these two forms. For the calculation of the left-hand side of Eq. (1) we took into account only the skeletal frequencies (except π) which were assigned as shown in Table V. The assignment was made on the basis of our experimental result stated above that the Raman lines or absorption peaks of the two isomers behave differently in various solvents or with change of state and of temperature. Of these frequencies, δ_1 was considered to be common to the two forms, because the corresponding Raman line behaves just as two different vibrations are overlapped on the same position.

The value of the left-hand side of Eq. (1) calculated from observed frequencies of Table V is 0.88. If, therefore, we compare this value with the ratio of *G* matrices shown in Table VI, we can conclude that the azimuthal angle of the less polar form is not much different from 150° and that of the more polar form is between 0° and 30°, taking into account the result of dipole measurement. Here the origin of the azimuthal angle was taken at the *trans*-position, as referred to above.

The results obtained above are summarized in Table VII. It is worthy of note that the less stable form in the liquid state becomes much more abundant than the other form in the gaseous state. This is quite interesting as compared with the results so far obtained by us for substances showing rotational isomerism.

In our previous paper[8] we stated that the nature of hindering potential is generally determined by the steric repulsion and the electrostatic interaction between the movable groups. If we assume that the steric repulsion between Cl-atom and O-atom is much less than that between two Cl-atoms, or between Cl-atom and CH_3-group, both of the molecules of $ClH_2C-COCl$ and $ClH_2C-COCH_3$ tend to take the *trans*-form ($\theta=0°$) with respect to two Cl-atoms or Cl-atom and CH_3-group caused by this repulsive force. However, the electrostatic interaction favors the other form with $\theta=$ *ca* 150° in $ClH_2C-COCH_3$, since in this form the two large bond moments, μ_{C-Cl} and $\mu_{C=O}$, are almost in opposite direction. In the case of $ClH_2C-COCl$ we have another C−Cl bond which makes the difference in moment value between the two molecular forms much less significant than in the case of $ClH_2C-COCH_3$. From this we can understand the experimental result found in the gaseous state that in $ClH_2C-COCH_3$ the 150° form (or the less polar form) is more abundant than the 0° form (or the more polar form), while in the case of the $ClH_2C-COCl$ the abundance ratio is just reversed. Moreover, we can see why the isomeric ratio of $ClH_2C-COCH_3$ changes much more markedly on condensation than that of $ClH_2C-COCl$ does, because in the liquid state the difference in electrostatic energy between the rotational isomers of $ClH_2C-COCH_3$ will be decreased much more conspicuously than that of $ClH_2C-COCl$.

Based on many experimental results of spectroscopic and electric measurements, we concluded in our previous paper that the steric repulsion between atoms contained in different movable groups plays the most important role in determining the azimuthal angle of stable forms, but the electrostatic force can affect the energy difference of stable forms considerably.[2,8]

In the case of dihalogenoethanes, the stable forms as determined by the steric repulsion were also stable from the electrostatic point of view. However, in the case of the molecules containing the C=O group, the form which is electrostatically more stable becomes less stable from the steric repulsive potential. The different behavior in rotational isomerism between 1,2-dihalogenoethanes and chloroacetone or halogenoacetyl halides is caused by this situation. The difference in internal rotation between chloroacetone and chloroacetyl chloride can be explained by a similar discussion, as stated previously. These molecules have similar skeletal structures which correspond to the similar steric potential of internal rotation, but there is a large difference in electrostatic potential to which the remarkable difference in the isomeric ratio of these two substances is due.

[8] Mizushima, Morino, and Shimanouchi, J. Phys. Chem. **56**, 324 (1952).

The Ultrasonic Velocity, Density, and Compressibility of Supercooled H_2O and D_2O

R. T. LAGEMANN AND L. W. GILLEY
Vanderbilt University, Nashville, Tennessee

AND

E. G. MCLEROY*
Emory University, Emory University, Georgia

(Received January 12, 1953)

The velocity of compressional waves in liquid water (H_2O and D_2O) has been measured over a range of temperature extending to some six degrees below the nominal freezing point, using a fixed-frequency variable-path sonic interferometer. The density of heavy water in the supercooled state has been determined and values of the adiabatic compressibility calculated. The curves representing the variation of density with temperature are symmetrical and congruent for the two isotopic liquids. It is confirmed that the compressibility of D_2O is greater than that for ordinary water. The new measurements of the three properties yield values which fall on smooth extrapolations of the previously known data, indicating that there is no partial ordering of the liquid structure into the solid structure at temperatures below the nominal freezing point, at least none at times removed from the start of observed freezing.

WATER is a unique substance in so far as its ultrasonic velocity is concerned. Whereas all other pure liquids studied show a linear variation of velocity with temperature and a negative temperature coefficient, water displays a maximum velocity (H_2O at 73° and D_2O at 79°) and a parabolic relationship. Frequently this anomalous behavior of water is attributed to association; yet methyl alcohol and those other associative compounds examined do not give a similar variation. Therefore, it was thought of interest to examine the velocity of ultrasonic compressional waves in liquid water below its normal freezing point, a region uninvestigated previously.

It is well known that water can be easily supercooled, sometimes to as low as minus 20°C. Dorsey,[1] while pointing out the lack of agreement on the causes for the freezing of supercooled water, says that a sufficient cause is the introduction of a piece of the solid or the rubbing of the interface separating the water and its container. Other reports[2,3] indicate that shaking or rapid vibration do not of themselves cause solidification, and this is supported by our experience that the passage of low power ultrasonic waves of frequency 500 kc/sec did not, generally, cause freezing in supercooled water down to some six degrees below the freezing point. Furthermore, below 6 degrees the freezing of the supercooled water could not be unequivocally associated with the application of the ultrasonic beam. With the equipment used it was possible to cool the water slowly to desired temperatures down to 6 degrees below the freezing point and maintain it in the liquid state for hours at a time, while measurements were made of the sonic velocity and density. It was found that brass and glass containers[4] for the water were equally satisfactory. It was further noted that outgassing of the water immediately prior to the measurements affected neither the values obtained nor the capacity of the water to be supercooled. A rough estimate indicates that less than one watt of power was sent into the water by the quartz crystal.

TABLE I. Some physical properties of liquid H_2O and D_2O at temperatures below the accepted freezing point.

Compound	Temperature (°C)	Ultrasonic velocity (m/sec)	Absolute density[a] (g/cc)	Adiabatic compressibility (cm-dyne^{-1} $\times 10^{12}$)
H_2O	−5.05	1379		
	−5.00	1381	0.99927	52.47
	−4.00	1386	0.99942	52.09
	−3.00	1393	0.99955	51.56
	−2.00	1396	0.99967	51.33
	−1.00	1402	0.99976	50.89
	0.00	1408	0.99984	50.44
	5.00	1428	0.99996	49.04
D_2O	−2.00	1297	1.1043	53.83
	−1.00	1303	1.1048	53.31
	0.00	1307	1.1049	52.98
	1.00	1313		
	2.00	1317	1.1054	52.16
	3.00	1322		
	3.50	1325		
	3.81	1326	1.1056	51.44
	4.00	1327		
	5.00	1332		
	6.00	1336	1.1060	50.65
	8.00	1344		
	10.00	1352	1.1061	49.46
	12.00	1360	1.1061	48.88
	16.00		1.1058	
	20.00	1386	1.1056	47.36
	25.00	1401	1.1045	46.13

[a] The values for H_2O are calculated from the specific gravity data given in the *Smithsonian Physical Tables*, (The Smithsonian Institution, Washington, D. C., 1927) Seventh Revised Edition, p. 106, using $d_4 = 0.999973$ g/cm^3.

* Now at the U. S. Navy Mine Countermeasures Station, Panama City, Florida.

[1] N. D. Dorsey, *Properties of Ordinary Water Substance* (Reinhold Publishing Corporation, New York, 1940).

[2] E. C. McCracken, Science **106**, 453 (1947).

[3] R. Smith-Johannsen, Science **108**, 652 (1948).

[4] R. T. Lagemann, J. Acoust. Soc. Am. **24**, 86 (1952).

EXPERIMENTAL

The measurements of the ultrasonic velocity were made by use of an ultrasonic interferometer described earlier.[5] A quartz crystal, energized by a constant-frequency, crystal-controlled oscillator of 500 kc/sec, was used as a source. Values of the half-wavelength were measured on a precision micrometer possessing a least count of 0.0001 inch. The temperature was controlled to ±0.05°C by immersing the entire interferometer in a water bath cooled by thermostated refrigerator coils. Temperatures were measured by means of a Bureau of Standards calibrated thermometer whose bulb and stem were inserted directly through the wall of the interferometer and placed in the water sample under study. The probable error of the velocity measurements was ±1.0 m/sec.

Densities were measured by means of a 5 cc double arm pycnometer described by Lipkin *et al.*[6] No difficulty was involved in maintaining the water in the liquid state, while bringing the pycnometer and its contents to temperature equilibrium and while reading the levels in the arms. It is believed that the density values for D_2O were determined with a probable error of ±0.0002 g/cc. The D_2O was used as it came from the Stuart Oxygen Company. It was described as 99.77 percent D_2O. The ordinary water used was first distilled in a 30-plate column.

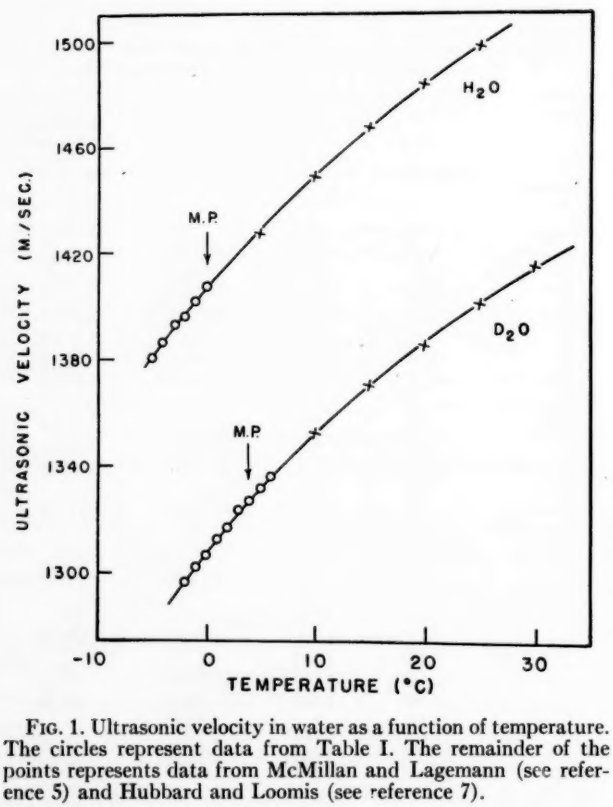

FIG. 1. Ultrasonic velocity in water as a function of temperature. The circles represent data from Table I. The remainder of the points represents data from McMillan and Lagemann (see reference 5) and Hubbard and Loomis (see reference 7).

RESULTS

The measured values of the density and the ultrasonic velocity for D_2O and H_2O are given in Table I. They have not been corrected for the percentage H_2O present. In most cases, each velocity given represents the average of several measurements made on separate samples. Our value at 0° for the velocity of H_2O, 1408 m/sec, agrees well with 1407 m/sec found by Hubbard and Loomis.[7]

The density of heavy water has not been reported for temperatures below 10°C, although the accepted freezing point is 3.81°C. The densities for D_2O, given in Table I, duplicate in a few cases work by Stokland, Ronaess, and Tronstad.[8] Although their work is more precise, the agreement is good where comparison can be made, when one considers the precision of the measurements. For example, Stokland and his coworkers obtained 0.998589 for the density of D_2O at 25° relative to its density at 11.23°C, the point of maximum density. They give the density of D_2O at 11.23°C relative to that of H_2O at 4°C to be 1.10596, from which we calculate the absolute density of D_2O at 11.23° to be 1.10593 g/cc and the absolute density of

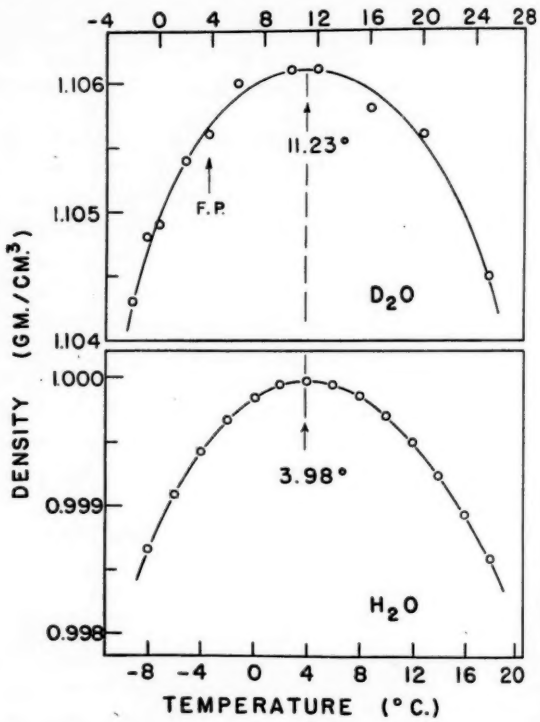

FIG. 2. The absolute density of H_2O and D_2O as a function of temperature. The data for H_2O are from the *Smithsonian Physical Tables*. The data for D_2O are from the present study.

[5] D. R. McMillan and R. T. Lagemann, J. Acoust. Soc. Am. **19**, 956 (1947).

[6] Lipkin, Davison, Harvey and Kurtz, Ind. Eng. Chem., Anal. Ed., **16**, 55 (1944).

[7] J. C. Hubbard and A. L. Loomis, Phil. Mag. **5**, 1177 (1928).

[8] Stokland, Ronaess and Tronstad, Trans. Faraday Soc. **35**, 312 (1939).

D_2O at 25° to be 1.10437 g/cc. Our own measured value at 25° is 1.1045 g/cc. For d_{25}^{25} (D_2O relative to H_2O) we obtain 1.1078, whereas Taylor and Selwood[9] give 1.1079 and Stokland *et al.*[8] give 1.10764 for 100 percent D_2O with the normal ratio of the oxygen isotopes.

In the last column of Table I are given the values of the adiabatic compressibility calculated from the measured density and sound velocity. The value of 50.44×10^{-12} cm-dyne^{-1} at 0°C, for example, compares favorably with the value 50.93×10^{-12} cm-dyne^{-1} (50.28×10^{-6} atmospheres^{-1}) found by Tyrer[10] from the direct determination of this property for H_2O. Although it is reported[11] that D_2O has a lower compressibility at 30° than does ordinary water, our results indicate the contrary and are in agreement with Bar.[12]

[9] H. S. Taylor and P. W. Selwood, J. Am. Chem. Soc. **56**, 998 (1934).
[10] D. Tyrer, J. Chem. Soc. **103**, 1675 (1913).
[11] S. Bhagavantam and C. V. J. Rao, Nature **140**, 1099 (1937).
[12] R. Bar, Helv. Phys. Acta **8**, 500 (1935).

Figures 1 and 2 show that the values of ultrasonic velocity and density of supercooled water, through the 6 degree range studied, lie on curves which are reasonable extrapolations of the respective measurements above the freezing point. No discontinuity or abrupt change of slope is noted, and seemingly there is no partial ordering of the liquid structure into the solid structure when the fluid is at temperatures below the nominal freezing point. (If there were, one would expect a larger velocity approaching that of ice, which has an ultrasonic velocity of about 3 km/sec at 0°C.) The equipment did not permit measurements of the velocity during a short time interval immediately prior to or during actual freezing, since some 15 minutes are required for a measurement.

Finally, it is interesting to note that the curves representing the variation of density with temperature for H_2O and D_2O are symmetrical and congruent within the limits of error involved and over the range of temperatures examined.

THE JOURNAL OF CHEMICAL PHYSICS VOLUME 21, NUMBER 5 MAY, 1953

Electronic Conduction in Silicon Carbide

J. T. KENDALL
Department of Electrical Engineering, Imperial College of Science and Technology, London, England
(Received November 4, 1952)

Pure silicon carbide was prepared by decomposition of the vapors of silicon tetrachloride and toluene on a hot carbon filament. Various *n*- and *p*-type impurity atoms were introduced by the addition of volatile metallic chlorides during the preparation. For the pure substance either *n*- or *p*-type crystals could be obtained by varying the ratio of the reaction constituents. The results show that semiconductivity in silicon carbide may be due either to nonstoichiometric proportions of silicon and carbon, or to the presence of impurity atoms, or (as probably occurs in the commercial product) to both circumstances simultaneously.

A theoretical model for electronic conduction in silicon carbide is proposed, which satisfactorily explains the magnitude of the low and high temperature activation energies observed, their different ratios in *n*- and *p*-type crystals, the occurrence of conduction at one of the disturbance energy levels, and the anomalous low Hall constant at low temperatures found in black but not in green silicon carbide. The model may be applicable to other semiconductors in which disturbance centers can give rise to electrons in unlocalized excited states.

1. INTRODUCTION

SILICON carbide is a solid in which the bonding is intermediate between homopolar and heteropolar. It is similar in its properties to the typically homopolar substance diamond and has a similar crystal structure, but with half the carbon atoms replaced by silicon. Because of the different electron affinities of carbon and silicon, this gives rise to a certain degree of heteropolarity in the crystalline bonds. According to Pauling[1] the SiC bond in silicon carbide is approximately 12 percent ionic in character. It will be shown in Sec. 7 how this may help to explain semiconductivity in silicon carbide.

[1] L. Pauling, *Nature of the Chemical Bond* (Cornell University Press, Ithaca, 1940), pp. 58–75.

It is noteworthy that electronic conduction in silicon carbide may be of *n*- or *p*-type. In the commercial material crystals which are colored green are *n*-type conductors, and blue or black crystals are *p*-type. The commercial material is made in the same way as the original synthesis of Acheson in 1886 by heating together sand and coke in an electric furnace. Many impurities, chiefly aluminum and iron, are introduced in this way, and an investigation by Lundquist[2] has indicated that aluminum as impurity may give rise to black *p*-type crystals and that iron may give rise to green *n*-type crystals. The interpretation of Lundquist is not, however, clear cut, since all commercial crystals contain considerable quantities of both iron and alumi-

[2] D. Lundquist, Acta Chemica Scand. **2**, 177 (1948).

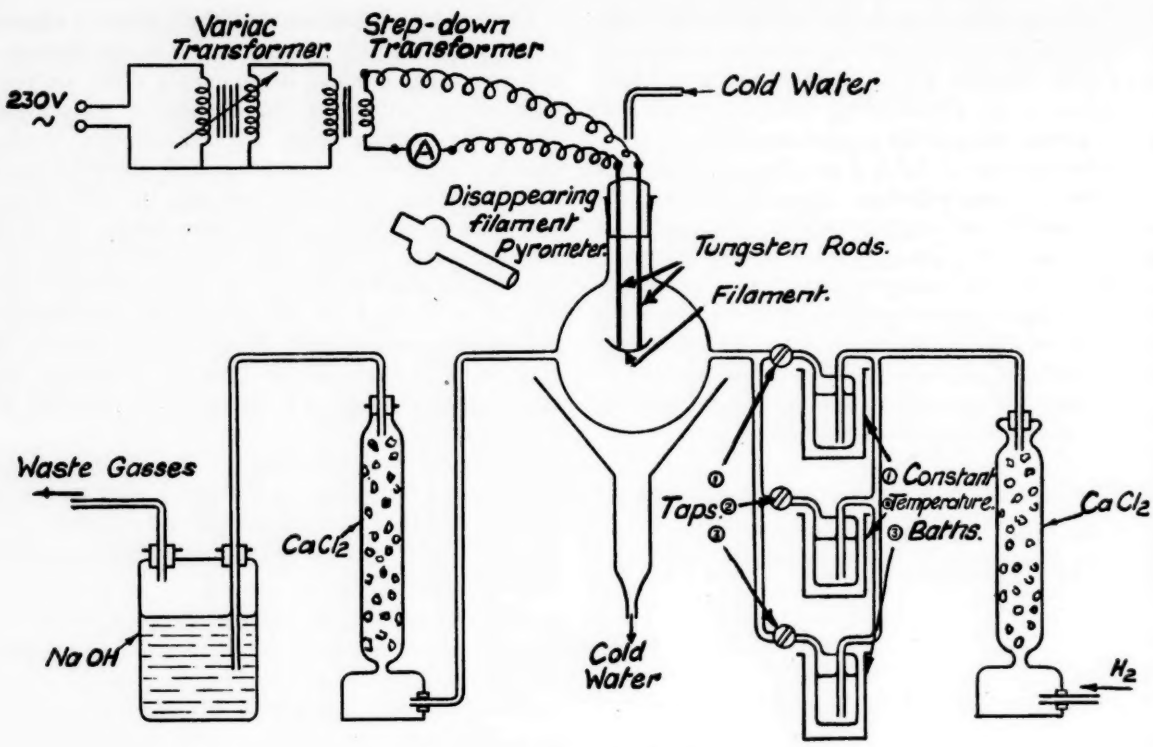

FIG. 1. Apparatus for preparing silicon carbide.

num as well as other elements. Moreover, the preparation of pure silicon carbide by Kendall and Yeo[3] showed that the presence of impurities is not essential for semiconductivity in silicon carbide.

The present research was, therefore, directed to the following points: (1) preparation of pure and impure specimens of silicon carbide, (2) determination of the type of semiconductivity produced by changes in the conditions of formation of the crystals and by the introduction of specific impurities, (3) spectrographic analysis of various specimens of commercial silicon carbide, with a view to determining the relevant impurities.

2. PREPARATION OF PURE SILICON CARBIDE

A method of preparing pure crystalline material has been described by Moers[4] and by Kendall and Yeo.[3] Briefly, a carbon filament 0.025 cm in diameter and about 1.5 cm long is heated in a stream of hydrogen containing the vapors of silicon tetrachloride and a hydrocarbon such as toluene. The proportions of the reaction constituents and the temperature of the filament can both be varied, and specific impurities can be introduced by means of volatile chlorides. A detailed description of the method has not been published, and, since considerable improvements have been made since the publication of the papers previously cited, a detailed description of the method as it is practiced at present will now be given.

The apparatus is illustrated in diagram form in Fig. 1. A stream of hydrogen (free from oxygen) is dried by passing over calcium chloride and then passes through three bubbling bottles arranged in parallel. In the first is put toluene, in the second, silicon tetrachloride, and in the third, concentrated sulfuric acid. The bottles are immersed in liquid baths maintained at constant temperature. The amounts of toluene and silicon chloride vapor picked up by the hydrogen stream can thus be separately varied by regulating the rate of bubbling through each bottle and the temperature of its contents. By the addition of volatile chlorides to a fourth bubbling bottle, specific impurities may be introduced. The hydrogen and vapors then pass through the reaction vessel, where a carbon filament is maintained at a temperature in the range 1500 to 2400°C. Decomposition of the vapors occurs on the filament with the deposition of crystalline silicon carbide and the formation of hydrogen chloride. The waste gas finally passes through a second calcium chloride column and then aqueous caustic soda to absorb the hydrogen chloride and excess silicon tetrachloride.

The current to the filament is supplied from the ac mains through a step-down transformer, with a 0-50 amp-ammeter in series with the secondary winding, controlled by a variable transformer. The temperature of the center of the filament is measured by a disappearing filament pyrometer. During the build-up of a

[3] J. T. Kendall, and D. Yeo, Proc. Intern. Congr. Pure Appl. Chem. **11**, 167 (1947).
[4] K. Moers, Z. anorg. u allgem. Chem. **198**, 243 (1931).

deposit on the filament the resistance of the filament decreases, and the variable transformer must be continually turned up (by hand) to maintain the filament at the desired temperature. After some experience it is not difficult to maintain the filament temperature constant to at least ±50°C.

Two tungsten rods are sealed into the stopper of the reaction vessel, and the carbon filament (supplied by Edison-Swan Electric Company, Ltd.) is secured at each end by means of Aquadag. It has been found best to build up a considerable thickness of Aquadag at the junctions with a series of thin layers, drying off each layer by passing a small current through the filament before applying the next. After some experience was obtained in making these junctions, it was found that an overheated filament invariably burnt out in the center and never at the junctions. It was found necessary to cool the outside of the reaction vessel with running cold water.

A typical preparation was carried out as follows: Bubbling bottle number 1 was half-filled with toluene, number 2 with silicon tetrachloride, number 3 with concentrated sulfuric acid. Bubbling bottles numbers 1 and 2 were immersed in water baths at 18°C. A carbon filament was secured to the tungsten leads and the whole apparatus flushed out with hydrogen. Taps 2 and 3 were then closed so that only hydrogen and toluene vapor passed through the reaction vessel at the rate of approximately 3 bubbles per second. The filament was then maintained at 1800°C until it had increased in diameter approximately three times (i.e., to a thickness of about 0.075 cm). This usually took about 3 minutes and required a final filament current of about 25 amp. This preliminary building up of the filament by deposition of carbon was found to be necessary to produce a robustness and decreased tendency to burn out at higher temperatures. Tap 3 was then opened and tap 1 closed so that only pure hydrogen passed through the reaction vessel. The filament temperature was then raised to (say) 2000°C and all the taps opened to (say) the following extents: through the toluene bottle—1 bubble per sec, through the silicon tetrachloride bottle—2 bubbles per sec, through the sulfuric acid bottle—2 bubbles per sec. The filament temperature was maintained constant for about 15 minutes (although it frequently burnt out at a weak spot before that time). By the end of the experiment the filament current was usually about 40 amp.

Crystalline silicon carbide was deposited on the filament, and a photograph of a typical deposit is shown in Fig. 2. The size of the crystals increases towards the center, since that part is considerably hotter than the ends. A number of variations in the experimental conditions were tried out, and the results of a large number of experimental runs are shown in summarized form below.

(a) Variation of Filament Temperature. (Bubbling Rates 1:2. C_7H_8: $SiCl_4$)

1500–1700°C	Black amorphous deposit, mostly C, but x-ray investigation indicated small amounts of SiC near the center of the filament.
1700–1900°C	Black crystalline deposit of SiC at center plus amorphous deposit of C+SiC (very small crystals).
1900–2100°C	Yellow crystalline SiC at center of filament (larger crystals), black crystalline SiC away from center (small crystals), amorphous C+SiC at ends.
2100–2200°C	Best temperature for formation of largest crystals of yellow SiC.
2200–2400°C	Filament usually burnt out quickly, otherwise large yellow crystals obtained.

(b) Variation of Bubbling Rates through Toluene and Silicon Tetrachloride

>5:1, C_7H_8:$SiCl_4$	C deposited at all temperatures.
4:1–2:1, C_7H_8:$SiCl_4$	C deposited below 2200°C; a little SiC (black) detected by x-ray investigation in deposits formed above 2200°C.
1.5:1–1:1, C_7H_8:$SiCl_4$	C deposited below 1900°C; a little black SiC detected by x-ray investigation in deposits formed from 1900–2100; black crystals formed at center of filaments above 2100°C.

FIG. 2. Photograph of part of a yellow deposit (magnification × 17) showing the variation in crystal size along the length. The size of crystal increases toward the center of the filament.

TABLE I. Spectrographic analysis of silicon carbide specimens.

No.	Specimen Type	Impurity elements[a] Al	Fe	Mg	Mn	Cu	Ag	Na	Ca	V	Zn	Ni	Totals Al+Fe	All elements
1	Norwegian, black	3	3	3	2	2	2	1	2	2	—	—	6	20
2	Swiss, black	4	4	3	2	2	1	1	2	3	—	—	8	22
3	Norwegian, blue-black	2	2	3	2	3	4	1	2	—	—	—	5	20
4	Norwegian, blue	5	5	4	4	4	2	2	3	1	—	—	10	30
5	Norwegian, green	2	3	3	1	5	1	2	1	1	—	1	5	20
6	Swiss, green	3	2	3	2	5	1	1	2	1	1	—	5	21
7	Swiss, pale green	2	2	3	3	1	1	1	3	—	—	—	4	16
8	Norwegian, pale green	3	3	3	2	3	3	1	2	—	—	—	6	20
9	Kendall, yellow	2	2	4	2	3	1	1	3	—	—	—	4	19

[a] 5 = Very heavy line. 4 = Heavy line. 3 = Medium line. 2 = Faint line. 1 = Very faint line. — = No line observed.

1:1.5–1:3, C_7H_8:$SiCl_4$ As described above under (a).

1:4–1:10, C_7H_8:$SiCl_4$ Black amorphous deposit of SiC deposited at 1500–1700°C; small yellow crystals deposited at 1800–2200°C; no deposition above 2200°C.

<1:10, C_7H_8:$SiCl_4$ Small yellow microcrystalline deposit at 1500–1800°C. No deposit above 1800°C.

(c) Variation of Bubbling Rate through Sulfuric Acid

This only affected the rate of deposition, not the nature of the deposit. A maximum rate of decomposition was found if about 2 bubbles per sec were passed through the sulfuric acid, although there was little variation up to 5 bubbles per sec after which the deposition rate fell off significantly.

It should be noted that the vapor pressures of toluene and silicon tetrachloride at 18°C are as follows:

C_7H_8 19.5 mm; $SiCl_4$ 175 mm.

The latter vapor is therefore in considerable excess in the reaction vessel for the best conditions of formation of silicon carbide.

In all cases, β-SiC (the cubic modification) was obtained. This is in agreement with the results of Taylor and Laidler,[5] who found that the hexagonal type was only produced at very high temperatures.

3. PREPARATION OF IMPURE SILICON CARBIDE

Volatile chlorides of the following elements were introduced during the preparation: Ge, Sn, B, Al, P, As, Sb, Bi, Cu, Fe. They were each placed separately in a fourth bubbling bottle in parallel with the other three, and the bottle immersed in a liquid bath at a temperature which would give a reasonable vapor pressure.

In all cases, the introduction of an impurity did not appear to affect the appearance of the final product, black and yellow crystals being formed as previously.

4. INVESTIGATION OF ELECTRICAL PROPERTIES OF SILICON CARBIDE PREPARATIONS

The crystals produced were all too small for any satisfactory measurements to be made of conductivity and Hall constant. It was, however, possible to make a qualitative determination of the sign of the thermoelectric coefficient at room temperature. This information determines whether the crystals are *n*- or *p*-type. A crystal was held between two phosphor-bronze electrodes, one of which was heated. The electrodes were connected externally through a sensitive dc galvanometer, and the direction of movement of the needle gave the sign of the thermoelectric coefficient.

It was found that all yellow crystals (whether pure or contaminated with *n*- or *p*-type impurities) were *n*-type semiconductors. Most black crystals were also *n*-type (although commercial black silicon carbide is *p*-type), but a few black crystals were found to be *p*-type. These were obtained only in those deposits formed when the ratio of the bubbling rates through toluene and silicon tetrachloride was equal to or greater than 1:1 and when the deposits were pure or contaminated with boron or aluminum. Crystals prepared in the same way, but contaminated by germanium, tin, phosphorus, arsenic, antimony, bismuth, copper, or iron, were found to be *n*-type, although identical in appearance. These *p*-type black crystals were formed at temperatures above 2100°C. The black crystals formed at lower temperatures and hence with a lower ratio of toluene: silicon tetrachloride, were all found to be *n*-type even when contaminated by boron or aluminium.

The conclusions from this would seem to be as follows:

(1) In the preparation of silicon carbide by reaction of silicon tetrachloride and toluene vapors on a hot carbon filament, silicon is normally present in great excess over carbon, and the resultant silicon carbide is *n*-type, even when pure, as a result of a stoichiometric excess of silicon. It does not appear possible to introduce sufficient boron or aluminum to neutralize this excess silicon.

(2) If the toluene:silicon tetrachloride ratio is increased, pure silicon carbide crystals can be deposited which are *p*-type, presumably because there is now a stoichiometric excess of carbon. In this case, however, the introduction of *n*-type impurities appears to reverse the effect of the excess carbon. (3) It thus appears that *n*- and *p*-type conductivity in silicon carbide can be caused by nonstoichiometric proportions of silicon and carbon and also by the introduction of impurities. (4) The temperature of formation of the silicon carbide

[5] A. Taylor and D. S. Laidler, Brit. J. Appl. Phys. 1, 174 (1950).

appears to have no influence on the type of conductivity.

5. PREPARATION OF EVAPORATED SILICON CARBIDE FILMS

It is of interest that films of silicon carbide can be prepared by evaporating at a high temperature in a vacuum. The carbon filament on which silicon carbide had been deposited was heated to 2500°C in a vacuum approximately 1 cm away from a silica plate. In most cases the filament burnt out quickly, but in a few cases it remained complete for a sufficient length of time for a thin evaporated layer of silicon carbide to be deposited on the silica plate. In all cases this layer was contaminated with carbon evaporated simultaneously. The films produced were yellow or black in color, depending on the degree of carbon contamination and on the color of the original silicon carbide. It was hoped to prepare evaporated films for measurement of conductivity and Hall constant, but it was not found possible to prepare films of sufficient thickness for this purpose. Since thick films could not be built up, the method was not further developed.

6. SPECTROGRAPHIC ANALYSIS OF COMMERCIAL SILICON CARBIDE CRYSTALS

Various specimens of commercial silicon carbide were analyzed spectrographically, using the sensitive "cathode layer" technique. A powdered specimen was placed in a small graphite cathode. The intensities of the lines observed on a photographic film were measured by a photoelectric densitometer and compared with each other. The experimental results are summarized in Table I.

It will be seen that all the crystals contain iron and aluminum in approximately constant ratios, and there does not appear to be any clear-cut correlation between color or conductivity type and nature of impurities.

7. THEORETICAL SPECULATION

(a) General Theoretical Model

We may describe the ionic-homopolar structure[1] of silicon carbide as some resonant combination of Si=C and $[Si]^{4+}\cdot[C]^{4-}$. The relevant atomic and ionic radii are C=0.77A, C^{4-}=2.60A, Si=1.18A, Si^{4+} =0.39A. We may therefore have, in the ionic form, missing Si^{4+} ions (cf. CuO) or interstitial Si^{4+} ions (compare with ZnO). The ionization energy of these "impurity" centers may be calculated from the usual relation $E_I=2\pi^2me^4/\epsilon^2h^2$, where m=mass of free electrons or hole, e=magnitude of electronic charge, ϵ=dielectric constant, h=Planck's constant. For silicon carbide ϵ may be taken as 7. Therefore $E_I=0.275$ ev.

This value for the ionization energy of an "impurity" center will be the same whether the "impurity" arises from the presence of foreign atoms (electron donators or acceptors), or from nonstoichiometric proportions of carbon and silicon, or from both causes.

At temperatures above absolute zero some of the "impurity" centers will be in excited states. At low concentrations of impurity the electronic levels of these excited states will be localized, and, since the number of electrons in them will be small, they may generally be neglected in considering the process of activation of free electrons. However, at high concentrations of impurity the excited-state levels will broaden out into bands, as shown by Erginsoy.[6] If this occurs we have the possibility of an electron conduction band, since the excited-state impurity electrons will no longer be localized. This can be shown actually to occur in silicon carbide as follows: The radii of the normal and excited orbits of the impurity electron can be calculated. In a medium of dielectric constant ϵ the normal radius of the carbon atom, 0.77×10^{-8} cm, will expand to $r=\epsilon\times q^2\times$Bohr radius (where q=principal quantum number of the orbit, i.e., 1 for the ground state and 2 for the first excited level). For successive values of q, and $\epsilon=7.0$, we thus have $r=5.4\times10^{-8}$, 22×10^{-8}, 49×10^{-8} cm, and these will have activation energies of E_I/q^2, i.e., 0.275, 0.07, 0.03 ev. These expanded orbits will allow electronic conduction to take place if the mean distance between disturbing centers is less than twice the orbital radius of the "impurity" electron, for the orbits around neighboring centers will then overlap as shown in Fig. 3.

Now, from the experimental results of Busch[7] all crystals of black silicon carbide have approximately the same number of *holes*, bound and free, approximately 10^{20} per cc, and the number of missing silicon atoms

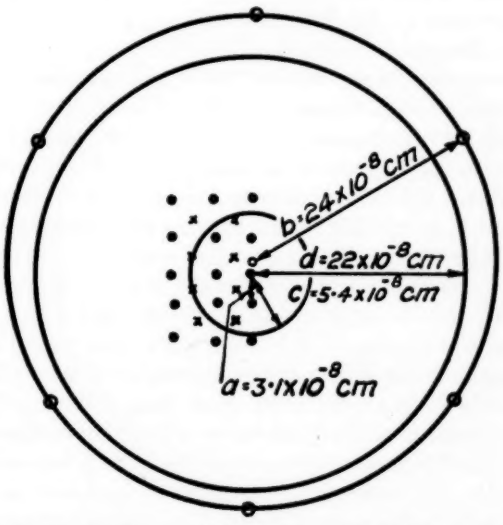

FIG. 3. Black silicon carbide showing radii of holes in ground and excited states. a=carbon-carbon distance=3.1×10^{-8} cm (shown ● and ×); b=missing silicon-missing silicon distance =24×10^{-8} cm (shown ○); c=radius of hole in ground state =5.4×10^{-8} cm; d=radius of hole in excited state =22×10^{-8} cm.

[6] C. Erginsoy, Phys. Rev. **80**, 1104 (1950).
[7] G. Busch, Helv. Phys. Acta **19**, 167 (1946).

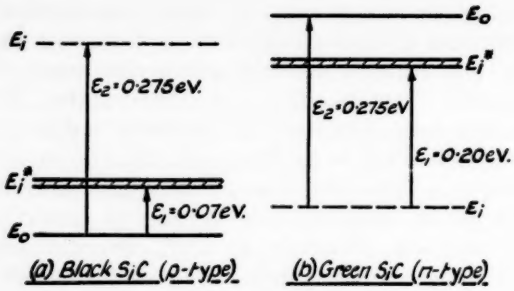

FIG. 4. Energy levels in SiC.

(or electron-acceptor impurities) must therefore be the same. Knowing the lattice parameters of silicon carbide, the mean distance between acceptor centers can therefore be calculated as about 24×10^{-8} cm. This situation is depicted in Fig. 3, and it can be seen that electrons excited to the level corresponding to $q=2$ will have overlapping orbits and therefore sufficient mobility to form a conduction band, while electrons corresponding to $q=1$ will be held in localized energy levels. A similar situation arises for p-type semiconduction in silicon and germanium, but in their cases the activation energies are much lower and, for $q>1$, become so small as to be indistinguishable at ordinary temperatures from the top of the full conduction band. In the case of silicon carbide there is an appreciable activation energy corresponding to $q=2$ (and even higher), so that at lower temperatures one may expect to find narrow conduction bands corresponding to $q=2, 3, \cdots$. We are therefore led to propose an energy level diagram for black silicon carbide as in Fig. 4(a), in which disturbing centers of one kind (missing silicon atoms or electron acceptors) give rise to more than one energy level, and the mobility of electrons in the E_i^* level will be dependent on the mean distance between disturbing centers.

For green silicon carbide (an n-type semiconductor) analogous calculations, assuming interstitial silicon atoms or electron-donator impurities, lead to an energy-level diagram as shown in Fig. 4(b). There is a significant difference in the two diagrams for black and green silicon carbide. In the former case electrons may be thermally excited from the normally full band, first to the excited level E_i^* with an activation energy of 0.07, and second to the localized level E_i with an activation energy of 0.275 ev. (We may neglect the transition from E_i^* to E_i as the number of electrons at the level E_0 is always very much greater than at E_i^*.) Measurement of conductivity as a function of temperature should therefore give these two activation energies ε_1 and ε_2 and, moreover, the ratio of $\varepsilon_1/\varepsilon_2$ should be 0.25. However, in the case of green silicon carbide, electrons must be excited initially from E_i to E_i^*, and subsequently from E_i to E_0. The activation energies observed should therefore be $\varepsilon_1=0.20$ ev and $\varepsilon_2=0.275$ ev, and the ratio of $\varepsilon_1/\varepsilon_2$ should be 0.75.

We are thus assuming that for p-type SiC the current carriers are holes in the normally full band and electrons in the impurity conduction band; while for n-type SiC they are electrons in both the normally empty band and in the impurity conduction band.

(b) Comparison with Experiment

The experimental results of Busch[7] for a number of different crystals of silicon carbide are given in Table II, and there is seen to be a qualitative correlation with the model given above. To examine the properties of the proposed model in more detail, we may consider the experimental results of Busch and Labhart[8] on black silicon carbide, as shown in Fig. 5. According to these results, the conductivity is given by

$$\sigma=A_1\exp[-\varepsilon_1/2KT]+A_2\exp[-\varepsilon_2/2KT]$$

over ranges I and II of Fig. 5, and a maximum conductivity over range III was explained by them as being the result of degeneration in the conduction band. The presence of two different activation energies was explained by them on the assumption of two kinds of disturbance centers having different energy levels, and it was found necessary, in order to explain the anomalous Hall constant at low temperatures, to assume that conduction could take place at one of these levels, although there seemed no particular reason why this should occur. The necessity of postulating two kinds of disturbing center has been avoided in the present model, which turns out to have properties similar to Busch and Labhart's, and moreover, provides a satisfactory explanation for the magnitude of the activation energies observed, for their different ratios in n- and p-type crystals and for the occurrence of conduction at one of the disturbance energy levels. Furthermore, the anomalous low Hall constant at low temperature found in black but not in green silicon carbide may also be accounted for, as will be shown below.

In the temperature range I of Fig. 5, conduction will be due to *holes* in the normally full band and to an equal number of *electrons* in the disturbance conduction band at E_i^*. The conductivity may be expressed as

$$\sigma=en_+b_++en_-b_-,$$

TABLE II. Experimental activation energies (Busch).

Black silicon carbide (8 different crystals)			Green silicon carbide (7 different crystals)		
ε_1	ε_2	$\varepsilon_1/\varepsilon_2$	ε_1	ε_2	$\varepsilon_1/\varepsilon_2$
0.044	0.270	0.16	0.120	0.215	0.56
0.038	0.281	0.14	0.185	0.246	0.75
0.044	0.272	0.16	0.133	0.285	0.47
0.042	0.282	0.15	0.191	0.265	0.72
0.051	0.248	0.21	0.147	0.263	0.56
0.050	0.231	0.22	0.057	0.157	0.36
0.050	0.231	0.22	0.097	0.198	0.49
0.052	0.226	0.23			
Theoretical activation energies (Kendall)					
0.07	0.275	0.25	0.20	0.275	0.75

[8] G. Busch and H. Labhart, Helv. Phys. Acta **19**, 463 (1946).

where e is the magnitude of the electronic charge, n_+ and n_- are the number of holes and electrons, and b_+ and b_- are their respective mobilities, i.e.,

$$\sigma = en(b_+ + b_-)$$

since in this temperature range $n_+ = n_-(=n)$. The situation will thus be very similar to that obtaining for intrinsic semiconductors, except that electrons in the disturbance conduction band would not be expected to have such a high mobility as would normal conduction electrons owing to the comparatively large mean distance between disturbance centers. For intrinsic semiconductors b_- is always greater than b_+, while in the present case the sign and magnitude of the Hall constant show that b_+ is greater than b_-. The Hall constant will be given by $R = 3\pi/8en(b_+ - b_-)/(b_+ + b_-)$. Thus its sign and magnitude will depend on the relative mobilities of holes and electrons, as well as on their number. Since Busch and Labhart obtained abnormally low values of the Hall constant at low temperatures, it seems that b_+ is nearly equal to b_-, and also, since there is no change in the sign of the Hall emf, the hole mobility must be slightly higher than the electron mobility. It can also be deduced that b_+ and b_- must vary with temperature, as otherwise the curve for $\log R$ against $1/T$ would show a small constant positive slope.

In the higher temperature range II, electrons will be excited from the normally full band to localized energy levels at E_i. Hole conduction will therefore become predominant, since n_+ will increase without a corresponding increase in n_-. Finally, when $n_+ \gg n_-$, the conductivity will be wholly p-type and will be given by the equation $\sigma = en_+b_+$, and the Hall constant by $R = 3\pi/8en_+$.

For green silicon carbide Busch and Labhart did not observe the anomalous low Hall constant in the low temperature range (see Figs. 4–7 of their paper, but note that Figs. 6 and 7 have been inadvertently transposed), and this is easily understood, since in the present model at both high and low temperatures, conduction in green silicon carbide is due to *electrons* exclusively, and we do not have the simultaneous hole and electron conduction in the low temperature range. Refinements to the theoretical model may make it possible to determine with more certainty the nature of the disturbance centers causing n- and p-type conduction in silicon carbide.

For other semiconductors the same model may be applicable, and its properties will be largely dependent on the dielectric constant of the crystal. For large values of dielectric constant (for example, germanium and silicon) the activation energies will be low, and the disturbance conduction bands will lie very close to the normally full (or empty) band of the crystal. For small values the activation energies will be high, and there will be additional localized energy levels as a result of the excited states, which do not develop into disturbance conduction bands. For intermediate values (e.g., silicon carbide) an additional energy level may occur which, as indicated above, will contain electrons which are localized or free according to the crystal parameters and the concentration of disturbance centers.

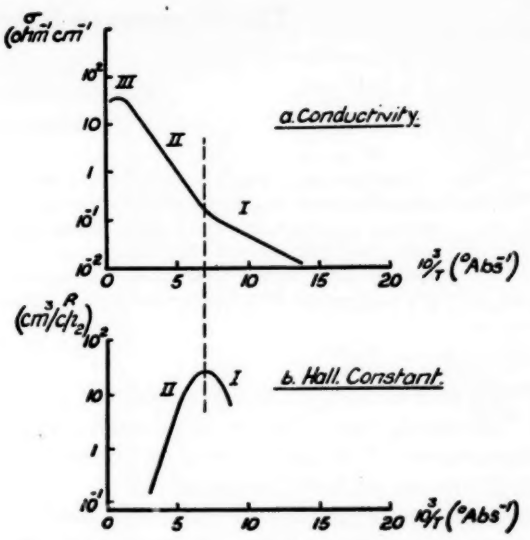

FIG. 5. Conductivity and Hall constant of black SiC. (Experimental results of Busch and Labhart.)

ACKNOWLEDGMENTS

The author wishes to acknowledge the award of a Leverhulme Research Fellowship (1949–1951) and to thank the Directors of Metropolitan-Vickers Electrical Company, Ltd., Manchester for granting him extended leave of absence. He also wishes to thank Professor Willis Jackson in whose department the work has been carried out and the D.S.I.R. for a grant for equipment. The spectrographic analyses were carried out in the Research Department of Metropolitan-Vickers Electrical Company Ltd. by Miss J. M. Rooke. Specimens of commercial silicon carbide were kindly supplied by the Gotthardwerke A. G., Bodio, Switzerland and the Arendal Smeltewerk, Eydehavn, Norway.

The Microwave Spectrum of Arsenic Trifluoride*

P. KISLIUK† AND S. GESCHWIND†
Columbia University, New York, New York

(Received December 29, 1952)

The microwave spectrum of AsF_3 is re-examined under high resolution permitting the evaluation of small interactions due to centrifugal distortion and $I\cdot J$ effects, as well as a more precise determination of the rotational constant and quadrupole interaction. The constants determined are: $B=5878.971\pm0.002$ Mc, $(eqQ)_{As}=-236.23\pm0.05$ Mc, $D_{JK}=-9.\pm2.$ kc, $a=-6.\pm7.$ kc, $b=6.\pm2.$ kc, $\alpha_2=-5.\pm1.$ Mc, and $\alpha_4=-0.16\pm0.04$ Mc. In addition, the bond angle is estimated from the quadrupole interaction by means of a comparison with $AsCl_3$, yielding $\angle F-As-F=102°\pm2°$.

THE microwave spectrum of arsenic trifluoride has previously been observed and its most important features noted.[1] However, a detailed account of this work has not as yet been published.

Among those pyramidal XY_3 molecules having pure rotational transitions in the microwave region, AsF_3 is especially convenient for the study of small interactions, such as the $I\cdot J$ interaction between the nuclear magnetic moment and the molecular magnetic field, for the following reasons:

(1) The combination of large dipole moment and the particular nuclear masses and internuclear distances gives a strong and easily interpreted transition ($J=1\rightarrow2$) in an easily available microwave region.

(2) The quadrupole interaction of the arsenic nucleus removes some of the degeneracy of the rotational levels (designated by the quantum numbers K and F), allowing detailed examination of the resolved components.

(3) Complications due to the interactions of the fluorine nuclei are expected to be small because the spin of 1/2 precludes quadrupole interactions. Accordingly, the high resolution microwave spectrometer developed at the Columbia Radiation Laboratory[2] was utilized for a more precise measurement of this spectrum.

TABLE I.

Transition K	F_i	F_f	Measured frequency (Mc)	Calculated frequency
0	5/2	5/2	23 461.905±0.010	23 461.901
1	3/2	5/2	23 471.334±0.010	23 471.332
1	3/2	3/2	23 492.423±0.010	23 492.425
1	5/2	5/2	23 500.834±0.010	23 500.833
0	1/2	1/2	23 515.865±0.010	23 515.860
0	{3/2 / 5/2}	{5/2 / 7/2}	23 520.965±0.010	23 520.972[a]
1	5/2	7/2	23 530.318±0.010	23 530.320
1	1/2	3/2	23 545.596±0.015	23 545.594
0	3/2	3/2	23 563.222±0.010	23 563.222

[a] Calculated assuming the two components to be completely unresolved.

The frequencies of the $J=1\rightarrow2$ transition of the ground vibrational state thus measured are given in Table I, together with calculated frequencies obtained by choosing certain interaction parameters to obtain the best possible fit with the measurements. These parameters are: (1) the rotational constant[3] $B=h/8\pi^2I=5878.971\pm0.002$ Mc, (2) the quadrupole coupling constant[4] $(eqQ)_{As}=-236.230\pm0.050$ Mc, (3) the centrifugal distortion constant[3] $D_{JK}=-0.009\pm0.002$ Mc, and (4) the $I\cdot J$ interaction constants[5] $a=-0.006\pm0.007$ Mc and $b=0.006\pm0.002$ Mc, where the shift of the energy level resulting from the $I\cdot J$ interaction is given by

$$W_{IJ}=h\left[a\frac{K^2}{J(J+1)}+b\right][F(F+1)-J(J+1)-I(I+1)].$$

The limits of error quoted for the measured frequencies are those obtained from the internal consistency of several measurements, while those quoted for the various interaction constants are those which would alter at least one of the calculated frequencies by the experimental limit of error. Somewhat greater deviations could be tolerated within this limit by varying several parameters simultaneously, so that the quoted limits are better interpreted as probable than as maximum errors.

Second-order quadrupole effects[6] are taken into account and amount to 160 kc in the largest case among the lines of Table I. The largest shift resulting from $I\cdot J$ interaction is 24 kc, arising entirely from the constant b. The largest shift due to the constant a is 10 kc.

The value of -9 kc for D_{JK} in AsF_3 may be compared with -11.7 kc for PF_3 and -25.7 for NF_3.[7] It is to be expected that, as is the case for these molecules, D_{JK} will tend to be smaller for heavier molecules, since the dimensional dependence is as $(\text{mass})^{-2}$, but the precise expression depends on internuclear distances and force constants in a complicated manner.

* Work supported jointly by the U. S. Signal Corps and the U. S. Office of Naval Research.

† Present address: Bell Telephone Laboratories, Inc., Murray Hill, N. J.

[1] Dailey, Rusinow, Shulman, and Townes, Phys. Rev. **74**, 1245 (1948).

[2] S. Geschwind, thesis, Columbia University (1951).

[3] G. Herzberg, *Infra Red and Raman Spectra* (D. Van Nostrand Company, Inc., New York, 1945), p. 400.

[4] J. Bardeen and C. H. Townes, Phys. Rev. **73**, 97 (1948).

[5] R. S. Henderson, Phys. Rev. **74**, 107 (1948).

[6] J. Bardeen and C. H. Townes, Phys. Rev. **73**, 627 (1948).

[7] Johnson, Trambarulo, and Gordy, Phys. Rev. **84**, 1178 (1951).

The part of the $I \cdot J$ interaction which is independent of K, i.e., that depending on the constant b, is analogous to $I \cdot J$ interaction in diatomic case treated by Foley.[8] On the basis of this model, b and its equivalent in the diatomic case should be positive if the nuclear g factor is positive. This is the case in the few examples for which the sign has been determined.[9–14] The results for AsF_3 may perhaps be compared to those for ammonia, where it is found that $a=0.4$ kc and $b=6.1$ kc.[14] Thus b is nearly the same in the two cases, although the ratio of a to b appears to differ considerably. It should be remembered that a is only roughly determined for AsF_3 in this experiment.

At low pressures (near 10^{-4}-mm Hg) and low power levels it was possible to reduce the half-width of the lines at half-maximum to 40 ± 5 kc at dry ice temperature. It is not certain, however, that this is the minimum possible width, as the gas adheres quite strongly to the metal walls of the wave-guide absorption cell, and there may not have been time enough during a run to lower the pressure sufficiently to eliminate collision broadening. The half-width of the line due to Doppler effect at this temperature is 10 kc, and wall collisions would account for an additional 6 or 7 kc in wave guide of the dimensions used. Thus, additional apparent broadening effects may well be present, a possibility being interactions involving the fluorine nuclei which might split the line into several unresolved components.

With the aid of a conventional Stark modulation type microwave spectrometer,[15] several of the hitherto unobserved weak lines were seen, including some due to higher vibrational states. Several of these are attributed to the vibrational state $v_2=1$,[16] yielding the vibration-rotation interaction constant $a_2=-5$. Mc. In addition, with the high resolution instrument, lines about 0.7 Mc higher in frequency than each of the three strongest lines, and about one tenth as intense, were observed. These are attributed to the vibrational state $v_4=1$, giving $a_4=-0.16$ Mc. All absorption frequencies thus far observed are given in Table II, together with tentative assignments of the vibrational states and calculated intensities. The intensities were computed on the assumption that the half-width is 25 Mc at a pressure of 1 mm Hg and that the observation is made at room temperature.

These measurements do not alter the earlier result that the distance AsF is 1.712 ± 0.005A[1], nor the later conclusion of Townes and Dailey[17] that AsF_3 is predominantly of the structure

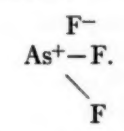

The bond angle is not determinable directly from the microwave data as there is but one naturally occurring isotopic species for each of the nuclei. However, the angle can be estimated indirectly, using the fact that for arsenic trichloride both the quadrupole coupling and bond angle can be measured by microwave methods.[18,19] Comparison of the quadrupole coupling of the arsenic nuclei for the two molecules permits a quantitative comparison between the amount of $s-p$ hybridization in the As—F bond and that in the As—Cl bond.[17] This may be used directly to calculate the bond angle, using the criterion of Hultgren.[20] The result is $\angle F-As-F=102°$ with an estimated limit of error of about 2°.

In conclusion, the authors would like to thank Professor C. H. Townes for his interest and encouragement.

TABLE II. Observed lines in the $J=1\rightarrow2$ transition of AsF_3.

Vibrational state	K	F_i	F_f	Frequency (Mc)	Intensity (cm^{-1})
ground	0	1/2	3/2	23 457	1.9×10^{-7}
		5/2	5/2	23 461.90	2.1×10^{-7}
		1/2	1/2	23 515.86	1.9×10^{-7}
		3/2	5/2	23 520.97	1.4×10^{-6}
		5/2	7/2		
		3/2	3/2	23 563.22	2.5×10^{-7}
		3/2	1/2	23 622.2	3.9×10^{-8}
	1	3/2	5/2	23 471.33	3.7×10^{-7}
		3/2	3/2	23 492.42	1.9×10^{-7}
		5/2	5/2	23 500.83	1.6×10^{-7}
		5/2	7/2	23 530.32	7.0×10^{-7}
		1/2	3/2	23 545.60	1.5×10^{-7}
		1/2	1/2	23 575	1.5×10^{-7}
$v_2=1$	0	5/2	5/2	23 482	4×10^{-8}
		5/2	7/2	23 543	3×10^{-7}
		3/2	5/2		
		3/2	3/2	23 584	5×10^{-8}
	1	3/2	3/2	23 513	4×10^{-8}
		5/2	7/2	23 553	1.4×10^{-7}
		1/2	1/2	23 595	3×10^{-8}
$v_4=1$	0	3/2	5/2	23 521	4×10^{-7}
		5/2	7/2		
	1	5/2	7/2	23 531	2×10^{-7}
?	1			23 509	5×10^{-8}

[8] H. M. Foley, Phys. Rev. **72**, 504 (1947).
[9] See reference 5 and erratum, Phys. Rev. **74**, 626 (1948).
[10] Gilbert, Roberts, and Griswold, Phys. Rev. **76**, 1723 (1949).
[11] J. Trischka, Phys. Rev. **74**, 718 (1948).
[12] Carlson, Lee, and Fabricand, Phys. Rev. **85**, 784 (1952).
[13] J. C. Swartz and J. W. Trischka, Bull. Am. Phys. Soc. **27**, 1, 31 (1952).
[14] R. G. Gunther-Mohr, thesis, Columbia University (1953).
[15] McAfee, Hughes, and Wilson, Rev. Sci. Instr. **20**, 821 (1949).
[16] The notation is that of reference 3.
[17] C. H. Townes and B. P. Dailey, J. Chem. Phys. **17**, 782 (1949).
[18] P. Kisliuk and C. H. Townes, J. Chem. Phys. **18**, 1109 (1950).
[19] P. Kisliuk and C. H. Townes, Phys. Rev. **83**, 210 (1951).
[20] R. Hultgren, Phys. Rev. **40**, 891 (1932).

Rotation-Vibration Spectra of Diatomic and Simple Polyatomic Molecules with Long Absorbing Paths. X. The Spectrum of Tri-Deuteromethane in the Photographic Infrared

L. F. H. Bovey*
Division of Physics, National Research Council of Canada, Ottawa, Canada
(Received December 8, 1952)

The absorption spectrum of CD_3H has been investigated under high resolution in the photographic infrared with absorbing paths of up to 7 m atmos obtained by multiple reflection. Two simple parallel bands were observed at 8870A and 11590A. The K structure in the former was clearly resolved. The rotational structure of the two bands was analyzed yielding

$$B_0 = 3.278_7 \pm 0.001_0 \text{ cm}^{-1}.$$

On the assumption of tetrahedral symmetry for the CD_3H molecule this value leads to a C−H distance

$$r_0 = (1.0919_3 \pm 0.0001_7) \times 10^{-8} \text{ cm}.$$

This value is compared with the corresponding values obtained by other authors from studies of CH_4 and CH_3D.

I. INTRODUCTION

THE spectrum of methane has been obtained with high resolution instruments by several workers. Nielsen and Nielsen[1] and Boyd, Thompson, and Williams[2] have observed the fundamentals in the infrared; Nelson, Plyler, and Benedict;[3] McMath, Mohler, and Goldberg;[4] Vedder and Mecke;[5] and Childs[6] have observed overtone and combination bands in the near infrared and photographic infrared regions; and Dickinson, Dillon, and Rassetti;[7] and Stoicheff, Cumming, St. John, and Welsh[8] have studied the Raman spectrum. The determination of the molecular constants, and particularly of the internuclear distances from the CH_4 spectra, encounters difficulties on account of the effect of Coriolis forces. Even though these difficulties seem to have been overcome in the recent work of Stoicheff *et al.*,[8] it seems still worth while to obtain an independent check by a study of appropriate deuterium-substituted methanes. In mono- and tri-deuteromethane the symmetry is reduced from T_d to C_{3v}; that is, these isotopic molecules are symmetric rather than spherical tops; and consequently, many of the degeneracies which cause difficulties in CH_4 are removed. In particular, parallel bands of C_{3v} molecules, unlike perpendicular bands, are not influenced by first-order Coriolis effects, and they should therefore yield reliable values for the rotational constants.

Ginsburg and Barker[9] and, quite recently, Boyd and Thompson[10] have studied the fundamentals of CH_3D, and Childs and Jahn[11] have measured an overtone band in the photographic region. The present paper describes an investigation of the photographic infrared spectrum of CD_3H. Two simple absorption bands at 8870A and 11590A have been found, and their measurement has yielded precise values of the rotational constants of CD_3H and of the C−H distance in methane.

II. EXPERIMENTAL

After an unsuccessful attempt to obtain CD_3H by the reaction of heavy water with aluminum carbide (Al_4C_3), two liters of the gas at 20-cm pressure were obtained by the Grignard synthesis:

$$CD_3MgBr + H_2O = CD_3H + MgBrOH.$$

The Grignard compound was prepared from small quantities of CD_3Br and CD_3I (of approximate composition $CD_{2.7}H_{0.3}X$), which were kindly supplied by Dr. Nolan and Dr. Leitch of the Chemistry Division. The technique used was similar to that described by Childs and Jahn[11] who used CH_3I for the preparation of CH_3D. Mass spectroscopic analysis of the sample showed it to contain about 70 percent CD_3H, the remainder being mainly CD_2H_2. Neither CH_4 nor CD_4 was present in detectable amounts.

The gas was briefly studied in the wavelength region 2μ–14μ by means of a Perkin-Elmer spectrometer. Much of the spectrum of CD_3H above 5μ is masked by the much stronger absorption of CD_2H_2, but the fundamental ν_1 of the C−H stretching vibration is clearly present as a strong parallel band at 2992 cm^{-1}. This observation confirms the suggestion of Herzberg[12]

* National Research Laboratories Postdoctorate Fellow. Contribution No. 2995 from the National Research Council, Ottawa, Canada. Present address: Emission Spectroscopy Group, Atomic Energy Research Establishment, Harwell, England.

[1] A. H. Nielsen and H. H. Nielsen, Phys. Rev. **48**, 864 (1935).
[2] Boyd, Thompson, Williams, Proc. Roy. Soc. (London) **A213**, 42 (1952).
[3] Nelson, Plyler, and Benedict, J. Research Natl. Bur. Standards **41**, 615 (1948).
[4] McMath, Mohler, and Goldberg, Astrophys. J. **109**, 17 (1949).
[5] H. Vedder and R. Mecke, Z. Physik **86**, 137 (1933).
[6] W. H. J. Childs, Proc. Roy. Soc. (London) **A153**, 555 (1936).
[7] Dickinson, Dillon, and Rasetti, Phys. Rev. **34**, 582 (1929).
[8] Stoicheff, Cumming, St. John, and Welsh, J. Chem. Phys. **20**, 498 (1952).
[9] N. Ginsburg and E. F. Barker, J. Chem. Phys. **3**, 668 (1935).
[10] D. R. Boyd and H. W. Thompson, Proc. Roy. Soc. (London) **A216**, 143 (1953).
[11] W. H. J. Childs and H. A. Jahn, Proc. Roy. Soc. (London) **A169**, 428 (1939).
[12] G. Herzberg, *Molecular Spectra and Molecular Structure II. Infrared and Raman Spectra of Polyatomic Molecules* (D. Van Nostrand Company, Inc., New York, 1945).

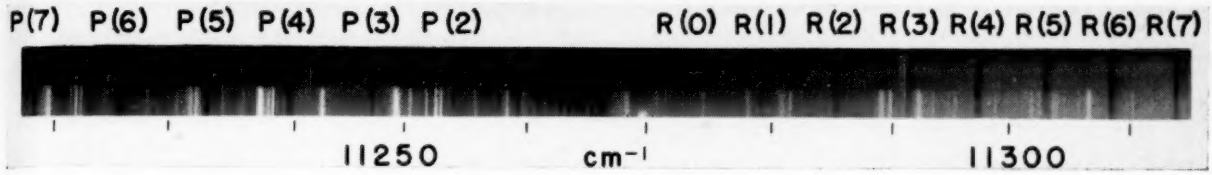

FIG. 1. Central part of the 8870A band of CD_3H photographed in the second order of a 21-ft grating. The iron arc spectrum is visible in the lower half of the photograph.

that a band first found by Nielsen and Nielsen[13] at the same wave number in CD_4 is really due to CD_3H.

The absorption tube for the study in the photographic infrared was in all respects similar to those described in earlier papers of this series[14] except that it was smaller in size (100 cm long, 3 cm in diameter) in order to reduce the amount of gas required. Up to 28 traversals through this tube were obtained at a pressure of about 20 cm, so that the equivalent absorbing path was about 7 m atmos.

Two bands were found, one at 8870A and the other at 11590A. The former was photographed in the second order of the 21-ft grating spectrograph of this laboratory on *IV–N* plates; the latter was photographed only in the first order on *I–Z* plates.

Both bands showed a *P*, *Q*, and *R* structure. A portion of the 8870A band is shown in Fig. 1. For the higher *J* values the "lines" of the *P* and *R* branches are resolved into a number of components. This is shown more clearly in Fig. 2 in which a part of the *R* branch is reproduced under higher magnification. For the second band at 11590A no clear resolution of the "lines" of the branches into components was obtained, but a shading of each line to shorter wavelengths was noted. The 8870A band was measured on two different plates; the 11590A band, on one plate. Except for a slight systematic difference (about $+0.03$ cm^{-1}), presumably caused by a shift of the iron arc comparison spectrum, the two sets of measurements of the 8870A band agreed in a most satisfactory manner.

III. ANALYSIS OF THE BANDS

The simple *P*, *Q*, *R* structure of the two photographic infrared bands at 8623.3 cm^{-1} (11590A) and 11266.9 cm^{-1} (8870A) shows clearly that they are parallel bands. Indeed they fit well as the second and third overtone, respectively, of the C—H stretching vibration whose fundamental ν_1 is at 2992 cm^{-1}. This assignment gives a reasonable anharmonicity: one finds that the three bands can be represented by

$$\nu = 3047.2v_1 - 57.6v_1^2.$$

As is well known[12] the parallel bands of symmetric top molecules consist of a series of sub-bands, one for each value of *K*, which almost coincide. Until a short time ago the *K* fine structure had been resolved only for the 950 cm^{-1} NH_3 band,[15] but very recently Boyd and Thompson[10] have resolved the *K* fine structure of a band of CH_3D. The observed fine structure of the 8870A CD_3H band is clearly such a *K* structure. In the 11590A band this structure is not resolved, partly because of the lower resolution possible in this spectral region.

In Tables I and II the observed wave numbers of all the measured lines of the two bands and their assignments are given. The *J* numbering of the lines was immediately obtained from the position of the lines relative to the central *Q* branch. The *K* numbering is less obvious but could readily be obtained when certain theoretical relationships were taken into account as outlined below.

The rotational energy levels of a symmetric top molecule in a given vibrational level are given by

$$F(J,K) = BJ(J+1) + (A-B)K^2 - D_J J^2(J+1)^2 - D_{JK}J(J+1)K^2 - D_K K^4, \quad (1)$$

where *A*, *B*, and *D* have their usual meanings.[12] For a parallel band $\Delta K = 0$, and therefore one has for the *P*

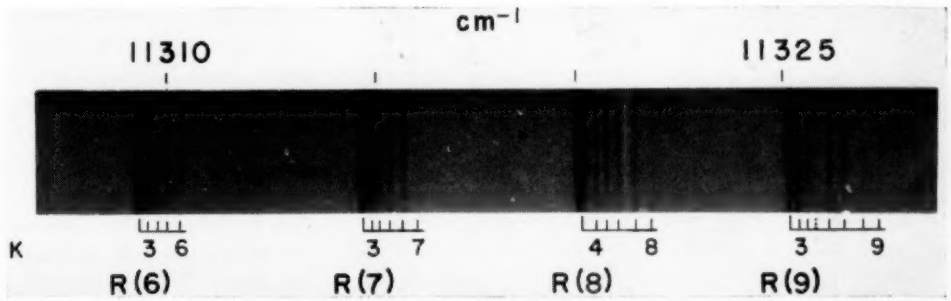

FIG. 2. Part of the *R* branch of the 8870A band under high magnification, showing the *K* fine structure.

[13] A. H. Nielsen and H. H. Nielsen, Phys. Rev. **54**, 118 (1938).
[14] H. J. Bernstein and G. Herzberg, J. Chem. Phys. **16**, 30 (1948).
[15] Sheng, Barker, and Dennison, Phys. Rev. **60**, 786 (1941).

TABLE I. Observed and calculated wave numbers (ν_{vac}) of the lines in the 8900A band.

		$P(J, K)$		$R(J, K)$	
J	K	Obs	Calc	Obs	Calc
0	0			11273.36	11273.37
1	0, 1			279.67	279.68
2	0, 1	11253.71	11253.71	285.88	285.85
3	0, 1, 2	246.93	246.94	292.00	291.92
4	0, 1, 2	239.98	240.00	297.84	297.82
	3	240.19	240.21	298.05	298.04
	4			298.26	298.24
5	0, 1, 2	233.04	232.94	303.56	303.59
	3	233.33	233.15	303.81	303.81
	4			304.03	304.01
6	0, 1, 2	225.77	225.75	309.19	309.22
	3	225.97	225.96	309.43	309.43
	4	226.18	226.16	309.63	309.64
	5	226.43	226.42	309.90	309.90
	6			310.24	310.23
7	0, 1, 2	218.41	218.45	314.69	314.71
	3	218.66	218.65	314.92	314.92
	4	218.86	218.85	315.12	315.13
	5	—	—	315.39	315.39
	6	219.40	219.42	315.70	315.71
8	0, 1, 2	210.99	211.01	320.09	320.05
	3	211.22	211.22	—	—
	4	211.41	211.42	320.48	320.47
	5	211.66	211.67	320.75	320.74
	6	212.00	211.98	321.04	321.06
	7	212.30	212.35	321.43	321.44
	8			321.82	321.88
9	0, 1, 2	203.44	203.46	325.25	325.26
	3	203.68	203.66	325.47	325.47
	4	203.87	203.86	325.70	325.67
	5	204.10	204.11	—	—
	6	204.42	204.42	326.24	326.26
	7			326.62	326.64
	8			327.06	327.08
10	0, 1, 2	11195.81	11195.78	11330.38	11330.31
	3	—	—	—	—
	4	196.19	196.18	330.70	330.73
	5	196.43	196.43	331.02	330.99
	6	196.75	196.74	331.30	331.31
	7	197.10	197.10	331.70	331.69
	8	197.54	197.52	332.16	332.13
	9	197.97	198.00	332.65	332.63
	10			333.16	333.18
11	0, 1, 2	188.00	187.98	335.31	335.21
	3	188.21	188.18	—	—
	4	—	—	—	—
	5	—	—	—	—
	6	188.94	188.93	—	—
	7	189.27	189.29	336.60	336.59
	8	189.72	189.71	337.07	337.03
	9			337.56	337.53
	10			338.14	338.08
12	0, 1, 2	180.11	180.05	340.14	339.97
	3	—	—	—	—
	4	180.45	180.45	—	—
	5	180.72	180.69	340.66	340.64
	6	180.98	181.00	341.07	340.96
	7	181.36	181.36	—	—
	8	—	—	—	—
	9	182.31	182.24	342.38	342.27
13	0, 1, 2	172.11	172.00	—	—

and R branches

$$P(J,K)=[\nu_0-(B'+B'')J+(B'-B''-D_J'+D_J'')J^2 +2(D_J'+D_J'')J^3-(D_J'-D_J'')J^4] +[(A'-A'')-(B'-B'')-D_{JK}'J(J-1) +D_{JK}''J(J+1)]K^2-(D_K'-D_K'')K^4 \quad (2)$$

$$R(J,K)=[\nu_0+2B'-4D_J'+(3B'-B''-12D_J')J +(B'-B''-13D_J'+D_J'')J^2 -(6D_J'-2D_J'')J^3-(D_J'-D_J'')J^4] +[(A'-A'')-(B'-B'') -D_{JK}'(J+1)(J+2) +D_{JK}''J(J+1)]K^2-(D_K'-D_K'')K^4. \quad (3)$$

Here the first term gives essentially the positions of the unresolved P and R lines; the second term gives the splitting; the third term is presumably quite small. Therefore, when the wave numbers of the components of a "line" are plotted against K^2, a very nearly straight line should be obtained if the correct numbering is chosen. Only for one numbering was this the case. For this numbering one must assume that the components corresponding to $K=0$, 1, 2 are unresolved. This assumption is confirmed by the fact that for the R "lines" with $J=0$, 1, 2, and for the P "lines" with $J=0$, 1, 2, 3 which have only components with $K\leq 2$, no fine structure is observed.

TABLE II. Observed wave numbers (ν_{vac}) of the lines in the 11590A band.

J	$P(J)$	$R(J)$
0	—	—
1	—	8636.10
2	8610.11	42.37
3	03.36	48.53
4	8596.48	54.60
5	89.61	60.54
6	82.53	66.43
7	75.41	72.03
8	68.21	77.64
9	60.84	83.20
10	53.43	88.60
11	45.91	93.81
12		99.03
13		8703.14
14		08.96
15		13.62

A further confirmation of the K numbering is obtained from the intensity alternation in each group of given J. As is well known,[12] for a C_{3v} molecule the levels with K a multiple of 3 have a higher statistical weight than the other levels. If the nuclear spin of the three identical atoms is 1, as in the present case, the ratio of statistical weights and therefore the intensity ratio of the corresponding lines is 11:8. While no quantitative investigation was made, the microphotometer tracing of the P branch in Fig. 3 shows that the lines with $K=3$, 6, 9, $\cdots$ are, in general, stronger than the neighboring lines.

For the 8870A band it was possible to obtain the

rotational constants of the ground state from combination differences $\Delta_2F''(J, K)=R(J-1, K)-P(J+1, K)$ formed for each K value. From Eq. (1) we have

$$\Delta_2F(J, K)=F(J+1, K)-F(J-1, K)$$
$$=(4B-6D_J-4D_{JK}K^2)(J+\tfrac{1}{2})-8D_J(J+\tfrac{1}{2})^3. \quad (4)$$

In Fig. 4 $\Delta_2F''(J, K)/(J+\frac{1}{2})$ is plotted as a function of $(J+\frac{1}{2})^2$. It is seen that the points for higher K values deviate increasingly from the straight line formed by the points for $K=0$, 1, 2. The slope of the latter line gives $D_J''=0.000046$ cm^{-1}. If the $\Delta_2F''(J, K)/(J+\frac{1}{2})$ values for a given J are plotted against K^2, a straight line is obtained (with considerable scatter) whose slope, according to Eq. (4), gives $-4D_{JK}''$. In this way $D_{JK}''=-0.00003_5$ cm^{-1} was obtained. Based on this D_{JK}'' value, the parallel lines on which the points for higher K values in Fig. 4 should lie, according to Eq. (4), are indicated (broken lines). The deviations of the individual points from these lines are appreciable. Nevertheless, the general agreement with Eq. (4) is apparent. The intercept of the line for $K=0$, 1, 2, corrected to $K=0$, gives $B''=3.278_7\pm0.001_0$ cm^{-1}.

When $\Delta_2F'(J, K)/(J+\frac{1}{2})$ is plotted against $(J+\frac{1}{2})^2$, a somewhat larger scatter is found than for $\Delta_2F''(J, K)/(J+\frac{1}{2})$.

Another way of determining the rotational constants of the upper state is by means of the combination sums $R(J-1, K)+P(J, K)$. One finds from Eq. (1)

$$R(J-1, K)+P(J, K)$$
$$=2\nu_0+2[(A'-B')-(A''-B'')]K^2$$
$$-2(D_K'-D_K'')K^4+2[(B'-B'')$$
$$-(D_{JK}'-D_{JK}'')K^2]J^2-2(D_J'-D_J'')J^2(J^2+1) \quad (5)$$

In Fig. 5, $R(J-1, K)+P(J, K)$ is plotted against J^2 for the different K values. The scatter of the points is again rather larger than would have been expected from the accuracy of the measurements and points to perturbations in the upper state of the band. Nevertheless, a slight difference in slope for different K values is noticeable which is clearly due to the term $2(D_{JK}'-D_{JK}'')K^2$ in the coefficient of J^2 in Eq. (5). In this way an approximate value for D_{JK}' has been obtained. Taking this into account a precise value for $B'-B''$, and therefore B', is obtained from the slopes of the lines in Fig. 5.

The rotational constant A cannot be determined from a parallel band. But $A'-A''$ can be determined either from the slope of the plot of $P(J, K)$ or $R(J, K)$ against K^2 for a fixed J according to Eqs. (2) and (3), or from the slope of a plot of the intercepts in Fig. 5 against K^2 according to Eq. (5). The latter plot also leads to a precise value for ν_0. The molecular constants obtained in this way are collected in Table III.

As mentioned above, the K structure of the 11590A band is not resolved. This is partly due to the fact that the quantity $(A'-B')-(A''-B'')$, which, according to Eqs. (2) and (3), determines the K splitting, is

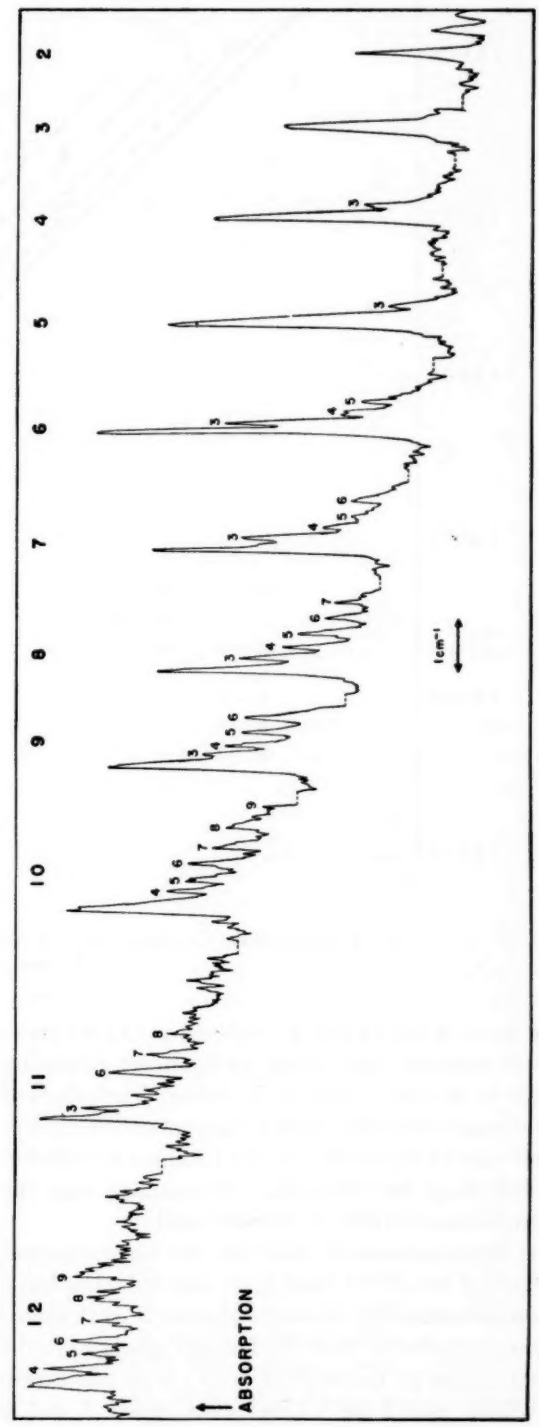

FIG. 3. Microphotometer record of the P branch. In order to decrease the horizontal dimension, the portion of the record between the lines has been cut out. The J numering is shown along the top and the K numbers are given near the associated peaks.

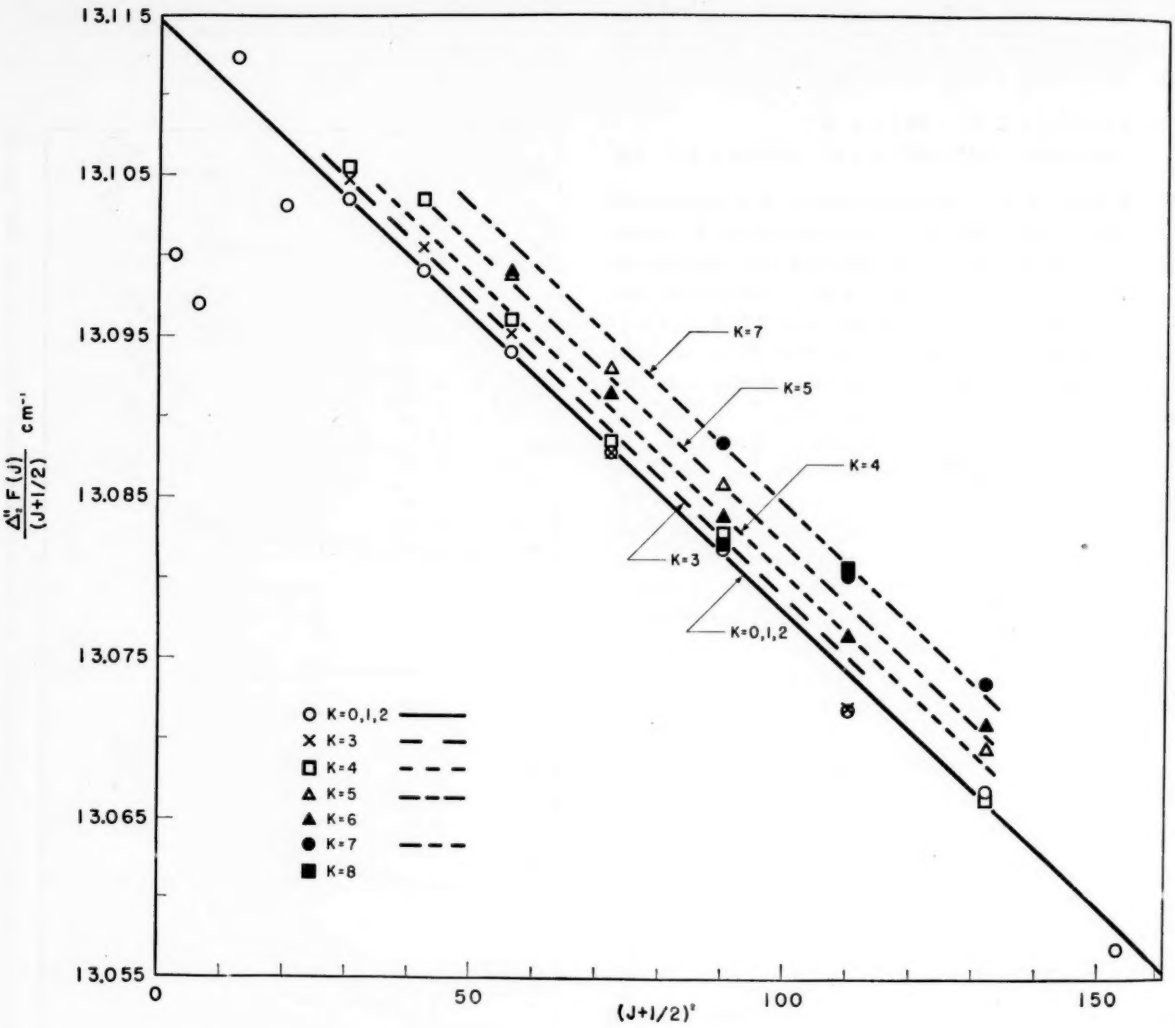

FIG. 4. Combination differences $\Delta_2 F''(J, K)/(J+\frac{1}{2})$ for the ground state of CD_3H obtained from the data of the 8870A band.

smaller than for the 8870A band since the 11590A band is a lower overtone, and partly to the lower resolution available in the long wavelength region. The values of the rotational constants (except D_{JK}) were obtained in the same way as for the 8870A band and are included in Table III. They are somewhat less accurate than the constants obtained from the 8870A band.

Using the constants of Table III the wave numbers of the lines of the 8870A band have been calculated as a check on the reliability of the constants. The calculated values are included in Table I. The agreement with the observed values up to $J=10$, $K=7$ is, with two exceptions, within ± 0.02 cm^{-1}. Lines with higher J and K values are weak and, therefore, less accurately measured. The two exceptions at low J are the lines $P(5)$ and $R(3)$ which are shifted by about 0.12 cm^{-1} to higher wave numbers indicating a perturbation of the $J'=4$ levels by this amount. The intensities of the lines also show a few perturbations which occur in pairs in lines of the type $P(J+1, K)$ and $R(J-1, K)$, that is, these intensity perturbations are also due to a perturbation of the upper state.

The occurrence of perturbations in the upper state emphasizes the importance of determining ground state rotational constants by the method of combination differences rather than by trying to represent all the lines in a band by a power series and subsequent derivation of the rotational constants from the coefficients of the power series.

IV. THE C–H DISTANCE IN METHANE

From the rotational constant in the ground state of CD_3H

$$B_0 = 3.278_7 \pm 0.001_0 \text{ cm}^{-1},$$

one obtains for the moment of inertia about an axis

perpendicular to the symmetry axis

$$I_B{}^0=\frac{27.98_{30}\times10^{-40}}{B_0}=8.534_7\times10^{-40}\text{ g cm}^2.$$

This moment of inertia is related to the internuclear distance r_0(C−H) by

$$I_B{}^0=\frac{4m_D(3m_D+5m_H)+m_C(5m_D+3m_H)}{3(m_H+3m_D+m_C)}r_0{}^2,$$

where m_H, m_D, m_C are the masses of the H, D, C atoms, respectively. Here the assumption has been made that the C−H and C−D distances are exactly the same. Actually this assumption can be expected to hold rigorously only for the equilibrium distances r_e(C−H) and r_e(C−D). The zero-point vibration will cause a slight difference between r_0(C−H) and r_0(C−D) which we shall have to neglect. Only if all the rotational

TABLE III. Rotational constants of CD_3H.

	8870A band	11590A band
$B_0=B''$	3.27_{87}	3.278_4
B'	3.21_{46}	3.228_5
$A'-A''$	−0.0350	
ν_0	11266.94	8623.31
D_J''	0.000046	0.00005
D_J'	0.000052	0.00004
D_{JK}''	-0.00003_5	
D_{JK}'	-0.00003_0	
α_1	0.0160 cm^{-1}	0.016_6 cm^{-1}

constants α_i in

$$B_{[v]}=B_e-\Sigma\alpha_i\left[v_i+\frac{d_i}{2}\right]$$

were known, could B_e, and therefore the equilibrium r_e, be determined, and one could thus be free of the neglect just mentioned. Unfortunately at present only α_1 is known.

One obtains for the effective internuclear distance in the lowest vibrational level under the assumption r_0(C−H)=r_0(C−D)

$$r_0(\text{C}-\text{H})=(1.0919_3\pm0.0001_7)\times10^{-8}\text{ cm}.$$

The error quoted is due solely to the error in the determination of $B_0(CD_3H)$ and does not take account of inaccuracies in the assumed fundamental constants (taken from Herzberg[16]) nor of the systematic error resulting from the assumption r_0(C−H)=r_0(C−D).

In the case of diatomic CH, the difference between r_0(C−H) and r_0(C−D) can be obtained directly from the observed B_0 values. One finds r_0(C−H)−r_0(C−D) =0.0028A. The corresponding difference for CH_4 would

[16] G. Herzberg, *Molecular Spectra and Molecular Structure I. Spectra of Diatomic Molecules* (D. Van Nostrand Company, Inc., New York, 1950).

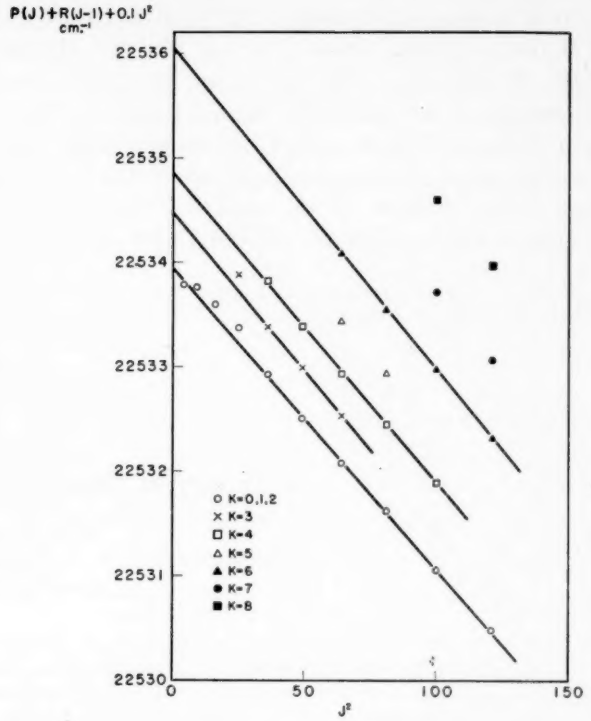

FIG. 5. Combination sums $R(J-1, K)+P(J, K)$ for the 8870A band. The perturbed lines with $J=3$ and 5 have been omitted.

be expected to be of the same order of magnitude. In Table IV, the B_0 values, moments of inertia, and internuclear distances obtained for the three species CH_4, CH_3D, and CD_3H are collected together (all based on the same fundamental constants used before[16]). The small differences found between the r_0(C−H) values are indeed of the order found for r_0(C−H)−r_0(C−D) in free CH, even though somewhat smaller differences might have been expected. The observed differences are much greater than would correspond to the experimental accuracy of the individual values. In agreement with expectation the r_0(C−H) value from CD_3H is smaller than that from CH_3D, but contrary to expectation the value from CH_4 is intermediate between those from CD_3H and CH_3D. It seems probable that the complications arising in the case of CH_4, and believed to be solved by Stoicheff *et al.*,[8] still remain and have led to an incorrect value for the moment of inertia of CH_4.

TABLE IV. B_0 values, moments of inertia, and internuclear distances in isotopic methanes.

	B_0	$I_B{}^0$	r_0(C−H)	Reference
CH_4	5.249	5.3311	1.0930_7	Stroicheff *et al.*[8]
CH_3D	3.878_0	7.2158	1.0935_6	Boyd and Thompson[10]
				Childs and Jahn[11]
CD_3H	3.278_7	8.5347 $\times10^{-40}$ g cm^2	1.0919_3 $\times10^{-8}$ cm	this paper

It is tempting to represent the data on CD_3H and CH_3D by slightly different values of $r_0(C-H)$ and $r_0(C-D)$ (but neglecting the change in angle), as was attempted in the case of the methyl halides by Miller *et al.*[17] However, here again a surprisingly large difference has to be assumed: one finds $r_0(C-H)=1.0972_4$A, $r_0(C-D)=1.0902_1$A. At the same time the moment of inertia of CH_4 would have to be 5.3719×10^{-40}, which deviates widely from the observed value. Clearly the effect of zero-point vibration cannot be taken into account in such a simple way.

The author wishes to thank Dr. A. E. Douglas for suggesting the problem and for giving experimental and theoretical help. He is grateful to Dr. G. Herzberg for much helpful discussion. The cooperation of Dr. J. A. B. Nolin and Dr. L. C. Leitch in supplying the deuterated methyl halides and of Dr. F. P. Lossing in analyzing the gases by mass-spectroscopic methods is also greatly appreciated.

[17] Miller, Aamodt, Dousmanis, Townes, and Kraitchman, J. Chem. Phys. **20**, 1112 (1952).

THE JOURNAL OF CHEMICAL PHYSICS VOLUME 21, NUMBER 5 MAY, 1953

A Theory of Sensitized Luminescence in Solids

D. L. DEXTER*
Metallurgy Division, Naval Research Laboratory, Washington, D. C.
(Received November 3, 1952)

The term "sensitized luminescence" in crystalline phosphors refers to the phenomenon whereby an impurity (activator, or emitter) is enabled to luminesce upon the absorption of light in a different type of center (sensitizer, or absorber) and upon the subsequent radiationless transfer of energy from the sensitizer to the activator. The resonance theory of Förster, which involves only allowed transitions, is extended to include transfer by means of forbidden transitions which, it is concluded, are responsible for the transfer in all inorganic systems yet investigated. The transfer mechanisms of importance are, in order of decreasing strength, the overlapping of the electric dipole fields of the sensitizer and the activator, the overlapping of the dipole field of the sensitizer with the quadrupole field of the activator, and exchange effects. These mechanisms will give rise to "sensitization" of about 10^3–10^4, 10^2, and 30 lattice sites surrounding each sensitizer in typical systems. The dependence of transfer efficiency upon sensitizer and activator concentrations and on temperature are discussed. Application is made of the theory to experimental results on inorganic phosphors, and further experiments are suggested.

I. INTRODUCTION

ONE of the important problems of solid state physics is that of a description of the processes which follow the absorption of visible or ultraviolet light by an insulating crystal. Of the several possible general processes, luminescence has received the most experimental attention, although unfortunately there seems to be no simple crystal yet investigated for which luminescence associated with the undistorted lattice has been unambiguously demonstrated.[1] Consequently most experimental work on luminescence has dealt with systems consisting of a host lattice and one or more types of impurity atoms.[2,3] The theoretical work in this field has not kept up with experiment for two main reasons: (1) The development of the field of luminescence, because of its commercial significance, has been guided largely by practical considerations, with a resulting reduction in the attention directed towards development and investigation of the simplest possible luminescent systems, which might be more easily interpreted. (2) The theoretical problems of luminescence are exceedingly difficult to treat even in their simplest form, not only because they involve the simultaneous interactions among radiation, matter and phonons, but also because the specific details of the wave functions are of first-order importance. The experimental results on luminophors consisting of electronically similar impurity atoms in the same host lattice and of the same impurity atom in similar host lattices demonstrate the strong influence of the details of the coupling between the impurity atom and its surroundings and thus emphasize the "many-body" nature of the problems to be solved.

A branch of luminescence investigated in recent years, namely, "sensitized luminescence,"[4–13] appears at first,

* Present address: Institute of Optics, University of Rochester, Rochester, New York.

[1] The edge emission of CdS [F. A. Kröger, reference 31, C. C. Klick, Phys. Rev. **89**, 274 (1953)] may prove to be an example of true lattice emission. A number of more complicated inorganic crystals, $CaMoO_4$ and $CaWO_4$, for example (see references 8 and 12), apparently luminesce even in the absence of imperfections, as do a number of organic crystals, e.g., anthracene and napthalene.

[2] P. Pringsheim, *Fluorescence and Phosphorescence* (Interscience Publishers, Inc., New York, 1949).

[3] H. W. Leverenz, *Introduction to Luminescence of Solids* (John Wiley and Sons, Inc., New York, 1950).

[4] S. Rothschild, Physik. Z. **35**, 557 (1934); **37**, 757 (1936).

[5] Schulman, Evans, Ginther, and Murata, J. Appl. Phys. **18**, 732 (1947).

[6] J. B. Merrill and J. H. Schulman, J. Opt. Soc. Am. **38**, 471 (1948).

[7] H. C. Froelich, J. Electrochem. Soc. **93**, 101 (1948).

[8] F. A. Kröger, *Some Aspects of the Luminescence of Solids* (Elsevier Publishing Company, Inc., Houston, Texas, 1948).

perhaps, to be even more complicated than the more common forms. That this is not the case is, as we shall see, a result of the difference in the questions that we may ask regarding the various processes.

According to common usage, sensitized luminescence refers to the process whereby an impurity atom (activator) having no appreciable absorption band in a given region of the (visible or uv) spectrum is made to emit radiation upon excitation in this region as a result of absorption by and transfer from another impurity atom (sensitizer) or from the host lattice. We shall refer to these distinct processes as impurity-sensitized and host-sensitized luminescence, respectively.

We may now see the relatively simple nature of the problems to be investigated. If we accept the experimental facts regarding the positions and strengths of the absorption band of the activator and the emission band of the sensitizer, we may isolate the most fundamental problem peculiar to *sensitized* luminescence as follows: What is the mechanism of the process by which the excitation energy is transferred from sensitizer to activator, and what is its efficiency as a function of temperature and of activator and sensitizer concentrations? That is, we may in this case avoid all of the difficult problems of common luminescence and concentrate on those of sensitized luminescence alone.

The purpose of this paper is to examine the above questions regarding sensitized luminescence in insulating crystals on the basis of a resonance theory of energy transfer. Such a theory does not involve transitions to or from the conduction band and hence does not take account of photoconductivity. Other theoretical work on sensitized luminescence in solids includes Mott and Gurney's[14] suggestion that electrons and holes which are freed by absorption of light at the sensitizer travel through the conduction and valence bands, eventually to recombine at the activator. Such processes, involving photoconductivity, are not included within the present theory.

A resonance theory of energy transfer is of course not new. Franck, Cario, and many others have demonstrated the mechanism in gases,[15] and a quantum theory was given by Kallmann and F. London.[16] Transfer has similarly been shown in solutions containing organic molecules,[15] and both classical[17] and quantum-mechanical[18,19] theories have been formulated for transfer processes involving allowed transitions. Investigations of the propagation of excitons in insulators have likewise been based on resonance theories,[20] as has a theory of the annihilation of F centers by excitons.[21]

Previous theoretical work has been concerned with resonance between two allowed (electric dipole) transitions. In the common organic systems the transitions involved are allowed, and the significance of Förster's work[19] has been generally recognized by workers in the organic field. However, one of the principal reasons for the interest in sensitized luminescence in inorganic solids has been that resonant transfer can be obtained between an allowed transition in the sensitizer and a forbidden transition in the activator. That is, an activator with a suitable emission spectrum (for example, manganese with a forbidden transition) can be made to luminesce after energy transfer from an absorbing sensitizer, although the activator will not absorb the energy directly.[22] Clearly a description of forbidden transitions is essential.

Several authors have suggested, on the basis of the above analogies in gases and liquids, that resonant transfer occurs in the systems they have investigated.[4–13] Some of these writers state that the transfer probability is determined by the overlapping of the wave functions of the sensitizer and activator[9–11] and that only when activator and sensitizer occupy adjacent lattice sites may transfer occur.[9,10] Inspection of the above-mentioned resonance theories shows that overlap integrals between activator and sensitizer occur only in the normalization of the wave functions and are of minor importance. Furthermore, in the case of impurity-sensitization exchange intervals (which depend partially on overlap) are unimportant when strong electric dipole transitions are allowed. Previous treatments of sensitized luminescence therefore have not included exchange effects and are concerned with the overlapping of the "near-zone" electric fields, and not the wave functions. It will be shown that exchange effects become important for magnetic dipole (and higher order) transitions.

Section II contains discussions of the physical model employed here and of the procedure for normalization of the wave functions. Sections III, IV, and V treat electric dipole-dipole, dipole-quadrupole, and exchange effects and electric dipole-magnetic dipole transitions, respectively. The above all refer to impurity-sensitization, whereas Sec. VI discusses host-sensitization.

[9] Th. P. J. Botden and F. A. Kröger, Physica **XIV**, 553 (1948).
[10] F. A. Kröger, Physica **XV**, 801 (1949).
[11] Schulman, Ginther, and Klick, J. Electrochem. Soc. **97**, 123 (1950).
[12] Th. P. J. Botden, Philips Research Repts. **6**, 425 (1951).
[13] J. Franck and R. Livingston, Revs. Modern Phys. **21**, 505 (1949). This paper contains references to work on organic systems.
[14] N. F. Mott and R. W. Gurney, *Electronic Process in Ionic Crystals* (Oxford University Press, New York, 1940), p. 207.
[15] For references to the original work see, for example, references 2 and 13.
[16] H. Kallmann and F. London, Z. Physik. Chem. **B2**, 207 (1929).
[17] J. Perrin, Compt. rend. Paris, **184**, 1097 (1927).
[18] F. Perrin, J. phys. et radium **7**, 1 (1936).
[19] Th. Förster, (a) Ann. Physik **2**, 55 (1948); (b) *Fluoreszenz organische Verbindungen* (Vandenhoeck and Ruprecht, Göttingen, 1951); (c) Z. Elektrochem. **53**, 93 (1949).
[20] The latest paper on this subject, W. R. Heller and A. Marcus, Phys. Rev. **84**, 809 (1951), contains references to other previous work.
[21] D. L. Dexter and W. R. Heller, Phys. Rev. **84**, 377 (1951).
[22] A second practical benefit of sensitization comes from the double degradation of the absorbed energy, as a result of a Stokes' shift in both the sensitizing and activating center. For example, the Hg 2537 line can be used for excitation, and emission can be obtained in the visible, as in the ordinary fluorescent lamp. (In this example it is probable that internal transitions to lower excited states of the Mn ion are responsible for part of the shift.)

The transfer probabilities are evaluated from optical data in Eqs. (16), (17), (25), (26), and (30). Section VII contains a discussion of the application of the theory to experiment.

II. NORMALIZATION PROCEDURE

For the next four sections we shall be concerned with impurity sensitization in an insulating crystal. The natural physical model is that of an atomic fraction x_s of sensitizing impurity atoms or ions arranged at random on the suitable lattice sites of the crystal, without appreciable mutual interaction, and a fraction x_a of activators similarly arranged. For the present we shall assume weak concentrations x_s and x_a, such that the transfer probability from one sensitizer to another is negligible, such that the probability of the formation of new crystalline phases is negligible, and such that effects depending on pairs or clusters of activators are unimportant. Interactions of the lattice vibrations with the sensitizer and with the activator will be accounted for experimentally. Interactions between impurities and the charged bodies of the lattice will be taken into account by means of a suitable dielectric constant. A further restriction is the assumption that no photoconductivity occurs. Clearly none of these assumptions is universally valid, and certain additional effects will be discussed later.

The entire transfer process consists of five stages: (1) absorption of a photon of energy $\sim E_0$ by the sensitizer, (2) relaxation of the lattice surrounding the sensitizer by an amount such that the available electronic energy in a radiative transition from the sensitizer is $E_1<E_0$, (3) transfer of energy E_1 to the activator, (4a) relaxation around the activator such that the available electronic energy in a radiative transition is $E_2<E_1$, (4b) relaxation around the sensitizer to a state similar (but not necessarily identical) to its original unexcited state, (5) emission of energy E_2.

Step 2 occurs in about 10^{-13} seconds or longer, the excess energy being dissipated to the lattice by phonons. This is the process associated with the Stokes' shift. Step 3 requires a time which depends on the distances to the surrounding activators, i.e., on the concentration x_a. If these distances are too large, we may expect the energy E_1 to appear: (a) as a photon which may or may not be absorbed by an activator atom depending on its absorption cross section and on the total number (not the concentration) of activators in the crystal, (b) as a photon which may be reabsorbed by another sensitizer, depending on whether or not the absorption and emission bands of the sensitizer overlap and upon the total number of sensitizers in the crystal, (c) as electronic excitation energy E_1 on a different sensitizer atom without a photon as intermediary, depending on the concentration x_s and on the overlap between emission and absorption bands of the sensitizer, or (d) as thermal energy following a nonradiative transition. For the present we shall not discuss these various processes, and shall be concerned only with the probability of direct transfer to an activator.

Assuming that the latter transfer has occurred, step (4) again requires a time $\gtrsim 10^{-13}$ seconds, and step (5) a time 10^{-8} seconds or much longer, depending on the forbiddenness of the transition. Since in almost all cases the Stokes' shifts are sizable, it is clear why the activator represents a "trap" for the electronic excitation energy: the activator, when excited, is not in resonance with the sensitizer, i.e., $E_2<E_0$. Thus when appreciable relaxation occurs, as seems to be the case for most systems of interest in solids, the energy must stay on the activator atoms, and we need not concern ourselves with transfer in the opposite direction. A further stage or series of stages which may occur between steps 4 and 5, namely, radiative and nonradiative transitions to lower excited electronic states of the activator, may further decrease the probability of back-transfer, as would transfer to more distant activators. (If the activator and sensitizer are sufficiently close together, back-transfer may take place before relaxation, step 4, has time to occur. We shall not treat this case at the present time.)

We now consider the wave functions describing the above model. According to the time-dependent perturbation theory of quantum mechanics,[23] the well-known expression for the transition probability is $(2\pi/\hbar)|\langle H_1\rangle|^2\rho_E$ where $\hbar$ is Planck's constant, ρ_E is the density of states, and $\langle H_1\rangle$ is the matrix element of the perturbation to the Hamiltonian, between the initial and final states of the system. In our case, we ascribe the initial state Ψ_I to the configuration in which the sensitizer S is excited, ψ_s', while the activator A is in its ground state, ψ_a; and the final state Ψ_F to that in which S is in its ground state, ψ_s, while A is excited, ψ_a'. (Primed quantities will refer throughout to excited states.) Thus the probability that the energy is transferred from a particular sensitizer S to a particular activator A is of the form

$$P_{sa}=(2\pi/\hbar)\rho_E\left|\int\Psi_I^*H_1\Psi_F d\tau\right|^2, \qquad (1)$$

as long as the states Ψ_I and Ψ_F are of the same energy.

Because of lattice vibrations, of course, neither the initial nor final levels of S or A are well defined. We may therefore normalize our wave functions on an energy scale as we would for continuum wave functions[24] and absorb the density of states factor ρ_E within the normalization parameters. It will be convenient to normalize the initial (excited) state of S and the initial (ground) state of A in the usual manner and to introduce probability functions $p_s'(w_s')$ and $p_a(w_a)$ to ex-

[23] See, for example, L. I. Schiff, *Quantum Mechanics* (McGraw-Hill Book Company, Inc., New York, 1949), p. 189.

[24] For a discussion of this type of normalization see, for example, H. Bethe, *Handbuch der Physik* (1933), (2) **24/1**, p. 273, and references contained therein. The discussion of normalization given below is similar to that in reference 19.

press the probabilities that S is in the particular energy state denoted by w_s' and that A is in the state w_a. Therefore consider

$$\int|\psi_s'(w_s')|^2d\tau=\int|\psi_a(w_a)|^2d\tau=1,$$
$$\int_0^\infty p_s'(w_s')dw_s'=\int_0^\infty p_a(w_a)dw_a=1. \tag{2}$$

For the final states we normalize the wave functions on an energy scale as follows:

$$\frac{1}{\Delta w}\int_w^{w+\Delta w}dw_s\int|\psi_s(w_s)|^2d\tau=1,$$
$$\frac{1}{\Delta w}\int_w^{w+\Delta w}dw_a'\int|\psi_a'(w_a')|^2d\tau=1. \tag{3}$$

Now the properly antisymmetrized initial and final states wave functions describing S and A can be written

$$\begin{aligned}&\sqrt{2}\Psi_I(w_s',w_a)\\&\quad=\psi_s'(\mathbf{r}_1,w_s')\psi_a(\mathbf{r}_2,w_a)-\psi_s'(\mathbf{r}_2,w_s')\psi_a(\mathbf{r}_1,w_a)\\&\sqrt{2}\Psi_F(w_s,w_a')\\&\quad=\psi_s(\mathbf{r}_1,w_s)\psi_a'(\mathbf{r}_2,w_a')-\psi_s(\mathbf{r}_2,w_s)\psi_a'(\mathbf{r}_1,w_a'),\end{aligned} \tag{4}$$

if only two electrons are involved in the transitions. If more than two electrons should be involved, Eq. (4) could easily be extended to express all of the possible permutations of the electrons; Eq. (4) as written will serve to show the type of term that enters because of antisymmetrization, i.e., the exchange term. The other terms, namely, Coulomb terms, are correctly given even without antisymmetrization of the wave functions. In the following $\mathbf{r}_1$ and $\mathbf{r}_2$ will be used to denote the coordinates of all the electrons involved. The atomic wave functions in (4) are normalized according to Eq. (2) and (3). If overlapping of the wave functions such as $\psi_s'(\mathbf{r}_1)$ and $\psi_a(\mathbf{r}_1)$ were appreciable, the squares of the normalization factors $\sqrt{2}$ should be reduced by quantities such as $(\int\psi_s'(\mathbf{r}_1)^*\psi_a(\mathbf{r}_1)d\tau_1\int\psi_a(\mathbf{r}_2)^*\psi_s'(\mathbf{r}_2)d\tau_2)$; such effects are small and will henceforth be ignored. In general there will be several possible states Ψ_I and Ψ_F from and to which the system may make transitions contributing to the transfer process, depending, for example, on the polarization of the atomic functions. Then $\langle H_1(w_s',w_a;w_s,w_a')\rangle_{IF}$ is the matrix element of H_1 between particular states $\Psi_I(w_s',w_a)$ and $\Psi_F(w_s,w_a')$. It should be noticed that as a result of our type of normalization $\langle H_1\rangle$ is now a dimensionless quantity, not an energy.

The electronic excitation energy on S in the state Ψ_I is $E=w_s'-w_s$, and that on A in the state Ψ_F is $w_a'-w_a$. According to the Franck-Condon principle, there is small probability of an electronic transition in which electronic excitation energy is lost to the lattice, so that the energy principle requires that the transition probability P_{sa} contain a Dirac delta-function $\delta[(w_s'-w_s)-(w_a'-w_a)]$. We therefore obtain for the total probability of energy transfer from S to A the result,

$$\begin{aligned}P_{sa}=&(2\pi/\hbar)\sum_I\sum_F(g_s'g_a)^{-1}\\&\times\int dw_a'\int dw_s\int dw_a p_a(w_a)\int dw_s' p_s'(w_s')\\&\times|\langle H_1(w_s',w_a;w_s,w_a')\rangle_{IF}|^2\\&\times\delta[(w_s'-w_s)-(w_a'-w_a)],\end{aligned}$$

where we omit the indices I and F on the energy parameters for the sake of brevity. The factor g_s', the degeneracy of the level of the excited S atom or ion, is necessary to take account of the fact that only one of the possible excited states of S is occupied, whereas we subsequently sum over them all, similarly for g_a. The sums over I and F represent a sum over all possible transitions that can contribute to the transfer, that is, sums over i_s, i_a, f_s, and f_a. If the ground state of A is nondegenerate, the summation over i_a may be removed and g_a set equal to unity. Carrying out the integration over w_s by means of the delta-function and substituting $E=w_a'-w_a=w_s'-w_s$, we obtain

$$\begin{aligned}P_{sa}=&(2\pi/\hbar)\sum_I\sum_F(g_s'g_a)^{-1}\\&\times\int dE\int dw_a p_a(w_a)\int dw_s' p_s'(w_s')\\&\times|\langle H_1(w_s',w_a;w_s'-E,w_a+E)\rangle_{IF}|^2.\end{aligned} \tag{5}$$

III. ELECTRIC DIPOLE-DIPOLE INTERACTION

In order to compute the transfer probability [Eq. (5)] we require H_1, the interaction between A and S. This interaction may be expressed as the sum of all the Coulomb interactions of the outer electrons and core of A with those of S, suitably reduced by the dielectric constant κ of the medium. When this sum is expanded in a Taylor series about the vector $\mathbf{R}$, the separation of the nuclei of A and S, the interaction energy is found to be

$$\begin{aligned}H_1(\mathbf{R})=&(e^2/\kappa R^3)\{\mathbf{r}_s\cdot\mathbf{r}_a-3(\mathbf{r}_s\cdot\mathbf{R})(\mathbf{r}_a\cdot\mathbf{R})/R^2\}\\&+(3e^2/2\kappa R^4)\{\sum_{i=1}^{3}(R_i/R)r_{ai}^2r_{si}(-3+5R_i^2/R^2)\\&+10(XYZ/R^3)(x_ay_az_s+x_az_ay_s+y_az_ax_s)\\&+\sum_{i\neq j}^{3}\sum^{3}[(R_j/R)-5R_i^2R_j/R^3]\\&\qquad\times[-r_{ai}^2r_{sj}-2r_{ai}r_{aj}r_{si}]\}\\&+\cdots.\end{aligned} \tag{6}$$

This is, of course, the interaction that gives rise to van der Waals' forces. The first curly brackets contain the

dipole-dipole interaction, and the second the dipole-quadrupole interaction; higher order interactions, including quadrupole-dipole, have been omitted. (We shall assume throughout that the sensitizer has an allowed transition, so that the dipole term for S gives the largest contribution.) In Eq. (6) $\mathbf{r}_s=\sum_m \mathbf{r}_{s,m}$ refers to all the electrons on S, measured from its nucleus, and similarly with $\mathbf{r}_a=\sum_n \mathbf{r}_{a,n}$; e is the magnitude of the electronic charge.

Inserting the first bracket of Eq. (6) into Eq. (5), we obtain

$$P_{sa}(dd)=(2\pi/\hbar)\sum_I\sum_F(e^4/\kappa^2R^6)(g_s'g_a)^{-1}\times\int dE\int dw_a p_a(w_a)\int dw_s' p_s'(w_s')\times|\langle\mathbf{r}_s\rangle\cdot\langle\mathbf{r}_a\rangle-3(\langle\mathbf{r}_s\rangle\cdot\mathbf{R})(\langle\mathbf{r}_a\rangle\cdot\mathbf{R})|^2, \quad (7)$$

where each matrix element, such as $\langle\mathbf{r}_s\rangle$, should be written as a function of two of the energy parameters, as $\langle\mathbf{r}_s(w_s', w_s'-E)\rangle_{i_sf_s}$. Note that the dimensions of $\langle\mathbf{r}\rangle^2$ are length squared per unit energy; note also the familiar R^{-6} dependence found in the van der Waals' energy. In Eq. (7) we have neglected all terms associated with the antisymmetrization of the wave functions. If we look at the interaction terms before expanding, we find we must compute the matrix elements of terms of the form e^2/R, $e^2/|\mathbf{R}+\mathbf{r}_a|$ and $e^2/|\mathbf{R}+\mathbf{r}_a-\mathbf{r}_s|$. Neither of the first two terms gives a nonzero matrix element in view of our neglect of overlap effects, i.e., the first two terms contain two and one factors, respectively, of the form $\int\psi_a^*(2)\psi_s(2)d\tau_2$. The third term gives rise to Eq. (7) and also to typical exchange integrals of the form $-e^2\int\psi_s'(1)^*\psi_a(2)^*(1/r_{12})\psi_s(2)\psi_a'(1)$. Such terms will be discussed in Sec. V; they are unimportant when dipole-dipole interactions are present. It should also be noted that each matrix element $\langle\mathbf{r}\rangle=\int\psi'^*\mathbf{r}\psi d\tau$ vanishes in the event that the electron spin flips during the transition. Spin-flip transitions will likewise be discussed in Sec. V.

We now average the absolute square of the matrix element in Eq. (7) over all possible orientations of $\mathbf{R}$ and obtain

$$\langle|\langle\mathbf{r}_s\rangle\cdot\langle\mathbf{r}_a\rangle-(3/\mathbf{R}^2)(\langle\mathbf{r}_s\rangle\cdot\mathbf{R})(\langle\mathbf{r}_a\rangle\cdot\mathbf{R})|^2\rangle_{\text{Av}}=(2/3)|\langle\mathbf{r}_s\rangle|^2|\langle\mathbf{r}_a\rangle|^2, \quad (8)$$

where

$$|\langle\mathbf{r}\rangle|^2=|\langle x\rangle|^2+|\langle y\rangle|^2+|\langle z\rangle|^2.$$

Thus the transfer probability becomes

$$P_{sa}(dd)=\frac{4\pi e^4}{3\hbar\kappa^2R^6g_s'g_a}\sum_I\sum_F\int dE\times\left\{\int dw_s' p_s'(w_s')|\langle\mathbf{r}_s(w_s', w_s'-E)\rangle|^2\right\}\times\left\{\int dw_a p_a(w_a)|\langle\mathbf{r}_a(w_a, w_a+E)\rangle|^2\right\}. \quad (9)$$

An evaluation of these matrix elements as a function of energy is of course the foremost problem of luminescence, a problem which, as we have stated, we do not propose to discuss here. Knowing the wave functions, it would be a trivial matter to evaluate the integrals; not knowing them, it is expedient to evaluate the matrix elements directly from experiment. These same matrix elements determine oscillator strengths, absorption coefficients, and decay times, all of which are measurable quantities. We shall now express Eq. (9) in terms of these experimental parameters.

The probability of a spontaneous radiative transition of an isolated atom from a state i to a state f is given by[25]

$$A(if)=\frac{4e^2E^3}{3\hbar^4c^3}|\langle\mathbf{r}_{if}\rangle|^2, \quad (10)$$

where c is the velocity of light. For an atom in a crystalline medium this expression is to be changed in several ways. First, the energies of the initial and final states, because of vibrations of the surroundings, are not well defined, so that we introduce a probability function $p'(w')$, as in Sec. II, and normalize the final states on an energy scale. Second, we must change the expression to take account of the dielectric properties of the medium. Since the transition probability is proportional to the square of the matrix elements of the electric field dotted into the electric moment at the atom, the expression on the right-hand side of Eq. (10) is to be multiplied by the square of the ratio of the field within the crystal to that at an isolated atom, that is, by $(\mathcal{E}_c/\mathcal{E})^2$. The average value of $\mathcal{E}_c$ within the crystal and the value of $\mathcal{E}$ in a vacuum are to be chosen so as to correspond to the same photon density. Further, the transition probability is proportional to the density of states in momentum space, or to k^2dk, where k is the propagation vector of photons in the medium. Since k is increased in a medium by the factor n (index of refraction), (10) is also to be multiplied by the factor n^3.

In view of the above arguments, the probability of emission of a photon of energy E is

$$A(E)=\sum_i\sum_f\frac{4e^2E^3}{3\hbar^4c^3g'}\left(\frac{\mathcal{E}_c}{\mathcal{E}}\right)^2n^3\times\int|\langle\mathbf{r}_{if}(w', w'-E)\rangle|^2p'(w')dw', \quad (11)$$

where the sum is over all transitions, and the degeneracy factor g' is introduced for the same purpose as in Eq. (5). The shape of the function $A(E)$ is given by the emission spectrum of the atom, and the integral $\int A(E)dE$ is equal to the decay constant of the level, $1/\tau$. Let the

[25] See, for example, N. F. Mott and I. N. Sneddon, *Wave Mechanics and Its Applications* (Oxford University Press, New York, 1948), p. 253 *ff*; note that there are several misprints on p. 257.

normalized function $f(E)$ represent the observed shape of the emission band, so that $\int f(E)dE=1$. Then from Eq. (11) we have the result,

$$\sum_i\sum_f\int|\langle\mathbf{r}_{if}(w',w'-E)\rangle|^2p'(w')dw'=\frac{3\hbar^4c^3g'}{4n^3e^2E^3}\left(\frac{\mathcal{E}}{\mathcal{E}_c}\right)^2\frac{1}{\tau}f(E). \quad (12)$$

Equation (12) is of course general and refers to either S or A. The left-hand side of Eq. (12), which refers to S in Eq. (9), may be evaluated experimentally by measuring the decay time and emission spectrum of S in a crystal containing a low concentration of S as its only impurity. Note that we assume no interactions between S and any other impurity in the derivation of Eq. (12). If interactions occur and change the band shape or decay time or if any competing processes occur to affect the decay time, Eq. (12) is not applicable. In general, Eq. (12) will be applicable if the concentration x_s is weak and if the quantum yield for luminescence of S is unity. If for some reason Eq. (12) cannot be applied, the left-hand side may be evaluated through absorption experiments as follows:

The usual expression for the Einstein B coefficient[25] for induced transitions in an isolated atom is

$$B(if)=\frac{2\pi e^2}{3\hbar^2}|\langle\mathbf{r}_{if}\rangle|^2.$$

In the event that the absorption band becomes broad, we may normalize the wave functions as previously and speak of the induced transition probability per unit energy range. Including the effect of the changed electric field in the medium, we obtain

$$B(E)=\sum_i\sum_f\frac{2\pi e^2}{3\hbar^2g}\left(\frac{\mathcal{E}_c}{\mathcal{E}}\right)^2\int p(w)dw|\langle\mathbf{r}_{if}(w,w+E)\rangle|^2.$$

The absorption cross section then becomes

$$\sigma(E)=\sum_i\sum_f\frac{4\pi^2e^2nE}{3\hbar cg}\left(\frac{\mathcal{E}_c}{\mathcal{E}}\right)^2\int p(w)dw\times|\langle\mathbf{r}_{if}(w,w+E)\rangle|^2, \quad (13)$$

where the factor n appears because we have divided the transition probability B by a photon flux $v=c/n$. The absorption cross section, which will not in general be greatly distorted except by very large concentrations, can be measured as the ratio of the absorption coefficient (cm^{-1}) to the number density of impurities in the medium (cm^{-3}). Let us introduce therefore the normalized function $F(E)$ such that $\sigma(E)=QF(E)$, where $\int F(E)dE=1$. Then we obtain from Eq. (13) the result,

$$\sum_i\sum_f\int p(w)dw|\langle\mathbf{r}_{if}(w,w+E)\rangle|^2=\frac{3\hbar cg}{4\pi^2e^2nE}\left(\frac{\mathcal{E}}{\mathcal{E}_c}\right)^2QF(E). \quad (14)$$

By applying this equation to the activator, if it has an observable absorption band, we may evaluate the remaining matrix elements in Eq. (9). $Q=\int\sigma(E)dE$ is measured as the area under the absorption band.

Equation (14) may also be useful for the evaluation of the sensitizer's matrix elements in the event that the quantum yield of S when present by itself is less than unity, or when the decay rate either cannot be measured or is not a simple exponential function. In such cases, we may still measure the (normalized) shape of the emission band $f_s(E)$ but may express the "strength" of the line in terms of the absorption area, Q_s. Thus we obtain the relation,

$$\sum_{i_s}\sum_{f_s}\int p_s'(w_s')dw_s'|\langle\mathbf{r}_{if}(w_s',w_s'-E)\rangle|^2=\frac{3g_s\hbar c}{4\pi^2e^2nE}\left(\frac{\mathcal{E}}{\mathcal{E}_c}\right)^2Q_sf_s(E). \quad (15)$$

It should be borne in mind that this last result is only approximate; the quantity Q_s is determined by the wave functions of S when its surroundings are in the positions characteristic of the unexcited state, whereas τ_s should be computed using wave functions in the "relaxed" lattice. Since these wave functions will in general be different in the two configurations of the lattice, the transition strength as measured by Q_s will be inexact.

Making use of Eqs. (12), (14), and (15), we may express Eq. (9) as

$$P_{sa}(dd)=\frac{3\hbar^4c^4Q_a}{4\pi R^6n^4\tau_s}\left(\frac{\mathcal{E}}{\kappa^{\frac{1}{2}}\mathcal{E}_c}\right)^4\int\frac{f_s(E)F_a(E)}{E^4}dE \quad (16)$$

with absorption data for A and emission data for S, or as

$$P_{sa}(dd)=\frac{3\hbar c^2Q_aQ_s}{4\pi^3n^2R^6}\left(\frac{g_s}{g_s'}\right)\left(\frac{\mathcal{E}}{\kappa^{\frac{1}{2}}\mathcal{E}_c}\right)^4\int\frac{f_s(E)F_a(E)}{E^2}dE, \quad (17)$$

making use also of absorption data for S. We could similarly use an emission time τ_a to express the line strength for the activator, but if A has an allowed transition as assumed, Q_a can be easily measured.

The transfer probability is thus given by the strengths of the individual transitions in terms of decay times τ and absorption band areas Q and by the energy overlap of the absorption and emission bands of A and S. These quantities are all directly measurable optically except for the ratio $\mathcal{E}/\mathcal{E}_c$. We know that the average field

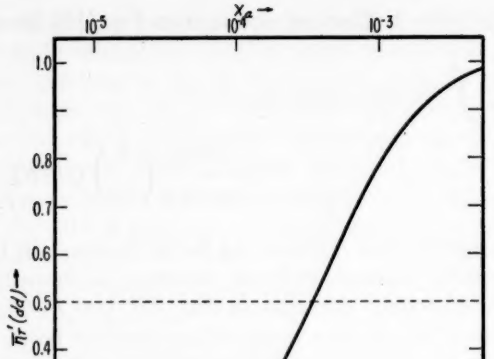

FIG. 1. Quantum yield for *dd* transfer as a function of the reduced concentration y of the activator. The upper abscissa represents the numerical value of the atomic concentration x_a in a typical case.

strength within the medium is reduced in the ratio $(\bar{\mathcal{E}}_c/\mathcal{E})^2=1/\kappa$, and we shall set the quantity $(\mathcal{E}/\kappa^{\frac{1}{2}}\mathcal{E}_c)^4$ equal to unity in the following numerical evaluation.

The foregoing discussion of the dipole-dipole transfer, based on a physical model similar to that of Förster,[19] has proceeded in a manner similar to, although somewhat more general than, the development by him. It has been included here in detail for the sake of completeness and for the sake of clarity in the treatments of transfer by forbidden transitions.

Let us evaluate Eq. (16) for a typical pair of impurities. With good overlap we may expect $F_a(E)$ to overlap $f_s(E)$ with an overlap integral of $\sim 1/(3\text{ ev})$, E to be about 5 ev, $n^4\sim 6$, and $Q_a\sim 10^{-16}$ cm^2 ev. Then P_{sa} becomes $(27/R)^6\ (1/\tau_s)$, where R is expressed in Angstrom units. In order that appreciable transfer occur before S luminesces, $P_{sa}\tau_s$ must be $\gtrsim 1$, or transfer will occur if S and A are separated by not more than about 25A. For $\tau_s\sim 10^{-8}$ sec and for S and A in adjacent positive ion sites in NaCl ($R=3.97$A), the jump time would be of the order 10^{-12} or 10^{-13} sec.

The experimentally significant quantity is the quantum yield for transfer, η_T. If we neglect nonradiative transitions in S and also neglect transfers from S to S, this quantity becomes $\eta_T=P_{sa}\tau_s/(1+P_{sa}\tau_s)$. Defining $v=(4/3)\pi R^3$, we obtain $\eta_T=\beta^2/v^2+\beta^2$, where β is defined through the relation $P_{sa}=\beta^2/\tau_s v^2$. In the typical case just discussed, β is 8.26×10^{-20} cm^3, and η_T as defined is the quantum yield for transfer from an excited center S to an activator at distance $R=(3v/4\pi)^{\frac{1}{3}}$. To obtain the average yield $\bar{\eta}_T$ in a crystal, we require the integral over-all space of η_T times the probability that the nearest activator is at distance R. Let C^+ be the number density of lattice sites of the type that can accommodate A, and let v_0 be the volume excluded by the presence of the sensitizer. Introducing the parameter $y=x_aC^+\beta$, we find the average yield to be given by

$$\bar{\eta}_T=ye^{x_aC^+v_0}\{y^{-1}[e^{-x_aC^+v_0}-1]+\mathrm{Ci}(y)\sin y - \mathrm{Si}(y)\cos y+(\pi/2)\cos y\}, \quad (18)$$

where Ci and Si are the cosine- and sine-integral functions. For concentrations $x_a\lesssim 1$ percent ($y\lesssim 20$) we may set equal to unity the factors $\exp\pm(x_aC^+v_0)$ and obtain a function of y alone,

$$\bar{\eta}_T'=y\{\mathrm{Ci}(y)\sin y-\mathrm{Si}(y)\cos y+(\pi/2)\cos y\}. \quad (19)$$

A similar expression has been derived by Förster.[19b] This function is shown in Fig. 1. For small concentrations ($y\ll 1$) $\bar{\eta}_T'$ varies as $y(\pi/2+y\ln y-0.4228y)$, thus demonstrating the expected linear dependence on concentration for small x_a. For $y\gg 1$, i.e., high concentrations, $\bar{\eta}_T\to 1$, as may be seen from Eq. (18). Since $\bar{\eta}_T'$ is equal to $\frac{1}{2}$ for $y=0.65$, according to Fig. 1, we may arbitrarily define a "critical" concentration by the relation $\bar{\eta}_T'=\frac{1}{2}$, or by

$$x_a^*=\frac{0.65}{C^+\beta}. \quad (20)$$

For β equal to 8.3×10^{-20} cm^3 and $C^+=2.25\times 10^{22}$ cm^{-3} (as in NaCl), x_a^* becomes 3.5×10^{-4}, and we may say that in this case S is able to sensitize 2900 sites. This large number will evidently be diminished if the overlap between emission of S and absorption of A is less than assumed above, if nonradiative processes in S reduce the natural lifetime τ_s, or if the strength of the transition in A is less than assumed above. It will clearly be further increased if S atoms are present in sufficient concentration that the excitation energy may be transferred from S to S until it resides nearer than average to an activator. For sufficiently weak concentrations x_s, of course, the transfer probability P_{sa} is independent of x_s.

Note that the critical concentration varies inversely as β, and hence as the inverse square root of the coupling integral $\int f_s(E)F_a(E)dE/E^4$ and as the inverse square root of the line strength of A. Thus even systems with poor overlap and with weak electric dipole transitions in A may take part in transfer with low concentration x_a.

It should be borne in mind that the above development is applicable not only to $S-A$ transfer, but also to $S-S$ and $A-A$ transfer. In the latter two cases the usual Stokes' shift will in general greatly reduce the overlap between emission and absorption, so that concentrations an order of magnitude higher than the above value of 3×10^{-4} may be required. The treatment is also applicable, of course, to liquid systems. The primary differences between solid and liquid systems seem to lie in the relative smallness of the index of refraction in liquid solutions and in the relative smallness of the Stokes' shifts in the liquids.

The temperature dependence of the transfer probability can be inferred from Eqs. (16) and (17). In general the strengths of the transitions as indicated by Q_a and τ_s or Q_s are roughly independent of temperature. Thus the main temperature dependence occurs in the amount of overlap between f_s and F_a. Both of these functions broaden with temperature, and in the event that they overlap perfectly at all temperatures the transfer probability will decrease with increasing temperature. However, if their centers are well separated, the broadening associated with increasing temperature will increase the overlap and hence the transfer probability. At low temperatures the broadening is negligible as compared with natural, zero-point widths, and the transfer probability should be independent of temperature. A further effect is the possible shift of the center of one function relative to the other, an effect which may either increase or decrease the probability. Such effects as these will vary from one case to the next, and are extremely difficult to calculate accurately from first principles.

Kröger[8] has suggested that energy transfer be visualized on a "configurational coordinate" diagram, in which the energy of the center is plotted in the configuration space of the nuclear coordinates of the lattice neighbors. He presents such a diagram (in two dimensions) showing both the energy of a sensitizer and that of an activator as a function of the same configurational coordinate, and concludes that energy transfer can occur only at the point in configuration space where the curves cross, and that this point in general corresponds to specific excited vibrational states for both centers. He further concludes that the transfer process requires an activation energy and that the probability of transfer contains an exponential dependence on the reciprocal temperature, $P\sim\exp -W_s/kT$, where W_s is the energy difference between the crossing-point and the minimum of the curve representing the excited sensitizer atom. (See reference 8, p. 210.) These ideas have been developed in further detail by Botden.[12]

In two dimensions such a diagram is of course almost meaningless as is recognized by the authors. Specifically the one coordinate, if important for the sensitizer, will in general not be important for the activator, so that, whereas the sensitizer curve may be a rapidly varying function of the coordinate, the activator function will not; and the curves will in general not intersect. Also, the generalized energy surfaces for the two centers when plotted simultaneously in a multidimensional space will in general intersect at an infinite number of points with energy parameters, W_s, ranging from very close to zero (depending on the separation) up to infinity. Furthermore, these points do not represent the configurations for which transfer may occur.

With suitable modification, however, an interpretation based on configurational coordinate diagrams may be useful in some instances. The only restriction on the transfer is that the virtual photon emitted by the sensitizer be equal in energy to that absorbed by the activator. That is, if one plots the *difference* between the energies of the excited electronic state and of the ground electronic state of the sensitizer center, and simultaneously the analogous energy difference for the activator, in the generalized coordinate space, transfer may occur with appreciable probability, according to the Franck-Condon principle, only at the intersections of these generalized surfaces of energy difference. Again there will in general exist an infinite number of such intersections; these intersections appear for all values of the energy W_s as defined above.

For example, if the low temperature emission band of S occurs at higher energy than the absorption band of A and if the centers are sufficiently far apart that the coordinates important to A do not greatly influence S, transfer may occur from S to A with no appreciable thermal activation W_s of S, but with activation only of A. The probability of achieving one of the possible configurations for transfer may in some cases be roughly proportional to $\exp -W_a/kT^*$, where $T^*=\theta\coth\theta/T$ is the "effective temperature" which takes account, through the Debye θ, of the zero-point broadening of the levels.[26] T^* and hence P_{sa} are independent of T for low T.

Transfer will also be possible for configurations corresponding to "activation energies" of all higher values than the minimum. Further, if S and A are close together, the minimum activation energy may be either greater or smaller than the above. In so far as the exponential dependence on W/T^* is valid, the value for W will be the smallest amount of thermal energy needed to bring S and A into resonance. The energy W_a, if present at A, may be sufficient to bring about resonance, whereas an energy W_s may be required at S. In general W_a and W_s will not be equal, and if S and A are not identical atoms, it is not possible *a priori* to say which of W_s and W_a is the smaller. If S and A are identical atoms, as in $S-S$ transfer, the least thermal energy sufficient to bring about resonance will usually be required at the excited atom, since the energy of the more spatially extended excited atom is not as strong a function of neighboring displacements as is that of the ground state. To repeat, in so far as W/kT^* represents the temperature dependence of P_{sa}, W will be the smaller of W_s and W_a. In the absence of detailed calculations we may not say which is the smaller. It should further be borne in mind that there exist many more configurations of all higher values of energy for which transfer may occur, so that the approximation by a single activation energy is expected to be valid only over a limited temperature range where W/kT^* is $\gg 1$. These complicated averaging processes over activation energies are taken account of empirically in Eqs. (5),

[26] K. Husimi, Proc. Phys. Math. Soc. Japan **22**, 264 (1940).

(16), and (17). A transfer probability with simple exponential dependence on the reciprocal *absolute* temperature, $\exp(-W/kT)$, over a wide range of T, where W is independent of concentration x_a, seems extremely unlikely in view of the above considerations, whatever the interpretation given to W. A simple dependence on the *effective* temperature of the form $P_{sa}\sim\exp -W/kT^*$ could best be sought in systems of low concentration x_a and x_s having well-separated low temperature emission and absorption bands. It should be emphasized that all of the above considerations refer to the transfer probability itself and not to the quantum yield for the transfer process. The quantum yield will of course exhibit other temperature variation depending on nonradiative transitions within S.

An assumption that has been made throughout the foregoing treatment is that the presence of the activator does not alter the shape or position of the emission spectrum of the sensitizer. That this assumption is not precisely valid is clear both experimentally[10] and theoretically. The reason for the changes in the spectra is based on the difference in the interaction between the activator and the sensitizer and that between the ion normally occupying the activator site and the sensitizer. This difference is of the same order of magnitude as each interaction alone. Each interaction is the difference between the energy perturbation to the ground state and that to the excited state of S by the other ion. Again the difference is of the same order as each energy perturbation. Thus the shift in the peak of the emission band of S must be of the same order as, or less than, the van der Waals' interaction between S and A at distance R. This energy is of the order of $\Delta E\sim E\alpha_a\alpha_s/R^6$, where E is the energy of the transition and α_a and α_s are the polarizabilities of A and S. Since α is of the order 10^{-24} cm^3, it is clear that for separations R larger than nearest neighbor separations the perturbation by van der Waals forces is negligible. If A and S are nearest neighbors in the NaCl lattice, the relative energy shift $\Delta E/E$ is of the order $(2.8)^{-6}\sim 2\times 10^{-3}$. Such a shift would be of importance in the case of very poor overlap between absorption and emission bands, but not otherwise. The perturbation for nearest neighbors and for nearest like neighbors might in some cases be somewhat larger than the above estimate as a result of exchange effects, particularly in crystals of high dielectric constant, but it seems safe to treat these perturbation effects on the spectra as of second-order importance.

IV. ELECTRIC DIPOLE-QUADRUPOLE INTERACTION

To determine the transfer probability when S makes an allowed transition and A makes a forbidden, quadrupole transition, we insert into Eq. (5) the absolute square of the matrix element $|\langle H_1\rangle|^2$ computed from the second bracket of Eq. (6). Before inserting $|\langle H_1\rangle|^2$ however we average over all orientations of $\mathbf{R}$. This process results in

$$\langle|\langle H_1\rangle|^2\rangle_{Av}=\frac{9e^4}{4\kappa^2R^8}|\langle\mathbf{r}_s\rangle|^2 \times\left\{\frac{71}{36}[|\langle x_a^2\rangle|^2+|\langle y_a^2\rangle|^2+|\langle z_a^2\rangle|^2] +\frac{4}{3}[|\langle x_ay_a\rangle|^2+|\langle y_az_a\rangle|^2+|\langle z_ax_a\rangle|^2] -\frac{8}{21}[|\langle x_a^2\rangle\langle y_a^2\rangle|+|\langle y_a^2\rangle\langle z_a^2\rangle| +|\langle z_a^2\rangle\langle x_a^2\rangle|]\right\}, \quad (21)$$

where, as before, we omit exchange terms. The usual expression for the quadrupole transition probabilities are given in terms of the double dot product of the dyadic[27]

$$|\langle N\rangle|^2=|\langle x^2\rangle|^2+|\langle y^2\rangle|^2+|\langle z^2\rangle|^2 +2|\langle xy\rangle|^2+2|\langle yz\rangle|^2+2|\langle zx\rangle|^2.$$

By summing $|\langle H_1\rangle|_{Av}^2$ and $|\langle N_a\rangle|^2$ over all D and S states we obtain the numerical relation between their matrix elements,

$$\langle|\langle H_1\rangle|^2\rangle_{Av}=\frac{9e^4\alpha}{4R^8\kappa^2}|\langle\mathbf{r}_s\rangle|^2|\langle N_a\rangle|^2, \quad (22)$$

where $\alpha=1.266$. Thus we obtain the transfer probability from Eqs. (5) and (22):

$$P_{sa}(dq)=\frac{9e^4\pi\alpha}{2\hbar\kappa^2R^8g_s'g_a}\sum_I\sum_F\int dE \times\left\{\int dw_s'p_s'(w_s')|\langle\mathbf{r}_s(w_s',w_s'-E)\rangle|^2\right\} \times\left\{\int dw_ap_a(w_a)|\langle N_a(w_a,w_a+E)\rangle|^2\right\}. \quad (23)$$

We may relate the quantities in the brackets in Eq. (23) to either absorption or emission data as in Sec. III. The first quantity, referring to the sensitizer, can be expressed either as in Eq. (12) or as in Eq. (15), depending on whether or not the decay time τ_s is known and meaningful. The quadrupole matrix elements should properly be expressed in terms of absorption curves, but unfortunately there is little hope of obtaining such data for the following reasons. The strength of a quadrupole transition is ordinarily weaker by a factor of $(a/\lambda)^2$ than an electric dipole transition, where a is the radius of the atom and λ the wavelength of the ab-

[27] E. U. Condon and G. H. Shortley, *The Theory of Atomic Spectra* (Cambridge University Press, Cambridge, 1935), p. 96.

sorbed light, or is weaker by a factor $\sim 10^{-7}$. Since the absorption coefficient resulting from a ten percent impurity with an allowed transition is of the order 10^4 cm^{-1}, ten atomic percent of the activator with a forbidden, quadrupole transition will have an absorption coefficient of only 10^{-3} per cm and thus will not be measurable. We may relate the matrix elements to the emission band, however, since decay times of the order $(10^{-8})/(10^{-7})=0.1$ sec can easily be observed. The spontaneous emission probability[27] is related to $|\langle N\rangle|^2$ through the relation,

$$\sum_{i_a}\sum_{f_a}\int p_a(w_a)dw_a|\langle N(w_a, w_a+E)\rangle|^2 = \frac{10\hbar^6c^5g_a'}{E^5e^2\tau_a n^3}\left(\frac{\mathcal{E}}{\mathcal{E}_c}\right)^2 F_a(E), \quad (24)$$

where we have included the effects of the medium and of broadening as in Eq. (11). Using Eqs. (22), (12), and (23), we find

$$P_{sa}(dq)=\frac{135\pi\alpha\hbar^9c^8}{4n^6R^8\tau_s\tau_a}\frac{g_a'}{g_a}\left(\frac{\mathcal{E}}{\kappa^{\frac{1}{2}}\mathcal{E}_c}\right)^4\int\frac{f_s(E)F_a(E)}{E^8}dE. \quad (25)$$

If τ_s is not obtainable or significant, we may use Eq. (15) instead of Eq. (12), with the result

$$P_{sa}(dq)=\frac{135\alpha\hbar^6c^6}{4\pi n^4R^8}\frac{Q_s}{\tau_a} \times\frac{g_a'g_s}{g_ag_s'}\left(\frac{\mathcal{E}}{\kappa^{\frac{1}{2}}\mathcal{E}_c}\right)^4\int\frac{f_s(E)F_a(E)}{E^6}dE. \quad (26)$$

Again it should be recalled that these line strengths are given only approximately by Q_s and τ_a for the same reason as that given following Eq. (15); that is, the strengths should be properly expressed in terms of τ_s and Q_a if these parameters were known. Note the inverse eighth-power dependence on R.

The ratio of the dipole-quadrupole transfer probability to the dipole-dipole probability is found from Eqs. (25) and (16) to be $(45\alpha/4\pi^2)(n\lambda/R)^2\tau_a(d)/\tau_a(q)$, where we have made use of Eqs. (12) and (14). Now a quadrupole radiative transition [compare Eqs. (24) and (12)] has a probability of the order $(a/\lambda)^2$ times that for a dipole transition. Inserting $\tau_a(d)/\tau_a(q)\sim(a/\lambda)^2$, we find $P_{sa}{}^{(dq)}/P_{sa}{}^{(dd)}$ to be of the order $(a/R)^2$, which amounts to only an order of magnitude or so reduction for close neighbors. We see therefore that resonance transfer can easily occur from a sensitizer to a nearby activator if the latter has a quadrupole transition in the suitable frequency range; on the other hand, direct absorption of radiation in the activator occurs with a probability only $\sim 10^{-7}$ of that in an impurity with an allowed transition.

The dependence on concentration is found as in the last section. We define γ through the relation $P_{sa}(dq)=\gamma^{8/3}/v^{8/3}\tau_s$, and letting $y=\gamma C^+x_a$, we find

$$\bar{\eta}_T=ye^{x_aC^+v_0}\left\{y^{-1}[e^{-x_aC^+v_0}-1]+\int_0^\infty\frac{e^{-yt}}{1+t^{8/3}}dt\right\}, \quad (27)$$

$$\bar{\eta}_T'=y\int_0^\infty\frac{e^{-yt}}{1+t^{8/3}}dt. \quad (27')$$

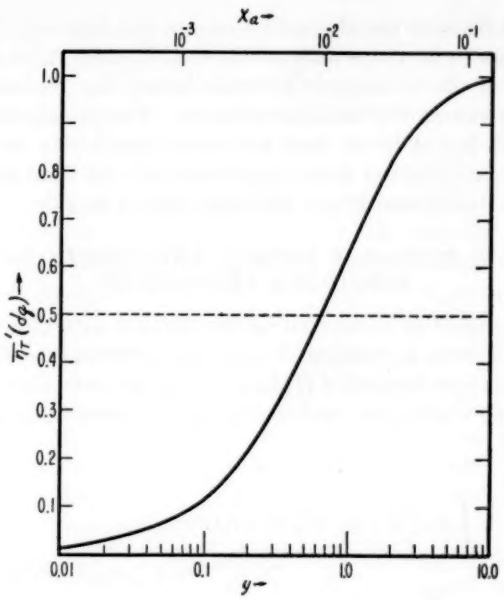

FIG. 2. Quantum yield for dq transfer as a function of the reduced concentration y of the activator, as in Fig. 1. Typical atomic concentrations are shown on the upper abscissa scale. Note the more rapid variation of $\bar{\eta}_T'$ with concentration in the dq case than in the dd case.

The integral has been evaluated numerically as a function of y and is shown in Fig. 2. Since concentrations x_a higher than 1 percent may be of interest in the dq transfer, it is not permissible to replace $\exp\pm(x_aC^+v_0)$ by unity in the general case, and consequently $\bar{\eta}_T$ is not a function of y alone in part of the range of interest. Figure 2 shows therefore the function $\bar{\eta}_T'(y)$, and for high concentrations ($x_a>1$ percent), $\bar{\eta}_T$ will require the indicated corrections. If we accept $\bar{\eta}_T'=\frac{1}{2}$ as the criterion for appreciable transfer, we find again that $y=0.65$ determines a critical concentration, $x_a{}^*=0.65/\gamma C^+$. In a typical case [Eq. (25)] we may expect $E=5$ ev, $n^6=13$, $\tau_a=0.1$ sec, $g_a'/g_a=5$, $\int f_s(E)F_a(E)dE=1/(3\text{ ev})$, and $C^+=2.25\times10^{22}$ cm^{-3}, so that γ becomes 3×10^{-21} cm^3 and x_a is 0.96×10^{-2}. Thus S may be expected to sensitize about 100 sites. As is to be expected from the stronger R dependence in the dq case, $\bar{\eta}_T'$ is a somewhat more rapidly varying function of x_a in the dq case than in the dd case. The discussion of the temperature dependence given in the last section is also applicable to dq transfer.

One final remark should be made regarding the function $F_a(E)$, the absorption shape function for A. This function cannot be determined directly from experi-

ment because the absorption cannot be observed. Some idea as to its shape may be inferred in some cases from that of the observable emission band, but the energy of its center will still be unknown. The calculation of $F_a(E)$ is a difficult task, but some qualitative success may be expected from application of the methods of Lax, Huang and Rhys, Williams, and others.[28]

V. EXCHANGE EFFECTS AND ADDITIONAL FORBIDDEN TRANSITIONS

We shall be concerned in this section with effects of the electron spin and shall therefore write out explicitly the matrix element of H_1 in terms of the wave functions $\psi(\mathbf{r}, \boldsymbol{\sigma})=\varphi(\mathbf{r})\chi(\boldsymbol{\sigma})$, where $\chi(\boldsymbol{\sigma})$ are the spin wave functions.

$$\langle H_1\rangle=\int \varphi_s'^*(\mathbf{r}_1)\varphi_a^*(\mathbf{r}_2)H_1\varphi_s(\mathbf{r}_1)\varphi_a'(\mathbf{r}_2) \times\chi_s'^*(\boldsymbol{\sigma}_1)\chi^*_a(\boldsymbol{\sigma}_2)\chi_s(\boldsymbol{\sigma}_1)\chi_a'(\boldsymbol{\sigma}_2) -\int \varphi_s'^*(\mathbf{r}_1)\varphi_a^*(\mathbf{r}_2)H_1\varphi_a'(\mathbf{r}_1)\varphi_s(\mathbf{r}_2) \times\chi_s'^*(\boldsymbol{\sigma}_1)\chi_a^*(\boldsymbol{\sigma}_2)\chi_a'(\boldsymbol{\sigma}_1)\chi_s(\boldsymbol{\sigma}_2).$$

The first term in $\langle H_1\rangle$ is the Coulomb term with which we have been concerned in the last two sections. Since in the approximation of Eq. (6) H_1 does not operate on the χ's, we see the previously mentioned selection rule against spin-flip transitions, i.e., unless $\chi_s'=\chi_s$ and $\chi_a=\chi_a'$, the first integral vanishes. Thus all our results so far are applicable only to transitions in which all the spins are unchanged. The second integral is an exchange integral with $H_1=e^2/\kappa r_{12}$. Ignoring the χ's for the moment, we see that this integral merely represents the electrostatic interaction between the two charge clouds $Q'(\mathbf{r}_1)=\varphi_s'^*(\mathbf{r}_1)\varphi_a'(\mathbf{r}_1)$ and $Q(\mathbf{r}_2)=\varphi_a^*(\mathbf{r}_2)\varphi_s(\mathbf{r}_2)$; since each function φ dies off exponentially with distance from S or A, it is clear that each product Q will be very small throughout all space unless S and A have small separation. If the separation is small, both functions Q will be sizeable in the same region of space, namely, between S and A where r_{12} is small; thus the integral $\int Q'(\mathbf{r}_1)(1/r_{12})Q(\mathbf{r}_2)d\tau_{12}$ may well be sizeable (for small R) even though the overlap integrals $\int Q(\mathbf{r})d\tau$, which enter in normalization, are negligibly small.

Let us now look at the selection rules in the exchange integrals. Unless $\chi_s'=\chi_a'$ and $\chi_a=\chi_s$ the integral vanishes. However χ' is not necessarily equal to χ, so that the spin functions on both atoms may change simultaneously. If such a transition is forbidden on S (or A) by the Pauli principle, however, the spin function on A (or S) may not change either.

Other selection rules occur in the exchange integrals over the spatial variables, but in each case they forbid only specific transitions and do not preclude all transitions in any symmetry class. Thus, although all Coulomb integrals may vanish, exchange will allow transfer to and excitation of A by all types of allowed and forbidden transitions, including, for example, $L=0$ to $L=0$ transitions.

The transfer probability by the exchange mechanism may be written in the form

$$P_{sa}(ex)=(2\pi/\hbar)Z^2\int f_s(E)F_a(E)dE, \qquad (28)$$

where Z^2, a quantity that cannot be directly related to optical experiments, is defined by

$$Z^2=\sum_I\sum_F \frac{e^4}{g_s'g_a\kappa^2}\left|\int Q'(\mathbf{r}_1)\frac{1}{r_{12}}Q(\mathbf{r}_2)d\tau_{12}\right|^2_{IF}. \qquad (29)$$

Note that the φ's and Q's are normalized over space (and not on an energy scale) so that Z^2 has the dimensions of energy squared. The separation and concentration dependences are hidden in Z^2, which varies approximately as $Y(e^4/\kappa^2R_0^2)\exp(-2R/L)$, where L is an effective average Bohr radius for the excited and unexcited states of the atoms S and A, and Y is a dimensionless quantity $\ll 1$ which takes account of the cancellation as a result of sign changes in the wave functions. If S and A occupy nearest like lattice sites in an ionic crystal such as NaCl, a typical transfer time would be of the order $10^{-10}-10^{-11}$ seconds; if S and A occupy second nearest like lattice sites, the probability would be reduced by a factor of the order of 10^{-2}. In insulators with large dielectric constants the excited state wave functions may extend over very large volumes, so that Q' is sizeable even for R of the order 2 or 3 R_0; nevertheless the ground-state wave functions are relatively little influenced by the dielectric constant, are much more compact, and make Q negligibly small for $R\sim 2R_0$. Thus it seems unlikely even in a crystal of large κ that exchange may transfer excitation energy farther than the shell of third nearest like lattice sites. The NaCl structure contains, in the first shell, 12, in the second shell, 6, and in the third shell, 24 like lattice sites. Thus probably about 40 is an upper limit for the number of sites sensitizable by the exchange mechanism, or in other words the exchange mechanism is slightly less efficient than is dq transfer.

Another type of transfer mechanism may be investigated by including magnetic fields in the Hamiltonian. We may thereby obtain transfer by an electric dipole-magnetic dipole (em) process. The probability for this process will be seen to be negligibly small compared to that for exchange transfer when exchange is allowed by the spin selection rules.

The most important term in H_1 involving the magnetic field is of the form

$$\frac{e\hbar}{2mc}\mathbf{H}\cdot(\mathbf{r}_a\times\boldsymbol{\nabla}_a+i\boldsymbol{\sigma}_a),$$

[28] See M. Lax, J. Chem. Phys. **20**, 1752 (1952) for further references.

where $\mathbf{H}$ is the magnetic field at A due to the motion of charge at S. The largest term in $\mathbf{H}$ is of the order $(e/c)\mathbf{R}\times\mathbf{v}_s/R^3$, or $(eh/mc)\mathbf{R}\times\boldsymbol{\nabla}_s/R^3$. Thus $\langle H_1\rangle$ has the magnitude $(e^2h^2/2m^2c^2R^2)\langle\boldsymbol{\nabla}_s\rangle$ or, since $\langle\boldsymbol{\nabla}_s\rangle=mE\langle\mathbf{r}_s\rangle/\hbar^2$, we find

$$|\langle H_1(em)\rangle|^2/|\langle H_1(dd)\rangle|^2\sim(e^2/\hbar c)^4E^2/(e^2/R)^2. \quad (30)$$

For nearest neighbors therefore the *em* transfer probability is of the order 10^{-8} times that for the *dd* process, or of the order 10^4 sec^{-1}, and is clearly negligibly small.

VI. HOST-SENSITIZATION

From the viewpoint of the theory of solids, sensitization by the lattice itself rather than by impurities is the more interesting type, since such experiments are in principle capable of yielding information characteristic of the pure lattice, specifically information about excitons. Most of what has been said in the last four sections is likewise applicable to host-sensitization, except for the obviously nonvalid assumption that x_s is small enough that $S-S$ transfers do not occur. In general the transition in S will be an allowed, electric dipole transition as before; however, with concentrations x_s equal to unity a magnetic dipole transition in S having a probability $\sim10^{-5}$ that of an allowed transition will give rise to an absorption coefficient of the order 10 per cm, so that appreciable radiation may be absorbed in a 1-mm thick crystal. In the latter case of course the transfer mechanism from S to S is by exchange, and similarly from S to A. If S has an allowed transition the transfer mechanism will usually be a *dd* process from S to S and, depending on the degree of forbiddenness of the transition in A, either a *dd* process, a competition between *dq* and exchange, or exchange from S to A. For the same reasons as previously mentioned, transfer from A to S will in many cases be highly improbable because of relaxation effects.

It is important to distinguish between two types of exciton propagation from S to S. In one case, where the transition in S is strong, with an oscillator strength of order unity, the jump time is of the same order as, or shorter than, nuclear readjustment times, namely, 10^{-13} sec [see Eq. (16)]; in this case step 2 in Sec. II, i.e., lattice relaxation, does not occur, and S' remains in resonance with all other S atoms so that P_{ss} is not greatly influenced by the temperature. (With the effective mass of the exciton independent of T and its kinetic energy proportional to kT for high T, its velocity and hence reciprocal jump time vary as $T^{\frac{1}{2}}$, after the exciton becomes thermalized.) For this type of transfer the use of configurational coordinates, based on the adiabatic approximation, is not justified.[29] Thus the exciton travels rapidly through the lattice, being scattered frequently by lattice vibrations, until it is thermally decomposed,[30] until it recombines optically or thermally, or until it meets with an imperfection.[21] If the transition in A is in resonance with that in S, the probability of transfer to A is large, $\sim10^{13}$ sec^{-1} for nearest neighbors if A has an allowed transition, $\lesssim10^{11}$ sec^{-1} if not. In the former event there is likewise high probability for transfer back to some S before the occurrence of lattice relaxation which would end the transfer process. In the latter case the transfer probability P_{sa} will in general be less than, say, 10^{-1} or 10^{-2} times the probability that the energy will be transferred to another S; on the other hand the distortion of the lattice associated with the presence of A may tend to keep the exciton in its vicinity, and of course if $S-A$ transfer should occur, nuclear readjustments would have time to occur and would assist in preventing transfer back to an S atom. Both of these effects will tend to keep the efficiency of sensitization high.

In the second type of propagation, where the oscillator strength for the transition in S is small, nuclear readjustment will take place on S before transfer occurs. In this case P_{ss} may be strongly temperature dependent (except at low T) since the excited atom S' in the relaxed lattice may be far from resonance with its neighbors S. The exciton will in this case move with an effective mass characteristic of nuclear masses, and P_{ss} may be reduced by many orders of magnitude from that for the other case discussed. If A is in resonance with the excited S in the relaxed lattice, however, P_{sa} may still be of the same magnitude as above, namely, $10^{13}-10^{10}$ sec^{-1} depending on the forbiddenness of the transition.

For either type of propagation S to S, the dependence of $\bar{\eta}_T$ on x_a is complicated greatly by the existence of other mechanisms for destroying the excitons. If thermal annihilation is unimportant, we might expect $\bar{\eta}_T$ to become and remain close to unity for $x_a\gg$ the concentration of other imperfections x_i since, experimentally, radiative processes in S are usually unimportant for x_i as small as attainable. For appreciable transfer to occur when thermal processes are important, however, the concentration x_a must be sufficiently large that $(x_aC^+)^{-\frac{1}{3}}$ is as small as the diffusion length of the exciton.

The temperature dependence of P_{sa} is about the same as was discussed in Sec. III, with the added complication that with increasing temperature the trapping of the exciton around A becomes less probable. The temperature dependence of P_{ss} may be weak, as in the first type of $S-S$ transfer above, or may be strong and complicated as for P_{sa}, in the second type. Botden[12] has presented an interpretation of host-sensitization data on Sm-activated $CaWO_4$ and $SrWO_4$ along the lines of Kröger's arguments[8] discussed in Sec. III. His interpretation of the temperature dependence is as follows: At low temperatures he believes that only the radiative energy absorbed at the tungstate (S) sites nearest neighbors to the Sm (A) can be transferred to the Sm and that the transfer occurs without an activation energy. From all other WO_4 sites, he supposes an activation energy to be required in order to transfer to

[29] R. Peierls, Ann. Physik **13**, 905 (1932).
[30] Paul Leurgans, thesis, to be published.

the nearest WO_4 sites, so that at higher temperatures ($\lesssim$200K) the quantum yield increases. In order to explain the low temperature behavior Botden postulates *ad hoc* that in the $S-A$ transfer the Sm is raised to an excited electronic state exactly in resonance with the WO_4 transition, from which it jumps to a lower excited electronic state and from which finally the Sm emits. An alternative interpretation may be made which avoids the above assumption and still fits the temperature data: The postulate of more than one excited electronic state is unnecessary since relaxation around the Sm will prevent back-transfer, and the assumption of precise resonance to explain the absence of a temperature dependence at low temperature is unnecessary since thermal broadening of absorption and emission lines is small in comparison with zero-point widths at low T.

In the above system the oscillator strength for the transition in S is small, since the transition probability in the WO_4 group is $\sim 10^5$ per sec. Thus the second type of $S-S$ transfer is operative, and as we have seen above and in Section III, this type of transfer will also have a probability independent of T for low T. We might expect then a total probability of transfer from the initial tungstate ion to the Sm to depend on the temperature through a factor of the type $\exp-(W_{sa}+nW_{ss})/kT^*$, where n is the number of $S-S$ transfers required. A simple dependence such as this is to be expected only when complicating factors of the type discussed in Section III are unimportant.

VII. CONNECTION WITH EXPERIMENT

Sensitized luminescence experiments on the simplest transfer mechanism discussed above, namely, the *dd* transfer mechanism, do not seem to have been reported in the literature for simple inorganic systems. Probably this experiment has been neglected for two reasons: (1) If A has an allowed transition, it can absorb radiation itself and hence requires no sensitizer in order to be excited. It should be recalled, however, that the second reason for the practical interest in sensitization, namely, a double degradation of the energy, is still operative, so that, for example, the 2537 Hg line could be used to excite visible emission of short lifetime in the event that two sizeable Stokes' shifts ($\sim$1 ev each) can be employed. (2) In some experimental systems there might be difficulty in distinguishing *dd* transfer from a cascade phenomenon. In the latter process, where a photon is emitted by S and reabsorbed by A, the quantum yield for transfer depends not on the concentration x_a alone but also on the size and shape of the system. Neglecting *dd* transfer, we find the quantum yield for transfer by the cascade mechanism is equal to

$$\bar{\eta}_T(C)=Av\int f_s(E)[1-e^{-C+x_a l\sigma(E)}]dE,$$

where the average is performed over the linear dimension l of the sample. $1-\bar{\eta}_T(C)$ is the probability that a photon emitted from S will leave the system. We neglect $S-S$ transfer of all types. Note that the critical concentration for this process varies inversely as the strength of the transition in A and inversely as the average size of the sample. See Eq. (20) for a comparison with *dd* transfer. The quantity x_aC^+l represents the number of activators per cm squared projected on a plane perpendicular to the path of the photon. In a spherical system of a given volume containing a given concentration x_a the quantum yield will be much larger than for the same system flattened out into a thin film. We found $\bar{\eta}_T(dd)$ to be independent of the shape of the sample, or of its size. As an example to illustrate the orders of magnitude involved, let us consider a spherical sample of 1-mm radius, containing a concentration $x_a=3\times10^{-4}$. Let us further assume the system to be characterized by those parameters given in Sec. III so that $\bar{\eta}_T(dd)$ is equal to $\frac{1}{2}$. For convenience let us assume that both $f_s(E)$ and $\sigma(E)$ are step functions each 1 ev wide, and that they overlap by $\frac{1}{3}$ ev. These specific assumptions are in agreement with the value of the overlap integral between emission and absorption assumed in Sec. III. We find $\bar{\eta}_T(C)$ to be $\frac{1}{3}$, as corresponds to the circumstance that practically all of the radiation emitted in a frequency range which can be absorbed by A is absorbed, and all the rest is transmitted. If the concentration x_a is increased to 3×10^{-3}, $\bar{\eta}_T(dd)$ is increased to almost 1 (see Fig. 1), but $\bar{\eta}_T(C)$ is still $\frac{1}{3}$. This example serves to illustrate the difference in the dependence of the two transfer mechanisms upon overlap of emission and absorption. If the emission band of S were 1 ev wide and the absorption band of A were 3 ev wide and covered the S emission range, the overlap integral $\int f_s(E)F_a(E)dE$ would be unchanged, and hence $\bar{\eta}_T(dd)$ would be unchanged. On the other hand the quantum yield $\bar{\eta}_T(C)$ would now be >0.99 for $x_a>3.1\times10^{-5}$. If the sphere were flattened out into a thin film, say 10^{-4} cm thick, $\bar{\eta}_T(dd)$ would still be $\frac{1}{2}$ for $x_a=3\times10^{-4}$, but $\bar{\eta}_T(C)$ would be close to zero regardless of the particular shape of the overlap integrand.

Thus the two distinctions between cascade and resonant transfer occur in the dependence of the cascade transfer probability on the size and shape of the sample and on the details of the overlap of the absorption and emission spectra of A and S. Cascade effects can be made unimportant experimentally by dealing with thin samples of systems in which the overlapping of spectra is poor. For further discussion of this topic the reader is referred to reference 19(b), (c).

A second point should be emphasized in connection with the *dd* transfer: Because of the high efficiency of the transfer mechanism, it should be possible to utilize as a sensitizer an impurity which, even when present by itself, will not luminesce appreciably because of competing nonradiative processes. For example, let the thermal lifetime be denoted by τ_N, so that the quantum

yield for transfer becomes

$$\bar{\eta}_T' = \int_0^\infty \frac{\tau_s P_{sa} x_a C^+ dv e^{-x_a C+v}}{1+\tau_s/\tau_N+P_{sa}\tau_s}.$$

The value of the integral is given by Eq. (19) in which y is to be replaced by $y(1+\tau_s/\tau_N)^{-\frac{1}{3}}$. Hence if nonradiative processes within S are one hundred times more probable than emission from S, a concentration x_a ten times larger than the value of 3×10^{-4} obtained previously will result in efficient transfer. Thus though S, when present alone in the lattice, may luminesce with an efficiency as low as one percent, it may still serve as an excellent sensitizer for several hundred lattice sites. These considerations have only partial applicability to the *dq* and exchange processes. If $\tau_s/\tau_N\sim10^2$, concentrations of the order ten percent are required for appreciable transfer.

An experimentally important process has so far been entirely neglected, i.e., concentration quenching.[30a] Although the precise mechanism for this process is not understood, it is nevertheless clear experimentally that quenching effects occur for concentrations x_a as large as those required for efficient transfer by means of the *dq* and exchange mechanisms. Thus it is impossible in many cases to isolate experimentally the $S-A$ transfer process from quenching phenomena. This circumstance is a further argument for the investigation of simple *dd* systems in attempting to understand sensitized luminescence in general; such systems might consist of impurities such as Tl, Pb, Ag, Cu in the alkali halide lattices.

One of the commonly used luminescent impurities is Mn, which exhibits visible emission in a wide variety of host lattices,[6–11,31] as well as in manganese salts.[8,32] Klick and Schulman[32] have compared the absorption spectrum of Mn^{++} in $MnCl_2$ with the atomic absorption spectrum, and have correlated the levels in solids with the corresponding levels in the isolated atoms. This correlation shows a number of spin-flip and quadrupole transitions in the wavelength range of 2370–5500A; these transitions are probably those of importance in the process of transfer to Mn when used as an activator. It seems probable that the Mn ion when excited by any of these transitions is able to undergo nonradiative transitions into the lowest excited electronic state, from which it emits with a large Stokes' shift. It is difficult in practice to distinguish transfer by the *dq* process from that by the exchange process (which alone may excite the Mn in a spin-flip transition) since the critical concentration of Mn would be of the same order of magnitude for both processes and since the absorption shape $F_a(E)$, and hence P_{sa}, are unknown. Quenching effects will also make difficult such a separation. If in any particular case the critical concentration turns out to be $\gtrsim$ one percent, it would appear safe to assert that transfer is by the *dq*, rather than the exchange, process; if x_a is $>$ two percent it might *a priori* be either mechanism if both types of levels were known to exist in the general energy region capable of exciton by S. Critical concentrations of Mn of the order of three percent have been observed experimentally in $CaSiO_3$:Pb+Mn[9,11] and in $Ca_3(PO_4)_2$:Ce+Mn.[9] Botden and Kröger[9] have assumed that transfer may occur only to nearest neighbors and have accepted the relatively low critical concentration of Mn as evidence for the preferential formation of pairs Ce+Mn and Pb+Mn. Since transfer is not restricted to nearest neighbors, however, preferential pair formation is not necessarily indicated by these experiments.

From host-sensitization experiments one hopes to obtain information on several aspects of excitons: (1) From the use of activators with measurable absorption spectra can be determined the amount of Stokes' shift, if any, within the host-sensitizer. Since most pure lattices do not emit, the above information is not obtainable by direct means. (2) By varying the concentration x_a the diffusion length of the exciton may be found. (3) If such measurements are made as a function of temperature, indirect evidence may be inferred as to the thermal processes of the exciton. (4) Experiments that utilize directly the detecting properties of the activator for excitons may readily be imagined. For example, assume that a suitable activator has been found, say in the course of experiment (1) above, such that upon its introduction as an impurity some particular crystal becomes luminescent upon irradiation in the first fundamental absorption band. Then evaporate onto one face of a thin "perfect" crystal a layer of the same material containing the activator in high concentration, irradiate the other face of the crystal in the first fundamental absorption band, and measure the resulting luminescence. For a crystal of thickness much greater than 10^{-6} cm essentially none of the incident light will remain unabsorbed, and if luminescence is observed on the back face (and if photoconductivity is absent) the excitons must have travelled through the crystal. Such an experiment is in principle capable of measuring directly the diffusion length for an exciton, and if successful would be the first experimental proof of its motion. (The elegant experiments by Apker and Taft[33] on alkali halides were performed with a concentration of imperfections so large that, were there reasons to doubt the motion of excitons, the same interpretation[21] which has been based on their motion could

[30a] A manuscript is in preparation discussing concentration quenching from the point of view of resonance transfer of energy, i.e., S–S transfer, in ordinary systems containing one impurity. It is concluded that S–S transfer is the critical process for systems of low dielectric constant and small Stokes' shift.

[31] F. A. Kröger, *Luminescence in Solids Containing Manganese* (Van Campen, Amsterdam, 1940).

[32] C. C. Klick and J. H. Schulman, J. Opt. Soc. Am. **42**, 910 (1952).

[33] L. Apker and E. Taft, Phys. Rev. **83**, 479 (1951), and several earlier papers.

also be satisfactorily based on the nearness of every halide ion to a vacancy or F center.)

The difficulty of the above experiment of course resides in obtaining a "perfect" crystal sufficiently thin. An evaporated film would surely be so full of imperfections that the exciton's diffusion length would be less than or about the absorption depth of the incident light. If the diffusion length D in a good single crystal should be much larger than Heller and Marcus' estimate,[20] 10^{-4} cm, a crystal could probably be cleaved and annealed successfully, but if D is $<10^{-4}$ cm the experiment must await new methods of preparation of perfect thin films. Since the interaction between excitons and ionic crystals is large,[21,30] the experiment might best be performed with non-ionic materials.

The most thoroughly investigated systems so far reported are the tungstates of Cd and Zn and the tungstate and molybdate of Ca, all activated with Sm.[12] The WO_4 and MoO_4 ions are the sensitizers in these crystals. The interpretation by Botden and Kröger of the temperature dependence has been discussed above in Section VI, and modifications have been presented. Several tentative conclusions may be drawn from these experiments. With a radiative decay time of $\sim 10^{-5}$ sec in the WO_4 ion, or an oscillator strength of the order 10^{-3}, the exchange mechanism is probably the operative method for $S-S$ transfer, and in the absence of relaxation effects, each jump time would be perhaps 10^{-10} sec. However, the tungstate excitation and reflection spectra[12] indicate that the tungstate absorption peaks at $\lesssim$2400A, whereas the emission occurs at 4200A. Thus the lattice relaxation around the excited tungstate ion gives rise to a large Stokes' shift of 2.2 ev, throwing the excited tungstate ion far out of resonance with its neighbors. Consequently, we expect exceedingly slow migration of the energy from S to S, and, since the exciton must arrive within two or three shells of the Sm for $S-A$ transfer to occur, it is not surprising that the transfer yield is low ($\sim$5 percent) even for concentrations x_a as large as a tenth of a percent. The transfer to the Sm occurs by means of the short-range exchange mechanism since the transition within the Sm ion is forbidden, and that in the WO_4 ion is weak. That the Sm transition is a magnetic dipole transition is indicated by the decay time of the Sm luminescence, 10^{-3} sec, and by the weakness of the Sm absorption bands in the crystal. The relatively weak exchange mechanism is made still weaker by the poor overlap between the absorption of the Sm ion (centered at 3650A) and the WO_4 emission (4200A). We nevertheless expect a much higher probability for energy transfer from WO_4' to a nearby Sm than from WO_4' to WO_4 because of the large Stokes' shift in the tungstate ion.

Subsequent to the preparation of this manuscript a paper by Botden[34] has appeared, containing new experimental results for the impurity-sensitized systems $Ca_3(PO_4)_2$:Ce + Mn, $Sr_3(PO_4)_2$:Sn + Mn, $3Ca_3(PO_4)_2CaF_2$:Sb + Mn, $Ca_2P_2O_7$:Sn + Mn, and $CaCO_3$: (Pb or Tl)+Mn. Botden has analyzed his results on the basis of resonant transfer from S to A and includes S to S transfer in his interpretation. Experimentally he finds that about 30 or 40 sites may be sensitized by S, in agreement with our expectations above on the basis of the exchange mechanism (in the absence of an allowed transition in the Mn). He also finds experimentally that $S-S$ transfer may occur to one of the 150 nearest neighbors. Using Eq. (17) one may predict a critical separation of 23A. From the $Ca_3(PO_4)_2$ molecular weight (310) and macroscopic density (3.14 gm/cm^3), the present writer estimates the cation site concentration to be 1.8×10^{22} cm^{-3}, and thus about 1000 sites to be within 23A of the sensitizer. Such a discrepancy, about a factor of 6, would be too large to overlook in a careful interpretation. Since Botden's determination of the number of sites depends on the zeroth, first and second derivatives of the experimental curves of transfer efficiency *versus* S concentration, and depends in a complicated and unknown way on a number of drastic simplifying assumptions, it is probably not profitable to emphasize the discrepancy at this time.

In addition to the statistical analysis to obtain the number of sites sensitized by S, Botden[34] discusses the temperature dependence of the transfer probability along the same lines as in references 8 and 12. The same modifications are suggested here as were made to references 8 and 12 in Secs. III and VI.

ACKNOWLEDGMENTS

The writer takes great pleasure in expressing his appreciation to Mr. Paul H. Egli, Dr. Paul L. Smith, and to other members of the Crystal Branch for helping to make his stay at this laboratory both enjoyable and profitable. He is indebted to Dr. C. C. Klick and especially to Dr. J. H. Schulman for their kind interest in this work and for their many helpful discussions of experimental material. He would also like to thank the Applied Mathematics Group for the numerical integration of Eq. (27′).

[34] Th. Botden, Philips Research Rept. **7**, 197 (1952).

The Molecular Structure, Dipole Moment, and g Factor of Ozone from Its Microwave Spectrum*

R. TRAMBARULO,† S. N. GHOSH,‡ C. A. BURRUS, JR., AND W. GORDY
Department of Physics, Duke University, Durham, North Carolina

(Received December 8, 1952)

Four low-J rotational transitions of O_3^{16} have been measured in the region from 42 to 118 kmc. The rotational spectroscopic constants found are $A=106{,}530.0\pm1.1$ Mc, $B=13{,}349.06\pm0.06$ Mc, $C=11{,}834.3\pm1.1$ Mc. The oxygen nuclei form an isosceles triangle with an apex angle of $116°49'\pm30'$, and the two equal internuclear distances are 1.278 ± 0.003A. From the Stark splitting of the $2_{0,2}\rightarrow1_{1,1}$ transition the dipole moment is 0.53 ± 0.02 debye. Zeeman splittings of this transition show that ozone is not significantly paramagnetic.

INTRODUCTION

ALTHOUGH the structure of ozone has been the subject of many investigations, no consistent and definitive assignment of the molecular dimensions has been accomplished until the recent microwave investigations made by Hughes[1] of Westinghouse, and those made concurrently in this laboratory[2] and reported here.

By the electron diffraction method Shand and Spurr[3] assigned an apex angle of $127°\pm3°$ and the two similar O-O distances as 1.26 ± 0.02A. Although their assignment of the bond lengths is within the upper limit of their estimated error the apex angle which they assigned is 10° too large.

Difficulties have been encountered in assigning the fundamental vibrational frequencies from the infrared spectrum,[4,5] and it would appear from the fine structure of the vibrational bands examined by Adel and Dennison[4] that the apex angle is acute. However, the recent discovery of a new fundamental band by Wilson and Badger[6] favors a model with an obtuse apex angle.

In the microwave region from 9 to 44 kmc Hughes[1] identified eighteen rotational transitions of ozone for which two lines involved values of J lower than nine. From these results Hughes obtained an angle of 116.5°–117° and two like distances of 1.276–1.279A. In the present work three additional lines involving $J=4$ or lower were found and identified in the region from 96 to 118 kmc. These lines, along with the low-J transition at 42 kmc, allow the parameters of the molecule to be unquestionably assigned. Although only one transition, that at 42 kmc, included in our study was measured also by Hughes, his assignment of the structural parameters from the lower frequency lines which he measured are in essential agreement with our assignment from the high frequency low-J transitions. There is some discrepancy, however, in the two electric dipole moment determinations.

EXPERIMENTAL PROCEDURE

A Stark-modulation spectrograph[7] with 4 kc square wave modulation was employed. The cell was 94.5 cm long from window to window and was made of gold-plated K-band wave guide with a silver Stark electrode supported by Teflon spacers. Sources of energy were crystal harmonic generators[8] driven by Ratheon klystrons. Second, third, fourth, and fifth harmonics were utilized. At the higher frequencies the cell loss was about 10 db. To increase the strength of the lines the cell was cooled with dry ice. The absorption lines were detected by a Sylvania type 1N53 crystal and were displayed on a recorder preceded by a lock-in amplifier. Frequencies were measured with harmonics from a crystal controlled oscillator[9] which was monitored by comparison with station WWV.

Ozone was prepared in the small quantities required by passing a silent discharge through electrolytic oxygen which had been dried with sulfuric acid and phosphorus pentoxide. Oxygen was admitted to the discharge chamber to a pressure of about half an atmosphere. As ozone was formed, it was condensed with liquid air; and after the discharge had taken place for about 20 minutes, unconverted oxygen was pumped off. The ozone was admitted to the cell to pressures of about 10^{-1} mm of Hg from the discharge chamber which was cooled with liquid air. In preliminary experiments formaldehyde lines were found. The formaldehyde was apparently produced by reaction of the ozone with stopcock grease in the vacuum system.

* The research reported in this paper has been sponsored by the Geophysics Research Directorate of Air Force Cambridge Research Center, Air Research and Development Command.

† Present address: Department of Physics, The Pennsylvania State College, State College, Pennsylvania.

‡ On leave from the University of Calcutta.

[1] R. H. Hughes, Phys. Rev. **85**, 717 (1952); *Symposium on Molecular Structure and Spectroscopy*, Ohio State University, June 1952.

[2] Preliminary results given in Quarterly Progress Reports, Air Force Contract No. W19-122-ac-35, November, 1950, February, 1951, March, 1952.

[3] W. Shand and R. A. Spurr, J. Am. Chem. Soc. **65**, 179 (1943).

[4] A. Adel and D. M. Dennison, J. Chem. Phys. **14**, 379 (1946).

[5] D. M. Simpson, Trans. Faraday Soc. **41**, 209 (1945); J. Chem. Phys. **15**, 846 (1947).

[6] M. K. Wilson and R. M. Badger, J. Chem. Phys. **16**, 741 (1948).

[7] R. H. Hughes and E. B. Wilson, Jr., Phys. Rev. **71**, 562 (1947).

[8] The multipliers used in most measurements were modified forms suggested by C. M. Johnson of crossed wave-guide designs already described. For references to the earlier designs see Johnson, Trambarulo and Gordy, Phys. Rev. **84**, 1178 (1951).

[9] R. R. Unterberger and W. V. Smith, Rev. Sci. Instr. **19**, 580 (1948).

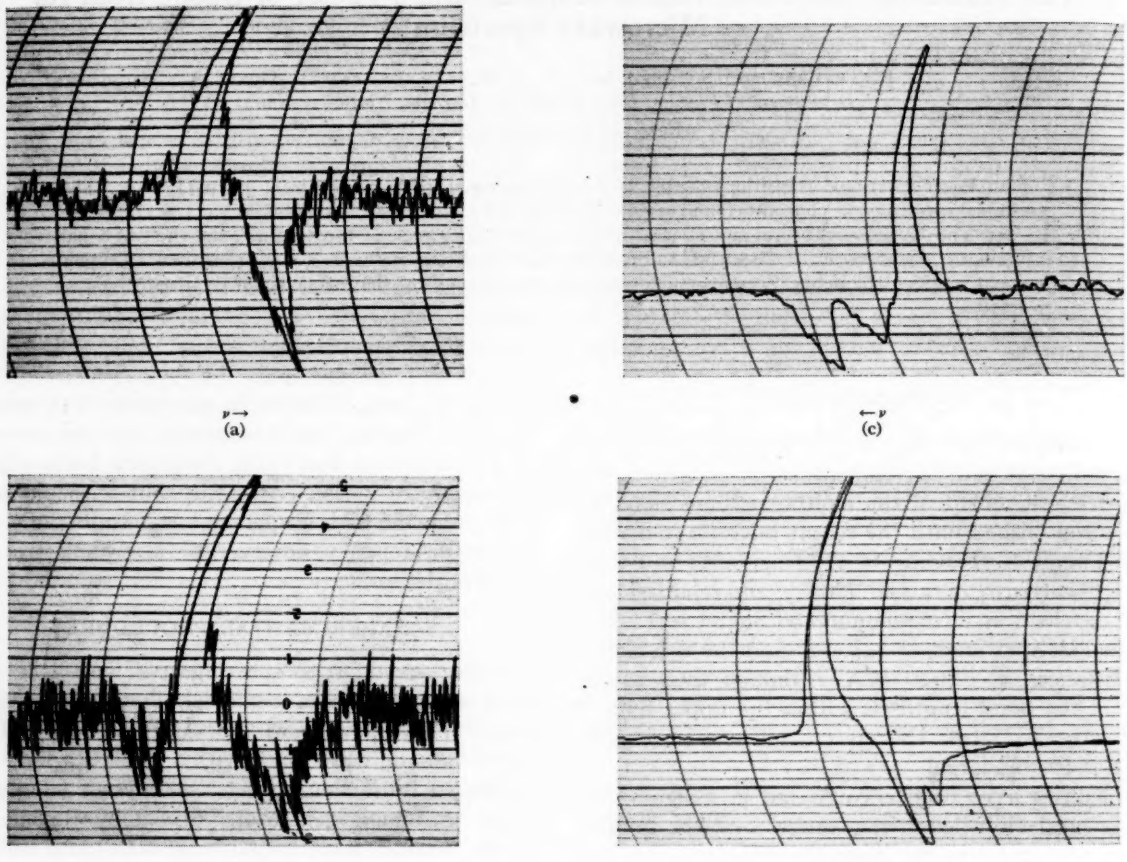

FIG. 1. Recordings of four low-J ozone lines and their Stark components. (a) The $0_{0,0}\rightarrow 1_{1,1}$ transition at 118 364 Mc. (b) The $4_{0,3}\rightarrow 4_{1,3}$ transition at 101 736 Mc. (c) The $2_{0,2}\rightarrow 2_{1,1}$ transition at 96 229 Mc. (d) The $2_{0,2}\rightarrow 1_{1,1}$ transition at 42 833 Mc. Stark components point downward, undisplaced line upward.

Ozone lines appeared immediately upon introduction of the gas to the cell, and they gradually became weaker, whereas formaldehyde lines did not appear until after several minutes and grew stronger. This behavior served as a convenient means of distinguishing new ozone lines from those of formaldehyde.

The $2_{0,2}\rightarrow 1_{1,1}$ transition near 43 kmc was split by a magnetic field of about 3000 oersteds which was formed by placing nine similar magnetron magnets side by side with soft iron strips linking the similar pole pieces of each individual magnet. By arranging the magnetron magnets and by placing shims between their pole pieces and the iron strips, it was possible to attain a field which varied by less than 5 percent over a distance of 60 centimeters. This magnet could be oriented along the wave-guide cell with the field parallel to either the wide or narrow dimension of the guide.

THE OZONE SPECTRUM

Recordings of the four low-J lines are shown in Fig. 1. Frequencies of the lines and identifications are given in Table I. Also listed in Table I is the harmonic of the klystron frequency used to obtain each line. The transitions were identified as to the values of J involved from the Stark patterns and as to the particular sublevels from a comparison with the energy level scheme. Since the O^{16} nucleus has a spin of zero and ozone has a C_{2v} symmetry, with the dipole moment along the axis of intermediate moment of inertia, only $++$ and $--$ levels are possible. This restriction prevents ozone from having more lines of low J in the microwave region.

Table II lists the spectroscopic constants A, B, C and the asymmetry parameter, $\delta=(B-C)/(A-C)$, which were obtained from the three transitions, $0_{0,0}\rightarrow 1_{1,1}$, $2_{0,2}\rightarrow 1_{1,1}$, and $2_{0,2}\rightarrow 2_{1,1}$, with centrifugal distortions neglected. Errors listed result from uncertainties in the

TABLE I. Observed transitions of ozone.

Transition	Frequency (Mc)	Klystron harmonic used
$2_{0,2}\rightarrow 1_{1,1}$	42 832.62±0.07	2
$2_{0,2}\rightarrow 2_{1,1}$	96 228.84±0.18	4
$4_{0,4}\rightarrow 4_{1,3}$	101 736.83±0.14	3
$0_{0,0}\rightarrow 1_{1,1}$	118 364.3 ±0.5	5

line frequency measurements. From the constants so obtained, the $4_{0,4}\rightarrow 4_{1,3}$ transition is calculated to occur at 101,738.63 Mc as compared with the measured frequency of 101,736.83 Mc. This small discrepancy results partly from centrifugal distortions.

MAGNETIC SPLITTINGS OF THE $2_{0,2}\rightarrow 1_{1,1}$ TRANSITION

It is difficult to measure accurately the paramagnetic susceptibility of liquid ozone because of the presence of small amounts of dissolved oxygen which is strongly paramagnetic. Nevertheless from susceptibility measurements Laine[10] obtained evidence which he interpreted to indicate that ozone is slightly paramagnetic. A sensitive indicator of paramagnetism, one which is not influenced by paramagnetic impurities, is the Zeeman splitting of microwave absorption lines. As is seen from Fig. 2, the Zeeman splitting of the $2_{0,2}\rightarrow 1_{1,1}$ rotational line of ozone is not very large at a field strength of about 3 kilo-oersteds, and consequently ozone is at most only weakly paramagnetic. The analysis of this splitting given below indicates that the magnetism of ozone arises principally from its molecular rotation. Evidently the electronic ground state of ozone is $^1\Sigma$.

For the alternating electric field vector parallel to the stationary magnetic field $\Delta M=0$ transitions (π-type) are induced while $\Delta M=\pm 1$ transitions (σ-type) occur for the electric field vector perpendicular to the imposed magnetic field. The shifts, $\Delta\nu$, in the transition frequency for the two magnetic field orientations are

$$\Delta\nu(\pi)=-M(g'-g)\beta_I H/h$$

and

$$\Delta\nu(\sigma)=-(M'g'-Mg)\beta_I H/h,$$

where the primes correspond to the upper rotational state of the transition and β_I is the nuclear magneton. Other symbols have the usual significance. Thus, if the g factors of the two rotational states are sensibly different, and neither is equal to zero, three lines are expected for the π-transition and six for the σ-transition from the $2_{0,2}$ to the $1_{1,1}$ levels. However, only three resolved lines are observed for the σ-transition [Fig. 2(a)]. This can be explained if the g factor for the $2_{0,2}$ state is much smaller than that for the $1_{1,1}$ state. The

TABLE II. Molecular constants of ozone.

$A=106\,530.0\pm 1.1$ Mc	$I_a=7.8749\times 10^{-40}$ g cm^2
$B=13\,349.06\pm 0.06$ Mc	$I_b=62.844\times 10^{-40}$ g cm^2
$C=11\,834.3\pm 1.1$ Mc	$I_c=70.888\times 10^{-40}$ g cm^2
$\delta=0.015996\pm 0.000012$	
Electric dipole moment $\mu=0.53\pm 0.02$ debye	
g factor $=1.54\pm 0.09$ n.m. for $1_{1,1}$ state	
$=0.15\pm 0.03$ n.m., for $2_{0,2}$ state	
Structure: isosceles triangle	
Two equal OO bond lengths $=1.278\pm 0.003$A	
Angle between bonds $=116°49'\pm 30'$	

[10] P. Lainé, Ann. phys. **3**, 461 (1935).

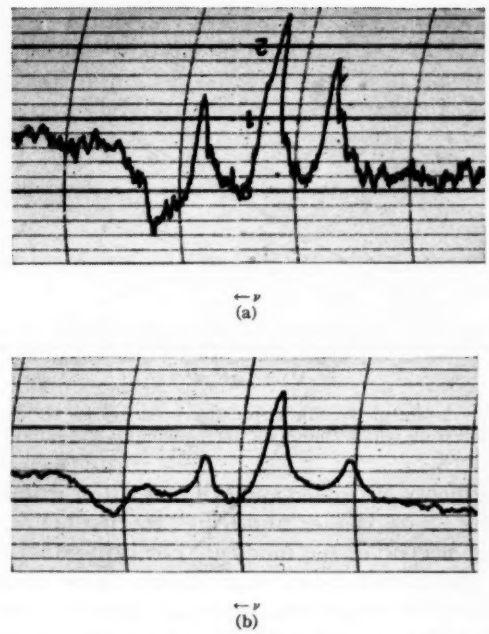

(a)

(b)

FIG. 2. Zeeman splittings of the $2_{0,2}\rightarrow 1_{1,1}$ transition of ozone. Stark components have been pulled out far enough not to interfere with the magnetic splitting of the lines. (a) Magnetic field perpendicular to the electric component of the radiation. (b) Magnetic field parallel to the electric component of the radiation.

center line on each tracing of Fig. 2 is more intense than would be expected since the magnetic field included only 65 percent of the absorbing path of the radiation. For a field of 2.93 ± 0.07 kilo-oersteds the component spacing for the σ-transitions is 2.78 ± 0.05 Mc and for the π-transitions is 3.12 ± 0.05 Mc. If it is assumed that the g factors of both rotational states have the same sign, then the factors are 1.54 ± 0.09 for the $1_{1,1}$ state and 0.15 ± 0.03 for the $2_{0,2}$ state. The large dependence of g factors upon the rotational state is interesting. The g factor for the $1_{1,1}$ state of ozone is considerably larger than those found by Jen[11] for other molecules in singlet sigma-states. If the ozone magnetism arises from contributions of excited electronic states, then the electronic structure of the molecule depends to a surprising extent upon rotation. From the formal charges on the atoms in the most probable electronic ground state (see structures I and II below) one would expect a significant magnetic moment to be generated by rotation about the symmetry axes.

ELECTRIC DIPOLE MOMENT

Stark splitting of the $2_{0,2}\rightarrow 1_{1,1}$ transition yield a value of the dipole moment of 0.53 ± 0.02 debye which is in agreement with the values 0.49 debye found by Lewis and Smyth[12] and 0.52 debye reported by Epprecht,[13] but not with the value 0.65 ± 0.05 debye given by Hughes.[1]

[11] C. K. Jen, Phys. Rev. **81**, 197 (1951).
[12] G. L. Lewis and C. P. Smyth, J. Am. Chem. Soc. **61**, 3063 (1939).
[13] G. W. Epprecht, Z. angew. Math. Physik **1**, 138 (1950).

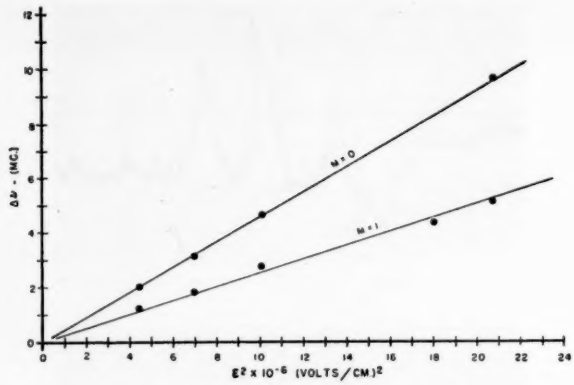

FIG. 3. A plot of the Stark splitting versus $\mathcal{E}^2$ for the $2_{0,2}\rightarrow 1_{1,1}$ transition from which the dipole moment of O_3 was obtained.

The theory of Golden and Wilson[14] with the intensity tables of Cross, Hainer, and King[15] was used in evaluating the electric dipole moment. For calibration of the Stark spectrometer, OCS with known dipole moment[16] 0.7085 ± 0.004 debye was employed. Since the observed Stark effect is second order, the plot of the component displacements against the field strength squared, $\mathcal{E}^2$, is a straight line. With the imposed field parallel to the electric vector of the microwave radiation only $\Delta M=0$ components are observed. Figure 3 shows a plot of the line splitting *versus* $\mathcal{E}^2$ for the $2_{0,2}\rightarrow 1_{1,1}$ transition from which the dipole moment was obtained.

THE MOLECULAR DIMENSIONS

The three principal moments of inertia and other properties are given in Table II. For a rigid planar molecule the moment of inertia I_c should be the sum of the moments I_a and I_b; however, in the ground vibrational state this relationship breaks down because of zero-point vibrations. A measure of this departure is the quantum defect, $I_c-(I_a+I_b)$ which for ozone is 0.169×10^{-40} g cm^2.

The molecular structure obtained from our results is an isosceles triangle with 1.278 ± 0.003A for the two similar sides and an apex angle of $116°49'\pm30'$. These values represent the mean of the structures calculated from the three moments of inertia taken two at a time, and the errors quoted are the maximum deviation from the mean.

ELECTRONIC STRUCTURE

The molecular dimensions and dipole moment of ozone throw light on the complex electronic structure of the molecule. Qualitatively, the electronic structure can be discussed most conveniently in terms of the valence bond resonance concepts of Pauling. The most reasonable contributing structures are I and II with perhaps small contributions from III and IV. The observed bond angle is near the 120° trigonal bonds formed by sp^2 hybrid orbitals. This and other facts suggest that to a first approximation the four valence orbitals of the apex oxygen consist of three sp^2 hybrids which lie in a plane and a pure p orbital which is normal to this plane. Two of the sp^2 orbitals presumably form bonds to the two end oxygens in all forms I–IV, and the p orbital forms the second component of the double bond in forms I and II. The third sp^2 hybrid of the apex oxygen is directed upward along the symmetry axis and has an unshared electron pair in all forms I–IV.

It is significant that the bond length in ozone, 1.278A, is intermediate between the double bond length in oxygen, 1.21A, and the single bond length in hydrogen peroxide, 1.47A. It is somewhat nearer, however, to the double bond than to the single bond value. The observed lengths with the Pauling rule[17] indicate that the bonds have almost 50 percent double bond character. Thus the two equivalent resonating forms I and II essentially represent the electronic structure of ozone. The fact that the apex angle is slightly less than 120° may, however, indicate some contributions from forms III and IV because the unlike charge on the end oxygens in these forms would tend to decrease the apex angle.

In molecular orbitals terminology, each of the bonding sp^2 orbitals would form a localized σ-molecular orbital by combination with a bonding orbital of an end oxygen, while the p orbital would be combined with orbitals of both end oxygens to form π-molecular orbitals. The electrons in the π-orbitals are not then considered as localized in a pair bond, as in the hypothetical forms I and II, but as moving throughout the molecule. If the π-molecular orbital is represented by the linear combination,

$$\psi=a\psi_1+b\psi_2+c\psi_3,$$

of the atomic orbital where ψ_1 refers to the apex oxygen, then from the previous structural considerations it is evident that $b^2=c^2\approx a^2/2$.

If it is assumed that the positive and negative charges in I and II are separated by the bond length, the primary dipole moment resulting from these forms

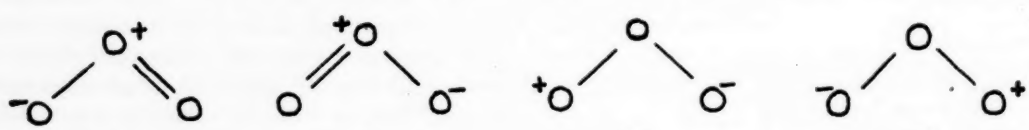

I II III IV

[14] S. Golden and E. B. Wilson, Jr., J. Chem. Phys. **16**, 669 (1948).
[15] Cross, Hainer, and King, J. Chem. Phys. **12**, 210 (1944).
[16] R. G. Shulman and C. H. Townes, Phys. Rev. **77**, 500 (1950).
[17] L. Pauling, *The Nature of the Chemical Bond* (Cornell University Press, 1945), pp. 164, 195.

would be about 3.0 debye. This primary component evidently is mostly canceled by the large, oppositely-directed atomic hybridization moment of the apex oxygen. If we subtract the observed moment from the primary moment, an approximate value for the atomic moment, 2.5 debye, is obtained. This value is not unreasonable, considering the one unbalanced electron in the sp^2 orbital directed along the symmetry axis. However, hybridization in the end oxygens, which is neglected, may be important.

THE JOURNAL OF CHEMICAL PHYSICS VOLUME 21, NUMBER 5 MAY, 1953

The Vibration Frequencies of the Halogenated Methanes and the Substitution Product Rule*

KENNETH S. PITZER AND EDWARD GELLES
Department of Chemistry and Chemical Engineering, University of California, Berkeley, California
(Received January 16, 1953)

The extension of the Teller-Redlich product rule to the substitution of different atoms or groups, which was previously applied to the methyl benzenes, is here applied to the halogenated methanes. The rule is found to hold accurately enough to be useful in assigning fundamental frequencies or in computing unobserved fundamentals.

SEVERAL years ago Pitzer and Scott extended the Teller-Redlich product rule to the substitution of methyl groups for hydrogen atoms in certain hydrocarbons.[1] Similar extensions of the isotopic product rule have been made by others.[2] The present paper presents the results of applying the substitution product rule to the halogen derivatives of methane.

The recent force constant-frequency calculations of Stepanov,[3] Decius,[4] Pace,[5] and others[6–8] yield more detailed information on these simple compounds. The application of these force constants to more complex molecules would give, in principle, the desired guidance to spectral assignments. However, normal coordinate calculations become very laborious for larger molecules of low symmetry. Consequently, while the product rule yields less information, its ease of application makes it particularly valuable. This will be illustrated with some methane derivatives of low symmetry in the present paper.

In the earlier paper the product ratio τ was defined as

$$\tau=\prod_i\left(\frac{\nu_i'}{\nu_i}\right)\left[\prod_j\left(\frac{I_j}{I_j'}\right)\prod_k\left(\frac{M_k}{M_k'}\right)\right]^{\frac{1}{2}}, \qquad (1)$$

where the prime mark indicates the substituted molecule and where the indices i, j, and k cover all the vibrations, rotations, and translations, respectively, of a given symmetry type. The other symbols ν, I, and M refer to vibration frequencies, moments of inertia, and molecular masses, respectively.

An examination of normal coordinate theory shows that in every case τ will be given by a product of mass and bond distance ratios and a ratio of force constants. In isotopic substitution one assumes no change in bond distances or force constants, hence the factors depending on these quantities are unity. Then it is customary to combine the mass ratio with the terms in square brackets in Eq. (1) so as to yield a theoretical value for the ratio of frequencies.

However, the substitution of new atoms changes bond distances and force constants as well as masses. Thus, a reliable theoretical value of τ is not available. It seems best to combine all of the observable quantities in the form of Eq. (1), so that the τ-values for similar substitutions will be comparable. Furthermore, the theory does not indicate exactly the same τ-value for all examples of a given substitution. The cross terms in the potential expression enter in different ways. Also the distances and principal force constants for a given bond may vary slightly from one molecule to another. Consequently, we do not expect exact constancy of these substitution product ratios but rather will wish to see whether the variation is small enough to make them useful. The vibration frequency assignments for CH_4, CH_3F, CH_3Cl, CH_3Br, CH_2F_2, CH_2Cl_2, CH_2Br_2, CHF_3, $CHCl_3$, $CHBr_3$, CF_4, CCl_4, CBr_4, CF_3Cl, CF_2Cl_2, $CFCl_3$, CF_3Br, CF_2Br_2, $CFBr_3$, CCl_3Br, CCl_2Br_2, and $CClBr_3$ seem sufficiently reliable to be used in the determination of the τ-values and their constancy.

The experimental frequency values adopted in the

* This research was a part of the program of Research Project 50 of the American Petroleum Institute.
[1] K. S. Pitzer and D. W. Scott, J. Am. Chem. Soc. **65**, 803 (1943).
[2] See, for example, Mizushima, Morino, and Shimanouchi, Sci. Papers Inst. Phys. Chem. Research (Tokyo) **40**, 87 (1942).
[3] B. Stepanov, Acta Physicochim. U.R.S.S. **20**, 174 (1945).
[4] J. C. Decius, J. Chem. Phys. **16**, 214 (1948).
[5] E. L. Pace, J. Chem. Phys. **18**, 881 (1950).
[6] Meister, Rosser, and Cleveland, J. Chem. Phys. **18**, 346 (1950).
[7] Zietlow, Cleveland, and Meister, J. Chem. Phys. **18**, 1076 (1950).
[8] E. K. Plyler and W. S. Benedict, J. Research Natl. Bur. Standards **47**, 202 (1951).

TABLE I. Product ratios for the substitution of Y for X.

Compounds	Sym. type	F for H	Cl for F	Br for Cl
(Examples with one stretching motion)				
CX_4, CY_4	A_1	0.31	0.51	0.59
CH_3X, CH_3Y	A_1	0.27	0.52	0.59
CF_3X, CF_3Y	A_1	0.27	0.53	0.59
CCl_3X, CCl_3Y	A_1	0.25	0.53	0.58
CBr_3X, CBr_3Y	A_1	0.25	0.55	0.58
average for one stretching		0.27	0.53	0.58
(Examples with one bending motion)				
CX_4, CY_4	E	0.29	0.50	0.56
CH_3X, CH_3Y	E	0.25	0.53	0.54
CF_3X, CF_3Y	E	0.29	0.48	0.56
CCl_3X, CCl_3Y	E	0.27	0.53	0.59
CBr_3X, CBr_3Y	E	0.26	0.52	0.59
CH_2X_2, CH_2Y_2	A_2	0.22	0.51	0.59
CF_2X_2, CF_2Y_2	A_2	0.25	0.50	0.59
CCl_2X_2, CCl_2Y_2	A_2	0.25	0.56	0.58
CBr_2X_2, CBr_2Y_2	A_2	0.25	0.56	0.58
CH_2X_2, CH_2Y_2	B_1	0.28	0.48	0.59
CF_2X_2, CF_2Y_2	B_1	0.31	0.50	0.52
CCl_2X_2, CCl_2Y_2	B_1	0.31	0.49	0.59
CBr_2X_2, CBr_2Y_2	B_1	0.30	0.49	0.59
average for one bending		0.27	0.51	0.58
(Examples with one stretching and one bending motion)				
CX_4, CY_4	T_2	0.086	0.23	0.34
CHX_3, CHY_3	A_1	0.102	0.23	0.34
CFX_3, CFY_3	A_1	0.098	0.22	0.33
$CClX_3$, $CClY_3$	A_1	0.099	0.23	0.34
$CBrX_3$, $CBrY_3$	A_1	0.099	0.22	0.34
CH_2X_2, CH_2Y_2	A_1	0.085	0.25	0.34
CF_2X_2, CF_2Y_2	A_1	0.093	0.24	0.33
CCl_2X_2, CCl_2Y_2	A_1	0.087	0.25	0.33
CBr_2X_2, CBr_2Y_2	A_1	0.083	0.26	0.34
CH_2X_2, CH_2Y_2	B_2	0.054	0.27	0.36
CF_2X_2, CF_2Y_2	B_2	0.058	0.27	0.34
CCl_2X_2, CCl_2Y_2	B_2	0.060	0.26	0.35
CBr_2X_2, CBr_2Y_2	B_2	0.054	0.29	0.36
av for 1 stretching and 1 bending		0.082	0.25	0.34
(av stretching)×(av bending)		0.073	0.27	0.34
(Examples with one stretching and two bending motions)				
CHX_3, CHY_3	E	0.016	0.13	0.20
CFX_3, CFY_3	E	0.019	0.12	0.20
$CClX_3$, $CClY_3$	E	0.017	0.13	0.20
$CBrX_3$, $CBrY_3$	E	0.018	0.14	0.20
av for 1 stretching and 2 bendings		0.017	0.13	0.20
(av stretching)×(av bending)^2		0.020	0.14	0.20

TABLE II. Spectral assignments and product ratios for CX_2YZ molecules. (Revised assignments marked *r*.)

Molecule	CH_2FCl[8]	CH_2FBr[10]	CH_2ClBr[8]	CF_2HCl[8]
A′	2993	2993	2987	3023
	1470	1461	1402	1311
	1351	1313(*r*)	1225	1178
	1068	1050	728	809
	760	630	606	595
	385	314	226	422
A″	3048	3053	3060	1347
	1236	1227	1130	1116
	1004	940(*r*)	852	365
Mole wt	68.5	113.0	129.4	86.5
$I_z\times10^{39}$	16.1	23.3	40.5	17.2
$I_xI_y\times10^{78}$	29.3	45.3	112.0	200.0
Reference	CH_2F_2	CH_2F_2	CH_2Cl_2	CF_3H
Ratio (obs) A′	0.26	0.078	0.35	0.27
expected	0.27	0.092	0.34	0.27
Ratio (obs) A″	0.49	0.28	0.59	0.50
expected	0.51	0.30	0.58	0.51

Molecule	CF_2HBr[12]	CF_2BrCl[12]	CCl_2HF[8]	CCl_2HBr[8]
A′	3003	1102	3023	3040
	1280	872	1304	1168
	1135	648	1079	719
	718	(400)	742	604
	576	(380)	458	330
	(380)calc	(200)	276	220
A″	1344	1150	1242	1211
	1108	440	804	760
	323	300	368	215
Mole wt	130.9	165.4	102.9	163.9
$I_z\times10^{39}$	28.2	56.0	12.2	44.4
$I_xI_y\times10^{78}$	291.5	1085	890	1690
Reference	CF_3H	CF_3Cl	CH_2Cl_2	$CHCl_3$
Ratio (obs) A′	0.097	0.081	0.066	0.34
expected	0.092	0.092	0.073	0.34
Ratio (obs) A″	0.28	0.31	0.27	0.60
expected	0.30	0.30	0.27	0.58

Molecule	CCl_2FBr[10]	CBr_2HF[10]	CBr_2HCl[8]	CBr_2FCl[10]
A′	1069	3015	3034	1063
	779(*r*)	1295(*r*)	1189	802
	501	1063	746	462
	334	620	570	340(*r*)
	303(*r*)	358(*r*)	278	267(*r*)
	215	171	168	160
A″	825(*r*)	1170(*r*)	1144	741
	390	704	657	306(*r*)
	203(*r*)	295(*r*)	201	195(*r*)
Mole wt	181.9	191.9	208.3	226.3
$I_z\times10^{39}$	54.8	14.9	32.2	42.7
$I_xI_y\times10^{78}$	2380	5370	6550	7540
Reference	CCl_2HBr	CBr_2H_2	CBr_2H_2	CBr_2HCl
Ratio (obs) A′	0.077	0.064	0.018	0.063
expected	0.073	0.073	0.020	0.073
Ratio (obs) A″	0.27	0.26	0.14	0.27
expected	0.27	0.27	0.14	0.27

force constant treatments mentioned above are used in the present calculations, the latest vapor phase data being employed where available.

We accept the recent assignment for CF_3Br.[9] The general assignment for CCl_2Br_2 given by Plyler and Benedict is correct, but we have substituted the more precise Raman frequencies listed in the *Landolt-Börnstein Tabellen*.[10] This involves the interchange of the 174 and 230 cm^{-1} frequencies in the Landolt-Börnstein assignment. The new assignment for CF_2Cl_2[8] must replace that of Thompson and Temple,[11] whose assignments for CF_3Cl and $CFCl_3$ are accepted, however.

The moments of inertia were obtained from various sources in the literature or calculated from the appropriate bond distances and angles. Values are quoted in g-cm^2 units. Since these values contribute little uncertainty, they will not be discussed in detail.

Table I contains the calculated product ratios for the compounds listed above. For a single motion the average deviation from the mean is about 8 percent for

[9] W. F. Edgell and C. E. May, J. Chem. Phys. **20**, 1822 (1952).
[10] *Landolt-Börnstein Tabellen* (Verlag Julius Springer, Berlin, 1951), Sixth Edition, Vol. I, parts 2 and 3.
[11] H. W. Thompson and R. B. Temple, J. Chem. Soc. 1422 (1948).

the substitution of F for H but only about 3 percent for the substitution of one halogen for another. Where more than one motion is involved one would expect the variation to be greater. This is found particularly in the case of one bending and one stretching motion with substitution of F for H. Here we find examples equivalent to the combination of the extreme ratios for the single component motions. It may be noted, however, that for a given symmetry type a higher degree of constancy obtains for each type of motion. Also it appears that the ratios for the substitution of Cl for H would be more nearly constant than those for F for H. This is readily verified by observing that the higher values of τ for F for H substitution are followed by relatively low values for Cl for F substitution. It may be seen from Table I that the average product ratios for two or more motions closely approximate the product of the averages for the single component motions. We believe the agreement found in Table I is good enough to allow the method to be used in interpreting other spectra.

The assignments for the CX_2YZ molecules are given in Table II. The frequencies are in cm^{-1} and the moments of inertia in g-cm^2 units. All possible molecules of this type (with H, F, Cl, or Br) are included. A number of the assignments given in the *Landolt-Börnstein Tabellen*[10] are inconsistent with the polarization of the Raman bands. The present assignments have removed all these inconsistencies. No changes were required in the assignments of Plyler and Benedict[8] or of Plyler and Acquista.[12] For the four molecules not investigated by Plyler, revision of the previous assignments was necessary. In one case a single pair of frequencies was interchanged as indicated by (r), and in the other three cases two pairs of frequencies were interchanged in order to obtain satisfactory agreement with the τ-values and the polarization data. For CF_2HBr one frequency was not observed, but the value calculated by Stepanov appears to be quite satisfactory. The three lowest frequencies of A′ symmetry in CF_2BrCl were estimated from combination and overtone bands.[12]

The completely unsymmetrical compound CHFClBr has been studied recently,[13] the observed frequencies and other relevant data being given in Table III. The agreement between observed and expected product ratios is very satisfactory.

TABLE III. Spectral frequencies and product ratio for $CHFClBr^{13}$.

Frequencies	3023, 1299, 1202, 1060, 772, 655, 426, 313, 220 cm^{-1}
Mole wt	147.4
$I_1I_2I_3\times10^{111}$	26800
Reference	$CHFCl_2$
Ratio (obs)	0.194
expected	0.20

[12] E. K. Plyler and N. Acquista, J. Research Natl. Bur. Standards 48, 92 (1952).

[13] E. K. Plyler and M. A. Lamb, J. Research Natl. Bur. Standards 46, 382 (1951).

TABLE IV. Spectral assignments and product ratios for iodomethanes. (Revised assignments marked r.)

Molecule	CH_3I[10]	CF_3I[9]	CH_2I_2[10]
	2950	1073	2970
	A_1 1240	A_1 740	A_1 1348
	525	265(r)	485
			120
	3050	1185	A_2 1103(r)
	E 1420	E 540	
	890	286(r)	B_1 3050
			714(r)
			B_2 1028(r)
			567
Mole wt	142.0	195.9	267.9
$I\times10^{39}$	I_A= 0.55	I_A=14.8	I_x=131.2
	I_B=10.0	I_B=55.1	I_y= 3.20
			I_z=135.5
Reference	CH_3Br	CF_3Br	CH_2Br_2
Ratio (obs)	(A_1) 0.67	(A_1) 0.63	(A_1) 0.47
expected		0.67	0.47
Ratio (obs)	(E) 0.70	(E) 0.67	(B_2) 0.47
expected		0.70	0.47
Ratio (obs)			(A_2) 0.72
expected			0.70
Ratio (obs)			(B_1) 0.69
expected			0.70

Molecule	CH_2BrI[10]	CH_2ClI[10]
	2978	2978
	1374	1392
	A′ 1065(r)	A′ 1126(r)
	616	718
	517	527
	144	194
	3053	3048
	A″ 1150	A″ 1183
	754(r)	801(r)
Mole wt	220.9	176.4
$I\times10^{39}$	I_z= 92.5	I_z= 51.9
	I_xI_y=336	I_xI_y=170
Reference	CH_2Br_2	CH_2Cl_2
Ratio (obs)	(A′) 0.45	(A′) 0.15
expected	0.47	0.16
Ratio (obs)	(A″) 0.68	(A″) 0.40
expected	0.70	0.41

We find throughout Tables II and III that the τ values agree within a few percent with the relevant average τ-values from Table I.

The data for iodine compounds are generally less extensive or certain than those considered heretofore. The values available are included in Table IV. As before, the symbol (r) indicates a rearrangement of fundamental frequencies from an earlier assignment.

The reversal of the assignment of the two lowest frequencies of CF_3I is suggested by the product ratios. In the absence of polarization data and in view of the proximity of the two frequencies, this new assignment cannot be considered certain.

As we stated above, it is not possible to calculate reliable theoretical values for these ratios unless the detailed potential systems are known for each molecule. However, we may indicate the form that the ratios

TABLE V. Comparison of observed and calculated product ratios.

Substitution	F for H	Cl for F	Br for Cl	I for Br
Stretching				
Calc for no change in potential constant	0.23	0.73	0.67	0.79
Calc with average potential constant	0.26	0.54	0.61	0.69
Average obs	0.27	0.53	0.58	0.67
Bending				
Calc for no change in potential constant	0.19	0.57	0.61	0.72
Calc with average potential constant	0.33	0.50	0.58	···
Average obs	0.27	0.51	0.58	0.70

take when a simple valence potential system is assumed with no off-diagonal terms. Also we assume that the substitution concerns a terminal atom, i.e., one connected to the rest of the molecule by just one bond. We obtain from the usual theory

$$\tau\ (\text{theory, stretching}) = \left(\frac{m}{m'}\right)^{\frac{1}{2}}\left(\frac{k'_{\text{str.}}}{k_{\text{str.}}}\right)^{\frac{1}{2}}, \qquad (2)$$

$$\tau\ (\text{theory, bending}) = \frac{d}{d'}\left(\frac{m}{m'}\right)^{\frac{1}{2}}\left(\frac{k'_{\text{bend.}}}{k_{\text{bend.}}}\right)^{\frac{1}{2}}. \qquad (3)$$

Here the primed quantities refer in each case to the substituted molecule, and d, k, and m refer to the bond distance, potential constant, and atomic mass, respectively. It is of interest to compare the observed average product ratios with those calculated from the above equations. The stretching force constants given by Pace[5] are used together with a value of 2.20×10^{-5} dyne/cm for the carbon-iodine stretching constant. The appropriate X−C−Y bending constants, averaged over all types of substitution shown in Table I, are taken from the above-mentioned force-constant treatments.[4–8]

Table V gives these calculated product ratios together with the observed average values. The theoretical product ratios with the potential constants k' and k equal in each case are also listed for comparison.

The agreement between observed and calculated product ratios is very satisfactory. In connection with the averaged product ratios for the bending motions in the substitution of fluorine for hydrogen it must be remembered that there is a considerable variation with symmetry type in the relevant product ratios of Table I.

The observed τ-values are practically identical for both bending and stretching motion. This leads to an interesting relationship between force constants and bond distances

$$d\left(\frac{k_{\text{str.}}}{k_{\text{bend.}}}\right)^{\frac{1}{2}} \cong d'\left(\frac{k'_{\text{str.}}}{k'_{\text{bend.}}}\right)^{\frac{1}{2}}. \qquad (4)$$

This relationship would appear to hold within about 4 percent, so far as the observed product ratios are concerned. Since the use of the principal force constants of Decius and Pace gives more variation when substituted into Eq. (4), it is apparent that the off-diagonal potential terms must play a role in the close agreement found above.

CONCLUSIONS

We believe the tables presented above illustrate the value of the substitution product rule for halogen derivatives of hydrocarbons. This principle makes it possible to check an assignment or to calculate a single missing frequency with much less labor than that required for a force constant—normal coordinate treatment.

We intend to use these assignments as a basis for calculating the thermodynamic properties of the halogenated methanes. We are also continuing to apply the substitution product rule to halogen derivatives of higher hydrocarbons.

Effect of $3p$ Atomic Orbital on Energy of the Double Bond*

J. S. DOOLING
Department of Chemistry, The Catholic University of America, Washington, D. C.

(Received March 5, 1951)

The energy of the $\pi-\pi$ part of the double bond is calculated by (1) the perturbation method using the "united atom" model, and (2) the MO method where the wave function used is constructed as a linear combination of atomic orbitals, as a function of internuclear distance. In each case the wave function includes the $3p$ atomic orbital. The results of the investigation indicate (1) that the wave function ordinarily used in the MO method is not appreciably improved by the inclusion of the $3p$ atomic orbital, and (2) that the absolute value of the energy calculated by the MO method using p functions centered at the nuclei, is at least 20 percent too low at the distances occurring in the C—C bond.

CONSIDERABLE work has been done in recent years in calculating the energy values and wave functions of molecules with double bonds. A double bond consists of a $\sigma-\sigma$ part and a $\pi-\pi$ part; it is only the latter with which we are concerned in this paper.

One of the methods frequently used is the molecular orbital method[1] in which one constructs one-electron molecular orbitals (MO) as linear combinations of atomic orbitals. In some cases, the coefficients of the atomic orbitals as they appear in a MO are found by symmetry alone, e.g., in H_2CCH_2; in other cases, they must be found by minimizing the energy. Up to now, the orbitals used in the MO for the $\pi-\pi$ bond involving carbon atoms have always been simple atomic $2p$ orbitals.

As Hund[2] has pointed out, an actual molecule can be approached from two points of view; from that of the "united atom" which contains the nuclei pushed together in a single nucleus, and from that of the nuclei separated infinitely far apart. If one starts from the united atoms, one slowly pulls the nuclei apart. It is clear that this is the better approach for small internuclear distances. The H_2^+ ion, for which Hylleraas[3] has solved the wave function directly, would come in this range. If one starts with the separated atoms at infinite distance apart, one then brings the atoms to the distance of interest. This approach gives a better approximation for large distances of separation. The double-bond calculations for actual molecules fall in this range.

In the present paper both methods of approach are used in calculating the energy of the $\pi-\pi$ bond. For small distances, a perturbation method is used; for large distances, a variational method is used. In both methods the symmetry properties of the $\pi-\pi$ bond must be preserved. The $\pi-\pi$ bonding MO has symmetry species Π_u. If the axes are chosen as in Fig. 1, then the Π_z MO is even with respect to reflections at the YZ and XY planes and odd with respect to reflections at the YZ planes. We consider a single electron in the field of bare nuclei, so that our model is an H_2^+ ion with arbitrary nuclear distance and charge.

METHOD STARTING FROM UNITED ATOM MODEL

In this perturbation method, we start with a nucleus of charge $2Z'$. An electron moving in the field of this nucleus would have the following Hamiltonian:

$$H_0=-\frac{h^2}{8\pi^2 m}\Delta-\frac{2Z'e^2}{r}. \tag{1}$$

The nucleus is now separated forming two nuclei with displacements $\pm a$ along the Z axis and with equal charges Z'. The Hamiltonian for the electron may now be expressed as $H=H_0+H_1$ where H_0 is given by (1),

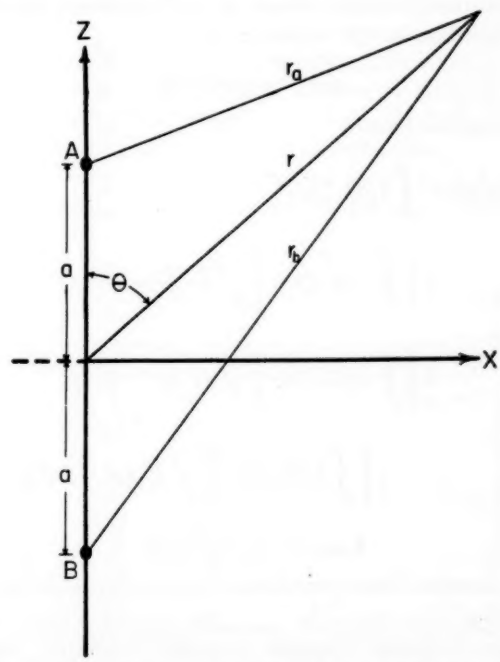

FIG. 1. Polar coordinates for an electron at P in an atomic orbital of atom A or B. In addition, $\phi=\phi_A=\phi_B$.

*This work has been supported in part by the U. S. Office of Naval Research under contract N6onr-2551. From a thesis submitted in partial fulfillment of the requirements for the Ph.D. degree at The Catholic University of America.

[1] A review of the molecular orbital method is given by J. H. Van Vleck and A. Sherman, Revs. Modern Phys. 7, 167 (1935).
[2] F. Hund, Z. Physik 73, 1 (1931).
[3] E. A. Hylleraas, Z. Physik 73, 739 (1931).

TABLE I. Energy of the $\pi-\pi$ bond in $Z'^2e^2/2a_0$ units calculated from "united atom" model.

$Z'R/a_0$	E°	E^1	E_1^2	E_2^2	E_3^2	E_H	A_3/A_2
0.0	−1.000	−1.000	−1.000	−1.000	−1.000	−1.000	0.00
0.5	−1.000	−0.984	−0.984	−0.984	−0.984	−0.984	0.00
1.0	−1.000	−0.946	−0.948	−0.948	−0.948	−0.948	0.02
1.5	−1.000	−0.897	−0.905	−0.915	−0.917	−0.919	0.03
2.5	−1.000	−0.787	−0.847				0.08
5.0	−1.000	−0.449	−0.679				0.18

and the perturbation function H_1 is

$$H_1=Z'e^2\left(\frac{2}{r}-\frac{1}{r_a}-\frac{1}{r_b}\right), \tag{2}$$

where r_a and r_b are the distances from the electron to nucleus A and B, respectively. The sum $(1/r_a)+(1/r_b)$ may be expanded in terms of the Legendre polynomials. Using these series gives

$$H_1=-\frac{2Z'e^2}{r}\sum_{s=1}\frac{a^{2s}}{r^{2s}}P_{2s}(\cos\theta) \quad r>a, \tag{2a}$$

$$H_1=-\frac{2Z'e^2}{r}-\frac{2'Ze^2}{a}\sum_{s=0}\frac{r^{2s}}{a^{2s}}P_{2s}(\cos\theta) \quad r<a. \tag{2b}$$

The desired solution of the Schrödinger equation will contain only those wave functions having the symmetry of the $\pi-\pi$ bond in the ground state as discussed in the introduction. The unperturbed atomic wave function, $2p=R_{2,1}(r)P_1^1(\cos\theta)\cos\phi$, has this required symmetry. Because of the symmetry of the molecule, the only other wave functions which will give a node in the required plane are those whose angular momentum is characterized by odd quantum numbers. The solution of the equation is

$$\psi=A_2 2p+A_3 3p, \tag{3}$$

with eigenvalues of

$$E=E(2p)+\int 2pH_1 2p d\tau + \left[\int 3pH_1 2p d\tau\right]^2 \Big/ E(2p)-E(3p) + \left[\int 4pH_1 2p d\tau\right]^2 \Big/ E(2p)-E(4p) + \left[\int 5pH_1 2p d\tau\right]^2 \Big/ E(2p)-E(5p). \tag{4}$$

TABLE II. $S_{sj}=\int a_s b_j d\tau$.

$Z'R/a_0$	5	8	10	15	20
S_{22}	0.5780	0.2869	0.1640	0.0327	0.0053
S_{23}	−0.1794	−0.2458	−0.2361	−0.1365	−0.0551
S_{33}	0.8089	0.6630	0.5830	0.3106	0.1782

In Table I are given the values of the energy as calculated from the above expressions for various values of the internuclear distance. The energy is in the units of $(Z'^2e^2)/(2a_0)$ for charge Z' on each nucleus; the internuclear distance is given in terms of $Z'R/a_0$. E° represents the unperturbed energy; E^1, the energy correct to the first-order perturbation; E_1^2, E_2^2, and E_3^2, the energy including the first, second, and third term, respectively, of the second-order perturbation. These values are compared with those calculated by Hylleraas who has solved the wave equation directly. His values are designated by E_H. In the last column are given the ratio of the coefficients A_3/A_2. In Table I, the energy is 1.0 for distance zero, since this corresponds, in Z^2 hydrogen units, to a nucleus of charge, $2Z$, and a wave function of principal quantum number 2.

METHOD STARTING WITH SEPARATED NUCLEI

Instead of using simply the unperturbed atomic $2p$ orbital of each nucleus in building up the MO, it was decided to build the MO as follows:

$$\psi=\sum_s A_s(a_s+b_s),$$

TABLE III. $C_{sj}=\int\frac{a_s a_j}{r_b}d\tau$.

$Z'R/a_0$	5	8	10	15	20
C_{22}	0.3293	0.2274	0.1881	0.1298	0.0985
C_{23}	0.0428	0.0170	0.0096	0.0030	0.0013
C_{33}	0.2787	0.1708	0.1459	0.1129	0.0918

where a_s refers to the atomic wave functions of atom A, and b_s to atom B. The coefficient A_s will be the same for a_s and b_s because of the symmetry properties. In this method we do not break the Hamiltonian into two parts, H_0 and H_1, but use

$$H=-\frac{h^2}{8\pi^2 m}\Delta-\frac{Z'e^2}{r_a}-\frac{Z'e^2}{r_b}, \tag{5}$$

where the coordinates are defined in Fig. 1.

The wave functions are the solution of

$$\psi^*H\psi=\psi^*E\psi. \tag{6}$$

The general expression for the energy from Eq. (6) is

$$E=\frac{\sum_{s=2}A_s^2W_s+\sum_{s=2}\sum_{j=2}A_jA_sS_{sj}-Z'e^2\sum_{s=2}\sum_{j=2}A_jA_s(C_{sj}+Q_{sj})}{\sum_{s=2}A_s^2+\sum_{s=2}\sum_{j=2}A_sA_jS_{sj}}, \tag{7}$$

where W_s is the energy of the electron in atomic state s

and

$$S_{sj}=S_{js}=\int a_s b_j d\tau,$$

$$C_{sj}=C_{js}=\int \frac{a_s a_j}{r_b} d\tau,$$

$$Q_{sj}=\int \frac{a_s b_j}{r_b} d\tau.$$

In considering the effect of the $3p$ atomic orbital, the wave function to be used reduces to

$$\psi=A_2(a_2+b_2)+A_3(a_3+b_3),$$

where

$$a_2=2p(A);\ a_3=3p(A);\ b_2=2p(B);\ \text{and}\ b_3=3p(B).$$

Equation (7) for the energy is then given by

$$E=\frac{A_2^2W_2+A_3^2W_3+2A_2A_3S_{23}-2Z'e^2A_2A_3C_{23}-Z'e^2A_2A_3(Q_{23}+Q_{32})}{A_2^2+A_3^2+2A_2A_3S_{23}}.$$

The energy must then be minimized with respect to the coefficients A_2 and A_3, giving two simultaneous equations. The energy E and the ratio of the coefficients A_3/A_2 were then calculated. The values of the overlap and Coulomb integrals were calculated[4] and are given in Tables II, III, IV, and V for various values of the internuclear distance. In Table V, which gives the energy values, $E(1)$ is the energy given by the usual first-order approximation using $2p$ atomic orbitals, and $E(2)$ is that calculated with the modified wave function. The energy is given in units of $Z'^2e^2/2a_0$. In the separated atoms, the limiting value for $R=\infty$ is 0.25 corresponding in Z^2 hydrogen units to a $2p$ electron on one Z fold hydrogen nucleus.

TABLE IV. $Q_{sj}=\int(a_sb_j/r_a)d\tau$.

$Z'R/a_0$	5	8	10	15	20
Q_{22}	0.2292	0.0946	0.0483	0.0074	0.0010
Q_{23}	−0.0236	−0.0872	−0.0703	−0.0384	−0.0008
Q_{32}	0.0013	0.0358	−0.0374	−0.0194	−0.0113
Q_{33}	0.1298	0.0916	0.0787	0.0539	0.0308

TABLE V. Energy of the $\pi-\pi$ bond in $Z'^2e^2/2a_0$ units calculated from the separated nuclei model.

$Z'R/a_0$	5	8	10	15	20	∞
$E(1)$	−0.582	−0.500	−0.453	−0.383	−0.349	−0.250
$E(2)$	−0.612	−0.503	−0.454	−0.383	−0.349	−0.250

DISCUSSION OF RESULTS

It is difficult to determine the convergence of the series used in the perturbation calculation. The following general criterion may be used: if the shift in the energy level caused by the perturbation is small compared to the energy separation of the unperturbed level from its nearest neighbor, the perturbation method yields a good approximation to the energy of the system. In the calculations carried out in this paper, the method starting from the "united atom" gave excellent results for internuclear distances up to $Z'R/a_0=1.5$. At the distance $Z'R/a_0=5.0$, the energy shift caused by the perturbation was of the same order of magnitude as the energy difference between the unperturbed atomic $2p$ and $3p$ states. Certainly, the series for this internuclear distance does not converge. It is doubtful whether the series for $Z'R/a_0=2.5$ converges.

However, although these series do not converge, the value for the energy obtained by taking any given number of terms in either of the series will be greater than the true value of the energy. This is so because we have used the exact Hamiltonian and $\int\psi^*H\psi d\tau\geq E$. The statement, that any approximate wave function must give energies which are too high, is true without further qualification only for the lowest state. For any higher state, it is true only if the approximate wave function used does not have any admixture from the lower state, i.e., is orthogonal to the true wave functions of all lower states. This is the case in our problem, where we are dealing with p functions which have one plane node passing through the molecular axis. Any lower state would have cylindrical symmetry around the molecular axis, and would, therefore, be necessarily orthogonal to all the wave functions used here.

The following conclusions may be drawn from Fig. 2, in which the points on 3 are the values found starting

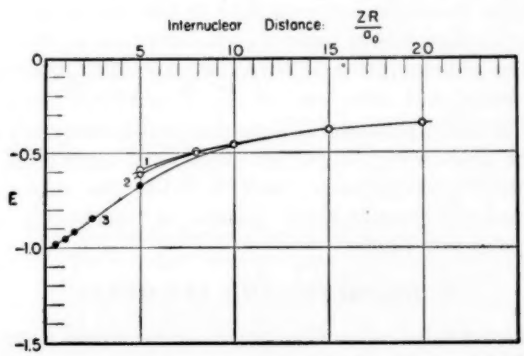

FIG. 2. Energy plotted against internuclear distance. The points on curve 1 are calculated using only $2p$ functions; those on curve 2, using $2p$ and $3p$ functions. Both are calculated starting from the separated atoms. The points on curve 3 are calculated starting from the "united atom" model.

[4] These values, calculated from hydrogen-like wave functions were compared where possible with values calculated by Mulliken, Rieke, Orloff and Orloff, using Slater orbitals, J. Chem. Phys. **17**, 1265 (1949).

from the "united atom"; the points on 1 and 2 are those from the separated atoms. The points on 1 are found by using the $2p$ functions (usual method); those on 2, by including $2p$ and $3p$ functions. In the curve the point at $Z'R/a_0=0$ (united atom) is exact, and the next three points, agreeing with Hylleraas' calculation, are very nearly so. On the other hand, for large values of R (separated atoms), 0.25 is exact. All the other points must lie too high, although because of the large nuclear separation, the points at 15 and 20 probably do not lie much too high. But the energy value at $Z'R/a_0=5$, calculated by the MO method, by using a linear combination of $2p$ functions only, must be considerably too high, since it is lying 0.1 units above the point calculated by the "united atom" method which itself is too high. It is difficult to judge by how much the point S (usual method) at 7.83 (double bond distance) is too high. By a reasonable interpolation of the curve from the points on 3 to the points on 1 from 10 on, one would estimate that at 7.8, the point on 1 lies about 0.05 unit (i.e., about 20 percent of the binding energy) above the interpolation curve, which itself must be too high by an unknown amount, i.e., the absolute value calculated is too low.

Accordingly, the one-electron double-bond absolute energy, calculated by p functions centered at the nuclei, is at least 20 percent too low at the distances occurring in the double bond.

ACKNOWLEDGMENTS

The author gratefully acknowledges his indebtedness to Professor Karl Herzfeld, under whose direction the work was carried out, and to Dr. V. Griffing for many helpful discussions and advice concerning this paper. The author also wishes to thank Dr. D. Beard for reading the manuscript.

THE JOURNAL OF CHEMICAL PHYSICS VOLUME 21, NUMBER 5 MAY, 1953

The Bipyramidal XY_5 Molecular Model. Part I. Classical Vibration Problem

JOSEPH S. ZIOMEK AND CECIL B. MAST *
De Paul University, Chicago 14, Illinois
(Received December 2, 1952)

Symmetry coordinates are set up from the standpoint of group theory for describing the normal modes of oscillation of the XY_5 molecular model in such a manner that maximum factorization of the secular determinant is accomplished. The cubic and quartic portions of the anharmonic potential function are derived, and the components of vibrational angular momentum are set down. The complete valence-type potential function is discussed. Explicit relations are derived between the force constants occurring in the secular determinant and the physical valence force constants.

I. INTRODUCTION

THE bipyramidal XY_5 molecular model has the symmetry D_{3h} and includes, as examples, the pentahalides of phosphorus and others. The normal vibrations of this molecular model and the quantum-mechanical evaluation of its allowed rotation-vibration energies have not been treated in the literature. This paper is intended to form the classical part of the basis for the interpretation of both the gross vibrational and fine rotational structure of the Raman and infrared spectra of bipyramidal XY_5 molecule. Furthermore this paper deals with the purely vibrational aspects of the problem and includes discussions of the molecular symmetry, characteristic modes of vibrations, and potential functions.

II. GEOMETRY AND SYMMETRY

The equilibrium configuration of the model assumed for the bipyramidal XY_5 is shown in Fig. 1, along with a right-handed rectangular coordinate system, xyz, whose origin coincides with the center of mass and whose axes are principal axes of inertia. The respective atoms are indicated by an arbitrary index $i(i=1, 2 \cdots 6)$ for reference. The three Y atoms (1, 2, 3) and the atom $X(4)$ lie in the xy plane, and the two Y atoms (5, 6) lie in the xz plane, and Y atoms 5 and 6 and X atom lie on the z axis. The masses (m_i) and equilibrium coordinates (x_{0i}, y_{0i}, z_{0i}) of the respective atoms are listed in Table I.

The twelve covering operations of symmetry point group D_{3h} form six classes as follows: E, the identity operation; $2C_3$, rotations by $\pm 2\pi/3$ around the z axis; $2S_3$, rotations by $\pm 2\pi/3$ around the z axis plus reflection in the xy plane; $3C_2'$, rotation by π around the axes passing through atoms $Y(1, 2, 3)$ and X atom, respectively; $3\sigma_v$, reflection in the xz plane, in the plane containing z axis and atom $Y2$, and in the plane containing z axis and atom $Y3$; and σ_h, a reflection in the xy plane. Table II contains the characters of the various classes of covering operations performed on the six possible types $(A_1', A_2', A_1'', A_2'', E', E'')$ of physical quantities. The types A are nondegenerate and E are twofold degenerate. Quantities associated with the

* Now at the Notre Dame University, Nore Dame, Indiana.

vibrations and rotations of the XY_5 model have the following species assignments: (a) of the components of linear displacement, x and y form an E' pair and z is A_2''; (b) of the components of angular momentum, P_x and P_y form an E'' pair and P_z is A_2'; (c) of the components of the electric dipole moment, M_x and M_y form an E' pair and M_z is A_2''; (d) the polarizability tensor has components of species A_1', E', and E''.

III. COORDINATES FOR INFINITESMAL VIBRATIONS

The body-fixed rectangular coordinate system, which was introduced in Sec. II for the description of the equilibrium configuration, is suitable for analytical discussion of the rotations and modes of vibration of the molecular model if it moves with the molecular framework subject to the following two conditions:[1,2] (a) the coordinate origin remains at the center of mass, and (b) none of the modes of vibration results in angular momentum of rotation of the molecular framework as a whole inside the coordinate system. The instantaneous coordinates of the ith atoms during infinitesmal vibrations will be given by $x_i=x_{0i}+x_i'$, etc., where x_{0i},

TABLE I. Masses and equilibrium coordinates.

Atom	i	m_i	x_{0i}	y_{0i}	z_{0i}
Y	1	m	d_0	0	0
Y	2	m	$-\frac{d_0}{2}$	$\frac{(3)^{\frac{1}{2}}}{2}d_0$	0
Y	3	m	$-\frac{d_0}{2}$	$-\frac{(3)^{\frac{1}{2}}}{2}d_0$	0
X	4	M	0	0	0
Y	5	m	0	0	D_0
Y	6	m	0	0	$-D_0$

y_{0i}, and z_{0i} denote the equilibrium values of the coordinates and x_i', y_i', z_i' denote components of displacement from the equilibrium position. The conditions (a) and (b) are satisfied by the following relations which are given in terms of the displacement coordinates:

$$\sum_i m_i x_i' = \sum_i m_i y_i' = \sum_i m_i z_i' = 0, \tag{1}$$

$$p_{0x} = \sum_i m_i (y_{0i}\dot{z}_i' - z_{0i}\dot{y}_i') = 0, \tag{2a}$$

$$p_{0y} = \sum_i m_i (z_{0i}\dot{x}_i' - x_{0i}\dot{z}_i') = 0, \tag{2b}$$

$$p_{0z} = \sum_i m_i (x_{0i}\dot{y}_i' - y_{0i}\dot{x}_i') = 0. \tag{2c}$$

For the XY_5 model these conditions are satisfied by the following equations:

$$m(x_1'+x_2'+x_3'+x_5'+x_6')+Mx_4'=0, \quad \text{etc.}, \tag{1'}$$

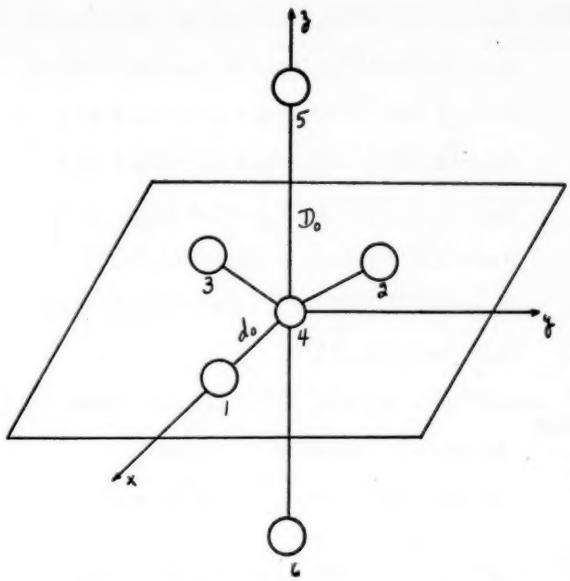

FIG. 1. The equilibrium configuration of the XY_5 molecule.

and

$$((3)^{\frac{1}{2}}/2)md_0(z_2'-z_3')+mD_0(y_6'-y_5')=0, \tag{2'a}$$

$$(\tfrac{1}{2})md_0(-2z_1'+z_2'+z_3')+mD_0(x_5'-x_6')=0, \tag{2'b}$$

$$(m/2)d_0[2y_1'-y_2'-y_3'+(3)^{\frac{1}{2}}(x_2'-x_2')]=0. \tag{2'c}$$

The methods of group theory show that the twelve normal modes of vibration of the XY_5 molecule of symmetry D_{3h} have the following species classifications: two of A_1', none of A_2', none of A_1'', two of A_2'', three pairs of E', and one pair of E''. The complete vibrational secular determinant can accordingly be broken up at once, if one uses generalized coordinates with proper symmetry properties, into steps as follows: two twofold, two identical threefold, and two identical onefold steps. It can be shown with the aid of group theory methods that the following twelve linear combinations of displacement coordinates form a set of orthonormal generalized coordinates of appropriate symmetries for setting up the normal vibration problem:

$$A_1': \quad S_1=(1/2\cdot 3^{\frac{1}{2}})[2\xi_1-\xi_2-\xi_3+3^{\frac{1}{2}}(\eta_2-\eta_3)],$$

$$S_2=(1/2^{\frac{1}{2}})[\zeta_5-\zeta_6],$$

$$A_2'': \quad S_3=(1/30^{\frac{1}{2}})[-2(\zeta_1+\zeta_2+\zeta_3)+3(\zeta_5+\zeta_6)],$$

$$S_4=(a/5)^{\frac{1}{2}}[M^{\frac{1}{2}}(\zeta_1+\zeta_2+\zeta_3+\zeta_5+\zeta_6)-5m^{\frac{1}{2}}\zeta_4],$$

TABLE II. Characters of point group D_{3h}

	E	σ_h	$2C_3$	$2S_3$	$3C_2'$	$3\sigma_v$
A_1'	1	1	1	1	1	1
A_2'	1	1	1	1	−1	−1
A_1''	1	−1	1	−1	1	−1
A_2''	1	−1	1	−1	−1	1
E'	2	2	−1	−1	0	0
E''	2	−2	−1	1	0	0

[1] C. Eckart, Phys. Rev. **47**, 552 (1932).
[2] E. B. Wilson, Jr., and J. B. Howard, J. Chem. Phys. **4**, 260 (1936).

E': $S_{5a}=(a/5)^{\frac{1}{2}}[M^{\frac{1}{2}}(\xi_1+\xi_2+\xi_3+\xi_5+\xi_6)-5m^{\frac{1}{2}}\xi_4]$,

$S_{5b}=(a/5)^{\frac{1}{2}}[M^{\frac{1}{2}}(\eta_1+\eta_2+\eta_3+\eta_5+\eta_6)-5m^{\frac{1}{2}}\eta_4]$,

$S_{6a}=(1/30^{\frac{1}{2}})[-2(\xi_1+\xi_2+\xi_3)+3(\xi_5+\xi_6)]$,

$S_{6b}=(1/30^{\frac{1}{2}})[-2(\eta_1+\eta_2+\eta_3)+3(\eta_5+\eta_6)]$,

$S_{7a}=(1/2\cdot 3^{\frac{1}{2}})[-2\xi_1+\xi_2+\xi_3+3^{\frac{1}{2}}(\eta_2-\eta_3)]$,

$S_{7b}=(1/2\cdot 3^{\frac{1}{2}})[2\eta_1-\eta_2-\eta_3+3^{\frac{1}{2}}(\xi_2-\xi_3)]$,

E'': $S_{8a}=[m/2I_{ex}^{\frac{1}{2}}][2D_0(\zeta_2-\zeta_3)+3^{\frac{1}{2}}d_0(\eta_5-\eta_6)]$,

$S_{8b}=[m/2(3I_{ex})^{\frac{1}{2}}]$

$\times[2D_0(-2\zeta_1+\zeta_2+\zeta_3)-3d_0(\xi_5-\xi_6)]$,

where

$\xi_i=m_i^{\frac{1}{2}}x_i'$; $\eta_i=m_i^{\frac{1}{2}}y_i'$; $\zeta_i=m_i^{\frac{1}{2}}z_i'$,

$m=m_i$ for $i=1, 2, 3, 5, 6$, $m_4=M$,

$a=\dfrac{1}{M+5m}$, and $I_{ex}=m(\frac{3}{2}d_0^2+2D_0^2)$.

The vibrational kinetic energy T_v must be of symmetry species A_1' and is given by the expression

$$2T_v=\sum_{i=1}^{12}m_i(\dot{x}_i^2+\dot{y}_i^2+\dot{z}_i^2). \tag{3}$$

In terms of the symmetry coordinates this becomes

$$T_v=\sum_{i=1}^{4}\dot{S}_i^2+\sum_{j=5}^{8}(\dot{S}_{ja}^2+\dot{S}_{jb}^2). \tag{4}$$

The harmonic or zero-order potential energy U_0 must be of the symmetry species A_1' and is given by the following expression:

$$2U_0=\sum_{i,i'=1}^{2}\frac{k_{ii'}S_iS_{i'}}{(\mu_i\mu_{i'})^{\frac{1}{2}}}+\sum_{j,j'=3}^{4}\frac{k_{jj'}S_jS_{j'}}{(\mu_j\mu_{j'})^{\frac{1}{2}}}+\sum_{k,k'=5}^{7}\frac{k_{kk'}(S_{ka}S_{k'a}+S_{kb}S_{k'b})}{(\mu_k\mu_{k'})^{\frac{1}{2}}}+\frac{k_{88}(S_{8a}^2+S_{8b}^2)}{m}, \tag{5}$$

where

$$\mu_1=\mu_2=\mu_3=\mu_6=\mu_7=m \quad \text{and} \quad \mu_5=\mu_4=\mu=\frac{5mM}{M+5m}.$$

Since there are thirteen force constants and only eight fundamental frequencies, an approximation must be made in the evaluation of the five force constants or these five must be evaluated from data on isotopic molecules.

IV. THE NORMAL MODES OF VIBRATION

The frequencies ω_n of the normal or characteristic modes of vibration of the molecular model are obtained from the solution of Lagrange's determinantal equation, $|\lambda T_v-U_0|=0$, where $\lambda_n=4\pi^2c^2\omega_n^2$, if c is the velocity of light in cm/sec and ω_n is the frequency in cm^{-1}. The steps of the secular determinant associated with the various symmetry species have the following forms:

$$A_1'\text{:}\quad\begin{vmatrix}\lambda-\dfrac{k_{11}}{m} & -\dfrac{k_{12}}{m}\\ -\dfrac{k_{12}}{m} & \lambda-\dfrac{k_{22}}{m}\end{vmatrix}=0\,. \tag{5a}$$

A_2': none.

A_1'': none.

$$A_2''\text{:}\quad\begin{vmatrix}\lambda-k_{33}/m & -k_{34}/(\mu m)^{\frac{1}{2}}\\ -k_{34}/(\mu m)^{\frac{1}{2}} & \lambda-k_{44}/\mu\end{vmatrix}=0 \tag{5b}$$

$$E'\text{:}\quad\begin{vmatrix}\lambda-k_{55}/\mu & -k_{56}/(\mu m)^{\frac{1}{2}} & -k_{57}/(\mu m)^{\frac{1}{2}}\\ -k_{56}/(\mu m)^{\frac{1}{2}} & \lambda-k_{66}/m & -k_{67}/m\\ -k_{57}/(\mu m)^{\frac{1}{2}} & -k_{67}/m & \lambda-k_{77}/m\end{vmatrix}=0. \tag{5c}$$

E'': $\lambda-k_{88}/m=0$. (5d)

The following relations among the frequencies of various symmetry species can be obtained from the expansion of the steps of the secular determinant:

A_1':
$$\lambda_1+\lambda_2=(k_{11}+k_{22})/m,$$
$$\lambda_1\lambda_2=(k_{11}k_{22}-k_{12}^2)/m^2, \tag{6a}$$

A_2'':
$$\lambda_3+\lambda_4=k_{33}/m+k_{44}/\mu,$$
$$\lambda_3\lambda_4=(k_{33}k_{44}-k_{34}^2)/m\mu; \tag{6b}$$

E':
$$\lambda_5+\lambda_6+\lambda_7=k_{55}/\mu+(k_{66}+k_{77})/m,$$
$$\lambda_5\lambda_6+\lambda_5\lambda_7+\lambda_6\lambda_7=(k_{55}k_{66}-k_{56}^2)/\mu m+(k_{55}k_{77}-k_{57}^2)/\mu m+(k_{66}k_{77}-k_{67}^2)/m^2, \tag{6c}$$
$$\lambda_5\lambda_6\lambda_7=\begin{vmatrix}k_{55}/\mu & k_{56}/(\mu m)^{\frac{1}{2}} & k_{57}/(\mu m)^{\frac{1}{2}}\\ k_{56}/(\mu m)^{\frac{1}{2}} & k_{66}/m & k_{67}/m\\ k_{57}/(\mu m)^{\frac{1}{2}} & k_{67}/m & k_{77}/m\end{vmatrix},$$

E'': $\lambda_8=k_{88}/m$. (6d)

The following equations give the transformation from the symmetry coordinates of Eq. (3) to the normal coordinates Q_n for the species A_1':

$$S_i=\sum_{k=1}^{2}n_{ik}Q_k, \quad i=1, 2 \tag{7}$$

where n_{ik} is the normalized cofactor of the ki element of the secular determinant in Eq. (5a) with $\lambda=\lambda_k$; for

species A_2''

$$S_l=\sum_{m=3}^{4} n_{lm}Q_m, \quad l=3, 4 \tag{8}$$

where n_{lm} is the normalized cofactor of the ml element of the secular determinant in Eq. (5b) with $\lambda=\lambda_m$; for species E'

$$S_{ja}=\sum_{l=5}^{7} n_{jl}Q_{la},$$

$$S_{jb}=\sum_{l=5}^{7} n_{jl}Q_{lb}, \quad j=5, 6, 7 \tag{9}$$

where n_{jl} is the normalized cofactor of the lj element of the secular determinant in Eq. (5c) with $\lambda=\lambda_l$. Finally S_{8a} and S_{8b} are already normal coordinates. In terms of the normal coordinates, the kinetic and harmonic potential energies of vibration become

$$T_v=\tfrac{1}{2}\left[\sum_{i=1}^{4}\dot{Q}_i^2+\sum_{l=5}^{8}(\dot{Q}_{la}^2+\dot{Q}_{lb}^2)\right], \tag{10}$$

and

$$U_0=\tfrac{1}{2}\left\{\sum_{i=1}^{4}\lambda_i Q_i^2+\sum_{l=5}^{7}\lambda_l(Q_{la}^2+Q_{lb}^2)\right\}. \tag{11}$$

It is convenient to introduce dimensionless coordinates q_n, which are given by the transformation, $Q_n=(\hbar/2\pi C\omega_n)^{\frac{1}{2}}q_n$, and in terms of which the zero-order vibrational energy is given in the Hamiltonian form as

$$H_{0v}=\left(\frac{hc}{2}\right)\left\{\sum_{i=1}^{4}\omega_i\left[\left(\frac{p_i^2}{\hbar^2}\right)+q_i^2\right]+\sum_{k=5}^{8}\omega_k\left[\left(\frac{p_{ka}^2+p_{kb}^2}{\hbar^2}\right)+(q_{ka}^2+q_{kb}^2)\right]\right\}. \tag{12}$$

V. ANHARMONIC POTENTIAL FUNCTION

Since each term in the expression for the total energy must belong to the symmetry type A_1', it can be shown by direct multiplication of the characters in Table II that the cubic combinations of normal coordinates occurring in the anharmonic potential function of a molecule belonging to symmetry group D_{3h} are $A_1'^3$, $A_1'^2A_1'$, $[A_2'^2A_1']$, $[A_1''^2A_1']$, $A_2''^2A_1'$, $A_1'^{(2)}A_1'$, $[A_2'^{(2)}A_2']$, $[A_1''^{(2)}A_1'']$, $A_2''^{(2)}A_2''$, and $A_1'^{(3)}$. Likewise the quartic combinations occurring are $A_1'^4$, $A_1'^3A_1'$, $A_1'^2A_1'^2$, $[A_1'^2A_1''^2]$, $[A_1'^2A_2'^2]$, $A_1'^2A_2''^2$, $[A_2'^4]$, $[A_2'^1A_1''^2]$, $[A_2'^2A_2''^2]$, $[A_1''^4]$, $[A_1''^2A_2''^2]$, $A_2''^4$, $(A_1'^{(2)})^2$, $A_1'^{(2)}A_1'^2$, $[A_1'^{(2)}A_1''^2]$, $[A_1'^{(2)}A_2'^2]$, $A_1'^{(2)}A_2''^2$, $(A_2'^{(2)})^2$, $(A_1''^{(2)})^2$, $(A_2''^{(2)})^2$, $A_1'^{(3)}A_1'$, $[A_2'^{(3)}A_2']$, $[A_1''^{(3)}A_1'']$, and $A_2''^{(3)}A_2''$. The terms in square brackets, such as $[A_2'^2A_1''^2]$, do not occur in the case of the XY_5 because there is no normal coordinate of the first degree of the type A_2' and A_1'', respectively. The designations $X^{(n)}$ are used to refer to the quadratic or cubic combinations of degenerate normal coordinates of the various symmetry types.[3] The most general cubic portion U_1 of the anharmonic potential function of the XY_5 molecular model is given by[4]

$$\begin{aligned}U_1/hc=&\sum_{i=1}^{2}\Big\{\beta_{iii}q_i^3+\sum_{i'}\beta_{iii'}q_i^2q_{i'}+\sum_{j}\beta_{ijj}q_iq_j^2\\&+\sum_{j'>j}\beta_{ijj'}q_iq_jq_{j'}+\sum_{k}\beta_{ikk}q_i(q_{ka}^2+q_{kb}^2)\\&+\sum_{\substack{k'\\(k'>k)}}\sum_{k}\beta_{ikk'}q_i(q_{ka}q_{k'a}+q_{kb}q_{k'b})\\&+\beta_{i88}q_i(q_{8a}^2+q_{8b}^2)\Big\}+\sum_{j}\sum_{k}\beta_{jk8}q_j(q_{ka}q_{8b}+q_{kb}q_{8a})\\&+\sum_{k}\beta_{k88}[2q_{8a}q_{8b}q_{ka}+(q_{8a}^2-q_{8b}^2)q_{kb}]\\&+\sum_{k''}\sum_{k'}\sum_{k}\beta_{kk'k''}\{(q_{ka}q_{k'b}+q_{kb}q_{k'a})q_{k''b}\\&-(q_{ka}q_{k'a}-q_{kb}q_{k'b})q_{k''a}\}.\end{aligned} \tag{13}$$

To second-order approximation[5] the quartic portion U_2, of the anharmonic potential function is given by

$$\begin{aligned}U_2/kc=&\sum_{i}\left\{\gamma_{iiii}q_i^4+\sum_{i'}\gamma_{iii'i'}q_i^2q_{i'}^2\right\}\\&+\sum_{j}\left\{\gamma_{jjjj}q_j^4+\sum_{j'}\gamma_{jjj'j'}q_j^2q_{j'}^2\right\}\\&+\sum_{k}\left\{\gamma_{kkkk}(q_{ka}^2+q_{kb}^2)^2\right.\end{aligned}$$

Equation 14 continued on next page.

[3] The quadratic combinations are as follows: $(q_{ka}^2+q_{kb}^2)$ and $(q_{ka}q_{k'a}+q_{kb}q_{k'b})$ of type $A_1'^{(2)}$; $q_{ka}q_{k'b}-q_{kb}q_{k'a}$ of type $A_2'^{(2)}$; $q_{ka}q_{8a}-q_{kb}q_{8b}$ of type $A_1''^{(2)}$; and $q_{ka}q_{8b}+q_{kb}q_{8a}$ of type $A_2''^{(2)}$. The cubic combinations are as follows: $(q_{ka}q_{k'b}+q_{kb}q_{k'a})q_{k''b}-(q_{ka}q_{k'a}-q_{kb}q_{k'b})q_{k''a}$ of type $A_1'^{(3)}$; $(q_{ka}q_{k'b}+q_{kb}q_{k'a})q_{k''a}+(q_{ka}q_{k'a}-q_{kb}q_{k'b})q_{k''b}$ of type $A_2'^{(3)}$; $(q_{ka}q_{8b}-q_{kb}q_{8a})q_{k'a}-(q_{ka}q_{8a}+q_{kb}q_{8b})q_{k'b}$ of type $A_2''^{(3)}$; $(q_{ka}q_{8b}-q_{kb}q_{8a})q_{k'b}+(q_{ka}q_{8a}+q_{kb}q_{8b})q_{k'a}$ of type $A_1''^{(3)}$; and $2q_{8a}q_{8b}q_{ka}+(q_{8a}^2-q_{8b}^2)q_{kb}$ of type $A_1'^{(3)}$.

[4] In the remainder of this paper, coordinates of type A_1' will be denoted by subscripts $i=1, 2$; A_2'' by $j=3, 4$; E' by $k=5, 6, 7$; and E'' by $1=8$. Primed and unprimed subscripts in a given summation refer to different coordinates of the same symmetry type. Each combination of subscripts may occur only once, i.e., permutations are not allowed.

[5] The most general quartic portion of the anharmonic potential function contains the following additional terms which are of odd degree in at least one coordinate and do not ordinarily contribute to the allowed energies:

$q_i^3q_{i'}$, $q_j^3q_{j'}$, $(q_{ka}^2+q_{kb}^2)(q_{ka}q_{k'a}+q_{kb}q_{k'b})$,
$(q_{ka}^2+q_{kb}^2)(q_{k'a}q_{k''a}+q_{k'b}q_{k''b})$,
$(q_{ka}q_{k'a}+q_{kb}q_{k'b})(q_{ka}q_{k''a}+q_{kb}q_{k''b})$, $q_iq_{i'}(q_{ka}q_{k'a}+q_{kb}q_{k'b})$,
$q_i^2(q_{ka}q_{k'a}+q_{kb}q_{k'b})$, $q_j^2(q_{ka}q_{k'a}+q_{kb}q_{k'b})$, $q_{jj'}(q_{ka}q_{k'a}+q_{kb}q_{k'b})$,
$q_iq_{i'}(q_{8a}^2+q_{8b}^2)$, $q_iq_j(q_{ka}q_{8b}+q_{kb}q_{8a})$,
$(q_{kb}q_{k'b}-q_{kb}q_{k'a})(q_{ka}q_{k''b}-q_{kb}q_{k''a})$, $(q_{8a}^2+q_{8b}^2)(q_{ka}q_{k'a}+q_{kb}q_{k'b})$,
$(q_{ka}q_{8a}-q_{kb}q_{8b})(q_{k'a}q_{8a}-q_{k'b}q_{8b})$, $(q_{ka}q_{8b}+q_{kb}q_{8a})(q_{k'a}q_{8b}+q_{k'b}q_{8a})$,
$[(q_{ka}q_{k'b}+q_{kb}q_{k'a})q_{k''b}-(q_{ka}q_{k'a}-q_{kb}q_{k'b})q_{k''a}]q_i$,
$[2q_{8a}q_{8b}q_{ka}+(q_{8a}^2-q_{8b}^2)q_{kb}]q_i$, and
$[(q_{ka}q_{8b}-q_{kb}q_{8a})q_{k'a}-(q_{ka}q_{8a}+q_{ka}q_{8b})q_{k'b}]q_j$.

$$+\sum_{k'>k}\gamma_{kkk'k'}(q_{ka}q_{k'a}+q_{kb}q_{k'b})^2$$

$$+\sum_{k'>k}\gamma_{kkk'k'}(q_{ka}^2+q_{kb}^2)(q_{k'a}^2+q_{k'b}^2)$$

$$+\sum_{k'>k}\gamma_{kkk'k'}(q_{ka}q_{k'b}-q_{kb}q_{k'a})^2\Big\}$$

$$+\sum_j\Big\{\sum_k\gamma_{jjkk}q_j^2(q_{ka}^2+q_{kb}^2)$$

$$+\gamma_{jj88}q_j^2(q_{8a}^2+q_{8b}^2)\Big\}+\sum_i\Big\{\sum_j\gamma_{iijj}q_i^2q_j^2$$

$$+\sum_k\gamma_{iikk}q_i^2(q_{ka}^2+q_{kb}^2)+\gamma_{ii88}q_i^2(q_{8a}^2+q_{8b}^2)\Big\}$$

$$+\sum_k\Big\{\gamma_{kk88}(q_{ka}^2+q_{kb}^2)(q_{8a}^2+q_{8b}^2)$$

$$+\gamma_{k8k8}(q_{ka}q_{8a}-q_{kb}q_{8b})^2$$

$$+\gamma_{k8k8}(q_{ka}q_{8b}+q_{kb}q_{8a})^2\Big\}+\gamma_{8888}(q_{8a}^2+q_{8b}^2)^2. \quad (14)$$

VI. VIBRATIONAL ANGULAR MOMENTUM

The components of internal angular momentum of vibration p_x, p_y, and p_z have importance in connection with the Coriolis interaction between the total and internal angular moments and are of the same symmetry type as the components of total angular momentum. An E'' pair is formed between p_x and p_y and while p_z is of the type A_2'. These components are defined as

$$p_x=\sum_{i=1}^{6}m_i(y_i'\dot{z}_i'-z_i'\dot{y}_i'),$$

$$p_y=\sum_{i=1}^{6}m_i(z_i'\dot{x}_i'-x_i'\dot{z}_i'),$$

$$p_z=\sum_{i=1}^{6}m_i(x_i'\dot{y}_i'-y_i'\dot{x}_i'),$$

and are expressed in terms of the dimensionless normal coordinates q_i and conjugate moments p_i as follows:

$$p_x=\sum_{i=1}^{2}\xi_i\left[\left(\frac{\omega_{8a}}{\omega_i}\right)^{\frac{1}{2}}p_{8a}q_i-\left(\frac{\omega_i}{\omega_{8a}}\right)^{\frac{1}{2}}p_iq_{8a}\right]$$

$$+\sum_{k=5}^{7}\xi_k\left[\left(\frac{\omega_{8a}}{\omega_{ka}}\right)^{\frac{1}{2}}p_{8a}q_{ka}-\left(\frac{\omega_{ka}}{\omega_{8a}}\right)^{\frac{1}{2}}p_{ka}q_{8a}\right]$$

$$+\sum_{k'}\xi_{k'}\left[\left(\frac{\omega_{8b}}{\omega_{k'b}}\right)^{\frac{1}{2}}p_{8b}q_{k'b}-\left(\frac{\omega_{k'b}}{\omega_{8b}}\right)^{\frac{1}{2}}p_{k'b}q_{8b}\right]$$

$$+\sum_k\sum_i\xi_{kj}\left[\left(\frac{\omega_j}{\omega_{kb}}\right)^{\frac{1}{2}}p_jq_{kb}-\left(\frac{\omega_{kb}}{\omega_j}\right)^{\frac{1}{2}}p_{kb}q_j\right], \quad (15)$$

$$p_y=\sum_{i=1}^{2}\eta_i\left[\left(\frac{\omega_{8b}}{\omega_i}\right)^{\frac{1}{2}}p_{8b}q_i-\left(\frac{\omega_i}{\omega_{8b}}\right)^{\frac{1}{2}}p_iq_{8b}\right]$$

$$+\sum_{k=5}^{7}\eta_k\left[\left(\frac{\omega_{8b}}{\omega_{kb}}\right)^{\frac{1}{2}}p_{8b}q_{kb}-\left(\frac{\omega_{kb}}{\omega_{8b}}\right)^{\frac{1}{2}}p_{kb}q_{8b}\right]$$

$$+\sum_{k'}\eta_{k'}\left[\left(\frac{\omega_{8a}}{\omega_{k'a}}\right)^{\frac{1}{2}}p_{8a}q_{k'a}-\left(\frac{\omega_{k'a}}{\omega_{8a}}\right)^{\frac{1}{2}}p_{k'a}q_{8a}\right]$$

$$+\sum_k\sum_j\eta_{kj}\left[\left(\frac{\omega_j}{\omega_{ka}}\right)^{\frac{1}{2}}p_jq_{ka}-\left(\frac{\omega_{ka}}{\omega_j}\right)^{\frac{1}{2}}p_{ka}q_j\right],$$

and

$$p_z=\sum_{k',k=5}^{7}\zeta_{kk'}\left[\left(\frac{\omega_{k'b}}{\omega_{ka}}\right)^{\frac{1}{2}}p_{kb}q_{k'a}-\left(\frac{\omega_{k'a}}{\omega_{kb}}\right)^{\frac{1}{2}}p_{k'a}q_{kb}\right]$$

$$+\zeta_8\left[\left(\frac{\omega_{8b}}{\omega_{8a}}\right)^{\frac{1}{2}}q_{8a}p_{8b}-\left(\frac{\omega_{8a}}{\omega_{8b}}\right)^{\frac{1}{2}}q_{8b}p_{8a}\right],$$

where

$$\xi_i=(m/I_{ex}^{\frac{1}{2}})[n_{1i}D_0-(\tfrac{3}{2})^{\frac{1}{2}}n_{2i}d_0]=\eta_i,$$

$$\xi_k=(m/I_{ex}^{\frac{1}{2}})D_0n_{7k}=-\eta_k=-\xi_{k'}=\eta_{k'},$$

$$\xi_{kj}=n_{5k}n_{4j}+n_{6k}n_{3j}=\eta_{kj},\quad j=3,4;\quad k=5,6,7,$$

$$\zeta_{kk'}=n_{5k}n_{5k'}+n_{6k}n_{6k'}-n_{7k}n_{7k'}\quad\text{for}\quad k',\quad k=5,6,7.$$

VII. VALENCE SYMMETRY COORDINATES

The generalized symmetry coordinates defined in Eqs. (3) were used in setting up the general quadratic potential function given in Eq. (5). The generalized force constants occurring in Eq. (5) do not have obvious physical significance and are not appropriate for use in the analysis of experimental data. It has been found in many cases that a suitable potential function for analysis of data is based on so-called valence coordinates which are changes in the length of valence bonds and changes in the included valence angles. For infinitesmal displacements there are linear relationships between the valence coordinates and the generalized symmetry coordinates defined in Eqs. (3). One can obtain linear relations between the generalized force constants in Eq. (5) and those in a valence type quadratic potential function.

The valence coordinates can best be described in terms of changes in distances between pairs of atoms. The infinitesmal change in distance δp_{mn} between the mth and nth atoms is given in terms of the original rectangular coordinates and displacements as follows:

$$\delta p_{mn}=[(x_{0m}-x_{0n})(x_m'-x_n')+(y_{0m}-y_{0n})(y_m'-y_n')+(z_{0m}-z_{0n})(z_m'-z_n')]/p_{0mn}. \quad (16)$$

The valence coordinates suitable for description of infinitesmal vibrations of a group of three atoms (m, n, and a central atom) are illustrated in Fig. 2, where $r_m=r_{0m}+\delta r_m$, $r_n=r_{0n}+\delta r_n$, and $\beta_{mn}=\beta_{0mn}+\delta\beta_{mn}$; r_m, r_n, and β_{mn} denote, respectively, the instantaneous values of the two valence bond lengths and the included bond angle, while r_{0m}, r_{0n}, and β_{0mn} denote their equilibrium values, and δr_m, δr_n, and $\delta\beta_{mn}$ denote changes occurring during vibrations. The quantity $\delta\beta_{mn}$ is given for infinitesmal vibrations by

$$\delta\beta_{mn}=[p_{0mn}\delta p_{mn}-(r_{0m}-r_{0n}\cos\beta_{0mn})\delta r_m -(r_{0n}-r_{0m}\cos\beta_{0mn})\delta r_n]/r_{0m}r_{0n}\sin\beta_{0mn}, \quad (17)$$

where p_{mn} is the distance between atoms m and n.

Following a procedure similar to that outlined by Shaffer and Herman,[6] it is possible to obtain the combination of valence coordinates (orthonormal) listed below for the XY_5 molecular model which belong to the various symmetry types.

Type A_1':

$$\Delta_1=1/(3)^{\frac{1}{2}}(\delta r_1+\delta r_2+\delta r_3)=a_1S_1,$$

$$\Delta_2=1/(2)^{\frac{1}{2}}(\delta r_5+\delta r_6)=a_2S_2,$$

$$\Delta_{01}=1/(3)^{\frac{1}{2}}(\delta\alpha_{12}+\delta\alpha_{13}+\delta\alpha_{23})\equiv 0,$$

$$(\text{redundant coordinate})=a_0S_1,$$

$$\Delta_{02}=1/(6)^{\frac{1}{2}}(\delta\beta_{15}+\delta\beta_{16}+\delta\beta_{25}+\delta\beta_{26}+\delta\beta_{35}+\delta\beta_{36})$$

$$\equiv 0\ (\text{redundant coordinate})=\sum_{i=1}^{2}a_{0i}S_i.$$

Type A_2': none.

Type A_1'': none.

Type A_2'':

$$\Delta_3=1/(2)^{\frac{1}{2}}(\delta r_5-\delta r_6)=\sum_{j=3}^{4}a_{3j}S_j,$$

$$\Delta_4=1/(6)^{\frac{1}{2}}(\delta\beta_{15}-\delta\beta_{16}+\delta\beta_{25}-\delta\beta_{26}+\delta\beta_{35}-\delta\beta_{36})$$

$$=\sum_{j=3}^{4}a_{4j}S_j. \quad (18)$$

Type E':

$$\Delta_{5a}=1/(6)^{\frac{1}{2}}(2\delta r_1-\delta r_2-\delta r_3)=\sum_{k=5}^{7}a_{5k}S_{ka},$$

$$\Delta_{5b}=1/(2)^{\frac{1}{2}}(\delta r_2-\delta r_3)=\sum_{k=5}^{7}a_{5k}S_{kb},$$

$$\Delta_{6a}=1(6)^{\frac{1}{2}}(\delta\alpha_{12}+\delta\alpha_{23}-2\delta\alpha_{13})=\sum_{k=5}^{7}a_{6k}S_{ka},$$

$$\Delta_{6b}=1(2)^{\frac{1}{2}}(\delta\alpha_{23}-\delta\alpha_{12})=\sum_{k=5}^{7}a_{6k}S_{kb},$$

$$\Delta_{7a}=1(12)^{\frac{1}{2}}(2\delta\beta_{15}-\delta\beta_{25}-\delta\beta_{35}+2\delta\beta_{16}-\delta\beta_{26}-\delta\beta_{36})$$

$$=\sum_{k=5}^{7}a_{7k}S_{ka},$$

$$\Delta_{7b}=1/2(\delta\beta_{25}-\delta\beta_{35}+\delta\beta_{26}-\delta\beta_{36})=\sum_{k=5}^{7}a_{7k}S_{kb}.$$

Type E'':

$$\Delta_{8a}=(1/12)^{\frac{1}{2}}(2\delta\beta_{15}-\delta\beta_{25}-\delta\beta_{35}-2\delta\beta_{16}+\delta\beta_{26}+\delta\beta_{36})$$

$$=a_8S_{8b},$$

$$\Delta_{8b}=1/2(\delta\beta_{25}-\delta\beta_{35}-\delta\beta_{26}+\delta\beta_{36})=-a_8S_{8a},$$

where

$$a_1=a_2=\left(\frac{1}{m}\right)^{\frac{1}{2}},\quad a_{01}=\left(\frac{2}{m}\right)^{\frac{1}{2}}\frac{\cot\beta_{015}}{d_0},$$

$$a_{02}=\left(\frac{3}{m}\right)^{\frac{1}{2}}\frac{\cot\beta_{015}}{d_0},$$

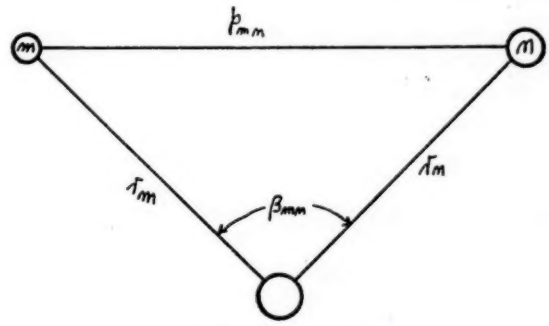

FIG. 2. Valence coordinates.

$$a_0=\frac{1+2\cos\alpha_{012}}{m^{\frac{1}{2}}d_0\sin\alpha_{012}},$$

$$a_{33}=\left(\frac{3}{5m}\right)^{\frac{1}{2}},\quad a_{43}=\frac{2}{(5m)^{\frac{1}{2}}d_0\sin\beta_{015}},$$

$$a_{34}=\left(\frac{2}{\mu}\right)^{\frac{1}{2}},\quad a_{44}=-\gamma_0\left(\frac{6}{\mu}\right)^{\frac{1}{2}},$$

$$a_{55}=\left(\frac{3}{2\mu}\right)^{\frac{1}{2}},\quad a_{65}=\frac{\alpha_0}{2}\left(\frac{3}{2\mu}\right)^{\frac{1}{2}},\quad a_{75}=-\gamma_0\left(\frac{3}{\mu}\right)^{\frac{1}{2}},$$

$$a_{57}=-\left(\frac{1}{2m}\right)^{\frac{1}{2}},\quad a_{67}=\frac{\beta_0}{2}\left(\frac{1}{2m}\right)^{\frac{1}{2}},$$

$$a_{77}=-\epsilon_0\left(\frac{1}{m}\right)^{\frac{1}{2}}, \quad (19)$$

$$a_{56}=-\left(\frac{1}{5m}\right)^{\frac{1}{2}},\quad a_{66}=-\frac{\alpha_0}{2}\left(\frac{1}{5m}\right)^{\frac{1}{2}},$$

$$a_{76}=-\delta_0\left(\frac{2}{5m}\right)^{\frac{1}{2}},$$

Equation 19 continued on next page.

[6] W. H. Shaffer and R. C. Herman, J. Chem. Phys. **12**, 494 (1944); R. C. Herman and W. H. Shaffer, J. Chem. Phys. **17**, 30 (1949).

$$a_8=\frac{1}{d_0D_0\sin\beta_{015}}\left(\frac{I_{ex}}{m^2}\right)^{\frac{1}{2}},\quad \alpha_0\equiv\frac{1-\cos\alpha_{012}}{d_0\sin\alpha_{012}},$$

$$\beta_0\equiv\frac{2+\cos\alpha_{012}}{d_0\sin\alpha_{012}},$$

$$\gamma_0\equiv\frac{1}{\sin\beta_{015}}\left(\frac{1}{d_0}-\frac{\cos\beta_{015}}{D_0}\right),$$

$$\delta_0\equiv\frac{1}{\sin\beta_{015}}\left(\frac{3}{2D_0}+\frac{\cos\beta_{015}}{d_0}\right),$$

$$\text{and}\quad \epsilon_0\equiv\frac{\cos\beta_{015}}{d_0\sin\beta_{015}}.$$

One needs the inverse transformations giving the intermediate symmetry coordinates, S_i's, defined in Eqs. (3) in terms of the valence symmetry coordinates defined above, in order to set up the kinetic and potential energy expressions in terms of the valence coordinates. These relations are given below.

$$\begin{aligned}
S_i&=(m)^{\frac{1}{2}}\Delta_i \quad \text{for} \quad i=1,2,\\
S_j&=\sum_{j'=3}^{4} b_{jj'}\Delta_{j'} \quad \text{for} \quad j=3,4,\\
S_{ka}&=\sum_{k'} b_{kk'}\Delta_{k'a} \quad \text{for} \quad k=5,6,7,\\
S_{kb}&=\sum_{k'} b_{kk'}\Delta_{k'b} \quad \text{for} \quad k=5,6,7,\\
S_{8a}&=b_8\Delta_{8b},\\
S_{8b}&=b_9\Delta_{8a},
\end{aligned}\tag{20}$$

where

$$b_{33}=\frac{(15m)^{\frac{1}{2}}\gamma_0\sin\beta_{015}}{\sigma_0},\quad b_{34}=\frac{(5m)^{\frac{1}{2}}\sin\beta_{015}}{\sigma_0},$$

$$b_{43}=\frac{(2\mu)^{\frac{1}{2}}}{d_0\sigma_0},\quad b_{44}=-\left(\frac{3\mu}{2}\right)^{\frac{1}{2}}\frac{\sin\beta_{015}}{\sigma_0},$$

$$b_{55}=\left(\frac{2\mu}{3}\right)^{\frac{1}{2}}\left(\frac{\beta_0\delta_0+\alpha_0\epsilon_0}{\rho_0}\right),$$

$$b_{56}=-2\left(\frac{2\mu}{3}\right)^{\frac{1}{2}}\left(\frac{\epsilon_0-\delta_0}{\rho_0}\right),$$

$$b_{57}=-\left(\frac{\mu}{3}\right)^{\frac{1}{2}}\frac{1}{(\gamma_0+\delta_0)},$$

$$b_{65}=\frac{(5m)^{\frac{1}{2}}(\alpha_0\epsilon_0+\beta_0\gamma_0)}{\rho_0},\quad b_{66}=-\frac{2(5m)^{\frac{1}{2}}(\epsilon_0+\gamma_0)}{\rho_0},\tag{21}$$

$$b_{67}=-\left(\frac{5m}{2}\right)^{\frac{1}{2}}\frac{1}{(\gamma_0+\delta_0)},$$

$$b_{75}=-\frac{(2m)^{\frac{1}{2}}\alpha_0}{\alpha_0+\beta_0},\quad b_{76}=\frac{2(2m)^{\frac{1}{2}}}{\alpha_0+\beta_0},\quad b_{77}=0,$$

$$b_8=-(1/I_{ex})^{\frac{1}{2}}md_0D_0\sin\beta_{015}=-b_9,$$

where

$$\sigma_0\equiv\frac{5}{d_0}-\frac{3\cos\beta_{015}}{D_0}\quad\text{and}\quad \rho_0\equiv(\alpha_0+\beta_0)(\gamma_0+\delta_0).$$

The vibrational kinetic energy T_v can be written in terms of the valence symmetry coordinates with the aid of Eqs. (20) and (4) and is given by the following expression:

$$\begin{aligned}
2T_v=&\sum_{i=1}^{2} M_i\dot{\Delta}_i^2+\sum_{j=3}^{4}\left\{M_j\dot{\Delta}_j^2+2\sum_{j'>j}M_{jj'}\dot{\Delta}_j\dot{\Delta}_{j'}\right\}\\
&+\sum_k\left\{M_k(\dot{\Delta}_{ka}^2+\dot{\Delta}_{kb}^2)\right.\\
&\left.+2\sum_{k'>k}M_{kk'}(\dot{\Delta}_{ka}\dot{\Delta}_{k'a}+\dot{\Delta}_{kb}\dot{\Delta}_{k'b})\right\}\\
&+M_8(\dot{\Delta}_{8a}^2+\dot{\Delta}_{8b}^2),
\end{aligned}\tag{22}$$

where

$$\begin{aligned}
M_1&=m=M_2,\\
M_3&=(5m/\sigma_0^2d_0^2)[\gamma_0^2d_0^2\sin^2\beta_{015}\\
&\qquad+(2M/(5m+M))],\\
M_4&=[(25m)\sin^2\beta_{015}/2\sigma_0^2][(2m+M)/(5m+M)],\\
M_{34}&=[(3^{\frac{1}{2}}(5m)\sin^2\beta_{015})/\sigma_0^2d_0]\\
&\qquad\times[d_0\gamma_0-M/(5m+M)];
\end{aligned}\tag{23}$$

$$M_k=\sum_{k'}2b_{k'k}^2,$$

$$M_{kk'}=\sum_{k''}2(b_{k''k}b_{k''k'}+b_{k''k'}b_{k''k})$$

for $k'>k$, and

$$M_8=(I_{ex})/(md_0D_0\sin\beta_{015})^2.$$

VIII. VALENCE POTENTIAL FUNCTION

The most general quadratic potential function, U_0, satisfying the symmetry conditions is given in terms of the valence symmetry coordinates by

$$\begin{aligned}
2U_0=&\sum_i\left\{K_i\Delta_i^2+2\sum_{i'>i}K_{ii'}\Delta_i\Delta_{i'}\right\}\\
&+\sum_j\left\{K_j\Delta_j^2+2\sum_{j'>j}K_{jj'}\Delta_j\Delta_{j'}\right\}\\
&+\sum_k\left\{K_k(\Delta_{ka}^2+\Delta_{kb}^2)\right.\\
&\left.+2\sum_{k'>k}K_{kk'}(\Delta_{ka}\Delta_{k'a}+\Delta_{kb}\Delta_{k'b})\right\}\\
&+K_8(\Delta_{8a}^2+\Delta_{8b}^2),
\end{aligned}\tag{24}$$

in which the cross products occur only among symmetry coordinates of the same type. The complete valence-type potential function U_0 for the XY_5 molecular model

can be written in terms of the valence coordinates as

$$
\begin{aligned}
2U_0 = {} & c_1(\delta r_1^2+\delta r_2^2+\delta r_3^2) \\
& +c_2(\delta r_5^2+\delta r_6^2)+c_3 d_0^2(\delta\alpha_{12}^2+\delta\alpha_{13}^2+\delta\alpha_{23}^2) \\
& +c_4(d_0D_0)(\delta\beta_{15}^2+\delta\beta_{25}^2+\delta\beta_{35}^2+\delta\beta_{16}^2+\delta\beta_{26}^2 \\
& +\delta\beta_{36}^2)+2c_1'(\delta r_1\delta r_2+\delta r_1\delta r_3+\delta r_2\delta r_3) \\
& +2c_2'\delta r_5\delta r_6+2c_3' d_0^2(\delta\alpha_{12}\delta\alpha_{13}+\delta\alpha_{12}\delta\alpha_{23} \\
& +\delta\alpha_{13}\delta\alpha_{23})+2d_0D_0[\delta\beta_{15}\{c_4'(\delta\beta_{25}+\delta\beta_{35}) \\
& +c_4'''(\delta\beta_{26}+\delta\beta_{36})\}+\delta\beta_{25}\{c_4'\delta\beta_{35} \\
& +c_4'''(\delta\beta_{16}+\delta\beta_{36})+c_4''\delta\beta_{26}\} \\
& +\delta\beta_{35}\{c_4''\delta\beta_{36}+c_4'''(\delta\beta_{16}+\delta\beta_{26})\} \\
& +c_4'\delta\beta_{16}(\delta\beta_{26}+\delta\beta_{36})+c_4'\delta\beta_{26}\delta\beta_{36}] \\
& +2d_0[\delta r_1\{c_{13}'\delta\alpha_{23}+c_{13}(\delta\alpha_{12}+\delta\alpha_{13})\} \\
& +\delta r_2\{c_{13}'\delta\alpha_{13}+c_{13}(\delta\alpha_{12}+\delta\alpha_{23})\} \qquad (25) \\
& +\delta r_3\{c_{13}'\delta\alpha_{12}+c_{13}(\delta\alpha_{13}+\delta\alpha_{23})\}] \\
& +2(d_0D_0)^{\frac{1}{2}}\{(\delta\beta_{15}+\delta\beta_{16})[c_{14}\delta r_1+c_{14}'(\delta r_2+\delta r_3) \\
& +d_0\{c_{34}'\delta\alpha_{23}+c_{34}(\delta\alpha_{12}+\delta\alpha_{13})\}] \\
& +(\delta\beta_{25}+\delta\beta_{26})[c_{14}\delta r_2+c_{14}'(\delta r_1+\delta r_3) \\
& +d_0\{c_{34}'\delta\alpha_{13}+c_{34}(\delta\alpha_{12}+\delta\alpha_{23})\}] \\
& +(\delta\beta_{35}+\delta\beta_{36})[c_{14}\delta r_3+c_{14}'(\delta r_1+\delta r_2) \\
& +d_0\{c_{34}'\delta\alpha_{12}+c_{34}(\delta\alpha_{13}+\delta\alpha_{23})\}]\} \\
& +2c_{23}d_0(\delta r_5+\delta r_6)(\delta\alpha_{12}+\delta\alpha_{13}+\delta\alpha_{23}) \\
& +2(d_0D_0)^{\frac{1}{2}}[(\delta\beta_{15}+\delta\beta_{25}+\delta\beta_{35})(c_{24}\delta r_5+c_{24}'\delta r_6) \\
& +(\delta\beta_{16}+\delta\beta_{26}+\delta\beta_{36})(c_{24}\delta r_6+c_{24}'\delta r_5)] \\
& +2c_{12}(\delta r_1+\delta r_2+\delta r_3)(\delta r_5+\delta r_6),
\end{aligned}
$$

$$
\begin{aligned}
& K_1=c_1+2c_1', \quad K_{12}=6^{\frac{1}{2}}c_{12}, \quad K_{1,01}=(\tfrac{1}{3})(5c_{13}+3c_{13}'), \\
& \qquad\qquad K_{1,02}=2^{\frac{1}{2}}(c_{14}+2c_{14}'), \\
& K_2=c_2+c_2', \quad K_{2,01}=6^{\frac{1}{2}}c_{23}, \quad K_{2,02}=3^{\frac{1}{2}}(c_{24}+c_{24}'), \\
& \qquad K_{01}=c_3+2c_3', \quad K_{01,02}=2^{\frac{1}{2}}(2c_{34}+c_{34}'), \\
& \qquad K_{02}=c_4+c_4''+2(c_4'+c_4'''), \qquad (26) \\
& K_3=c_2+c_2', \quad K_{34}=3^{\frac{1}{2}}(c_{24}-c_{24}'), \\
& K_4=c_4-c_4''+2(c_4'-c_4''), \\
& K_5=c_1-c_1', \quad K_{56}=(\tfrac{1}{2})(c_{13}'-c_{13}), \quad K_{57}=2^{\frac{1}{2}}(c_{14}-c_{14}'), \\
& K_6=c_3-c_3', \quad K_{67}=(2^{\frac{1}{2}}/2)(c_{34}'-c_{34}), \\
& K_7=c_4-c_4'+c_4''-c_4''', \\
& K_8=c_4-c_4'-c_4''+c_4'''.
\end{aligned}
$$

Substitutions of Eqs. (18) into Eq. (24) and comparison of the resulting expression with Eq. (5) lead to the relations between the K's of Eqs. (18) and the generalized force constants of Eqs. (5); substitution of Eq. (26) into the latter relations yields the expressions for the generalized force constants of Eq. (5) in terms of the valence force constants.

In the analysis of experimental data it is necessary to assume that some force constants are negligible as a first approximation since sufficient data are not available. In this respect it is necessary to examine similar molecules so that it is possible to make a judgment as to which constants to neglect.

In conclusion the authors wish to thank Mrs. J. S. Ziomek and Miss J. Schaefer for their aid in the preparation of the manuscript.

Collisional Excitation of F_2O*

HENRY AROESTE†‡
Cornell University, Ithaca, New York
(Received October 3, 1952)

The quantum mechanics is applied to the calculation of the intrinsic probability of excitation of vibration and rotation of an idealized F_2O molecule by a neon atom. Comparisons are made of the excitation of the three normal vibrations from the zeroth to the first states. The probabilities of excitation of rotation accompanying vibrational excitation are explicitly shown and discussed. Further, excitations involving a change of two and four vibrational quantum numbers are approximated.

THE decomposition of F_2O has been studied experimentally by Koblitz and Schumacher, and it has been termed unimolecular in its decomposition phase.[1] This implication has been drawn from the experimental fact that inert gases serve almost equally well in the energization or second-order phase, the rates of which have been measured at low pressures (about 0.1 to 0.5 atmosphere) and at temperatures of 250° to 270°C. Much evidence that the reaction is indeed homogeneous has been presented by these researchers, who varied the surface area of the reaction vessel and also the composition of the surface using glass, quartz, and magnesium. Further, the reaction was not followed by pressure measurements but by gas analysis, withdrawing by gas pipette samples of mixture and titrating for F_2O with Hi ($F_2O+4HI\rightarrow 2I_2+4HF+H_2O$). Relative rates were experimentally determined for helium, argon, and various inert molecules.

Though the calculations here are for neon and F_2O, they are with slight modification applicable to other inert gases. The theory of Zener,[2] which is largely applied here, is at variance with the Koblitz-Schumacher result that argon is more effective than helium. Zener's theory in this respect corroborates the predictions of Eucken that the lighter atom is more effective.[3] Koblitz and Schumacher report 0.52 to 0.40 for the relative effectiveness of argon to helium. It should be noted, however, that Volmer and Bogdan, in their work on N_2O get the results 0.66, 0.47, 0.20, (0.18), 0.16 for He, Ne, A, Kr, X in that order (the Kr value being a bit dubious), so that the lighter the inert atom the more effective it is.[4] Since the work of Volmer and Bogdan on N_2O represents a review of their previous work in which the argon value appeared as 0.12, one would tend to regard Koblitz and Schumacher's incomplete data as within the experimental error or as an error in calculation or parameter value assumptions.

The mathematical complexity of the quantum mechanical problem precludes its exact solution. We have thus been led to make assumptions which will simplify the mathematics and still retain the essential physical features. Our primary aim here is to discuss excitation of the normal vibrational modes of F_2O and to consider excitation of rotation only as it intertwines with that of vibration. Since F_2O, as a nonlinear symmetric molecule, has all its normal vibrational modes in the plane, a useful approximation may be to treat the idealized case of motion in the plane of the molecule and to regard F_2O as a plane rotor. We have also considered the translation as restricted to one dimension.

Further, the intermolecular potential between neon and F_2O has been approximated as if each atom in the molecule were a neon atom and interacted separately with the exciting neon atom. This has its basis in that the fluorine and oxygen atoms, though with different core charges and different masses, present closed neon-like valence shells to the exciting neon atom. The Ne−Ne interaction which has been adopted is that of the theoretical calculation of Bleick and Mayer,[5] as approximated in the region 1.8 to 3.2A by an exponential function which they suggest, and which they claim to be consistent with their data by about 10 percent. It is consistent with extensions of experimental data valid in the region 2.6 to 3.1A by about a factor of 2. Bleick and Mayer suggest the form $be^{(2r_0-r)/\rho}$, where $b=10^{-12}$ erg, $\rho=0.2091$A, $r_0=1.029$A. If $P=be^{2r_0/\rho}$ and $a=1/\rho$, this is $Pe^{-ar}=188\times10^{-10}\ e^{-4.78r}$ erg.

Since the initial and final state wave functions are orthogonal for this problem, we may use the usual result of the first-order Dirac time-dependent perturbation theory to calculate transition probabilities. Thus w, the probability per unit time of transition from a specific initial state to a continuum of final translational states, may be written

$$w=(4\pi^2/h)\rho(E_j^f)\,|\,V_{jm}\,|^2,$$

if $\rho(E_j^f)$ and V_{jm} are assumed to be slowly varying functions of the final relative translational energy, E_j^f. The density of final translational states, $\rho(E_j^f)$, is

* Based on part of a thesis submitted in partial fulfillment of the requirements for the degree of Doctor of Philosophy in the Graduate School of Cornell University in 1952.
† Present address: Institute for Nuclear Studies, University of Chicago, Chicago, Illinois.
‡ Du Pont Postgraduate Fellow 1950–1951.
[1] W. Koblitz and H. Schumacher, Z. physik. Chem. **B25**, 283 (1934).
[2] C. Zener, Phys. Rev. **37**, 556 (1931).
[3] A. Eucken and R. Becker, Z. physik. Chem. **B27**, 235 (1934).
[4] M. Volmer and M. Bogdan, Z. physik. Chem. **B21**, 257 (1933).
[5] W. E. Bleick and J. E. Mayer, J. Chem. Phys. **2**, 252 (1934).

taken as $(D/h)(\mu/2E_j^f)^{\frac{1}{2}}$ for two molecules of reduced mass μ in a one-dimensional box of extension D. Here, $V_{jm}=\int \chi_j^{f*} V \chi_m^i d\tau$, where V is the perturbation, and χ_j^f and χ_m^i, the final and initial wave functions, respectively.

The perturbing potential may be written as

$$V=P\sum_{i=1}^{3}\exp[-a|(\mathbf{R}-\boldsymbol{\gamma}_i-\boldsymbol{\varrho}_i)|]=P\sum_{i=1}^{3}V_i, \quad (1)$$

where $\mathbf{R}$ is the vector from the center of gravity of the F_2O molecule to the center of gravity of the neon atom, $\boldsymbol{\gamma}_i$ is the vector from the center of gravity of the molecule to the equilibrium position of the ith atom of the molecule, and $\boldsymbol{\varrho}_i$ is the vibrational displacement vector of the ith atom. (See Fig. 1.)

If, considering the ith atom, we place $\mathbf{R}-\boldsymbol{\gamma}_i=\mathbf{Q}_i$ and expand about $\rho_{ix}=0$ and $\rho_{iy}=0$ in a Taylor's series in two variables, we obtain

$$V_i=\sum_{j=0}^{n}(1/j!)(\rho_{ix}\partial/\partial Q_{ix}+\rho_{iy}\partial/\partial Q_{iy})^j V_i(Q_{ix}, Q_{iy}). \quad (2)$$

If $|Q_i|=(Q_{ix}^2+Q_{iy}^2)^{\frac{1}{2}}$, to the second term this is

$$e^{-a|Q_i|}+(a/|Q_i|)e^{-a|Q_i|}(Q_{ix}\rho_{ix}+Q_{iy}\rho_{iy})+\cdots.$$

On putting $Q_{ix}=|Q_i|\cos\theta$, and $Q_{iy}=|Q_i|\sin\theta$ we have

$$e^{-a|Q_i|}+ae^{-a|Q_i|}(\rho_{ix}\cos\theta+\rho_{iy}\sin\theta)+\cdots.$$

In the special case considered here $\mathbf{R}$ will be chosen to be directed parallel to the x axis. Then θ is the angle between $\mathbf{Q}_i$ and the x axis.

For ease of calculation the nuclear wave function of F_2O has been taken as separable into rotational, vibrational, and translational parts. The wave function for rotation, normalized in the interval $0-2\pi$, is

$$\psi_r=(1/\pi)^{\frac{1}{2}}\cos K\varphi \quad (K\geq 0)$$

or

$$\psi_r=(1/\pi)^{\frac{1}{2}}\sin K\varphi \quad (K\geq 1),$$

where K is an integer, and φ is the angle between the space fixed x axis and γ of the oxygen atom. The wave function for vibration has been taken as $\psi_v=\psi_{v_1}\psi_{v_2}\psi_{v_3}$, where ψ_{v_p} is the Hermite function representing the normal coordinate p: $\psi_{v_p}=N_{n_p}\exp(-\frac{1}{2}\alpha_p\xi_p^2)H_{n_p}$, where $\alpha_p=2\pi\nu_p/h$, $N_{n_p}=[(\alpha_p/\pi)^{\frac{1}{2}}/2^{n_p}n_p!]$, and V_p is the normal frequency. The translational wave functions have been taken as plane waves of a particle of mass μ, the reduced mass of the system, F_2O-Ne: $\psi_t=N\exp i\mathbf{k}\cdot\mathbf{R}$, where N is an appropriate normalizing constant. It has been further assumed that the neon atom may not approach any of the atoms of the F_2O closer than the classical closest distance of approach, b, which is a function of k, i.e., the potential has been taken as infinite in the region within b. In order that the cutoff, b, may be easily applied in the computation, it is necessary to put $\mathbf{Q}_i=\mathbf{R}-\boldsymbol{\gamma}_i$, as has been done for the perturbing potential, so that

$$\psi_t=N\exp[i\mathbf{k}\cdot(\mathbf{Q}_i+\boldsymbol{\gamma}_i)].$$

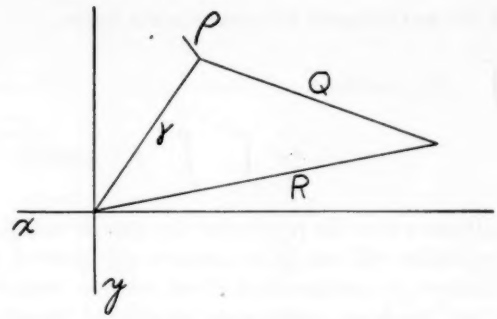

FIG. 1. Relationship of vectors.

If we further take the translational motion to be directed only parallel to the axis, we have

$$\psi_t=N\exp[ik_x(Q_{ix}+\gamma_{ix})].$$

We have taken $k_x=k_0/\sqrt{2}$ where k_0 is the wave number of a free particle of mass μ. This approximate result may be derived by applying a very rough modification of the W. K. B. procedure. If we consider the one-dimensional Schrödinger equation,

$$\psi''+(2\mu/\hbar^2)(E-V(x))\psi=0 \quad (3)$$

and look for solutions of the form $N\exp[ig(x)x/\hbar]$, we obtain on substituting this form of ψ in (3)

$$ih[2g'(x)+xg''(x)]-[g^2(x)+2xg'(x)g(x)+x^2g''(x)]+2\mu[E-V(x)]=0. \quad (4)$$

Though we may now set $g=g_0(x)+\hbar g_2(x)+\cdots$, we may as a very rough first approximation take $g'=0$ so that $g=(2\mu[E-V(x)])^{\frac{1}{2}}$. Even this form proves to be too difficult to handle analytically and $V(x)$, which varies between 0 and E, is taken as $E/2$, so that $g=(\mu E)^{\frac{1}{2}}$. Defining $k=g/\hbar$ and $k_0=(2\mu E)^{\frac{1}{2}}/\hbar$, we have $k=k_0/\sqrt{2}$.

Certain approximations have to be made in the choice of the cutoff, b, in order to simplify the calculation.

(a) Screening fractions: It may be assumed that for certain orientations b is larger than the usual Ne−Ne distance by virtue of one of the atoms of the F_2O shielding another from the exciting neon atom. b will therefore be approximately an angstrom larger for some angles, and integrations over these regions prove to be negligible. It is therefore necessary to calculate only over a certain fraction of the angles φ and θ. We therefore have integrals of the sort

$$\int_0^{\beta_1}\int_0^{\beta_2} f(\theta, \varphi)d\theta d\varphi,$$

where β_1 and β_2 are the angles over which the integrations are not negligible. Further, because of the complexities involved in the exact calculation of such in-

tegrals, we have chosen to approximate them:

$$\int_0^{\beta_1}\int_0^{\beta_2} f(\theta,\varphi)d\theta d\varphi = \beta_1\beta_2/4\pi^2 \int_0^{2\pi}\int_0^{2\pi} f(\theta,\varphi)d\theta d\varphi. \quad (5)$$

This will mean that the results for any specific rotational state transition will not have absolute significance. It is fair, however, to assume that if not too few rotational states are involved, sums over rotational transitions will have some absolute significance.

(b) Approximation of the component error: If, as suggested, the translational motion is taken parallel to the x axis, the atoms of the F_2O not necessarily in the line of translational motion, it is the component of translation in the direction of one of the atoms that should determine the cutoff, b. This component is, of course, a function of the angles, θ and φ. Fortunately, for the energies considered here the variation is very small and, if necessary, can be approximated for intermediary angles.

(c) Neglect of rotational energy: If the rotational energy is not too large, which is true for most of the cases considered here, one may assume that the lack of consideration of rotational energy in choosing the cutoff, b, is reasonable, since the actual $b(\theta,\varphi)$ will be larger than the b so chosen for certain rotational orientations and smaller for others. Therefore, the b so chosen roughly represents an average value of the actual $b(\theta,\varphi)$.

We now consider the excitation probability by translation from the zeroth to the first vibrational state of each of the three normal coordinates. We have seen previously that $w=(4\pi^2/h^2)(\mu/2E_j)^{\frac{1}{2}}D|V_{jm}|^2$. Consider the form of $|V_{jm}|$ for this case: $|V_{jm}|=|\sum_i V_{jm_i}|$, where

$$V_{jm_i}=P\int \psi_{t_j}^*\psi_{v_j}^*\psi_{r_j}^* V_i \psi_{t_m}\psi_{v_m}\psi_{r_m} d\tau. \quad (6)$$

Substituting for the wave functions and the perturbation potential, we have

$$V_{jm_i}=A\int_b^\infty\int_{-\infty}^\infty\int_0^{2\pi}\int_0^{2\pi} F(\theta,Q_i) \times G(\varphi,\xi_p)Q_i dQ_i d\xi_p d\theta d\varphi, \quad (7)$$

where

$$F=\exp[i(k_x{}^i-k_x{}^f)Q_i\cos\theta-aQ_i]\cos\theta,$$

$$G=\exp[i(k_x{}^i-k_x{}^f)\gamma_i\cos\Phi_i-\alpha_p\xi_p{}^2] \times H0_pH1_p\rho_{t_x}\sin K\varphi\sin N\varphi,$$

and

$$A=BN0_pN1_p\beta_i/\pi.\S$$

Here we have put $B=P\beta_i'a/D^2$, and β_i', β_i represent screening fractions on θ and φ, respectively. Also Φ_i is the angle between γ_i and the fixed x axis and is related to $\varphi=\Phi_O$, the Φ_i for the oxygen atom, through a constant, δ_i; i.e., $\Phi_i=\varphi-\delta_i$, where $\delta_O=0$. Using the orientation of G. Herzberg, we have $\rho_{t_x}=y_i\cos\varphi+x_i\sin\varphi$.[6] See also Fig. 2 in (a) of Appendix. There, y_i and x_i are determined as linear functions of the ξ_p. We may now write

$$V_{jm_i}=I_{t_i}[I_v(y_i)I_{r_i}(\cos\varphi)+I_v(x_i)I_{r_i}(\sin\varphi),$$

where I_t is the integral over Q_i and θ; I_r, over φ; and I_v, over ξ_p. Explicitly, we have

$$I_{t_i}=B\int_b^\infty\int_0^{2\pi}\exp(ik_xQ_i\cos\theta-aQ_i)\cos\theta Q_i dQ_i d\theta, \quad (8)$$

where $k_x=k_x{}^i-k_x{}^f$, and b is a function of k_x;

$$I_{r_i}(\cos\varphi)=(\beta_i/\pi)\int_0^{2\pi} I(\varphi)\cos\varphi d\varphi, \quad (9a)$$

and

$$I_{r_i}(\sin\varphi)=(\beta_i/\pi)\int_0^{2\pi} I(\varphi)\sin\varphi d\varphi, \quad (9b)$$

where

$$I(\varphi)=\exp(ik_x\gamma_i\cos\Phi_i)\sin K\varphi\sin N\varphi; \quad (9c)$$

$$I_v(x_i)=N0_pN1_p\int_{-\infty}^\infty x_iM(\xi_p)d\xi_p, \quad (10a)$$

and

$$I_v(y_i)=N0_pN1_p\int_{-\infty}^\infty y_iM(\xi_p)d\xi_p, \quad (10b)$$

where $M(\xi_p)=H0_pH1_pe^{-\alpha_p\xi_p{}^2}$, and x_i and y_i are $c_i\xi_p$ and $d_i\xi_p$, respectively.

Now, we have

$$I_{t_i}=2\pi iBI_t(Q_i), \quad (11)$$

where

$$I_t(Q_i)=e^{-aQ_i}J_1(k_xQ_i)Q_idQ_i, \quad (12)$$

since

$$J_1(k_xQ_i)=(1/2\pi)\int_0^{2\pi}\sin(k_xQ_i\cos\theta)\cos\theta d\theta. \quad (13)$$

If we put $k_xQ_i=z$, then the first term of the asymptotic series for $J_1(z)$ is

$$(2/\pi z)^{\frac{1}{2}}[\cos(3\pi/4)\cos z+\sin(3\pi/4)\sin z].$$

Then, also putting

$$\cos z=\tfrac{1}{2}(e^{iz}+e^{-iz})$$

and

$$\sin z=\tfrac{1}{2}i(e^{-iz}-e^{iz}),$$

we have

$$I_t(Q_i)\cong(1/2\pi k_x)^{\frac{1}{2}}\Big[\cos(3\pi/4)\Big(\int^+ +\int^-\Big) +i\sin(3\pi/4)\Big(\int^+ -\int^-\Big)\Big], \quad (14)$$

§ See (b) in Appendix. Also, for a discussion of the neglect of the higher terms in the potential, see (c).

[6] G. Herzberg, *Molecular Spectra and Molecular Structure* (D. Van Nostrand Company, Inc., New York, 1945), Volume II.

where

$$\int^{\pm} = \int_b^{\infty} \exp[Q(-a \pm ik_x)]Q^{\frac{1}{2}}dQ.$$

If we integrate this latter integral by parts and take the leading term, the other terms being at least one or two orders of magnitude less, we have

$$\int^{\pm} \cong -\exp[b(-a \pm ik]b^{\frac{1}{2}}/(-a \pm ik). \quad (15)$$

Thus we obtain

$$I_i(Q_i) \cong -[e^{-ab}(b/\pi k)^{\frac{1}{2}}/(a^2+k^2)] \times [(a-k)\cos kb - (a+k)\sin kb]. \quad (16)$$

As a special case we have chosen to calculate the transition probabilities from the first rotational state. We may therefore set $N=1$ in $I_{ri}(\cos\varphi)$ and $I_{ri}(\sin\varphi)$. Then, for instance, under the cut-off approximations discussed previously, we have

$$I_{ri}(\cos\varphi) = \tfrac{1}{2}\beta_i\{\cos[(K-2)\delta_i]J_{K-2}(k_x\gamma_i) - \cos[(K+2)\delta_i]J_{K+2}(k_x\gamma_i)\} \quad (17)$$

if K and $\frac{1}{2}K$ are even; if K is even and $\frac{1}{2}K$ is odd, it is the negative of the above; if K is odd and $\frac{1}{2}(K-1)$ is even, it is i times the above; and finally if K is odd and $\frac{1}{2}(K-1)$ is odd, it is $-i$ times the above. Similar formulas may be derived for $I_{ri}(\sin\varphi)$ and for cases where other than sine rotational wave functions are used.

Finally, very simply,

$$I_v(x_i) = c_i/(2\alpha_p)^{\frac{1}{2}} \quad (18)$$

and

$$I_v(y_i) = d_i/(2\alpha_p)^{\frac{1}{2}}.^{7} \quad (19)$$

RESULTS FOR THE ZERO-TO-ONE EXCITATION

We first compare the results for the three normal coordinates, ξ_1, ξ_2, ξ_3, the "stretching," "bending," and antisymmetric coordinates, respectively, for the same initial relative translational energy. We then consider the sensitivity to change of the initial relative translational energy on a particular rotational term. From these two considerations we may also draw some qualitative inferences with regard to the distribution of final rotational states in actual collisions.

For the first comparison we have chosen the initial relative translational energy equal to one quantum of the antisymmetric vibration ξ_3 and 45 rotational quanta. The initial rotational state is $N=1$. For ξ_1 and ξ_2 sine functions were chosen as initial and final rotational state functions; for ξ_3 a cosine function was chosen as initial state and sine functions as final states. In Table I we report for all vibrations $U_{jm} = |V'_{jm}|^2/(E_j)^{\frac{1}{2}}$, where V'_{jm} is $V_{jm}D^2$. We can also define $F = D^3\sum_K w$

[7] L. Pauling and E. B. Wilson, *Introduction to Quantum Mechanics* (McGraw-Hill Book Company, New York, 1935).

TABLE I. Contributions from the various final rotational states to the sum over final rotational states for each of the vibrational modes.

Final rotational state	$U_{jm}\times10^{30}$ ξ_1	ξ_2	ξ_3
1	99	1900	15
2	0.0018	1.2	15
3	53	80	44
4	57	1100	11
5	8.0	280*	0.62
6	34	110	45
7	9.1	84	60
8	3.1	83	210
9	12	0.31	140
10	9.0	1.0	130
11	0.13	0.076	14
12	0.15	$46(0.1)^6$	1.7
13	3.9	$81(0.1)^{11}$	0.77
14	2.8	$70(0.1)^8$	0.0010
15	8.0	$31(0.1)^8$	0.012
16	0.11	$54(0.1)^{11}$	0.31
17	0.55		0.31
18	0.040		0.0061
19	$67(0.1)^8$		$12(0.1)^5$
20	$32(0.1)^5$		$44(0.1)^6$
21	0.0020		$11(0.1)^7$
22	$92(0.1)^5$		$15(0.1)^8$
23	$71(0.1)^9$		$14(0.1)^6$
24	$79(0.1)^7$		$32(0.1)^7$
25	$73(0.1)^7$		$43(0.1)^9$

$= D^3C\sum_K U_{jm}$, where $C = 4\pi^2(\frac{1}{2}\mu)^{\frac{1}{2}}/h^2$. We report here

$$F_{\xi_1} = 0.95\times10^{15} \text{ angstroms}^3/\text{sec}$$
$$F_{\xi_2} = 11 \times10^{15} \text{ angstroms}^3/\text{sec}$$
$$F_{\xi_3} = 2.2 \times10^{15} \text{ angstroms}^3/\text{sec}.$$

As expected, the lower is the frequency, the more easily excited is the vibration. These results may be put in more usual form by taking $D \cong 10^5$A (the approximate free path at 0.3 atmos) and multiplying $\sum_K w$ by an approximate average time between collisions $\cong 10^{-8}$ sec. Thus, defining T as probability of transition per collision at 0.3 atmosphere, we obtain

$$T_1 = 0.95\times10^{-8}$$
$$T_2 = 11 \times10^{-8}$$
$$T_3 = 2.2 \times10^{-8}.$$

For the second consideration, that of the effect of varying the initial relative translational energy, we have chosen the fifth (starred) term in the ξ_2 calculation. Table II represents the results of calculations of U_{jm} for that term with differing initial relative translational energies. This table does not represent the complete range of energies, but is included merely to indicate the sensitivity to change of initial relative translational energy. The curve in the complete range has many more extrema than are given. The range given here is approximately from one of the maxima to one of the minima.

It is seen from Table I that for a specific initial relative translational energy, the contributions of the final rotational states go through various extrema, with the

contributions from the states farthest from the initial rotational state diminishing rapidly. The points at which these extrema occur are largely dependent on the choice of initial relative translational energy. Table II shows the effect of variation of the initial relative translational energy on a random contribution in Table I. It is to be expected that when the results are averaged statistically over an initial distribution of translational states, a function with only one maximum will result. In the meantime it is interesting to note from Table I (comparing ξ_1 and ξ_2) that the lower is the frequency of vibration, the fewer rotational states are excited, but that the contributions are larger per state for the lower frequency vibration. Thus, although larger changes in rotational quantum number are more probable upon excitation of the higher frequency vibration, the sum over rotational states is larger for the lower frequency vibration.

RESULTS FOR HIGHER EXCITATIONS

It is the purpose here to develop very rough approximations for the higher excitations and to apply them to the calculation of the excitation of the normal coordinate ξ_1 from the zeroth to the second and fourth states. We have again

$$w=(4\pi^2/h^2)(\mu/2E_j)^{\frac{1}{2}}D|V_{jm}|^2.$$

Since we are interested only in order of magnitude accuracy, we may consider

$$\sum_K w=(4\pi^2D/h^2)(\mu/2E_{Ja})^{\frac{1}{2}}\sum_K|V_{jm}|^2, \qquad (20)$$

where K is the quantum number of final rotational states, and an approximately average value has been taken for E_j, which strictly depends on K. We therefore consider $\sum_K|V_{jm}|^2$. For order of magnitude accuracy we may take one of the leading terms of the expansion of V_i. The term chosen is $(-a\rho_{iy}\sin\theta)^m e^{-aQ}$, where m is the quantum number of the final vibrational state. With this choice of V_i we may write, for instance, for the case of excitation of ξ_1 from the zeroth to the second state:

$$\sum_K|V_{jm}|^2=\sum_K\left|\sum_i A\int_b^\infty\int_{-\infty}^{\infty}\int_0^{2\pi}\int_0^{2\pi} F(\theta,Q_i)G(\varphi,\xi_1)Q_i dQ_i d\xi_1 d\theta d\varphi\right|^2, \qquad (21)$$

where

$$A=a^2\beta_i'\beta_i N_{01}N_{21}P/\pi D^2,$$
$$F=\exp(ik_xQ_i\cos\theta-aQ_i)\sin^2\theta,$$
$$G=\exp(ik_x\gamma_i\cos\Phi_i-\alpha_1\xi_1^2)\rho_{iy}{}^2H_{21}H_{01}\sin K\varphi\sin\varphi.$$

If we further substitute for $\rho_{iy}{}^2$ only the terms in x_i^2, as those in y_i are much smaller, we have

$$\rho_{iy}{}^2=(1.21\times10^{11}\xi_1\cos\varphi)^2.$$

Approximating the integral over φ as equal to some J_a, where J_a represents an approximate value for the actual combinations of Bessel functions averaged over the states $K=1$ to $K=L$ which contribute, we may then write

$$\sum_K|V_{jm}|^2\cong10^{45}K_LJ_a{}^2B^2\times\left|\int_{b_a}^\infty\int_0^{2\pi}FQdQd\theta\int_{-\infty}^{+\infty}I(\xi_1)d\xi_1\right|^2, \qquad (22)$$

where

$$I(\xi_1)=N_{01}N_{21}H_{01}H_{21}\exp(-\alpha_1\xi_1^2),$$

and $B=\pi A/N_{01}N_{21}$; further, approximate average values have been taken for k_x and b. Also, if k_{x_a} is somewhat larger than a, as it will be for ξ_1, the absolute value of the integral over Q and θ may be approximated as $2\sqrt{\pi}(k_{x_a}{}^{-5}b_a{}^{-1})^{\frac{1}{2}}e^{-ab_a}$. The integral over ξ_1 is $(\alpha_1\sqrt{2})^{-1}$ so that

$$\sum_K|V_{jm}|^2\cong10^{46}B^2K_LJ_a{}^2\alpha_1{}^{-2}b_a{}^{-1}k_{x_a}{}^{-5}e^{-2ab_a}. \qquad (23)$$

A similar formula for the transition from the zeroth to the fourth state is

$$\sum_K|V_{jm}|^2\cong10^{92}B^2K_LJ_a{}^2\alpha_1{}^{-4}a^4b_a{}^{-3}k_{x_a}{}^{-7}e^{-2ab_a}. \qquad (24)$$

We consider the initial relative translational energy equal to four vibrational quanta and forty-five rotational quanta and report for such a collision $F=D^2\sum_K w$ for the vibrational excitation of two and four quanta, respectively,

$$F_2\cong10^{15}\text{ angstroms}^3/\text{sec}$$
$$F_4\cong10^{7}\text{ angstroms}^3/\text{sec}.$$

Taking D at 0.3 atmos$\cong5\times10^5$A and the time between collisions$\cong10^{-8}$ sec, we have

$$T_2\cong10^{-10}$$
$$T_4\cong10^{-18}.$$

TABLE II. Effect of variation of initial relative translational energy on the contribution from a particular final rotational state to the sum over final rotational states.

Initial relative translational energy $\times10^{13}$ ergs	$U_{jm}\times10^{30}$
2.83	280
2.93	240
3.03	140
3.13	61
3.23	9
3.33	3

|| See (d) in Appendix.

ACKNOWLEDGMENT

The author wishes to thank Dr. John K. Bragg of the General Electric Company Research Laboratory for much helpful discussion and assistance during the course of the research.

APPENDIX

(a) Expression of the ρ_{ix} and ρ_{iy} in terms of normal coordinates: We use here the orientation of G. Herzberg[8] (see Fig. 2), where the y axis coincides with γ_O. Then we have

$$\left.\begin{aligned}\rho_{ix}&=y_i\cos\varphi+x_i\sin\varphi\\ \rho_{iy}&=y_i\sin\varphi-x_i\cos\varphi,\quad \text{where } i=1,2\end{aligned}\right\} \tag{25}$$

refer to the fluorine atoms and $i=3$ refers to the oxygen atom. We then can also write[9] in terms of the usual symmetry coordinates:

$$\left.\begin{aligned}x_1&=S_1-S_3\sin\alpha & x_2&=-S_1-S_3\sin\alpha\\ y_1&=S_2-S_3\cos\alpha & y_2&=S_2+S_3\cos\alpha\\ x_3&=(2m_F/m_O)S_3\sin\alpha & y_3&=-(2m_F/m_O)S_2.\end{aligned}\right\} \tag{26}$$

Also, with the new frequencies as determined by Bernstein and Powling[10] and Jones, Kirby-Smith, Woltz, and Nielsen,[11] $\nu_1=928\ \text{cm}^{-1}$, $\nu_2=461\ \text{cm}^{-1}$, $\nu_3=830\ \text{cm}^{-1}$, and using $\lambda_i=4\pi^2\nu_i^2$, one may obtain with the aid of the formulas G. Herzberg,[12]

$$\left.\begin{aligned}\lambda_3&=[1+(2m_F/m_O)\sin^2\alpha]k_1/m_F\\ \lambda_1\lambda_2&=2(1+2m_F/m_O)k_1k_\delta/m_F{}^2l^2\end{aligned}\right\}, \tag{27}$$

the new valence force constants

$$k_1=3.12\times10^{-5}\ \text{dyne/cm}$$
$$k_\delta/l^2=1.10\times10^{-5}\ \text{dyne/cm}.$$

Then, using the formula,[13]

$$\frac{S_1}{S_2}=\frac{2pk_1\cos^2\alpha+4p\sin^2\alpha k_\delta/l^2-2\lambda_i m_F}{-2\sin\alpha\cos\alpha(k_1-2k_\delta/l^2)}, \tag{28}$$

where $p=1+2m_F/m_O$, one can obtain that

$$\left.\begin{aligned}\xi_1&\sim\ \ 2.35S_1+S_2\\ \xi_2&\sim-13.9\ S_1+S_2\\ \xi_3&\sim S_3\end{aligned}\right\}. \tag{29}$$

Finally, combining the formulas (26) and (29) one may derive

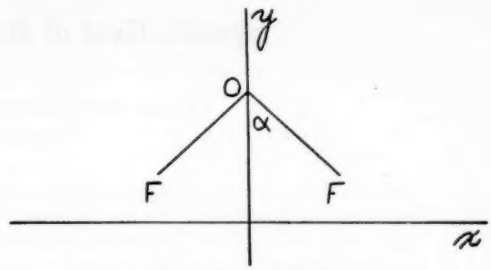

FIG. 2. Orientation of axes.

$$\left.\begin{aligned}x_1&=10^{11}(1.21\xi_1-1.26\xi_2-1.26\xi_3)\\ x_2&=10^{11}(-1.21\xi_1+1.26\xi_2-1.26\xi_3)\\ x_3&=10^{11}(2.99\xi_3)\\ y_1&=10^{11}(0.215\xi_1+0.04\xi_2-0.983\xi_3)\\ y_2&=10^{11}(0.215\xi_1+0.04\xi_2+0.983\xi_3)\\ y_3&=10^{11}(-0.51\xi_1-0.09\xi_2),\end{aligned}\right\}, \tag{30}$$

where the c_i and d_i defined in the body of the paper are in units of grams$^{-\frac{1}{2}}$.

(b) If in the excitation of one normal coordinate the others are taken to remain the same, we omit integrations over these coordinates, since they would be equal to unity. As for the transformations involving the external coordinates, the Jacobian of the transformation from $dR_xdR_yd\varphi$ to $dQ_{ix}dQ_{iy}d\varphi$ is 1. The wave function in y direction has been taken as $1/D^{\frac{1}{2}}$, i.e., $k_y=0$, and $D_y=D_x=D$. Further, the upper limit for the Q_i integrations has been taken as ∞ since $D\gg b$.

(c) We discuss here the approximation of neglect of the higher terms such as in the calculation of the excitation from the zeroth to the first state neglecting $c_i{}^3a^3\int H_0\xi_i{}^3H_1d\xi_i$ compared to $c_iaSH_0\xi_iH_1d\xi_i$. Approximately, we should compare $c_i{}^3a^3/(\alpha_i)^{\frac{1}{2}}$ to $c_ia/(\alpha_i)^{\frac{1}{2}}$. $a\cong5$ and $(\alpha_i)^{\frac{1}{2}}/c_i\cong100$ so that the first is about 1/400 of the second.

(d) For order of magnitude accuracy one can, besides neglecting the terms discussed in (c), take the leading terms for a particular $\xi_i{}^m$. For instance, for the $0-2(m=2)$ case in the differentiation of e^{-aQ} one obtains leading terms in a^2 as compared to the next largest in a/Q. Taking Q at the least to be 2A, a^2 is 25 compared to 2.5 for a/Q. A further approximation has been made to take only one of the leading terms, i.e., for $0-2$, one has $\rho_y{}^2\sin^2\theta$, $\rho_y\rho_x\sin\theta\cos\theta$, and $\rho_x{}^2\cos^2\theta$. In reality, the term in $\cos^2\theta$ is largest since only small θ should be considered, but our screening fractions approximation does not take this into account so that the term in $\sin^n\theta$, a bit easier to calculate, may be used to estimate relative orders of magnitude for $n=2$ and $n=4$.

[8] See reference 6, p. 146.
[9] See reference 6, p. 149.
[10] H. Bernstein and J. Powling, J. Chem. Phys. **18**, 685 (1950).
[11] Jones, Kirby-Smith, Woltz, and Nielsen, J. Chem. Phys. **19**, 337 (1951).
[12] See reference 6, II, 189, II, 191.
[13] See reference 6, II, 193.

Specific Heat of Diamond at Low Temperatures

WARREN DESORBO
General Electric Research Laboratory, Schenectady, New York
(Received November 25, 1952)

Specific heat data on diamond at temperatures between 20° and 300°K are reported. Comparisons of the data have been made with the predictions of the Debye theory. The deviation of the specific heat from the value given by the three-dimensional continuum theory in the low temperature region can be qualitatively described in terms of a superposition of a simple Einstein frequency. It has been found that variations that occur in expressing reduced characteristic temperatures as a function of reduced temperatures for diamond are qualitatively similar to those of the face-centered cubic metals Al, Cu, and Ag.

The values of entropy, enthalpy, and free energy have been determined and tabulated at integral values of temperature from 25° to 300°K. The entropy of diamond at 298.16°K is 0.568±0.005 cal/g-atom/deg.

FOREWORD

AN extension of the measurements on the specific heat of diamond to liquid hydrogen temperature regions is herein reported. Continuous determinations up to room temperature are also included. These measurements were undertaken in pursuance of a general program of determining thermodynamic properties of various modifications of carbon.[1]

Prior to this investigation, the specific heat of diamond had not been successfully studied below liquid nitrogen temperatures. The other three diamond-structure elements, germanium, silicon, and (gray) tin have all recently been studied down to liquid helium temperatures.[2,3] The specific heats of these three elements all show striking variations from the Debye theory.

Pitzer[4] compared his measurements on diamond with the Debye theory calculations and found small deviations which were outside his experimental errors. These measurements extended down to 70°K. Since the Debye characteristic temperature for diamond is high, there is a possibility that the temperature below which the three-dimensional elastic continuum idea is applicable[5] might be in the liquid hydrogen region.

EXPERIMENTAL

The sample used in this study consisted of approximately 80 grams of "fragmented boart" size −10, +14 mesh obtained from the Carboloy Department of the General Electric Company.* Spectroscopic analysis carried out by Mrs. A. P. O'Hara, Schenectady Works Laboratory showed the sample to contain "traces" of Mg, and Al, and "low" concentrations of Si and Fe. Laue x-ray photographs taken by Mrs. B. F. Decker showed a variation in intensity across some of the spots. This variation indicates that the crystal contained regions of misalignment. No attempt has been made to determine the proportions of the sample that exist as type I and type II diamond. About 20 percent of the crystals selected at random were fluorescent.

The calorimeter used in this investigation is the same as that used previously and is described elsewhere.[1] The accuracy of these measurements compares with the accuracy of the measurements described earlier, except for the temperatures near the liquid nitrogen region and below. The inaccuracy in the results at 70°K may be as large as 5 percent. This inaccuracy increases with decreasing temperature, amounting to about 30 percent at 40°K. Because of the extremely small values of the specific heat in the region of these lower temperatures, the data below approximately 30°K are, of necessity, of heuristic value only. Two independent determinations of the specific heat were undertaken in the region 20°−75°K. The first experiment was carried out in the usual manner with helium exchange gas in the calorimeter can at one atmosphere of pressure. In the second experiment, the calorimeter containing the sample was left open to the high vacuum of the cryostat. Under this latter condition the drift rates were normal up to about 100°K, indicative of the high thermal conductivity of the granular diamond specimen. Prior to these measurements, a complete recalibration of the empty calorimeter had been completed.

RESULTS

The experimental results are presented in Table I. These data along with those obtained by previous investigators are shown in Fig. 1. The specific heat values at the lower temperatures appear on a much enlarged scale.

The values of the thermodynamic functions listed in Table II were obtained from a smooth curve of large graphs of specific heat *versus* T and specific heat *versus* $\log T$ with the aid of Simpson's rule. The Debye characteristic temperatures deduced from the smooth specific heat data are also listed. The difference be-

[1] W. DeSorbo "Heat Capacity of Chromium Carbide (Cr_3C_2) from 13° to 300°K," J. Am. Chem. Soc. (to be published).
[2] R. W. Hill and D. H. Parkinson, Phil. Mag. **43**, 309 (1952).
[3] I. Estermann and S. A. Friedberg, Carnegie Institute of Technology, Technical Report No. 8, U. S. Office of Naval Research Contract N60R1-47, June 30, 1951.
[4] K. S. Pitzer, J. Chem. Phys. **6**, 68 (1938).
[5] M. Blackman, Proc. Roy. Soc. (London) **A148**, 365, 384 (1935); **A149**, 117, 126 (1935); **A159**, 416 (1937).
* The author is grateful to Mr. A. J. DeCarlo for the loan of this sample.

tween C_p and C_v, calculated by Magnus' formula,[6] was smaller than the experimental error throughout the temperature range studied. In Table III the entropy results are summarized.

DISCUSSION OF RESULTS

The specific heat values presented above are somewhat lower than those obtained by Pitzer in the temperature region 190°−260°K. The maximum difference between the two studies amounts to approximately 2 percent at 230°K. Such a difference is larger than the experimental error of both investigations. Outside this temperature region better agreement exists, although the present results are slightly lower throughout.

The variation could be due to differences in (1) impurities, (2) lattice imperfections, or (3) relative amounts of type I or type II diamonds present in the respective samples.

The influence of each of these factors is difficult to assay. It seems probable that the impurity factor is the least important. Pitzer states that the cyrstals used in his work were reasonably clear. Some of the diamond crystals used in this investigation had some coloration and were presumably less pure. If this is correct, a less pure sample should give higher rather than lower results.

Differences in "degree" of lattice imperfections could help to account for some of the discrepancy. Since diamond has such a high Debye characteristic temperature, any thermal effects caused by lattice irregularities could tend to be more pronounced than in a monatomic lattice having a much lower characteristic temperature.

As for the third factor, Robertson, Fox, and Martin[7] indicate slight differences between the specific heats of type I and type II diamonds. More recently, Willardson and Danielson[8] indicate that a single diamond crystal may be partly type I and partly type II. Data are insufficient at this time to evaluate this point.

A comparison of our data with the Debye theory is shown in Fig. 2. Smooth data were used in calculating the Debye characteristic temperatures. The results of previous investigations on diamond are also presented. A peak in the curve is revealed below 160°K. The maximum for this peak occurs at approximately 60°K. Above 160°K the Debye theory can describe the data quite accurately. This agreement obviates the need for "thermal quantum jumps"[9] used to describe the deviations appearing in the earlier data.

Expressing specific heat data in terms of θ_D *vs* T curves has often revealed variations from constant values. Estermann[3] has pointed out large deviations from the Debye theory found among face-centered and hexagonal close packed crystals. Body-centered cubic structures have a nearly constant θ_D *vs* T relationship. While one would expect the variation of θ_D with T to be similar for elements having similar structures, no simple generalization for the temperature dependence of θ_D for crystals of a given structure has been made. Hill and Parkinson[2] have recently pointed out a similarity, involving this function, in the diamond-structure elements. The peak observed in the θ_D *vs* T curve for diamond in this study is somewhat similar to those previously observed in the liquid helium temperature region in the studies of the specific heat of the three face-centered metals, Al, Cu, and Ag.[10] This similarity is illustrated in Fig. 3, where the reduced Debye temperature θ_D/θ_∞ is plotted against the reduced temperature T/θ_∞. The temperature θ_∞ represents the high temperature value of θ_D. The maximum in the peaks fall approximately at the same reduced temperatures. For the three metals the lattice specific heat only is considered.

Peaks as well as dips in the θ_D *vs* T curves have been observed for other substances in the lower temperature

TABLE I. Specific heat of diamond

Mean Temp.(°K)	ΔT	C_p cal/g-atom/°K	Mean temp.(°K)	ΔT	C_p cal/g-atom/°K
Corrected for helium exchange gas					
17.40	1.280	(0.0001)	134.78	3.890	0.168
23.12	2.060	(0.0004)	141.28	4.259	0.197
25.26	2.056	(0.0015)	146.55	4.134	0.223
27.22	1.971	(0.0014)	152.64	3.983	0.255
31.00	1.977	0.0021	158.46	3.846	0.288
33.08	2.049	0.0020	164.10	3.725	0.325
62.54	3.538	0.0107	169.53	4.129	0.349
73.20	3.680	0.0178	175.06	4.022	0.377
76.16	3.494	0.0222	179.78	3.904	0.418
79.57	3.337	0.0260	185.29	3.788	0.454
82.36	6.088	0.0307	191.11	3.932	0.497
87.34	4.388	0.0356	196.00	3.832	0.532
93.70	3.776	0.0478	200.29	3.735	0.561
100.33	4.079	0.0576	205.77	3.883	0.606
106.71	3.869	0.0758	210.85	3.784	0.643
112.68	3.701	0.0932	213.09	3.600	0.660
118.02	3.812	0.105	216.67	3.523	0.694
123.42	3.680	0.124	226.77	3.463	0.785
129.11	4.043	0.145	231.79	3.613	0.812
Mean Temp.(°K)	ΔT	C_p cal/g-atom/°K	Mean temp.(°K)	ΔT	C_p cal/g-atom/°K
Corrected for helium exchange gas			No helium exchange gas used		
236.78	3.510	0.864	29.47	2.118	0.0020
241.93	3.816	0.914	36.53	2.679	0.0024
246.39	3.738	0.945	41.63	2.427	0.0032
250.76	3.643	0.989	44.07	2.472	0.0039
257.11	3.318	1.048	52.18	2.806	0.0054
265.99	2.250	1.142	55.20	3.250	0.0068
271.55	3.243	1.200	58.31	2.978	0.0086
277.48	2.707	1.252	66.40	2.774	0.0127
281.26	2.652	1.295	69.30	3.022	0.0156
285.22	2.787	1.341	74.91	2.736	0.0204
290.80	2.788	1.379			
293.51	2.501	1.407			
299.07	2.337	1.469			
300.57	2.330	1.481			

[6] A. Magnus, Ann. Physik **70**, 320 (1923).
[7] Robertson, Fox, and Martin, Proc. Roy. Soc. (London) **A157**, 579 (1936).
[8] R. K. Willardson and G. C. Danielson, J. Opt. Soc. Am. **42**, 42 (1952).
[9] F. E. Simon, Sitzber. preuss, Akad. Wiss. **33**, 477 (1926).
[10] Burton, Grayson-Smith, Wilhelm, *Phenomena at the Temperature of Liquid Helium* (Reinhold Publishing Corporation, New York, 1940), p. 136 (contains references).

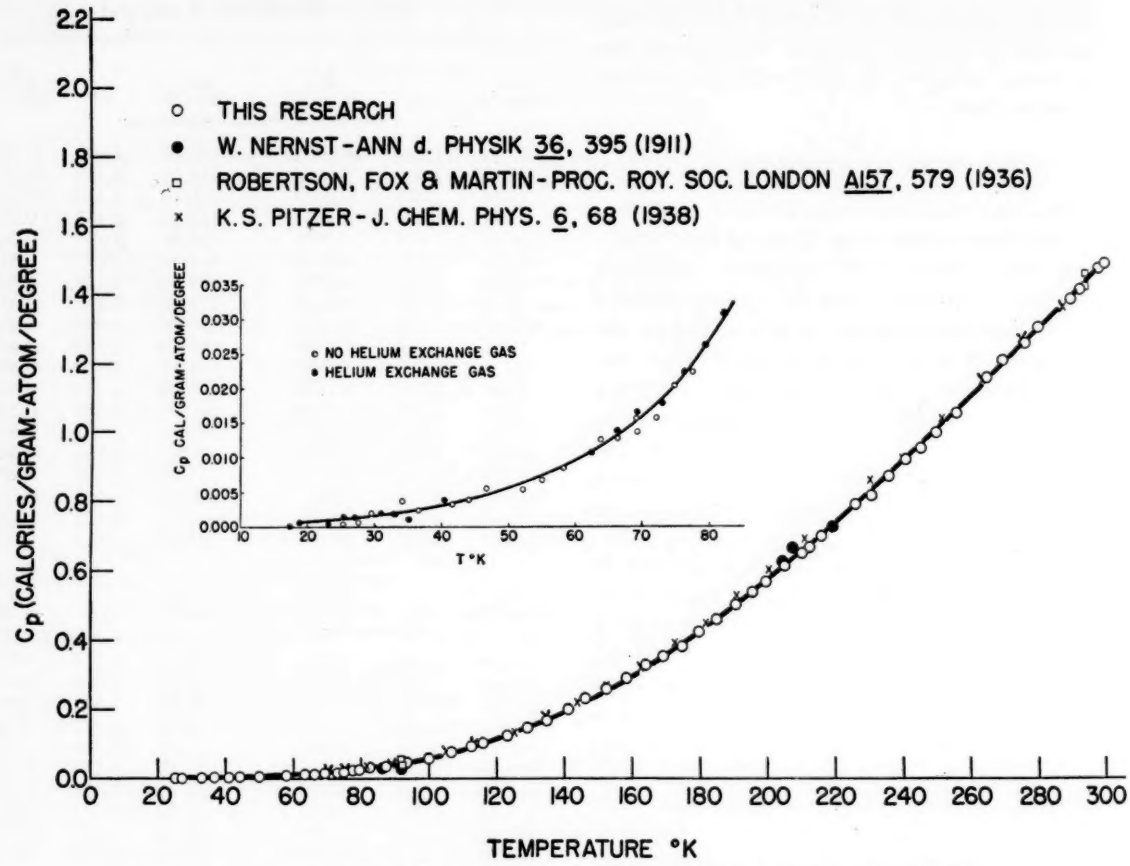
THIS RESEARCH
W. NERNST-ANN d. PHYSIK 36, 395 (1911)
ROBERTSON, FOX & MARTIN-PROC. ROY. SOC. LONDON A157, 579 (1936)
K.S. PITZER-J. CHEM. PHYS. 6, 68 (1938)
NO HELIUM EXCHANGE GAS
HELIUM EXCHANGE GAS
C_p CAL/GRAM-ATOM/DEGREE
T °K
C_p (CALORIES/GRAM-ATOM/DEGREE)
TEMPERATURE °K

FIG. 1. Low temperature specific heat of diamond; this research and previous investigations.

TABLE II. Thermodynamic functions of diamond based on the smooth curve of specific heats

T(°K)	C_p cal/g-atom/°K	θ_D	S° cal/g-atom/°K	$H^\circ-H_0^\circ$ cal/g-atom/°K	$\frac{H^\circ-H_0^\circ}{T}$ cal/g-atom/°K	$\frac{-(F^\circ-H_0^\circ)}{T}$ cal/g-atom/°K
25	(0.0012)	1822	(0.0007)	(0.0062)	(0.0002)	(0.0005)
30	(0.0018)	1910				
40	0.0034	2060				
50	0.0054	2207	0.0032	0.0832	0.0017	0.0015
60	0.0089	2242				
70	0.0154	2179				
75	0.0203	2129	0.0083	0.3593	0.0048	0.0035
80	0.0262	2086				
90	0.0418	2005				
100	0.0590	1989	0.0192	1.3095	0.0130	0.0062
110	0.0820	1961				
120	0.1120	1928				
125	0.1295	1919	0.0393	3.5749	0.0286	0.0107
130	0.1481	1903				
140	0.1899	1886				
150	0.2391	1869	0.0722	8.0875	0.0538	0.0184
160	0.2941	1858				
170	0.3516	1856				
175	0.3829	1855	0.1202	15.805	0.0902	0.0300
180	0.4156	1854				
190	0.4842	1854				
200	0.5584	1854	0.1828	27.502	0.1374	0.0453
210	0.6382	1853				
220	0.7223	1852				
225	0.7653	1852	0.2601	44.001	0.1955	0.0646
230	0.8078	1854				
240	0.8953	1858				
250	0.9884	1859	0.3524	65.859	0.2635	0.0889
260	1.0859	1857				
270	1.1829	1858				
275	1.2319	1862	0.4596	93.614	0.3403	0.1192
280	1.2810	1859				
290	1.3790	1862				
298.16	1.4615	1861	0.5684	124.785	0.4185	0.1499
300	1.4805	1861	0.5775	127.492	0.4250	0.1526

region. Katz[11] has recently attempted to explain some of these variations in terms of single Einstein frequencies which are added to or subtracted from a simple Debye spectrum. He shows that the relative deviation from a constant Debye θ for the low temperature range $0<T<\theta/10$ may be given by

$$\delta=\frac{\theta-\theta_0}{\theta_0}=-\frac{5}{12\pi^4}\sum_i\frac{\beta_i}{q_i^3}\frac{x_i^5e^{x_i}}{(e^{x_i}-1)^2}, \quad (1)$$

where $x_i=q_i\theta_0/T$. θ_0 is interpreted as the value of θ_D at 0°K. $q_i=\nu_i/\nu_0$, where ν_i is the Einstein frequency and ν_0 is the frequency corresponding to θ_0. β_i refer to small "weight factors," which may be positive or negative depending on whether the Einstein frequency is added to or subtracted from the Debye spectrum.

If only one Einstein frequency is involved the temperature T_m at which δ has an extreme (maximum or mini-

TABLE III. The molal entropy of diamond

0–25°K (Extrapolated)	0.0004 cal/g-atom/deg
25–298.16°K (Graphical)	0.5680
$S^\circ_{298.16}$	0.568±0.005

[11] E. Katz, J. Chem. Phys. 19, 488 (1951).

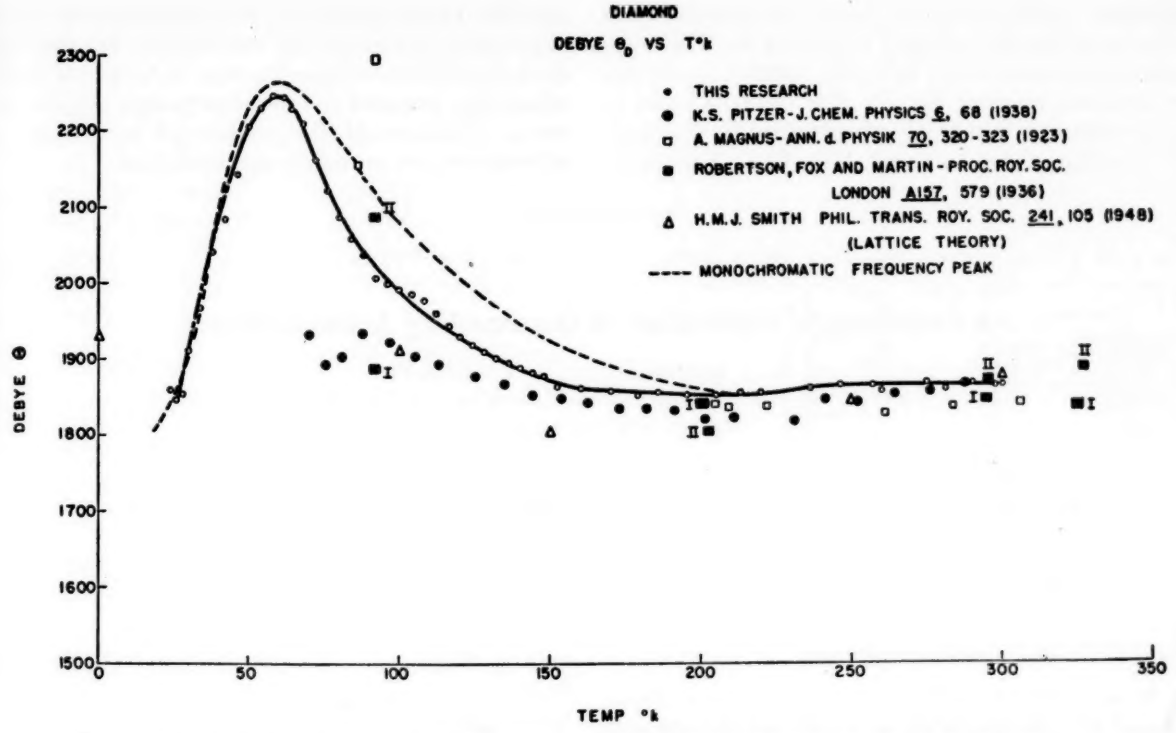
DIAMOND
DEBYE θ_D VS T°k
THIS RESEARCH
K.S. PITZER - J. CHEM. PHYSICS 6, 68 (1938)
A. MAGNUS - ANN. d. PHYSIK 70, 320 - 323 (1923)
ROBERTSON, FOX AND MARTIN - PROC. ROY. SOC. LONDON A157, 579 (1936)
H.M.J. SMITH PHIL. TRANS. ROY. SOC. 241, 105 (1948) (LATTICE THEORY)
MONOCHROMATIC FREQUENCY PEAK
DEBYE Θ
TEMP °k

FIG. 2. Characteristic Debye temperatures for diamond calculated from various investigations.

mum) value is given by

$$T_m = \theta_0 q/4.93. \tag{2}$$

Furthermore, the extreme value of δ is given by

$$\delta_m = -7.3\cdot 10^{-4}\beta_i\theta_0^3/T_m^3. \tag{3}$$

This analysis is applied to the peak observed in the θ_D *vs* T curve for diamond. The temperature T_m has the observed value of 60°K. If the θ_0-value for diamond is assumed to be approximately equal to 1800°K, then $\delta_m = 0.247$. The values calculated for q_i and β_i have the values 0.16 and -1.25×10^{-2}, respectively. Thus, by subtracting an Einstein frequency $\nu_i = 0.16\nu_0$ from a Debye spectrum with $\theta = 1800$°K, one gets a rough fit to the data. This is shown in Fig. 2. Whether or not this treatment has real physical significance is questionable.

From the relationship shown in Eq. (2), the temperature at which the maximum (or minimum) is observed in the θ_D *vs* T curve is directly proportional to θ_0, or frequency $(\nu_0)_{max}$, for an ideal lattice provided the q's are fixed. If one makes the assumption that θ_0 is equal approximately to the "constant" θ_D value in the higher temperature region for each of the three metals Ag, Al, and Cu and for diamond, one finds that the temperature T_m for the major peak observed in each of these

TABLE IV. Peak temperatures in the θ_D *vs* T curve

Element	$\theta_0 \simeq \theta_D$	T_m°K(obs)	T_m(calc)
Ag	216	~6	7
Cu	313	~9	10
Al	419	~14	13.6
Diamond	1800	60	—

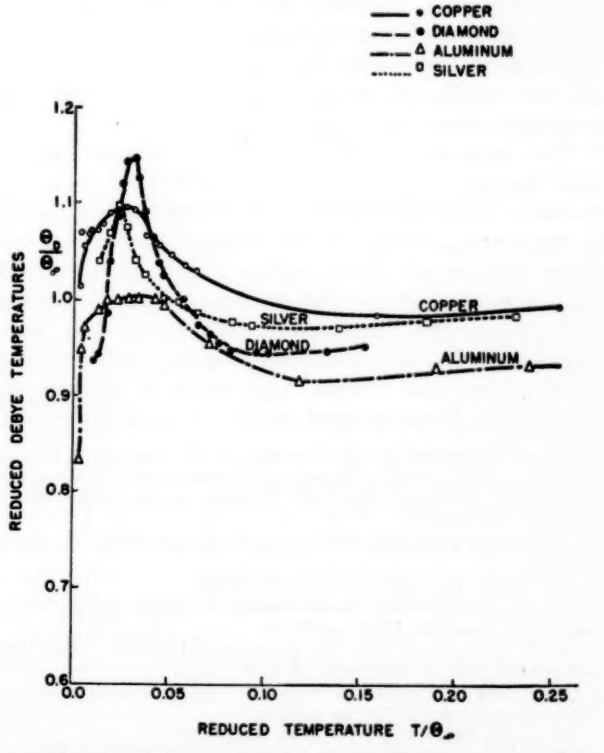

FIG. 3. Reduced Debye characteristic temperatures as a function of reduced temperatures for diamond and three *fcc* metals Cu, Al, and Ag.

monatomic solids forms a linear relationship when plotted as a function of their respective θ_D. This relationship is summarized in Table IV, where T_m(calc) has been obtained by using Eq. (2). The value "q" used in the calculations is that previously obtained for diamond.

The author wishes to thank Mrs. E. L. Fontanella and Mr. Frank Hudda for their assistance in the experimental work and in the calculations. For the latter, the author is also indebted to Mrs. N. V. Doyle and the calculating group of the Metallurgy Research Department. Criticisms of the manuscript by Dr. R. W. Schmitt are also gratefully acknowledged.

THE JOURNAL OF CHEMICAL PHYSICS VOLUME 21, NUMBER 5 MAY, 1953

A Calorimetric Calibration of Gamma-Ray Actinometers*†

C. J. Hochanadel and J. A. Ghormley
Chemistry Division, Oak Ridge National Laboratory, Oak Ridge, Tennessee
(Received November 24, 1952)

The yield for gamma-ray oxidation of ferrous sulfate in air saturated 0.4M sulfuric acid was found to be 15.6±0.3 ferrous ions oxidized per 100 electron volts absorbed. This value was based on calorimetric measurements of cobalt gamma-ray energy absorption in water at intensities of 25 r/sec, 74 r/sec, and 225 r/sec. The yield for reduction of ceric sulfate in air saturated 0.4M sulfuric acid solution, determined by comparison with the ferrous sulfate yield was 2.52±0.05 ceric ions reduced per 100 ev absorbed. The effects of several variables on these yields were investigated.

I. INTRODUCTION

An accurate determination of the amount of chemical change produced in a suitable actinometer solution as a function of the x-ray energy absorbed affords a simple and rapid method for determining the dose received by other solutions. In the past, calibration of chemical actinometers has been carried out by comparing the ionization current observed in an air-filled ionization chamber and the chemical change produced in a solution contained in a similar chamber placed in the same radiation field. The energy absorbed in the condensed system was calculated from the measured ionization in air.

The oxidation of ferrous sulfate in 0.4 molar sulfuric acid has been chosen for an actinometer by a number of workers. Miller[1] measured the yield for this system using a rigorous application of the Bragg[2]-Gray[3] cavity ion-chamber principle. Using radium gamma-rays and 200-kv x-rays at about 2 r per second he found a yield of 19.7 micromoles/liter/1000 r (G[4]∼20.6). The same value has also been obtained recently by Hardwick[5] using x-rays and γ-rays. This value is significantly higher than those reported earlier by Fricke[6] (G∼18.3) and by Shishacow[7] (G∼16). Recently Hummell and Spinks[8] reported yields of 15.8 for 24.5-Mev betatron x-rays and 16.8 for radium gamma-rays.

It seemed to us that this wide discrepancy in values could best be resolved by direct calorimetric measurement of the gamma-ray energy absorbed in the condensed system. Using a 300-curie cobalt-60 source[9] at intensities of 25 r/sec and 75 r/sec and a 1500-curie source at an intensity of 225 r/sec, we have found it feasible to measure by means of an adiabatic calorimeter the heat liberated in a sample of water during exposure to gamma-radiation. Following this measurement the water in the calorimeter was replaced with an air-saturated 10^{-3} M ferrous sulfate solution in 0.4 molar sulfuric acid and the rate of oxidation of ferrous ions measured. From these measurements the absolute yield was calculated.

Two other methods were used for calibrating the yield for ferrous oxidation. Measurements were made using a cavity ionization chamber. Based on available information on relative electron stopping powers for various materials, the energy necessary to form an ion pair in air and relative gamma-ray absorption coefficients, a yield for ferrous oxidation was calculated. Perhaps more to the point is the calculation of these quantities from the yield for ferrous oxidation measured calorimetrically.

Measurements were also made using 1.33-mv Van de Graaff electrons. The energy absorbed in solution was calculated from voltage and charge input measurements.

The reduction of ceric sulfate solution also provides a

* Paper presented in the meeting on Dosimetry in Intense Radiation Fields at the Conference on Fission Product Utilization, Brookhaven National Laboratory, Upton, Long Island, New York, February 18, 1952.

† This work was performed for the U. S. Atomic Energy Commission.

[1] N. Miller, J. Chem. Phys. **18**, 79 (1950).

[2] W. H. Bragg, *Studies in Radioactivity* (MacMillan and Company, Ltd., London, 1912), p. 94.

[3] L. H. Gray, Proc. Roy. Soc. (London) **A122**, 647 (1929); **156**, 578 (1936); Brit. J. Radiology **27**, 677 (1949).

[4] The yield (G) refers to ferrous ions oxidized per 100 electron volts energy absorbed by the solution.

[5] T. J. Hardwick, Can. J. Chem. **30**, 17 (1952).

[6] H. Fricke and S. Morse, Am. J. Roentgenol. Radium Therapy **18**, 430 (1927); Phil. Mag. **7**, 129 (1929); H. Fricke and E. Hart, J. Chem. Phys. **3**, 60 (1935).

[7] N. A. Shishacow, Phil. Mag. **14**, 198 (1932).

[8] R. W. Hummell and J. W. T. Spinks, J. Chem. Phys. **20**, 1056 (1952).

[9] J. A. Ghormley and C. J. Hochanadel, Rev. Sci. Instr. **22**, 473 (1951).

useful actinometer, especially for more intense radiation fields since the yield is lower than that for ferrous oxidation. The yield for reduction of ceric sulfate in air saturated 0.4 molar sulfuric acid solution was determined by comparing the rate of reduction of ceric ion with the rate of oxidation of a ferrous sulfate solution irradiated under identical conditions. The most recent study of ceric sulfate reduction by x-rays and γ-rays was made by Hardwick[10] who reported a yield 3.3 ceric ions reduced per 100 ev over a wide range of intensities.

II. CALIBRATION OF ACTINOMETER

A. Preparation of Solutions

Solutions were prepared using especially purified water. Water from a Barnstead still was redistilled from acid permanganate and then from alkaline permanganate. A further distillation was made in an all silica system, and the water was stored in silica vessels.

Baker's cp analyzed ferrous ammonium sulfate and ferrous sulfate were used. Recrystallization produced no change in the yield.

Several preparations of sulfuric acid were used, including Baker and Adamson reagent cp, Baker's analyzed reagent and Baker's analyzed reagent 20 percent fuming. Solutions prepared from each of these acids gave the same yield. However, with solutions prepared using the fuming sulfuric acid an initial low yield was observed which was traced to the presence of sulfurous acid.

G. Frederick Smith reagent ceric ammonium sulfate was used without further purification.

B. Analytical Methods

The solutions were analyzed before and after irradiation. Two methods were used for ferrous ion determination: direct titration with ceric sulfate using orthophenanthroline indicator and colorimetric determination using the absorption of the orthophenanthroline complex measured at 5100A with a Beckmann model DU spectrophotometer. Ferric ion was determined either by absorption of the thiocyanate complex at 4800A or by absorption of the ferric ion[11] directly at 3050A. The latter analysis is the most convenient and satisfactory and is in use at the present time. The ferrous and ferric analyses were standardized independently, and results obtained with the different methods agreed within about 2 percent. The molar extinction coefficient for ferric ion in 0.4*M* sulfuric acid measured at 3050A at 25°C was found to be 2240. The extinction coefficient is temperature sensitive, this being the only inconvenient feature of the method. Ferrous ion and H_2O_2 do not interfere.

Ceric ion was determined either by titration with ferrous sulfate or by direct measurement of the absorption of ceric ion[11] at 3200A. The latter method is the most convenient and is used at present. There is no interference by cerous ion and little effect of temperature on the extinction. The molar extinction coefficient for ceric ion in 0.4*M* sulfuric acid measured at 3200A at 25°C was found to be 5580.

The extinction coefficient reported here for ferric ion is 3 percent higher than that reported by Hardwick.[5] Our value for ceric ion is 8 percent lower than that reported by Hardwick[10] but is in agreement with the value reported by Medalia and Byrne.[12]

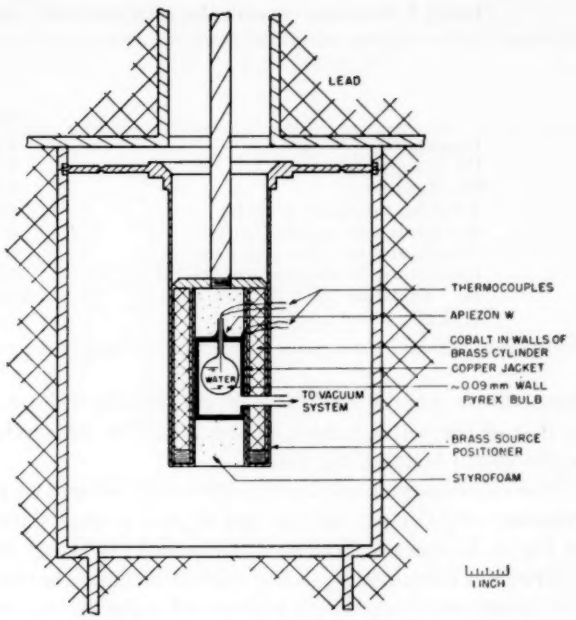

FIG. 1. Calorimeter for measurement of gamma-ray energy absorbed in water.

C. Calorimetric Measurements

Calorimetric measurements were made using both a 300-curie and a 1500-curie cobalt source. The 300-curie source has been described.[9] The 1500-curie source consisted of three cobalt cylinders (1 in. diameter×4 in.) arranged around the base of a 1½-in. brass tube immersed in ten feet of water.

The calorimeter shown in Fig. 1 for the 300-curie source consisted of a cylindrical copper jacket which surrounded a thin-walled silvered Pyrex bulb containing the water sample. The calorimeter was placed in the center of the cylindrical cobalt source for measurements at 75 r per second and placed at the side of the source for measurements at 25 r per second.

Temperatures were followed during irradiation by means of copper constantan thermocouples placed in the water and in the copper jacket. A white potentiometer was used for measuring thermocouple potential differences with reference junctions at 0°C. The

[10] T. J. Hardwick, Can. J. Chem. **30**, 23 (1952).

[11] Direct spectrophotometric determination of ferric ion and ceric ion was suggested to us by T. J. Hardwick.

[12] A. I. Medalia and B. J. Byrne, Anal. Chem. **23**, 453 (1951).

TABLE I. Summary of results for calorimetrically determined yield for ferrous sulfate oxidation by gamma-rays.

	300-curie source ~75 r/sec August 1950	300-curie source ~75 r/sec June 1951	~25 r/sec/ June 1951	1500-curie source ~225 r/sec/ June 1951
Heating rate (°C/min)	0.0104	0.00936	0.00333	0.0340
Wt of water (g)	5.98	5.18	5.18	2.72
Wt of glass (g)	0.30	0.26	0.26	0.17
Total heat capacity (cal/deg)	6.03	5.22	5.22	2.74
Energy abs. in system (cal/min)	0.0628	0.0488	0.0174	0.0932
Energy abs. in water (cal/g/min)	0.0100	0.00898	0.00320	0.0323
Energy abs. in solution (cal/ml/min)	0.0102	0.00925	0.00330	0.0332
Fe^{++} oxidation (10^{-6} M/liter/min)	69.0	62.5	21.8	229
G (Fe^{++}/100 ev)	15.5±0.3	15.6±0.3	15.2±0.5	15.9±0.4

temperature of the jacket was continually adjusted to that of the water using a heater placed in the cavity of the shield housing the cobalt.

The calorimeter used for the 1500-curie source at an intensity of 225 r per second was similar to that shown in Fig. 1. It was not, however, convenient to pump the calorimeter continually, so the system including a charcoal getter was evacuated and sealed immediately before the experiment. The temperature of the calorimeter jacket was controlled by means of a heater wound directly on the copper jacket.

Temperatures were followed over three to five hour periods during which time steady-state concentrations of products of water decomposition (H_2, O_2, H_2O_2) were attained, thereby eliminating the small effect of heat of chemical reaction. Figure 2 shows a 90-minute portion of the time-temperature plot for a typical calorimeter experiment (75 r/sec, June, 1951). Actually the slope over a four-hour period was exactly the same as that shown in the plot for the shorter period of time. After the heater was turned off, the sample temperature

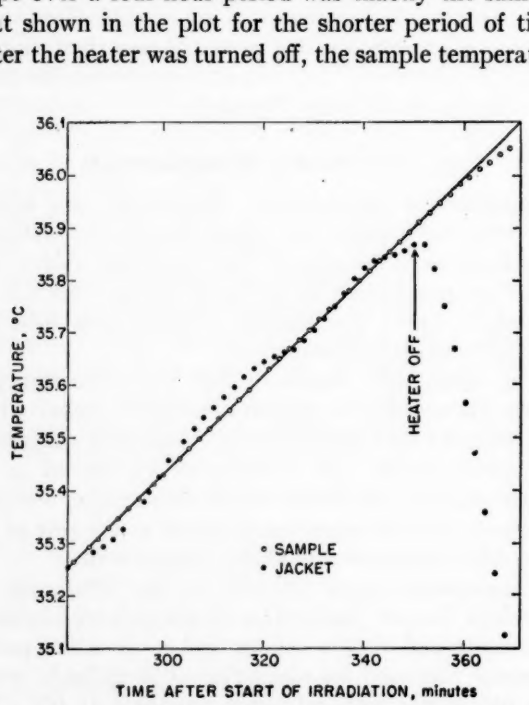

FIG. 2. Portion of the plot of a typical calorimeter experiment (~75 r/sec, June, 1951).

was followed until it started to decrease (not shown on the plot). From the temperature difference between jacket and sample at this point the rate of heat leakage of the calorimeter was calculated. The value obtained, 0.0204 cal/min/deg, indicated that this calorimeter assembly was considerably better than the previous one, (August, 1950), which had a heat loss rate of 0.145 cal/min/deg. The calorimeter used in the experiments with the 1500-curie source also had a relatively low heat loss of 0.022 cal/min/deg.

In our measurements the assumption was made that the temperature of the thermocouple junction immersed in the water was the same as the temperature of the water and of the bulb from which heat would be exchanged with the surrounding jacket. The validity of this assumption is indicated by the fact that the same yield was observed in the two experiments at the center of the 300-curie source, although quite different rates of heat leakage were observed for the two calorimeter assemblies.

The rate of energy absorption in the system (at 34°C) was calculated from the measured rate of temperature rise and the calculated heat capacity of the system. The rate of energy absorption in the water alone was calculated from this assuming the amount of energy absorbed by the glass was proportional to its fraction (4.8 percent to 5.9 percent) of the weight of the system. It is believed that this correction is valid within one percent. The heat capacity and energy absorption by the thermocouple (*B* and *S* No. 40 copper and No. 30 constantan) was negligible since the total mass of wire within the calorimeter was only 0.016 g. Likewise, the mass of the thin silver coating on the outside of the Pyrex bulb was also negligible (0.001 g). The rate of energy absorption in the ferrous sulfate solution was taken to be greater than that in water by the ratio of densities. The calorimetric measurements are summarized in Table I.

The average yield at intensities from 25 r/sec to 225 r/sec is calculated to be 15.6±0.3 ferrous ions oxidized per 100 ev absorbed. This value, based on calorimetric measurement of energy absorption, is believed to be more reliable than those based on ion-chamber measurements, since the uncertainties inherent in calculating energy absorbed in the condensed

medium from the measured ionization in air are eliminated.

D. Comparison with Other Methods

1. Ion Chamber Measurements

In an attempt to explain the serious discrepancy between the value reported here and the recent values reported by Miller[1] and by Hardwick,[5] the yield for ferrous oxidation was also determined using ion-chamber measurements of energy absorption. The uniform intensity distribution inside the cylindrical source provided ideal conditions for this type of measurement. The polystyrene ion chamber shown in Fig. 3 is similar to that used by Miller. Ferrous sulfate solutions were irradiated in a polysytrene vessel identical with the ion chamber except without the "dag" coatings and small lead wire holes.

The air volume in the chamber was determined by weighing mercury. The ion current was determined by measuring with a vibrating reed electrometer the potential drop across a calibrated precision one-megohm resistor. The same current was observed with 200 and 300 volts across the ion chamber with either polarity, indicating that saturation current was attained below 200 volts.

In Table II are listed measurements made with the chamber surrounded by cobalt in the position shown for the calorimeter in Fig. 1 (75 r per second) along with values for constants used in calculating energy absorption.

From these data the rate of energy absorption in water in terms of ev/sec/g was calculated using the expression

$$0.985(IP)(W)\left[\frac{(\rho_e S_e)_{\text{poly.}}}{(\rho_e S_e)_{\text{air}}}\right]\left[\frac{(\sigma_a+\tau)_{\text{water}}}{(\sigma_a+\tau)_{\text{poly.}}}\right],$$

where IP=ion pairs per gram of air, $(\sigma_a+\tau)$=mass absorption coefficient neglecting σ_s, corresponding to

TABLE II. Summary of measurements and constants used for ion chamber determination of yield for ferrous sulfate oxidation by gamma-rays.

Volume of chamber	6.38 cc
Temperature	27°C
Pressure	746 mm
Density of air	0.001155 g/cc
Ion current	1.262×10^{-7} amp
Energy per ion pair (W)	32
Electron density of air (ρ_e) air	3.01×10^{23} electrons/g
Electron density of polystyrene (ρ_e)poly.	3.24×10^{23} electrons/g
Electron stopping power ratio $\frac{(S_e)_{\text{poly.}}}{(S_e)_{\text{air}}}$	1.03
Gamma-absorption ratio $\frac{(\sigma_a+\tau)_{\text{water}}}{(\sigma_a+\tau)_{\text{poly.}}}$	1.03
Density of solution	1.023 g/cc
Attenuation by solution	1.5%
Fe^{++} oxidation	66.0×10^{-6} moles/liter/min
G	16.7 Fe^{++}/100 ev

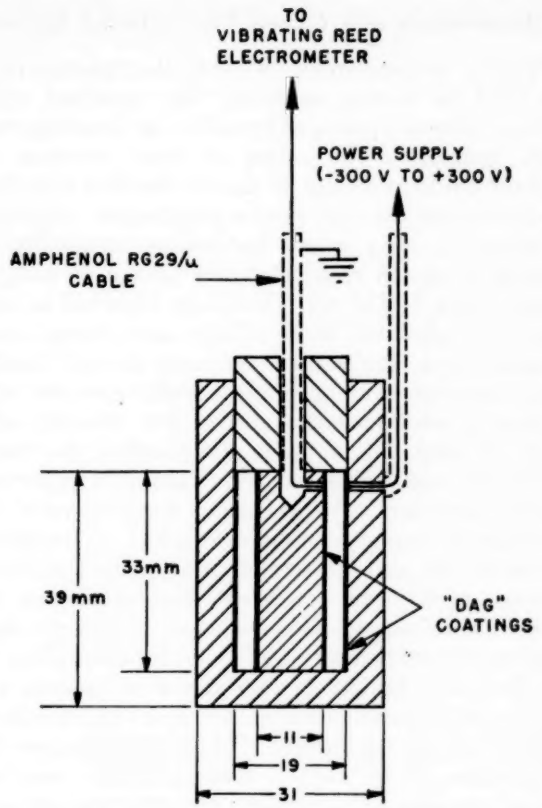

FIG. 3. Section through center of cylindrical polystyrene ion chamber.

energy of the scattered radiation, and 0.985=correction for attenuation by water.

The yield of 16.7 calculated on the basis of chosen values for the various quantities involved is 7 percent higher than the yield measured calorimetrically. Gerbes[13,14] value for energy per ion pair in air (W) was chosen and is probably accurate to ±2 percent. For the low "Z" materials and high gamma-ray energies involved here, the ratio of absorption coefficients is the same as the ratio of number of electrons per gram.[15] The value taken for the ratio of gamma-ray absorption of water to polystyrene is probably not in error by more than 1 percent. Relative electron stopping powers for polystyrene and air were taken from values given by Gray[3] for electronic stopping power as a function of atomic number. These values are not accurately known and it is believed that the discrepancy in yield values between 16.7 and 15.6 can be explained by inaccuracy in the chosen values for relative stopping powers. On this basis, in order to make the yield values obtained by the two methods consistent, the ratio of electronic stopping powers for polystyrene to air would be 1.10 rather than 1.03.

[13] W. Gerbes, Ann. Physik **23**, 648 (1935).
[14] Theodore J. Wang, Nucleonics **7**, 55 (1950).
[15] D. E. Lea, *Action of Radiations on Living Cells* (Macmillan Company, New York, 1947), pp. 345–349.

2. Measurements with 1.33-mv Van de Graaff Electrons

Prior to the measurements using cobalt gamma-rays, the yield for ferrous oxidation was measured using 1.33-mv electrons provided by a Van de Graaff electrostatic generator. The action of these electrons on aqueous solutions should be almost identical with that for cobalt gamma-rays (under comparable conditions of intensity, etc.) where the energy absorption is through Compton recoil electrons having an average initial energy of 0.63 mv. The energy absorbed in solution was calculated from voltage and charge input measurements. The vertical generator allowed irradiation of solution in an open 50-ml beaker provided with a glass encased magnetic stirring bar rotating on a tungsten point. The tungsten also provided the charge measuring lead which was connected to a calibrated charge integrator. The voltmeter was calibrated by members of the physics division at the (γ, n) thresholds for beryllium and deuterium (1.63 and 2.18 Mev). The use of an open irradiation vessel eliminated the correction for energy loss in a window, however, a small correction ($\sim$1 percent) was made for absorption by air. The yield obtained in a series of five irradiations of 40 ml of 10^{-3} molar ferrous sulfate in 0.4 molar sulfuric acid at an electron current of 0.065 microampere for total doses of 2.7 to 14.7 microcoulombs was 16.8 with a precision of ± 2 percent. The yield was the same at intensities of 0.065, 0.5, and 1.5 microamperes.

This value is about 8 percent higher than that observed in the calorimetric measurements using gamma-rays. We believe this difference to be due to an error in measurement of charge entering the solution. The current leads were properly insulated and shielded, however, there was undoubtedly some backscatter (electrons which entered the solution, produced some chemical effect, then escaped without being measured), the magnitude of which was not determined. With the low "Z" target (solution) used in these measurements this effect was minimized.

E. Yield for Reduction of Ceric Sulfate

The yield for reduction of ceric sulfate in air saturated 0.4 M sulfuric acid solution was determined by comparison with the yield for ferrous sulfate oxidation. The value determined in this manner was 2.52 ± 0.05 ceric ions reduced per 100 ev.

The ratio of yields for ferrous oxidation (2×10^{-3} M) to ceric reduction (2×10^{-4} M) was measured in glass vessels and found to be the same, 6.2 ± 0.2, at all intensities from 0.2 r/sec to 225 r/sec. Since Hardwick reported the yield for ceric reduction to be independent of intensity over a wide range, the constant ratios obtained here would imply that the ferrous yield is independent of intensity over the range studied (from 0.2 r/sec to 225 r/sec).

III. EFFECTS OF SEVERAL VARIABLES ON FERROUS OXIDATION

A. Gamma-Ray Intensity

Other ion-chamber measurements were made at intensities of 20 r/sec, 4 r/sec, 1 r/sec, and 0.2 r/sec by placing the chamber at various distances from the source and by using lead shielding. The first results indicated that the yield increased with decreasing intensity. However, it was observed that ferrous ion was oxidized appreciably just on standing in the polystyrene vessel for times comparable with those required for irradiation at low intensity. Oxidation of ferrous ion in the solution standing in a glass vessel for corresponding times was negligible. In addition, it was shown that something had dissolved (presumably organic material which is known to increase the yield[16]) which increased the yield for ferrous oxidation. For example, after allowing solution to stand in the polystyrene chamber for $5\frac{1}{2}$ hours, measuring the blank, then irradiating for 3 minutes at 75 r/sec, the rate was 70 micromoles/liter/min. The rate in the same polystyrene chamber using solution taken directly from the Pyrex container was only 59.5 micromoles/liter/min. In another experiment, after the solution stood for 16 hours in the polystyrene chamber, the rate during the first 3 minutes was 71 micromoles/liter/min, during the second 3 minutes 64.5 micromoles/liter/min, and during the third 3 minutes 64.5 micromoles/liter/min compared with a rate of 59.5 micromoles/liter/min for solution stored in Pyrex and irradiated in the polystyrene chamber. The relative rates at various intensities for samples irradiated in Pyrex containers and in the polystyrene vessel were different, again indicating the effect of polystyrene at low intensity and long irradiation.

Although several authors[5,17] reported no effect of polystyrene on yield, our results suggest that higher yields obtained in polystyrene vessels at low intensities may result from dissolved organic matter.

B. Solute Concentration

Complete dose *vs* concentration curves were run for many solutions, both air saturated and oxygen saturated at concentrations from 10^{-4} M to 5×10^{-2} M. No significant difference in yield was found over this concentration range at intensities of 5 r/sec, 75 r/sec, and 225 r/sec. Typical dose *vs* concentration curves are shown in Fig. 4 for ferrous sulfate oxidation and ceric sulfate reduction. The results are plotted as concentrations of ferric ion or cerous ion produced for various times of irradiation. The horizontal lines on the graph indicate complete oxidations of ferrous ion or complete reduction of ceric ion.

[16] H. A. Dewhurst, J. Chem. Phys. **19**, 1329 (1951).
[17] N. Miller and J. Wilkinson, paper presented before Faraday Society, Leeds, England, April 1952.

C. Oxygen Concentration

The yield for ferrous oxidation has been reported by several authors to be independent of oxygen concentration as long as some oxygen is present in solution. We have found that air-saturated and oxygen-saturated solutions gave the same yield within experimental error of a few percent and that the yield was still the same with 40-lb pressure of oxygen maintained over the solution. For evacuated solutions the yield was much lower. Several authors[1] reported a ratio (yield with oxygen present/yield in vacuum) of about 2.6, although others have reported ratios as high as 3.8. We found for 10^{-3} *M* ferrous sulfate in 0.4 *M* sulfuric acid a ratio of 2.0 for the yields in air saturated solution *versus* that in solution through which purified helium was swept in order to remove the oxygen. Sweeping hydrogen through the solution reduced the yield 8 to 10 percent below that for helium swept solutions, indicating some competition of hydrogen molecules with ferrous ions for hydroxyl free radicals.[18]

D. Long-Lived Intermediates

The direct spectrophotometric determination of ferric ion permitted observation of oxidation of ferrous ion following the termination of irradiation of ferrous sulfate solution. In a 7.2×10^{-5} *M* ferrous sulfate solution irradiated 50 seconds at 75 r/sec only one-half of the final ferric ion concentration was observed immediately after irradiation, and the balance of the ferric ion appeared at a rate comparable with the rate of oxidation of ferrous ion by hydrogen peroxide under similar conditions. The full yield, corresponding to that found at higher concentrations, was obtained on allowing the solution to stand sufficiently long after irradiation for complete reaction to occur. At the higher concentrations of ferrous normally used, oxidation by hydrogen peroxide was so rapid that no delayed formation of ferric was observed. In order to determine whether build-up of peroxide in ferrous solutions irradiated at high intensities could affect the yield, some experiments were carried out in which samples were given a series of short irradiations (10 sec) with relatively long periods (2 min) between. Pulsed exposures and equivalent continuous exposures of 3×10^{-4} *M* solutions showed no significant difference in yield either at 75 r/sec or 225 r/sec.

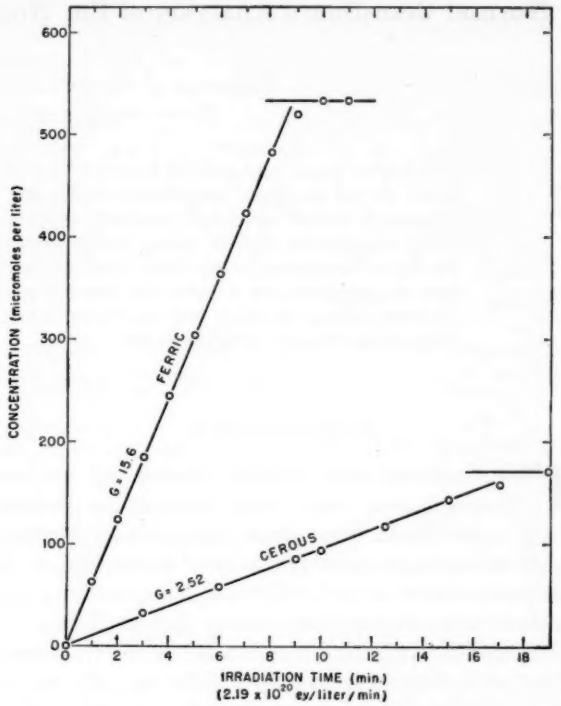

FIG. 4. Typical concentration *vs* dose curves for the oxidation of ferrous sulfate and the reduction of ceric sulfate by cobalt gamma-rays.

E. Temperature

The difference in yield for ferrous oxidation in 10^{-3} *M* solution irradiated at 25° and 65°C was found to be negligible. This is in agreement with the results of Minder and Leichti.[19]

[18] See Rigg, Stein, and Weiss, Proc. Roy. Soc. (London) **A211**, 375 (1952).

[19] W. Minder and A. Leichti, Experimentia **2**, 410 (1946).

Normal Coordinate Analysis of the Nonplanar Vibrations of 1,3,5-Trifluorobenzene*

ELDON FERGUSON
Department of Physics, University of Oklahoma, Norman, Oklahoma
(Received November 25, 1952)

A normal coordinate analysis has been carried out of the nonplanar vibrations of 1,3,5-trifluorobenzene based on the frequency assignments of Nielsen, Liang, and Smith and utilizing results from Miller and Crawford's normal coordinate treatment of the nonplanar vibrations of benzene. The analysis has furnished strong support for Nielsen, Liang, and Smith's tentative assignment of the lowest A_2'' fundamental and has led to the conclusion that their value for the highest E'' fundamental is too high. The spectral data have been re-examined, and a reasonable new assignment has been given for this E'' fundamental. A plausible reinterpretation consistent with the change in assignment of the E'' fundamental has been given of several of the combination and overtone bands.

INTRODUCTION

THE infrared and Raman spectra of 1,3,5-trifluorobenzene have been studied by Nielsen, Liang, and Smith[1] who made quite complete assignments of fundamentals. The normal vibrations of this molecule, which undoubtedly has the symmetry D_{3h}, divide into the following symmetry species: $4A_1'+3A_2'+7E'$ (planar vibrations) and $3A_2''+3E''$ (nonplanar vibrations). The vibrations of species A_1', E', and E'' are Raman active, those of species A_2'' and E' are infrared active, and the three vibrations of species A_2' are inactive both in infrared absorption and in the Raman effect.

The lowest A_2'' fundamental was inferred by Nielsen *et al.* from combination bands and hence was somewhat uncertain. There was also considerable uncertainty in the E'' highest fundamental assignment. The present investigation was undertaken for the purpose of checking these two uncertain assignments and evaluating force constants.

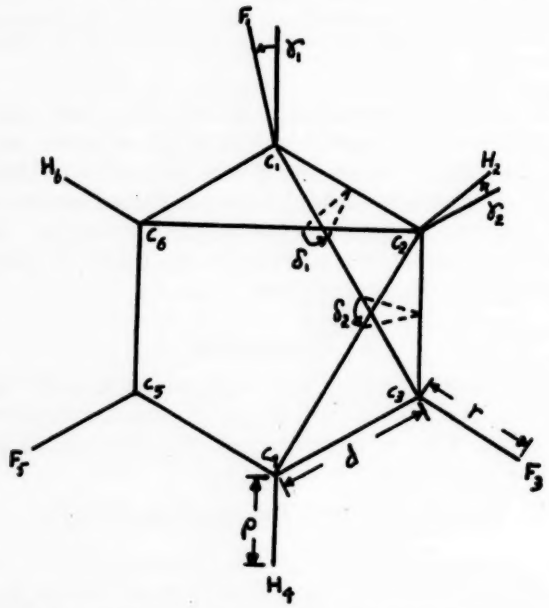

FIG. 1. Internal coordinates. Three types of nonplanar internal (or valence) coordinates are used: (1) The perpendicular displaceplacement of the ith fluorine atom out of the plane defined by the two adjacent C−C bonds is termed $r\gamma_i$, where γ_i is the angle thus defined and r is the equilibrium C−F bond length; (2) The analogous coordinate $\rho\gamma_i$ for hydrogen motion where ρ is the equilibrium C−H bond length; (3) The nonplanar ring bending deformations are regarded as torsions around C−C bonds, for example, C atoms 1, 2, and 3 form a plane and C atoms 6, 1, 2 form another plane, and the angle between these is called δ_1. The corresponding internal coordinate is $d\delta_1$, where d is the equilibrium C−C bond distance.

TABLE I. Symmetry coordinates.

Species	Symmetry coordinate	Corresponds to Miller and Crawford's
	$S_1=\frac{1}{(6)^{\frac{1}{2}}}(r\gamma_1+r\gamma_3+r\gamma_5+\rho\gamma_2+\rho\gamma_4+\rho\gamma_6)$	S_{11}
A_2''	$S_2=\frac{1}{(6)^{\frac{1}{2}}}(r\gamma_1+r\gamma_3+r\gamma_5-\rho\gamma_2-\rho\gamma_4-\rho\gamma_6)$	S_5
	$S_3=\frac{d}{(6)^{\frac{1}{2}}}(\delta_1+\delta_3+\delta_5-\delta_2-\delta_4-\delta_6)$	S_4
	$S_{1a}=\frac{1}{2}(r\gamma_3-r\gamma_5+\rho\gamma_6-\rho\gamma_2)$	S_{17a}
	$S_{2a}=\frac{1}{2}(r\gamma_3-r\gamma_5-\rho\gamma_6+\rho\gamma_2)$	S_{10a}
	$S_{3a}=\frac{d}{(12)^{\frac{1}{2}}}(2\delta_5-\delta_1-\delta_3+2\delta_2-\delta_4-\delta_6)$	S_{16a}
E''	$S_{1b}=\frac{1}{(12)^{\frac{1}{2}}}(-2r\gamma_1+r\gamma_3+r\gamma_5-2\rho\gamma_4+\rho\gamma_2+\rho\gamma_6)$	S_{17b}
	$S_{2b}=\frac{1}{(12)^{\frac{1}{2}}}(-2r\gamma_1+r\gamma_3+r\gamma_5+2\rho\gamma_4-\rho\gamma_2-\rho\gamma_6)$	S_{10b}
	$S_{3b}=\frac{d}{2}(\delta_1-\delta_3+\delta_4-\delta_6)$	S_{16b}

* Supported by the U. S. Atomic Energy Commission under Contract No. AT-(40-1)-1074.

[1] Nielsen, Liang, and Smith, Trans. Faraday Soc. No. 9, 177 (1950).

TABLE II. *f* matrix of valence force constants.

	$r\gamma_1$	$r\gamma_3$	$r\gamma_5$	$\rho\gamma_2$	$\rho\gamma_4$	$\rho\gamma_6$	$d\delta_1$	$d\delta_2$	$d\delta_3$	$d\delta_4$	$d\delta_5$	$d\delta_6$
$r\gamma_1$	H	h_m	h_m	$\bar{a}_o$	$\bar{a}_p$	$\bar{a}_o$	$-\bar{c}_o$	$-\bar{c}_m$	$-\bar{c}_p$	$+\bar{c}_p$	$+\bar{c}_m$	$+\bar{c}_o$
$r\gamma_3$		H	h_m	$\bar{a}_o$	$\bar{a}_o$	$\bar{a}_p$	$+\bar{c}_m$	$+\bar{c}_o$	$-\bar{c}_o$	$-\bar{c}_m$	$-\bar{c}_p$	$+\bar{c}_p$
$r\gamma_5$			H	$\bar{a}_p$	$\bar{a}_o$	$\bar{a}_o$	$-\bar{c}_p$	$+\bar{c}_p$	$+\bar{c}_m$	$+\bar{c}_o$	$-\bar{c}_o$	$-\bar{c}_m$
$\rho\gamma_2$				A	a_m	a_m	$+c_o$	$-c_o$	$-c_m$	$-c_p$	$+c_p$	$+c_m$
$\rho\gamma_4$					A	a_m	$+c_p$	$+c_m$	$+c_o$	$-c_o$	$-c_m$	$-c_p$
$\rho\gamma_6$						A	$-c_m$	$-c_p$	$+c_p$	$+c_m$	$+c_o$	$-c_o$
$d\delta_1$							B	b_o	b_m	b_p	b_m	b_o
$d\delta_2$								B	b_o	b_m	b_p	b_m
$d\delta_3$			symmetric						B	b_o	b_m	b_p
$d\delta_4$										B	b_o	b_m
$d\delta_5$											B	b_o
$d\delta_6$												B

TABLE III. *G* matrices.

Species	Matrix element[a]	Numerical value
A_2''	$G_{11}=\frac{1}{2}(\mu_F+\mu_H)+\mu_C[1+4(\rho_H-\rho_F)^2]$	0.6173
	$G_{12}=\frac{1}{2}(\mu_F-\mu_H)+2\mu_C(\rho_F-\rho_H)[1+2(\rho_H+\rho_F)]$	−0.3302
	$G_{13}=8\sqrt{3}\mu_C(\rho_H-\rho_F)$	−0.2157
	$G_{22}=\frac{1}{2}(\mu_F+\mu_H)+\mu_C(1+2\rho_F+2\rho_H)^2$	2.1949
	$G_{23}=-4\sqrt{3}\mu_C(2\rho_F+2\rho_H+1)$	−2.5855
	$G_{33}=48\mu_C$	3.9965
E''	$G_{11}=\frac{1}{2}[\mu_H+\mu_F+\mu_C\{(2\rho_F+\rho_H+1)^2+(2\rho_H+\rho_F+1)^2\}]$	1.6090
	$G_{12}=\frac{1}{2}[\mu_F-\mu_H+\mu_C\{5\rho_F^2+4\rho_F-5\rho_H^2-4\rho_H\}]$	−0.3708
	$G_{13}=2\mu_C(3\rho_F+3\rho_H+2)$	1.2028
	$G_{22}=\frac{1}{2}[\mu_F+\mu_H+\mu_C\{(1+2\rho_F-\rho_H)^2+(1+2\rho_H-\rho_F)^2\}]$	0.8202
	$G_{23}=6\mu_C(\rho_F-\rho_H)$	0.0934
	$G_{33}=16\mu_C$	1.3322

[a] $\mu_F=0.05263$, $\mu_H=0.99206$, $\mu_C=0.08326$. $\rho_H=1.08/1.39=0.7770$, $\rho_F=1.34/1.39=0.9640$. μ's are the reciprocal atomic masses in atomic weight units. ρ_H is the ratio of the equilibrium C−H bond distance to the C−C bond distance. ρ_F is the ratio of the equilibrium C−F bond distance to the C−C bond distance.

PROCEDURE

A normal coordinate analysis of the nonplanar vibrations of benzene and its deuterium derivatives has been carried out by Miller and Crawford.[2] In order to utilize their work, internal coordinates and symmetry coordinates were chosen to conform to theirs. The internal coordinates are defined and illustrated in Fig. 1. The symmetry coordinates and their correspondence to Miller and Crawford's coordinates are given in Table I.

Table II gives the *f* matrix which defines the valence force constants. The notation of Miller and Crawford is retained for the ring deformation and the applicable hydrogen bending constants. The subscripts *o*, *m*, and *p* refer to *ortho*, *meta*, and *para* relationship between the internal coordinates.

TABLE V. *F* matrix for species E''.

Matrix elements	Corresponds to Miller and Crawford's		Numerical values ($F\times10^{-5}$ dynes/cm)[a] (a)	(b)
$F_{22}=\frac{1}{2}(A-a_m+H-h_m+2\bar{a}_o-2\bar{a}_p)$	φ	E_g	0.226	3.565
$F_{12}=\frac{1}{2}(H-h_m-A+a_m)$	0		0.006	2.445
$F_{23}=\sqrt{3}/2(\bar{c}_o-c_o-\bar{c}_p+c_p)$	0		(0)	(0)
$F_{11}=\frac{1}{2}(A-a_m+H-h_m-2\bar{a}_o+2\bar{a}_p)$	σ	E_u	0.427	2.067
$F_{13}=\sqrt{3}/2(\bar{c}_o+c_o-\bar{c}_p-c_p)$	ω	E_u	(−0.515)	(−0.515)
$F_{33}=B-b_o-b_m+b_p$	θ	E_u	(0.757)	(0.757)
	Calculated frequency		852 cm^{-1}	2600 cm^{-1}

[a] Miller and Crawford's set 2 constants used in (a) and (b). Set 1 did not give real solutions. ( ) Force constant borrowed from benzene.

The *G* matrices for the A_2'' and E'' species, found by the method of Wilson,[3] are given in Table III. With the valence forces of Table II the *F* matrices given in Tables IV and V are obtained. The corresponding *F* matrices of Miller and Crawford are also given in these tables to show the correlation. Corresponding to the three vibrations of species A_2'' of 1,3,5-trifluorobenzene, the benzene molecule of higher symmetry (D_{6h}) has one vibration of species B_{2g} and two vibrations of species A_{2u}. Similarly, the three E'' vibrations of 1,3,5-trifluorobenzene split into one vibration of species E_u and two vibrations of species E_g in benzene.

With only two reasonably certain frequency assignments for each species, one is forced to make several assumptions in order to determine the six force constants of each species. The assumptions made here were the following: It was assumed that the forces involved in the distortion of the benzene ring are essentially the same in 1,3,5-trifluorobenzene as in benzene. This makes F_{33} for the species A_2'' equal to Miller and Crawford's β, and F_{33} for the species E'' equal to their θ. It was further assumed, on the basis of preliminary calculations, that $\bar{c}_o=c_o$, $\bar{c}_m=c_m$, and $\bar{c}_p=c_p$. This is equivalent to the assumption that the interaction between a

TABLE IV. *F* matrix for species A_2''.

Matrix elements	Corresponds to Miller and Crawford's		Numerical values ($F\times10^{-5}$ dynes/cm)[a] (a)	(b)	(c)	(d)
$F_{11}=\frac{1}{2}A+a_m+\frac{1}{2}H+h_m+2\bar{a}_o+\bar{a}_p$	α	A_{2u}	0.294	0.461	0.223	0.006
$F_{12}=\frac{1}{2}H+h_m-\frac{1}{2}A-a_m$	0		−0.006	0.067	−0.023	−0.127
$F_{13}=(c_o+c_p-c_m)-(\bar{c}_o+\bar{c}_p-\bar{c}_m)$	0		(0)	(0)	(0)	(0)
$F_{22}=\frac{1}{2}A+a_m+\frac{1}{2}H+h_m-2\bar{a}_o-\bar{a}_p$	ϵ	B_{2g}	0.478	0.457	0.515	0.524
$F_{23}=-(c_o+c_p-c_m+\bar{c}_o+\bar{c}_p-\bar{c}_m)$	η	B_{2g}	(0.258)	(0.258)	(0.373)	(0.373)
$F_{33}=B+2b_m-2b_o-b_p$	β	B_{2g}	(0.203)	(0.203)	(0.339)	(0.339)
	Calculated frequency		226 cm^{-1}	257 cm^{-1}	213 cm^{-1}	no real solution

[a] Miller and Crawford's set 1 constants used fh (a) and (b); set 2 in (c) and (d). ( ) force constant borrowed from benzene.

[2] F. A. Miller and B. L. Crawford, Jr., J. Chem. Phys. **14**, 282 (1946).
[3] E. Bright Wilson, Jr., J. Chem. Phys. **7**, 1047 (1939); **9**, 76 (1941).

fluorine motion out of the plane and a nonplanar ring deformation is equal to the interaction between a hydrogen motion out of the plane and a nonplanar ring deformation. With this assumption the F matrix for species A_2'' simplifies as follows: F_{13} is equal to zero, and F_{23} is equal to Miller and Crawford's η. The F matrix for species E'' similarly simplifies, F_{23} becoming equal to zero and F_{13} to Miller and Crawford's ω. Actually, the assumption made is less stringent than stated, being only that $\bar{c}_o-\bar{c}_p=c_o-c_p$ and $\bar{c}_o+\bar{c}_p-\bar{c}_m=c_o+c_p-c_m$.

It was further assumed that the constants A and a_m may be carried over from benzene. In the F matrix for species A_2'' there remain then two unknown combinations of valence force constants, namely, $\frac{1}{2}H+h_m$ and $2\bar{a}_o+\bar{a}_p$. In the E'' part of the F matrix there remain also two unknown combinations, namely, $H-h_m$ and $\bar{a}_o-\bar{a}_p$. Hence, for each species these two unknown combinations can be determined from the two certain assignments, and the third fundamental frequency can then be calculated. It should be noted that the calculations for the two species are independent. Miller and Crawford found two sets of values for the force constants η, β and ω, θ. The values of η, β are related and the values of ω, θ are related, but the two sets are independent of each other.

TABLE VI. Valence force constants for out-of-plane motion.

$H=0.303\times10^5$ dynes/cm	fluorine bending diagonal constant
$h_m=0.021$	interaction constant between fluorine bendings
$\bar{a}_o=-0.082$	interaction between a fluorine bending and an adjacent (*ortho*) hydrogen bending
$\bar{a}_p=0.019$	interaction between a fluorine atom bending and a *meta* hydrogen atom bending
Corresponding constants of Miller and Crawford for benzene	
$A=0.378$	hydrogen bending diagonal constant
$a_m=0.007$	hydrogen bending interaction constants. Relative positions indicated by subscripts (*ortho*, *meta*, or *para*).
$a_o=-0.057$	
$a_p=-0.026$	

VIBRATIONS OF SPECIES A_2''

The two fundamental frequencies that have been assigned with considerable certainty to species A_2'' are 665 cm^{-1} and 845 cm^{-1}. The uncertain assignment was of the lowest fundamental for which the value 214 cm^{-1} was inferred from observed combination bands. Using Miller and Crawford's first set of constants for species B_{2g}, one gets two sets of force constants and the two calculated frequencies 226 cm^{-1} and 257 cm^{-1}. The two solutions arise because of the quadratic nature of the equations. The solution leading to the frequency 257 cm^{-1} may be discarded on the following physical grounds. This solution (Table IV) yields a diagonal term F_{11} which exceeds F_{22} slightly (0.461 as compared to 0.457). However, F_{11} refers to the "dish-like" symmetry coordinate representing bending of all fluorines and hydrogens together above and below the plane of the ring, while F_{22} refers to the "puckered" coordinate corresponding to a motion where fluorines and hydrogens are displaced to opposite sides of the ring, and as in benzene the energy required for the "dish-like" distortion must be less than that for the "puckered" displacement. The distance between neighboring fluorine and hydrogen atoms is approximately 2.6A while the van der Waals radius of hydrogen is 1.2±0.1A and that of fluorine is 1.35±0.10.[4] Hence the argument advanced by Miller and Crawford that attractive forces may predominate might be expected to hold here also, and, since hydrogen is electropositive and fluorine electronegative with respect to carbon,[4] the argument may even be stronger here. The second set of constants of Miller and Crawford yield a value of 213 cm^{-1} for the lowest A_2'' fundamental. The other quadratic solution in this case does not yield a positive definite F matrix and does not give a real solution for ν. The resulting F matrices are shown in Table IV.

VIBRATIONS OF SPECIES E''

The assignments for the E'' species which seem quite certain are 253 cm^{-1} and 595 cm^{-1}. Here Miller and Crawford's first set of constants (for species E_u) yielded imaginary force constants. Their second set yielded a value for the highest E'' frequency of 852 cm^{-1} which is considerably lower than the frequency 1191 cm^{-1} assigned tentatively by Nielsen *et al.*[1] This discrepancy is so great, and such drastic changes in the potential function would be required in order to attain a value as high as 1191 cm^{-1} that it must be concluded that this assignment is in error. The second solution in this last case is not physically reasonable, leading to force constants larger than unity, and hence is discarded. The numerical values of the F matrix elements of species E'' are given in Table V. By combining the F constants of species A_2'' and E'' it is possible to calculate the valence force constants for the nonplanar motion of hydrogen and fluorine. The results of these calculations are shown in Table VI. Because of the approximations involved little significance is attached to the individual force constants.

RESULTS

The normal coordinate analysis of the nonplanar vibrations of 1,3,5-trifluorobenzene has yielded two physically reasonable values for the lowest A_2'' fundamental corresponding to two sets of force constants determined for benzene by Miller and Crawford and carried over to this work. These values are 213 cm^{-1} and 226 cm^{-1}. This is considered to be strong evidence for the assignment of 214 cm^{-1} for this fundamental by Nielsen *et al.* on the basis of observed infrared combination bands.

[4] L. Pauling, *The Nature of the Chemical Bond* (Cornell University Press, Ithaca, 1940), second edition, p. 189.

TABLE VII. Reinterpretation of certain combination bands depending on the highest E'' fundamental.

Wave number	Spectrum	Old interpretation	New interpretation
2389	Raman	$2\times1191=2382(A_1'+E')$	$[1540+\ 847=2387(E'')]$[a]
2500		$1191+1300=2491(E'')$	$1631+\ 847=2478(A_1''+A_2''+E'')$
2664		$1191+1471=2662(A_1''+A_2''+E'')$	$[1122+1540=2662E']$
1709	Infrared	$503+1191=1694(A_1''+A_2''+E'')$	$2\times847=1694(A_1'+E')$
2667		$1191+1471=2662(A_1''+A_2''+E'')$	$[1122+1540=2662E']$
2801		$1191+1610=2801(A_1''+A_2''+E'')$	$1350+1471=2821(E')$
1058			$847+\ 214=1061(E')$
2326			$847+1471=2318(A_1''+A_2''+E'')$
2469 (l)		$993+1471=2464(A_1'+A_2'+E')$	$847+1610=2457(A_1''+A_2''+E'')$
2481 (g)			$847+1631=2478(A_1''+A_2''+E'')$

[a] Interpretations in brackets involve the inactive A_2' fundamental tentatively accepted as 1540 cm^{-1}.

The results also indicate strongly that the highest E'' fundamental has been incorrectly assigned. The one reasonable calculated value is 852 cm^{-1} as compared to the value 1191 cm^{-1} assigned tentatively by Nielsen *et al.* There is some evidence that the second set of constants in Miller and Crawford's treatment of benzene are preferable in the case of the degenerate species. This is contrary to the results found by Crawford and Parr[5] who obtained these constants by a molecular orbital calculation. However, the evidence there was weak, since such calculations are necessarily very crude.

The value of the diagonal fluorine wagging constant H (Table VI) is found to be 0.303. This is significantly lower than the corresponding hydrogen constant $A=0.378$ in benzene. This implies that it is energetically easier to displace a fluorine atom out of the plane of the trifluorobenzene molecule than to displace a hydrogen atom out of the plane of the benzene ring. This is in accord with previous findings from spectral data[6] indicating that fluorine substitution in aromatic compounds reduces the directional properties of the bonds and hence decreases the out-of-plane restoring forces. However, it must be admitted that such evidence may also indicate that the hydrogen bending constant borrowed from benzene is higher than it should be in 1,3,5-trifluorobenzene. This is not a serious defect however, because a calculation showed that lowering the borrowed hydrogen bending constant by as much as 22½ percent caused the predicted highest E'' fundamental to be lowered less than 6 percent. This, of course, emphasizes the discrepancy between the calculated value and the value assigned by Nielsen *et al.*

REINTERPRETATION OF SPECTRAL DATA

The Raman spectrum of 1,3,5-trifluorobenzene was re-examined with a view toward proposing an alternative assignment of the highest E'' fundamental. It was observed that the band at 1191 cm^{-1} is strongly polarized. Because of the strongly polarized character of the band, much of the intensity should be due to a vibration of species A_1'. This is undoubtedly the overtone of the E'' fundamental occurring at 595 cm^{-1}, an alternative interpretation proposed by Nielsen *et al.* A band at 1192 cm^{-1} occurs also in the infrared spectrum of the liquid where the E'' fundamental is inactive but the E'' overtones of species $A_1'+E'$ are active.

The most likely value of the highest E'' fundamental is undoubtedly that of either the weak diffuse Raman band at 829 cm^{-1} or of the equally weak band at 847 cm^{-1}. The band at 829 cm^{-1} was given the alternative assignments $253+578=831$ E'' and $326+503=829$ $(A_1'+A_2'+E')$ in the previous work. The band at 847 cm^{-1} appears to be slightly polarized, although quantitative polarization measurements were not possible because of the low intensity of the band. However, this band appears quite diffuse and hence may be the E'' fundamental overlapping with the combination band $253+595=848$ $(A_1'+A_2'+E')$, the interpretation given for it by Nielsen *et al.* No assistance can be obtained from the infrared spectrum as to the species of 847 cm^{-1}, because an A_2'' fundamental occurs at this frequency.

If the value of 1191 cm^{-1} for the highest E'' fundamental is discarded, the reinterpretation of three Raman and three infrared bands which had been interpreted as combination bands involving 1191 cm^{-1} is necessary. The value 847 cm^{-1} for the highest E'' fundamental allows a more satisfactory interpretation of these bands than does the value 829 cm^{-1} and is therefore preferred. A revised assignment is given for these six combination bands in Table VII. Two of these combination frequencies utilize the value 1540 cm^{-1} proposed for one of the inactive A_2' fundamentals by Nielsen *et al.*, making a total of four assignments now dependent on this proposed A_2' fundamental.

The proposed value 847 cm^{-1} for the highest E'' fundamental is utilized in interpreting three of these bands. In addition, the extremely weak infrared band at 1058 cm^{-1} in the liquid spectrum, which was not previously interpreted, is readily interpreted as $847+214=1061(E')$. The very weak infrared band at 2326 cm^{-1}, the interpretation of which by Nielsen, Liang, and Smith contained a numerical error, may be interpreted

[5] B. L. Crawford, Jr., and R. G. Parr, J. Chem. Phys. **17**, 726 (1949).

[6] Smith, Nielsen, Berryman, Claassen, and Hudson, "Spectroscopic properties of fluorocarbons and fluorinated hydrocarbons," NRL Report 3567, September 15, 1949, p. 157.

as $847+1471=2318(A_1''+A_2''+E'')$. A similar error was noticed in the interpretation of the infrared band occurring at 2481 cm^{-1} in the gas spectrum and at 2469 cm^{-1} in the spectrum of the liquid, although an alternative assignment was listed in this case. However, the proposed assignment $847+1631=2478(A_1''+A_2''+E'')$ is somewhat more plausible than that previously given.

In at least one case (the Raman band at 2478 cm^{-1}) the revised assignment does not seem as reasonable as the original assignment of Nielsen *et al.* However, since two additional bands can be interpreted and a more reasonable assignment given for one other band, the new assignment of the observed combination bands, on the basis of the value 847 cm^{-1} for the highest E'' fundamental, seems considerably more reasonable than that proposed by Nielsen *et al.* using the value 1191 cm^{-1}. Moreover, the fact that a value of 847 cm^{-1} can explain five observed bands that could not otherwise be interpreted as binary sums strongly supports the assignment of this frequency to the highest E'' fundamental.

The writer wishes to acknowledge his indebtedness to Professor J. Rud Nielsen for suggesting the problem and for much helpful criticism.

THE JOURNAL OF CHEMICAL PHYSICS VOLUME 21, NUMBER 5 MAY, 1953

The Magnetic Properties of Some Anhydrous Chlorides*

NORMAN ELLIOTT
Department of Chemistry, Brookhaven National Laboratory, Upton, Long Island, New York
(Received December 23, 1952)

The magnetic susceptibility of $CoCl_2$ and of solid solutions of $CoCl_2$ with $ZnCl_2$ and $CdCl_2$ have been measured over the temperature range 76°–296°K. The susceptibility of $CoCl_2$ is very little affected by dilution with isomorphous chlorides. The results are interpreted as showing that $CoCl_2$ deviates from Curie's law in its behavior because of a crystalline field Stark effect rather than Heisenberg spin-spin exchange.

An examination of the magnetic susceptibility data of the anhydrous chlorides $MnCl_2$, $FeCl_2$, $CoCl_2$, and $NiCl_2$[1] reveals that $MnCl_2$ obeys Curie's law rather closely ($\Delta=3°$) over a wide temperature range, whereas the other chlorides follow the Weiss-Curie law.

In the sequence Mn^{++}, Fe^{++}, Co^{++}, and Ni^{++}, divalent manganese is the only ion in an S state. The magnetic moment of Mn^{++} is therefore not affected by crystalline fields, to a first approximation, and the magnetic susceptibilities of divalent manganese salts are given by Curie's law when electron exchange interaction is absent. On the other hand, Fe^{++}, Co^{++}, and Ni^{++} have orbital magnetic moments which interact with the crystal electric fields, and produce deviations in the susceptibilities from Curie's law.

The close adherence of $MnCl_2$ to Curie's law probably shows that the Mn^{++} ion is in a ${}^6S_{5/2}$ state and that there is little or no exchange interaction. One is inclined, therefore, to attribute the interaction terms observed for the other chlorides to crystalline field effects. This has been subjected to experimental test in the case of $CoCl_2$.

TABLE I.

$CoCl_2$	T°K	···	162.5°	192°	297°
	$\chi_{mole}\times10^6$	···	24000	20000	12420
23.4 mole % $CoCl_2$	T°K	76°	162.5°	194°	296°
76.6 mole % $ZnCl_2$	$\chi_{mole}\times10^6$	54800	23600	19800	12510
18.6 mole % $CoCl_2$	T°K	···	···	194°	296°
81.4 mole % $CdCl_2$	$\chi_{mole}\times10^6$	···	···	20700	12900

It has been shown[2,3] for magnetically concentrated salts of Mn^{++} and Fe^{+++} that deviations from Curie's law are due to exchange interaction of electron spins and that this interaction may be reduced and made to disappear by dilution of the salt with an appropriate isomorphous diamagnetic salt. On the other hand, dilution of a paramagnetic salt in which the interaction was primarily caused by the crystalline field would not be expected to have much effect on the susceptibility.

The magnetic susceptibilities of $CoCl_2$ and solid solutions of $CoCl_2$ in $ZnCl_2$ and $CdCl_2$ were measured as a function of temperature and compared.

Anhydrous $CoCl_2$ was prepared from $CoCl_2\cdot6H_2O$ (Baker's CP Analyzed $CoCl_2\cdot6H_2O$) by heating to 300°C in an atmosphere of dry HCl. Solid solutions with $ZnCl_2$ and $CdCl_2$ (Baker and Adamson, Reagent Grade Chemicals) were made by fusing mixtures of the anhydrous salts at 350°C and 550°C, respectively, in an HCl atmosphere. All subsequent operations were performed in a dry box. The $CoCl_2$ and the $CoCl_2$-$ZnCl_2$ and $CoCl_2$-$CdCl_2$ solutions were analyzed for cobalt by

* Research carried out under the auspices of the U. S. Atomic Energy Commission.
[1] Starr, Bitter, and Kaufmann, Phys. Rev. **58**, 977 (1940).
[2] H. Bizette, Colloq. intern. centre. natl. recherche. sci. (Paris) **27**, 18 (1951).
[3] Corliss, Delabarre, and Elliott, J. Chem. Phys. **18**, 1256 (1950).

a method given in Swift's *System of Chemical Analysis*.[4] The homogeneity of the solid solutions was determined from x-ray powder photographs.

The magnetic measurements were made by the Gouy method and a modification of the Curie method.[5] The Gouy method was found to be unsuitable for the $CoCl_2$-$CdCl_2$ solution which readily cleaves to form soft plate-like crystals that are not randomly oriented in the susceptibility tube. Identical results were, however, obtained for pure $CoCl_2$ and the $CoCl_2$-$ZnCl_2$ solid solution by the two methods. The magnetic susceptibility of $Fe(NH_4)_2(SO_4)_2 \cdot 6H_2O$ (Baker and Adamson Reagent Grade Chemical) was used as a reference standard.[6] Three specimens of each substance were measured. The data were consistent to ± 1 percent.

The molar magnetic susceptibilities of $CoCl_2$ and its solid solutions with $ZnCl_2$ and $CdCl_2$, corrected for diamagnetism,[7] are given in Table I.

The results obtained are shown graphically in Fig. 1. For comparison the susceptibilities of $CoCl_2$ found by De Haas and Schultz[8] are also given. The largest difference observed in susceptibility, between $CoCl_2$ and its solution in $CdCl_2$, is less than 4 percent. This is the limit of the experimental error generally obtained by the Gouy method. Some difference is to be expected, however, when Co is replaced by Cd or Zn and is not necessarily ascribed to error.

Magnetic measurements on solid solutions of $CoCl_2$ and $CdCl_2$ have been reported by Fehrenbach[9] whose results were decidedly different from those reported here. The very easy cleavage of $CdCl_2$ in the basal plane and the formation of plate-like crystals made it difficult to measure susceptibilities of powdered samples containing large amounts of $CdCl_2$. Results similar to Fehrenbach's were obtained until precautions were taken to get randomly oriented crystals. This was done by using a modification of Curie's method of measurement with a sample of the powdered material gently sprinkled into a small cup and measured in an inhomogeneous field. Without this precaution the susceptibility one measures is mainly that in the basal plane of the hexagonal crystals, and this susceptibility apparently differs from that along the hexagonal axis.

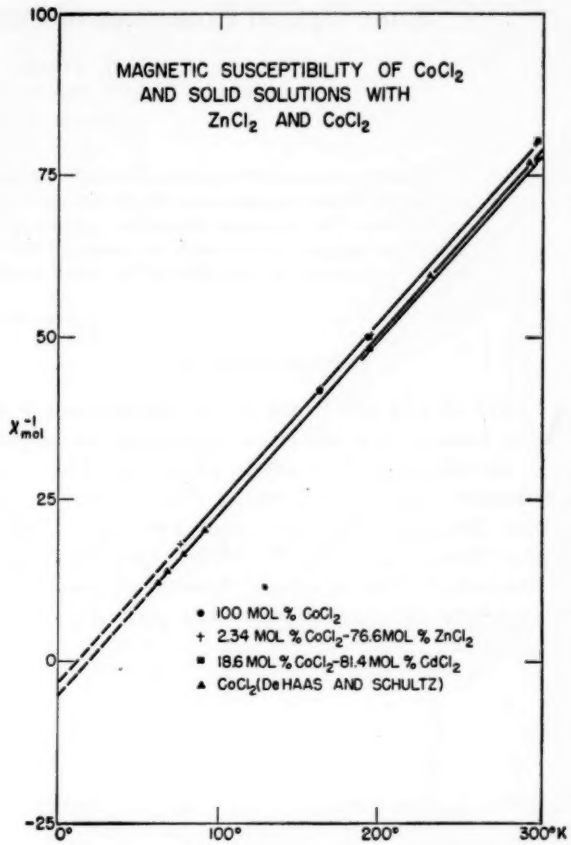

FIG. 1. Magnetic susceptibility of $CoCl_2$ and solid solutions with $ZnCl_2$ and $CoCl_2$.

The susceptibilities of $CoCl_2$ and solid solutions of $CoCl_2$ with $ZnCl_2$ and $CdCl_2$ show that $CoCl_2$ follows the Weiss-Curie law,

$$\chi_{\text{mole}} = \frac{C}{T+\theta},$$

between liquid nitrogen and room temperatures and that the θ's arise from a crystalline field Stark effect within the accuracy of the experiment. The Curie constant is the same for the three specimens and has the value $c = 3.59$. The magnetic moment of the Co^{++} ion is 5.37 Bohr magnetons. The value of θ obtained for $CoCl_2$ and its solution in $ZnCl_2$ is -10.8°K. For the solid solution $CoCl_2$-$CdCl_2$, a value -20.5°K was found.

[4] E. H. Swift, *A System of Chemical Analysis* (Prentice-Hall, Inc., New York, 1939), p. 344.
[5] E. C. Stoner, *Magnetism and Matter* (Methuen and Company, Ltd., London), Chap. III.
[6] C. Hutchison and N. Elliott, J. Chem. Phys. **16**, 920 (1948).
[7] W. R. Angus, Proc. Roy. Soc. (London) **A136**, 569 (1932).
[8] W. J. De Haas and B. H. Schultz, Physica **6**, 481 (1939).
[9] C. Fehrenbach, J. phys. et radium **8**, 11 (1937).

Some Optical Properties of Potassium Iodide-Thallium Phosphors

PHILIP H. YUSTER AND CHARLES J. DELBECQ
Chemistry Division, Argonne National Laboratory, Chicago, Illinois

(Received September 22, 1952)

The absorption spectra of potassium iodide-thallium phosphors have been studied at both liquid nitrogen and liquid helium temperatures. Eight absorption bands have been observed which are due to the presence of thallium. The maximum absorption coefficients of four of these bands appear to vary linearly, while the other four appear to vary with the square of the thallium concentration. The origin of these bands is discussed in terms of an extension of the model proposed by Seitz.

I. INTRODUCTION

A CONSIDERABLE amount of information is to be found in the literature concerning the properties of the alkali halide-thallium phosphors. The early experimental work was done by Pohl[1,2] and his coworkers Buenger,[3] Buenger and Flechsig,[4] Forro,[5] Hilsch,[1,6] Koch,[2,7] Lorentz,[8] MacMahon,[9] von Meyeren,[10] and Smakula,[11] while the first theoretical explanation of the properties of the phosphors was given by Seitz.[12]

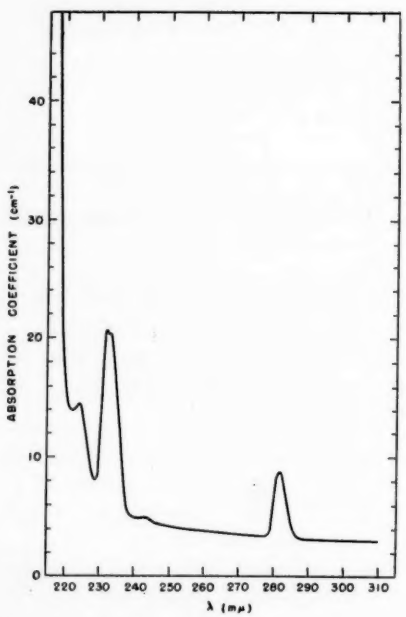

FIG. 1a. Absorption spectrum taken at liquid nitrogen temperature of a potassium iodide crystal containing 1.2×10^{-4} mole percent of thallium.

Recently, Williams[13,14] has made calculations concerning the position of one of the absorption bands in the KCl—Tl phosphor.

Seitz[12] postulated that the absorption bands observed in single crystals of these phosphors are due to the excitation of thallous ions which occupy lattice sites normally occupied by alkali metal ions. The structure of the observed bands was interpreted in terms of the details of the spectrum of the thallous ion and the probable effect of the crystalline field.

The present paper is concerned with the optical properties of potassium iodide containing various concentrations of thallous ion. This work was originally undertaken in an effort to discover whether the presence of a thallous ion in a potassium iodide crystal perturbs the transition in the neighboring iodide ions in a manner similar to the perturbation caused by the presence of an *F* center or a negative ion vacancy.[15] Such a perturbed transition is believed to have been found, but also, in the course of this investigation, a number of new absorption bands were observed, and their origin is discussed in terms of an extension of the model used by Seitz.

II. EXPERIMENTAL PROCEDURE

Single crystals of potassium iodide, containing various concentrations of thallous ion, were obtained from the Harshaw Chemical Company or were grown in this laboratory by the Kyropoulos method. The crystals obtained from the Harshaw Chemical Company contained a high concentration of thallium but covered a fairly limited concentration range, while the crystals grown in this laboratory covered the range of very high to very low concentrations. Crystals obtained from these two different sources agreed quite well in their absorption spectra. The potassium iodide used in the Kyropoulos method was Baker and Adamson reagent grade without further purification, while the thallous iodide was obtained from Eimer and Amend cp thallous chloride by an iodide precipitation. The thallous iodide obtained in this manner proved to be of quite high purity according to chemical tests.

[1] R. Hilsch and R. W. Pohl, Z. Physik **48**, 384 (1928); **57**, 145 (1929); **59**, 812 (1930).
[2] W. Koch and R. W. Pohl, Nachr. Ges. Wiss. Gott. (1929).
[3] W. Buenger, Z. Physik **66**, 311 (1930).
[4] W. Buenger and W. Flechsig, Z. Physik **67**, 42 (1931); **69**, 637 (1932).
[5] M. Forro, Z. Physik **56**, 235 (1929); **56**, 534 (1929); **58**, 613 (1930).
[6] R. Hilsch, Z. Physik **44**, 860 (1927).
[7] W. Koch, Z. Physik **57**, 638 (1929); **59**, 378 (1930).
[8] H. Lorentz, Z. Physik **46**, 558 (1927).
[9] A. M. MacMahon, Z. Physik **52**, 336 (1928).
[10] W. v. Meyeren, Z. Physik **61**, 321 (1930).
[11] A. Smakula, Z. Physik **45**, 1 (1927).
[12] F. Seitz, J. Chem. Phys. **6**, 163 (1938).
[13] F. E. Williams, J. Chem. Phys. **19**, 457 (1951).
[14] P. D. Johnson and F. E. Williams, J. Chem. Phys. **20**, 124 (1952).
[15] Delbecq, Pringsheim, and Yuster, J. Chem. Phys. **19**, 574 (1951).

The absorption spectra of these crystals cooled with liquid nitrogen or liquid helium were measured using a Beckman Model DU Spectrophotometer or a Cary Recording Spectrophotometer. The Dewar flask used for the measurements with liquid helium is in principle the same as that described previously[16] for use with liquid nitrogen except that it has an outer jacket which holds liquid nitrogen to shield the liquid helium.

A Central Research Laboratory double monochromator in conjunction with an AH-4 or AH-6 mercury lamp was used to obtain spectrally pure light for luminescence excitation measurements. The beam of light which emerges from the exit slit of the monochromator falls on the front side of the crystal to be investigated. The intensity of luminescence excited by this beam is measured from the back side of the crystal after the luminescence has passed through a filter which transmits the luminescence and absorbs the exciting light.

In order to study the variation of the absorption coefficient at the peak of an absorption band with concentration of thallium, a method for determining the amount of thallium in a crystal was developed. This method[17] involves the exposure of the crystal to neutron irradiation and, after appropriate chemical separations, the determination of the amount of Tl^{204} in the crystal. The results obtained are accurate to within ± 5 percent in the range down to 10^{-6} gram of thallium.

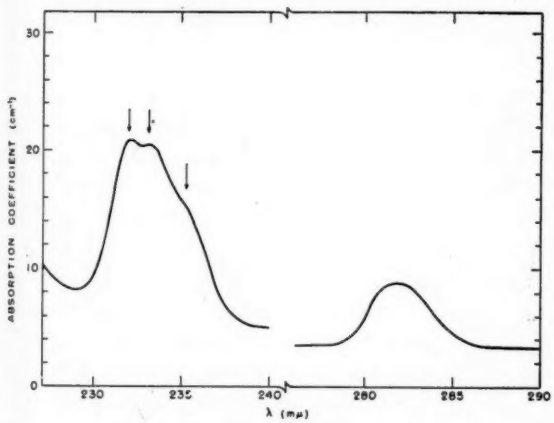

FIG. 1b. An expansion of the absorption spectrum in Fig. 1a showing the bands at 233 mμ and 282 mμ.

III. RESULTS

Figure 1a shows an absorption spectrum at liquid nitrogen temperature of a potassium iodide crystal containing a low concentration of thallium. The band at 224 mμ is superimposed on the rapidly rising long wavelength tail of the first fundamental absorption band of potassium iodide, while the bands at 233 mμ and 282 mμ are in a region in which there is relatively little absorption in the potassium iodide. Figure 1b is an expansion of Fig. 1a in the regions around 233 and 282 mμ. It shows clearly that the absorption around 233 mμ is not one single band but very likely consists of three bands, while the band at 282 mμ appears to be single. On a similarly expanded scale the band at 224 mμ also appears to be single in nature. Figure 2a shows an absorption spectrum of the same crystal when cooled with liquid helium. The peaks are observed to be considerably higher, narrower, and better resolved. Figure 2b, an expansion of Fig. 2a in the regions around 233 and 282 mμ, again shows that the band at 233 is triple in nature and that the band at 282 is single. On a similarly expanded scale the band at 224 mμ also appears to be single.

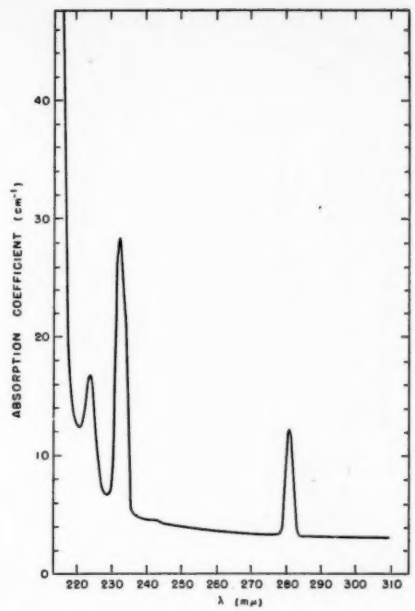

FIG. 2a. Absorption spectrum of the same crystal used in Fig. 1 but taken at liquid helium temperature.

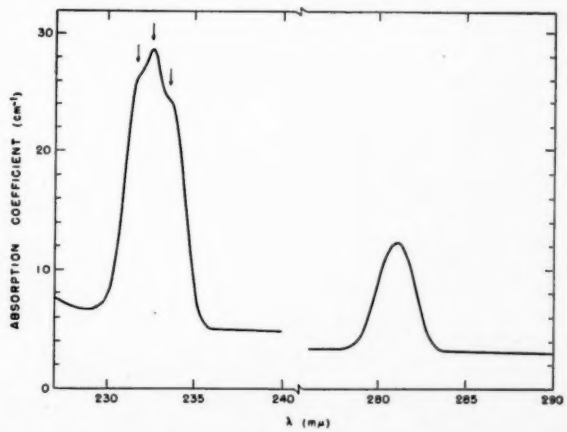

FIG. 2b. An expansion of the absorption spectrum in Fig. 2a showing the bands at 233 mμ and 282 mμ.

[16] Casler, Pringsheim, and Yuster, J. Chem. Phys. **18**, 887 (1950).

[17] Delbecq, Glendenin, and Yuster, Anal. Chem. (to be published).

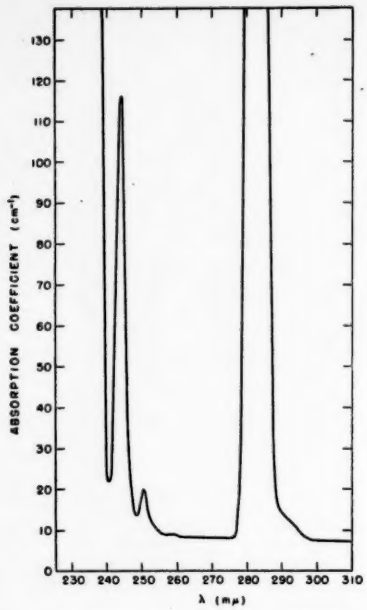

FIG. 3. Absorption spectrum taken at liquid nitrogen temperature of a potassium iodide crystal containing 3.7×10^{-2} mole percent of thallium.

Figure 3 shows an absorption spectrum, taken with liquid nitrogen as coolant, of a crystal of potassium iodide containing a higher concentration of thallium. At this higher concentration, the peak heights of the bands at 224 mμ, 233 mμ, and 282 mμ cannot be measured with our instruments, but new bands have appeared with peaks at 244 mμ and 250 mμ. Also it is obvious that a new band near 290 mμ is developing on the long wavelength tail of the 282 mμ absorption band. When this same crystal is cooled with liquid helium and

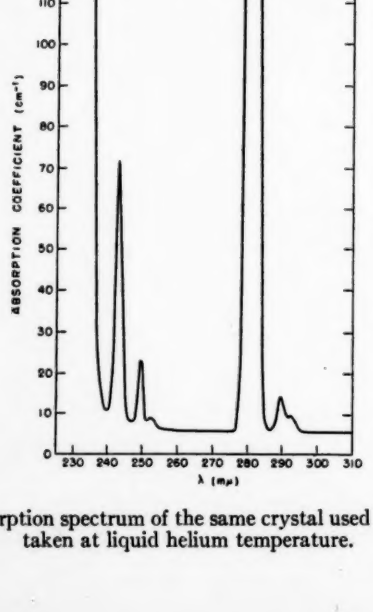

FIG. 4. Absorption spectrum of the same crystal used in Fig. 3 but taken at liquid helium temperature.

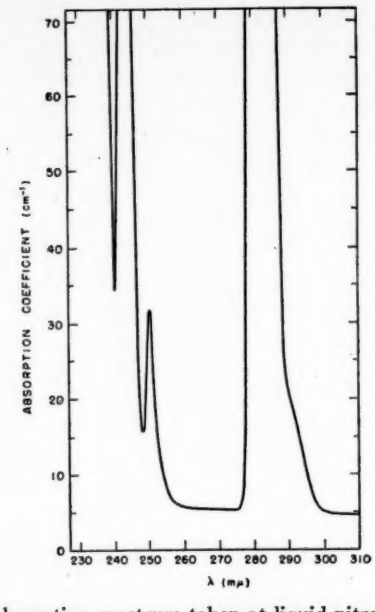

FIG. 5. Absorption spectrum taken at liquid nitrogen temperature of a potassium iodide crystal containing 7×10^{-2} mole percent of thallium.

an absorption spectrum is taken (Fig. 4), it is observed that the peak at 244 mμ drops by 40 percent; the band with peak at 250 mμ is seen to be composed of two bands with peaks at 250 mμ and 252 mμ; and the unresolved absorption near 290 mμ is now resolved into two bands with peaks at 290 mμ and 293 mμ.

Figures 5 and 6 show the absorption spectra, with liquid nitrogen and liquid helium as coolant, respectively, of a potassium iodide crystal containing a still higher concentration of thallium. The peaks of the bands at 224, 233, 244, and 282 mμ were too high to be

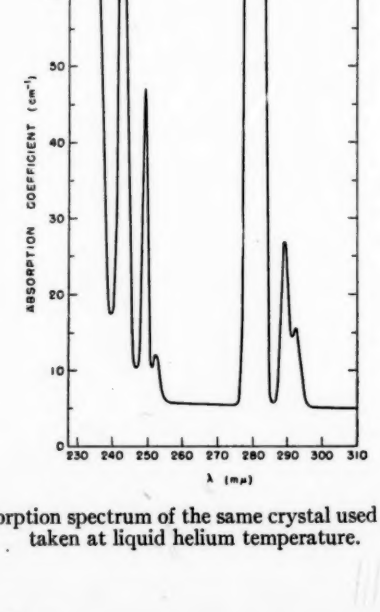

FIG. 6. Absorption spectrum of the same crystal used in Fig. 5 but taken at liquid helium temperature.

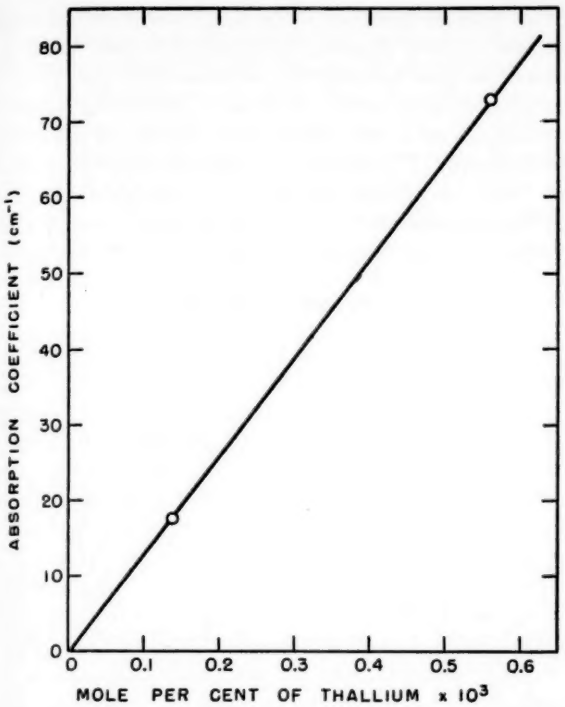

FIG. 7. Variation of maximum absorption coefficient, at liquid nitrogen temperature, as a function of thallium concentration for the composite band at 233 mμ.

measured with our instruments. It is seen that no new absorption bands appear as the concentration of thallium is increased.

It has been found that the areas under the absorption bands at 282 mμ, 233 mμ, and also the composite bands at 250–252 mμ remain quite constant in cooling from liquid nitrogen to liquid helium temperature. The band at 224 mμ and the composite band at 290–293 mμ are not completely resolved at liquid nitrogen temperature so that their change in area could not be checked. However, it seems quite clear from the absorption spectra that if any change in area has occurred in the case of the band at 224 mμ, it is very slight. The area

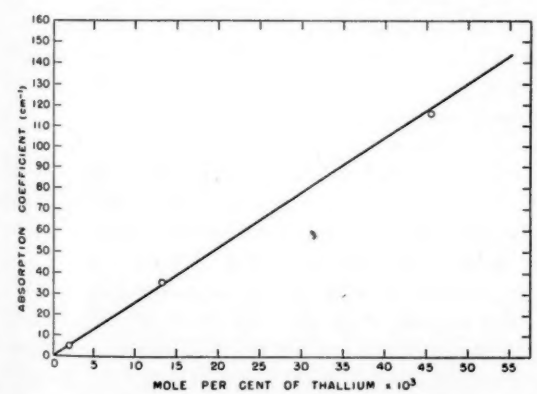

FIG. 8. Variation of maximum absorption coefficient, at liquid nitrogen temperature, as a function of thallium concentration for the band at 244 mμ.

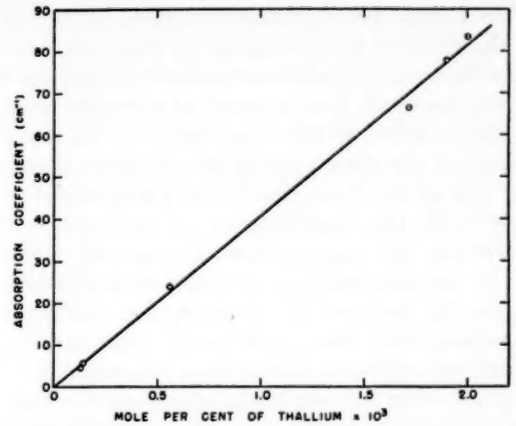

FIG. 9. Variation of maximum absorption coefficient, at liquid nitrogen temperature, as a function of thallium concentration for the band at 282 mμ.

under the absorption band at 244 mμ is found to decrease by 61 percent in going from liquid nitrogen to liquid helium temperature.

Figures 7 through 10 show the variation of maximum absorption coefficient, at liquid nitrogen temperature, as a function of thallium concentration for the bands at 233 mμ (composite), 244 mμ, 282 mμ, and 250 mμ (composite), respectively. Within the concentration range studied the maximum absorption coefficients of the bands at 233 mμ, 244 mμ, and 282 mμ obviously vary linearly with concentration of thallium. On the other hand, it is seen that the maximum absorption coefficient of the composite band at 250 mμ does not vary in the above fashion but appears to vary as the square of the thallium concentration. The peaks at 290 mμ and 293 mμ are proportional in height to the peaks at 250 mμ and 252 mμ and therefore also vary with the second power of the concentration. The band at 224 mμ, as mentioned before, is superimposed on the steeply rising tail of the fundamental band of potassium iodide, and consequently, it is more difficult to obtain accurate data concerning its peak height; however, it appears to grow linearly with the concentration of thallium.

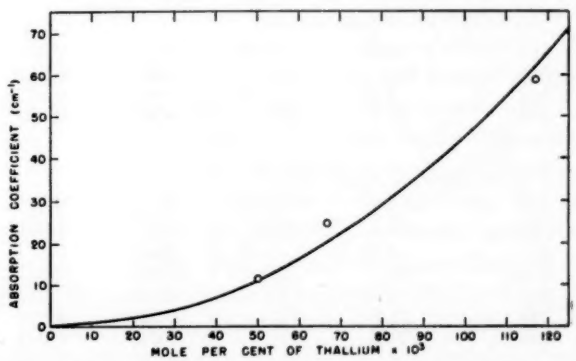

FIG. 10. Variation of maximum absorption coefficient, at liquid nitrogen temperature, as a function of thallium concentration for the composite band at 250 mμ.

Table I lists the oscillator strengths, as calculated from the classical formula given by Smakula,[18] of the various absorption transitions assumed to take place in a thallous ion which is substituted for a potassium ion in a potassium iodide lattice. Also listed are the essential data used in the calculation of the oscillator strengths. In the case of the absorption bands whose heights vary linearly with the concentration of thallium, it was assumed that the concentration of absorbing centers is equal to the concentration of thallium in the crystal. However, in the case of the absorption bands whose heights vary with the square of the concentration of thallium, an additional assumption was made in order to determine the number of absorbing centers; namely, that all positive ion lattice sites are equally probable to a thallous ion. With this assumption the number of thallous ion pairs (nearest neighbors) was calculated. The values for the oscillator strengths listed in Table I are probably good to ± 15 percent.

It has been shown that the fluorescence spectrum of potassium iodide-thallium phosphors consists of a single band with maximum in the violet.[10,19] In the present investigation a fluorescence spectrum was taken, at room temperature, of the most concentrated sample and confirmed the previous results. The exciting light used was that from an AH-4 mercury lamp filtered with Corning No. 9863 filters. The character of the fluorescence excited, at liquid nitrogen temperature, by light absorbed in each of the absorption bands at 224, 233, 244, 250 (composite), 282, and 290 (composite) mμ was examined with the use of filters and was shown to be the same in all cases. Also, the yield of fluorescence was high and about the same for absorption in any of the bands. At room temperature no phosphorescence was excited which was visible to the eye by absorption in any of the above bands. However, the fact that phosphorescence was actually excited, but was either too short in lifetime or too weak in intensity to be seen, was shown through the use of glow curves. Such glow curves, taken by others[20] in this laboratory, indicate that the yield of phosphorescence *versus* wavelength of exciting light has a maximum at about 233 mμ and falls off on either side fairly sharply. This result is similar to that obtained on the yield of phosphorescence in potassium chloride-thallium phosphors.[3] No phosphorescence was excited by absorption of light in the 250, 282, or 290 mμ bands.

TABLE I. Oscillator strengths of the various absorption transitions.

Band (mμ)	k (cm^{-1}) at absorp. max.	N = Number of thallium atoms/cm^3 $\times 10^{-16}$	Half-width (ev)	f = Oscillator strength
At temperature of liquid nitrogen				
233	14.9	1.59	0.118	0.80
244	116	543	0.065	0.011
282	5.30	1.59	0.061	0.17
250 (composite)	25.1	775	0.053	0.080
At temperature of liquid helium				
233	23.3	1.59	0.078	0.82
244	68.5	543	0.042	0.0042
282	8.70	1.59	0.038	0.17
250	39.9	775	0.030	0.072
252	6.04	775	0.046	0.017
290	21.8	775	0.040	0.056
293	10.6	775	0.046	0.032

IV. DISCUSSION

The fact that maximum absorption coefficients of the absorption bands at 233, 244, and 282 mμ vary linearly with thallium concentration (Figs. 7, 8, and 9) indicates that the absorptions are due to the presence of single isolated thallous ions in the crystal. As was mentioned above, Seitz has suggested that these absorptions are due to transitions in the thallous ions which have taken the position of normal positive ions in the lattice. It is assumed that the thallous ions, at low concentration, are surrounded by the cubic symmetry of the potassium iodide crystal. Consequently the transitions in question are those allowed between the levels into which the states of a free thallous ion are split by a crystalline field of cubic symmetry. This splitting is described qualitatively in Fig. 11. Under perfect cubic symmetry, the only electric dipole radiation transitions permitted from the ground level A_1 are to the T_1 levels. Since the levels retain some of their spin characteristics, the transition to the $^1T_1$ level should be more probable than the transition to the $^3T_1$ level. Thus there would arise only two absorption bands under the above conditions. However, the results indicate that in crystals of potassium iodide with fairly low concentrations of thallium, there are at least three absorption bands whose peaks vary linearly with concentration of thallium (233, 244, and 282 mμ). Since the band at 233 mμ has the highest oscillator strength (0.80), it is associated with the transition $^1A_1 \rightarrow {}^1T_1$, while the band at 282 mμ, of lower energy and lower oscillator strength (0.17), is associated with the transition $^1A_1 \rightarrow {}^3T_1$. This assignment is equivalent to the one given by Seitz[12] and later confirmed quantitatively by Williams[13] in the case of KCl—Tl. Seitz[12] has proposed that the transition corresponding to the band at 244 mμ is allowed because the symmetry surrounding the thallous ion is disturbed by lattice vibrations and is no longer cubic. This band is probably associated with a transition from the $^1A_1$ state to the $^3T_2$ state. The fact that the absorption at 244 mμ is dependent upon lattice vibrations and thus on temperature is seen by comparing Fig. 3 with Fig. 4. These figures, which are absorption measurements made on the same crystal, show that the 244 mμ band decreases in area by 61 percent when the measurement temperature is changed from that of liquid nitrogen to that of liquid helium. Measurements on the curves in Figs. 1

[18] A. Smakula, Z. Physik **59**, 603 (1930).
[19] A. Chatterjee, Indian J. Phys. **24**, 331 (1950).
[20] B. Smaller and E. Avery (to be published).

and 2 show that the areas under the bands at 282 and 233 mμ remain essentially constant as is to be expected when the measurement temperature is changed from that of liquid nitrogen to that of liquid helium.

As can be seen from Figs. 1b and 2b, the band at 233 mμ is triple, while if the symmetry were perfectly cubic it should be single. Under cubic symmetry the level $^1T_1$ is triply degenerate, and perhaps lattice vibrations can change the symmetry enough to remove the degeneracy and allow transitions to all three components. Figures 1b and 2b seem to indicate that the above may be true, since the absorption around 233 mμ looks more nearly like a single band at liquid helium temperature than it does at liquid nitrogen temperature. However, it is not as yet understood why the absorption at 282 mμ, which, similar to the absorption at 233 mμ, is a transition to a T_1 level, remains single under the above conditions.

As already stated, although it is difficult to estimate the exact height of the absorption band at 224 mμ because it is on top of the rising fundamental band of potassium iodide, it seems fairly certain that the maximum absorption coefficient of this band also varies linearly with concentration of thallium. From Figs. 1 and 2, it is seen that the 224 mμ band is fairly sharp, and that it narrows in half-width and rises in height as the temperature is lowered. These facts indicate that the transition is to a discrete upper level. Two possible explanations for the origin of this absorption band are (1) a transition to some higher excited state in the thallous ion, or (2) a perturbed transition due to the presence of the thallous ion. If the absorption were due to a transition in the thallous ion to some higher level than the one responsible for the 233 mμ band, it should lie farther toward shorter wavelength and would be obscured by the fundamental absorption of the potassium iodide.[12] For this reason it is believed that this absorption corresponds to a perturbed transition of the valence electrons of the iodide ions adjacent to a thallous ion, similar to the α- and β-bands described previously.[15]

An interesting fact in view of the above hypothesis for the origin of the 224 mμ absorption band is that fluorescence characteristic of thallium in high yield is excited by absorption in the band. This would indicate that when an iodide ion which has a thallous ion as a nearest neighbor absorbs energy it can transfer that energy quite efficiently to the neighboring thallous ion and cause fluorescence.

The bands at 250, 252, 290, and 293 mμ, which appear at fairly high thallium concentrations, seem to vary with the square of the thallium concentration, and it is assumed that these bands arise when two thallous ions are nearest neighbors. Recently,[21] a similar effect has been observed in crystals of sodium chloride containing traces of silver chloride in which the maximum absorption coefficient of an absorption band was also found to vary with the square of the concentration of silver. When a thallous ion is isolated in the potassium iodide lattice, it is surrounded by cubic symmetry. The symmetry surrounding a thallous ion having another thallous ion as a nearest neighbor is no longer cubic but is reduced to C_{2v} symmetry. C_{2v} symmetry removes all degeneracy and splits the levels of the thallous ion as shown in Fig. 11. The size of the splitting and the position and order of the levels as shown are purely arbitrary. Electric dipole radiation transitions are allowed between the ground level and all the levels but A_2.

The number of allowed transitions is sufficient to account for the observed absorptions. Symmetry considerations permit nine absorption bands which may vary with the square of the concentration. The three

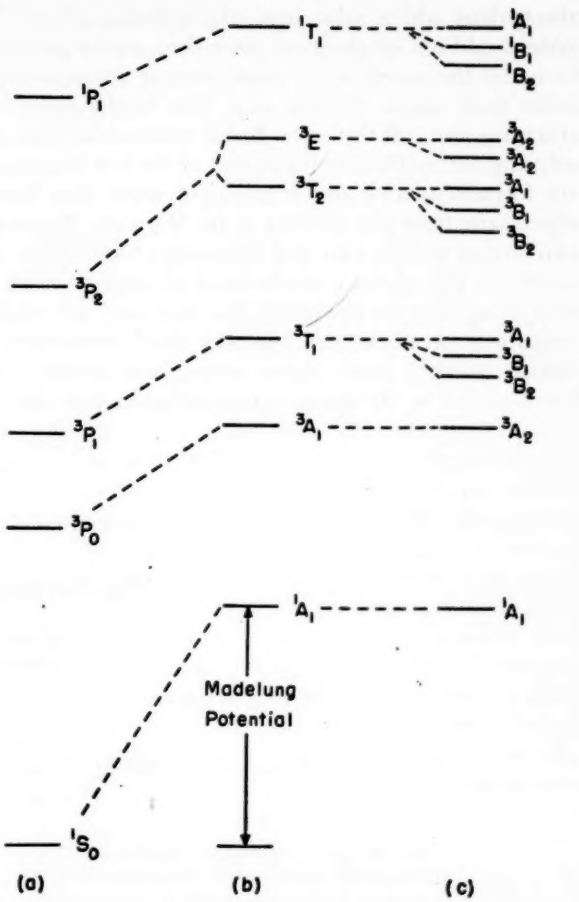

FIG. 11. Schematic diagram showing the effect of the symmetry of the surrounding field on the energy levels of the thallous ion. (a) The free thallous ion. (b) Cubic symmetry—a single thallous ion occupying a positive ion site in a sodium chloride type lattice (see reference 12). (c) C_{2v} symmetry—two thallous ions occupying adjacent positive ion lattice sites in a sodium chloride type lattice. The level notation follows that used by Eyring, Walter, and Kimball, in their book *Quantum Chemistry* (John Wiley and Sons Inc., New York, 1944). The anterior superscript denotes the multiplicity.

[21] Etzel, Schulman, Ginther, and Claffy, Phys. Rev. **85**, 1063 (1952).

absorptions which arise from the splitting of the $^1P_1$ state would not be observed since they would probably be under the much larger absorption at 233 mμ which arises from single thallous ions. One might expect to observe a group of three new bands which arise from the splitting of the $^3P_2$ state (since two of the five transitions are forbidden) and also a group of three new bands which arise from the splitting of the $^3P_1$ state. However, two groups of only two new absorption bands each are observed. The absence of the third absorption band in each group may be due to the fact that they are weaker transitions or it may be that the third component is hidden under a much higher absorption, namely, the bands at 244 or 282 mμ. It is interesting to note that no transition is possible between the A_1 and A_2 levels which would correspond to a transition in the free ion $^1S_0 \rightarrow {}^3P_0$.

The pattern of absorption bands which has been discussed should not be peculiar to potassium iodide-thallium phosphors but should be observable in other alkali halide-thallium phosphors. Preliminary investigations on sodium iodide- and potassium chloride-thallium phosphors indicate that the pattern of absorptions discussed above can also be found in these two phosphors.

V. ACKNOWLEDGMENT

The authors wish to thank Dr. M. Goldsmith, Dr. M. Hamermesh, Dr. C. A. Hutchison, and Dr. P. Pringsheim for helpful discussions in connection with this work.

THE JOURNAL OF CHEMICAL PHYSICS VOLUME 21, NUMBER 5 MAY, 1953

The Structure of Phosphine

MARSHALL H. SIRVETZ
Department of Physics

AND

RALPH E. WESTON, JR.
Department of Chemistry, Brookhaven National Laboratory, Upton, New York*

(Received November 24, 1952)

Several low J microwave transitions of PH_2D and PHD_2 have been observed in the K band. The effect of centrifugal distortion on the rotational levels has been taken into account approximately, with the result that errors in the computed structure due to this cause now appear to be negligible in comparison with those due to vibration-rotation interaction. One obtains for the P—H distance 1.4177 and 1.4116A in the two cases; for the H—P—H angle, 93°21.6′ and 93°15.4′. The dipole moment has been measured for both species with agreement within experimental error.

1. INTRODUCTION

BECAUSE even the lowest rotational transitions of the pyramidal molecule phosphine occur at frequencies unattainably high to most workers in microwave spectroscopy, no complete microwave determination of its structure has been reported. If, however, one makes the usual assumption of constancy of structural parameters with respect to isotopic substitution, it is possible to circumvent this difficulty by working with the monodeuterated or dideuterated molecules. These asymmetric top molecules each have several low J lines in the microwave K band. The present report, dealing with the K band spectra of PH_2D and PHD_2, thus yields two independent structural determinations together with some indication of the validity of the above assumption.

In 1940 Stevenson[1] made an estimate of the structure of PH_3 on the basis of covalent radii and the value of I_b given by infrared studies.[2] Recently Loomis and Strandberg[3] have observed a single microwave transition ($3_{0,3} \rightarrow 3_{1,3}$) in PH_2D; combining this datum with I_b for PH_3 they obtained values for the bond length, $r = 1.419$A, and the interbond angle, $\alpha = 93.5°$, in good agreement with Stevenson's predictions. Nielsen[4] has essentially confirmed these results ($r = 1.424$A, $\alpha = 93°50'$) on the basis of an analysis of the infrared vibration-rotation spectrum of PH_3 which determined both I_b and I_c.

The general program adopted in the present work is the following. We want to get r and α from the rotational frequencies of each of the two species, PH_2D and PHD_2. We also want to make some estimate of the limits of error which can be put on these quantities; as will be seen, these limits can be narrowed considerably if special precautions are taken. This program is readily carried through in each case if two observed frequencies are assigned to definite transitions and if the assumption is made that the molecule is effectively a rigid structure. The observed spectra led to three assign-

* Under contract with U. S. Atomic Energy Commission.
[1] D. P. Stevenson, J. Chem. Phys. 8, 285 (1940).
[2] N. Wright and H. M. Randall, Phys. Rev. 44, 391 (1933).
[3] C. C. Loomis and M. W. P. Standberg, Phys. Rev. 81, 798 (1951).
[4] H. H. Nielsen, J. Chem. Phys. 20, 759 (1952).

ments for each species with J values ranging between $J=1$ and $J=5$. The rigid rotor approximation could thus be tested and was found to give rather poor results when two lines were used to fix the rotational parameters, and these in turn were used to compute the third.

This was not, of course, unexpected. Recent work by Strandberg and co-workers[5] on deuterated ammonias and other rotationally light molecules shows that even the low J transitions of such molecules may include centrifugal distortion shifts of the order of 100 mc. They also propose methods of taking into account these effects, provided that enough frequencies are available to determine the large number of empirical constants involved. The condition is not met in the limited frequency range in which we worked. Consequently we were led to make a theoretical calculation of the centrifugal distortion constants. This type of computation is somewhat tedious to carry out and, moreover, cannot be considered completely reliable because of the many approximations that must be made. On the other hand, had this not been done, we would have been left with the necessity of stating that the observed frequencies contain effective uncertainties of the order of 100 mc as far as the structural interpretation is concerned. At the conclusion of the calculation, we found that having used the first two frequencies of each species to fix the rotational parameters as empirical constants, we could compute the third with considerably improved accuracy. The indication is that the frequencies used in the structural computation are in effective error by amounts less than, or of the order of, 5 mc. Although the r and α obtained after this centrifugal distortion computation are only very slightly different from those obtained using the rigid rotor approximation, we feel that they can now be stated with increased confidence and with a more reliable estimate of the errors involved.

2. EXPERIMENTAL DETAILS

The Stark effect microwave spectrograph has been described previously.[6] It ordinarily is operated between 18 000 and 30 000 mc. At usual gas pressures, lines are rather less than 1 mc wide, but frequency measurements, made with the aid of a frequency standard, are always reproducible to better than 0.05 mc. For the dipole moment determination, the voltmeter of the 100 kc square wave generator was calibrated by means of Stark effect measurements on OCS, its dipole moment taken equal to 0.7085 debye as given by Shulman and Townes.[7]

The PH_2D and PHD_2 used in this work were prepared by the equilibration of ordinary phosphine with deuterium oxide-hydrogen oxide mixtures, using sulfuric acid as catalyst.[8] Phosphine was prepared by the alkaline hydrolysis of resublimed phosphonium iodide, which was made by a standard procedure.[9] This preparation leads to phosphine of a high degree of purity, which does not contain other phosphorus hydrides.[10] The relative pressures of the isotopic species PH_3, PH_2D, PHD_2, and PD_3, present in the two gas samples were calculated to be as follows: (a) "PH_2D" sample, 1:0.19:0.001:0.0002; (b) "PHD_2" sample, 1:1.7:0.95:0.18. During the period of several days during which measurements were made no change in the isotopic constitution, from reaction with possible contaminants on the wave guide, was noticed.

TABLE I. Observed frequencies and assignments.

Isotopic species	ν (mc)	Transition
PH_2D	18070.96	$2_{1,2}\rightarrow 2_{1,1}$
	28158.53	$3_{0,3}\rightarrow 3_{1,3}$
	20815.38	$4_{0,4}\rightarrow 4_{1,4}$
	20754.57	
	22821.90	
PHD_2	29073.21	$1_{0,1}\rightarrow 1_{1,0}$
	19415.19	$3_{1,2}\rightarrow 3_{2,2}$
	24079.48	$5_{2,3}\rightarrow 5_{3,3}$
	28759.35[a]	
	29833.95[a]	
	30531.33[a]	

[a] Assignment to isotopic species not certain.

3. ROTATIONAL SPECTRA

Because quite reliable structural data were at hand at the beginning of the investigation, the transitions to be expected could be computed with some accuracy on the basis of well-known rigid rotor theory.[11] In the frequency range of interest only $\Delta J=0$ transitions need be considered. In addition, the molecular symmetry permits only a and c type transitions for PH_2D, and b and c transitions for PHD_2. The orientation with respect to the dipole moment of the two principal axes in the plane of symmetry shows that for PHD_2 the two types of transitions are of roughly equal intensity, while for PH_2D the a transitions are about one-fifth as strong as the c transitions. Energy level computations were made initially by interpolation in the King, Hainer, and Cross tables, and later by the convenient and precise method of continued fractions.

The transitions which have been assigned and which are used in the structural determination are given in Table I. A few other lines, with unresolved Stark effect, were observed. They are presumably of higher J and nothing more was done with them. The correctness of the assignments is attested to in various ways. First,

[5] M. T. Weiss and M. W. P. Strandberg, Phys. Rev. **83**, 567 (1951); R. B. Lawrance and M. W. P. Strandberg, Phys. Rev. **83**, 363 (1951).
[6] Wentink, Koski, and Cohen, Phys. Rev. **81**, 948 (1951).
[7] R. G. Shulman and C. H. Townes, Phys. Rev. **77**, 500 (1950).
[8] R. E. Weston, Jr., and J. Bigeleisen, J. Chem. Phys. **20**, 1400 (1952).
[9] *Inorganic Syntheses*, W. C. Fernelius, editor (McGraw-Hill Book Company, Inc., New York, 1946), Vol. 2, p. 141.
[10] C. C. Stephenson and W. F. Giauque, J. Chem. Phys. **5**, 149 (1937).
[11] King, Hainer, and Cross, J. Chem. Phys. **11**. 27 (1943).

TABLE II. Computed[a] vibrational frequencies (cm^{-1}).

Isotopic species	Symmetry species	
	a'	a''
PH_2D	2325	2329
	1672	969
	1096	
	888	
PHD_2	2327	1675
	1669	978
	909	
	761	

[a] The force constants used were (in 10^5 dynes/cm): $k_1=3.1128$, $k_\delta/l^2=0.3341$, $k_\delta'/l^2=-0.0214$.

one can take two lines of a given species, solve for $(A-C)/2$ and κ, and with these compute the third correctly (except for a discrepancy assumed due to the centrifugal stretching effect). Also the r and α obtained for the two species are the same to within several 0.001A and a few minutes of angle, respectively, as was expected to be the case. Second, the intensity of all PHD_2 transitions (b and c transitions) was roughly the same whereas in PH_2D the $J=2$ transition (a transition) was weaker than the other two (c transitions) in about the expected ratio. It might be mentioned here that in the sample labeled "PH_2D" only the PH_2D lines were observed. In "PHD_2," on the other hand, all six lines were seen and, indeed, the PH_2D lines with greater intensity. This is consistent with the estimated compositions of the two samples. Third, the Stark effect can be used where there are three or more resolved components to give the J value immediately.[12] For $J<3$, this sort of check is not possible, but here an accurate theoretical calculation of the Stark effect displacements is easily made on the basis of the tentative rotational assignment, and it was found that the two such lines, $J=2$ for PH_2D and $J=1$ for PHD_2, gave the same value of the dipole moment.

The inadequacy of the rigid rotor approximation for accurate computation can be demonstrated by means of an example. The first lines measured were $J=3$ and $J=4$ of PH_2D, the measured frequencies leading to the result: $(A-C)/2=23321.03$ mc and $\kappa=-0.740114$. On this basis one predicts a $J=2$ transition at 18182.43 mc, a prediction which turns out to be in error by 111.47 mc.

4. CENTRIFUGAL DISTORTION

In the formulation of centrifugal distortion theory given by Wilson[13] the usual rigid rotor Hamiltonian, $\sum_\alpha A_\alpha P_\alpha^2$, is supplemented by a centrifugal distortion term, $\frac{1}{4}\sum_{\alpha\beta\gamma\delta}\tau_{\alpha\beta\gamma\delta}P_\alpha P_\beta P_\gamma P_\delta$. Here P_α is the component of rotational angular momentum along the molecular principal axis α, and the τ's are constants discussed below. In general, the later treatments[14] based on this theory concentrate on obtaining approximate expressions for the eigenvalues as functions of the τ-coefficients, these being evaluated from the experimental data as empirical constants. This problem does not concern us here, since the order of the matrices considered is not greater than three, and exact diagonalization is therefore not difficult. On the other hand, because we are limited to a small number of transitions, the τ's, thirteen in number for each species, cannot be obtained from the data and must be computed from vibrational and structural information.

The constants $\tau_{\alpha\beta\gamma\delta}$ are defined by[13]

$$\tau_{\alpha\beta\gamma\delta}=-\tfrac{1}{2}\sum_k[(\partial\mu_{\alpha\beta}/\partial Q_k)(\partial\mu_{\gamma\delta}/\partial Q_k)]/4\pi^2\nu_k^2,$$

where ν_k is the kth fundamental vibration frequency and Q_k is the associated normal coordinate; $\mu_{\alpha\beta}$ is an element of the matrix inverse to the inertial matrix I. Evaluation of these constants requires (1) knowledge of the molecular structure, which we, of course, have from the rigid rotor analysis to sufficient accuracy; (2) knowledge of the vibrational frequencies and modes of vibration. For the latter aspect of the problem a modified valence force field (including cross terms in the angular displacements) was assumed. Some confidence in this approximation is obtained from the fact that the set of 3 force constants derived from the PH_3 vibrational spectrum could be used to compute frequencies for all four isotopic species in 1 percent agreement with experiment.[15] The frequencies used in this work are given in Table II.

Calculation of the $\partial\mu_{\alpha\beta}/\partial Q_k$ is rather straightforward but lengthy. The first stage consists of evaluating $\partial\mu_{\alpha\beta}/\partial S_i$, where the S_i are suitably chosen symmetry

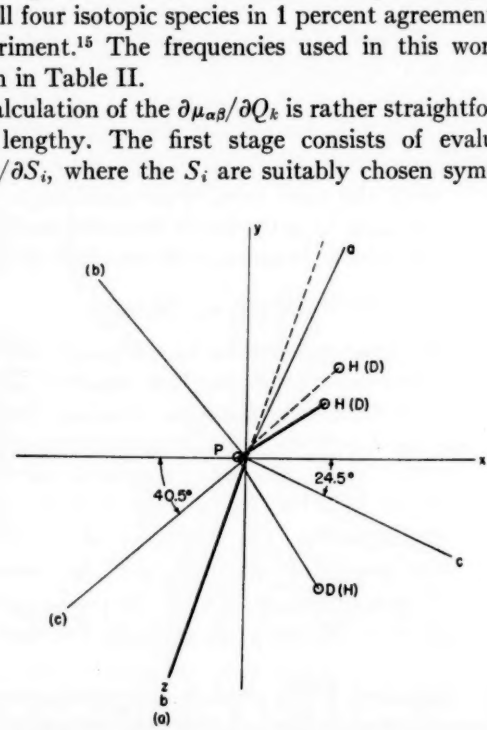

FIG. 1. The axis system xyz is chosen so that x coincides with the "symmetry axis" while z is perpendicular to the plane of symmetry. The axes a, b, c are principal axes of inertia. Symbols in in parentheses refer to PHD_2, others to PH_2D.

[12] S. Golden and E. B. Wilson, Jr., J. Chem. Phys. **16**, 669 (1948).

[13] E. B. Wilson, Jr., J. Chem. Phys. **5**, 617 (1937).

[14] Daniel Kivelson and E. B. Wilson, Jr., **20**, 1575 (1952); also see reference 5.

[15] R. E. Weston, Jr., and M. H. Sirvetz, J. Chem. Phys. **20**, 1820 (1952).

coordinates. Those depicted in Herzberg[16] for pyramidal XY_3 are convenient for the purpose when modified in a simple way. The equations connecting the S_i with the Cartesian displacement coordinates enable us to write the position of any atom, initially at x_n^0, as $x_n^0+\sum a_{ni}S_i$. The elements of I are then $I_{\alpha\beta}^0$ and $I_{\alpha\beta}$ in the equilibrium and displaced configurations, respectively, with these quantities related by an equation of the form

$$I_{\alpha\beta}=I_{\alpha\beta}^0+\sum\rho_{\alpha\beta;i}S_i+\sum\sigma_{\alpha\beta;ij}S_iS_j.$$

We can now identify $\rho_{\alpha\beta;i}$ with $\partial I_{\alpha\beta}/\partial S_i$. Since the $\mu_{\alpha\beta}$ are easily expressed in terms of the elements of I, the $\partial\mu_{\alpha\beta}/\partial S_i$ are now evaluated from the $I_{\alpha\beta}$ and the $\partial I_{\alpha\beta}/\partial S_i$. One further point should be mentioned. In actually computing moments of inertia it is convenient to consider the molecule in a coordinate system (See Fig. 1) with z axis perpendicular to the plane of symmetry and one other axis, x axis, coinciding with the "symmetry axis." The equations are then identical for PH_2D and PHD_2, involving masses m_1 and m_2, which are interpreted as m_H and m_D, respectively, or the reverse. The matrix I is then, of course, not diagonal. The quantities computed in this coordinate system are not precisely the $\partial\mu_{\alpha\beta}/\partial S_i$, for the indices α, β run by definition through the labels of the *principal* axes, a, b, c. We actually have $\partial\mu_{x_j,x_k}/\partial S_i$, where x_j, x_k are x, y, z. This discrepancy is, of course, readily removed. One simply constructs an orthogonal transformation matrix A, such that $A^{-1}IA$ is diagonal. Then the transform of the matrix with x_j, x_k element $\partial\mu_{x_j,x_k}/\partial S_i$ has elements $\partial\mu_{\alpha\beta}/\partial S_i$ as needed.

To get the quantities $\partial\mu_{\alpha\beta}/\partial Q_k$ one now needs the vibrational eigenvectors γ_k. They are defined in the following way. If the kinetic and potential energy matrices are D and C in terms of the symmetry coordinates, then $D^{-1}C\gamma_k=(4\pi^2\nu_k^2)\gamma_k$, with the column matrix γ_k normalized according to $\tilde{\gamma}_kD\gamma_k=1$. It is now easily shown from the above definition that the γ_k are the columns of the transformation matrix from the Q's to the S's: $S_i=\sum Q_k(\gamma_k)_i$, so that we may write

$$\partial\mu_{\alpha\beta}/\partial Q_k=\sum(\partial\mu_{\alpha\beta}/\partial S_i)(\partial S_i/\partial Q_k),$$

with

$$\partial S_i/\partial Q_k=(\gamma_k)_i.$$

This gives us everything needed for the $\tau_{\alpha\beta\gamma\delta}$. We may note that in general a nonvanishing result is obtained only if both $\mu_{\alpha\beta}$ and $\mu_{\gamma\delta}$ change in first order with displacements of the same symmetry class. For example, for PHD_2 the μ_{aa} and μ_{bc} change only with symmetrical (infinitesimal) motions; but μ_{ab} and μ_{ac}, only with antisymmetrical ones. In this way one immediately sees that certain τ's vanish, and that of the 21 possible distinct ones only 13 remain. These are given in Table III.

One further point must be mentioned, this in connection with constructing the Hamiltonian matrices.

[16] G. Herzberg, *Infrared and Raman Spectra of Polyatomic Molecules* (D. Van Nostrand Company, Inc., New York, 1945), p. 155.

TABLE III. Centrifugal distortion constants $\tau'_{\alpha\beta\gamma\delta}$.[a]

$\alpha\beta\gamma\delta$	PH_2D	PHD_2
aaaa	-9.3104×10^{-5}	3.0351×10^{-4}
bbbb	−5.7623	2.1705
cccc	−5.2589	0.6050
aabb	−1.2113	−1.2524
aacc	−1.2169	0.2930
bbcc	−1.7001	0.5409
abab	−7.4415	0.4829
acac	−5.8452	0.5103
bcbc	−0.4429	0.4150
abbc	0.6206	
acbb	0.3821	
aaac	−2.6031	
accc	1.2971	
aabc		−0.2660
bbbc		0.0645
bccc		0.1631
abac		−0.1376

[a] The quantities $\tau'_{\alpha\beta\gamma\delta}$ are dimensionless. In this set of units P_α is measured in units of $\hbar$. For PH_2D $\tau'_{\alpha\beta\gamma\delta}=\tau_{\alpha\beta\gamma\delta}/[(A-C)/2]$; for PHD_2 $\tau'_{\alpha\beta\gamma\delta}=\tau_{\alpha\beta\gamma\delta}/[(C-B)/2]$.

It is well known that a very great simplification in the theory of rigid asymmetric rotors was provided by Wang's[17] introduction of the basis functions, $2^{-\frac{1}{2}}[\psi(K)\pm\psi(-K)]$, in place of the usual symmetric rotor functions $\psi(K)$. In terms of the Wang functions the rigid rotor matrix factors into four blocks of roughly equal dimensionality. For a general nonrigid rotor this factorization is not possible, as is immediately seen by considering a term of the form $\tau_{\alpha\beta\gamma\gamma}P_\alpha P_\beta P_\gamma^2$, which is not invariant to the characteristic symmetry operations of the rigid rotor. Consequently the matrices in general will be of order $2J+1$. In the case under consideration, however, a partial factorization is still permitted. This corresponds to the fact that the modified Hamiltonian still possesses invariance with respect to a rotation about one of the principal axes, that perpendicular to the plane of symmetry. It then follows that if one takes the representation in which the component of angular momentum perpendicular to the symmetry plane is diagonal (P_b for PH_2D, P_a for PHD_2), there are no matrix elements coupling odd and even K. This may be considered the first step in the Wang factorization, although in the rigid rotor case it is valid in any representation. For computational purposes it is now convenient to go all the way to the Wang functions. When the Wang blocks are now diagonalized there will remain off-diagonal elements connecting levels of different Wang symmetry, but only two blocks will be involved. These off-diagonal elements are purely centrifugal distortion terms, hence small and usually accurately handled by second order perturbation theory. For the levels used, it was found that the contribution of these elements was essentially negligible, at most of the order of a few 0.1 mc. The magnitude of this contribution rises

[17] S. C. Wang, Phys. Rev. **34**, 243 (1929).

TABLE IV. Comparison of observed and computed frequencies.

Isotopic species	Transition	ν_{obs}	ν_{RR}	ν_{CD}	$\delta\nu$
PH_2D	$2_{1,2}\rightarrow 2_{1,1}$	18070.96			−0.7
	$3_{0,3}\rightarrow 3_{1,3}$	28158.53			−41.4
	$4_{0,4}\rightarrow 4_{1,4}$	20815.38	20843.61	20811.13	−68.5
PHD_2	$1_{0,1}\rightarrow 1_{1,0}$	29073.21			1.0
	$3_{1,2}\rightarrow 3_{2,2}$	19415.19			52.9
	$5_{2,3}\rightarrow 5_{3,3}$	24079.48	23926.36	24095.88	265.2

rapidly with J, however, and would probably be noticeable for slightly higher J.

The above considerations, leading to preferred representations different for each case, have as a consequence that the rotational constants obtained directly from the experimental data are $(A-C)/2$ and κ (as usual) for PH_2D, but $(C-B)/2$ and $\kappa'=[A-(B+C)/2]/[(C-B)/2]$ for PHD_2.

5. RESULTS

The results of the computations are given in Table IV. The ν_{RR} are the frequencies computed using the rigid rotor Hamiltonian, the ν_{CD} those obtained when the centrifugal distortion terms are included. Though discrepancies between the computed and observed frequencies still exist in the second case, a considerable improvement has been made. It moreover seems possible to place limits of error on the subsequently obtained structural parameters in the following way. The remaining errors in the computed rotational frequencies are of the order of a few percent of the centrifugal distortion corrections, $\delta\nu$. They presumably are to be attributed to errors in the τ's, and indeed uncertainties of this order of magnitude are to be expected. For example, the vibrational frequencies are uncertain to about 1 percent, and these uncertainties lead to errors in the vibrational eigenvectors. Now for each isotopic species the two lines of lowest J, which are used to fix the rotational constants, naturally show no error. It seems reasonable, however, to say that when these frequencies are used to compute rotation parameters, the fact that the τ's are in error introduces an effective uncertainty in the observed frequencies of the order of a few percent of the centrifugal distortion contribution to these frequencies. Thus for PH_2D the $J=4$ transition is in error by 4.25 mc, or 6.2 percent of the $\delta\nu$. Then we expect that the observed frequency for $J=3$ contains an effective uncertainty not greater than 6 percent of its $\delta\nu$, or 2.6 mc, while $J=1$ is essentially correct.

These effective probable errors in the frequencies can be used to estimate the probable errors in the rotational parameters, and eventually in r and α. In this way we obtain

(a) PH_2D: $\kappa=-0.741384\pm0.000016$,
$(A-C)/2=23292.6\pm1.4$ mc,
$r=1.4177$A,
$\alpha=93°21.6'$;

(b) PHD_2: $\kappa'=-2.40671\pm0.00023$,
$(C-B)/2=-8533.81\pm0.58$ mc,
$r=1.4116$A,
$\alpha=93°15.4'$.

The probable error in α is of the order of 0.1′ in each case, in r of the order of 0.0001A. These errors are, of course, only those produced by inexact handling of the rotational problem. The above work shows that they are essentially negligible compared to those due to neglect of the vibration-rotation interaction. The inadequacy of the assumption that rotational constants may be interpreted as reciprocal equilibrium moments of inertia is indicated by the extent to which the two structural determinations disagree.

For the dipole moment measurement the lines $J=1$ of PHD_2 and $J=2$ of PH_2D were used. Since the dipole moment has components along two principal axes, two contributions to the Stark shift must be computed separately, weighted by the squared cosine of the angle between the principal axis and the dipole moment ("symmetry") axis, and added. There is thus an explicit dependence on the structural model, in contrast to the case where the dipole moment coincides with a principal axis, and where, therefore, only the empirical rotational constants enter. Since the change in dipole moment caused by change in isotopic composition is expected to be well within the experimental error, it is gratifying that the two determinations are in good agreement. We obtain (a) PH_2D: $\mu=0.579\pm0.012$ debye, (b) PHD_2: $\mu=0.565\pm0.008$ debye. This result is in satisfactory agreement with values previously obtained by two methods.[3,18]

No evidence of inversion doubling was obtained. The resolving power of our instrument thus places an upper limit of about 0.5 mc on the splitting in the ground vibrational state. A recent calculation for PH_3 by Costain and Sutherland[19] seemed to indicate a possibility of observing this splitting for PH_2D in the microwave region. On attempting to repeat this calculation, however, we found the splitting to be so sensitive to the value of the bending force constant that it seemed impossible to make a definite statement on the magnitude of splitting to be expected. It is to be hoped that in the future this spectrum will be reinvestigated under conditions of higher resolution than possible in this laboratory.

We want to thank Miss Jean Snover for aid in the computational work.

[18] H. E. Watson, Proc. Roy. Soc. (London) **A117**, 43 (1927).
[19] C. C. Costain and G. B. B. M. Sutherland, J. Phys. Chem. 56, 321 (1952).

Application of the Fermi-Thomas Model in Computing the Dipole Moment of Iodine Chloride*

HERBERT GLAZER† AND HOWARD REISS‡
Chemistry Department, Boston University, Boston, Massachusetts
(Received November 24, 1952)

The Fermi-Thomas statistical method is applied to the molecule ICl and the nonlinear boundary value problem solved by means of the relaxation method of Southwell. In this manner it is possible to construct an electron density map for ICl and to compute its diploe moment. The computed moment compares favorably in magnitude with the measured and has the correct sense.

It appears as though the statistical method will be useful in estimating the senses of dipole moments when they are not clearly evident from experiment.

I. INTRODUCTION

THE general trend of research in the quantum mechanics of molecules is in the direction of the more exact solution. With the advent of modern computers the crude models which served in the past are (at least in so far as simple molecules are concerned) rapidly becoming objects of historical interest. However, the chemist more than the physicist often derives valuable assistance from the semiquantitative sort of information which these models are capable of yielding. It is therefore fitting to consider whether or not any suitable problems remain to be solved before the models are discarded.

One's attention is immediately drawn to the Fermi-Thomas statistical model[1–3] which has been used so successfully in the treatment of atoms. Very little attempt has been made to extend this method to the treatment of even the simplest molecules. The reasons for this are threefold:

(1) It seems probable that in the regions of phase space occupied by valence electrons (the most important electrons in a molecular problem) the "maximum density"[4] requirement is not fulfilled, i.e., all of the lowest quantum states are not occupied by electrons. Since the Fermi-Thomas method is founded on the assumption that the electrons constitute a totally degenerate gas[4] its validity is weakened by this circumstance.

(2) The Fermi-Thomas model does not take proper account of exchange effects.[5]

(3) The application of the method to molecules (nonspherical fields) involves the solution of a nonlinear boundary value problem in more than one dimension. Such problems, when they are amenable to solution, are only so through the use of tedious numerical procedures.

Some objection can be raised against the complaint that the maximum density requirement is not fulfilled. Although there is little doubt that this is true when the valence electrons in an isolated atom are considered, the situation may not be so bad in a molecule where there is a concentration of electron density in the direction of a bond. Also, point (3) in the above list is not as serious as it seems, for the labor involved in the solution of a nonlinear boundary value problem, although appreciable, is still small compared to that in the more refined wave mechanical treatments.[6] As a matter of fact, we shall show below how this work can be performed without the aid of computing machines.

Hund[7] was the first to apply the Fermi-Thomas method in its original form to molecules. He employed the Ritz variation method to investigate the nonlinear problem for N_2. He was able to conclude that the solution could be closely approximated by a superposition of two spherically symmetric fields, centered at each nucleus which were related through an interpolation function to the isolated atom solutions. It was also possible for him to show that the difference between the true solution and the one obtained by superposition was small. More recently, March[8] and Coulson, March, and Altmann[9] have investigated the electron distribution in benzene using the Fermi-Thomas method as employed by Hund. Comparison with the distribution calculated by the molecular orbital method was reasonably good, and both theoretical methods were in reasonable agreement with the experimental results of Robertson and coworkers[10] for naphthalene, as far as comparison was valid. March has also applied the Fermi-Thomas method to molecules with tetrahedral and octahedral symmetry[11] in the approximation in which the nuclei of the outer atoms are smeared over the surface of a sphere. Comparison with the results of the Hartree

* Supported by Air Force Cambridge Research Center.
† Part of dissertation for Ph.D. degree, Boston University.
‡ Present address: Bell Telephone Laboratories, Murray Hill, New Jersey.
[1] L. H. Thomas, Proc. Cambridge Phil. Soc. **23**, 542 (1927).
[2] E. Fermi, Z. Physik **48**, 73 (1928).
[3] E. Fermi, Z. Physik **49**, 550 (1928).
[4] Mayer and Mayer, *Statistical Mechanics* (John Wiley and Sons, Inc., New York, 1940), Chap. 16.
[5] P. A. M. Dirac, Proc. Cambridge Phil. Soc. **26**, 376 (1930).
[6] J. Mulligan, J. Chem. Phys. **19**, 347 (1951).
[7] F. Hund, Z. Physik **77**, 12 (1932).
[8] N. H. March, Acta Cryst. **5**, 187 (1952).
[9] Coulson, March, and Altmann, Proc. Natl. Acad. Sci. **38**, 372 (1952).
[10] Abrahams, Robertson, and White, Acta Cryst. **2**, 233, 238 (1949).
[11] N. H. March, Proc. Cambridge Phil. Soc. **48**, 665 (1952).

self-consistent field method for methane[12] shows that the charge distribution is somewhat poor while the potential is in good agreement. The method appears to break down for CCl_4.

The solution of a hybrid problem in which wave mechanics is applied accurately in one part while the statistical method is applied in another is exemplified by the work of Jensen[13] and of Bonet andBushkovitch.[14]

The superposition of two neutral spherically symmetric atomic charge distributions cannot produce a result having a dipole moment. Since the nitrogen molecule has no dipole moment, Hund's solution, when referred to it, possesses desirable properties but might not be satisfactory for highly polar molecules. Also, the small error in the total distribution which Hund says his superposition solution introduces may actually be large, relative to the valence electrons alone, in molecules where these electrons constitute only a small fraction of the total. Therefore, it seemed worth while to solve the problem for a heavy polar diatomic molecule having a moment whose value was known experimentally in the vapor phase. For this purpose we chose iodine chloride. Two values for its moment have been estimated from infrared intensity measurements (20–40 percent error), the average being $0.57D$;[15,16] the normal assignment of direction being I^+Cl^-. Other values for the moment have been inferred from other data.[17–20] In addition, since we were primarily interested in electron distributions, it seemed advisable to abandon the Ritz method of solution in favor of one which dealt with distribution more directly. In this manner we hoped to increase the accuracy of the final result. Consequently the problem was set up in finite difference form and solved by the relaxation method of Southwell.[21]

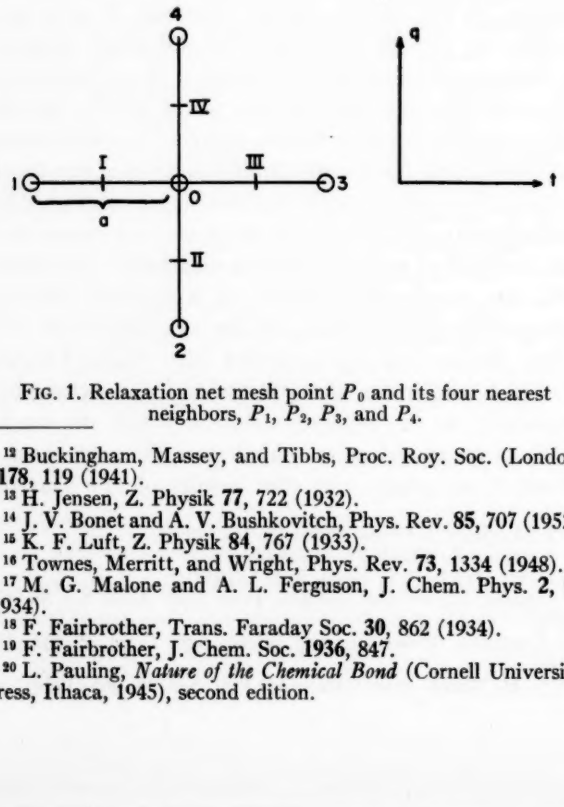

FIG. 1. Relaxation net mesh point P_0 and its four nearest neighbors, P_1, P_2, P_3, and P_4.

In closing this section it is worth mentioning that one of the most important services that calculations of this sort can provide is that of a quick independent method of estimating the signs of dipole moments in cases where such information is not clearly available from experiment. Of course, the reliability of the method must be assessed, and this can be achieved by applying it to cases where experiment furnishes a clear answer. If the calculated magnitude of the dipole moment is of the right order (in addition to the reasonableness of its sign) our confidence should be increased.

II. FORMULATION OF THE PROBLEM

In a completely degenerate electron gas, the number density ρ of electrons at a point of configuration space, where the potential is V, is given by

$$\rho=[2^{9/2}\pi(me)^{3/2}/3h^3]V^{3/2}, \tag{1}$$

where m=mass of the electron, $-e$=charge on the electron, and h=Planck's constant. In view of Eq. (1), Poisson's equation[22] for the potential V can be written in the form

$$\nabla^2V=[2^{13/2}\pi^2m^{3/2}e^{5/2}/3h^3]V^{3/2}=\alpha V^{3/2}. \tag{2}$$

Applied to the spherically symmetric case of the isolated atom, Eq (3) assumes the form

$$d^2V/dr^2+(2/r)dV/dr=\alpha V^{3/2}, \tag{3}$$

where r is the magnitude of the radius vector originating at the nucleus.

For the treatment of diatomic molecules it is convenient to use confocal elliptic coordinates.[23] Taking account of axial symmetry, Eq. (2) in this coordinate system assumes the form,

$$\frac{4}{R^2(s^2-t^2)}\left[\frac{\partial}{\partial s}(s^2-1)\frac{\partial V}{\partial s}+\frac{\partial}{\partial t}(1-t^2)\frac{\partial V}{\partial t}\right]=\alpha V^{\frac{1}{2}}. \tag{4}$$

The ranges of the variables s and t are $1\leq s\leq\infty$ and $-1\leq t\leq 1$. To Eq. (4) are appended the boundary conditions

$$\begin{aligned} &V=0, && s=\infty, \\ &\lim Vr_a=Z_ae, && s=1, \quad t=1, \\ &\lim Vr_b=Z_be, && s=1, \quad t=1. \end{aligned} \tag{5}$$

The solution of the spherical equation (3) subject to the boundary conditions

$$\begin{aligned} &V=0, && r=\infty, \\ &\lim Vr=Ze, && r=0, \end{aligned} \tag{6}$$

[12] Buckingham, Massey, and Tibbs, Proc. Roy. Soc. (London) **A178**, 119 (1941).
[13] H. Jensen, Z. Physik **77**, 722 (1932).
[14] J. V. Bonet and A. V. Bushkovitch, Phys. Rev. **85**, 707 (1952).
[15] K. F. Luft, Z. Physik **84**, 767 (1933).
[16] Townes, Merritt, and Wright, Phys. Rev. **73**, 1334 (1948).
[17] M. G. Malone and A. L. Ferguson, J. Chem. Phys. **2**, 99 (1934).
[18] F. Fairbrother, Trans. Faraday Soc. **30**, 862 (1934).
[19] F. Fairbrother, J. Chem. Soc. **1936**, 847.
[20] L. Pauling, *Nature of the Chemical Bond* (Cornell University Press, Ithaca, 1945), second edition.
[21] R. V. Southwell, *Relaxation Methods in Theoretical Physics*, (Oxford University Press, London, 1946).
[22] J. C. Slater and N. H. Frank, *Introduction to Theoretical Physics* (McGraw-Hill Book Company, Inc., New York, 1933), p. 212.
[23] L. Pauling and E. B. Wilson, *Introduction to Quantum Mechanics* (McGraw-Hill Book Company, Inc., New York, 1935), p. 444.

has been thoroughly worked out. It has been tabulated by Baker[24] and others[25] in dimensionless form. Consequently, it is convenient to rephrase our problem in Baker's notation. Baker tabulates the function $\phi(x)$, where

$$\gamma\phi = xV = x\gamma\psi, \qquad \mu x = r, \tag{7}$$

and

$$\gamma = 2^{13/3}\pi^{4/3}me^3Z^{4/3}/3^{2/3}h^2, \qquad \mu = 3^{2/3}h^2/2^{13/3}\pi^{4/3}me^2Z^{1/3}, \tag{8}$$

so that

$$\alpha\gamma^{\frac{1}{2}} = 1/\mu^2.$$

In this notation (where either Z_a or Z_b is used)

$$R = \mu L, \qquad r_a = \mu x_a, \qquad r_b = \mu x_b, \tag{9}$$

and Eq. (4) assumes the form

$$\frac{4}{L^2(s^2-t^2)}\left[\frac{\partial}{\partial s}(s^2-1)\frac{\partial\psi}{\partial s}+\frac{\partial}{\partial t}(1-t^2)\frac{\partial\psi}{\partial t}\right]=\psi^{\frac{1}{2}}. \tag{10}$$

If Z_a is used in Eqs. (8) and (9), Eqs. (5) become

$$\psi = 0, \quad s=\infty, \qquad \lim\psi x_a = 1, \quad s=1, \quad t=-1, \qquad \lim\psi Z_a x_b/Z_b = 1, \quad s=1, \quad t=1. \tag{11}$$

If Z_b is used in Eqs. (8) and (9), an opposite state of affairs will exist.

III. METHOD OF SOLUTION

In order to refer the problem contained in Eqs. (10) and (11) to iodine chloride, it is necessary to choose the magnitudes of L, Z_a, and Z_b so that they correspond to the measured bond distance (reduced from R, of course,) in ICl and the atomic numbers of iodine and chlorine, respectively. To set the problem up in finite difference form, a rectangular net of uniform mesh size must be constructed from the coordinate lines s and t. (The net must be rectangular despite the fact that physically s and t are not actually rectangular coordinates.) Reference to Eqs. (5) shows that one of the physically important boundaries of the problem lies at $s=\infty$. This demands that the net be of infinite extent in the s direction. Since a numerical operation must be performed at each mesh point this represents an untenable situation.

The difficulty can be obviated if we employ the transformation

$$s = 1-\ln q. \tag{12}$$

[24] E. Baker, Phys. Rev. **36** 632 (1930).
[25] See P. Gombas, *Die Statistische Theorie des Atoms* (Springer-Verlag, Vienna, 1949).

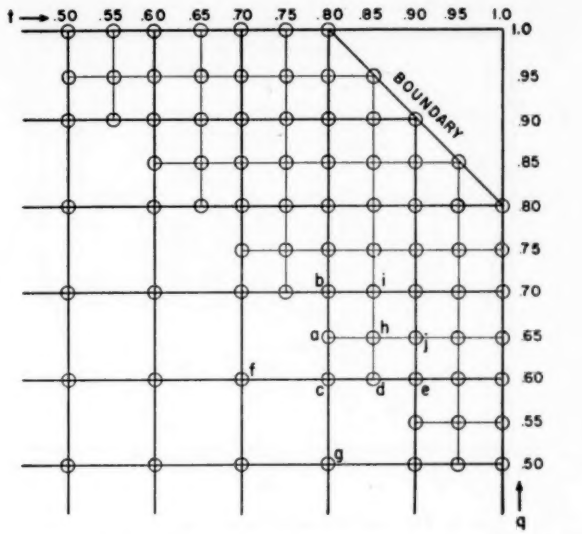

FIG. 2. Graded portion of relaxation net and excluded singularity.

The limits on q will then be finite:

$$s=1, \quad q=1, \qquad s=\infty, \quad q=0. \tag{13}$$

With this transformation Eq. (10) can be written as

$$\frac{\partial}{\partial q}\left[q\ln q(\ln q-2)\frac{\partial\psi}{\partial q}\right]+\frac{\partial}{\partial t}\left[\frac{1-t^2}{q}\frac{\partial\psi}{\partial t}\right] = \frac{L^2[(1-\ln q)^2-t^2]}{4q}\psi^{\frac{1}{2}} \tag{14}$$

or

$$\frac{\partial}{\partial q}\left[A(q)\frac{\partial\psi}{\partial q}\right]+\frac{\partial}{\partial t}\left[B(q,t)\frac{\partial\psi}{\partial t}\right]=C(q,t)\psi^{\frac{1}{2}}. \tag{15}$$

In Fig. 1 we have drawn a mesh point P_0 and its four nearest neighbors, P_1, P_2, P_3, and P_4. The Roman numerals refer to the corresponding mid-points of the lines joining nearest neighbors, and a is the distance between nearest neighbors. In terms of this notation the finite difference approximation to Eq. (15) at P_0 is

$$B_{\rm I}\psi_1+A_{\rm II}\psi_2+B_{\rm III}\psi_3+A_{\rm IV}\psi_4 -\psi_0(B_{\rm I}+A_{\rm II}+B_{\rm III}+A_{\rm IV})=a^2C_0\psi_0^{\frac{1}{2}}, \tag{16}$$

where the quantities A, B, C, and ψ have the values they assume at the points located by their subscripts.

At points lying along the boundaries of the net, prescribed conditions are imposed on ψ. In the present problem the net covers a rectangular area bounded by the lines $t=1$, $t=-1$, $q=1$, and $q=0$. ψ is symmetric across $t=1$, $t=-1$, and $q=1$. In practice this boundary condition may be applied in the following manner. Suppose that the point P_0 in Fig. 1 lies on the boundary $t=1$, the line $t=1$ running through P_2 and P_4. Then the point P_1 will not really appear in the net. Nevertheless, the condition of symmetry demands that,

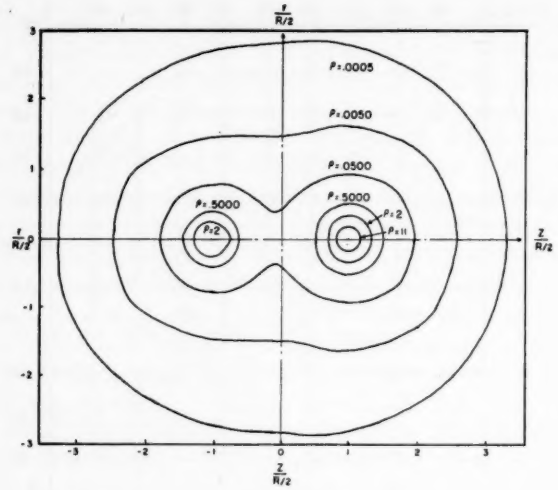

FIG. 3. The electron distribution function contours for iodine chloride.

in carrying out the relaxation procedure described below, we imagine that P_1 exists, that ψ_1 always equals ψ_3, and that $B_{\mathrm{I}}=B_{\mathrm{III}}$. The same considerations apply to $t=-1$ and $q=1$. By Eq. (11) the condition at $q=0$ is simply $\psi=0$.

Several features complicate our problem. In the first place, the solution possesses singularities at the locations of the nuclei, i.e., at $t=-1$, $q=1$ and $t=1$, $q=1$. These were eliminated from consideration by constructing (in real space) a small volume about each nucleus and employing the surfaces of the volumes as part of the boundary surface of the problem. On the q,t net this corresponds to excluding the upper corners as shown in Fig. 2. Of course, it is necessary to know the value of ψ at points along these new boundaries. If the volumes are chosen small enough (deep within the kernels of the atoms) the solution on their surfaces will be almost spherically symmetric.[26,27] In fact, an almost perfect approximation can be obtained by superposing two spherically symmetric solutions ψ_a and ψ_b centered respectively at nuclei a and b, where ψ_a is the solution for the isolated iodine atom and ψ_b, the solution for the isolated chlorine atom. Thus along the small volume surfaces we fix ψ as

$$\psi=\psi_a+\psi_b. \tag{17}$$

A second complicating feature lies in the fact that the transformation (12) which removes the infinite boundary performs a somewhat illusory service, because it can be argued that the convergence of an iterative procedure like the finite difference method is severely hampered when the differential coefficients A and B in Eq. (15) are of greatly unequal magnitude. The transformation (12) tends to produce this effect at values of q close to zero. On the other hand, if the mesh size is chosen so that q decreases from 1 to 0 in intervals of 0.1, it turns out that at $q=0.1$ the real distance from either nucleus is at most about two ICl bond distances, i.e., about $2R$. Therefore in the last step as q passes from 0.1 to zero, the distance from the nucleus increases from $2R$ to ∞. Consequently, all points on the net at which calculations are performed lie fairly close to the nuclei, and as a result the disparity is never too marked in the regions of operation.

A third difficulty arises because the solution ψ is changing rapidly close to either nucleus. To make the treatment more accurate we have used a graded net (shown in Fig. 2) in these regions. At a point such as a in Fig. 2, ψ is always assumed to have a value intermediate to its values at b and c. In applying the relaxation method to point c, for example, b and e are considered to be nearest neighbors along with f and g. In applying this method to the point h, points a, d, j, and i are regarded as nearest neighbors, but a and d are never themselves relaxed. In accordance with our assumtpion they always possess values intermediate to b and c, and c and e, respectively.

In applying the relaxation method, one begins by guessing the value of the solution ψ at each mesh point. The more accurate the initial guess the more rapidly will the subsequent iterative process converge. This matter is adequately discussed in Southwell's book. For our initial guess we chose the momentless distribution (17) in accordance with Hund's observation that a superposition of neutral atom solutions represents a fairly good approximation. It can be shown by general consideration of Eq. (10)§ to be most seriously in error midway between the two nuclei where the bond forms but quite accurate in the intermediate vicinity of either nucleus.

The finite difference problem is solved, when at each point the difference between the left and right sides of Eq. (16) (the "residual") has been made as small as possible by suitable readjustment of ψ. Referring to Fig. 1, if P_0 is a typical point, then with ψ_1, ψ_2, ψ_3, and ψ_4 fixed, ψ_0 is adjusted until the residual vanishes. However, this procedure may worsen the residuals at P_1, P_2, P_3, and P_4 when they in turn are considered as central points. Nevertheless, the continued successive suppression of residuals (the relaxation process), when carried over the entire net, always effects a general improvement (the process converges). The convergence is more rapid if the largest residuals are relaxed first. These matters are all discussed by Southwell.

It is interesting to note that in the parlance of the relaxation method this problem is one involving a net with an anisotropically variable "tension." To the authors' knowledge no other problem in the literature has been solved by the relaxation method in which the tension varies anisotropically. Furthermore, the lateral "pressure" appearing on the right of Eq. (16) is not

[26] H. Reiss and H. Saltsbrug, J. Chem. Phys. **18**, 1461 (1950).
[27] J. Lopuszanski, Acta Phys. Polon. **10** 213 (1950).

§ Transform to coordinates r_a and r_b and substitute $\psi=\psi_a(r_a)+\psi_b(r_b)$.

prescribed, as usual, but depends on the local displacement ψ_0.

IV. RESULTS

Every point on the relaxation net was relaxed four times with a relative decrease in all residuals of a hundredfold or better. The improvement which the fourth relaxation effected over the third was inappreciable, and so the process was halted.

The total charge in the region where the dipole moment was determined was summed from the net using Simpson's rule for mechanical cubature.[28] It was found to constitute 99 percent of the total charge in the molecule indicating that only 1 percent of the charge was not accounted for by moving the boundary from infinity and excluding the singularities at the nuclei. The actual contribution to the dipole moment of the excluded charge at great distances is, of course, very much less than 1 percent, since this charge is for the most part distributed symmetrically.

Taking account of axial symmetry the dipole moment in elliptical coordinates is given by[29]

$$\mu=\frac{2\pi eR^4}{16}\int\int\rho(s,t)st(s^2-t^2)dsdt, \qquad (18)$$

where ρ is the number density of electrons and is defined by Eq. (1). In terms of the transformation (12), Eq. (18) becomes

$$\mu=\frac{2\pi eR^4}{16}\int\int\frac{-\rho(q,t)}{q}[t(1-\ln q)][(1-\ln q)^2-t^2]dqdt. \qquad (19)$$

In this case ρ is actually the difference between the final net value and the sum of atomic densities, i.e., $\rho_I+\rho_{Cl}$. This integral was calculated, again, using mechanical cubature, with the result

$$\mu=0.3D[I^+Cl^-]. \qquad (20)$$

[28] J. B. Scarborough, *Numerical Mathematical Analysis* (The Johns Hopkins Press, Baltimore, 1950), second edition, p. 163.
[29] J. A. Stratton, *Electromagnetic Theory* (McGraw-Hill Book Company, Inc., New York, 1941), p. 174.

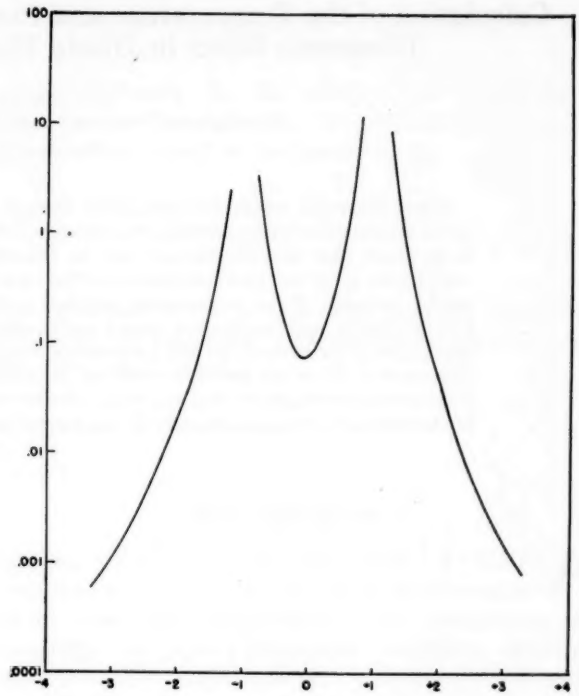

FIG. 4. Semilogarithmic plot of $\rho\times10^{-25}$ as ordinate *vs* $Z/(R/2)$ as abscissa for iodine chloride.

Besides having a reasonable sign this value compares numerically with the estimated experimental value,

$$\mu=0.57D.$$

Better results might have been obtained, of course, through the use of a finer net, but it is questionable whether the crudeness of the model justifies the additional labor.

Figure 3 contains the final electron density contour map of $\rho\times10^{-25}$, as given by Eq. (1), as a function of r, the radial distance from the center of the bond axis, and of z, the distance along the bond axis, for Cl···I.

Figure 4 is a semilogarithmic plot of $\rho\times10^{-25}$ as a function of distance along the bond axis in terms of $Z/(R/2)$ for Cl···I.

Calculation of the Temperature and Pressure Coefficients of Conductivity and the Ultrasonic Effect in Dilute Electrolytes from Onsager's Theory

SIDNEY BARNARTT
Westinghouse Research Laboratories, East Pittsburgh, Pennsylvania
(Received January 2, 1953)

When ultrasonic waves are propagated through electrolytes, the periodic adiabatic compressions give rise to conductance changes which are a measure of the temperature and pressure coefficients of conductivity. It is shown that these coefficients can be calculated from Onsager's equation for symmetrical-valence electrolytes, if the coefficients at infinite dilution are known. Therefore, the magnitude of the ultrasonic effect can be computed. If the temperature coefficient at infinite dilution is known, then the pressure coefficient at infinite dilution may be obtained from a measurement of the ultrasonic effect at atmospheric pressure. The magnitude of the effect is derived for progressive and stationary plane waves in conductivity cells of uniform cross section. When the conductance of the electrolyte is determined with ac, the ultrasonic waves produce two side-band voltages of equal amplitude. For $10^{-4}M$ KCl at 25°C in a favorable cell, the side-band voltages are computed to be approximately 53 microvolts per atmosphere acoustic pressure per volt applied.

I. INTRODUCTION

ACOUSTIC waves are associated with periodic compressions of the medium through which they are propagated. The compressions take place under virtually adiabatic conditions even at ultrasonic (inaudible) frequencies. In electrolytic solutions these adiabatic compressions produce periodic variations in conductivity.[1,2] An infinitesimal adiabatic compression changes the conductivity of the solution by a fraction

$$d\kappa/\kappa=\gamma dP+\delta dT, \tag{1}$$

where $\gamma=\partial\kappa/\kappa\partial P$ is the pressure coefficient and $\delta=\partial\kappa/\kappa\partial T$ the temperature coefficient of conductivity. The temperature and pressure changes are related by the thermodynamic equation

$$(dT/dP)_S=\alpha T/c_p d, \tag{2}$$

where $\alpha=1/V(\partial V/\partial T)_p$ is the coefficient of (cubic) thermal expansion of the solution, c_p its specific heat at constant pressure, and d its density. Substitution for dT in Eq. (1) yields the relationship

$$\frac{d\kappa}{\kappa}=\left(\gamma+\frac{\delta\alpha T}{c_p d}\right)dP. \tag{3}$$

The pressure changes in an ultrasonic wave are determined from intensity measurements, according to the well-known equation

$$I=p^2/2ud, \tag{4}$$

where I is the average energy flow per cm^2, p is the pressure amplitude, and u the velocity of sound in the solution. Thus the conductance changes can be calculated, if the coefficients γ and δ are known; it will be shown below that these coefficients can be computed from the interionic attraction theory of Debye and Hückel[3] and Onsager[4] for dilute solutions.

[1] Fox, Herzfeld, and Rock, Phys. Rev. **70**, 329 (1946).
[2] Y. I. Lichter and S. E. Khaikin, J. Exptl. Theoret. Phys. (U.S.S.R.) **18**, 651 (1948).
[3] P. Debye and E. Hückel, Physik. Z. **24**, 185, 305 (1923).
[4] L. Onsager, Physik. Z. **27**, 388 (1926); **28**, 277 (1928).

II. THE PRESSURE COEFFICIENT OF CONDUCTIVITY

For simplicity only salts of the symmetrical-valence type will be considered. Onsager's equation for dilute solutions of such a salt may be written

$$\Lambda=f_\Lambda\Lambda_\infty=\left[1-\left(\frac{8.160\times10^5 z^3}{(D_0T)^{\frac{3}{2}}}+\frac{81.97z^2}{\eta_0\Lambda_\infty(D_0T)^{\frac{1}{2}}}\right)c^{\frac{1}{2}}\right]\Lambda_\infty, \tag{5}$$

where Λ is the equivalent conductance of the solution at molarity c, Λ_∞ the limiting value at infinite dilution; $z=|z^+|=|z^-|$ is the ionic valence; D_0 and η_0 are the dielectric constant and viscosity, respectively, of the pure solvent. The specific conductance of the solution may then be written as

$$\kappa=10^{-3}zf_\Lambda\Lambda_\infty c. \tag{6}$$

Upon taking natural logarithms and differentiating with respect to pressure, one obtains

$$\gamma=\frac{\partial\ln f_\Lambda}{\partial P}+\frac{\partial\ln\Lambda_\infty}{\partial P}+\beta, \tag{7}$$

where

$$\beta=-\frac{1}{V}\left(\frac{\partial V}{\partial P}\right)_T=\frac{1}{c}\left(\frac{\partial c}{\partial P}\right)_T,$$

the isothermal compressibility of the solution.

Over the concentration range to which the limiting Onsager theory applies, the factor f_Λ is equal to unity minus a relatively small fraction. The differentiation of $\ln f_\Lambda$ can be simplified, therefore, by introducing the approximation

$$\ln f_\Lambda=-\left[\frac{k_1}{(D_0T)^{\frac{3}{2}}}+\frac{k_2}{\eta_0\Lambda_\infty(D_0T)^{\frac{1}{2}}}\right]c^{\frac{1}{2}}, \tag{8}$$

where k_1 replaces $8.160\times10^5z^3$ and k_2 replaces $81.97z^2$. Differentiation of Eq. (8), with respect to pressure, and

insertion into Eq. (7) leads to the result

$$\gamma=\frac{\partial \ln\Lambda_\infty}{\partial P}\left[1+\frac{k_2}{\eta_0\Lambda_\infty}\left(\frac{c}{D_0T}\right)^{\frac{1}{2}}\right]+\beta\left[1-\left(\frac{k_1}{2D_0T}+\frac{k_2}{2\eta_0\Lambda_\infty}\right)\left(\frac{c}{D_0T}\right)^{\frac{1}{2}}\right]+\frac{\partial \ln D_0}{\partial P}\left(\frac{3k_1}{2D_0T}+\frac{k_2}{2\eta_0\Lambda_\infty}\right)\left(\frac{c}{D_0T}\right)^{\frac{1}{2}}+\frac{\partial \ln\eta_0}{\partial P}\left(\frac{k_2}{\eta_0\Lambda_\infty}\right)\left(\frac{c}{D_0T}\right)^{\frac{1}{2}}. \quad (9)$$

It is anticipated that β will be considerably less than $\partial \ln\Lambda_\infty/\partial P$ for many solutions. At low concentrations β differs little from β_0, the compressibility of the pure solvent, and the quantity which it multiplies differs little from unity. Therefore, Eq. (9) may be approximated in such cases by

$$\gamma=\frac{\partial \ln\Lambda_\infty}{\partial P}\left[1+\frac{k_2}{\eta_0\Lambda_\infty}\left(\frac{c}{D_0T}\right)^{\frac{1}{2}}\right]+\beta_0+\frac{\partial \ln D_0}{\partial P}\left(\frac{3k_1}{2D_0T}+\frac{k_2}{2\eta_0\Lambda_\infty}\right)\left(\frac{c}{D_0T}\right)^{\frac{1}{2}}+\frac{\partial \ln\eta_0}{\partial P}\left(\frac{k_2}{\eta_0\Lambda_\infty}\right)\left(\frac{c}{D_0T}\right)^{\frac{1}{2}}. \quad (10)$$

This equation permits computation of γ from constants characteristic of the solvent, provided the pressure dependence of Λ_∞ is known. Thus for aqueous solutions at 25°C and atmospheric pressure, with the following numerical values of the solvent parameters:

$D_0=78.54$,[5] $\partial \ln D_0/\partial P=5.9_3\times10^{-5}$/atmos,[6]
$\beta_0=4.61\times10^{-5}$/atmos,[7]
$\eta_0=8.95\times10^{-3}$ poise,[8] $\partial \ln\eta_0/\partial P=3\times10^{-5}$/atmos,[9]

Eq. (10) reduces to

$$\gamma=\frac{\partial \ln\Lambda_\infty}{\partial P}\left(1+\frac{59.8z^2}{\Lambda_\infty}c^{\frac{1}{2}}\right)+4.61\times10^{-5}+\left(2.0_5\times10^{-5}z^3+\frac{3.6\times10^{-3}z^2}{\Lambda_\infty}\right)c^{\frac{1}{2}}. \quad (11)$$

[5] J. Wyman and E. N. Ingalls, J. Am. Chem. Soc. **60**, 1182 (1938).
[6] B. B. Owen and S. R. Brinkley, Ann. N. Y. Acad. Sci. **51**, 753 (1949).
[7] R. E. Gibson, J. Am. Chem. Soc. **56**, 4 (1934).
[8] *International Critical Tables*, Vol. V (McGraw-Hill Book Company, Inc., New York, 1929), p. 10.
[9] N. E. Dorsey, *Properties of Ordinary Water-Substance* (Reinhold Publishing Corporation, New York, 1940), p. 186.

III. THE TEMPERATURE COEFFICIENT OF CONDUCTIVITY

The expression for the temperature coefficient is obtained by differentiating the logarithmic form of Eq. (6) with respect to temperature, *viz.*,

$$\delta=\frac{\partial \ln f_\Lambda}{\partial T}+\frac{\partial \ln\Lambda_\infty}{\partial T}-\alpha. \quad (12)$$

The expansion of $\partial \ln f_\Lambda/\partial T$ follows from Eq. (8). When the expanded expression is inserted into Eq. (12), the following result is obtained:

$$\delta=\frac{\partial \ln\Lambda_\infty}{\partial T}\left[1+\frac{k_2}{\eta_0\Lambda_\infty}\left(\frac{c}{D_0T}\right)^{\frac{1}{2}}\right]-\alpha\left[1-\left(\frac{k_1}{2D_0T}+\frac{k_2}{2\eta_0\Lambda_\infty}\right)\left(\frac{c}{D_0T}\right)^{\frac{1}{2}}\right]+\left(\frac{\partial \ln D_0}{\partial T}+\frac{1}{T}\right)\left(\frac{3k_1}{2D_0T}+\frac{k_2}{2\eta_0\Lambda_\infty}\right)\left(\frac{c}{D_0T}\right)^{\frac{1}{2}}+\frac{\partial \ln\eta_0}{\partial T}\left(\frac{k_2}{\eta_0\Lambda_\infty}\right)\left(\frac{c}{D_0T}\right)^{\frac{1}{2}}. \quad (13)$$

For many solutions the term involving α may be approximated by α_0, the coefficient of thermal expansion of the pure solvent, since it is much smaller than the quantity $\partial \ln\Lambda_\infty/\partial T$. Equation (13) then becomes

$$\delta=\frac{\partial \ln\Lambda_\infty}{\partial T}\left[1+\frac{k_2}{\eta_0\Lambda_\infty}\left(\frac{c}{D_0T}\right)^{\frac{1}{2}}\right]-\alpha_0+\left(\frac{\partial \ln D_0}{\partial T}+\frac{1}{T}\right)\left(\frac{3k_1}{2D_0T}+\frac{k_2}{2\eta_0\Lambda_\infty}\right)\left(\frac{c}{D_0T}\right)^{\frac{1}{2}}+\frac{\partial \ln\eta_0}{\partial T}\left(\frac{k_2}{\eta_0\Lambda_\infty}\right)\left(\frac{c}{D_0T}\right)^{\frac{1}{2}}. \quad (14)$$

For aqueous solutions at 25°C,

$\alpha_0=2.57\times10^{-4}$/deg,[10]
$\partial \ln D_0/\partial T=-4.58\times10^{-3}$/deg,[5]
$\partial \ln\eta_0/\partial T=-2.32\times10^{-2}$/deg,[8]

and

$$\delta=\frac{\partial \ln\Lambda_\infty}{\partial T}\left(1+\frac{59.8z^2}{\Lambda_\infty}c^{\frac{1}{2}}\right)-2.57\times10^{-4}-\left(4.18\times10^{-4}z^3+\frac{1.43z^2}{\Lambda_\infty}\right)c^{\frac{1}{2}}. \quad (15)$$

[10] *International Critical Tables*, Vol. III (McGraw-Hill Book Company, Inc., New York, 1929), p. 24.

IV. THE ULTRASONIC EFFECT IN A CELL OF UNIFORM CROSS SECTION

(a) Resistance Changes When the Ultrasonic Waves Are Propagated in the Direction of Current Flow

Consider a conductivity cell consisting of two parallel electrodes covering the ends of a tube of length L which has the same cross-sectional area A all along its length (Fig. 1). Let plane, progressive ultrasonic waves be propagated through the solution in the direction x of current flow. Any element of solution Adx which is parallel to the electrodes is also parallel to the wave front, and consequently, represents a region of uniform acoustic pressure. The excess pressure in the element may be written[11]

$$dP=p\cos(\omega t-kx), \tag{16}$$

where $\omega=2\pi$ (frequency) and $k=2\pi/\lambda$, λ being the ultrasonic wavelength in the solution. Substitution for dP in Eq. (3), which is valid when p is not too high, yields

$$\frac{d\kappa}{\kappa}=-\frac{d\rho}{\rho}=\left(\gamma+\frac{\delta\alpha T}{c_p d}\right)p\cos(\omega t-kx). \tag{17}$$

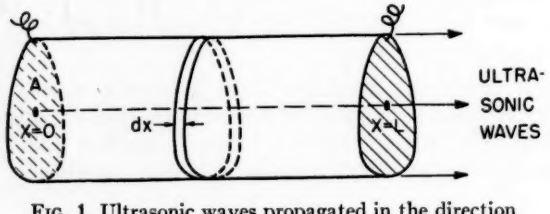

FIG. 1. Ultrasonic waves propagated in the direction of current flow.

Since the fractional resistivity changes resulting from ultrasonic irradiation are small, Eq. (17) may be replaced by

$$\rho_\epsilon=\rho_0\left[1-\left(\gamma+\frac{\delta\alpha T}{c_p d}\right)p\cos(\omega t-kx)\right], \tag{18}$$

where ρ_ϵ is the local resistivity within the element of solution and ρ_0 the resistivity in the absence of acoustic forces.

The total resistance of the cell during ultrasonic irradiation may now be evaluated as

$$R=\int_0^L\frac{\rho_\epsilon dx}{A}$$

$$=\frac{\rho_0}{A}\int_0^L\left[1-\left(\gamma+\frac{\delta\alpha T}{c_p d}\right)p\cos(\omega t-kx)\right]dx$$

$$=R_0\left[1-\frac{p(2-2\cos kL)^{\frac{1}{2}}}{kL}\left(\gamma+\frac{\delta\alpha T}{c_p d}\right)\sin(\omega t+\phi)\right], \tag{19}$$

where the phase angle is given by $\phi=\tan^{-1}\sin kL/(1-\cos kL)$. This result satisfies the condition that $R=R_0$, when L is an integral number of wavelengths, for then kL is a multiple of 2π and $(1-\cos kL)=0$.

(b) Resistance Changes When the Ultrasonic Waves Are Propagated Normal to the Direction of Current Flow in Rectangular Cells

Consider a conductivity cell comprising an insulating tube of rectangular cross section, with two parallel electrodes covering its ends (Fig. 2). Let plane, progressive ultrasonic waves be propagated parallel to the electrodes in the direction of the cell length L. The conductivity κ_ϵ within the element $MNdx$ is, from Eq. (17),

$$\kappa_\epsilon=\kappa_0\left[1+\left(\gamma+\frac{\delta\alpha T}{c_p d}\right)p\cos(\omega t-kx)\right]. \tag{20}$$

The total conductance is then

$$C=\int_0^L\frac{\kappa_\epsilon M dx}{N}$$

$$=C_0\left[1+\frac{p(2-2\cos kL)^{\frac{1}{2}}}{kL}\left(\gamma+\frac{\delta\alpha T}{c_p d}\right)\sin(\omega t+\phi)\right], \tag{21}$$

and therefore the resistance with this cell arrangement is also given by Eq. (19).

(c) Potential Drop Across the Cell

It is evident from Eq. (19) that the passage of a constant direct current through the cell produces a potential drop

$$E=E_0\left[1-\frac{p(2-2\cos kL)^{\frac{1}{2}}}{kL}\left(\gamma+\frac{\delta\alpha T}{c_p d}\right)\sin(\omega t+\phi)\right]. \tag{22}$$

Thus the ultrasonic effect produces an alternating potential having the same frequency as the ultrasonic waves. The amplitude of the ac potential varies with the distance L between the electrodes; it has a maximum value when L is an odd number of half-wavelengths and vanishes when L is a simple multiple of the wavelength.

The resistance of a conductivity cell is more generally measured with ac. Let a constant alternating current of relatively low frequency $\omega_1/2\pi$ be passed through the cell of Fig. 1 from a source of high internal impedance. The current, which may be written

$$i_0=E_0\sin\omega_1 t/R_0, \tag{23}$$

where $E_0\sin\omega_1 t$ is the voltage drop in the absence of ultrasonics, will remain unaffected by resistance changes produced by the acoustic waves. Hence the voltage

[11] A. Wood, *Acoustics* (Interscience Publishers, Inc., New York, 1941).

across the cell is

$$E=\frac{E_0\sin\omega_1 t}{R_0}\left[R_0-\frac{R_0 p}{kL}\left(\gamma+\frac{\delta\alpha T}{c_p d}\right)\times(2-2\cos kL)^{\frac{1}{2}}\sin(\omega t+\phi)\right]$$

$$=E_0\sin\omega_1 t-\frac{E_0 p}{kL}\left(\gamma+\frac{\delta\alpha T}{c_p d}\right)\left(\frac{1-\cos kL}{2}\right)^{\frac{1}{2}}\times[\cos\{(\omega-\omega_1)t+\phi\}-\cos\{(\omega+\omega_1)t+\phi\}]. \quad (24)$$

Thus the ultrasonic effect produces two equal side-band voltages, the frequencies of which are the sum and difference of the two frequencies, ultrasonic and electric. When $L=(2n-1)\lambda/2$, the side-band voltages have their maximum amplitude,

$$\frac{E_0 p}{(2n-1)\pi}\left(\gamma+\frac{\delta\alpha T}{c_p d}\right).$$

When the ultrasonic wavelength is large in comparison with the length of the cell, kL is a small angle and

$$\left(\frac{1-\cos kL}{2}\right)^{\frac{1}{2}}=\frac{kL}{2}. \quad (25)$$

The amplitude of the side-band voltages is then

$$\frac{E_0 p}{2}\left(\gamma+\frac{\delta\alpha T}{c_p d}\right).$$

This result is the same as that obtained by Fox, Herzfeld, and Rock[1] for a "detector" consisting of two fine wire electrodes brought close together, as expected.

Similarly it may be shown that, in the presence of stationary, plane ultrasonic waves the voltage across the cell, when ac is passed, becomes

$$E=E_0\sin\omega_1 t-\frac{E_0 p\sin kL}{2kL}\left(\gamma+\frac{\delta\alpha T}{c_p d}\right)\times\{\sin(\omega+\omega_1)t-\sin(\omega-\omega_1)t\}. \quad (26)$$

In this case the two side-bands have maximum amplitude when the length of the conductivity cell is an odd number of quarter wavelengths, and they vanish when it is a simple multiple of the half-wavelength.

V. DISCUSSION

The use of the interionic attraction theory to obtain the coefficients γ and δ permits computation of the side-band voltages for given values of E_0 and p. The literature contains little data on the pressure dependence of Λ_∞; hence one is generally unable to resort to the theory for the calculation of γ. If the temperature coefficient of Λ_∞ for a given electrolyte is known, however, $(\partial/\partial P)_T\ln\Lambda_\infty$ and γ for dilute solutions of that electrolyte may be obtained from a single measurement of the ultrasonic effect at atmospheric pressure.

If the dependence of Λ_∞ on both temperature and pressure are accurately determined for a given electrolyte, one could conceivably construct a hydrophone containing a solution of that electrolyte for precision calibration or exploration of ultrasonic fields in liquids.[1]

In order to indicate the magnitude of the side-band voltages, numerical data are given below for $10^{-4}M$ aqueous potassium chloride at 25°C. For this solution $\Lambda_\infty=149.85$ and $\partial/\partial T\ln\Lambda_\infty=0.01984$;[12] hence Eq. (15) gives $\delta=0.01956$/degree. Data are not available for the calculation of the pressure coefficient from Eq. (11); the approximate value $\gamma=13\times10^{-5}$/atmos was estimated from the data of Körber.[13] Substitution of these values into Eq. (24) gives, for $L=(2n-1)\lambda/2$, the maximum amplitude

$$5.3\times10^{-5}pE_0/(2n-1).$$

Thus the side-band voltages are predicted to be approximately 53 microvolts per atmosphere when unit voltage per half-wavelength is applied across the conductivity cell.

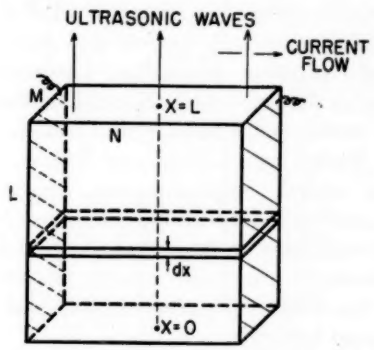

FIG. 2. Ultrasonic waves propagated normal to the direction of current flow.

[12] H. S. Harned and B. B. Owen, *The Physical Chemistry of Electrolytic Solutions* (Reinhold Publishing Corporation, New York, 1950), second edition, p. 590.

[13] F. Körber, Z. physik. Chem. **67**, 212 (1909).

A Study of Three-Center Integrals Useful in Molecular Quantum Mechanics*

ROLAND S. BARKER AND HENRY EYRING
Department of Chemistry, University of Utah, Salt Lake City, Utah, and Department of Chemistry, Princeton University, Princeton, New Jersey

(Received January 5, 1953)

An integrated equation for the three-center nuclear attraction integral has been formulated in a general way for Slater-type atomic s orbitals arising from any integral principle quantum number. No restrictions are placed on the effective nuclear charges or the interatomic distances. The formulation is expressed linearly in terms of certain auxiliary functions which are discussed in detail. Numerical values of some of the auxiliary functions for the triatomic hydrogen molecule are cited as examples of this exact formulation. An alternative approximate formulation is also given.

1. INTRODUCTION

THE accumulation of calculations of molecular quantum mechanics and the great need for further numerical work in this field has resulted in the systematic investigation of certain types of integrals. These integrals are needed for calculation of molecular energies, dipole moments, optical rotations, and other chemical and physical quantities. The two-center integrals used in diatomic molecular calculations are now (with the recent publications[1] of Coulson, Mullikan, Roothaan, Rudenberg, Kotani, and their co-workers) in fairly good shape. Such integrals, employing wave functions constructed by taking linear combinations of atomic orbitals, have in many cases convenient formulas. Furthermore, there are now available (for wide ranges of the basic parameters) tables[2] of values for many of these integrals.

Three- and four-center integrals needed for all polyatomic molecules, while not completely ignored, have received much less attention. Approximate formulas, it is true, have recently been investigated in some detail.[3] The undesirable, but in many cases useful, restriction of equal effective nuclear charges has been made in much of the comparatively little work done on the exact evaluation of multicentered integrals. James and Coolidge have evaluated a few by series methods,[4] while Hirschfelder, Eyring, and Rosen have (with the restriction of equal effective nuclear charges) evaluated several in closed form, using as a basis the three-center nuclear attraction integral.[5] This basic integral with the restriction of equal effective charges removed, and with generalization to higher orbitals is the subject of this paper.

2. GENERAL FORMULATION OF THE THREE-CENTER NUCLEAR ATTRACTION INTEGRAL

The general formula for the three-center nuclear attraction integral may be written

$$K_{g,AB}=\int \chi Z/r_g \chi' d\tau \equiv (\chi|Z/r_g|\chi'), \qquad (2.1)$$

where the functions χ, χ' represent the general AO's (atomic orbitals) on the nuclei A and B, respectively, and where r_g is the distance of an electron from nucleus g whose charge is Z. The integration is, of course, over the position coordinates of the electron. The Z/r_g is that part of the Hamiltonian operator derived from the potential energy of attraction of the electron and the g nucleus.

The choice of AO's for use in molecular quantum-mechanical calculations most consistent with published numerical tables and with the current literature would seem to be Slater-type AO's.[1] We have used special cases of Slater-type AO's in our current calculations of the triatomic hydrogen activated complex D−H−H as cited in later portions of this article. It should be noted that our formulas and auxiliary functions are here generalized to include any Slater-type atomic s orbitals in which both effective nuclear charges may be regarded as free parameters and in which only integral powers of the nuclear distance r occur. Atomic units (distances in units of the Bohr hydrogen atom radius and energies in units of twice the ionization energy of the hydrogen atom) are used. The centers are designated by A, B, and g; the distance between the centers of the AO's is taken as D, and the centers of the AO's are used as the foci of an elliptical coordinate system, defined[6] by

$$\mu=\frac{r_A+r_B}{D}; \quad \nu=\frac{r_A-r_B}{D},$$

ϕ = azimuthal angle of the electron.

* This work was assisted in part by a grant from the National Science Foundation.

[1] A comprehensive bibliography and an extensive literature survey may be found by consulting C. C. J. Roothaan, J. Chem. Phys. **19**, 1445 (1951) and K. Rudenberg, J. Chem. Phys. **19**, 1459 (1951).

[2] See Kotani, Amemiya, and Simose, Proc. Phys.-Math. Soc. Japan **20**, Extra No. 1 (1938); **22**, Extra No. 1 (1940); H. J. Kopineck, Z. Naturforsch. **5a**, 420 (1950).

[3] R. S. Mulliken, J. Chim. Phys. **46**, 497 (1949); K. Rudenberg, J. Chem. Phys. **19**, 1433 (1951).

[4] A. S. Coolidge, Phys. Rev. **42**, 189 (1932); A. S. Coolidge and James, J. Chem. Phys. **2**, 811 (1934).

[5] Hirschfelder, Eyring, and Rosen, J. Chem. Phys. **4**, 121 (1936); J. O. Hirschfelder and C. N. Weygandt, J. Chem. Phys. **6**, 806 (1938).

[6] The notation is that used in Eyring, Walter, and Kimball, *Quantum Chemistry* (John Wiley and Sons, Inc., New York, 1947), p. 367.

Conversely,

$$r_A=\tfrac{1}{2}D(\mu+\nu);\quad r_B=\tfrac{1}{2}D(\mu-\nu).$$

In these coordinates the volume element

$$d\tau=D^3/8(\mu^2-\nu^2)d\phi d\nu d\mu,$$

and the limits of integration for ϕ are from 0 to 2, for ν from -1 to 1, and for μ from 1 to ∞. The elliptical coordinates of the third fixed center are μ_g, ν_g, ϕ_g. (For the special case, when the three centers lie on a line with both external centers A and B the same distance R from the middle center g one has $D=R$; $\nu_g=1$; $\mu_g=3$.) The general formula for the three-center nuclear attraction integral using Slater-type s orbitals is

$$K_{g,AB}=C_1\int (r_A)^{n-1}e^{-\zeta r_A}(Z/r_g)(r_B)^{n'-1}e^{-\zeta' r_B}d\tau, \quad (2.2)$$

where

$C_1=(2\zeta)^{n+\frac{1}{2}}[(2n)!(2\pi)]^{-\frac{1}{2}}(2\zeta')^{n'+\frac{1}{2}}[(2n')!(2\pi)]^{-\frac{1}{2}}$,
n = principle quantum number of orbital A,
n' = principle quantum number of orbital B,
ζ = effective charge on nucleus of orbital A,
ζ' = effective charge on nucleus of orbital B.

When the AO's of the above integral are written in terms of an elliptical coordinate system with A and B taken as foci, one obtains a sum of integrals of the general type,

$$K=C_2\int\int\int Z/r_g\mu^p\nu^q e^{-\alpha\mu}e^{-\beta\nu}d\phi d\nu d\mu, \quad (2.3)$$

where

$\alpha=D/2(\zeta'+\zeta)$; $\beta=D/2(\zeta'-\zeta)$; C_2 = a constant.

For example, the triatomic hydrogen activated complex molecule may be formulated with $1s$ AO's with different effective charges on the middle and the end orbitals. In such a treatment one needs the integral

$$K_{a,bc}=C\int\int\int 1/r_g(\mu^2-\nu^2)e^{-\alpha\mu}e^{-\beta\nu}d\phi d\nu d\mu, \quad (2.4)$$

where

$C=D^3(Z_m^3Z_0^3)^{\frac{1}{2}}/8\pi$,
$\alpha=D/2(Z_m+Z_0)$; $\beta=D/2(Z_m-Z_0)$,
Z_m = effective charge on middle orbital,
Z_0 = effective charge on outer orbital.

It should be noted that formulas (2.3) and (2.4) are written in terms of hybrid coordinates, the inverse distance $1/r_g$ not as yet being expressed in elliptical coordinates. To perform the indicated integration this term may be expressed in terms of the fixed elliptical coordinates of the center g (μ_g, ν_g, and ϕ_g) and the coordinates (μ, ν, ϕ) of the electron, in the conventional manner by the Neumann[7] expansion. Thus,

$$1/r_g=2/D\sum_{\tau=0}^{\infty}\sum_{\eta=0}^{\tau}L_{\tau\eta}Q_\tau^\eta(\mu_+)P_\tau^\eta(\mu_-)P_\tau^\eta(\nu_g)P_\tau^\eta(\nu)\times\cos\eta(\phi_g-\phi), \quad (2.5)$$

where $L_{\tau 0}=(2\tau+1)$;

$$L_{\tau\eta}=(-1)^\eta 2(2\tau+1)\{(\tau-\eta)!/(\tau+\eta)!\}^2 \quad (\eta\geq 1),$$

and $\mu_+(\mu_-)$ is the larger (smaller) of μ_g and μ. The functions P_τ^η and Q_τ^η are the associated Legendre functions of the first and second kind.[8] On making the above substitution for $1/r_g$ in Eqs. (2.3) and (2.4) integration over the angle ϕ may be performed to give 2π for $\eta=0$ and zero for $\eta\geq 1$. The expression (2.3) then becomes

$$K=C_2\int\int\sum_{\tau=0}^{\infty}L_{\tau 0}Q_\tau(\mu_+)P_\tau(\mu_-)P_\tau(\nu_g)\times P_\tau(\nu)e^{-\alpha\mu}\mu^p e^{-\beta\nu}\nu^q d\nu d\mu \quad (2.6)$$

$$=C_2\sum_{\tau=0}^{\infty}L_{\tau 0}P_\tau(\nu_g)\times\left[\left(\int_1^\infty \mu^p e^{-\alpha\mu}Q_\tau(\mu_+)P_\tau(\mu_-)d\mu\right)\times\left(\int_{-1}^{1}\nu^q P_\tau(\nu)e^{-\beta\nu}d\nu\right)\right] \quad (2.7)$$

$$=C_2\sum_{\tau=0}^{\infty}L_\tau P_\tau(\nu_g)\cdot M_\tau(\mu_g,p,\alpha)\cdot G_\tau(q,\beta), \quad (2.8)$$

where one defines the auxiliary functions

$$M_\tau(\mu_g,p,\alpha)=P_\tau(\mu_g)\cdot\int_{\mu_g}^{\infty}\mu^p e^{-\alpha\mu}Q_\tau(\mu)d\mu+Q_\tau(\mu_g)\cdot\int_1^{\mu_g}\mu^p e^{-\alpha\mu}P_\tau(\mu)d\mu \quad (2.9)$$

$$=P_\tau(\mu_g)\cdot f_\tau(p,\mu_g,\infty,\alpha)+Q_\tau(\mu_g)\cdot G(p,1,\mu_g,\alpha), \quad (2.9')$$

$$G_\tau(q,\beta)=\int_{-1}^{1}\nu^q P_\tau(\nu)e^{-\beta\nu}d\nu \quad (2.10)$$

(values tabulated by Kotani).

Similarly, the three-center nuclear attraction integral of the triatomic hydrogen molecule (2.4) becomes

$$K_{a,bc}=C\sum_{\tau=0}^{\infty}L_\tau P_\tau(\nu_g)[M_\tau(\mu_g,2,\alpha)\cdot G_\tau(0,\beta)-M_\tau(\mu_g,0,\alpha)\cdot G_\tau(2,\beta)]. \quad (2.11)$$

[7] A short derivation of the Neumann expansion in elliptical coordinates has recently been given by K. Rudenberg. See reference 1.

[8] Our definitions are those of T. M. MacRobert, *Spherical Harmonics* (Dover Publications, New York, 1948) or E. Jahnke and F. Emde, *Tables of Functions* (Dover Publications, New York, 1945). It should be noted that the Legendre polynomials originally used by Neumann and later used in quantum-mechanical derivations by Sugiura (see reference 23) are just twice those used here, and that their L_τ term coefficient, must accordingly be adjusted.

where, $C=\frac{1}{2}D^2(Z_m{}^3Z_0{}^3)^{\frac{1}{2}}$. Any three-center nuclear attraction integral involving only Slater-type s orbitals may thus be obtained in terms of a rapidly converging series involving the two auxiliary functions $G_\tau(q, \beta)$ and $M_\tau(\mu_0, p, \alpha)$.

3. AUXILIARY FUNCTIONS

One of the two main auxiliary functions needed, $G_\tau(q, \beta)$, is well known. Recurrence relations[9] and tabulated values $\beta=0.0(0.25)5.50$ and $\beta=6.0(0.50)7.0$ have been given by Kotani.[10]

It might be mentioned at this point that these $G_\tau(q, \beta)$ functions are special cases of the $w_n{}^l(\beta)$ functions of Rudenberg,[1] which he pointed out would occur in the three-center nuclear attraction integrals.

The other auxilary function $M_\tau(\mu_0, p, \alpha)$ is used here for the first time to our knowledge. Recurrence formulas are given in later portions of this paper for the evaluation of this function in terms of the parameters ζ_a, ζ_b, and R. This new auxilary function has been defined by Eqs. (2.9) or (2.9′) in terms of Legendre polynomials of the first and second kind. Formulas for these polynomials in terms of fixed values of the parameters are well known.[11] The needed values may also be obtained from tables.[8] The evaluation of $M_\tau(\mu_0, p, \alpha)$ thus reduces to the evaluation of two secondary auxilary functions defined as

$$G_\tau(p, 1, \mu_0, \alpha)=\int_1^{\mu_0}\mu^p e^{-\alpha\mu}P_\tau(\mu)d\mu \qquad (3.1)$$

and

$$f_\tau(p, \mu_0, \infty, \alpha)=\int_{\mu_0}^{\infty}\mu^p e^{-\alpha\mu}Q_\tau(\mu)d\mu. \qquad (3.2)$$

The secondary auxilary function $G_\tau(p, 1, \mu_0, \alpha)$ is similar to the $G_\tau(p, \alpha)$ function used by Kotani and discussed before Eq. (2.10). In fact, except for the limits, it is the same function. It is not surprising, therefore, that the recurrence formulas for these functions are identical. That is,

$$(2\tau+1)G_\tau(m+1, 1, \mu_0, \alpha) = \tau G_{\tau-1}(m, 1, \mu_0, \alpha)+(\tau+1)G_{\tau+1}(m, 1, \mu_0, \alpha). \qquad (3\,3)$$

The initial members of the function for use in the above recurrence relation may be computed, as outlined in reference 10, by expanding (when α is small) the exponential component under the integral sign as a series and then integrating term by term, or by use of defined $B_m(1, \mu_0, \alpha)$ functions similar though differing in initial value and recurrence formula, to those used by Kotani.[2] These $B_m(1, \mu_0, \alpha)$ functions are here defined as

$$B_m(-, -, \alpha)=\int e^{-\alpha\mu}\mu^m d\mu,$$

$$B_m(1, \mu_0, \alpha)=\int_1^{\mu_0} e^{-\alpha\mu}\mu^m d\mu,$$

$$B_m(\mu_0, \infty, \alpha)=\int_{\mu_0}^{\infty} e^{-\alpha\mu}\mu^m d\mu.$$

They have the recurrence relations[12]

$$B_m(-, -, \alpha)=1/\alpha[mB_{m-1}(-, -, \alpha)-\mu^m e^{-\alpha\mu}], \qquad (3.4)$$

$$B_m(1, \mu_0, \alpha) = 1/\alpha[e^{-\alpha}-\mu_0{}^m e^{-\alpha\mu_0}+mB_{m-1}(1, \mu_0, \alpha)], \qquad (3.4')$$

$$B_m(\mu_0, \infty, \alpha) = 1/\alpha[\mu_0{}^m e^{-\alpha\mu_0}+mB_{m-1}(\mu_0, \infty, \alpha)]. \qquad (3.4'')$$

An outline similar to that given in reference 11 may then be followed to obtain any desired value of $G_\tau(p, 1, \mu_0, \alpha)$.

The other secondary auxilary function $f_\tau(p, \mu_0, \infty, \alpha)$ is defined by Eq. (3.2). This function is similar to Rosen's function[13] $f_\tau(p, \alpha)$. It may be evaluated by use of the relations (3.4), (3.5), and (3.6) given below. The general recurrence relationship[14] is

$$(\tau+1)f_{\tau+1}(m, \mu_0, \infty, \alpha) = (2\tau+1)f_\tau(m+1, \mu_0, \infty, \alpha) - \tau f_{\tau-1}(m, \mu_0, \infty, \alpha); \quad (\tau\geq 1). \qquad (3.4''')$$

Initial values of the functions needed for use in the above recurrence formula may be obtained by calculating $f_0(m, \mu_0, \infty, \alpha)$ and $f_1(m, \mu_0, \infty, \alpha)$. The first of these functions may be calculated[15] by Eq. (3.5),

$$f_0(m, \mu_0, \infty, \alpha)=\tfrac{1}{2}\int_{\mu_0}^{\infty}\mu^m e^{-\alpha\mu}\ln\left(\frac{\mu+1}{\mu-1}\right)d\mu = \tfrac{1}{2}\ln\left(\frac{\mu_0+1}{\mu_0-1}\right)\cdot B_m(\mu_0, \infty, \alpha) - T_m(\mu_0, \infty, \alpha), \qquad (3.5)$$

---

[9] The recurrence formula, $(2\tau+1)G_\tau(m+1, \alpha)=\tau G_{\tau-1}(m, \alpha)+(\tau+1)G_{\tau+1}(m, \alpha)$ is obtained directly from the definition of $G_\tau(m, \alpha)$ and the recurrence relation of Legendre polynomials, $(\tau+1)P_{\tau+1}(\mu)=(2\tau+1)\mu P_\tau(\mu)-\tau P_{\tau-1}(\mu)$. For properties and relations of Legendre polynomials see E. W. Hobson, *Spherical and Ellipsoidal Harmonics* (Cambridge University Press, Cambridge, 1931).

[10] See reference 2. Kotani evaluated his tabulated values of $G_\tau(q, \beta)$ by calculating a set of values of $G_\tau(0, \beta)$ [by either expanding the exponential term in the integral as a series and integrating or by use of defined $B_m(\beta)$ functions]. Then using the relation given in reference 10 he calculated a set of $\tau-1$ values of $G_\tau(1, \beta)$. This set of $G_\tau(1, \beta)$'s was then used to calculate a $\tau-2$ set of $G_\tau(2, \beta)$'s and so forth. The final function $G_0(\tau, \beta)$ obtained was checked against the value of $B_\tau(\beta)$.

[11] See, for example, W. E. Byerly, *Fourier's Series and Spherical, Cylindrical, and Ellipsoidal Harmonics* (Ginn and Company, Boston, 1893), pp. 151, 190.

[12] These equations follow from definition, and an elementary integration formula. See, for example, B. O. Peirce *A Short Table of Integrals* (Ginn and Company, Boston, 1929), p. 53, No. 403.

[13] N. Rosen, Phys. Rev. 38, 507 (1931).

[14] This relation may be derived from the definition Eq. (3.2) and the recurrence formula for Legendre polynomials of the second kind. See, for example, reference 11, p. 190, No. 9.

[15] The equation is obtained on integration by parts and use of definition (3.5′) and (3.5″).

in which

$$B_m(\mu_0, \infty, \alpha) = \int_{\mu_0}^{\infty} e^{-\alpha\mu}\mu^m d\mu$$

(see recurrence formula 3.4″),

$$T_m(\mu_0, \infty, \alpha) = \int_{\mu_0}^{\infty} B_m(-, -, \alpha)\cdot\tfrac{1}{2}d\left\{\ln\left(\frac{\mu+1}{\mu-1}\right)\right\}$$

$$= (m/\alpha)T_{m-1}(\mu_0, \infty, \alpha) - (1/\alpha)N_m(\mu_0, \infty, \alpha). \quad (3.5')$$

The relationship (3.5′) follows from Eq. (3.4″) and the definition

$$N_m(\mu_0, \infty, \alpha) \equiv \int_{\mu_0}^{\infty} \mu^m e^{-\alpha\mu} d\{Q_0(\mu)\}$$

$$= -B_{m-2}(\mu_0, \infty, \alpha) + N_{m-2}(\mu_0, \infty, \alpha). \quad (3.5'')$$

The derivation of Eq. (3.5″) is long.[16]

The values

$$N_0(\mu_0, \infty, \alpha) = -e^{\alpha}/2Ei\{-\alpha(\mu_0+1)\} + e^{-\alpha}/2Ei\{-\alpha(\mu_0-1)\},$$

$$N_1(\mu_0, \infty, \alpha) = e^{\alpha}/2Ei\{-\alpha(\mu_0+1)\} + e^{-\alpha}/2Ei\{-\alpha(\mu_0-1)\}$$

may be obtained from the definition (3.5″) after a change of variable as outlined in reference 16 and use of the definition of the exponential integral. The exponential integral[17] (or integral logarithm) is defined as

$$Ei(x) = -\int_{x}^{\infty} e^{-x}/x dx.$$

[16] The derivation proceeds by replacing $Q_0(\mu)$ in the definition of $N_m(\mu_0, \infty, \alpha)$, Eq. (3.5″) by its value $Q_0(\mu) = \frac{1}{2}\ln(\mu+1)/(\mu-1)$. Integration of the two integrals resulting after such substitution and the splitting of the logarithm into the difference of the logarithms of its numerator and denominator is performed by change of the variable. Thus the integration of

$${}_nN_m(\mu_0, \infty, \alpha) = \tfrac{1}{2}\int_{\mu_0}^{\infty} \mu^m e^{-\alpha\mu} d\{\ln\alpha(\mu+1)\}$$

is made by letting $x = \alpha(\mu+1)$, $\mu^2 = ((x^2/\alpha^2) - (2x/\alpha) + 1)$. The integral then may be written as

$${}_nN_m(\mu_0, \infty, \alpha) = e^{\alpha}/2\int_{\mu_0}^{\infty} \mu^{m-2}(x^2/\alpha^2 - 2x/\alpha + 1)e^{-x}dx/x$$

and finally as the algebraic sum of three integrals. The integral resulting from the denominator part of the logarithm ${}_dN_m(\mu_0, \infty, \alpha)$ may be converted into a similar form by the substitution $y = \alpha(\mu-1)$, $\mu^2 = (y^2/\alpha^2 + 2y/\alpha + 1)$. Conversion of the variables x and y back to the original variable μ then allows collection of terms to give Eq. (3.5″) the recurrence relationship desired.

[17] For values of the exponential integral see the two volume set of tables *Tables of Sine, Cosine and Exponential Integral*, prepared by the Federal Works Agency under the sponsorship of the National Bureau of Standards (N.Y.M.T.P., 1940).

Values for $f_1(m, \mu_0, \infty, \alpha)$ are obtained from the relationship[18]

$$f_1(m, \mu_0, \infty, \alpha) = f_0(m+1, \mu_0, \infty, \alpha) - B_m(\mu_0, \infty, \alpha). \quad (3.6)$$

4. A SHORT DERIVATION OF THE EQUAL APPARENT CHARGE FORMULA

The above general method for evaluating three-center nuclear attraction integrals may now be illustrated by deriving the special case of formula (2.11) used by Hirschfelder,[5] (obtained as a by-product of Sugiura's work[19] and also obtained by Schuchowsky[20] and Gordadse,[21] where $\zeta_A = \zeta_B$.

The desired integral[22] is

$$K_{0,AB} = 1/\pi \int 1/r_{01} e^{-r_{a1}-r_{b1}} d\tau_1. \quad (4.1)$$

This expression is written in elliptical coordinates, the $1/r_0$ term expanded in the Neumann series and integration over the angle ϕ performed in the usual way to give

$$K_{0,AB} = k\sum_{\tau=0}^{\infty} L_\tau P_\tau(\nu_0)[M_\tau(\mu_0, 2, \alpha)\cdot G_\tau(0, 0) - M_\tau(\mu_0, 0, \alpha)\cdot G_\tau(2, 0)]. \quad (4.2)$$

In this expression

$$k = \frac{D^2}{2}; \quad L_\tau = 2\tau+1.$$

From the properties of Legendre polynomials, the definition of the function $G_\tau(p, 0)$ and the fact that any power τ of μ may be expressed as a sum of Legendre polynomials in μ of order no greater than τ, it follows that $G_\tau(p, 0) = 0$ for all $\tau > p$. The above series expansion of $K_{0,AB}$ is thus seen to be finite. The integral is

$$\begin{aligned} K_{0,AB} &= k[L_0P_0(\nu_0)\{M_0(\mu_0, 2, \alpha)\cdot G_0(0, 0) - M_0(\mu_0, 0, \alpha)\cdot G_0(2, 0)\} \\ &\quad + L_2P_2(\nu_0)\{0 - M_2(\mu_0, 0, \alpha)\cdot G_2(2, 0)\}] \\ &= k[M_0(\mu_0, 2, \alpha)\cdot G_0(0, 0) \\ &\quad - M_0(\mu_0, 0, \alpha)\cdot G_0(2, 0) \\ &\quad - 5\cdot\{\tfrac{1}{2}(3\nu_0^2 - 1)\}M_2(\mu_0, 0, \alpha)\cdot G_2(2, 0)]. \end{aligned} \quad (4.3)$$

The above expression may be further simplified by evaluating the $G_\tau(q, \beta)$'s in the equation. From the definition (2.10) and elementary integration it follows

[18] Equation (3.6) follows at once from definition (3.2) and the relation $Q_1(\mu) = \mu Q_0(\mu) - 1$.

[19] Y. Sugiura, Z. Physik **45**, 484 (1927).

[20] A. Schuchowsky, Acta Physicochim. U.R.S.S. **1**, 901 (1934).

[21] G. Gordadse, Z. Physik **96**, 542 (1935).

[22] If the ζ's are not equal to one, the integral may still be written as given above, if the substitution $\rho = \zeta r$ is made and the integral multiplied by ζ.

TABLE I. Values of $G_\tau(q, \beta)$ from Kotani. $\beta=0.25$.

τ	$G_\tau(0, 0.25)$	$G_\tau(2, 0.25)$
0	2.020 8985	0.679 2132
1	−0.167 7107	−0.100 7459
2	0.008 3706	0.273 8405
3	−0.000 2986	−0.028 9031
4	0.000 0083	0.001 5987
5	−0.000 0002	−0.000 0604
6	0.000 0000 04	0.000 0017 4

that

$$G_0(0, 0)=2,$$
$$G_0(2, 0)=2/3,$$
$$G_2(2, 0)=4/15.$$

The integral may then be written

$$K_{g,AB}=2k[\{M_0(\mu_g, 2, \alpha)-1/3M_0(\mu_g, 0, \alpha)+1/3M_2(\mu_g, 0, \alpha)\}-\nu_g^2M_2(\mu_g, 0, \alpha)]$$
$$=K_0(D, \mu_g)+\nu_g^2K_2(D, \mu_g). \quad (4.4)$$

Use of the auxilary functions given earlier in the paper allows one to obtain

$$M_0(\mu_g, 0, \alpha)=\frac{e^{-\alpha}}{\alpha}Q_0(\mu_g)+\frac{e^{-\alpha}}{2\alpha}Ei\{\alpha(\mu_g-1)\}-\frac{e^{\alpha}}{2\alpha}Ei\{-\alpha(\mu_g+1)\}, \quad (4.5)$$

$$M_0(\mu_g, 2, \alpha)=Q_0(\mu_g)B_2(1, \infty, \alpha)+\frac{2}{\alpha^3}\left[-\frac{e^{\alpha}}{2}Ei\{-\alpha(\mu_g+1)\}+\frac{e^{-\alpha}}{2}Ei\{-\alpha(\mu_g-1)\}\right]+\frac{2}{\alpha^2}\left[\frac{e}{2}Ei\{-\alpha(\mu_g+1)\}+\frac{e^{-\alpha}}{2}Ei\{-\alpha(\mu_g-1)\}\right]+\frac{1}{\alpha}\left[\frac{-e^{-\alpha\mu_g}}{\alpha}-\frac{e^{\alpha}}{2}Ei\{-\alpha(\mu_g+1)\}+\frac{e^{-\alpha}}{2}Ei\{-\alpha(\mu_g-1)\}\right], \quad (4.6)$$

$$M_2(\mu_g, 0, \alpha)=3/4(\mu_g^2-1/3)Q_0(\mu_g)\times[3B_2(1, \infty, \alpha)-B_0(1, P, \alpha)]-3/4(\mu_g^2-1/3)[3T_2(\mu_g, \infty, \alpha)-T_0(\mu_g, \infty, \alpha)+3B_1(\mu_g, \infty, \alpha)]-9/4\mu_gB_2(1, \mu_g, \alpha)+3/4\mu_gB_0(1, \mu_g, \alpha). \quad (4.7)$$

Putting the above values of $M_\tau(\mu_g, p, \alpha)$'s in Eq. (4.4) then leads to

$$K_0(D, \mu_g)=3/4D(\mu_g^2+1)U-3\mu_g/2D\cdot I(D)+e^{-D\mu_g}(3\mu_g/2D-\tfrac{1}{2}) \quad (4.8)$$

$$K_2(D, \mu_g)=-9/4D(\mu_g^2-1/3)U+9\mu_g/2D\cdot I(D)-3e^{-D\mu_g}(3\mu_g/2D+\tfrac{1}{2}), \quad (4.9)$$

where

$$U=I(D)\left[\ln\frac{\mu_g+1}{\mu_g-1}+Ei\{-D(\mu_g-1)\}\right]-F(D)Ei\{-D(\mu_g+1)\},$$
$$I(D)=e^{-D}(D^2/3+D+1); \quad F(D)=e^{D}(D^2/3-D+1).$$

These values of $K_0(D, \mu_g)$ and $K_2(D, \mu_g)$ in Eq. (4.4) give the formula for the special case of equal charges as cited by Hirschfelder.[5] This may be further restricted when the three centers lie on a line with both external centers A and B the same distance R from the middle center g (for example, $D=R$; $\nu_g=1$; $\mu_g=3$) to give the formula

$$K_{a,bc}=-12U/R+9/R\cdot I(R)+e^{-3R}(-2-9/R),$$

where

$$U=I(R)[\ln 2+Ei(-2R)]-F(R)Ei(-4R),$$
$$I(R)=e^{-R}(1+R+R^2/3); \quad F(R)=e^{R}(1-R+R^2/3).$$

5. AIDS IN EVALUATION OF THE GENERAL UNEQUAL CHARGE INTEGRAL

The general integral (2.11) is expressed as a series of terms. Values of $G_\tau(q, \beta)$ are available. Their rapid convergence may be seen from the values[2] given in Table I. For calculations of the three-center integral used in the linear symmetrical triatomic hydrogen molecule where $\nu_g=1$, $P_\tau(\nu_g)=1$ for all values of τ.

6. AN APPROXIMATE FORMULA FOR THE NUCLEAR ATTRACTION INTEGRAL

In some cases it is desirable to be able to evaluate nuclear attraction integrals with different effective charges approximately. This sacrifices exactness for some saving in time. As the two-center nuclear attraction integral formula for atomic orbitals for both equal and unequal effective charge have been obtained in closed form, these are used first as examples before extension to the three-center integral is made. The two-center nuclear attraction integral is

$$J_{a,ab}=Z(\zeta_a^3\zeta_b^3)^{\frac{1}{2}}/\pi\int 1/r_ae^{-(\zeta_ar_a+\zeta_br_b)}d\tau, \quad (6.1)$$

If $\zeta_a=\zeta_b=\zeta$, the well-known integration formula

$$J_{a,ab}=\zeta[e^{-\rho}(\rho+1)] \text{ is applicable,} \quad (6.2)$$
$$\rho=\zeta R; \quad R=\text{distance between centers.}$$

At first glance, one might expect that a fair approximation for different effective charges on centers a and b would be found using the average of ζ_a and ζ_b as ζ in formula (6.2). A much better approximate evaluation, however, was obtained using $\zeta=\zeta_a$ in this formula as was demonstrated by a direct comparison of the results from such evaluations against that obtained using the closed form integration formula of Coulson,[23]

$$J_{a,ab}=\frac{4(\zeta_a^3\zeta_b^3)}{RX^2}[2\zeta_b e^{-\zeta_a R}-(2\zeta_b+RX)e^{-\zeta_b R}], \quad (6.3)$$

where

$$X=(\zeta_b^2-\zeta_a^2).$$

[23] C. A. Coulson, Proc. Cambridge Phil. Soc. **38**, 210 (1942).

Similar results are obtained for the three-center nuclear attraction integral. Thus $K_{a,bc}$ evaluated by use of integration formula (4.4) in the form

$$K_{a,bc}=\zeta[K_0(\rho,\mu_\sigma)+\mu_\sigma^2 K_2(\rho,\mu_\sigma)],$$

($\rho=\zeta R$; $K_0(\rho,\mu_\sigma)$ and $K_2(\rho,\mu_\sigma)$ are defined by Eqs. (4.8) and (4.9)) with $\zeta=\zeta_a=\zeta_c$ is superior to the approximation obtained by taking $\zeta=\frac{1}{3}(\zeta_a+\zeta_b+\zeta_c)$, as may be verified using the exact formulation 2.11.

We would like to acknowledge helpful discussions of phases of this problem with Professor C. J. Thorne (Mathematics Department, University of Utah), Professor M. Kotani (Tokyo Imperial University, Japan), and Professor J. O. Hirschfelder (University of Wisconsin).

THE JOURNAL OF CHEMICAL PHYSICS VOLUME 21, NUMBER 5 MAY, 1953

Manometric Determination of the Density of Liquid Ozone

CALLAWAY BROWN AND KARL D. FRANSON
Laboratory of Ozone Technology, Armour Research Foundation of Illinois Institute of Technology, Chicago, Illinois

(Received October 22, 1952)

A manometric method for density of liquids at low temperatures is described and applied to liquid ozone. Results in g cm^{-3}: 1.571 at −183°C, 1.595 at −188°C, and 1.614 at −195°C with an average deviation from the mean of ±0.003. A simple method of test for magnetic susceptibility of low temperature liquid is described and used to detect residual oxygen in liquid ozone. Vacuum distilled liquid ozone is shown to contain less than 0.1 percent oxygen.

INTRODUCTION

IN the course of the development of an analytical method for liquid ozone-oxygen mixtures, the need arose for an accurate value of the density of pure liquid ozone in order to prepare analytical standards volumetrically. The literature revealed only the value 1.71±0.05 g cm^{-3} at 183°C, Riesenfeld and Schwab.[1] In view of the large uncertainty thus indicated in the density, it was decided to reinvestigate the problem.

A manometric method for density was devised, essentially the inverse of measurement of a pressure differential across a U-tube manometer. A known pressure difference is applied across a U-tube manometer containing liquid ozone and the density is calculated from the measured head of liquid.[2] This method proved especially suitable for liquid ozone since the measurement is independent of the amount of liquid used and requires only that the hydrostatic head of liquid produced by a known pressure be measured.

Ozone was purified by vacuum distillation and virtually complete removal of oxygen was demonstrated by the absence of measurable magnetic susceptibility in the liquid. Refrigeration of a strong permanent magnet in the cooling bath used for the liquid ozone permitted the use of a simple and novel method of test for magnetic susceptibility of liquid at low temperature.

EXPERIMENTAL PROCEDURE

Concentrated liquid ozone was obtained by passage of a stream of ozonized oxygen, from a laboratory ozonizer of the corona discharge type, through a receiver tube cooled in liquid oxygen. The liquid ozone was freed from oxygen by distillation in the all glass vacuum system shown schematically in Fig. 1.

The receiver tube R, containing approximately 1 cc of liquid ozone from the laboratory ozonizer, was connected to the system by means of a ground glass joint. The apparatus was evacuated with traps T_1, T_5, and T_6 cooled in liquid nitrogen and the liquid ozone in tube R cooled in liquid oxygen, so that ozone distilled slowly into trap T_1 at −195°C. The traps T_5 and T_6, packed with glass rod to increase the cold surface in contact with vapor, served to condense vapors from the pump side which might contaminate the ozone. After all the ozone had distilled into T_1, trap T_2 was cooled in liquid nitro-

[1] E. H. Riesenfeld and G-M. Schwab, Z. Physik **11**, 12 (1922).

[2] Since this work was completed it has been called to the attention of the writers that the Fisher-Davidson Gravitometer, marketed by the Fisher Scientific Company, Pittsburg, Pennsylvania, utilizes this principle to determine specific gravity of liquids at room temperature. This instrument is based on U. S. Patent 2,328,787 (1943) issued to D. Davidson, M. Popowski, and P. Rosenblatt.

gen and ozone was distilled slowly from T_1, either by substitution of liquid oxygen for liquid nitrogen in the cooling bath on T_1 or by dropping the level of the refrigerant below T_1. Similarly the ozone was distilled into T_3 from which it drained into the U-tube manometer M_1 (2 mm capillary tubing). The ozone was thus vacuum distilled and condensed three times under continual pumping to remove residual oxygen.

A pressure differential was applied across the two arms of the U-tube M_1 by admission of a low pressure of helium to the system with stopcock S_4 closed. The manometer M_2 containing concentrated sulfuric acid then permitted a direct comparison of the hydrostatic head of ozone h_1 with the head of sulfuric acid h_2. Since the product of the liquid head and density was equal for the two liquids, the density of liquid ozone, $d_1=h_2d_2/h_1$, where d_2 is the density of the sulfuric acid, predetermined accurately in a pycnometer. The heads of liquid in the two manometers, adjusted to fall in the range of 100 to 200 mm, were read with a cathetometer. The refrigerant for the liquid ozone in M_1 was contained in an unsilvered Dewar flask to permit direct reading of the head of liquid ozone with a cathetometer.

Helium was purified before admission to the system by passage through trap T_7 which was packed with activated charcoal and cooled in liquid nitrogen. A fine sintered glass filter in the inner tube of trap T_7 was inserted as a precaution against passage of traces of the activated charcoal into the liquid ozone. Component parts of the apparatus were cleaned carefully before assembly with chromic acid cleaning solution, followed by distilled water. Immediately prior to each run the apparatus was flamed with a Bunsen burner while a stream of oxygen flowed through it. At the end of a run ozone was distilled from the U-tube into the trap T_4, then allowed to evaporate into a stream of oxygen flowing from the pump side through stopcock S_1 and out into a ventilated hood through the joint at R.

MAGNETIC SUSCEPTIBILITY

The effectiveness of the vacuum distillation in the removal of oxygen was checked by tests of the magnetic susceptibility of the liquid collected in the manometer M_1. Lainé has shown that the magnetic susceptibility of pure liquid ozone is no more than 0.15×10^{-6} cgs units at -196°C,[3] a value less than 0.1 percent that of pure liquid oxygen. Significant paramagnetism in the liquid may therefore be taken as an indication that oxygen is incompletely removed.

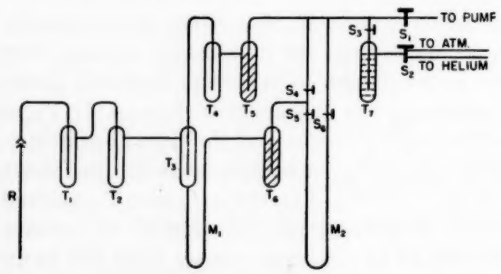

FIG. 1. Apparatus for density and magnetic susceptibility of liquid ozone.

The right arm of the U-tube M_1 was placed in the pole gap of a strong permanent magnet which was arranged for vertical adjustment by remote control in order to bring the ozone liquid-vapor boundary into the center of the magnet gap. The entire assembly was immersed in liquid nitrogen in a large, unsilvered Dewar flask. Refrigeration of the magnet along with the liquid ozone permitted use of a pole gap just wide enough to pass the 3-mm glass tubing used in the right arm of manometer M_1. In such a narrow pole gap a high magnetic flux density (*ca* 9000 gauss) was obtained with an Alnico V magnet of moderate size. The magnet used was the $A1007$ magnetizer magnet of the Indiana Steel Products Company, Valparaiso, Indiana, with pole pieces adjusted for $\frac{1}{8}$-in. pole gap.

With this assembly the magnetic susceptibility of liquid in the U-tube was measured by the height of the column of liquid supported by the magnetic field. The height of this column was read with a cathetometer. Liquid oxygen was used as a reference liquid and was lifted by the magnetic field approximately 100 mm. Liquid ozone, distilled as described above, showed a lift in the magnetic field of no more than 0.1 mm. Since this was approximately the limit of accuracy in reading, no conclusions concerning the paramagnetism of liquid ozone are attempted but it is concluded that the oxygen content of the triple distilled liquid ozone did not exceed 0.1 percent. Development of an analytical method for liquid ozone-oxygen mixtures based on the paramagnetism of liquid containing oxygen is now approaching completion and magnetic measurements will be discussed in more detail in a forthcoming publication.

DENSITY RESULTS

The results of six density runs at three different temperatures are given in Table I. Temperatures were read with an oxygen vapor pressure thermometer. Each result represents the average of at least four readings of the hydrostatic heads of liquid ozone and sulfuric acid. The deviations listed are the average deviation from the mean density calculated from these readings. The temperatures were maintained with boiling liquid nitrogen at -195.4°, boiling liquid oxygen at -183°C, and a boiling mixture of nitrogen and oxygen at -188.7° to -187.9°, listed in the table as -188°.

SOURCES OF ERROR

The manometric method for density is independent of the quantity of sample used, an advantageous feature in the handling of ozone which is subject to decomposition at normal temperatures. The method was checked for systematic error by measurement of the density of

[3] P. Lainé, Ann. phys. **3**, 461 (1935).

liquid oxygen. In four check runs on oxygen, the following values of density at −195°C were obtained: 1.190±0.004, 1.208±0.006, 1.212±0.008, 1.205±0.006 g/cc. These are to be compared with 1.201 at −195°, listed in the International Critical Tables.[4] More variable results were obtained with oxygen than with ozone because a steady pressure head of helium across the liquid in the U-tube was more difficult to hold with a volatile liquid.

Drift of the head of liquid during the course of measurement was the source of the deviations encountered. Since temperature throughout the system was nonuniform, slight changes in the level of the refrigerating liquids cause the pressure to change sufficiently to be reflected in the hydrostatic head of liquid. To prevent this source of error from being systematic, alternate readings of the four manometric liquid levels were made in reverse order. That is, first liquid ozone lower level, liquid ozone upper level, sulfuric acid lower level, sulfuric acid upper level then the same readings in reverse order were made. This procedure magnified the average deviation of the density calculated from the ratio of the heads of the two liquids, but assured the bracketing of the true ratio of the liquid heads.

The density of the concentrated sulfuric acid used as a reference liquid was determined gravimetrically with a pycnometer before use in the manometer and later by the manometric method using water as the reference liquid. The manometric density was about 0.3 percent higher than the original density measured gravimetrically, probably caused by loss of water during use in the vacuum apparatus. Since the manometric determinations were directly comparable, the manometric value of 1.8305±0.0025 g-cm^{-3} was used. The average deviation of ±0.14 percent is substantially larger than that of good gravimetric determinations, but is only about 30 percent of the average deviation of the sulfuric acid reference liquid in use in the vacuum system. The density determined manometrically with water as a reference liquid appears to be a safer reference standard. One run was made in which liquid ozone was compared directly with a water reference standard. The result at −195°C was 1.60±0.015 g-cm^{-3}. The average deviation was considerably higher than in the runs with nonvolatile sulfuric acid as a reference standard, due to a more rapidly drifting pressure head across the manometers. This run was made, however, with a pressure of one atmosphere of helium on both arms of the manometer and the liquid head was produced with a relatively small pressure differential across the manometers in contrast to the runs of Table I in which a vacuum was held on the low pressure arms of the manometers, the entire helium pressure being a differential pressure. Substantial agreement in the two cases indicates that there is no systematic error due to the temperature gradients in the system. The density of liquid ozone as reported in Table I thus appears reasonably certain to be correct within the limits of error indicated.

TABLE I. Density of liquid ozone. Reference liquid-sulphuric acid, d=1.8305 g/cc.

Temperature °C		Density g-cm^{-3}
−195.4°		1.615±0.003
−195.4°		1.613±0.003
−195.4°		1.613±0.004
−195.4°		1.615±0.005
−195.4°	Average	1.614±0.004
−188°		1.595±0.003
−183.0°		1.571±0.003

A search of the literature indicates that the only previous determination of the density of pure liquid ozone is that of Riesenfeld and Schwab.[1,5] These investigators measured the volume of a column of liquid ozone in a capillary tube and determined the mass gravimetrically. The results of six measurements at −183°C gave a value of 1.71±0.05 g-cm^{-3}, about 9 percent higher than the present results. No proof is reported that oxygen was entirely eliminated from the liquid ozone used. Since any oxygen in their samples would largely volatilize and be counted in the measured weight of ozone but not in the volume of the condensed liquid, the presence of oxygen may account for the higher value of the density obtained in their work. Incidentally this figure is 1.5 times the accepted value[4] for liquid oxygen of 1.14 at −183°, which is implausible as it would imply that triatomic ozone has the same molar volume as diatomic oxygen in the liquid state.

The writers are grateful to co-workers at Armour Research Foundation for many helpful suggestions on the handling of concentrated liquid ozone, especially C. E. Thorp, L. C. Kinney, and R. F. Remaly.

This work is part of a research program carried out under contract with the Air Reduction Company, New York, New York.

[4] *International Critical Tables* (McGraw-Hill Book Company, Inc., New York), Vol. 3, p. 20.

[5] G-M. Schwab, Z. physik. Chem. **110**, 599 (1924).

On Polarization in Liquid Dielectrics*

GEORGE JAFFÉ AND CHARLOTTE Z. LEMAY†
Louisiana State University, Baton Rouge, Louisiana
(Received August 15, 1952)

A theory of polarization originally developed for crystals is extended in such a way as to be applicable to dc measurements in liquid dielectrics. In Sec. II the general time dependent solution of the relevant differential equation is obtained by the method of eigenvalues. It leads to expressions for the "charging current" in Eq. (22) and the "discharge current" in Eq. (29), which are characteristic of liquids. In Sec. III the measurements and their results are described. They refer to solutions in hexane, and to pure hexane rendered conductive by radium radiation. Attempts to obtain photoconductivity were futile. In Sec. IV it is shown that the observations can be correlated by the theory of Sec. II provided the presence of two species of ions of different mobilities is assumed. A few cases of quantitative analysis are carried out. They lead to the determination of the mobility of the slower ions, and of the thickness of the polarization layers. In Sec. V some aspects of polarization in crystals are discussed in the light of the more recent development.

I. INTRODUCTION

POLARIZATION in electrical conduction is a very general phenomenon. It is observed in all media, whether they are good or poor conductors; metals are the only exception. It seems reasonable, to assume that the underlying cause is the same throughout, and it becomes desirable to develop a theory which brings into evidence such a common cause.

It is generally accepted that electrical conductance in all substances is caused by the motion of discrete, charged particles and, the phenomenon of polarization must be connected somehow with their motion. In 1933,[1] one of the authors based a theory of polarization on the concept that some of the carriers are unable to transport their charges through the boundaries. In this rigorous form, the theory accounted, in a general way, for the very strong phenomena of polarization which are observed in crystals. In recent years, with the aid of collaborators,[2] he has extended the theory to other media and has obtained new experimental material which confirms the theory. First the theory with its original boundary conditions was applied successfully to the case of semiconductors (J.II). Then the boundary conditions were generalized in such a way so as to be applicable to liquid media by the assumption that the discharge of the ions represents a rate process (J.III). Thereby the theory assumed a form in which it is able to correlate the rather complex phenomena which are observed in ordinary electrolyte solutions (J.IV).

Another group of media in which strong effects of polarization are observed is that of liquid dielectrics. Since their conductance is smaller than that of electrolytes by many orders of magnitude, it seemed desirable to extend the investigation to this group. It would give a strong support to the theory if it were feasible to correlate the experimental facts over such wide ranges of conductance.

Measurements in dielectrics are most easily performed by applying or removing an electric field and by observing the transient changes in current which occur.

II. THEORY, THE TIME DEPENDENT SOLUTION

(a) General Theory

The differential equations for the problem in question have been stated previously (J.II, Eqs. I–IV). They are nonlinear and have to be treated by successive approximations. They can be linearized, however, by the following two assumptions: (1) the electric field may be approximated by a homogeneous field $E \equiv E_0$; (2) the formation and recombination of ions may be neglected.

The linear differential equations which result from these assumptions have also been given previously. They are stated in the original paper (J.I, Eqs. 44–46); it shows how these equations can be used as the starting point for a procedure of successive approximations.

As a consequence of the previous two assumptions, (1) and (2), the differential equations for the various species of carriers become independent of each other, no matter how many there are. It will suffice to write down one of them, e.g., for a species of positive ions. Let p be their concentration (number per cc), b their mobility, and D their diffusivity. Then we will have

$$\partial p/\partial t - D\partial^2 p/\partial x^2 + bE_0 \partial p/\partial x = 0, \qquad (1)$$

where x is the distinguished direction of the linear problem. We assume that the conductor extends from $x=0$ to $x=l$, and we consider a column of one cm² cross section throughout.

The density of the current carried by the group of ions considered, j^+, is given by

$$j^+ = \epsilon(bpE_0 - D\partial p/\partial x), \qquad (2)$$

where ϵ is the charge on an ion (electronic charge or multiple of it).

* Work supported by U. S. Office of Naval Research.
† Now in Dallas, Texas, with Texas Instruments, Inc.
[1] G. Jaffé, Ann. phys. **16**, 217, 249 (1933). We are going to refer to this paper in the text by J.I and the page or the equation.
[2] G. Jaffé. Phys. Rev. **85**, 354 (1952); H. Chang and G. Jaffé, J. Chem. Phys. **20**, 1071 (1952); G. Jaffé and J. A. Rider, J. Chem. Phys. **20**, 1077 (1952). We are going to refer to these papers in the text with the symbols J.II, J.III, and J.IV. See also: Final Report of the Signal Corps Project No. 152(B), 14–74 (J.V).

The boundary conditions have been stated and discussed previously (J.III, p. 1073). For the p ions they reduce to

$$j^+ = -\epsilon\xi(p(0)-p^*), \quad \text{for} \quad x=0, \tag{3}$$

$$j^+ = \epsilon\xi(p(l)-p^*), \quad \text{for} \quad x=l. \tag{4}$$

Here ξ represents a rate constant, and p^* an equilibrium value which is supposed to be a constant, but in the case of solutions depends on the concentration of the solute.

Equations similar to Eqs. (1–4) hold for every species of ions.[3]

The problem represented by Eqs. (1–4) is similar to that of heat conduction "with external conduction."[4] It will suffice to indicate the general solution since it is easy to verify by direct substitution.[5] It assumes the form

$$p = p_{\text{stat}} + \sum_{m=1}^{\infty} A_m \exp(-\lambda_m t) X_m, \tag{5}$$

where p_{stat} is the solution of the stationary problem. Furthermore, the eigenfunctions X_m are defined by

$$X_m = \exp(vx/2l)[\cos(\nu_m x) + ((\rho+v/2)/z_m)\sin(\nu_m x)], \tag{6}$$

and the eigenvalues

$$z_m = \nu_m l \tag{7}$$

as the roots of the transcendental equation

$$\tan z = 2\rho z/(v^2/4+z^2-\rho^2). \tag{8}$$

We have introduced dimensionless parameters for the applied voltage V, and for the discharge constant ξ, namely

$$v = (b/D)E_0 l = (b/D)V, \tag{9}$$

and

$$\rho = \xi l/D. \tag{10}$$

λ_m is defined by

$$\lambda_m = (bE_0)^2/4D + D\nu_m^2 = (D/l^2)((v/2)^2+z_m^2). \tag{11}$$

The stationary solution, p_{stat}, has to be established separately and can be found in a straightforward way from Eqs. (1–4). In the applications, we shall require the solution only for values of v which are at least as large as 8. Under these circumstances terms of the order $\exp(-v)$ may be disregarded and the stationary solution assumes the simplified form

$$p_{\text{stat}} = p^*(\rho+2v\exp(-v(1-x/l)))/(\rho+v), \quad v>8, \tag{12}$$

and

$$j^+_{\text{stat}} = \epsilon b p^* E_0 \rho/(\rho+v). \tag{13}$$

Thus the stationary current (which is realized under all circumstances as $t\to\infty$) increases from zero to the normal value

$$j^+_{\max} = \epsilon b p^* E_0, \tag{14}$$

as the reduced discharge constant, ρ, increases from zero to ∞. This was to be expected since $\rho=0$ corresponds to a "completely blocked electrode," and $\rho=\infty$ to an "open electrode" (J.III, p. 1073).

There remains to determine the coefficients A_m in Eq. (5) from the initial distribution which is supposed to be known. Let p at time $t=0$ be given in the form

$$p = F(x), \quad \text{for} \quad t=0. \tag{15}$$

Since p_{stat} is no eigenfunction[5] $(F(x)-p_{\text{stat}})$ has to be developed into a series of the eigenfunctions (6), which yields

$$A_m = Z_m/N_m, \tag{16}$$

with

$$Z_m = \int_0^l \sigma(x)(F(x)-p_{\text{stat}})X_m dx, \tag{17}$$

and

$$N_m = \int_0^l \sigma(x)X_m^2 dx. \tag{18}$$

Here

$$\sigma(x) = \exp(-vx/l) \tag{19}$$

stands for the density factor required by the general theory.[5]

When the ionic distribution Eq. (5) is determined the current can be evaluated by straightforward, though somewhat lengthy computations. It is feasible to split the total transient current in a formal way into parts which are considered to be due to the various species of carriers. Thus the contribution of the p ions, j_{tr}^+, is given by[6]

$$j_{tr}^+(0) = -(\epsilon D/l)\int_0^l [\partial p/\partial x - (b/D)E_0 p]dx, \quad x=0. \tag{20}$$

$$J_{tr} = j_{tr}^+(0) + j_{tr}^-(0) \tag{21}$$

will represent the total transient current. If there are more groups of ions, the sum total of their contributions has to be formed in order to obtain the current of physical significance.

The measurements on which we are going to report are of two different kinds. Either the external field is applied to the liquid at a given time, say $t=0$, and the variation of the "charging current" is observed; or the field is applied until a stationary state is reached and then at a given time, again called $t=0$, the field is removed and the "discharge current" is observed. There-

[3] If the ions are negatively charged the signs of E and j have both to be changed.

[4] Max Planck, *Introduction to Theoretical Physics* (Macmillan and Company, Ltd., London, 1932), Vol. 5, Chap. 3, Part 2.

[5] Some complications arise from the two facts that the differential equation for the eigenfunctions Eq. (6) is not self-adjoint, and that the boundary conditions are not homogeneous. More details of the calculations involved are given in the Final Report, National Office of Naval Research-183(00), N.R. 017-301, of September 1, 1952.

[6] It should be noted that the parts due to the various species of ions are not independent of x and, hence, have to be evaluated all for the same value of x, say $x=0$.

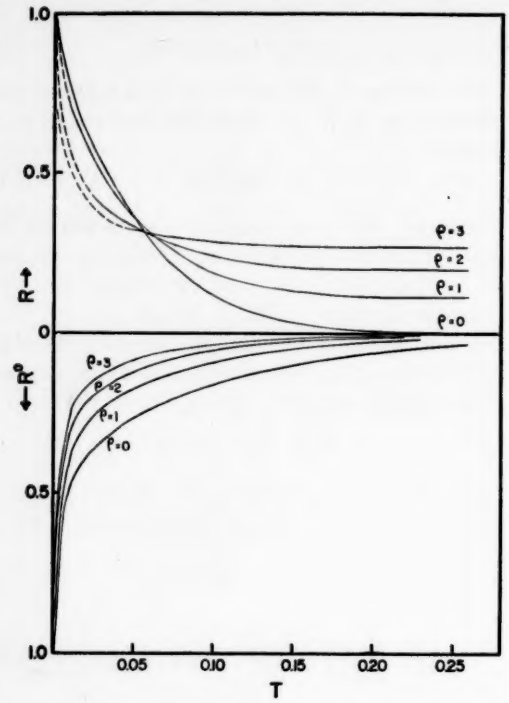

FIG. 1. Representation of theoretical charging and discharge currents for $v=8$ and various values of ρ. The reduced charging currents, R, and the reduced discharge currents, R^0, are plotted *versus* the reduced time variable T. The broken parts are extrapolated.

fore we are interested in applying our general solution to the two special cases corresponding to the modes of observation.

(b) First Special Case. Charging Current

We assume that in the initial state the distribution of the p ions is homogeneous up to the electrodes, $p=c_0$. Consequently we have to set $F(x)=c_0$ in Eqs. (16–18). The result is so involved that we are not going to give it here completely. In most practical cases the restrictions $\exp(-v/2)\ll 1$, and $(\rho/v)^2\ll 1$ represent sufficient approximations. We are going to accept them. Furthermore we assume that for the two species of ions the mobilities, diffusivities, and boundary conditions are the same. Then we obtain

$$J=2\epsilon b p^* E_0\Big[\rho/(\rho+v) - 2(c_0-p^* v/(\rho+v))\sum_{m=1}^{\infty}\exp(-\lambda_m' T)C_m\Big]. \quad (22)$$

The first term represents the time independent conduction current, and the sum the transient current. In Eq. (22) we have introduced a dimensionless time variable

$$T=(D/l^2)t. \quad (23)$$

Consequently λ_m' is given by

$$\lambda_m'=((v/2)^2+z_m^2). \quad (24)$$

Furthermore we have set

$$C_m=(-1)^m[1/(z_m^2(1+(v/2m)^2)^2)](D_m/E_m), \quad (25)$$

where

$$D_m=((v/2)^2+z_m^2+\rho^2)-\rho^2((5/4)v^2+z_m^2), \quad (26)$$

and

$$E_m=((v/2)^2+z_m^2+\rho^2)-\rho^2 v^2. \quad (27)$$

(c) Second Special Case. Discharge Current

Discharge phenomena are characterized by the absence of an external field, and that means in our approximation $E_0=0$. Thereby the problem represented by Eqs. (1) to (4) becomes identical to that of heat conduction with external conduction.[4] Our more general solution Eq. (5) remains valid if we set $v=0$ everywhere. The symbols referring to this case will be characterized by a superscript zero. Thus the general solution is given by

$$p^0=p^*+\sum_{m=1}^{\infty} A_m{}^0\exp(-\lambda_m{}'^0 T)X_m{}^0. \quad (28)$$

We have replaced p_{stat} in Eq. (5) by p^* since this is easily shown to be the only stationary solution for the present case. Furthermore, $X_m{}^0$, $\lambda_m{}'^0$, $A_m{}^0$ are obtained from Eqs. (6), (11), (16), (17), (18), and (24) by setting $v=0$ everywhere.

The second special case mentioned above is realized by choosing the initial state to be the stationary solution in Eq. (5). We take p_{stat} in the abbreviated form of Eq. (12). Then the final result for the total transient current carried by positive and negative ions of equal characteristics can be written in the form

$$J^0=-2\epsilon b p^* E_0(8/v^2)\sum_{n=0}^{\infty} G_n\exp(-(z_{2n+1})^2 T), \quad (29)$$

where

$$G_n=[(1+(z^0{}_{2n+1}/v)^2)(1+(\rho^2+2\rho)/(z^0{}_{2n+1})^2)]^{-1}. \quad (30)$$

In Fig. 1, we have represented reduced values of the charging and discharge currents for the unique value $v=8$, and various values of ρ, setting $c_0=p^*$. The reduced currents are defined as

$$R=J/(2\epsilon b p^* E_0), \quad (31)$$

and

$$R^0=J^0/(2\epsilon b p^* E_0), \quad (32)$$

respectively. The eigenvalues were found from Eq. (8) by graphical procedure, and the values of Eqs. (31) and (32) were then calculated from the theoretical formulas.[7]

The difference between these curves and those referring to $\rho=0$ (see J.I, Fig. 3) is quite marked and shows the effects which were anticipated in introducing

[7] Since $(\rho/v)^2$ is not sufficiently small for the application of the simplified formula of Eq. (22), we have used a more elaborate formula which assumes only $\exp(-v/2)$ to be small. Equation (29) is sufficiently accurate in itself.

finite rates of discharge. Whereas all charging currents tend towards zero (for $t\to\infty$), as long as $\rho=0$, now they approach asymptotically the constant values $\rho/(\rho+v)$ which increase with ρ. At the same time, the "back currents," i.e., R^0, decrease for $t=0$ and fall off more rapidly as ρ increases. As ρ approaches large values the charging current approximates the normal value $2\epsilon bp^*E_0$, and the back currents become more and more insignificant. These features describe exactly the behavior of liquid dielectrics in contradistinction from solid dielectrics which approximate the behavior for $\rho=0$. A more quantitative comparison between theory and experiment will be carried out in Sec. IV.

(d) Second Approximation

So far we have considered exclusively the first approximation which consists of treating the field as homogeneous. It will be seen in Sec. IV that the observations on the discharge clearly indicate a deviation from our formula Eq. (29) which can be accounted for by the next approximation. Therefore, a few words regarding this point have to be said.

We derived Eq. (29) by using Eq. (20) and by assuming that the field becomes zero instantaneously at time $t=0$. This cannot be true in a rigorous way. As long as there is space charge present near the electrodes, there will also be a field (though the applied voltage is zero). Therefore, there will be a term in J^0 of the form (see Eq. (20))

$$J_1{}^0=(\epsilon b/l)\int^l E_1(p+n)dx. \tag{33}$$

This represents a conduction term having the direction of E_1, where E_1 is the inhomogeneous field created by the first order charge distribution.

It is quite feasilbe to calculate E_1 from the Poisson equation and then evaluate Eq. (33). However, this complicated procedure is hardly worth while since Eq. (33) represents only a correction term. We can establish a sufficient approximation in the following way. The first-order densities are given by series of the form Eq. (28) and may be approximated by their first terms. This is legitimate as the other terms escape observability by their more rapid decrease. Consequently the field also becomes an expression of the form

$$E_1=\mathcal{E}_1\exp(-\lambda_1{}^0 l), \tag{34}$$

where $\mathcal{E}_1$ is a constant. Finally the correction term (33) can be written in the form

$$J_1{}^0=\epsilon b\langle(p+n)\rangle_{Av}\mathcal{E}_1\exp(-\lambda_1{}^0 l), \tag{35}$$

where $\langle(p+n)\rangle_{Av}$ is an average value which should not be very different from $2c_0$. This is the form that we are going to use in the applications, treating $\langle(p+n)\rangle_{Av}\mathcal{E}_1$ as a constant which has to be determined from the measurements.

III. MEASUREMENTS

The measurements were performed exclusively with hexane and solutions in hexane because it had been shown by previous work of one of the authors[8] that this is a liquid dielectric suitable for the present purpose. It can be brought to a high state of purity by repeated distillations, and can also be rendered more conductive by addition of known concentrations of solute. Furthermore, its behavior is typical of other liquid dielectrics such as benzene, CS_2, CCl_4, though these are more difficult to purify.

For the study of polarization effects a very natural way of operating is indicated, namely to purify the liquid until its conductance becomes negligible, and consequently the effects of polarization small, and then to increase them by the artificial production of ions. Three different ways of producing ions artificially suggest themselves: either by the addition of known quantities of solute, or by irradiation with radioactive radiation, or by a volume photoeffect if such proves to be observable. These three methods were used though the last of them was not successful and shall not be reported on here.

(a) Method of Observation

Since the currents to be observed were excessively small an electrometric device of dc measurement was adopted.[9] The electrometer used was of the Lindemann

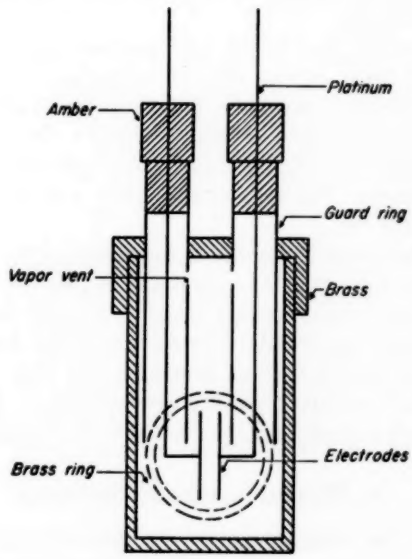

MEASURING CELL

FIG. 2. The measuring cell.

[8] G. Jaffé, Ann. phys. **25**, 257 (1908); **28**, 326 (1909); **32**, 148 (1910); **36**, 25 (1911). We are going to refer to these papers by the symbols A, B, C, and D.

[9] The details of the experimental procedure, as well as a much fuller account of the measurements are contained in the Doctoral thesis: Charlotte Z. LeMay, "Polarization in dielectric liquids," Lousiana State University, 1950.

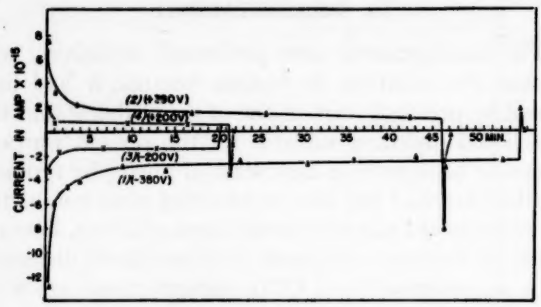

FIG. 3. Charging and discharge currents observed in a diphenylamine solution of $m=1.9\times10^{-4}$ mole/l at 2 voltages. The drawn-out curves are graphical interpolations.

type with its appropriate voltage supply unit (both obtained from the Cambridge Instrument Company). The equilibrium currents actually measured varied from 3.0×10^{-16} to 1.4×10^{-12} amp. The accuracy of the measurements at the highest sensitivity was not great. Individual observations taken during the initial stage of the polarization process may be out by 25 percent. In the later stages, say after 10 minutes, when the changes are less rapid, averages may be formed and the accuracy rises to about 5 percent.

It goes without saying that all parts of the system had to be screened carefully and were built as compact as possible to keep the capacity low (it was 19.6 $\mu\mu f$ for the entire system). External lead screening (about 1.7 cm thick) was added to cut down stray radiation. Dehumidification proved to be essential to maintain sufficient insulation.

The construction of the cell required particular care. The final form of the cell, of cylindrical shape with 3.02 cm internal diameter, is represented in Fig. 2. It was built completely of brass, with Pt electrodes and amber insulation and had long guard cylinders shielding the electrodes. The area of the latter was 4 cm^2, their distance 0.3 cm.

Nothing needs to be said here regarding the purification of the solvent and the solute. The procedure for the former has been described (B, p. 333), and the solutes were treated by standard procedures. The lead oleate had to be prepared from reagent grade oleic acid and lead acetate and recrystallized several times. A storage vessel with built-in pipette proved to be valuable.

(b) Measurements on Solutions

Before the measurements of solutions could be approached, a careful study of the solvent had to be made. The polarization effects in ordinary "pure hexane" are of exactly the same nature as those in solutions which will be described presently. They become less marked, however, with progressing purification and may disappear almost completely as the liquid approaches a conductivity of about 1 to 5×10^{-19} ohm^{-1} cm^{-1}.[10]

The solutes studied were diphenylamine, anthracene, and lead oleate. The concentrations of the diphenylamine solutions varied from $m=1.7\times10^{-4}$ to 6.5×10^{-4} mole/l. Ohm's law was verified in all cases up to the highest field used, i.e., about 1200 v/cm, and the specific conductivities reached after a time of 24 hours were of the order 10^{-18} ohm^{-1} cm^{-1} and were roughly proportional to the concentration. The conductivities given here and below are those after subtraction of the conductivity of the solvent.

The anthracene solutions were varied over a considerable range of concentrations from $m=3.6\times10^{-4}$ to 7.8×10^{-3} mole/l. The conductances were of the order of 1×10^{-19} ohm^{-1} cm^{-1} at the lowest concentration, and were proportional to the concentration, as was verified after 24 hr and after 48 hr of applied voltage.

Lead oleate solutions from $m=4.6\times10^{-7}$ to 7.9×10^{-6} mole/l were investigated and all showed the characteristic approach to saturability. The saturation currents varied from 2.6×10^{-14} to 1.43 to 10^{-12} amp. The dependence of the saturation current on the concentration has been studied previously. It is difficult to establish because the lead oleate changes its character with time losing its conductivity (D, p. 33). The present measurements confirm the older results in a general way.

As for polarization effects, "charging currents," i, as well as "discharge currents," i^0, were observed at varying voltages in both directions. The currents were never quite equal in the two directions and, therefore, both directions were observed in all cases. A large number of observations were made, altogether about 100 sets of runs, most of them at three different voltages. The results are so similar that it will suffice to illustate here one instance referring to a case where Ohm's law holds, and one instance where saturation is fairly complete.[11]

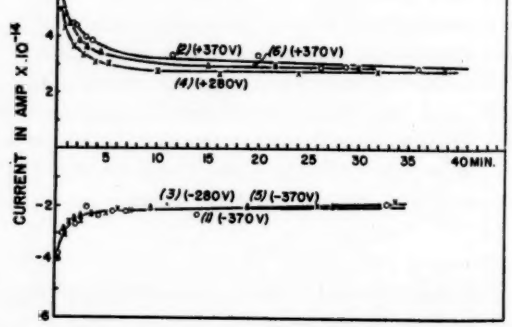

FIG. 4. Charging currents observed in a lead oleate solution of $m=4.6\times10^{-7}$ mole/l at two voltages. The drawnout curves are graphical interpolations.

[10] It is known that ultimately hexane behaves like a dense gas in exhibiting saturation currents (B, p. 349). Then there is no sense in assigning a specific conductivity to the liquid. But this state was not reached nor aimed at in the present investigation.

[11] The numbers assigned to the curves indicate the order in which they were taken. The two examples given here refer to two voltages only, as otherwise the diagrams become too involved. The drawn-out curves are graphical interpolations.

Figure 3 represents observations with a diphenylamine solution of $m=1.9\times10^{-4}$ mole/l. It shows the strong initial drop in the charging currents and the discharge currents of reverse direction. The decrease of current upon the application of the voltage is observable over an astonishingly long time, up to 45 min, whereas the discharge current dies out in a few minutes.

Figure 4 refers to a lead oleate solution of $m=4.6\times10^{-7}$ mole/l. The discharge currents have not been observed here but exist in oleate solutions (see Sec. IV). The charging currents are similar to those in Fig. 3 except that they indicate very little separation for the two voltages.

The examples here given are typical in all respects, and the observations on polarization may be summarized by the following statements.

If the final equilibrium values, i_∞, are subtracted the transient currents $(i-i_\infty)$ always fall off exponentially after the initial stage, say after 5 minutes. In the initial stage the decrease is more rapid. The exponent of the ultimate decrease varies somewhat from solution to solution, but is always of the same order of magnitude. The asymptotic values, i_∞, are not rigorously constant. They change, mostly decrease, at a much slower rate due to electrolysis or changes in the liquid. The ratios $(i-i_\infty)/i_\infty$ are almost the same for the various voltages (see Sec. IV), as long as the liquids remain the same, and do not vary strongly with concentration. They do vary, however, from one solute to another.

(c) Measurements with Radium Radiation

Two kinds of measurements were performed with the hard rays of a source of about 1.5 mg of radium. In the first set the source of radiation was maintained in position during the whole set of measurements. The results are so similar to those obtained with lead oleate solutions that they need not be discussed. The second set of measurements was made by bringing the radium into position at a fixed time, and by then removing it again after the equilibrium value has been reached. One set of observations referring to two strengths of the source (unshielded and shielded) and to two voltages is represented in Fig. 5.

Under these circumstances, anomalies are observed which have been reported previously (A, p. 280, 281) and which evidently are caused by changes in polarization. They will be discussed in Sec. IV.

IV. COMPARISON BETWEEN EXPERIMENT AND THEORY

The main feature by which polarization in dielectric liquids is distinguished from that in crystals is brought out distinctly by our theory, as was stated at the end of Sec. IIc. Apart from that, the characteristics summarized above are predicted in a general way by the theory. The charging and discharge currents both should be proportional to either the initial value, i_0, or

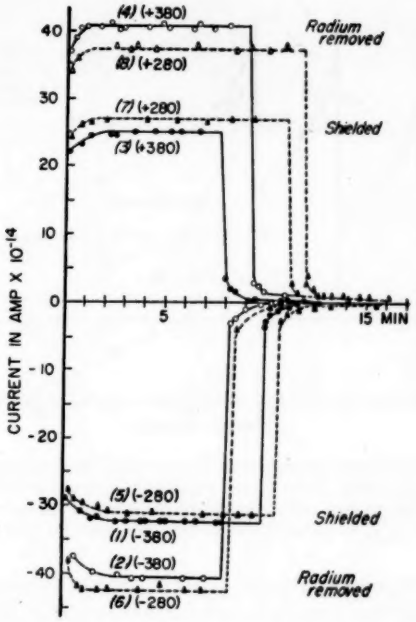

FIG. 5. Observations on pure hexane with the hard radiation of radium either brought into position or removed. Two voltages and two different intensities of the radiation. The drawn-out curves are graphical interpolations.

the final value, i_∞, as long as the thickness of the polarization layer does not change. Now it can be shown that this thickness is a slowly varying function of the concentration and the field strength (J.II, p. 360; J.V, p. 36), and this accounts for the similarity of all polarization effects. Finally, the distance between the two plates (if large enough) should be of no influence. This has been verified within the experimental error by measurements not reported on here.

So far the agreement between experiment and theory is very satisfactory. However, when an attempt is made to match the experimental curves with the theoretical ones quantitatively, the same difficulty is encountered as in the case of semiconductors and electrolytic solutions. It is impossible to match the curves completely if the presence of only one species of ions is assumed. Apart from ions of normal mobility at least one further group of ions, with a mobility about one order of magnitude less, has to be present.

We are going to confirm this conclusion by the detailed analysis of two sets of curves, one representing observations on the charging current, the other discharge currents. The numerical calculations involved are quite lengthy. Therefore, we have not attempted to choose individual parameters ρ and v for each set of observations, but have calculated all of them with the common values $\rho=2$ and $v=8$ which were found by trial and error, and which were also used in the computations leading to Fig. 1.

Figure 6 refers to observations on the charging current in a diphenylamine solution of $m=6.5\times10^{-4}$ mole/l, at three different voltages, and on four different

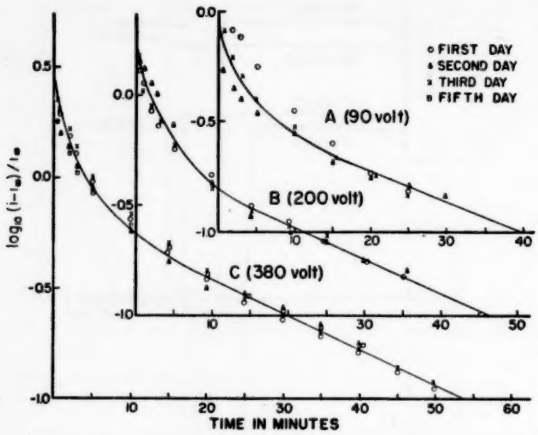

FIG. 6. Comparison between theory and measurements on the charging currents in a diphenylamine solution of $m=6.5\times10^{-4}$ mole/l. The drawn-out curves are theoretical (from Eq. (36)). $\mathrm{Log}_{10}(i-i_\infty)/i_\infty$ is plotted *versus* time in minutes.

days. The observational points were obtained by first averaging the positive and negative currents, and by then determining i_∞ by trial and error. The decadic logarithms of $(i-i_\infty)/i_\infty$ are plotted against time, in minutes, and the points should fall on one curve if the conclusions stated in Sec. IIIb are correct. The diagram indicates to what extent this is true. The observations referring to the three voltages, 380, 200, and 90 volts, are separated to avoid confusion, but they coincide almost as well as the observations with the same voltage on different days.

The drawn-out curves are theoretical ones, and are calculated under the assumption that there are two groups of ions, one of normal mobility b_1 and one of slower mobility b_2. It is assumed, furthermore, that the action of the slower ions may be represented with sufficient approximation by a simple exponential decrease. Hence the theoretical curves are given by the formula

$$i-i_\infty=C_1(R(\rho, v)-\rho/(\rho+v))+C_2\exp(-\lambda_1 t). \quad (36)$$

TABLE I. Constants used in the calculation of Fig. 6.

Curve	C_1	C_2	λ_1 (10^{-2} min^{-1})	b_1 (cm²/volt ×sec)	b_2	l_1 (cm)
A (90 volt)	0.77	0.36	3.16	$\delta_1\times10^{-4}$	$\delta_1\times1.4\times10^{-5}$	$\delta_1^{\frac{1}{2}}\times0.11$
B (200 volt)	1.63	0.52	3.51	$\delta_1\times10^{-4}$	$\delta_1\times1.6\times10^{-5}$	$\delta_1^{\frac{1}{2}}\times0.11$
C (380 volt)	2.67	0.76	3.78	$\delta_1\times10^{-4}$	$\delta_1\times1.7\times10^{-5}$	$\delta_1^{\frac{1}{2}}\times0.11$

	1st day	2nd day	3rd day	5th day
A i_∞ (amp $\times10^{-15}$)	1.9	1.8	···	1.6
B i_∞ (amp $\times10^{-15}$)	4.6	4.2	···	3.1
C i_∞ (amp $\times10^{-15}$)	8.5	7.3	6.8	6.4

For b_1 we have assumed the value $\delta_1\times10^{-4}$ cm²/v ×sec, where δ_1 is a numerical factor which should be of the order of unity if the mobility of the ions in diphenylamine solutions is of the same order as in lead oleate solutions (D, p. 42, 43) or of radiative ions (C, p. 160). The constants used in the calculation of the curves are collected in Table I. They indicate that i_∞, i.e., the equilibrium current, decreased with time but much more slowly than the decrease studied here.

It is somewhat difficult to observe discharge currents in dielectric liquids with our method of observation, since they are so insignificant and decay so rapidly (see Fig. 3). In many cases they escape observation altogether. Therefore, several series of observations were performed with the special object of studying this point. Solutions of lead oleate of relatively high concentration, and irradiation with a strong source of radium were used.

Figure 7 represents two observations with a lead oleate solution of $m=7.8\times10^{-6}$ mole/l. The one, *A*, refers to the discharge after applying a voltage of +370 volt until equilibrium is reached, the other one, *B*, refers to a charging voltage of −370 v. Both series reveal a rather surprising reversal of the current after about 40 sec. This is confirmed by measurements at different charging voltages and also by the measurements with a strong radiative source acting on pure hexane.

The explanation is to be found in the second order effect which is predicted by theory (see Eq. (35)). We have, therefore, calculated the full curves of Fig. 7 by a formula of the type

$$i^0=C_3R^0(\rho, v)-C_4\exp(-\lambda_1{}^0 t), \quad (37)$$

where R^0 is the ratio of Eq. (32). The constants used in the calculations are given in Table II. Since we are dealing with lead oleate here the mobility of the normal ions is known with a fair accuracy (D, p. 42, 43). The mobility of the slower group can then be derived from the knowledge of $\lambda_1{}^0$.

It will be seen that the theoretical curves represent the observed data with as good an accuracy as might be expected from the nature of the measurements. In all events, the initial rapid decrease, and the subsequent reversal of the current are well represented.

The thickness of the polarization layer l_1 can be derived from the comparison of the T scale and the t scale, provided D is known, (see Eq. (23)). Assuming Town-

TABLE II. Constants used in the calculation of Fig. 7.

Curve	C_3 (amp $\times10^{-14}$)	C_4	$\lambda_1{}^0$ (10^{-2} sec^{-1})	b_1 (cm²/volt ×sec)	b_2	l_1 (cm)
A (370 volt)	86.6	4.6	2.75	0.7×10^{-4}	2.6×10^{-5}	2.0×10^{-1}
B (−370 volt)	75.0	1.65	1.15	0.7×10^{-4}	1.1×10^{-5}	2.0×10^{-1}

send's relation to hold, we have calculated the l_1 values given in Tables I and II. They are much larger than in the case of semiconductors ($l_1 \sim 10^{-5}$ cm, J.II, Table IV) and electrolytic solutions ($l_1 \sim 10^{-5}$ cm, J.IV, p. 1083). This difference is caused by the extreme smallness of the conductance in the present case and is predicted by theory, since it can be shown that also for $\rho \neq 0$, the thickness of the polarization layer decreases as the concentration of the ions increases.

A few words should be said on the interpretation of the observations with a radiation source applied and removed while the field is being kept constant (see above Sec. III(c)). The time dependence which is observed upon the application of the source (see Fig. 5) can be understood as the superposition of two effects, the establishment of the saturation current, and the destruction of a state of polarization that existed before. In the final stationary state there will be saturation current, and consequently, a homogeneous field distribution.[12] Before application of the radium, however, there was a state of polarization which is being removed. Hence the observable current will consist of two parts: the saturation current (due to the radiation), and a current (caused by the liquid itself) which is in the direction of the field and rises from i_∞ to i_0. Vice versa, upon the removal of the source, there is at first a homogeneous field distribution and polarization is established. Hence the observable current will again be in the direction of the field, but it will decrease from i_0 to i_∞. These considerations explain the observations qualitatively.[13]

V. NOTE ON POLARIZATION IN SOLID DIELECTRICS

The theoretical treatment of Sec. II is applicable also to solid dielectrics. It was shown in J.I that the observations on crystals which are to a great extent due to A. Joffé and his school can be correlated in a satisfactory way by the theory in its original form, i.e., with $\rho = 0$. There remained, however, some difficulties in the quantitative application of the theory, and these difficulties can now be removed.

The first point in question is the dissymmetry with regard to direction of the field which is exhibited by some crystals. For instance in calcite a polarization layer, and a very marked one, is formed only at the cathode, none at all at the anode. This fact could not be explained by the theory in its original form. If, however, the positive ions in calcite are unable to discharge, i.e., if they satisfy the boundary condition with $\rho = 0$, whereas the negative ions may discharge (say $\rho \sim 3$) the result would be exactly the one observed. Furthermore, the crystal would lose negative charge while the field is applied, and would show a positive

[12] G. Jaffé, Ann. phys. **43**, 249 (1914).

[13] It would be feasible to adapt the general solution of Sec. II to these conditions, but it seems hardly worth while.

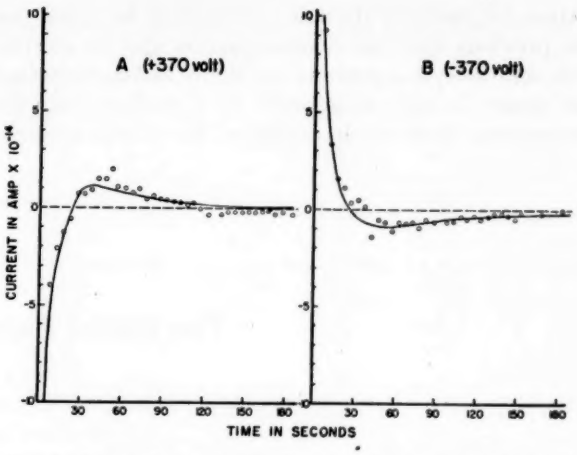

FIG. 7. Comparison between theory and measurements on the discharge current in a lead oleate solution of $m = 7.8 \times 10^{-6}$ mole/l. The drawn-out curves are theoretical (from Eq. (37)). The observed currents are plotted *versus* time in seconds

charge after the removal of the field. This, again, is observed (J.I, p. 275).

The second discrepancy which remained in the older treatment consisted of the fact that it led to values of b/D which were much smaller (10^3 to 10^4 times) than correspond to the Townsend relation (J.I, 271).

As has been recognized in the work on semiconductors and electrolytes it is necessary to determine the thickness of the polarization layer by special considerations as, otherwise, the bulk resistance of the medium cannot be taken into consideration. In the older work it was assumed that the solutions of the differential equations were valid over the whole thickness of the crystal L. It is easy to see that this circumstance accounts for the discrepancy mentioned above. The comparison between the empirical time scale and the dimensionless parameter T of the theory yields directly only the expression D/l_1^2. Thus, the Townsend relation can be maintained if l_1 is determined as distinct from L.

We shall illustrate this by one example. In the old paper one set of charging and discharging currents observed by Hochberg and Joffé on a $NaNO_3$ crystal[14] were subjected to a detailed analysis. We shall retain the values $c_0 = 4.5 \times 10^{12}$ and $b = 1.2 \times 10^{-6}$ cm²/volt ×sec as determined there. Now we determine the diffusivity from the Townsend relation which yields $D = 3.6 \times 10^{-8}$ cm²/sec. Finally the experimental value $T/t = 4.76 \times 10^{-3}$ permits of determining l_1. It comes out that $l_1 = 2.8 \times 10^{-3}$ cm which is in good agreement with the estimate of Hochberg and Joffé. This value also fits in with the determinations made above since the specific conductivity (at 80°C) was found to be much larger than those observed in our dielectric liquids, namely $\kappa = 1.7 \times 10^{-12}$ ohm^{-1} cm^{-1}.

If we summarize the complete recent work on polar-

[14] B. Hochberg and V. Joffé, Z. Physik **66**, 172 (1930).

ization, i.e., not only the work reported on here, but also the previous work on semiconductors and on electrolytic solutions, it appears to be highly satisfactory that the theory is able to account in a uniform way for phenomena observed in media of so widely different conductivity (from selenium, $\kappa\sim10^{-3}$ ohm^{-1} cm^{-1} down to hexane of $\kappa\sim1\times10^{-19}$ ohm^{-1} cm^{-1}), for ac as well as dc measurements. It does not seem hazardous to assert that the phenomenon of polarization is traced back to the finite rate of discharge of the ions at the electrodes.

THE JOURNAL OF CHEMICAL PHYSICS VOLUME 21, NUMBER 5 MAY, 1953

The United Atom Treatment of H_2^+

F. A. MATSEN*
Departments of Chemistry and Physics, The University of Texas, Austin, Texas
(Received January 12, 1953)

Using first-order perturbation theory on the united atom, closed expressions are obtained for the energies, and the charges which minimize those energies, of the following states: $1s\sigma$, $2p\sigma$, $2p\pi$, $3p\pi$, and $3d\delta$. Numerical calculations based on these expressions show, for the higher states, quite good agreement with the more exact calculations of Teller and Chakravarty.

IN the united atom treatment the Hamiltonian for the hydrogen molecule ion, neglecting nuclear repulsion, is written[1,2]

$$-\frac{1}{2}\nabla^2-\frac{Z}{r}+\left(\frac{Z}{r}-\frac{1}{r_a}-\frac{1}{r_b}\right).$$

Here r is the distance between the electron and the midpoint between atoms a and b. The first two terms make up the zero order and the last three the perturbation Hamiltonian. The zero-order wave functions are then hydrogenic functions of charge Z. For those states to which first-order nondegenerate perturbation theory can be applied,[3] the energy is

$$E_{n,1,\lambda}=\frac{Z^2}{2n^2}-2\int\frac{\psi^2_{n,1,m}d\tau}{r_a}.$$

Morse and Stueckelberg expanded $1/r_a$ in terms of Legendre polynomials and inverse powers of the internuclear distance R.[4] However, integration over elliptic coordinates yields expressions in closed form as given in Table I.

In the united atom He^+, $Z=2$. The use of this value of charge gives agreement with the more exact calculations[5,6] only at extremely small nuclear separations. Some improvement is obtained by using the value of Z which minimizes the ground state. The expression for this Z is given in Table I.

A significant improvement in the energy calculations can be obtained if some of the excited states are minimized separately. The states to which separate minimization can be applied are those which are orthogonal to the ground state and to all other states which lie below them.[7,8] To $n=3$ these states are $1s\sigma$, $2p\sigma$, $2p\pi$,

TABLE I. $a=ZR/2n$.

$1s\sigma$
$E=Z^2/2-(2Z/a)[1-e^{-2a}(1+a)]$
$Z=2e^{-2a}(1+2a)$

$2p\sigma$
$E=Z^2/8-(Z/2a^3)[6+2a^2-e^{-2a}(6+12a+14a^2+11a^3+6a^4+2a^5)]$
$Z=(2/a^3)[e^{-2a}(12+24a+24a^2+17a^3+10a^4+6a^5+4a^6)-12]$

$2p\pi$
$E=Z^2/8-(Z/2a^3)[-3+2a^2+e^{-2a}(3+6a+4a^2+a^3)]$
$Z=(4/a^3)[3-e^{-2a}(3+6a+6a^2+(7/2)a^3+a^4)]$

$3d\pi$
$E=Z^2/18-(Z/72a^5)[-2880+96a^2+48a^4+e^{-2a}(2880+5760a+5664a^2+3648a^3+1680a^4+560a^5+128a^6+16a^7)]$
$Z=(1/8^5)[11520-192a^2-e^{-2a}(11520+23040a+22848a^2+14976a^3+7296a^4+2800a^5+864a^6+208a^7+32a^8)]$

$3d\delta$
$E=Z^2/18-(Z/288a^5)[2880-768a^2+192a^4-e^{-2a}(2880+5760a+4992a^2+2304a^3+576a^4+64a^5)]$
$Z=(1/32a^5)[-11520+1536a^2+e^{-2a}(11520+23040a+21504a^2+12288a^3+4608a^4+1088a^5+128a^6-224a^7)]$

* Guggenheim Fellow 1951–1952, Kings College, London, and Wadham College, Oxford.

[1] B. N. Finkelstein and G. E. Horowitz, Z. Physik **48**, 118 (1928).

[2] P. M. Morse and E. C. G. Stueckelberg, Phys. Rev. **33**, 932 (1929).

[3] These include degenerage states whose nondiagonal matrix elements are zero.

[4] This limits the validity of their energy expression to R less than a_0.

[5] E. Teller, Z. Physik **61**, 458 (1930).

[6] S. K. Chakravarty, Phil. Mag. **28**, 423 (1939).

[7] C. Eckart, Phys. Rev. **36**, 878 (1930).

[8] Morse and Stueckelberg (reference 2) minimized some states which are not orthogonal to the ground state. To treat $2s\sigma$, for example, it is necessary to obtain expressions for the energy of the two orthogonal linear combinations of $2s\sigma$ and $1s\sigma$. Each of these energy expressions is then separately minimized with respect to the charge. The higher energy is found to lie above that obtained from a minimization of the $2s\sigma$ state alone. These states have separated atom designations of σ_g $1s$, σ_u $1s$, π_u $2p$, π_u $3p$, and δ_g $3d$.

$3d\pi$, and $3d\delta$, which all belong to different irreducible representations of the point group $D_{\infty h}$. The expressions obtained for Z by these separate minimizations are given in Table I. The numerical results together with those obtained by Teller are given in Table II and plotted in Fig. 1.

Since the charge, and consequently the energy, go to zero at infinite nuclear separation, the treatment is better for those molecular states which dissociate into atoms in excited states. The treatment also appears better for the excited molecular states because the electron density is spread far enough away from the two nuclei so that they appear united.

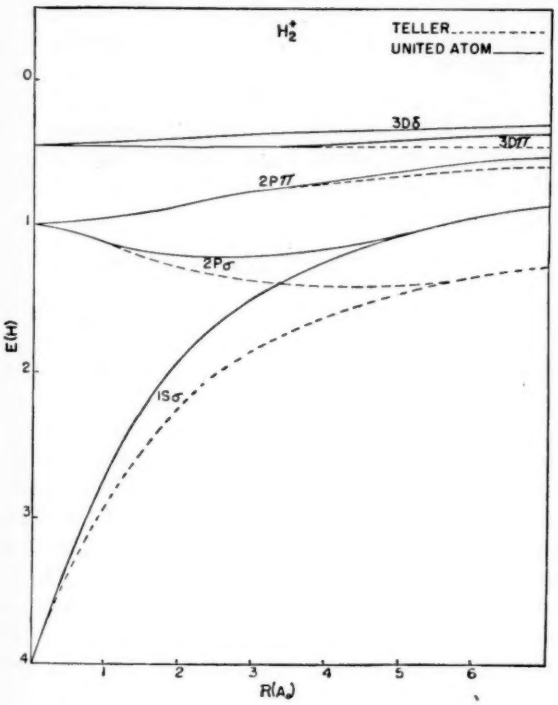

FIG. 1.

The energy obtained for the $3d\pi$ state lies about 0.05 of an electron volt below that calculated by Teller up to a nuclear separation of four Bohr radii. Teller used a variation method to solve one of his equations and estimates his error to be 0.1 electron volt. Consequently, since the united atom value must lie above the true value, it actually is a better result than Teller's. The $3d\delta$ state does not appear to have been calculated accurately before this. The result should be reliable to $R=4a_0$, since it correlates with separated atoms which are in the relatively high-lying $3d$ state.[9]

TABLE II. Electronic energy of H_2^+. $e^2/2a_0=1$.

$R(a_0)$	Teller $1s\sigma$	United atom		$2p\pi$	
0.0000	4.00	4.00	0.000	1.000	1.000
0.4964		3.3836	1.319	0.920	
0.599	3.35		1.3671		0.9092
0.895	3.00		1.9958		0.8449
0.9054		2.8210	2.18	0.839	
1.0+	2.896		2.3608		0.8088
1.1837		2.5272	2.7703		0.7706
1.3+	2.648		3.2287		0.7310
1.5240		2.2394	3.267	0.749	
1.9445		1.8812	3.7424		0.6907
2.0+	2.204		4.18	0.687	
2.4+	2.025		5.77	0.600	
2.4630		1.7170	6.4965		0.5300
2.95+	1.836		7.18	0.542	
3.1023		1.4758			
3.429	1.701			$3d\pi$	
	$2p\sigma$		0.000	0.444	0.4444
			1.1940		0.4464
0.0000	1.000	1.000	1.7888		0.4475
0.7338		1.0602	2.3944		0.4479
1.0769		1.1267	3.0255		0.4464
1.310	1.166		3.71126		0.4433
1.3809		1.1732	4.25	0.442	
1.7738		1.2045	5.3729		0.4225
1.789	1.250		6.00	0.443	
2.0086		1.2082	7.6980		0.3912
2.2778		1.2020	8.06	0.432	
2.439	1.347				
2.950	1.381			$3d\delta$	
3.808	1.380				
3.8912		1.0655	0.000		0.4444
5.503	1.326		1.3397		0.4042
			2.1250		0.3791
			2.9458		0.3588
			3.7967		0.3424
			6.8254		0.3009
			9.9254		0.2669

The $2p\pi$ and the $3d\delta$ states are of interest since they are the united atom analogs of the LCAO molecular orbital states $2p_a \pm 2p_b$ which are so often used in calculations on ethylene and other unsaturated molecules. In conjugated systems the molecular orbitals can be formed from linear combinations of united atom orbitals LCUAO, particularly the $2p\pi$ orbitals. The bond order is then expressible in terms of the squares of the coefficients of the united atom orbitals.

The writer is indebted to Professor C. A. Coulson for helpful discussions.

[9] For the states with $n=3$, Morse and Stueckelberg assumed that Z retained its united atom value of two. This is not a particularly good assumption for R greater than a_0.

Substituted Methanes. XIV.* Vibrational Spectra, Potential Constants, and Calculated Thermodynamic Properties of Bromochloromethane†

ALFONS WEBER, ARNOLD G. MEISTER, AND FORREST F. CLEVELAND
Spectroscopy Laboratory, Department of Physics, Illinois Institute of Technology, Chicago 16, Illinois
(Received December 1, 1952)

Raman displacements, semiquantitative relative intensities, quantitative depolarization factors, and wave numbers for the infrared bands in the region 400–3000 cm^{-1} have been obtained for CH_2BrCl. A reasonable set of potential constants has been determined using Wilson's *FG* matrix method. The thermodynamic properties—heat content, free energy, entropy, and heat capacity—have been calculated from the spectroscopic and molecular structure data for 11 temperatures from 100 to 1000°K.

RAMAN displacements, depolarization factors, and estimated relative intensities have been reported previously in three investigations.[1–3] Emschwiller and Lecomte,[4] and Plyler *et al.*,[5] have obtained the infrared spectrum.

A partial normal coordinate treatment was carried out by Plyler and Benedict[6] for the a'' vibrations, using potential constants taken from the work of Decius.[7] No experimental or calculated values for the thermodynamic properties could be found in the literature.

EXPERIMENTAL

The sample of CH_2BrCl was obtained from the Dow Chemical Company, Midland, Michigan. The purification of the sample was carried out as described by Davis *et al.*[8] The Raman spectrum obtained with the sample treated in this manner exhibited an exceedingly low continuous background and showed no evidence of impurities. The techniques employed and the equipment used in obtaining the Raman and infrared spectra have been described previously.[8]

TABLE I. Raman spectral data for liquid bromochloromethane (CH_2BrCl).[a]

Raman displacement (cm^{-1})				Relative intensity	Depolarization factor			
PR	BW	De	PV	PR	W	De	PR	PS
228	226	227	227	68	0.40	0.42	0.41	P
603	603	602	603	100	0.14	0.14	0.16	P
729	726	728	728	5	0.58	0.4	0.54	P
854	···	853	854	0	···	D	D	D
···	1034	···	···	···	···	···	···	···
1128	1130	1129	1129	1	0.87	0.8	0.85	D
1227	1224	1226	1226	1	P	0.3	0.32	P
1407	1403	1404	1405	5	0.65	0.5	0.66	P
···	1443	···	···	···	···	···	···	···
···	2854	···	···	···	···	···	···	···
2987	2986	2984	2986	44	0.20	P	0.23	P
3056	3054	3050	3053	4	···	D	0.84	D

[a] PR = present results; BW = Bacher and Wagner (reference 1); De = Delwaulle (reference 3); PV = probable values; W = Wagner (reference 2); and PS = polarization state (P, polarized; D, depolarized).

RESULTS AND ASSIGNMENTS

The Raman spectral data are summarized in Table I. The present results agree very well with previously reported work,[1–3] but fill in some gaps where quantitative data were not previously available. The 854 cm^{-1} fundamental is extremely weak and was found only after a 64-hr exposure on the 2-prism spectrograph.[8]

The infrared data are summarized in Table II. Table III contains the probable values of the Raman and infrared data, the calculated wave numbers, and the assignments. The two fundamentals found at 2987 and 3060 cm^{-1} by Plyler, Smith, and Acquista[5] were observed also in this laboratory with a Beckman IR-2 spectrophotometer with KBr optics but are not listed in view of the poor resolution in this region.

In view of the data existing in the literature, as well as the work done in this laboratory, one concludes that the Raman lines found by Bacher and Wagner[1] at 1034 and 2854 cm^{-1} are not due to CH_2BrCl. The Raman line at 1443 cm^{-1} reported by the same investigators could very well correspond to the 1453 cm^{-1} band appearing in the infrared. However, this band was not found in the previous investigations[2–4] and also was not found in the present investigation of the Raman spectrum, even though exposures were made in excess of 200 hr.

The CH_2BrCl molecule possesses the symmetry of the C_s point group; its nine fundamental vibrations break down therefore into six vibrations of type a' and three vibrations of type a''. The assignments given in Table III were made in view of the selection rules[9] and the observed depolarization factors.

* For previous papers in this series see J. Chem. Phys. **18**, 346, 1073, 1076, 1081 (1950); **19**, 119, 784, 1561 (1951); **20**, 454, 1949, 1979 (1952); **21**, 158, 189, 242 (1953).

† Partly presented at the Chicago meeting of the American Physical Society, November 1950; Abstract in Phys. Rev. **81**, 301 (1951).

[1] W. Bacher and J. Wagner, Z. physik. Chem. **B43**, 191 (1939).
[2] J. Wagner, Z. physik. Chem. **B45**, 69 (1939).
[3] M. L. Delwaulle, Compt. rend. **217**, 172 (1943).
[4] G. Emschwiller and J. Lecomte, J. phys. et radium **8**, 130 (1937).
[5] Plyler, Smith, and Acquista, J. Research Natl. Bur. Standards **44**, 503 (1950).
[6] E. K. Plyler and W. S. Benedict, J. Research Natl. Bur. Standards **47**, 202 (1951).
[7] J. C. Decius, J. Chem. Phys. **16**, 214 (1948).
[8] Davis, Cleveland, and Meister, J. Chem. Phys. **20**, 454 (1952).
[9] Pontarelli, Meister, Cleveland, Voelz, Bernstein, and Sherman, J. Chem. Phys. **20**, 1949 (1952).

NORMAL COORDINATE TREATMENT

As a check on the assignments, as well as to obtain reliable values of the potential constants, a normal coordinate treatment (Wilson's *FG* matrix method) was carried out using the most general quadratic potential function. The potential constants and the equilibrium coordinates are expressed in the descriptive notation introduced in paper VIII.[8] The symbols used for the equilibrium values of the bond distances and interbond angles are b=C−Br, c=C−Cl, h_1=C−H_1, h_2=C−H_2; bh_1=Br−C−H_1, bh_2=Br−C−H_2, bc=Br−C−Cl; h_1h_2=H_1−C−H_2, ch_1=Cl−C−H_1, and ch_2=Cl−C−H_2. The following orthonormal linear combinations of the changes in these quantities were used as the symmetry coordinates for the a' vibrations:

$$R_1=\Delta b,$$
$$R_2=\Delta c,$$
$$R_3=2^{-\frac{1}{2}}(\Delta h_1+\Delta h_2),$$
$$R_4=6^{-\frac{1}{2}}(\Delta h_1h_2+\Delta ch_1+\Delta ch_2-\Delta bh_1-\Delta bh_2-\Delta bc),$$
$$R_5=6^{-\frac{1}{2}}(\Delta ch_1+\Delta ch_2-2\Delta h_1h_2),$$
$$R_6=6^{-\frac{1}{2}}(\Delta bh_1-2\Delta bc+\Delta bh_2), \text{ and}$$
$$R'=6^{-\frac{1}{2}}(\Delta h_1h_2+\Delta ch_1+\Delta ch_2+\Delta bh_1+\Delta bh_2+\Delta bc)\equiv 0$$

for the redundant coordinate. It is to be noted that these symmetry coordinates are different from those employed by Pontarelli *et al.*[9] in the study of $CHClBr_2$ and $CDClBr_2$. The symmetry coordinates used here lead to simpler expressions for the elements of the *F* and *G* matrices, which makes the modification of the potential constants an easier task.

From the *f* matrix (formally the same as that given by Pontarelli *et al.*[9]) and the coefficients of the symmetry coordinates, the following elements of the *F* matrix were obtained for the a' vibrations:

$$F_{11}=f_b,$$
$$F_{12}=f_b{}^c,$$
$$F_{13}=2^{\frac{1}{2}}f_b{}^h,$$
$$F_{14}=6^{-\frac{1}{2}}(2f_b{}^{ch}-2f_b{}^{bh}-f_b{}^{bc}+f_b{}^{hh}),$$
$$F_{15}=6^{\frac{1}{2}}(f_b{}^{ch}-f_b{}^{hh})/3,$$
$$F_{16}=6^{\frac{1}{2}}(f_b{}^{bh}-f_b{}^{bc})/3,$$
$$F_{22}=f_c,$$
$$F_{23}=2^{\frac{1}{2}}f_c{}^h,$$
$$F_{24}=6^{-\frac{1}{2}}(2f_c{}^{ch}-f_c{}^{bc}-2f_c{}^{bh}+f_c{}^{hh}),$$
$$F_{25}=6^{\frac{1}{2}}(f_c{}^{ch}-f_c{}^{hh})/3,$$
$$F_{26}=6^{\frac{1}{2}}(f_c{}^{bh}-f_c{}^{bc})/3,$$
$$F_{33}=f_h+f_h{}^h,$$
$$F_{34}=3^{-\frac{1}{2}}(f_h{}^{ch}+f_h{}^{ch'}+f_h{}^{hh}-f_h{}^{bh}-f_h{}^{bh'}-f_h{}^{bc}),$$
$$F_{35}=3^{-\frac{1}{2}}(f_h{}^{ch}+f_h{}^{ch'}-2f_h{}^{hh}),$$
$$F_{36}=3^{-\frac{1}{2}}(f_h{}^{bh}+f_h{}^{bh'}-2f_h{}^{bc}),$$

TABLE II. Infrared spectral data for bromochloromethane (CH_2BrCl).[a]

	Liquid				Gas	
EL	PSA	PR	I	PV	PR	I
...	377	...	...	377	...	...
602	606	606	vs	604	618	s
636	638	640	vvw	638	...	...
729	728	725	vvs	727	737	vs
849	852	853	m	851	854	vvw
...	950	...	...	950	...	...
...	1130	1128	m	1129	1139	vw
1201	1225	1230	s	1227	1235	m
...	1261	...	...	1261	...	...
...	1331	...	...	1331	...	...
1404	1402	1406	m	1404	1421	w
...	1453[b]	1453	m	1453	...	...

[a] EL = Emschwiller and Lecomte (reference 4); PSA = Plyler, Smith, and Acquista (reference 5); PR = present results; I = present intensities (s = strong, m = medium, w = weak, v = very); and PV = probable values.
[b] Above 1453 cm^{-1}, PSA (reference 5) observed 14 bands, the two C−H stretching fundamentals at 2987 and 3060 cm^{-1}, and 12 binary combinations and overtones.

TABLE III. Probable values for the Raman and infrared fundamentals, calculated wave numbers, and assignments for liquid CH_2BrCl.[a]

Raman			Infrared		Calculated wave number			
RD	I	PS	cm^{-1}	I	PB	PR	Assignment[b]	Type
227	68	P	...	...	...	228	ν_6	a'
603	100	P	604	s	...	602	ν_5	a'
728	5	P	727	vvs	...	728	ν_4	a'
854	vvw	D	851	m	852	857	ν_9	a''
1129	1	D	1129	m	1142	1126	ν_8	a''
1226	1	P	1227	s	...	1226	ν_3	a'
1405	5	P	1404	m	...	1406	ν_2	a'
2986	44	P	2987	s	...	2986	ν_1	a'
3053	4	D	3060	m	3077	3055	ν_7	a''

[a] RD = Raman displacement in cm^{-1}, PB = Plyler and Benedict (reference 6). Other symbols have same meaning as in Tables I and II.
[b] PSA (reference 5) assigned satisfactorily all the bands found in the infrared spectrum as fundamentals, binary combinations, and overtones.

TABLE IV. Potential constants for CH_2BrCl.[a]

Constant	Value	Constant	Value
f_h	5.0656[b]	$f_h{}^{ch}$	0.27299
f_b	2.7305	$f_h{}^{ch'}$	−0.091001
f_c	3.3250	$f_h{}^{hh}$	0.22645
$f_h{}^h$	−0.0106	$f_h{}^{bh}$	0.23249
$f_b{}^c$	0.32037	$f_h{}^{bc}$	0
$f_b{}^h$	0.05890	$f_h{}^{bh'}$	−0.077498
$f_c{}^h$	0.08800	$f_b{}^{ch}$	−0.16400
f_{hh}	0.54715	$f_b{}^{hh}$	0
f_{ch}	0.83110	$f_b{}^{bh}$	0.25970
f_{bh}	0.60011	$f_b{}^{bc}$	0.33000
f_{bc}	1.1383	$f_c{}^{ch}$	0.18601
$f_{ch}{}^{hh}$	0.06768	$f_c{}^{hh}$	0
$f_{hh}{}^{bh'}$	−0.007312	$f_c{}^{bh}$	−0.15200
$f_{ch}{}^{ch'}$	0.06107	$f_c{}^{bc}$	0.3000
$f_{bh}{}^{ch}$	0.08350	$f_{bh}{}^{ch'}$	−0.02537
$f_{bc}{}^{ch}$	0.019661	$f_{bc}{}^{hh}$	0.053171
$f_{bc}{}^{bh}$	0.099639	$f_{bh}{}^{hh}$	0.06000

[a] Bond stretching and bond interaction constants are expressed in *md/A*; angle-bond interaction constants are in *md*/rad; and angle, and angle-angle interaction, constants are in *md A*/rad^2.
[b] This number of significant figures is not justified except that they are necessary to give the best reproduction of the observed wave numbers and to secure internal consistency in the calculations.

TABLE V. Observed wave numbers and degeneracies for the fundamental frequencies of CH_2BrCl.

Designation	Degeneracy	Type	Wave number in cm^{-1}
ν_1	1	a'	2986[a]
ν_2	1	a'	1421[b]
ν_3	1	a'	1235[b]
ν_4	1	a'	737[b]
ν_5	1	a'	618[b]
ν_6	1	a'	227[a]
ν_7	1	a''	3053[a]
ν_8	1	a''	1139[b]
ν_9	1	a''	854[b]

[a] For the liquid state.
[b] For the gaseous state.

$$F_{44}=(2f_{ch}-4f_{bc}{}^{ch}+2f_{ch}{}^{ch'}+f_{hh}-4f_{bh}{}^{ch}+4f_{ch}{}^{hh}-4f_{bh}{}^{ch'}-4f_{bh}{}^{hh}+2f_{bh}+2f_{bh}{}^{bh'}+4f_{bc}{}^{bh}+f_{bc}-2f_{bc}{}^{hh})/6,$$

$$F_{45}=(f_{ch}-f_{bc}{}^{ch}-f_{bh}{}^{ch}-f_{hh}+f_{ch}{}^{ch'}-f_{ch}{}^{hh}-f_{bh}{}^{ch'}+2f_{bh}{}^{hh}+f_{bc}{}^{hh})/3,$$

$$F_{46}=(f_{bh}{}^{ch}+f_{bh}{}^{ch'}+f_{bh}{}^{hh}-f_{bh}-f_{bh}{}^{bh'}+f_{bc}{}^{bh}-2f_{bc}{}^{ch}+f_{bc}-f_{bc}{}^{hh})/3,$$

$$F_{55}=(f_{ch}+2f_{hh}+f_{ch}{}^{ch'}-4f_{ch}{}^{hh})/3,$$

$$F_{56}=(f_{bh}{}^{ch}+f_{bh}{}^{ch'}-2f_{bh}{}^{hh}-2f_{bc}{}^{ch}+2f_{bc}{}^{hh})/3, \text{ and}$$

$$F_{66}=(f_{bh}+f_{bh}{}^{bh'}-4f_{bc}{}^{bh}+2f_{bc})/3.$$

The elements of the G matrix for the a' vibrations, obtained by use of Decius' tables[10] are as follows:

$$G_{11}=\mu_{Br}+\mu_C,$$

$$G_{12}=-\mu_C/3,$$

$$G_{13}=-2^{\frac{1}{2}}\mu_C/3,$$

$$G_{14}=4\mu_C 3^{\frac{1}{2}}(c^{-1}+2h^{-1})/9,$$

$$G_{15}=2\mu_C 3^{\frac{1}{2}}(c^{-1}-h^{-1})/9,$$

$$G_{16}=4\mu_C 3^{\frac{1}{2}}(c^{-1}-h^{-1})/9,$$

$$G_{22}=\mu_{Cl}+\mu_C,$$

$$G_{23}=-2^{\frac{1}{2}}\mu_C/3,$$

$$G_{24}=-4\mu_C 3^{\frac{1}{2}}h^{-1}/9,$$

$$G_{25}=-8\mu_C 3^{\frac{1}{2}}h^{-1}/9,$$

$$G_{26}=2\mu_C 3^{\frac{1}{2}}(3b^{-1}+h^{-1})/9,$$

$$G_{33}=2\mu_C/3+\mu_H,$$

$$G_{34}=-2\mu_C 6^{\frac{1}{2}}(c^{-1}+h^{-1})/9,$$

$$G_{35}=-\mu_C 6^{\frac{1}{2}}(c^{-1}-5h^{-1})/9,$$

$$G_{36}=-\mu_C 6^{\frac{1}{2}}(2c^{-1}+3b^{-1}-h^{-1})/9,$$

$$G_{44}=4\mu_H h^{-2}/3+2\mu_{Cl}c^{-2}/3+2(11h^{-2}+3c^{-2}+10h^{-1}c^{-1})\mu_C/9,$$

$$G_{45}=-\mu_H h^{-2}/3+\mu_{Cl}c^{-2}/3-\mu_C(h^{-2}-3c^{-2}+2h^{-1}c^{-1})/9,$$

$$G_{46}=-2\mu_H h^{-2}/3+2\mu_{Cl}c^{-2}/3-\mu_C(11h^{-2}-6c^{-2}-5h^{-1}c^{-1}+3h^{-1}b^{-1}-3b^{-1}c^{-1})/9,$$

$$G_{55}=7\mu_H h^{-2}/3+\mu_{Cl}c^{-2}/6+\mu_C(59h^{-2}+3c^{-2}-14h^{-1}c^{-1})/18,$$

$$G_{56}=\mu_H h^{-2}/6+\mu_{Cl}c^{-2}/3+\mu_C(h^{-2}+6c^{-2}-19h^{-1}c^{-1}+3b^{-1}c^{-1}-39b^{-1}h^{-1})/18, \text{ and}$$

$$G_{66}=\mu_H h^{-2}/3+2\mu_{Cl}c^{-2}/3+3\mu_{Br}b^{-2}/2+(11h^{-2}+27b^{-2}+12c^{-2}+6b^{-1}h^{-1}+12b^{-1}c^{-1}-20c^{-1}h^{-1})\mu_C/18.$$

Here $\mu_C(=5.0153\cdot10^{22}\ g^{-1})$, $\mu_{Br}(=7.5372\cdot10^{21}\ g^{-1})$, $\mu_{Cl}(=1.6988\cdot10^{22}\ g^{-1})$, and $\mu_H(=5.9762\cdot10^{23}\ g^{-1})$ are, respectively, the reciprocals of the masses of the C, Br, Cl, and H atoms, while $b(=1.91\text{A})$, $c(=1.76\text{A})$, and $h(=1.093\text{A})$ are the equilibrium values for the C−Br, C−Cl, and C−H bond lengths.[11]

For the a'' vibrations, the symmetry coordinates and the F and G matrix elements are not given since they are formally the same as those of Pontarelli *et al.*[9]

In order to obtain approximate potential constants, values were transferred from CCl_3X,[12] CBr_3X,[11] CBr_2Cl_2,[8] and $CHBr_2Cl$.[9] After several modifications, the resulting potential constants yielded calculated wave numbers (Table III) within 0.5 percent of the probable values for the liquid. These constants are listed in Table IV.

TABLE VI. Heat content, free energy, entropy, and heat capacity of CH_2BrCl for the ideal gaseous state at 1 atmos pressure.

T(°K)	$(H^0-E_0{}^0)/T$	$-(F^0-E_0{}^0)/T$	S^0	$C_p{}^0$
100	8.21[a]	49.25	57.46	8.85
200	8.93	55.15	64.08	10.53
273.16	9.56	58.03	67.59	12.06
298.16	9.79	58.88	68.67	12.60
400	10.77	61.89	72.66	14.64
500	11.71	64.40	76.11	16.27
600	12.59	66.61	79.20	17.58
700	13.38	68.61	81.99	18.64
800	14.09	70.45	84.54	19.52
900	14.74	72.14	86.88	20.26
1000	15.32	73.72	89.05	20.90

[a] Cal deg^{-1} $mole^{-1}$.

THERMODYNAMIC PROPERTIES

The heat content, free energy, entropy, and heat capacity at constant pressure were calculated for 11 temperatures from 100 to 1000°K, using the wave numbers listed in Table V. Vapor frequencies were used when possible. All frequencies are nondegenerate and the symmetry number is 1. Assuming tetrahedral angles, and using the bond distances and atomic masses given above, the product of the three principal moments of inertia is

$$I_A I_B I_C=1.0190\cdot10^6 \text{ awu}^3\ A^6.$$

The thermodynamic functions, calculated for a rigid rotor, harmonic oscillator model for the ideal gaseous

[10] J. C. Decius, J. Chem. Phys. **16**, 1025 (1948).

[11] Meister, Rosser, and Cleveland, J. Chem. Phys. **18**, 346 (1950).

[12] Zietlow, Cleveland, and Meister, J. Chem. Phys. **18**, 1076 (1950).

state at 1 atmos pressure, are listed in Table VI. Plyler and Benedict[13] have analyzed the rotational structure of the infrared spectrum in the region 1.6 to 3.2μ. Molecular dimensions deduced from that study are C−H=1.093A, C−Cl=1.766A, C−Br=1.911A, H−C−H=109°28′, and Br−C−Cl=112°. If these values are used to compute the product of the three principal moments of inertia, one finds that

$$I_A I_B I_C = 1.0179 \cdot 10^6 \text{ awu}^3 A^6.$$

[13] E. K. Plyler and W. S. Benedict, J. Research Natl. Bur. Standards **49**, 1 (1952).

The error in the thermodynamic functions as a result of using all angles as 109°28′ is then +0.0011 cal deg^{-1} mole^{-1} which, of course, is negligible in view of the accuracy of the present calculations.

ACKNOWLEDGMENTS

This work was part of a research program which has been aided by research grants from the Research Corporation, the Society of the Sigma Xi, and the American Academy of Arts and Sciences, and by a contract (DA-11-022-ORD-464) with the Office of Ordnance Research, U. S. Army.

THE JOURNAL OF CHEMICAL PHYSICS VOLUME 21, NUMBER 5 MAY, 1953

Note on the Nature of Conduction in Liquid Iron Oxide and Iron Silicates

M. T. Simnad and G. Derge
Metals Research Laboratory, Carnegie Institute of Technology, Pittsburgh, Pennsylvania
(Received January 20, 1953)

Current efficiency has been measured for the entire range of melts between iron oxide and the silica saturated slag. All compositions show some ionic conductivity, but the proportion of this type of conductance increases with the concentration of silica.

THE chemical constitution of liquid metal-oxide systems is still in an early state of development because of the considerable experimental difficulties involved in such work.[1,2] Recent electrochemical studies[3,4] and conductivity measurements[5–7] have indicated the presence of semiconduction in a number of molten silicate systems[3–6] and in pure iron oxide.[7]

A quantitative study of the ionic contribution to the mechanism of transport of current can be made by measuring the extent to which Faraday's law is obeyed during electrolysis of the liquid oxides. The experimental difficulties involved in such work[8] have now been met and experiments designed to test Faraday's law in the system liquid iron oxide-silica have been completed. The range of slags from pure iron oxide to iron oxide saturated with silica (42 percent silica) has been studied in iron crucibles. Direct current was passed through molten iron oxide and iron silicates at 1400°C using a pure iron rod as an anode and the crucible as the cathode. The melting and electrolysis were carried out under an argon atmosphere. Control runs showed negligible loss of weight at the anode when no current was passed. A copper coulometer was included in the circuit to measure the quantity of electricity passed during electrolysis. In this way, assuming that the cation involved is Fe^{++}, the theoretical quantity of Fe^{++} lost from the anode according to Faraday's law may be calculated, and this, when compared with the actual observed loss, gives an indication of the extent to which Faraday's law has been obeyed, and hence the amount of ionic conduction in the melt.

The results obtained are shown in Fig. 1. The main points of interest are as follows: (1) The proportion of ionic conductance does not change appreciably at compositions up to 10 percent silica. (2) There is a direct increase in ionic conductance with silica content be-

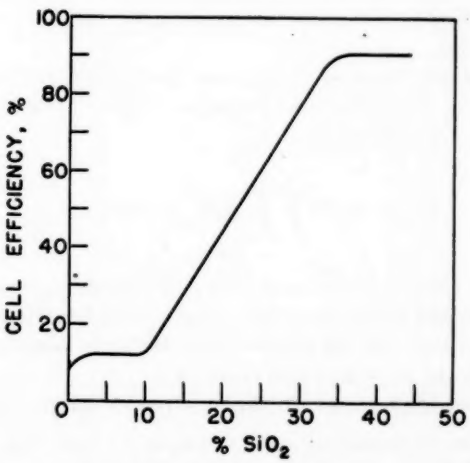

FIG. 1. Cell efficiency in the system—liquid FeO−SiO_2.

[1] John Chipman and L. C. Chang, Trans. Am. Inst. Mining Met. Engrs. **185**, 191–197 (1949).
[2] J. O'M. Bockris and J. W. Tomlinson, Research **2**, 362 (1949).
[3] Bockris, Kitchener, and Davies, Trans. Faraday Soc. **48**, 536 (1952).
[4] Bockris, Kitchener, and Davies, J. Chem. Phys. **19**, 255 (1951).
[5] Bockris, Kitchener, Ignatowicz, and Tomlinson, Trans. Faraday Soc. **48**, 75 (1952).
[6] A. E. Martin and G. Derge, Trans. Am. Inst. Mining Met. Engrs. **154**, 104 (1943).
[7] J. W. Tomlinson and H. Inouye, J. Chem. Phys. **20**, 193 (1952).
[8] Simnad, Dennis, and Derge, Rev. Sci. Instr. **23**, 248 (1952).

tween 10 percent and 34 percent silica. (3) The maximum ionic conductance begins at 34 percent silica and continues without change to saturation at 42 percent silica.

The following tentative explanations are put forward to account for these results. First, the authors agree with Richardson[9] in that there is no reason to apply any different picture to the liquid iron oxide than to the solid and thus no case for supposing the existence of distinct molecular species such as FeO and Fe_3O_4. The picture is one of ferrous and ferric ions in an oxygen ion network. The high disorder of the liquid state provides the equivalent of vacant oxygen sites in the solid crystal.[10] The concentration of ferric ions (about 10 percent in iron oxide) decreases with increase in silica content, reaching a minimum of 2 percent at about 10 percent silica.[11,12] The break in Fig. 1 at 10 percent silica may be related to this factor and indicates that above this the ions resulting from introduction of silica are increasingly effective in the conductance. The break at 34 percent silica may indicate the existence of some proportion of associated complex ions in the melts above this composition, which is close to the stoichiometric compound $2FeO \cdot SiO_2$. Our results corroborate the view that the melt consists mainly of ferrous and silicate ions.

Further discussion on the nature of the conducting ions will be postponed until transport number measurements are completed.

Support of this work has been given by a research program sponsored by the United States Atomic Energy Commission.

[9] F. D. Richardson, Disc. Faraday Soc. 4, 253 (1948).
[10] F. D. Richardson, Disc. Faraday Soc. 4, 257 (1948).
[11] N. L. Bowen and J. F. Schairer, Am. J. Sci. 5th Series, 24, 200 (1932).
[12] L. S. Darken and H. W. Gurry, J. Am. Chem. Soc. 68, 798 (1946).

THE JOURNAL OF CHEMICAL PHYSICS VOLUME 21, NUMBER 5 MAY, 1953

Simplified Relation Between Thermodynamics and Molecular Distribution Functions for a Mixture

BRUNO H. ZIMM
General Electric Research Laboratory, The Knolls, Schenectady, New York
(Received March 6, 1953)

An equation is presented connecting the chemical potential, the compressibility, and one of the molecular pair distribution function integrals of a binary mixture.

STATISTICAL mechanical techniques employing molecular distribution functions are a recent development that frequently may be used to advantage in place of the usual partition function methods. McMillan and Mayer[1] and Kirkwood and Buff[2] have published derivations of a number of formulas useful in the theory of solutions. In this note we derive from their results a simplified formula that is particularly useful for liquid solutions.

The quantities of interest are the cluster integrals, G_{11} and G_{22}, of molecules of species *1* and *2*, respectively. These are defined by

$$G_{xx}=(1/V)\int\int(F_2(i,j)-1)d(i)d(j), \tag{1}$$

where $F_2(i, j)$ is the molecular pair distribution function of specified molecules i and j and x may be either *1* or *2*. To convert to McMillan and Mayer's notation, we would use $G_{11}=2b_{20}$ and $G_{22}=2b_{02}$.

From Mayer and McMillan's power series [Eq. (57) of their paper] for the pressure p in terms of the fugacity z we may identify coefficients with the corresponding Taylor series to get

$$2b_{20}=\frac{1}{kT}\frac{z_1^2}{c_1^2}\left(\frac{\partial^2 p}{\partial z_1^2}\right)_{z_2,T}. \tag{2}$$

From Kirkwood and Buff [Eq. (19) of their paper], we have

$$G_{11}c_1=kT\left(\frac{\partial c_1}{\partial p}\right)_{T,\mu_2}-1. \tag{3}$$

In these equations c_1 is the molecular concentration, N_1/V, of component *1*, and the fugacity z_x is related to the chemical potential μ_x by the relation

$$\mu_x=kT(\ln z_x/z_{x0}), \tag{4}$$

with z_{x0} an arbitrary constant.

We may use the equation of differential calculus,

$$dc_1=\left(\frac{\partial c_1}{\partial p}\right)_{\mu_2}dp+\left(\frac{\partial c_1}{\partial \mu_2}\right)_{p}d\mu_2, \tag{5}$$

[1] W. G. McMillan, Jr., and J. E. Mayer, J. Chem. Phys. 13, 276 (1945).
[2] J. G. Kirkwood and F. P. Buff, J. Chem. Phys. 19, 774 (1951).

giving

$$(\partial c_1/\partial p)_{\mu_2}=(\partial c_1/\partial p)_{N_1/N_2} - (\partial c_1/\partial \mu_2)_p(\partial \mu_2/\partial p)_{N_1/N_2}, \quad (6)$$

and the thermodynamic equation for the Gibbs free energy G,

$$dG=d(\mu_1N_1+\mu_2N_2)=Vdp+\mu_1dN_1+\mu_2dN_2-SdT, \quad (7)$$

with the corollaries

$$\left(\frac{\partial \mu_2}{\partial p}\right)_{N_1,\,N_2,\,T}=\left(\frac{\partial \mu_2}{\partial p}\right)_{N_1/N_2,\,T} =\left(\frac{\partial V}{\partial N_2}\right)_{p,\,T,\,N_1}=v_2 \quad (8)$$

and

$$(\partial \mu_1/\partial \mu_2)_{p,\,T}=-N_2/N_1=-c_2/c_1, \quad (9)$$

the latter being the Gibbs-Duhem equation. With these we may transform either Eq. (2) or Eq. (3) into each other or into

$$\frac{G_{11}}{v_1}=kT\left[\frac{\kappa}{v_1}-\frac{v_2c_2}{v_1c_1^2}\left(\frac{\partial c_1}{\partial \mu_1}\right)_{p,\,T}\right]-\frac{1}{v_1c_1}, \quad (10)$$

where $\kappa=-(\partial \ln V/\partial p)$ is the isothermal compressibility and v_1 is the partial molecular volume.

For condensed systems the term containing the compressibility is usually negligible. With the neglect of this term and after the introduction of the volume fractions,

$$\varphi_x=c_xv_x, \quad (11)$$

Eq. (10) may be written simply in either of the two forms:

$$\frac{G_{11}}{v_1}=kT\left(\frac{\varphi_2}{\varphi_1}\right)\left(\frac{\partial \ln \varphi_1}{\partial \mu_1}\right)_{p,\,T}-\frac{1}{\varphi_1}, \quad (12)$$

$$\frac{G_{11}}{v_1}=-\varphi_2\left(\frac{\partial (z_1/\varphi_1)}{\partial z_1}\right)_{p,\,T}-1. \quad (13)$$

It can be seen that the cluster integral is exactly minus one molecular volume for any incompressible system in which the fugacity is proportional to the volume fraction. On the other hand, the integral is large and positive, indicating the presence of large clusters of molecules, in systems where the fugacity varies little with the volume fraction. Examples of such systems are liquid mixtures near the critical mixing point and dilute colloidal solutions.

These equations are simpler for condensed systems than those of Kirkwood and Buff[2] for the chemical potential. The latter contain two cluster integrals where ours contain one cluster integral and the compressibility term which is usually small or negligible.

Letters to the Editor

THIS section will accept reports of new work, provided these are terse and contain few figures, and especially few half-tone cuts. The Editorial Board will not hold itself responsible for opinions expressed by the correspondents. Contributions to this section should not exceed 600 words in length and must reach the office of the Editor not later than the 15th of the second month preceding that of the issue in which the Letter is to appear. No proof will be sent to the authors. A publication charge of $10.00 per Letter is made which, when honored, will entitle the Institution to 100 free reprints.

Burning Velocity Measurement

DOROTHY M. SIMON AND EDGAR L. WONG
Lewis Flight Propulsion Laboratory of the National Advisory Committee for Aeronautics, Cleveland, Ohio
(Received March 2, 1953)

IN a recent review of the status of burning velocity measurement Linnett[1] pointed out that there is a wide variation in the reported maximum burning velocities for methane-oxygen flames. The three values compared were (1) 620 cm/sec (Stevens, soap bubble); (2) 445 cm/sec (Singer and Heimel, Bunsen burner frustrum area with 1.5-mm burner); and (3) 330 cm/sec (Jahn, burner method total area).

Burning velocity by the soap bubble method is calculated from the rate of growth of the flame sphere radius, which should be uniform, divided by the expansion ratio of the gas mixture.[2] New work with the soap bubble method at the NACA has shown that methane in some oxygen-enriched air atmospheres and in pure oxygen at the concentration for maximum burning velocity (near stoichiometric) does not give a smoothly propagating flame. An irregular flame front develops accompanied by an increase in the rate of flame growth. For example, Fig. 1 shows representative

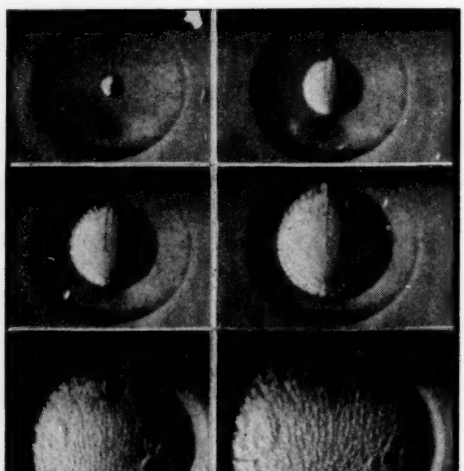

FIG. 1. Selected schlieren photographs of a flame propagating in a mixture of 28.3 percent methane, 18.0 percent nitrogen, and 53.7 percent oxygen in an aqueous soap bubble. Initial bubble diameter 4 inches. Time between frames in the original sequence 1.5×10^{-4} second.

schlieren photographs from a Fastax movie sequence of a flame propagating in a mixture of 28.3 percent methane (106 percent of stoichiometric), 53.7 percent oxygen, and 18.0 percent nitrogen in an aqueous soap bubble four inches in diameter. During approximately the first third of the flame travel the flame front is smooth, as shown in the first two photographs; during the second third the disturbed flame front develops; and for the final third a completely disturbed front as shown in the last two photographs exists. The solid curves in Fig. 2 show the increase in diameter of

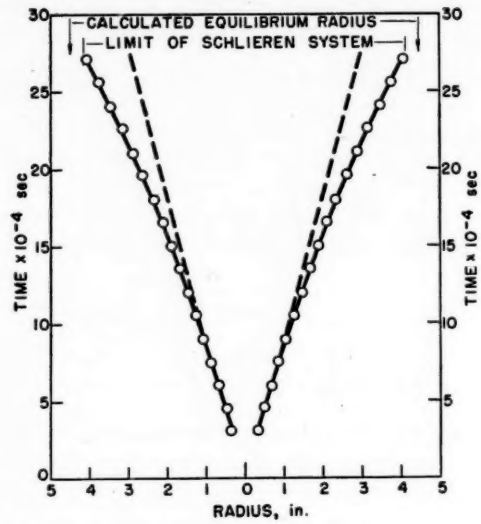

FIG. 2. Flame growth of a disturbed methane, oxygen, nitrogen flame measured from schlieren photographs of a Fastax movie sequence.

the flame sphere with time during the propagation of the flame measured from the Fastax films. The dotted lines are an extension of the initial rate of flame growth to emphasize the deviation of the experimental curves. The arrows at the top of the figure indicate the final radius of the completely burned gas calculated from equilibrium conditions. The average rate of linear propagation is about 1.5 times the initial rate for a four-inch bubble. For the same mixture in a two-inch bubble the completely disturbed flame front develops near the end of the process, and the measured average rate of linear propagation is only about 1.3 times the initial rate. Disturbed flames have also been observed for ethylene oxygen-enriched air and pure oxygen mixtures in water soap bubbles and in glycerine soap bubbles.

Visually the nature of these flames in the soap bubble is somewhat similar to the nonisotropic flames observed by Manton, Lewis, and von Elbe[3] in the spherical bomb, but the conditions are different. In the soap bubble the observed flames are fast (fundamental burning velocities 300–500 cm/sec), there is a negligible change in pressure during the course of the flame travel, and the low molecular weight component of the mixtures can be in excess. In the bomb the observed nonisotropic flames were slow (burning velocities 40–100 cm/sec), there was an appreciable change in pressure as the flames approached the bomb wall, and the low molecular weight component of the mixture was always deficient.

These observations of the nature of a flame in the soap bubble suggest that the burning velocities of methane in oxygen measured by the soap bubble method are not comparable with measurements made by the burner method, because in the former case the flame front is disturbed. The apparent burning velocity of the disturbed flame is greater than that of the undisturbed flame. Because the calculated burning velocity depends directly on the measured rate of flame propagation, the increased rate of the disturbed flame accounts for at least part of the difference between burning velocities of methane-oxygen flames measured by the soap bubble method and by a burner method.

[1] J. W. Linnett, Fourth Symposium on Combustion, Cambridge, Massachusetts, September, 1952.
[2] F. W. Stevens, J. Am. Chem. Soc. **48**, 1896 (1926).
[3] Manton, Lewis, and von Elbe, J. Chem. Phys. **20**, 153 (1952).

Nuclear Magnetic Relaxation in Viscous Liquids

ROBERT L. CONGER
U. S. Naval Ordnance Test Station, Inyokern, and Michelson Laboratory, China Lake, California
(Received March 9, 1953)

THIS work pertains to the effect of viscosity on the ability of paramagnetic ions to decrease proton relaxation time. The proton relaxation time of a paramagnetic ion solution is given by the equation[1]

$$1/T_1 = CN\mu_{eff}^2\eta/T, \quad (1)$$

where T_1 is the proton relaxation time, C is a constant, N is the concentration of paramagnetic ions, μ_{eff} is the effective magnetic moment of the paramagnetic ions, η is the viscosity, and T is the absolute temperature. The term η/T is proportional to the correlation time τ, which is the time required for the paramagnetic ions to diffuse a sufficient distance from the proton to reduce its effect substantially. A high viscosity η keeps the paramagnetic ion near the proton for a longer period and thereby increases the ion's effectiveness.

The term μ_{eff} is related to the magnetic moment μ as determined by magnetic susceptibility measurements but is not necessarily equal to μ. For example, μ_{eff} is less than $1/10\mu$ for Co^{++} ions. For any particular paramagnetic ion μ_{eff} has a value which represents the effectiveness of that ion in decreasing the proton relaxation time. μ_{eff} can be determined from proton relaxation time measurements by the use of Eq. (1). The value of μ_{eff} so determined should be a constant for any particular ion.

Figure 1 shows the effective moments of Mn^{++}, Cr^{+++}, and

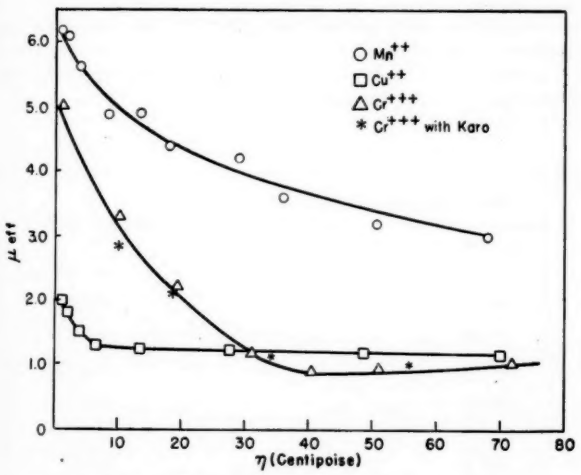

FIG. 1. Effective magnetic moment of Cu^{++}, Mn^{++}, and Cr^{+++} as a function of viscosity.

Cu^{++} ions in Bohr magnetons as a function of viscosity. The experimental points of these curves were determined by measuring the proton relaxation times of water-glycerin and water-corn syrup solutions containing the paramagnetic ions. Relaxation time measurments were made by a method described previously.[2] Water-corn syrup solutions were used for the experimental points marked with an *, while water-glycerin solutions were used for the other points. Viscosity values for the water-glycerin solutions were taken from Lange's *Handbook of Chemistry* and those of the water-corn syrup solutions were measured with a viscometer. The small concentrations of paramagnetic ions had no measurable effect on the viscosity.

The decrease in μ_{eff} with increasing viscosity for the Mn^{++} curve can be explained by the changing molecular environment of the protons as water is replaced by glycerin. The last point is for a solution which is over 80 percent glycerin, and thus the protons in the glycerin molecules are producing much of the effect. A similar effect was found by Bloembergen, Purcell, and Pound at Harvard University for water-glycerin solutions containing no paramagnetic ions. The proton relaxation time, which was much longer since no paramagnetic ions were present, did not decrease as fast as viscosity increased. Since μ_{eff} is proportional to $1/T_1\eta$, this effect would cause μ_{eff} to decrease with increasing viscosity. This could explain the shape of the curve of Fig. 1.

The curves for Cu^{++} and Cr^{+++} ions were prepared in the same way as the curve for the Mn^{++} ions except that different paramagnetic ions were used. Thus changing only the paramagnetic ions in solution has produced curves of different shapes.

The Harvard group has suggested that a short paramagnetic relaxation time may limit the value of τ when the correlation time τ is rather long. The relationship between the relaxation time for any particular ion and the correlation time is given by the equation

$$\frac{1}{T_1} = C\left[\frac{\tau}{1+\omega^2\tau^2} + \frac{2\tau}{1+4\omega^2\tau^2}\right], \quad (2)$$

where T_1 is the relaxation time, C is a constant, ω is the resonant frequency, and τ is the correlation time. From this equation we can see that when $\omega\tau \ll 1$, $T_1 = 1/3C\tau$ and T_1 will decrease with increasing τ. T_1 will reach a minimum at $\omega\tau = 1/\sqrt{2}$; and for $\omega\tau \gg 1$, $T_1 = 2\omega^2\tau/3C$ and T_1 will be proportional to τ. The resonant frequency ω for paramagnetic ions is about 2000 times larger than for protons because of the different gyromagnetic ratios and so the minimum in the T_1 *vs* τ curve is at a much shorter value τ for paramagnetic ions than for protons. It is possible that as viscosity and τ, which is proportional to viscosity, increase the paramagnetic relaxation times T_p of the Cu^{++}, and Cr^{+++} ions may decrease until they become less than τ and become the controlling factor in the values of μ_{eff}. With a further increase in viscosity T_p would reach a minimum and then increase with viscosity just as τ does. In this region where T_p is proportional to viscosity η, T_p will replace η in the equation for μ_{eff} and the dependence on η will be the same as before. This will account for the horizontal portion of the curves of Fig. 1. In the region where T_p is less than τ, but is still decreasing with increasing η, the values of μ_{eff} will decrease. This will account for the dip in the first part of the curves. Thus this mechanism will explain the shape of the Cu^{++} and Cr^{+++} ion curves.

Another possible explanation for the shape of these curves is the formation of complexes by the paramagnetic ions with either glycerin or corn sugar. Such complexes could decrease the effectiveness of the ions. It does not seem likely that glycerin and corn sugar would form complexes with Cr^{+++} ions in such a way that the experimental points would fall on the same curve. However, this is a possibility since glycerin and corn sugar have similar chemical structures. Most materials with chemical structures much different from glycerin or corn sugar cannot be used for this work since they are either insoluable in water or do not increase the viscosity of water.

Whatever the cause, the experimental curves show that the paramagnetic ions have different effects in water-glycerin or water-corn syrup solutions. These results may be of value in the study of liquids or possibly of chemical complexes.

[1] Bloembergen, Purcell, and Pound, Phys. Rev. **73**, 679 (1948).
[2] R. L. Conger and P. W. Selwood, J. Chem. Phys. **20**, 383 (1952).

The Deuterium Effect on Hydrogen Bond Distances in Crystals*

R. E. RUNDLE
Institute of Atomic Research and Department of Chemistry, Iowa State College, Ames, Iowa
(Received February 24, 1953)

SOME years ago Robertson and Ubbelohde found that strong O−H···O hydrogen bonds are lengthened when deuterium is substituted for hydrogen.[1] Though well substantiated,[2] this result is contrary to expectation and to results found for most

other substances.[3] Nordman and Lipscomb have recently suggested that the abnormal effect can be understood in terms of the broad, nearly square-well potential energy field for hydrogen in a strong hydrogen bond.[4] At a given (sufficiently high) temperature, the higher vibrational levels of the deuterium compound will be filled to a larger extent than the more widely spaced levels in the hydrogen compound, leading to a broadening of the deuterium distribution and thence to a broadening of the well.

The one point which offers hope for testing the Nordman-Lipscomb explanation of the Robertson-Ubbelohde effect is that it makes the effect temperature dependent. Thus, at sufficiently low temperatures essentially only the zero vibrational states will be occupied in both hydrogen and deuterium compounds, and then the substitution of deuterium for hydrogen should shorten, or at least not lengthen, strong hydrogen bonds. To test the proposal, it is necessary to have accurate lattice constants for strongly intermolecularly hydrogen-bonded crystals, deuterated and undeuterated, both at normal and low temperature. The only data in the literature which come close to fulfilling these requirements are those for ice and heavy ice. Megaw[5] reports lattice constants at 0° and −66°C as follows:

	0°		−66°	
H_2O	$a_0=4.5135$	$c_0=7.3521$A	$a_0=4.5085$	$c_0=7.338$A
D_2O	4.5165	7.3537	4.5055	7.338

Thus, the data support the Nordman-Lipscomb explanation, since there is a reversal of effect in this temperature range. The size of the effect is, however, about comparable with the experimental error in the lattice constants. It would be interesting to see the results for shorter hydrogen bonds where the changes should be more spectacular.

* Contribution from the Institute for Atomic Research and Department of Chemistry, Iowa State College, Ames, Iowa. Work was performed in the Ames Laboratory of the U. S. Atomic Energy Commission.

[1] J. M. Robertson and A. R. Ubbelohde, Proc. Roy. Soc. (London) **170A**, 222 (1939); A. R. Ubbelohde, *ibid.* **173A**, 417 (1939).
[2] A. R. Ubbelohde and I. Woodward, Proc. Roy. Soc. (London) **179A**, 399 (1942); D. H. W. Dickinson and A. R. Ubbelohde, Acta Cryst. **3**, 6 (1950).
[3] E. Zintl and A. Harder, Z. physik. Chem. **28B**, 478 (1935); R. E. Rundle, J. Am. Chem. Soc. **69**, 1719 (1947).
[4] C. E. Nordman and W. N. Lipscomb, J. Chem. Phys. **19**, 1422 (1951).
[5] H. D. Megaw, Nature **134**, 900 (1934).

On the Raman Spectrum of Monomeric Methyl Methacrylate at −180°C

S. C. Sirkar and N. K. Roy
Indian Association for the Cultivation of Science, Optics Department, Jadavpur, Calcutta, India
(Received March 3, 1953)

It was pointed out previously by Hibben[1] that the line 1638 cm^{-1} of monomeric methyl methacrylate disappears and several other new lines appear when the liquid is polymerized. Patel,[2] on the other hand, claimed to have observed a line at 1598 cm^{-1} in place of the line 1638 cm^{-1} in the Raman spectrum of the polymer and remarked that Hibben's conclusion that the polymerization takes place at the expense of C=C bond is to be revised. It was thought worth while to reinvestigate the problem. Further, the Raman spectrum of the monomer in the solid state at −180°C was not studied by any previous worker. We have, therefore, studied the Raman spectrum of the polymer in the form of Plexiglas supplied by I.C.I. Ltd. and have compared the results with those obtained with the monomer in the liquid state at about 28°C and in solid state at −180°C. The monomer was found not to undergo any change after the exposure, and the mass solidified and cooled to −180°C. When brought to room temperature, it was found to be a liquid having the same properties as those of the liquid before the exposure. The results are given in Table I. The visually estimated intensities are given in parentheses. The spectrograms due to the monomer in the liquid state at 28°C and in the solid state at −180°C are reproduced in Fig. 1(a) and Fig. 1(b), respectively.

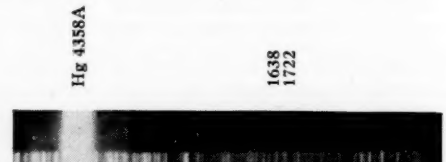

Fig. 1. (a) Raman spectrum of methyl methacrylate (liquid) at 28°C. (b) Raman spectrum of the same substance at −180°C.

It can be seen from Table I that the line 1638 cm^{-1} is the most intense line in the Raman spectrum of the liquid monomer, but this line as well as the line 1408 cm^{-1} is totally absent in the Raman spectrum of the polymer. These results are in agreement with those reported by Hibben. The lines 228, 282, and 2954 cm^{-1} observed in the case of the monomer were not reported by Hibben. These lines are not due to partial polymerization of the monomer during the exposure, as can be seen from the fact that the intense lines 976 and 816 cm^{-1} due to the polymer were not observed in the case of the monomer and also that the low frequency lines observed in the latter case are different from those observed in the former case. The line 1722 cm^{-1} is also observed to diminish in intensity with polymerization.

Table I.

Methyl methacrylate monomer		
Liquid at 28°C $\Delta\nu$ in cm^{-1}	Solid at −180°C $\Delta\nu$ in cm^{-1}	Plexiglas at 28°C $\Delta\nu$ in cm^{-1}
228 (2)		238 (0b)
282 (1b)		300 (1)
380 (5)	380 (0b)	380 (1b)
507 (2)	506 (0)	507 (2b)
603 (3)		600 (4)
658 (0)		
833 (8)	838 (2)	816 (5)
937 (2)	937 (0)	976 (5)
998 (1b)	998 (0)	
1012 (2)	1014 (1)	1002 (4) 1122 (0)
1335 (1)	1327 (2b) 1383 (1)	1188 (0) 1340 (0b)
1408 (5)	1408 (2)	
1448 (3b)	1460 (2b)	1462 (5b)
1638 (10)	1630 (3)	1731 (2)
1722 (8)	1700 (5)	2853 (2)
2850 (1)	2852 (0b)	2962 (8b)
2934 (3)	2934 (1) 2951 (0)	3024 (3b)
2954 (3)	2969 (0) 2991 (2)	
3002 (2)	3024 (2)	
3108 (2)	3103 (2)	3109 (0b)

Table I further shows that when the monomer is solidified and cooled to −180°C, the line 1638 cm^{-1} shifts to 1630 cm^{-1} and becomes much weaker than the line 1700 cm^{-1} corresponding to the line 1722 cm^{-1} due to the liquid. This indicates the formation of bonds between some of the neighboring molecules at the expense of the C=C bonds. This process is, however, different from the regular polymerization process, because the changes observed in the intensities and positions of some of the prominent lines, e.g., the lines 833, 998, and 2934 cm^{-1} are different from those observed in the case of the polymer.

These results thus furnish direct evidence regarding the formation of chemical bonds between neighboring molecules in the solid state at −180°C at the expense of the strong C=C bond. Details will be published elsewhere.

[1] J. H. Hibben, J. Chem. Phys. 5, 706 (1937).
[2] M. M. Patel, Current Science 18, 436 (1949).

Temperature Variation of the Paramagnetic Resonance Absorption of Two Free Radicals

L. S. Singer and E. G. Spencer
Electricity Division, Naval Research Laboratory, Washington, D. C.
(Received February 23, 1953)

PARAMAGNETIC resonance absorption in organic free radicals has been reported by several investigators.[1-3] The resonance in these substances is characterized by a very narrow line width, in some cases, the width at half-maximum absorption being one gauss or less. It has been suggested[2] that in these free radicals strong exchange forces manifest themselves by causing the fourth moment of the absorption line to increase, giving rise to a narrowing of the curve near the peak with a resulting broadening in the wings.

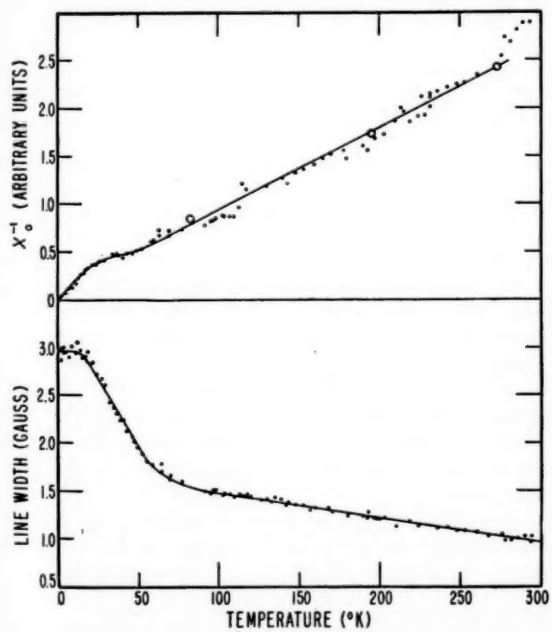

FIG. 1. Upper curve: variation of the reciprocal of the static susceptibility of *I* with temperature. Lower curve: variation of line width of *I* with temperature.

In order to obtain further information concerning the magnetic properties of these substances, we have measured the resonance absorption of two free radicals α,α-diphenyl-β-picryl hydrazyl (denoted *I*) and tris-*p*-nitro phenyl methyl (denoted *II*) as a function of temperature from 2.5°K to 295°K at a frequency of 25 mc.

The samples were inserted into the coil of a weakly oscillating regenerative oscillator, a length of inconel coaxial line serving as the connection between the coil and the rest of the circuit which was maintained at room temperature. The coil was placed at the center of a double Dewar along the axis of a large solenoid. To obtain temperatures between 80°K and room temperature, various amounts of liquid nitrogen were added to the outer Dewar, and several warming and cooling cycles were used over the same temperature range. The temperature variation in this region during a width and maximum intensity determination was kept less than 0.4°. Temperatures between 4.2° and 60° were obtained by controlling the rate of desorption of helium by activated charcoal surrounding the sample.[4] The estimated error in the temperature measurements, except for *II* between 150°K and room temperature, was less than 2°.

The results of a resonance measurement were displayed on a Leeds and Northrup X-Y recording potentiometer, the two variables being the output of a phase detector and the potential drop across a manganin resistance in series with the solenoid supplying the static magnetic field. The 280-cycle modulating field was 0.04 gauss for *I* and 0.02 gauss for *II*, a modulation small enough compared to the absorption line width to insure the output of the phase detector to be a measure of the slope of the absorption curve. In order to measure relative intensities, a calibrator circuit[5] was employed. The oscillator frequency for the experiments on *I* was 25.00±0.05 mc; for the experiments on *II*, the frequency was 27.50±0.05 mc.

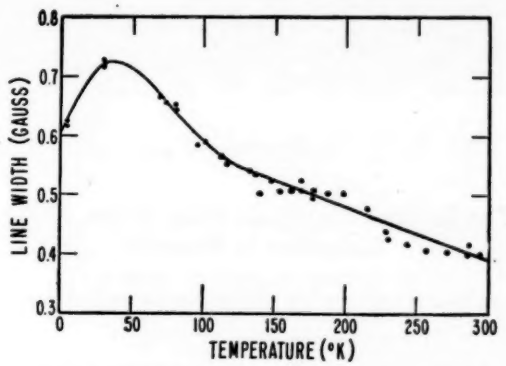

FIG. 2. Variation of line width of *II* with temperature.

The lower curve in Fig. 1 shows the variation of line width with temperature for sample *I*; the line width *vs* temperature curve for sample *II* is shown in Fig. 2. By line width we mean the total width in gauss between inflection points of the absorption curve.

In order to attach more significance to the line width measurements, line shapes were investigated in some detail. This was done by numerically integrating the slope curves obtained from the recorder charts and comparing the resulting absorption curves with both a Lorentzian and a Gaussian type curve. For *I*, the shape was intermediate between the two both at room and liquid helium temperatures. For *II*, the shape was much closer to Lorentzian. To obtain information concerning the variation of static susceptibility of *I* with temperature, it was assumed that an approximate form of the Kramers-Kronig[6] relations,

$$\chi_0=\frac{2}{\pi H_0}\int_0^\infty \chi''dH,$$

was applicable to our measurements. χ_0 is the static susceptibility, χ'' the imaginary part of the susceptibility, and H the magnetic field.

For an absorption curve of given shape, the product of the maximum slope and line width is directly proportional to the area of the χ'' *vs* H curve and thus proportional to χ_0. Since line width and maximum slope were obtained directly from our

recorder tracings, the reciprocal of the above-mentioned product denoted χ_0^{-1} is shown plotted *vs* temperature in Fig. 1. The circled points are taken from the static susceptibility measurements of Selwood and Turkevich[7] and are normalized so that the 273°K point would fall on the experimental curve.

The effective g values at 4.2°K for both *I* and *II* were approximately 0.1 percent lower than the g for *I* at room temperature; however, the average error in the g determinations was about 0.05 percent.

It was expected that the strong exchange forces postulated for these substances might produce some type of cooperative phenomenon at low temperatures. The apparent transition in line width for *I* between 20°K and 50°K was not accompanied by a sudden decrease in absorption intensity as has been observed in antiferromagnetic substances in the vicinity of the Curie temperature.[8]

The increase in line width with decreasing temperature for both *I* and *II* suggests that a mechanism similar to the "freezing out" of molecular motions in the case of nuclear resonance,[9] may be involved here.

The authors wish to thank Dr. C. A. Hutchison, Jr., and Mr. R. Pastor for the sample *II* used in these measurements.

[1] Holden, Kittel, Merritt, and Yager, Phys. Rev. **75**, 1614 (1949); **77**, 147 (1950).
[2] C. H. Townes and J. Turkevich, Phys. Rev. **77**, 148 (1950).
[3] Hutchison, Pastor, and Kowalsky, J. Chem. Phys. **20**, 534 (1952).
[4] This technique was suggested by R. T. Webber and P. B. Alers. A similar technique is described by Jackson and Preston-Thomas, J. Sci. Instr. **28**, 99 (1951).
[5] G. D. Watkins, Department of Physics, Harvard University, private communication.
[6] See, for example, Gorter, *Paramagnetic Relaxation* (Elsevier Publishing Company, Inc., Amsterdam, 1947), p. 21.
[7] Selwood and Turkevich, J. Am. Chem. Soc. **63**, 1077 (1941).
[8] Trounson, Bleil, Wangsness, and Maxwell, Phys. Rev. **79**, 542 (1950).
[9] Bloembergen, Purcell, and Pound, Phys. Rev. **73**, 679 (1948).

The Excited Electronic State of the 2600A Transition in Benzene

A. C. Albrecht and W. T. Simpson
Department of Chemistry and Chemical Engineering, University of Washington, Seattle, Washington
(Received March 16, 1953)

RECENTLY Parr, Craig, and Ross[1] have summarized the predictions made for benzene by the molecular orbital and the valence bond approximations and their refinements. Each of these methods indicates that the first singlet excited electronic state is of the symmetry species B_{2u}. In spite of claims to the contrary, we feel that the certainty of this assignment still awaits experimental confirmation.[2]

We have performed a series of experiments which are internally consistent and from which it is concluded that the excited electronic state involved does indeed belong to the species B_{2u}.[3]

The experiments deal with *para*-disubstituted benzene derivatives, including *p*-dimethoxybenzene. The derivatives were chosen because the absorption bands are strong and structureless; hence low resolution polarization measurements can be interpreted as giving directly information about the electronic part of the vibronic wave functions.

Essentially these derivatives belong to the symmetry group V_h.[4] The theoretical aspect of our experiments is based on the correlation between species of the groups D_{6h} and V_h. In the derivatives, the band which is related to the 2600A band of benzene represents a transition involving excitation to an upper state which we show to be of the species B_{3u} (the species of the translation "y," where "y" is in-plane and perpendicular to the line joining the substituents). Assuming that the 2600A transition of benzene is forbidden but made allowed on *para*-disubstitution, the B_{2u} assignment for benzene follows.[5] It remains to be shown how the B_{3u} assignment was obtained. We shall also indicate the reasons for believing that the absorption bands of benzene and the derivatives can be related, and that the benzene transition is one which is forbidden and made allowed on *para*-disubstitution.

In this preliminary report only one of a set of consistent results is described. The species of the excited electronic state is determined by a study of the crystal spectrum, obtained with polarized light, of *p*-dimethoxybenzene, a compound of known crystal structure.[6] We have been able to obtain crystal flakes (facing on the 001 plane, which contains the "a" and "b" axes) thin enough for absorption work by a sublimation procedure developed in this laboratory by Mr. R. C. Nelson.

The molecule in the crystal is oriented in a manner such that the square of the projection of the "y" component onto the "b" axis of the crystal is 2.03 times the square of its projection onto the "a" axis, while the square of the projection of the "x" component (in-plane, perpendicular to "y") onto the "b" axis is 150 times the square of its projection onto the "a" axis. Assuming an oriented gas model for the crystal,[7] and discounting the thermal motion of the molecules, these projections onto the axes are directly proportional to the appropriate extinction coefficients for polarized radiation incident on the 001 plane.

The crystal spectrum was obtained with a spectrophotometer consisting of a Bausch and Lomb grating monochromator and a Photovolt multiplier photometer, series 520-M. The source used was a Beckman No. 2230 hydrogen discharge lamp, and the light was polarized by reflection from a stack of quartz plates. The crystal was first viewed along the "a" axis, then along the "b" axis. Density measurements were obtained in the 2150A–3150A region and were properly corrected for incomplete polarization of the incident light. In this region two bands were evident; one centered about 2280A, and the other, which is related to the 2600A band of benzene, centered about 2950A. Our results show that over this latter band the "b" axis/"a" axis density ratio is 2.0 ± 0.1 (to be compared with 2.03 for pure "y") in the region 2900A to 3050A, becoming larger at both shorter and longer wavelengths (at 3100A the ratio is 2.6 ± 0.2). Additional studies show that absorption with the electric vector oriented in the "z" direction (figure axis), if present, plays a negligible role. Thus we can say that the 2950A transition, which gives rise to an intense and structureless absorption band, involves predominantly "y" absorption. Equivalently, the species of the upper level is B_{3u} of V_h.

Using the theory of Daub and Vandenbelt,[8] we have been able to identify positively the 2950A transition of *p*-dimethoxybenzene as being derived from the 2600A transition of benzene.

The vibrational analysis of the 2600A band of benzene by Sponer, Nordheim, Sklar, and Teller[9] and by Garforth, Ingold, Poole, and co-workers[10] has shown that the transition is forbidden and that the excited electronic state involved belongs either to the species B_{1u} or B_{2u}. We have shown that the B_{2u} assignment is the correct one.

Our experiments demonstrate the presence of both "x" and "y" absorption in the 2280A band, which corresponds to the 2035A band of benzene. At present we are investigating this spectrum more thoroughly and hope to present a quantitative interpretation at a later date.

We are grateful for the aid given us by Mr. J. D. Turner in matters dealing with the crystal structure of the sublimation flakes.

[1] Parr, Craig, and Ross, J. Chem. Phys. **18**, 1561 (1950).
[2] See also footnote 15a, C. C. J. Roothaan and R. S. Mulliken, J. Chem. Phys. **16**, 118 (1948).
[3] In this letter we assume, as is commonly done, that the transitions which we are considering always occur from a totally symmetric ground state.
[4] In order to classify *p*-dimethoxybenzene in this way, we must exclude the methyls. Our experiments indicate that this simplification is reasonable.
[5] The notation used is that found in H. Sponer, Revs. Modern Phys. **14**, 224 (1942), except that "x" and "y" are interchanged.
[6] Goodwin, Przybylska, and Robertson, Acta Cryst. **3**, 279 (1950).
[7] Evidence for the validity of this model is the near equality of absorption maxima in the solution and crystal spectra.
[8] L. Daub and J. M. Vandenbelt, J. Am. Chem. Soc. **69**, 2714 (1947).
[9] Sponer, Nordheim, Sklar, and Teller, J. Chem. Phys. **7**, 207 (1939).
[10] Garforth, Ingold, and Poole, J. Chem. Soc. **1948**, 406.

A Slot Burner Method for Studying Combustion Wave Instability*

G. H. MARKSTEIN AND L. M. SOMERS
Cornell Aeronautical Laboratory, Inc., Buffalo, New York
(Received March 2, 1953)

QUANTITATIVE studies of combustion wave instability[1] have been performed mainly by two methods: observation of polyhedral flames burning on circular ports[2–6] and of cellular flames burning in wide tubes.[7] Their primary objectives were determinations of limit conditions of instability and measurements of average cell sizes.

An ideal experimental procedure should yield data that would depend only on composition and state of the combustible mixture. The tube method approached this ideal closely, owing to the complete absence of entrainment of extraneous gases into the flame, and the lack of wall effects over a major portion of flame area. The technique turned out to be inapplicable, however, for burning velocities exceeding about 15 cm/sec. Moreover, cell sizes could be determined only by a cumbersome and subjective procedure that yielded merely a statistical average.

The study of polyhedral flames can be extended to much higher burning velocities, but it has other serious limitations. It seems obvious that the disturbances responsible for polyhedral structure originate at the flame base and thereafter merely propagate upward along generatrices of the flame "cone." The selection of the length of the polygon sides at the flame base as a measure of cell size[2,4] appears therefore justified. However, since the location of the flame base cannot be determined with precision, an appreciable uncertainty is introduced into the measurement of cell sizes. Furthermore, owing to its origin, the appearance of polyhedral structure depends predominantly on the complex conditions of wall quenching and entrainment near the flame base. This is borne out by the entirely different behavior of open and enclosed (Smithells) flames[2,3] and by the influence of flow rate and burner configuration on limits of polyhedral structure and on cell sizes.[4]

A search for methods that would eliminate the shortcomings of the tube technique without accepting all the drawbacks of polyhedral flame studies led to the slot burner design shown schematically in Fig. 1. The premixed combustible gases enter the

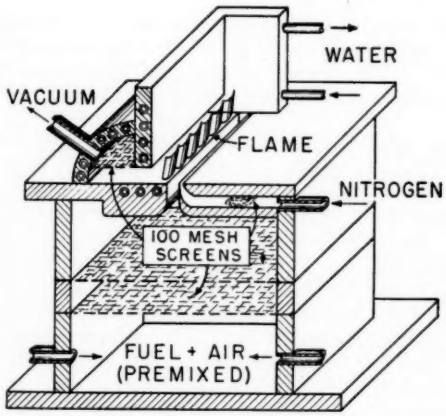

FIG. 1. Slot burner set-up.

narrow rectangular slot of adjustable width after passing through a settling chamber, calming screens, and a contracting section. A stream of nitrogen issuing from a parallel auxiliary slot prevents attachment of the flame on one side of the burner port. In the absence of instability the flame thus assumes the shape of a practically plane surface slanting inward from the other slot edge. In the case of instability, disturbances originate at the flame base, as in polyhedral flames, and propagate upward along its surface, but owing to the quasi two-dimensional flow the resulting ridges remain parallel throughout the flame height. Their spacing thus provides a convenient measure of cell size that can be determined with ease and accuracy.

Results obtained with open slot flames, however, depended strongly on flow rate and slot width. Further experiments showed that the influence of these variables was primarily due to air entrainment at the flame base. Enclosure of the flame did not remove this difficulty, as the resulting entrainment of burned gases caused highly unsteady burning or blow-off. Surprisingly steady flames were obtained, however, over wide ranges of composition and flow rate, by means of partial exhaust of burned gases through a suction slot incorporated near the flame base in the water-cooled enclosure (Fig. 1). Preliminary measurements indicated that this device reduced the influence of flow rate and slot width appreciably.

Figure 2 shows typical flames obtained with this burner. One unique feature of the technique is the possibility of determining

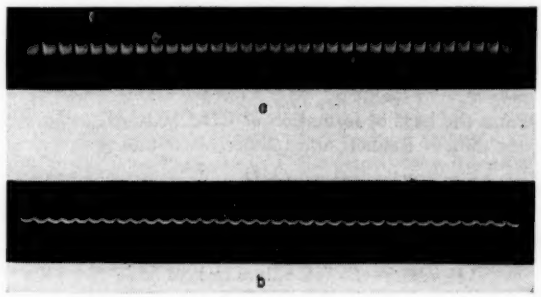

FIG. 2. Cellular slot burner flames; (a) front view; (b) edge-on view. Butane-air mixtures; fuel concentration about 1.4 times stoichiometric. Slot dimensions 16.2 × 0.25 cm.

amplitude in addition to wavelength of flame front distortion by taking edge-on photographs, thus arriving at a measure of intensity of the instability phenomenon. Further details and results of this work will be published later.

* This research was conducted under the auspices of Project SQUID, jointly sponsored by the U. S. Office of Naval Research and the U. S. Office of Air Research.

[1] G. H. Markstein, *Fourth Combustion Symposium* (Williams & Wilkins, Baltimore, to be published).
[2] F. A. Smith and S. F. Pickering, J. Research Natl. Bur. Standards **3**, 65 (1929).
[3] H. Behrens, Naturwiss. **32**, 297, 299 (1944); Z. physik. Chem. **196**, 78 (1950).
[4] G. W. Culshaw and J. E. Garside, Gas World **125**, 674 (1946); J. E. Garside and B. Jackson, *Fourth Combustion Symposium* (Williams & Wilkins, Baltimore, to be published).
[5] D. B. Leason, *Engines* (Department of Supply and Development, Melbourne, Australia, 1949). (Note 132).
[6] W. Jost and L. Sieg, Z. Naturforsch. **6a**, 403 (1951); Jost, Krug, and Sieg, *Fourth Combustion Symposium* (Williams & Wilkins, Baltimore, to be published).
[7] G. H. Markstein, J. Aero. Sci. **18**, 199 (1951); G. H. Markstein and L. M. Somers, *Fourth Combustion Symposium* (Williams & Wilkins, Baltimore, to be published).

Some Theoretical Considerations of Ether Decompositions

B. G. GOWENLOCK
Department of Chemistry, University College of Swansea, University of Wales, Swansea, Wales
(Received February 10, 1953)

BOND dissociation energy data for ethers and heat of formation data for radicals produced in ether decompositions have not been previously tabulated except for a recent publication by Rebbert and Laidler.[1] These authors give a value for the heat of formation of the ethoxy radical. Considering this value, together with the heat of formation data for diethyl ether, formaldehyde,

and methyl radical, they conclude that the pyrolysis of diethyl ether is best represented by the scheme

$$C_2H_5OC_2H_5 \rightarrow C_2H_5+OC_2H_5$$
$$OC_2H_5 \rightarrow HCHO+CH_3$$
$$C_2H_5+C_2H_5OC_2H_5 \rightarrow C_2H_6+CH_3CHOC_2H_5$$
$$CH_3+C_2H_5OC_2H_5 \rightarrow CH_4+CH_3CHOC_2H_5$$
$$CH_3CHOC_2H_5 \rightarrow CH_3CHO+C_2H_5.$$

The chain ending process is a reaction of $CH_3CHOC_2H_5$ radicals with methyl or ethyl radicals, first-order kinetics for the decomposition resulting. The authors prefer this scheme to that of Rice and Herzfeld[2] who give the initial reaction

$$C_2H_5OC_2H_5 \rightarrow CH_3+CH_2OC_2H_5.$$

It is our purpose to employ available thermochemical and kinetic data to elucidate the likelihood of these mechanisms.

Let us represent $D(CH_3CHO-C_2H_5)$ by D_1 and

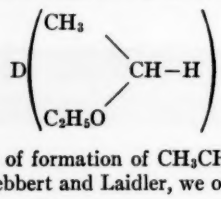

by D_2 and the heat of formation of $CH_3CHOC_2H_5$ as Q_1. Then, using the data of Rebbert and Laidler, we obtain

$$Q_1=18+D_1,$$
$$Q_1=111.5-D_2,$$

giving the expression

$$D_1=93.5-D_2 \text{ (all values in kcal mole}^{-1}).$$

Thus if $CH_3CHOC_2H_5$ is to have the necessary stability to take part in the mechanism cited by Rebbert and Laidler, D_2 must be much less than 93.5 kcal mole^{-1} and/or the activation energy for

$$CH_3CHO+C_2H_5 \rightarrow CH_3CHOC_2H_5$$

must be high. It is known[3] that $D[(CH_3)_2CH-H]$ is 94 kcal mole^{-1}, and it might be expected that there would be little difference for the secondary C—H bond in diethyl ether. If the $CH_3CHOC_2H_5$ radical is unstable, then chain ending will be due to methyl and ethyl radicals alone and the decomposition will no longer be first order.

We can apply similar thermochemical considerations to the Rice-Herzfeld mechanism as given by Smith and Hinshelwood,[4]

$$C_2H_5OC_2H_5 \rightarrow CH_3+CH_2OC_2H_5 \quad (1)$$
$$CH_2OC_2H_5 \rightarrow CH_3+CH_3CHO \quad (2)$$
$$CH_3+C_2H_5OC_2H_5 \rightarrow C_2H_6+CH_2OC_2H_5. \quad (3)$$

They consider that reaction (2) is slow compared with (3) to account for the observed differences in propylene and nitric oxide inhibition, the former mainly combining with CH_3 radicals, the latter with $CH_2OC_2H_5$ radicals. Let us represent $D(CH_3-CH_2OC_2H_5)$ as D_3, the endothermicity of (2) as D_4, and the heat of formation of $CH_2COC_2H_5$ as Q_2. Then, again using the data of Rebbert and Laidler, we have

$$D_3=90.6-Q_2,$$
$$D_4=Q_2-13,$$

giving the expression

$$D_3=77.6-D_4 \text{ (all values in kcal mole}^{-1}).$$

As Rebbert and Laidler[1] give $D(C_2H_5-OC_2H_5)$ as 77.5 kcal mole, if this mechanism is to occur it is necessary for D_3 to be less than 77.5, i.e., D_4 must be greater than zero (we assume the back reactions of both possible primary reactions to have zero activation energy). Rice and Johnston[5] determined the activation energy of the decomposition of diethyl ether into radicals to be 68.6 kcal mole^{-1}, and this may be taken as a lower limit.[6] Thus D_4 is between 0 and 9 kcal mole^{-1}, and for the $CH_2OC_2H_5$ radical to have the stability ascribed to it by Smith and Hinshelwood, the activation energy for

$$CH_3+CH_3CHO \rightarrow CH_2OC_2H_5$$

must be high.

Analogies can be provided from the available data for the decomposition of dimethyl ether. Let $D(CH_3OCH_2-H)$ be D_5, $D(CH_3-OCH_2)$ be D_6, and the heat of formation of CH_2OCH_3 be Q_3. Using the value 19 kcal mole^{-1} given by Marcus, Darwent, and Steacie[7] for the activation energy of

$$CH_3OCH_2 \rightarrow CH_3+HCHO$$

and signifying the activation energy of

$$CH_3+HCHO \rightarrow CH_3OCH_2$$

as E, we have the following relationships:

$$D_5+Q_3=97.3,$$
$$D_6=Q_3+2.3,$$
$$D_6=19-E,$$

giving the expression

$$D_5=80.6+E \text{ (all values in kcal mole}^{-1}).$$

The data of Rebbert and Laidler are used; the heat of formation of dimethyl ether is calculated from the heat of combustion value given by Kharasch.[8*]

If E is small (compare

$$CH_3+C_2H_4 \rightarrow C_3H_7,$$

activation energy 1–2 kcal mole, reference 6, page 312), then D_5 is decidedly low. Even if E is as high as 13 kcal mole^{-1} the value for $D(CH_3OCH_2-H)$ is still low compared with $D(C_2H_5-H)$.

The evidence available would therefore suggest that one or more of the three following conclusions is possible.

(1) Substitution of CH_3O and C_2H_5O for CH_3 in ethane and propane, respectively, leads to a considerable drop in the primary and secondary C—H bond dissociation energies, respectively.

(2) The activation energies for the reactions

$$HCHO+CH_3 \rightarrow CH_2OCH_3$$
$$CH_3+CH_3CHO \rightarrow CH_2OC_2H_5,$$

are in the 10–20 kcal mole^{-1} range.

(3) The heats of combustion (and hence of formation) for dimethyl and diethyl ethers are in error by as much as 10–20 kcal mole^{-1}. In the event of conclusion (3) being correct, there are no available accurate values for heats of dissociation of R—OR bonds.

It would therefore seem to be difficult on the basis of available evidence to decide between the two mechanisms cited for the decomposition of diethyl ether. If evidence is forthcoming to confirm that the radicals $CH_2OC_2H_5$ and $CH_3CHOC_2H_5$ are very unstable, then it becomes a matter of difficulty to account for the experimental data of Smith and Hinshelwood[4] of inhibition of diethyl ether decomposition by propylene and nitric oxide. Recent data[9,10] would suggest that at the temperatures involved in the work of Smith and Hinshelwood, the reaction of a methyl radical is faster with nitric oxide than with propylene by a factor of approximately 10. This would seem to imply a reconsideration of the inhibition mechanism proposed by these authors.

[1] R. E. Rebbert and K. J. Laidler, J. Chem. Phys. **20**, 574 (1952).
[2] Rice and Herzfeld, J. Am. Chem. Soc. **56**, 284 (1934).
[3] Szwarc, Disc. Faraday Soc. **10**, 336 (1951).
[4] Smith and Hinshelwood, Proc. Roy. Soc. (London) **A180**, 237 (1942).
[5] Rice and Johnston, J. Am. Chem. Soc. **56**, 214 (1934).
[6] E. W. R. Steacie, *Atomic and Free Radical Reactions* (Reinhold Publishing Corporation, New York, 1946), p. 113.
[7] Marcus, Darwent, and Steacie, J. Chem. Phys. **16**, 987 (1945).
[8] Kharasch, J. Research Natl. Bur. Standards **2**, 359 (1929).
[*] The value given in Tables of Selected Values of Chemical Thermodynamic Properties, Series I (National Bureau of Standards, Washington, 1948), is $D_5=79.5+E$.
[9] A. F. Trotman-Dickenson and E. W. R. Steacie, J. Chem. Phys. **19**, 169 (1951).
[10] R. W. Durham and E. W. R. Steacie, J. Chem. Phys. **20**, 582 (1952).

Relative Energies of Polar and Nonpolar Valence Bond Functions and Molecular Orbital Method. I*

MAX WOLFSBERG
Department of Chemistry, Brookhaven National Laboratory, Upton, Long Island, New York
(Received March 4, 1953)

THE introduction of configurational interaction into the molecular orbital theory treatment of molecules such as hydrogen, carbon, nitrogen, and cyclobutadiene has been found to lead in the ground states to an increase in the contribution of nonpolar valence bond functions with respect to polar valence bond functions. The relative contributions of polar and nonpolar structures to molecular wave functions will depend in part on their relative diagonal energies. The question then arises whether we calculate these relative energies correctly in view of the fact that we usually miscalculate these differences at infinite separation with the atomic orbitals employed in the LCAO molecular computations.

Moffit[1] has recently demonstrated that the energy matrix element between valence bond functions X and Y can be written in the form $H_{XY}=M_{XY}W_Y+V_{XY}$, if one uses the appropriate separated atom wave functions. Here M_{XY} is the overlap integral between X and Y, W_Y is the energy of the separated atoms corresponding to Y, and V_{XY} is an interaction term vanishing at infinite separation of the atoms. On the basis of his analysis, Moffit[2] applied correction terms to a molecular orbital calculation of the oxygen molecule. Three types of computations on H_2 and C_2H_4 (treated as a 2π-electron system[3]) have been undertaken here to investigate further such corrections of the molecular orbital method: (A) a valence bond approach employing experimental values of W but M_{XY} and V_{XY} computed with approximate wave functions; (B) addition of correction factors to molecular orbital computations based on the expansion of the molecular orbital functions in terms of valence bond functions and correcting on the assumption that terms $M_{XY}W_Y+V_{XY}$ appear in the molecular orbital matrix elements for each corresponding valence bond term; (The correction term is computed from the difference between the experimental value of W_Y and the one computed with the approximating atomic orbitals employed.) (C) a molecular orbital method with those correction factors employed at all separations which were calculated by method (B) at infinite separation. (This is the form of the correction employed by Moffit.) One of the purposes of these computations is to explore the effect of the form of the atomic orbitals on the results and to see if these methods give meaningful results if only one atomic orbital Z value is used for a given atom for all molecular states, as is usually done. In the one case where some work on the best Z values in different molecular states has been carried out for normal molecular orbital calculations, namely H_2, it is found that greatly different Z's must be used for different states at short internuclear distances.

Computations by method (A) on H_2 show that, while at large distances when the overlap integrals between s orbitals is of the order of 0.3 the interaction terms vary but little with the Z values, at short distances these variations become large indeed. With Z equal to 1, one finds, in the vicinity of the equilibrium distance, that the energies of polar valence bond functions become nearly equal to or even less than the energies of the corresponding nonpolar functions in computations by methods (A), (B), and (C). This apparent overcorrection[4] is remedied by lowering the Z values of ionic structure atomic orbitals. It must also be pointed out that at small distances, where method (A) becomes highly dependent on Z, methods (B) and (C) also become highly dependent on Z and do not too closely approximate method (A). At large internuclear distances however, methods (B) and (C) approximate method (A) quite well. One thus concludes that, at short distances, the correction factors as applied to a standard molecular orbital treatment with a single Z value is more empirical than one might have hoped.

It has already been stated by Moffit that the introduction of correction factors into the ethylene computation would force this calculation, as regards the first excited singlet-triplet separation, into closer agreement with experiment. Some of the results of our computations on ethylene are shown in Table I, and compared there with experiment and with the standard molecular orbital results. In the vicinity of $Z=3.18$, the dependence of method (A) on Z[5] is somewhat larger than that in the similar H_2 problem at corresponding overlap. Methods (B) and (C) approximate method (A) fairly well, probably largely because of the Mayer-Sklar approximations used in all of these computations.

TABLE I. Energies in ev.[a]

	Method (A)		Method (B)	Standard M.O.	
	$Z=3.18$	$Z=2.74$	$Z=3.18$	$Z=3.18$	Experiment[b]
H_{NN}	0.0	−1.3[e]	0.0	0.0	0.0
H_{ZZ}	10.0	11.9	12.5	15.0	···
H_{TT}	4.1	4.3	4.7	3.1	5.4
H_{VV}	6.3	7.1	7.2	11.5	7.6
$H_{BB}-H_{AA}$[d]	1.5	1.8	0.6	3.6	
C.I.[e]	0.1	0.1	0.04	1.3	

[a] The nomenclature of the matrix elements is that of Parr and Crawford, see reference 3.
[b] As interpreted by R. S. Mulliken and C. C. J. Roothaan, Chem. Revs. **41**, 219 (1947).
[c] This computation is given with respect to $H_{NN}(Z=3.18)=0$. All the other computations are given with respect to their own $H_{NN}=0$.
[d] $H_{BB}-H_{AA}$ is the energy difference between polar and nonpolar $^1A_{1g}$ valence bond functions.
[e] Configurational interaction, the energy difference between the lowest molecular orbital configuration and state N.

* Research carried out under the auspices of the U. S. Atomic Energy Commission.
[1] W. Moffit, Proc. Roy. Soc. (London) **A210**, 245 (1951).
[2] W. Moffit, Proc. Roy. Soc. (London) **A210**, 224 (1951).
[3] R. G. Parr and B. L. Crawford, J. Chem. Phys. **16**, 526 (1948).
[4] Since polar and nonpolar structures of the molecule do not differ in the same way as they do in the separated atoms, a basic overcorrection, independent of this Z value problem, should also be investigated here.
[5] One might have some basic doubts about the justification of varying Z in a Mayer-Sklar type of calculation.

Relative Energies of Polar and Nonpolar Valence Bond Functions and Molecular Orbital Method. II*

MAX WOLFSBERG
Department of Chemistry, Brookhaven National Laboratory, Upton, Long Island, New York
(Received March 4, 1953)

IN the preceding note,[1] it is shown that one could introduce correction factors into a molecular orbital theory treatment of the ethylene molecule which bring the results into closer agreement with experiment. These correction factors decrease the separation in energy between nonpolar and polar structures and were, therefore, found to decrease greatly the amount of configurational interaction in ethylene. Moreover, since state T of ethylene is purely nonpolar while state V is completely polar, the separation between these two states was decreased through the introduction of the correction, in agreement with experiment.

It appeared worthwhile to apply the correction methods B and C of I to a recalculation of one of the conjugated ring systems. The simplest of these systems is cyclobutadiene, which has been previously treated as a four π-electron problem by Craig.[2] It was found here, as in the case of H_2 and C_2H_4, that methods B and C result in exactly the same correction factors for diagonal molecular orbital matrix elements, differing only in the nondiagonal ones. It might be noted that in these three cases the molecular orbitals are completely determined by symmetry. The nondiagonal matrix elements do, of course, become the same at infinite separation. Since the π-overlap integrals are rather small in cyclobutadiene, it was found that the results of methods B and C differ only slightly. Some evidence was obtained in carrying out the calcula-

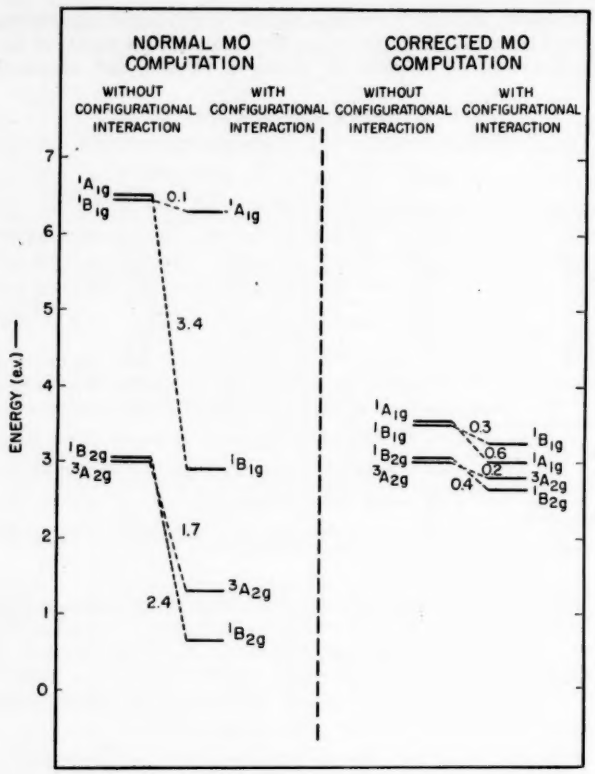

FIG. 1. Relative energies of electronic states of cyclobutadiene.

tions in I that method B more closely approximates method A than does method C. In Fig. 1 are shown the results of Craig's computations and of corrected molecular orbital computations using method B for the states arising from the lowest molecular orbital configuration of cyclobutadiene. It is relatively easy to take configurational interaction completely into account in calculations on this molecule, and therefore the results without and with configurational interaction are given. It is seen that, in general, the amount of configurational interaction is reduced through introduction of the correction factors and that, moreover, the states resulting from this one configuration now lie very closely together in energy.

Corrections have also been applied to the computation carried out by Parr and Mulliken[3] on *cis*-butadiene. Correction factors were computed only by method C and configurational interaction was not taken into account. The lowest singlet excitation energy was calculated by Parr and Mulliken to be 7.8 ev. The introduction of correction factors lowers this quantity to 6.17 ev, while experimentally it is about 6.00 ev. This agreement is much better than one would expect.

Standard molecular orbital calculations usually predict much higher intensities for transitions than one observes. This result is somewhat improved through the introduction of configurational interaction. In the corrected computations, where the amount of configurational interaction is lowered, it is to be expected that this improvement of predicted intensities becomes less. This is indeed found to be the case in ethylene for the $N \rightarrow V$ transition. On the other hand, in cyclobutadiene, approximately the same results were obtained with Craig's wave functions and the corrected ones for the $^1B_{2g} \rightarrow {}^1E_u$ transition.

The discussion of this and the preceding note will be detailed and extended in a future publication.

* Research carried out under the auspices of the U. S. Atomic Energy Commission.

[1] M. Wolfsberg, J. Chem. Phys. **21**, 943 (1953).
[2] D. P. Craig, Proc. Roy. Soc. (London) **A202**, 498 (1950).
[3] R. G. Parr and R. S. Mulliken, J. Chem. Phys. **18**, 1338 (1950).

The Raman Frequency of Bromine Monochloride

H. STAMMREICH AND ROBERTO FORNERIS
Department of Physics, Faculdade de Filosofia, Ciências, e Letras, University of São Paulo, São Paulo, Brasil
(Received March 2, 1953)

SINCE 1929 much experimental work has been done on the determination of the equilibrium constant and the heat content change for the reaction

$$Br_2 + Cl_2 \rightleftharpoons 2BrCl,$$

settling the well-known long-standing discussion over the existence or nonexistence of BrCl. But the impossibility of separating this diatomic halide from its dissociation products made the spectroscopic investigation difficult and, therefore, not much spectral data for the evaluation of the molecular constants are available. Cordes and Sponer,[1] investigating the absorption of bromine vapor, observed at pressures of about 0.08 mm three bands at 1657, 1671, and 1685A, and, at 1.1 mm, a new band at 1697A. These bands had to be ascribed to the BrCl molecule, formed by impurities of Cl_2 present in the bromine. The last of the mentioned bands was attributed to the ground state of the molecule and yielded a first vibrational quantum of about 435 cm^{-1}.

In a subsequent paper[2] the same authors reported observations on bromine-chlorine mixtures under improved conditions. They analyzed two band-systems in the region from 1629 to 1696A and from 1557 to 1635A as intercombinations between the ground state $^1\Sigma^+$ and the two components of the multiplet $^3\Pi_1$ and $^3\Pi_0$; however, according to Mulliken,[3] this assignment is problematic. Their measurements on the edges of these absorption bands yielded a probable value of $\omega = 430$ cm^{-1}, reported (as uncertain) in nearly all actual spectroscopic tables.

Smith, Tidwell, and Williams[4] observed the microwave spectrum of BrCl in the region of 9000 Mc sec^{-1}, corresponding to the $J = 0 \rightarrow 1$ transitions of the four isotopic species of the molecule and calculated the corresponding rotational constants B_e and α. From these data they derived the value of the internuclear distance $r = 2.138$A.

Recently Cole and Elverum[5] computed from the available data on BrCl (and other diatomic interhalogens), the thermodynamic properties and the vibrational and rotational constants of the molecule. For the vibrational constants ω was taken to be 430 cm^{-1}, and the value of $\omega_e x_e = 1.68$ cm^{-1} was obtained by interpolation from the known values of the anharmonicity constants for other diatomic halides as function of the reduced masses. The resulting calculated values of ω_e and $\omega_e x_e$, respectively, for the four isotopic species are 436.3 and 1.70 cm^{-1} for $Br^{79}Cl^{35}$, 434.7 and 1.69 cm^{-1} for $Br^{81}Cl^{35}$, 428.1 and 1.63 cm^{-1} for $Br^{79}Cl^{37}$, and 426.4 and 1.62 cm^{-1} for $Br^{81}Cl^{37}$. The internuclear separation was estimated to be 2.11A, which differs appreciably from the above-mentioned value obtained by Smith, Tidwell, and Williams, whose results were apparently not used.

In view of the existing uncertainty in the value of the first vibrational quantum of the BrCl molecule, we attempted at obtaining the Raman spectrum of the compound with an experimental technique used by one of us[6] for the determination of the Raman spectrum of bromine. Some details on the excitation of Raman spectra by helium-lamps in the red and near infrared region of the spectrum were given in a previous paper.[7] As a result of improvements in the experimental arrangement, we were able to use as exciting lines the He lines 6678.2, 7065.2, and 7281.4A. The first one was found suitable for the present work.

The Raman sample was a chlorine-bromine mixture dissolved in CCl_4. Twenty milliliters of the solution contained 3g of Br_2 and nearly the same quantity of Cl_2; the latter was used in excess to restrain the dissociation of BrCl.

We employed a Zeiss three-prism spectrograph with collimator $f = 30$ cm, 1:5 and an especially built camera with an $f/4.5$ lens, $f = 24$ cm; the reciprocal dispersion at 6874A, corresponding to the observed Raman shift, was 133A/mm. The spectra were recorded on Kodak I-F-3 plates which have the highest sensitivity in the

spectral region which is of interest here; exposure times ranged from 5 to 20 hours.

The Raman frequency corresponding to the first vibrational quantum of the BrCl molecule was found to be

$$\Delta G_{\frac{1}{2}} = 428 \pm 2 \text{ cm}^{-1}.$$

The observed Raman line is due in part to the presence of the four isotopic species of BrCl. The value of $\Delta G_{\frac{1}{2}}$ given above was obtained by measuring the maximum density of the line and corresponds certainly to the predominant contribution of the two species containing the Cl^{35} atom.

The Cl_2 frequency was found at 551 cm^{-1}; the Br_2 shift nearly coincides with the CCl_4 frequency 313 cm^{-1} and, therefore, was not observable. We hope soon to be able to investigate the gaseous system Br_2, Cl_2, and BrCl.

[1] H. Cordes and H. Sponer, Z. Physik **63**, 334 (1930).
[2] H. Cordes and H. Sponer, Z. Physik **79**, 170 (1932).
[3] R. S. Mulliken, Phys. Rev. **40**, 545 (1934).
[4] Smith, Tidwell, and Williams, Phys. Rev. **79**, 1007 (1950).
[5] L. G. Cole and G. W. Elverum, Jr., J. Chem. Phys. **20**, 1543 (1952).
[6] H. Stammreich, Phys. Rev. **78**, 79 (1950).
[7] H. Stammreich and R. Forneris, Z. Naturforsch. **7a**, 756 (1952).

The Raman Spectra of Hexamethyldisilane and Hexamethyldisiloxane

HIROMU MURATA,* *Osaka Municipal Technical Research Institute, Osaka, Japan*

AND

MAKOTO KUMADA, *Department of Chemistry, Osaka Municipal University, Osaka, Japan*

(Received February 26, 1953)

A SERIES of linear polysiloxanes have been prepared, and the Raman spectra of these are being measured in our laboratory. The infrared spectra of this series have been reported by several investigators.[1-3] The Raman data for the first compound of this series, hexamethyldisiloxane, are given in Table I, together

TABLE I. The Raman spectra of hexamethyldisilane and hexamethyldisiloxane.[a]

Hexamethyldisilane			Hexamethyldisiloxane		
$\Delta\nu$	I	Exciting line	$\Delta\nu$	I	Exciting line
178	(9b)	($e\pm$)	178	(7s)	($e\pm$)
250	(3s)	($e\pm$, k)	205	(2s)	(e)
403	(6s)	($e\pm$, k)	251	(4s)	($e\pm$, k)
638	(7s)	($e\pm$, k)	314	(1s)	(e, k)
689	(6s)	($e\pm$, k)	406	(1s)	(e)
754	(2s)	(e, k)	517	(6s)	($e\pm$, k)
833	(2s)	(e, k)	662	(5b)	($e\pm$, k)
883	(3s)	(e, k)	750	(2s)	(e, k)
			830	(3s)	(e, k)
			892	(1b)	(e)
			955	(1b)	(e)
			1045	(1b)	(e)
1245	(1s)	(e, k)	1252	(1s)	(e, k)
1317	(4s)	(e, k)	1322	(3s)	(e, k)
1373	(5s)	(e, k)	1393	(3b)	(e, k)
2893	(10s)	(e, k)	2898	(10s)	(e, k)
2955	(10s)	(e, k)	2957	(10s)	(e, k)

[a] $\Delta\nu$ = Raman displacement in cm^{-1}; I = relative intensity; b = broad; s = sharp; e = Hg 4358A; and k = Hg 4047A. The symbols + and − indicate Stokes and anti-Stokes lines, respectively.

with the results obtained for hexamethyldisilane. Cleveland, Lamport, and Mitchell[4] studied the Raman and infrared spectra of hexamethylethane and concluded that this molecule has a staggered configuration. Comparing with the structure of hexamethylethane, the Raman spectrum of hexamethyldisilane is interesting and a detailed investigation is in progress.

* Present address: Spectroscopy Laboratory, Department of Physics, Illinois Institute of Technology, Chicago 16, Illinois.

[1] N. Wright and M. J. Hunter, J. Am. Chem. Soc. **69**, 803 (1947).
[2] R. E. Richards and H. W. Thompson, J. Chem. Soc. **1949**, 124.
[3] I. Simon and H. O. McMahon, J. Chem. Phys. **20**, 905 (1952).
[4] Cleveland, Lamport, and Mitchell, J. Chem. Phys. **18**, 1321 (1950).

The Reaction Field of a Noncentral Dipole

B. K. P. SCAIFE

High Voltage Laboratory, Queen Mary College, University of London, London, England

(Received October 7, 1952)

THE purpose of this letter is to suggest a method whereby the average reaction field of a dipole, situated eccentrically in a spherical cavity embedded in a dielectric, may be obtained. This problem has already been considered very recently by Frood and Dekker.[1] It is suggested that their result may be obtained rather more directly as follows.

Use is made of the following Gaussian theorem[2] which states that the average field in a spherical volume resulting from a distribution of charges outside the spherical region is equal to the field at the center of the sphere. The theorem can be proved by considering the case of a single charge q, situated at a distance b from the center of a sphere whose radius is less than b.

The average field, $\mathbf{E}$ say, must be parallel to the line joining the center of the sphere to the charge q. If $\mathbf{K}$ is the unit vector in the direction of $\mathbf{E}$, we have

$$\mathbf{E} = \frac{q\mathbf{K}}{v_s}\int \nabla\left(\frac{1}{r}\right)\cdot \mathbf{K}\,dv_s = \frac{q\mathbf{K}}{v_s}\int \frac{\mathbf{K}\cdot d\mathbf{S}}{r} = \frac{q\mathbf{K}}{b^2},$$

where v_s is the volume of the sphere, and r is the distance between the charge q and an element of volume in the sphere dv_s. $\mathbf{dS}$ is an element of surface area.

Referring to Fig. 1 of reference 1 and considering one charge only ($+q$ say) we may write,

$$\varphi_0 = \sum_{n=0}^{\infty} B_n P_n(\cos \mathcal{J}_2) r^{-(n+1)};$$

and

$$\varphi_i = q\sum_{n=0}^{\infty} a_2{}^n r^{-(n+1)} P_n(\cos \mathcal{J}_2) + \sum_{n=0}^{\infty} A_n P_n(\cos \mathcal{J}_2) r^n \quad (r > a_2),$$

where φ_0 and φ_i denote the electric potentials outside and inside the cavity, respectively, A_n and B_n are constants, and $P_n(\cos \mathcal{J}_2)$ has its usual significance.

Using the theorem just proved, it is clear that we may calculate the average reaction field in the cavity provided A_1 is known; all other terms give no contribution when $r = 0$.

Assuming ϵ_i the dielectric constant of the cavity is unity, the following conditions hold for $r = R$:

$$\varphi_0 = \varphi_i \quad \text{and} \quad \epsilon_0(\partial\varphi_0/\partial r) = (\partial\varphi_i/\partial r),$$

ϵ_0 is the dielectric constant of the material surrounding the cavity.

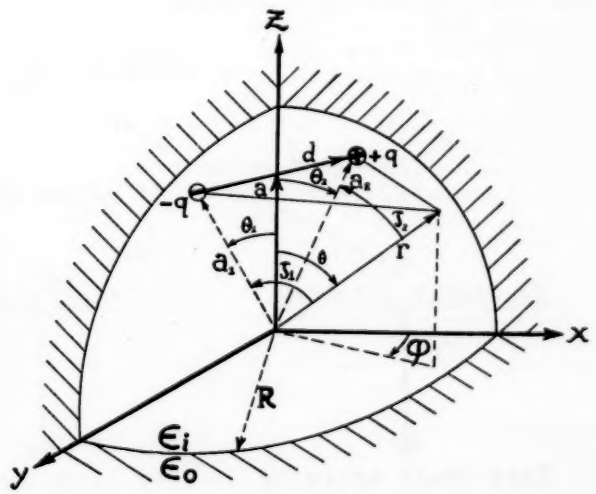

FIG. 1. The geometry of the electrostatic problem.

Using the fact that

$$\int_0^\pi P_n(\cos\mathcal{J})P_m(\cos\mathcal{J})\sin\mathcal{J}d\mathcal{J}=\frac{2\delta_{mn}}{2m+1},$$

where δ_{mn} is the Kronecker delta, we have the following relation

$$-qa_2^n(n+1)(\epsilon_0-1)R^{-(2n+1)}=A_n[\epsilon_0(n+1)+n].$$

Hence

$$A_1=-\frac{2(\epsilon_0-1)qa_2}{R^3(2\epsilon_0+1)}.$$

The field at the center of the cavity is obviously parallel to the direction of a_2. Therefore the average reaction field $\mathbf{R}$ arising from a dipole consisting of two unlike charges as illustrated in Fig. 1, is given by

$$\mathbf{R}=\frac{2(\epsilon_0-1)}{R^3(2\epsilon_0+1)}q(\mathbf{a}_2-\mathbf{a}_1)=\frac{2(\epsilon_0-1)}{R^3(2\epsilon_0+1)}q\mathbf{d}.$$

Putting $q\mathbf{d}=\boldsymbol{\mu}$, $\boldsymbol{\mu}$ the dipole moment, we have

$$\mathbf{R}=\frac{2(\epsilon_0-1)}{R^3(2\epsilon_0+1)}\boldsymbol{\mu}$$

which is the result obtained by Frood and Dekker.[1]

This work was carried out during the tenure of a maintenance allowance from the Department of Scientific and Industrial Research to which the writer is grateful; he also wishes to express his thanks to Dr. H. Tropper for his interest in this work.

[1] D. G. Frood and A. J. Dekker, J. Chem. Phys. **20**, 1030 (1952).
[2] Quoted in R. H. Fowler, *Statistical Mechanics* (Cambridge University Press, Cambridge, 1936), 2nd edition, p. 440.

Preliminary Experiments Using Mg^{28} as a Tracer with Chlorophylls, Plants, and their Extracts*

R. S. Becker and R. K. Sheline
Chemistry Department, The Florida State University, Tallahassee, Florida
(Received February 9, 1953)

A RECENTLY observed isotope of magnesium, Mg^{28}, with a half-life of 21.3 hours,[1] has been employed in exchange with chlorophylls and as a tracer in the plants bean and coleus (yellow-green variety). This work was done for the purpose of studying the reactions of chlorophylls and other plant materials and their possible role in photosynthesis.

Approximately 2.6 mg of Mg^*Cl_2 was added to 1–2 mg of pure freshly chromatographed chlorophyll *a* in absolute ethanol. After 7.2 hours, the chlorophyll was extracted with low boiling petroleum ether and washed 10–12 times with a 5 percent salt solution and water to remove the Mg^{*++}. The remaining chlorophyll had an activity of 1.03 ± 0.59 (standard deviation) counts per minute in a standard Geiger counter. An upper limit of 0.037 percent exchange is obtained using a value of $2.21(1.03+2\sigma)$ counts per minute and a minimum Mg^{*++} to chlorophyll *a* ratio. The lower limit on the half-time of exchange using these figures is 565 days.

Comparable quantities of Mg^*Cl_2 and pure, freshly chromatographed chlorophyll *b* were exchanged in absolute ethanol. After 6.4 hours, there was obtained a count of 0.63 ± 0.54 counts per minute. The upper limit on exchange in this case is 0.032 percent with a lower limit on the half-time of exchange of 581 days.

From the original work of Ruben *et al.*,[2] Myers and Prestwood[3] have computed half-times for the exchange of Mg^* with pure separated chlorophylls as >2.3 days. In view of the work of Barnes and Dorough,[4] in which divalent ions were found to be incapable of exchanging with the corresponding tetraphenylporphin metallo derivatives, the apparent failure of exchange in pure chlorophylls *a* and *b* is not surprising.

Experiments *in vitro* were carried out according to the simplified flow scheme shown in Fig. 1. It is notable in these experiments that there is some material(s) in each of the polar soluble and petroleum ether extracts that can associate magnesium. When these are both in competition for the Mg^{*++}, the polar soluble material effects by far the greater association.

In the investigation of Ruben *et al.*,[2] the site of association of Mg^{*++} is given as a coordination group of chlorophyll or another compound present in their crude mixtures of chlorophylls *a* and *b* (comparable to our nonpolar solubles). Since it appears that pure separated chlorophylls do not exchange or associate, it would seem doubtful that their first reason is the correct one. We believe the association to be due to material different from chlorophyll.

Additional experiments *in vivo* showed that no observable Mg^{*++} had exchanged, associated, or synthesized with chlorophylls after $11\frac{1}{3}$ hours in the case of a decapitated bean leaf or after approximately 65 hours in the case of a coleus plant.

Conclusions: (1) The experiments point to the fact that, either *in vitro* or *in vivo*, when polar soluble plant materials are present with nonpolar plant soluble materials, some fraction of the former complexes with Mg^{++} better and faster than any materials soluble in nonpolar solvents.

(2) Separated pure chlorophylls appear not to exchange with Mg^{*++}, but when other petroleum ether soluble plant compounds are present there is marked association of Mg^{*++}. Experiments are in progress to determine the site of the association.

(3) Our experiments to date indicate that, indeed, chlorophylls may not be the agents that exchange or associate radioactive Mg *in vivo* or *in vitro*.

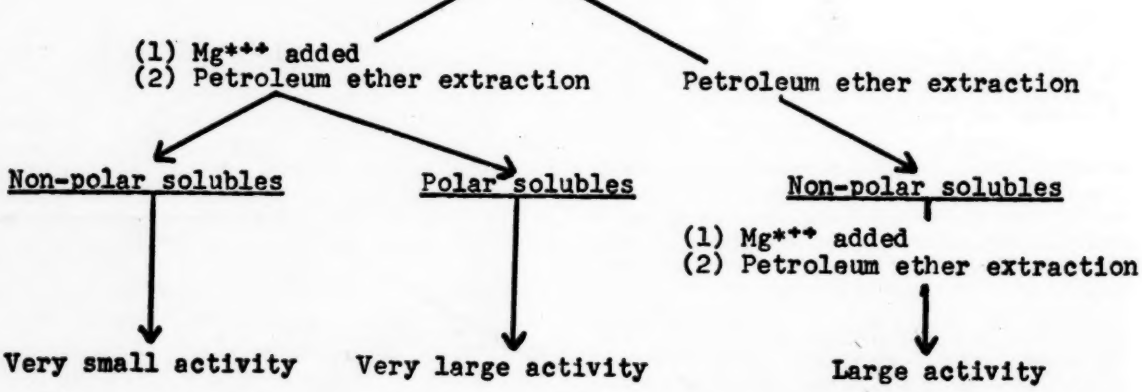

FIG. 1.

The authors wish to thank especially Dr. S. Aronoff of Iowa State College for his valuable advice and assistance and Dr. R. Hanks of the Botany Department in this university.

* This work was supported by the U. S. Atomic Energy Commission.
[1] R. K. Sheline and N. R. Johnson, Phys. Rev. **89**, 520 (1953).
[2] Ruben, Frenkel, and Kamen, J. Phys. Chem. **46**, 710 (1942).
[3] E. Myers and R. J. Prestwood, *Radioactivity Applied to Chemistry*, edited by A. C. Wahl and N. A. Bonner (John Wiley and Sons, Inc., New York, 1951), p. 243.
[4] J. W. Barnes and G. D. Dorough, J. Am. Chem. Soc. **72**, 4045 (1950).

Angular Distribution of the Light Scattered by Random Coils*

H. Benoit and Martin Goldstein
Department of Chemistry, Harvard University, Cambridge, Massachusetts
(Received February 17, 1953)

In many problems, it is assumed that a Gaussian coil (i.e., a coil with a large number of elements without correlations in their orientations) can be replaced by a spherical distribution of points around the center of gravity. Usually this is characterized by the probability function $4\pi r^2 w(r)dr$, which gives the probability of finding an element of the chain at the distance r from the center of gravity.

As a first approximation, one uses the Gaussian probability function, which can be written

$$w(r)=\left(\frac{9}{\pi b^2 N}\right)^{\frac{3}{2}} \exp-\frac{9r^2}{b^2 N}. \tag{1}$$

In this expression, b is the length of the statistical elements of the chain and N their number.

Recently Isihara[1] and Debye and Bueche[2] have given a more accurate expression based on the theory of Markoff chains:

$$w(r)=\int_0^1 \{(2/9)b^2N[u^3+(1-u)^2]\}^{+\frac{3}{2}} \times\exp-\frac{9r^2}{2b^2N[u^3+(1-u)^2]}du. \tag{2}$$

This expression cannot be integrated in closed form and Debye and Bueche give only expansions in power series.

It seems interesting to use these functions to calculate the angular distribution of the light scattered by random coils and to compare these with the classical expression obtained by using the distribution function for distances separating pairs of elements.[3] For this purpose one can show that for N points, distributed with spherical symmetry, each being at the distance r_i from the center-of-mass, the angular distribution of the light scattered is given by the expression

$$P(\theta)=\left[\Sigma_i \frac{\sin\mu r_i}{\mu r_i}\right]^2 \quad \text{with} \quad \mu=\frac{\pi}{\lambda}\sin\theta/2, \tag{3}$$

where θ is the angle between the incident and scattered beams and λ' the wavelength of the light in solution. Now if the probability function $w(r)$ is known, one can write

$$P(\theta)=\left[\int_0^\infty w(r)\frac{\sin\mu r}{\mu r}4\pi r^2 dr\right]^2. \tag{4}$$

Using this equation, it is possible to calculate the values of $P(\theta)$ with the function (1) or (2).

In the first case Hermans[4] has shown

$$P(\theta)=\exp(-u/3) \quad \text{with} \quad u=\mu^2\frac{b^2N}{6}. \tag{5}$$

In the second case, the integration is performed by inverting the order of integration; it is found that $P(\theta)$ is given by the very simple expression

$$P(\theta)=\frac{\pi}{u}\exp(-u/6)\left[\Theta\left(\frac{\sqrt{u}}{2}\right)\right]^2, \tag{6}$$

where Θ is the well-known probability integral

$$\Theta(x)=\frac{2}{\sqrt{\pi}}\int_0^x \exp(-t^2)dt. \tag{6'}$$

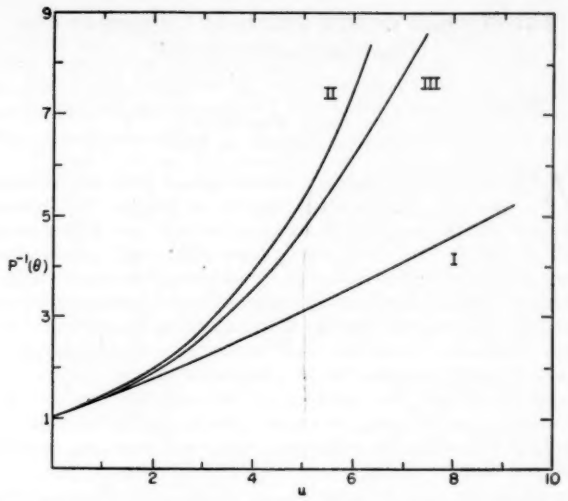

FIG. 1. $P^{-1}(\theta)$ as a function of $u=\mu^2(b^2N/6)$ in different cases. Curve I—the usual value from Eq. (7); curve II—assuming a Gaussian distribution of elements around the center of mass; Eq. (5); curve III—assuming the Debye distribution (2) around the center of mass; Eq. (6).

To compare these two functions and the usual Debye function

$$P(\theta)=(u-1+\exp-u)2/u^2, \tag{7}$$

we plot in Fig. 1 the reciprocal values $P^{-1}(\theta)$ as functions of u, because it is the usual form of the experimental data. One can see that, though they have the same initial slope, there are substantial differences. The two functions (5) and (6) differ the least; this is not surprising since they are obtained using the Eqs. (1) and (2), which as Debye and Bueche showed are very similar. But the discrepancy between these two functions and the function (7) is considerable for large values of u. The asymptotic behavior of $P(\theta)$ is not at all the same in the different cases.

Isihara has obtained the first two terms in the series expansion of $P(\theta)$ by integrating the expression (2) termwise: he observes that these are very similar to the first two terms of the series expansion of $P(\theta)$ given by Eq. (7). However, it is clear that the first few terms are inadequate to describe the behavior of the function at large values of the argument.

Accepting function (7) as the true result for a Gaussian chain, this discrepancy can only be explained by the approximations involved in the assumption that the molecule can be treated, through $w(r)$, as spherically symmetrical. Specifically, this function does not give the probability of relative positions of the segments of the molecule, but only the probability of finding them at the distance r from the center of mass. The large discrepancy obtained in calculating the angular distribution of the scattered light by this method shows that most of the configurations of Gaussian chains are far from possessing spherical symmetry and that perhaps the use of the distribution function (2) in other problems could also lead to inaccurate results.

* This work was supported by U. S. Office of Naval Research Contract N5ori-07654, T.O. 54 NR-330-025.
[1] A. Isihara, J. Polymer Sci. **8**, 574 (1952).
[2] P. Debye and F. Bueche, J. Chem. Phys. **20**, 1337 (1952).
[3] Zimm, Stein, and Doty, Polym. Bull. 1, 90 (1945).
[4] J. J. Hermans, Rec. trav. chim. **68**, 859 (1949).

The Normal Boiling Points of Oxygen on the Thermodynamic Scale*

J. G. ASTON AND G. W. MOESSEN
School of Chemistry and Physics, The Pennsylvania State College, State College, Pennsylvania
(Received February 19, 1953)

WE have recently made a comparison of seven platinum resistance thermometers against a helium thermometer between 10.4°K and 90.5°K using a 146 cm³ gas thermometer bulb similar to that of smaller volume (19.7 cm³) described by Hoge and Brickwedde[1] with the temperature held constant in a similar manner. A very precise manometer of 22-mm bore tubing thermostated and read exactly as described by Beattie *et al.*[2] was used. Meniscus covolumes were determined by Kistemaker's equation,[3] and meniscus height corrections were computed from Blaisdell's tables.[4] The accuracy of the corrected pressures was estimated as ±0.01 mm, the precision being ±0.003 mm, and the accuracy of reading the resistance thermometers on the specially designed Mueller bridge was ±0.00002Ω. In addition to the increased precision in manometry, the large bulb volume greatly reduced the dead space correction.

We estimate the uncertainty due to the dead space volume (excluding that portion within the thermostated manometer case) to be of the order of ±0.001°. The dead space volume within the manometer thermostat case, where the temperature is accurately known and constant, introduces negligible error if the meniscus covolume data of Kistemaker and the meniscus height data of Blaisdell are assumed correct.

The readings taken with an ice point pressure of 1 meter gave independent data for the normal boiling points of oxygen and hydrogen.

One thermometer loaned by the National Bureau of Standards (L and N 718158) had all its fixed points determined at the National Bureau of Standards, while the others (Pt-G3, etc.) had fixed point values determined independently at the Pennsylvania State College Cryogenic Laboratory. The method and apparatus described by Scott[5] was used for determining the oxygen point calibration,[6] and the method and apparatus described by Beattie *et al.*[7] were used to determine the ice, steam, and sulfur points.

The thermodynamic temperature of the ice point was taken as 273.16°K, and the values of the second virial coefficient used in reduction to the ideal gas scale were taken from the data of Keyes.[8]

Three independent readings of the gas thermometer against the platinum thermometers (only 3 of the platinum thermometers were read during the first point and all 7 of the platinum thermometers were read on the second and third points) gave 17 values for the normal boiling point of oxygen. The oxygen point values of all 7 thermometers were independent of the gas thermometer data since 6 of the thermometers were individually compared with an oxygen boiling point and for the 7th thermometer, the oxygen boiling point value was determined by separate intercomparison measurements (see reference 6). The results are given in Table I in three columns under the dates of the runs. At the head of each column is given the thermodynamic temperature in degrees Kelvin calculated from the pressure readings of the gas thermometer. This temperature was converted to degrees centigrade by subtracting 273.160, the value chosen for the thermodynamic temperature of the ice point, and subtracted from the temperature reading on the international temperature scale corresponding to the indications of each platinum thermometer. These values (t°C Int. $-t$°C) are listed in the columns for each run. The mean of all the values is +0.0359±0.0013°. The value assigned to the boiling point of oxygen on the international scale in deriving the equations for the thermometers was −182.970°. Thus the normal boiling point of oxygen in centigrade degrees on the thermodynamic scale is −183.006° or 90.154°K.

TABLE I. Comparison of the international temperature scale and the thermodynamic temperature scale at around 90°K, 0°C = 273.160°K.

Date	Feb. 2, 1951	March 17, 1951	March 18, 1951
Gas thermometer temperature °K	89.9378	90.0500	90.0962
Platinum resistance thermometer No.	t°C Int. $-t$°C[a,b]	t°C Int. $-t$°C[a,b]	t°C Int. $-t$°C[a,b]
NBS, L and N 718158	+0.0401	+0.0358	+0.0355
Pt-G12	+0.0393	+0.0353	+0.0346
Pt-A2	···	+0.0355	+0.0346
Pt-G10	···	+0.0350	+0.0342
Pt-G8	···	+0.0345	+0.0337
Pt-G7	···	+0.0355	+0.0349
Pt-G3	+0.0398	+0.0361	+0.0354

[a] Mean t°C Int. $-t$°C (Abs) = +0.0359±0.0013°.
[b] From gas thermometer data t°C = T°K − 273.16, where T°K has been calculated from the gas thermometer readings with reduction to the ideal gas scale as outlined in text.

A comparison of our values with other reported values of the normal boiling point of oxygen will be reserved for a later date. However, it seems certain that the Reichsanstalt values of 90.198°K[9] and 90.195°K[10] for the normal boiling point of oxygen are about 0.04°K too high.

* This work was assisted in part by the U. S. Office of Naval Research under Task Order III of contract N6-ONR-269 with the Pennsylvania State College.
[1] H. J. Hoge and F. C. Brickwedde, J. Research Natl. Bur. Standards **22**, 351 (1939).
[2] J. A. Beattie *et al.*, Proc. Amer. Acad. Arts and Sci. **74**, 327–398 (1941).
[3] J. A. Kistemaker, Leiden Commun. No. 268c.
[4] B. E. Blaisdell, J. Math. Phys. **19**, 217 (1940).
[5] R. B. Scott, J. Research Natl. Bur. Standards **25**, 459 (1940).
[6] Ten intercomparisons (other than those cited in this communication) of the 7 platinum thermometers at temperatures within a few hundredths of a degree of the oxygen point revealed a systematic error of 0.0088° in the determination of the oxygen point for one thermometer, Pt-A2. Accordingly an adjustment to the constant β equivalent to this amount was made. This is permissible since the precision of the intercomparisons is considerably greater than the precision of the determination of the oxygen point on the international temperature scale. An estimate of the over-all precision of the oxygen point determinations can be made by consideration of the data in Table I, bearing in mind that the constants for the thermometer National Bureau of Standards, L and N 718158, were determined at the National Bureau of Standards while the remaining constants were determined as part of the present investigation.
[7] J. A. Beattie *et al.*, Proc. Amer. Acad. Arts and Sci. **71**, 327–374 (1937).
[8] F. G. Keyes, in *Temperature, Its Measurement and Control in Science and Industry* (Reinhold Publishing Corporation, New York, 1941), p. 57.
[9] W. Heuse and J. Otto, Ann. Physik **9**, 486 (1931).
[10] W. Heuse and J. Otto, Ann. Physik **14**, 185 (1932).

Kinetics of Reaction between Ammonia and Oxygen in a Quartz Vessel*

HENRY WISE AND MAURICE F. FRECH
Jet Propulsion Laboratory, California Institute of Technology, Pasadena, California
(Received March 6, 1953)

ALTHOUGH the oxidation of ammonia in the presence of catalytic surfaces has been studied in great detail[1] because of its industrial importance, the reaction in the absence of a metallic catalyst has received little attention. Recently Stephens and Pease[2] reported some measurements on the slow oxidation of ammonia in a quartz vessel at temperatures between 400°C and 725°C which led to the interesting conclusion that the fraction of ammonia reacted increases rapidly as the concentration of ammonia is diminished. We wish to present some observations on the reaction between ammonia and oxygen which indicate the appearance of hydrogen as an intermediate in this reaction.

The experiments to be described were carried out in a static system composed of a quartz reaction vessel (volume = 1560 cc, surface-to-volume-ratio = 1.12 cm^{-1}). A homogeneous gas mixture containing the desired concentrations of NH_3 and O_2 was prepared at room temperature, an aliquot of which was admitted to the externally heated reactor where it was allowed to reside for a given time interval. Subsequently, the reaction products were transferred rapidly into a trap cooled by liquid nitrogen. The noncondensable gases were pumped off by means of a Toepler pump circuit and quantitatively analyzed for hydrogen by combustion

over a heated platinum filament. The results of these measurements at 1096°K are shown in Fig. 1.

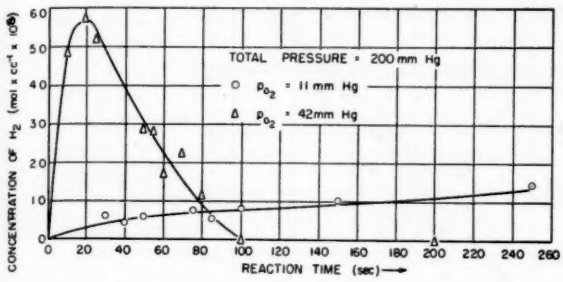
TOTAL PRESSURE = 200 mm Hg
P_{O_2} = 11 mm Hg
P_{O_2} = 42 mm Hg
CONCENTRATION OF H_2 (mol x cc^{-1} x 10^8)
REACTION TIME (sec)
0 20 40 60 80 100 120 140 160 180 200 220 240 260
0 10 20 30 40 50 60

FIG. 1. Variation in concentration of hydrogen with time for system ammonia-oxygen at 1096°K.

It is to be noted that the rate of formation of hydrogen is a function of the partial pressure of oxygen. However, as the concentration of oxygen in the gas mixture is increased, another reaction sets in which causes the depletion of this reaction intermediate with the formation of water as the final product. Thus, the mechanism of oxidation of ammonia involves first dehydrogenation of the ammonia molecule followed by oxidation of the hydrogen thus produced. Spectroscopic investigations of ammonia-oxygen diffusion flames[3] further substantiate the fact that ammonia does not react directly with oxygen but first undergoes decomposition to N_2 and H_2 via NH_2 and NH. The appearance of hydrogen as an intermediate may explain the apparent self-inhibition of ammonia in its oxidation process.[2] It is known that the thermal decomposition of pure ammonia is retarded by hydrogen.[4] Consequently, since in the oxidation of ammonia the rate of disappearance of hydrogen diminishes with increasing mole fractions of NH_3, the inhibition in rate will become more pronounced under these conditions. On the other hand, as the relative concentration of O_2 in the gas mixture is increased, the rate of oxidation of hydrogen produced by dehydrogenation of NH_3 is rapid, relative to its rate of formation, and no diminution in reaction rate due to hydrogen is obtained.

A more detailed analysis of the kinetics and mechanism of reaction between ammonia and oxygen will be presented in a subsequent publication.

* This paper presents the results of one phase of research carried out at the Jet Propulsion Laboratory, California Institute of Technology, under Contract No. DA-04-495-ORD 18, sponsored by the Department of the Army Ordnance Corps.

[1] R. Wendlandt [Z. Elektrochem. **53**, 307 (1949)] gives an interesting review of this process.

[2] E. R. Stephens and R. N. Pease, J. Am. Chem. Soc. **72**, 1188 (1950); **74**, 3480 (1952).

[3] H. G. Wolfhard and W. G. Parker, Proc. Phys. Soc. (London) **65**, 2 (1952).

[4] Hinshelwood and Burk, J. Chem. Soc. **127**, 1116 (1925).

Molecular Kinetics of Hydrogenation and Exchange Reactions of Ethylene at Surfaces

KEITH J. LAIDLER, *The Catholic University of America, Washington, D. C.*,
MARY COLMAN WALL, *Rosemont College, Rosemont, Pennsylvania,*
AND
MARIA CLARE MARKHAM, *St. Joseph College, West Hartford, Connecticut*

(Received March 6, 1953)

IN a recent letter[1] we have formulated mechanisms for the exchange and hydrogenation reactions of olefins at surfaces. We have subsequently derived, on the basis of absolute rate theory, the kinetic laws applicable to these mechanisms, and the details will be published elsewhere;[2] the present note summarizes the main conclusions we have reached, with special reference to the reactions of ethylene.

Ethylene is assumed to be adsorbed on dual surface sites, hydrogen (or deuterium) atoms on single sites. Adsorbed ethyl radicals may be formed by interaction between adsorbed ethylene and hydrogen atoms [reaction (3) of reference 1], and gaseous ethylene can be produced either by reaction between adsorbed ethyl and adsorbed H, or by dismutation between ethyls adsorbed on neighboring sites. The absolute rate equations obtained for both methods of production of ethane are similar, and indicate that the rate passes through rather a flat maximum as the ethylene pressure is raised; the maximum is appreciably flatter than is predicted by the simple treatment[3] in which the ethylene is assumed to be adsorbed on a single site. Twigg's mechanism,[4] according to which hydrogen only becomes adsorbed by reaction with ethylene, leads to no maximum but to a constant rate at high ethylene pressures.

The hydrogenation of ethylene has been studied extensively on a number of surfaces. In several cases[5–8] the data indicate a falling-off of the rate at high ethylene pressures, so that at least in these cases Twigg's mechanism is not applicable; in other cases the situation is uncertain. We have calculated absolute rates corresponding to our mechanism for four independent investigations[9–12] in all cases obtaining agreement with experiment within a factor of 10. It is to be emphasized, however, that the absolute rate calculations do not discriminate between our mechanism and Twigg's; his would give equally good agreement.

The situation regarding the exchange reaction between ethylene and deuterium calls for some more discussion of the experimental data. Twigg and Rideal[11] studied the reaction on a nickel surface and concluded that the rate was independent of the ethylene pressure and directly proportional to the first power of the deuterium pressure; evidently the deuterium covers the surface only sparsely while the ethylene coverage is considerable. According to Twigg[4] both hydrogenation and exchange occur by similar mechanisms involving adsorbed ethyl radicals. His mechanism, however, leads to difficulty; the activation energy of the exchange reaction is greater by about 9 kcal than that for hydrogenation, but the rate of exchange is about three times that of hydrogenation. On the basis of activation energy alone, the exchange rate is expected to be 10^{-5} that of hydrogenation, and there should therefore be a frequency factor ratio of this order; the source of such a ratio is not apparent. As seen above absolute rate calculations give good agreement for hydrogenation; the calculated exchange rates are, however, too low by 10^5.

The only way out of this difficulty would seem to be to conclude that, as with other exchange reactions,[13,14] the rate is really proportional to the square root of the deuterium pressure. Examination of the data of Twigg and Rideal does in fact reveal that the square root law is by no means incompatible with the results. Only two deuterium pressures were used, differing by a factor of two, and the large variations in catalytic activity from run to run were corrected for in terms of the variation in activity with respect to *hydrogenation*.

If the square root law is accepted the data admit of a ready interpretation. We suppose that ethyl radicals revert to ethylene by depositing an H or D atom on a bare neighboring site

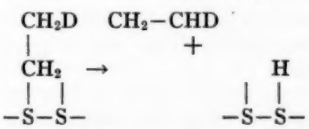

It is assumed that there is nearly always a bare site adjacent to an ethyl radical, so that the exchange rate can be considered a unimolecular reaction of adsorbed ethyl radicals. Under the usual conditions, H is in excess over D on the surface, so that the product is mainly CH_2CHD, and derivation of the rate equation for the formation of this leads us to the result that the activation energy for exchange should exceed that for hydrogenation by one-half the heat of adsorption of hydrogen. Support for our mechanism is provided by the fact that the heat of adsorption

on a covered surface is 17 kcal per mole,[15] which is close to twice the activation energy difference (9 kcal).

At 156°C and a deuterium pressure of 10.6 mm Twigg and Rideal obtained an activation energy of 12.2 kcal and an absolute rate of 1.36×10^{18} molecules cm^{-2} sec^{-1}. Our calculated rate is 8×10^{16}; the agreement is not as good as usual, but this could be due to a small error in the activation energy. The first power law gives $\sim10^{12}$, which is much too low.

[1] Markham, Wall, and Laidler, J. Chem. Phys. **20**, 1331 (1952).
[2] K. J. Laidler, chapters on "Kinetic laws in surface catalysis" and "Absolute rates of surface reactions," to be published in Vol. 1 of the forthcoming *Catalysis*, edited by P. H. Emmett (Reinhold Publishing Corporation, New York, 1953).
[3] K. J. Laidler, Disc. Faraday Soc. **8**, 47 (1950).
[4] G. H. Twigg, Disc. Faraday Soc. **8**, 152 (1950).
[5] R. N. Pease, J. Am. Chem. Soc. **45**, 1196 (1923).
[6] A. Farkas and L. Farkas, J. Am. Chem. Soc. **60**, 22 (1938).
[7] O. Toyama, Rev. Phys. Chem., Japan **11**, 153 (1937).
[8] O. Toyama, Rev. Phys. Chem., Japan **14**, 86 (1940).
[9] Farkas, Farkas, and Rideal, Proc. Roy. Soc. (London) **A146**, 630 (1934).
[10] O. Toyama, Rev. Phys. Chem., Japan **12**, 115 (1938).
[11] G. H. Twigg and E. K. Rideal, Proc. Roy. Soc. (London) **A171**, 55 (1939).
[12] G. M. Schwab and H. Zorn, Z. phys. Chem. **B32**, 169 (1936).
[13] J. Weber and K. J. Laidler, J. Chem. Phys. **19**, 1089 (1951).
[14] C. Kemball, Trans. Faraday Soc. **48**, 254 (1952).
[15] D. D. Eley, Disc. Faraday Soc. **8**, 352 (1950).

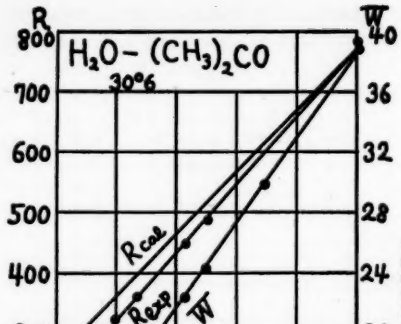

FIG. 1. Molecular sound velocity and molecular compressibility in dependence on molar fraction in water-acetone mixtures (sound velocity data by Rao).

Molecular Sound Velocity and Molecular Compressibility of Liquid Mixtures

OTOHIKO NOMOTO
Kobayasi Institute of Physical Research, Kokubunzi, Tokyo, Japan

(Received February 18, 1953)

RAO'S molecular sound velocity as defined by

$$R=(M/\rho)V^{1/3}, \tag{1}$$

where M means the molecular weight, ρ the density, and V the sound velocity, is known as a quantity independent of temperature[1] for each pure liquid and satisfying the additivity rule[2]

$$R=\Sigma_i a_i \tag{2}$$

or[3]

$$R=\Sigma_i b_i \tag{3}$$

with respect to the constitutive elements of the molecules of the liquid, though these rules do not hold true for halogen compounds.[4] Here a_i means the atomic increments and b_i the bond increments.

Another quantity of similar nature has been introduced by Wada[5] under the name of "molecular compressibility" and defined by

$$W=(M/\rho)\beta^{-1/7}, \tag{4}$$

where β means the adiabatic compressibility. This quantity is also independent of temperature for each liquid because of the relation

$$W=(M/\rho^{6/7})V^{2/7}=M^{1/7}R^{6/7}, \tag{5}$$

and this quantity also satisfies the additivity rule with respect to the constitutive elements of the molecule, according to Wada.

This note reports the result of calculations performed on R and W in binary mixtures of mutually soluble liquids. Calculations have been performed on forty such mixtures employing the existing ultrasonic velocity data (see Sette[6] and others[7–10]) and employing the number average molecular weight as M.

Liquid mixtures so far examined exhibit three types of R *vs* C_M curves, i.e., linear type (see Fig. 1), concave upwards type (Fig. 2), and water-alcohol type (Fig. 3). The $W-C_M$-curves are linear in the first two groups of mixtures (Fig. 1 and Fig. 2), while the general trend of these curves remains the same as the R *vs* C_M curves in the water-alcohol mixtures (Fig. 3). The following tabulates the mixtures belonging to these three groups. The deviation from straight lines of both these curves in type (1)

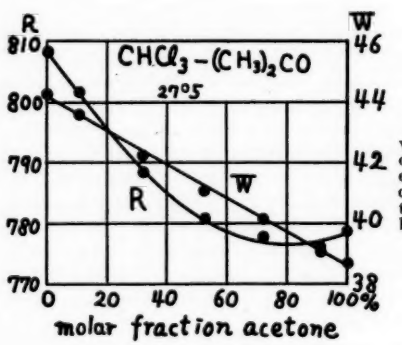

FIG. 2. Molecular sound velocity and molecular compressibility in dependence on molar fraction in chloroform-acetone mixtures (sound velocity data by Parshad).

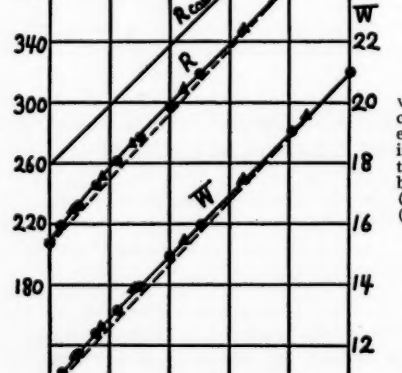

FIG. 3. Molecular sound velocity and molecular compressibility in dependence on molar fraction in water-methanol mixtures (sound velocity data by Pesce and Giacomini (25°) and by Parshad (26°).

mixtures and that of W-curves in type (2) mixtures are less than 0.5 percent, except in a few cases marked with asterisk. For the purpose of illustration, the mixtures are divided into six subgroups according to the form of the sound velocity *vs* molar fraction curves: (a) with maximum of V and minimum of β; (b) V-curve is convex upwards and β-curve concave upwards; (c) with point of inflection for V-curve; (d) with linear V-curve; (e) V-curve is concave upwards; (f) with minimum of V.

(1) Both R *vs* C_M curves and W *vs* C_M curves are linear (27 examples):
(a) water-formic acid, water-acetic acid, water-acetone;
(b) nitrobenzene-ethanol, nitrobenzene-methanol, ethanol-aniline, benzene-acetone, methanol-ethanol;
(c) benzene-ethanol, pentane-heptane;
(d) benzene-ethyl ether,* nitrobenzene-toluene*;
(e) benzene-chlorobenzene, benzene-carbon disulfide, benzene-toluene, heptane-benzene, heptane-chlorobenzene, *n*-heptane-*n*-buthanol, carbon disulfide-carbon tetrachloride, chloroform-carbon tetrachloride, ethanol-ether, methanol-ether, ethanol-cyclohexane, nitrobenzene-aniline;
(f) heptane-ethanol, heptane-dichloromethane, acetone-cyclohexane;
(2) R *vs* C_M curves are concave upwards, W *vs* C_M curves are linear (8 examples):
(d) carbon tetrachloride-tetraline*;
(e) benzene-dichloromethane, chloroform-benzene, benzene-carbon tetrachloride, heptane-carbon tetrachloride, chloroform-acetone;
(f) carbon tetrachloride-ethanol, chloroform-ether;
(3) Water-alcohol type (4 examples);
(a) water-methanol, water-ethanol, water-propanol, water-iso propanol.

One mixture (ethyl acetate-carbon tetrachloride) has exhibited somewhat irregular R-curve and W-curve; this may presumably be due to experimental errors.

It is to be noticed that all the mixtures of group (2) consist of one heavy liquid such as chloroform or carbon tetrachloride and one light liquid, and it seems that the deviation from linearity of the R-curve is a density effect. The W-curves for these liquids, on the other hand, are completely linear, presumably because of the reduced effect of density on this quantity as compared to R [see Eq. (1) and Eq. (5)].

Both the R-curves and the W-curves in water-alcohol mixtures deviate slightly upwards from the straight line with maximum deviation in the neighborhood of the velocity peak. This upward deviation may be due to the diminution of association by the mutual interaction between the molecules of water and those of alcohol, as was first pointed out by Parshad.[11] The values of R in water and in alcohol are lower than the values R cal computed from the additivity rules (2) [or (3)], and the effect of association is supposed to be the cause of these low values (see Weissler[12]). The decrease in association will cause R to decrease and to approach the normal value in greater or less extent.

Detailed accounts of this note will be published elsewhere.

[1] Rama Rao, Indian J. Phys. **14**, 109 (1940).
[2] Rama Rao, J. Chem. Phys. **9**, 682 (1941).
[3] R. T. Lagemann and J. E. Corey, J. Chem. Phys. **10**, 759 (1942).
[4] Lagemann, Evans, and McMillan, J. Am. Chem. Soc. **70**, 2996 (1948).
[5] Y. Wada, J. Phys. Soc. Japan **4**, 280 (1951).
[6] D. Sette, Ricerca sci. **19**, 1338 (1949).
[7] I. Gabrielli and G. Poiani, *Colloque international sur les ultrasons* (1951), 234.
[8] I. Gabrielli and G. Poiani, Ricerca sci. **22**, 1426 (1952).
[9] B. Jacobson, Arkiv Kemi **2**, 177 (1950).
[10] I. G. Mikhailov, Compt. rend. (Doklady) U.R.S.S. **31**, 324, 550 (1941).
[11] R. Parshad, J. Acoust. Soc. Am. **20**, 66 (1948); J. Chem. Phys. **15**, 418 (1947).
[12] A. Weissler, J. Chem. Phys. **15**, 210 (1947).

The General Relation between the Density Virial Coefficients and the Pressure Virial Coefficients

WILLIAM E. PUTNAM AND JOHN E. KILPATRICK
Department of Chemistry, The Rice Institute, Houston, Texas
(Received February 19, 1953)

APPARENTLY the general relation between the density (or inverse volume) virial coefficients and the pressure virial coefficients has not been published. It occurred to us that a technique used by one of us[1] to handle a somewhat related problem would also lead to the general solution in this case.

The two sets of virial coefficients may be defined by the equations

$$Pv=\sum_{j=0} C_jP^j \tag{1}$$

$$Pv=\sum_{k=0} D_kx^k \tag{2}$$

$$x=1/v. \tag{3}$$

It is apparent that $C_0=D_0=RT$ and that any particular C_n (or D_n) can be given in terms of the set $D_n, \cdots, D_0$ (or $C_n, \cdots, C_0$). Scatchard[2] has given such expressions for C_1, C_2, and C_3.

More recently Epstein[3] has deduced expressions for the second through the fifth virial coefficients of each sort in terms of the coefficients of the opposite sort.

The general solution can be found as follows: The equation

$$\sum_{j=0} D_jx^j=\sum_{k=0} C_kP^k \tag{4}$$

is multiplied by either $x^{-n-1}dx$ or $P^{-n-1}dP$ and is then integrated (as a complex variable) around the common origin of x and P. By application of Cauchy's theorem we find (after a few expansions by means of the multinominal theorem)

$$D_n=-n!\sum_{i=0}(i-1)C_i\sum_{(a_s)}\prod_{s=0}\frac{C_s^{a_s}}{a_s!}\begin{cases}\sum a_s=n\\ \sum sa_s=n-i\end{cases} \tag{5}$$

$$C_n=\sum_{i=0}\sum_{t=0}\frac{(-)^t(n+t-1)!(i+1)}{(n-1)!}\frac{D_i}{D_0^{n+t}}\sum_{(a_s)}\prod_{s=1}\frac{D_s^{a_s}}{a_s!}\begin{cases}\sum a_s=t\\ \sum sa_s=n-i.\end{cases} \tag{6}$$

The summation over i in Eq. (5) and the summations over i and t in Eq. (6) can be eliminated by the introduction of the net powers k_s

$$D_n=C_0\sum_{(k_s)} n!\prod_{s=0}\frac{C_s^{k_s}}{k_s!}\begin{cases}\sum k_s=n\\ \sum sk_s=n\end{cases} \tag{7}$$

$$C_n=\sum_{(k_s)}\frac{(-)^{n-k_0+1}(2n-k_0-2)!}{(n-1)!}\frac{D_0^{k_0}}{D_0^{2n-1}}\prod_{s=1}\frac{D_s^{k_s}}{k_s!}\begin{cases}\sum k_s=n\\ \sum sk_s=n.\end{cases} \tag{8}$$

The summations in Eqs. (7) and (8) are to be interpreted as: sum over all sets of integers k_s (positive or zero) satisfying the two restrictive conditions. The sets of powers k_s can very readily be found from the various ways the integer n can be partitioned into n parts, each zero or positive. For a given partition, k_s is equal to the number of times the integer s occurs.

The density virial expansion is often written in the form

$$Pv=RT\sum_{j=0} B_jx^j.$$

Since $D_n=RTB_n$, Eqs. (7) and (8) can readily be reduced to relations between B's and C's.

[1] J. E. Kilpatrick, J. Chem. Phys. **21**, 274 (1953).
[2] G. Scatchard, Proc. Natl. Acad. Sci. **16**, 811 (1930).
[3] L. F. Epstein, J. Chem. Phys. **20**, 1981 (1952). Equation (9), for E_p, is incorrect. It should read $E_p=(E_v-2C_v^3-4B_vD_v+10B_v^2C_v-5B_v^4)/(RT)^4$.

Studies by Infrared Spectra on the Initiation Process in Autoxidation of Methyl Linolenate

N. A. KHAN*
Hormel Institute, Austin, Minnesota
(Received March 12, 1953)

THE information on the mechanisms of autoxidation of methyl linolenate is still rather unsatisfactory. One of the chief difficulties is the very strong susceptibility of this substrate to autoxidation. The mechanism of autoxidation of methyl linoleate has only recently been clarified to a great extent by the physico-chemical approach of different investigators.[1-3] Methyl linoleate has only one methylenic group flanked on either side by two double bonds, whereas methyl linolenate has two such methylenic groups that make it so unstable. In the present investigations special precautions have been taken during the initial autoxidation and during the isolation of the products formed, so as to preserve intact their initial structures.

In the previous studies[3] in this laboratory, the initial products in the case of methyl linoleate have been characterized by means of infrared spectra. Two major types of products have been obtained: (a) *Cis-trans* conjugated (absorption at 10.55μ, or 948 cm^{-1}), and (b) *trans-trans* conjugated (absorption at 10.15μ, or 988 cm^{-1}), when autoxidation was conducted at or below 0°C. Hence it was considered that the similar studies on the initial autoxidation reaction of methyl linolenate would reveal some aspects of the mechanisms involved.

Methyl linolenate was prepared by separation of the urea-complex. One kilo of the mixed esters of linseed oil gave rise to a concentrate (filtrate) with an iodine number of 253.0 after twelve fractionations, six of which were conducted below room temperature (20° to −10°C), each time removing *ca* 5–6 percent ester with urea. The residues in the above filtrate were subjected to fractional distillation and 89 percent pure *cis-, cis-, cis*-linolenate was obtained. Since methyl linolenate produces unstable peroxides,[4] it was autoxidized at −10° to a peroxide value of 200 m.e./kg (*ca* 3 percent linolenate autoxidized) with dispersed oxygen in a shorter duration. Thus the preferential autoxidation of methyl linolenate was also insured.[5] The hydroperoxides thus formed were concentrated by countercurrent extraction (10–15°C), using 87 percent alcohol and skelly *F*, and a peroxide value of 6025 m.e./kg was obtained. These unstable peroxides in alcohol solution were reduced by stannous chloride without delay to the corresponding hydroxy linolenate which is more stable. The reduction by stannous chloride does not affect the isomeric structure of the peroxides.[6] This hydroxy linolenate (hydrogen uptake, 2.8 moles/mole; OH, one mole/mole) showed absorption in the same regions of the infrared spectrum as the linoleate, as far as the geometric isomers of the double bonds are concerned. It gave evidence for the presence of two major types of isomers: (a) *cis-trans* conjugated (10.55μ or 948 cm^{-1}), (b) *trans-trans* conjugated (10.15μ or 988 cm^{-1}). This may mean that methyl linolenate follows the same pattern of reactions as methyl linoleate during the initial stage of autoxidation. This will occur, when one active methylenic group (either 11 or 14) is attacked as follows:

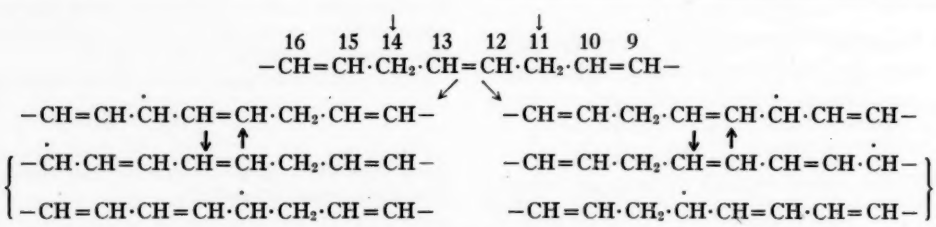

4 Conjugated isomers,
stabilized by resonance.

This initiation process lends support to the conclusions reached on the basis of the thermodynamic studies by Bolland and Gee.[7] These investigators predicted the identical processes for both methyl linoleate and linolenate. The complications arise, when both the active methylenic groups are attacked simultaneously, or when other side reactions follow due to the experimental conditions.

Further work is in progress and the details will be published later. The author wishes to thank Dr. D. H. Wheeler and Mr. W. E. Tolberg for the infrared analysis and Dr. W. O. Lundberg for his kind help. The work was possible due to the grants-in-aid from the U. S. Office of the Naval Research, the Department of Navy.

* Research Fellow.
[1] Dugan, Beadle, and Henick, J. Am. Oil Chemists' Soc. **26**, 681 (1949).
[2] Cannon, Zilch, Burket, and Dutton, J. Am. Oil Chemists' Soc. **29**, 447 (1952).
[3] Privett, Lundberg, Khan, Tolberg, and Wheeler, J. Am. Oil Chemists' Soc. **30**, 61 (1953).
[4] Farmer, Koch, and Sutton, J. Chem. Soc. **1943**, 541.
[5] N. A. Khan (to be published).
[6] Khan, Lundberg, Tolberg, and Wheeler (to be published).
[7] J. L. Bolland and G. Gee, Trans. Faraday Soc., Oxidation **42**, 236 (1946).

A Light Scattering Investigation of the Polymolybdates*

MICHAEL KESTIGIAN,† PAUL COLODNY,‡ AND RICHARD S. STEIN
Department of Chemistry, University of Massachusetts, Amherst, Massachusetts
(Received February 23, 1953)

IT is known that while the molybdate ion exists in the monomeric form, $MoO_4^=$ in basic solution, it aggregates to form higher molecular weight species in acid solution. The aggregation-disaggregation process has been studied by Jander and his school[1] by measuring diffusion coefficients of the polymolybdate ions and by conductiometric titration. They propose a stepwise aggregation of the molybdate ion with decreasing *p*H in the manner indicated in Fig. 1.

The ionic weights given by these workers might be criticized because an empirical equation is used to relate the diffusion constant to the molecular weight. This work is concerned with an absolute measurement of the molecular weight of some of these complex molybdates using the light scattering technique.[2]

The light scattering measurements were made using an apparatus patterned after that described by Zimm.[3] Light scattering intensities were measured at an angle of 90° from the incident beam for two sets of solutions of sodium molybdate (cp "Bakers Analyzed") in water. Absolute turbidities were obtained by calibrating the apparatus against redistilled, recrystallized thiophene-free benzene using the value of $\tau = 2.83 \times 10^{-4}$ for benzene obtained by Carr and Zimm.[4] The solutions were clarified by filtering through a thoroughly washed layer of activated charcoal supported on Corning ultrafine glass as suggested by Lochet[5] and used in his work on scattering from solutions of simple inorganic

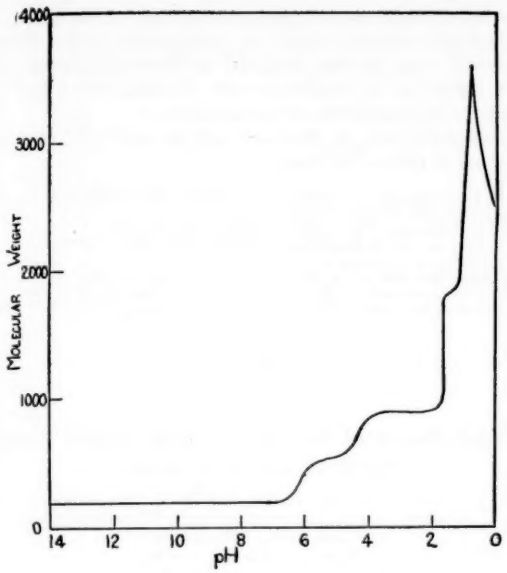

FIG. 1. The variation of the molecular weight of the molybdate ion with pH as determined by diffusion.

salts.[6] The solution was equilibrated with the charcoal before filtering, and the concentration was checked before and after filtering by measuring the refractive index of the solution.

The usual plot of c/τ_2 against c (in grams per cc) is given in Fig. 2. τ_2 is the difference between the turbidity of the solution and that of the solvent. Curve I is for a solution of sodium molybdate of unadjusted pH. The pH was found to be between 6.5 and 7.5 at all concentrations. Curve II was obtained using a solution whose pH was brought into the range 2.5 to 4.0 by adding a sufficient amount of filtered c.p. nitric acid to the filtered solution. The turbidity of the solvent in this latter case was taken as that of a solution of nitric acid in distilled water of concentration

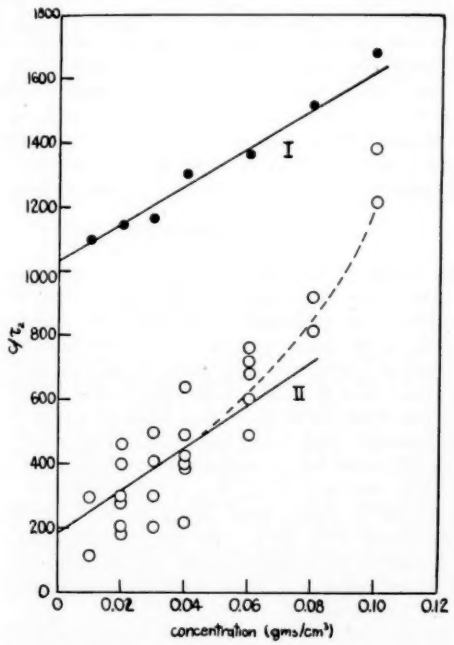

FIG. 2. The variation of the reduced turbidity of a sodium molybdate solution with concentration for two pH regions.

corresponding to that of the nitric acid in the sodium molybdate solution.

The molecular weight M was calculated from the intercept of these plots using Eq. (2).

$$H(c/\tau_2)_{c=0}=1/M$$

$$H=\frac{32\pi^3n^2(\partial n/\partial c)^2}{3\lambda^4 No}.$$

n is the refractive index of the solution, 1.339, λ the wavelength of the light (5.461×10^{-5} cm), and No is Avogadro's number. $(\partial n/\partial c)$ was determined from the slope of the plot of the refractive index against concentration. Some of these factors are listed in Table I.

TABLE I.

Solution	pH range	$(\partial n/\partial c)$	H	$(c/\tau_2)_{c=0}$	M
I	6.5–7.5	0.14	2.03×10^{-6}	1040 ± 30	480 ± 10
II	2.5–4.0	0.14	2.03×10^{-6}	200 ± 90	2500 ± 1000

While the precision of our results, especially in the acid region, is quite low, the light scattering data definitely confirm the greater association of the molybdate ion at lower pH. Our absolute molecular weights are greater by a factor of about 2–3 than those given by Jander. Further work at other pH's and at higher ionic strengths (corresponding to those of Jander's measurements) is contemplated.

* This paper includes part of the senior Honors research work of Mr. Kestigian and Mr. Colodny leading to the degree of B.S. in Chemistry at the University of Massachusetts.

† Present address: Department of Chemistry, University of Connecticut, Storrs, Connecticut.

‡ Present address: Department of Chemistry, Princet on University, Princeton, New Jersey.

[1] G. Jander, *et al.*, Z. anorg. Chem. **144**, 225 (1925); **187**, 60 (1930); **194**, 383 (1930); **201**, 361 (1931); **211**, 49 (1933); **212**, 1 (1933); **214**, 145, 275 (1933); **215**, 310 (1933); **217**, 65 (1934); **220**, 201 (1934); **225**, 162 (1934); **229**, 129 (1936); for summaries, see Kelloid Beihefte **411**, 297 (1934) or D. Van Nostrand Company, Inc., New York (1945), pp. 183–87.

[2] P. Debye, J. Appl. Phys. **15**, 338 (1944); Dotz, Zimm, and Mark, J. Chem. Phys. **13**, 159 (1945).

[3] B. H. Zimm, J. Chem. Phys. **16**, 1099 (1948).

[4] C. I. Carr and B. H. Zimm, J. Chem. Phys. **18**, 1616 (1950).

[5] Robert Locket, University of Bordeaux, private communication.

[6] R. Locket, Compt. rend. **230**, 437, 1657 (1950); **232**, 1084 (1951).

LCAO Self-Consistent Field Calculations of the π-Electrons Energy Levels and Electronic Structure of Fulvene

GASTON BERTHIER
Institut du Radium, 11 rue Pierre Curie, Paris, France
(Received March 2, 1953)

DURING the last years increasing interest has been centered on the theoretical study of aromatic nonbenzenoid hydrocarbons.[1] The properties of these compounds being generally quite different from those of the corresponding benzenoid isomers, their theoretical investigation may form a useful criteria for the validity of the different quantum methods of theoretical chemistry. We have now applied the LCAO self-consistent field method recently introduced by Roothaan[2] to the study of fulvene (Fig. 1), which is the cross-conjugated isomer of benzene. In order to facilitate the comparison with other results, the calculations have been carried out with the same approximations as those used by Parr and Mulliken in their study of butadiene:[3] the π-electrons are desscribed by molecular orbitals built up out of $2p\pi$ atomic orbitals of effective charge $Z=3.18$, independently of the other electrons of the molecule; three and four center integrals have

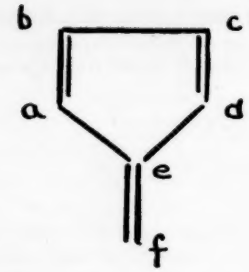

FIG. 1.

been included, approximated by Sklar's formula. The only empirical parameters introduced were the geometrical dimensions of the fulvene skeleton, for which C−C distances equal respectively to 1.35A and 1.46A for the double and single bonds of the usual formula were adopted. Table I contains the results obtained.

TABLE I.

Molecular orbitals (4)	ϵ_i
$\phi_1=0.3109(\chi_a+\chi_d)+0.2954(\chi_b+\chi_c)+0.4114\chi_e+0.2712\chi_f$	−2.668 ev
$\phi_2=0.1556(\chi_a+\chi_d)+0.3763(\chi_b+\chi_c)-0.4798\chi_e-0.5237\chi_f$	0.972
$\phi_3=0.5320(\chi_a-\chi_d)+0.4115(\chi_b-\chi_c)$	1.897
$\phi_4=0.3949(\chi_a+\chi_d)-0.3845(\chi_b+\chi_c)+0.3512\chi_e-0.6689\chi_f$	12.412
$\phi_5=0.5305(\chi_a-\chi_d)-0.7298(\chi_b-\chi_c)$	17.240
$\phi_6=0.5515(\chi_a+\chi_d)-0.2575(\chi_b+\chi_c)-0.8293\chi_e+0.5398\chi_f$	17.271

In the fundamental state of the molecule the six π-electrons occupy in pairs the three first levels of Table I and have the total energy W_π, whose difference with respect to the energy W_K of the structure represented in Fig. 1 gives the contribution of the π-electrons to the vertical resonance energy of fulvene R:

$$W_\pi=-113.93 \text{ ev}; \quad W_K=-113.05 \text{ ev};$$
$$R=0.88 \text{ ev } (20.3 \text{ kcal/mole}).$$

This value lies between those obtained for benzene (3.17 ev) and butadiene (0.3 ev).[5]

The molecular orbital ϕ_3, the highest filled in the fundamental state, gives the first ionization potential of fulvene I_1

$$I_1\simeq -W_{2p}-1.897\simeq 9.38 \text{ ev}.$$

The theoretical ionization potential of fulvene is thus slightly smaller than that of butadiene.[3] There are no experimental values as yet to check these predictions.

The distribution of electrical charge around all the carbon atoms is

$$q_a=q_d=1.0167; \quad q_b=q_c=1.0159; \quad q_e=1.0382; \quad q_f=0.8966.$$

This gives a dipole moment $\mu=1.13D$. It is thus seen that contrary to the usual approximation of the LCAO method which yields a moment of $4.8D$, the self-consistent field method yields a theoretical moment which is in perfect agreement with the experimental one of $1.2D$, measured by Wheland and Mann.[6] It seems thus that the π-electrons effectively determine the polar properties of fulvene.

The nonoccupied orbitals ϕ_4, ϕ_5, and ϕ_6 enable us to calculate the different $N\rightarrow V$ electronic transitions of fulvene. Table II contains

TABLE II.

	$N\rightarrow V$	f^a	$(N\rightarrow V)_{exp}$	f_{exp}
$^1B_2$	4.95 ev	0.013	3.4 ev	0.012
$^1A_1$	7.51	0.55	4.6	0.32

[a] Calculated with ν_{exp}.

the results for the first two transitions, best known experimentally.[7] Though these results indicate correctly a bathochromic shift of the longest wavelength of absorption of fulvene with respect to butadiene and benzene, the calculated energies of the transitions are, just as in butadiene and benzene, higher than the experimental ones. On the contrary, the theoretical intensities of the two bands are in agreement with the observed values; this confirms the interpretation of the spectrum.

A detailed account of this study will be published shortly in the *Journal de chimie physique.*

[1] See B. Pullman and A. Pullman, *Les Théories Electroniques de la Chimie Organique* (Masson Editeur, Paris, 1952).
[2] C. C. J. Roothaan, Revs. Modern Phys. **23**, 69 (1951).
[3] R. G. Parr and R. S. Mulliken, J. Chem. Phys. **18**, 1338 (1950).
[4] Notations as in reference 3.
[5] R. S. Mulliken and R. G. Parr, J. Chem. Phys. **19**, 1271 (1951).
[6] G. W. Wheland and D. E. Mann, J. Chem. Phys. **17**, 264 (1949).
[7] E. D. Bergmann and Y. Hirshberg, Bull. soc. chim. **17**, 1091 (1950).

T^2 Dependence of the Low Temperature Specific Heat of Boron Nitride

A. S. DWORKIN, D. J. SASMOR, AND E. R. VANARTSDALEN
Chemistry Division, Oak Ridge National Laboratory, Oak Ridge, Tennessee

(Received March 9, 1953)

RECENTLY DeSorbo and Tyler[1] demonstrated that at temperatures below about 40°K the heat capacity of graphite varies as the square of the absolute temperature rather than according to the usual Debye T^3 law. This was ascribed to the layered structure of graphite in which the interlayer restoring forces are quite weak thereby giving a quasi two dimensional crystal. Apparently Nernst[2] was the first to imply that a T^2 law might hold for layered lattices. The applicability of a T^2 law to graphite was discussed by Tarassov[3a] and more recently he considered it in dealing with a number of other substances.[3b,c,d] Gurney[4] has used the concept of a two-dimensional lattice in the otherwise usual Debye treatment to derive the expression

$$C_v=9.60RT^2/\theta^2 \tag{1}$$

for the heat capacity of a layered crystal and has shown good agreement between theory and experiment in the case of graphite. Very recently DeSorbo[5] called attention to the agreement with a T^2 law in the case of the heat capacity data for gallium below 40°K obtained by Adams, Johnston, and Kerr.[6]

We have just completed a determination of the heat capacity of high purity, crystalline boron nitride[7] which has a layered structure and lattice parameters[8] very like graphite. The heat capacity of boron nitride obeys a T^2 law quite exactly up to temperatures of about 60°K. The agreement of our data with the T^2 relationship is shown in Fig. 1, where we have plotted C_v *vs* T^2. C_v was calculated for each experimental C_p value by means of the equation

$$C_p-C_v=\alpha^2VT/\beta \tag{2}$$

where the coefficient of expansion α and the molar volume V were obtained from the x-ray crystallographic data of Pease.[8] The compressibility coefficient β has not been determined for boron nitride, so we have assumed it to be the same as that of graphite. This is admittedly an approximation; however, even a 20 percent error in β introduces only a small error in the derived values of C_v at these low temperatures where C_p and C_v differ but slightly in absolute magnitude. Since boron nitride and graphite have nearly the same lattice parameters we believe our approximation is well justified. Using Eq. (1) we calculate from our data that $\theta=348$°K with a mean deviation of 1.5 percent in the temperature range 20 to 60°K. This may be compared with the value of $\theta=608$°K for graphite given by DeSorbo and Tyler,[1] which, however, refers to 1 gram atom of C, while θ for boron nitride is for 1 mole of BN.

There are now examples of two elements, graphite and gallium, and a compound, boron nitride, all possessing layered structures and showing quite exact low temperature T^2 heat capacity de-

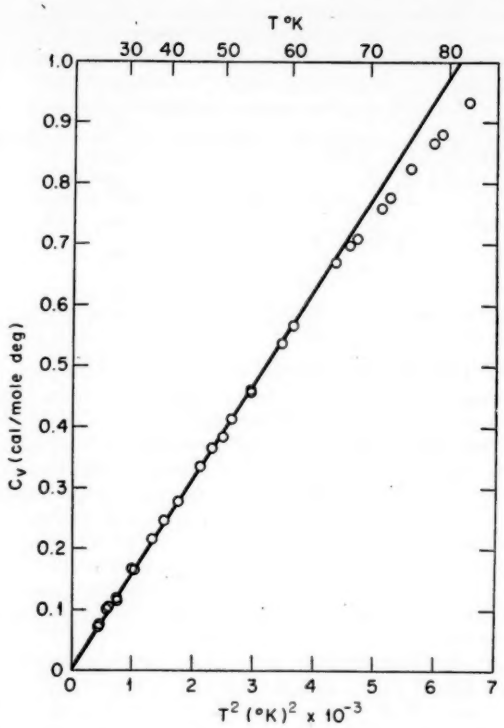

FIG. 1. Heat capacity of boron nitride.

pendence. Therefore we are inclined to the feeling that this is a rather general phenomenon for quasi two-dimensional crystals.

A detailed presentation and discussion of heat capacity as well as other thermodynamic data for boron nitride will be given by us at a later date.

[1] W. DeSorbo and W. W. Tyler, Phys. Rev. **83**, 878 (1951).
[2] W. Nernst, Ann. Physik **36**, 395 (1911).
[3] V. V. Tarassov, (a) Compt. rend. acad. sci. U.R.S.S. **46**, 20, 110 (1945); (b) *ibid.* **54**, 795 (1946); (c) Zhur. Fiz. Khim. **24**, 111 (1950); (d) Doklady Akad. Nauk. U.R.S.S. **58**, 577 (1947).
[4] R. W. Gurney, Phys. Rev. **88**, 465 (1952).
[5] W. DeSorbo, J. Chem. Phys. **21**, 168 (1953).
[6] Adams, Johnston, and Kerr, J. Am. Chem. Soc. **74**, 4784 (1952).
[7] We wish to thank Mr. C. W. Henson of the Norton Company for kindly placing this sample of boron nitride at our disposal.
[8] R. S. Pease, Acta Cryst. **5**, 356 (1952).

Sound Dispersion in *cis*- and *trans*-Dichloroethylene Vapors*

M. BOUDART
The James Forrestal Research Center, Princeton University, Princeton, New Jersey
(Received February 24, 1953)

SETTE *et al.* recently published in this Journal[1] a study on collisional energy transfer in *cis*- and *trans*-dichloroethylene vapors. They considered the latter as an ideal gas. This, however, is not justified as can be seen in Fig. 1, where the values of v^2, v being the measured sound velocity, are plotted against pressure for the *trans*-compound at the frequency $f=0.4251$ Mc/sec. A straight line is obtained, as befits an imperfect gas[2] with a non-zero second virial coefficient B. The latter can be calculated by means of the Berthelot equation, since the critical pressure and temperature of both isomers are available in the literature.[3] We get $B_{cis}=-960$ cm^3, $B_{trans}=-870$ cm^3. Then, the value v_0 of the sound velocity, reduced to zero pressure, can be obtained by means of the relation $v^2=v_0^2(1+ap)$, where $a=2B/RT$. We get $a_{cis}=1.0\cdot10^{-4}$ mm^{-1} and $a_{trans}=0.9\cdot10^{-4}$ mm^{-1}. The value of a_{trans} thus obtained practically coincides with that taken from the

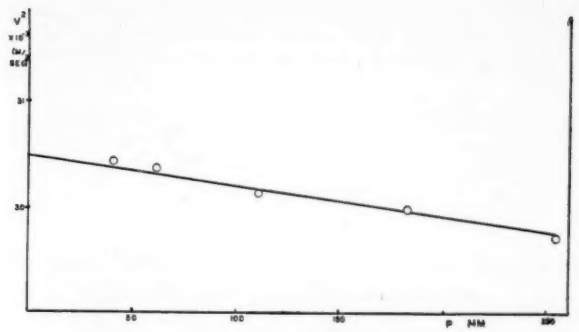

FIG. 1. Effect of pressure on sound velocity at a nondispersive frequency.

slope of the straight line in Fig. 1. The Berthelot equation is quite adequate in this case. The values of v_0 are shown in Tables I and II. In Fig. 2, we have plotted v_0^2 against $\log(f/p)$. It can be seen that a single dispersion wave is now well defined. Sette *et al.* believed that two separate waves were operative for each molecule. When corrected values of v are used, the data at low frequency and high pressure are smoothed out, so that this conclusion of Sette *et al.* seems incorrect. It can also be seen on Fig. 2 that the dispersion wave of both isomers starts practically at the same value of f/p. However, since both curves start from a different low value of v_0, the *trans*-curve appears to be shifted slightly toward higher values of f/p. Both curves subsequently converge as they should. In view of the scattering of experimental points due to the fact[2] that the precision of the measurements decreases when pressure is lowered, it appears extremely difficult to decide whether there is a significant difference in relaxation times for both compounds. The inflection point, for both curves, lies around 90 Mc/atom. The lack of any marked difference in the behavior of

TABLE I. *cis*-compound.

f Mc/sec	p mm Hg	v m/sec	v_0 m/sec
0.4250	195.6	173.0	174.7
0.4283	118.8	174.0	175.0
	79.2	174.2	174.9
	49.5	175.7	176.1
	29.5	176.8	177.0
2.9827	182.0	176.0	177.6
1.9868	93.1	177.5	178.3
2.9827	122.1	178.2	179.3
	75.9	179.4	180.1
	57.4	180.9	181.4
1.9868	30.4	182.0	182.3
2.9827	36.6	180.7	181.0
1.9868	21.2	181.5	181.7
2.9827	25.9	182.5	182.7
1.9868	14.9	182.6	182.7
	12.2	183.1	183.2

TABLE II. *trans*-compound.

f Mc/sec	p mm Hg	v m/sec	v_0 m/sec
0.4251	253.5	172.4	174.4
	181.9	173.0	174.4
	110.2	173.6	174.5
	61.1	174.3	174.8
1.9847	249.2	172.5	174.5
	231.0	173.1	174.9
	190.0	174.1	175.6
0.4251	40.5	174.5	174.8
1.9847	132.8	174.4	175.4
	97.0	175.7	176.5
	69.6	175.5	176.1
	48.7	175.3	175.7
1.9867	48.8	175.1	175.5
	35.4	177.3	177.6
1.9847	27.9	178.7	178.9
1.9867	20.4	179.4	179.6
1.9847	16.4	182.5	182.6
	13.9	181.3	181.4
1.9866	12.1	183.4	183.5

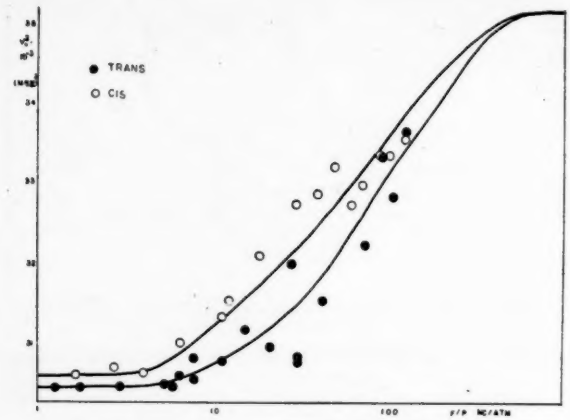

FIG. 2. Dispersion of sound in dichloroethylene isomers.

the isomers corroborates the theoretical conclusion of Sette *et al.* Only short-range forces seem to operate in vibrational energy exchange. The tables also show that the low frequency corrected values of v_0, 174.7 and 174.4, are still slightly higher than the theoretical values, 173.74 and 173.46, calculated by Sette *et al.* from spectroscopic data. The discrepancy may be explained by the presence of 1 or 2 percent of a lighter gas, e.g., C_2H_3Cl in the isomers investigated.†

It seems advisable, in the future, to correct sound data for departure from ideal gas law when a pressure dependence of v is observed.[2] Failure to do so may lead to difficulties, as illustrated here. The work on energy exchange in this laboratory is supported by Air Materiel Command, Contract No. AF 33(038)-23976.

* The work in energy exchange in this laboratory is supported by the Air Materiel Command.
[1] Sette, Busala, and Hubbard, J. Chem. Phys. **20**, 1899 (1952).
[2] N. Pusat, Rev. Fac. Sci. Univ. Istanbul **17**, 46 (1952).
[3] D. R. Stull, Ind. Eng. Chem. **39**, 517 (1947).
† The author is indebted to Professor K. F. Herzfeld and Dr. D. Sette for this suggestion.

The Mechanism of Acetone Pyrolysis

J. R. MCNESBY, T. W. DAVIS, AND A. S. GORDON
Michelson Laboratory, U. S. Naval Ordnance Test Station, Inyokern, China Lake, California
(Received March 16, 1953)

RECENT work by Moore and Wall[1] indicates that the mechanism of acetone pyrolysis may be largely intramolecular. When they pyrolyzed mixtures of normal and deutero-acetone, almost no CH_3D was observed in the early stages of the reaction; at the same time large amounts of CH_4 and CH_2D_2 were formed. As part of a larger program we have repeated and extended the results of Moore and Wall. Our results are quite consistent with the Rice-Herzfeld free radical mechanism.

The deutero-acetone analyzed 92.2 percent d_6, 7.2 percent d_5, and 0.6 percent d_4. Pyrolyses were carried out with 1:1 mixtures of normal and deuteroacetone at a total pressure of about 400 mm at 500°C.

The resulting methane ratios after various times of heating are given in Table I. Each ratio is the average of two analyses from the same run. The two values given for 20 minutes are averages from two separate runs and reveal the general precision of the methane ratios.

The acetones always exchanged during the reaction.

The d_5 acetone/d_6 acetone ratio was 7.8 percent at zero time; it increased to 11.6 percent at the end of the 5-minute run, and to 250 percent at the end of the 40-minute run. Nevertheless, the

TABLE I. Time in minutes of decomposition of 1:1.2 mixtures of deutero and normal acetone and resulting methane ratios.

Time (min)	5	10	20	40
$\frac{CD_3H}{CD_4}$	2.70	2.79	2.76 2.85	3.07
$\frac{CH_4}{CH_3D}$	3.13	2.72	2.47 2.59	1.49
$\frac{CH_4}{CD_4}$	7.82	7.96	7.29 7.65	6.20

CD_3H/CD_4 ratio remains remarkably constant with time. If the mechanism of methane formation were appreciably intramolecular, the above ratio should increase markedly as the d_5 acetone/d_6 acetone ratio increases. If the mechanism is essentially free radical, the CD_3H/CD_4 ratio should increase slowly with progressive exchange. The increasingly abundant CD_2H free radical forms relatively little CD_3H by abstraction of deuterium, since it preferentially abstracts hydrogen by a factor of about 3 (see Table I). Even after extensive exchange most of the CD_3H is formed by CD_3 abstracting H. When the data are roughly corrected for the CD_3H formed from CD_2H, the CD_3H/CD_4 ratio stays more constant with time of reaction.

From the Rice-Herzfeld mechanism, assuming equal steric factors[2] for the methyl radical extraction of H and D, it is readily shown that $CD_3H/CD_4=\exp\Delta E/RT$, where ΔE is the energy of activation difference between CD_3 abstracting a hydrogen and a deuterium from acetone. From the above experimental values $\Delta E=1.3$ kcal if the ratio of the frequency factors is about unity. Using a photochemical technique, Steacie and Trotman-Dickenson,[2] assuming no activation energy for the methyl-methyl reaction, obtained a value of 9.7 kcal for the energy of activation of the reaction $CH_3+CH_3COCH_3\rightarrow CH_4+CH_2COCH_3$ and a value of 10.3 for $CD_3+CD_3COCD_3\rightarrow CD_4+CD_2COCD_3$.

The CH_4/CH_3D value should decrease fairly rapidly with amount of exchange as is found experimentally, since the CH_2D free radical prefers to stabilize itself by abstraction of H.

If ΔE for the abstraction of hydrogen and deuterium by CH_3 were the same as for CD_3, the CH_4/CH_3D and CD_3H/CD_4 ratios should be equal when there is no acetone exchange. Experimentally the CH_4/CH_3D ratio is significantly higher at the 5-minute time than the CD_3H/CD_4 ratio. Any correction for the exchange will make these ratios diverge even more so that the difference is probably real. Further work is under way to check this point.

We intend to publish detailed results of more extensive work at a later date.

[1] W. J. Moore and L. A. Wall, J. Phys. Chem. **55**, 965 (1951).
[2] A. F. Trotman-Dickenson and E. W. R. Steacie, J. Chem. Phys. **18**, 1097 (1950).

Errata: A Hydrodynamic Method for the Measurement of Rates of Very Fast Reactions

S. H. BAUER
Department of Chemistry, Cornell University, Ithaca, New York
(Received March 6, 1953)

A NUMBER of errors were uncovered in a paper under the above title which appeared in the recently issued L. Farkas Memorial Volume.[1] I shall appreciate owners of copies of the book requesting reprints of this note for inserting the following corrections in their texts:

p. 98: Equation (3). The limits for the second integral in the right member should be from p_0 to p_1.

p. 99: Several lines were deleted at the bottom of the page. The last sentence should read as follows: "In Eqs. (2) and (3) delete the subscript 1; these quantities then become functions of x. Two additional relations are required to permit a complete solution. They are . . .".

p. 102: Equation (11). Replace K_n by K_p, in both parts.

p. 103: Equation (19). Delete the [1+] from the bracket in the right member. The equation should read

$$\left(\frac{\partial \alpha_e}{\partial T}\right)_p = \frac{p}{2}\frac{\alpha_e^3}{RT^2K_n}\left[\frac{\Delta H^0}{RT}\right].$$

p. 104: Middle of page—an extra sentence was inserted. Delete the statement just above Eq. (23) . . . "The steady state condition (valid at each position x along the stream line),"

p. 106: In the first line, replace t_0 by T_0. Equation (30) delete the [1+] from the first bracket in the second term of the right member.

p. 108: Figure 4. Delete the entire bracket in the lower equation for C_p''. That equation should read

$$C_p'' = \frac{2p}{K_p}\frac{\Delta H^0}{RT^2}\alpha_e^3.$$

The curves in this figure are correct.

p. 108: Figure 5. All the curves in this figure, except the one labeled p_2, are essentially correct. The numerical magnitude of p_2 was obtained by taking a difference between large quantities (Eqs. (30), (32)). It is regrettable that the latter were not carried to a sufficient number of significant figures in a self-consistent procedure. Also, use of an inconsistent set of symbols introduced further errors. Hence the values for p_2 indicated in Fig. 5 are much too large.

p. 109: As a consequence of the above error, two statements on this page are incorrect.

Delete from the text the last sentence in the first paragraph, which starts with the words, "The rather unexpected . . .."

Also, delete the paragraph marked (b), and insert instead: "It should not prove difficult to distinguish between heat capacity lag due to vibration alone, to dissociation alone, and to dissociation plus vibration. The computed magnitudes of the maximum pressure defects for the $NO_2-N_2O_4$ reaction, for the last two cases are 1.2×10^{-3} atmos and 5.6×10^{-3} atmos, respectively. Since the lag in dissociation cannot be less than the lag in vibrational equilibration involving the bond being broken, study of the pressure defect as a function of nozzle length and impact tube diameter will show two regions, if these are resolvable. Starting with a short characteristic time constant for the apparatus, and proceeding to the longer ones, the case where both reaction and vibration lag will be encountered first and then the case where reaction only lags."

p. 114: Delete the last two sentences on this page.

Comment on the method of solution by successive approximation (p. 105):

Although the proposed procedure for solving the three simultaneous differential equations by successive approximations is entirely feasible, it appears to be very lengthy and involved from the point of view of analyzing numerically appreciable amounts of experimental data. We have now set up a much simpler procedure, in which relaxation theory is utilized. Approximations are thus inherently introduced, but these may be justified in terms of our limiting experimental errors. Details of the experimental procedures, data on the $NO_2-N_2O_4$ reaction, and their analysis in terms of characteristic relaxation times will be shortly submitted for publication. This research has been supported, in part, by the U. S. Office of Naval Research.

[1] *L. Farkas Memorial Volume*, Research Council of Israel, Special publication No. 1 (Jerusalem, 1952), p. 95 ff

The Iron Catalyzed Reaction between Nitrosyl Disulfonate and Hydroxylamine Monosulfonate Ions

WILLIAM J. RAMSEY AND DON M. YOST
Gates and Crellin Laboratories of Chemistry, California Institute of Technology, Pasadena, California
(Received February 17, 1953)

POTASSIUM nitrosyl disulfonate, $K_2NO(SO_3)_2$, is noteworthy because the solid salt is orange in color and diamagnetic while its neutral aqueous solutions are purple in color and paramagnetic. These neutral solutions hydrolyze slowly to form N_2O and hydroxylamine sulfonates; on the addition of acid the rate of hydrolysis is markedly increased. The mechanism of the hydrolytic reaction is unexpectedly complex as was found by Murib and Ritter[1] and, independently, by us. In order to obtain a more comprehensive picture of the mechanism of the hydrolytic reaction we have explored additional reactions which may play a part in the hydrolysis.

We have found in particular that the reaction in aqueous solution between nitrosyl disulfonate and hydroxylamine monosulfonate ion, $ON(SO_3)_2^=$ and $HONHSO_3^-$, respectively, is catalyzed by iron salts. The reaction is of interest for two reasons. First, very small concentrations of iron cause the reaction to proceed at an easily measurable rate. Second, the rate of the catalyzed reaction is dependent upon hydrogen ion concentration in a way that indicates that predominantly one of the hydrolyzed species of iron (III), $Fe(OH)^{++}$, is responsible for the catalysis. The stoichiometry of the iron catalyzed reaction is represented by the equation,

$$4ON(SO_3)_2^= + 2HONHSO_3^- + H_2O = N_2O + 4HON(SO_3)_2^= + 2HSO_4^-. \quad (1)$$

Rates of disappearance of nitrosyl disulfonate ion were measured spectrophotometrically (by means of a Beckman Model DU spectrophotometer) under the following initial conditions: Perchloric acid concentration, between 2.5×10^{-4} and 2.5×10^{-3} VF (formula weights per liter of solution); ferric perchlorate concentration, as high as 1.46×10^{-6} VF; sodium hydroxylamine monosulfonate concentration, between 1.03 and 4.59×10^{-5} VF; potassium nitrosyl disulfonate concentration, between 1.4 and 4.7 $\times10^{-5}$ VF; various concentrations of potassium perchlorate and lanthanum perchlorate to adjust the ionic strength; and at temperatures of 20.00 ± 0.03 and 30.00 ± 0.03°C. The details of this investigation are to be published at a later date.

In the majority of cases only the initial rate of disappearance of nitrosyl disulfonate ion was measured, because as the reaction proceeds, side reactions become important.

At a given hydrogen ion concentration, temperature, and ionic strength, and at iron concentrations less than 3.5×10^{-7} VF; the rate of disappearance of nitrosyl disulfonate ion is well represented by the equation

$$-\frac{d(ON(SO_3)_2^=)}{dt} = k_0(\Sigma Fe^{+3})(HONHSO_3^-), \quad (2)$$

where (ΣFe^{+3}) represents the total concentration of iron in the reaction solution.

The value of k_0 increases with increasing hydrogen ion concentration up to a value of 1.4×10^{-3} VF and then decreases with increasing hydrogen ion concentration.

The following mechanism is in accord with the experimental data:

$$Fe^{+++}+H_2O \overset{h_1}{\rightleftharpoons} Fe(OH)^{++}+H^+, \quad (3)$$

$$Fe(OH)^{++}+H_2O \overset{h_2}{\rightleftharpoons} Fe(OH)_2^{+}+H^+, \quad (4)$$

$$Fe(OH)^{++}+HONHSO_3^- \overset{k_2}{\rightarrow} \text{reactive products}+Fe^{++}, \quad (5)$$

$$Fe(OH)_2^{+}+HONHSO_3^- \overset{k_3}{\rightarrow} \text{reactive products}+Fe^{++}, \quad (6)$$

$$\text{reactive products}+ON(SO_3)_2^= \rightarrow N_2O+HON(SO_3)_2^=, \quad (7)$$

$$\text{reactive products}+Fe(III) \rightarrow N_2O+Fe^{++}, \quad (8)$$

$$Fe^{++}+H_2O+ON(SO_3)_2^= \rightarrow Fe(OH)^{++}+HON(SO_3)_2^=, \quad (9)$$

where h_1 and h_2 are the first and second hydrolysis constants for iron (III), and k_2 and k_3 are the specific rate constants for the reactions represented by Eqs. (5) and (6). Equation (8) summarizes the reactions which may take place between the various species of iron (III) and the reactive products of the initial oxidation of hydroxylamine monosulfonate ion. The reactions represented by Eqs. (9) and either (7), (8), or both must be fast compared to those represented by Eqs. (5) and (6). The rate of disappearance of nitrosyl disulfonate ion under the conditions stated above is then described by the equation

$$-\frac{d(ON(SO_3)_2^=)}{dt}=2\left\{\frac{k_2h_1(H^+)+k_3h_1h_2}{(H^+)^2+h_1(H^+)+h_1h_2}\right\} \times(\Sigma Fe^{+3})(HONHSO_3^-). \quad (10)$$

The value for the constant h_1 was taken from the work of Siddall and Vosburgh.[2]

The values obtained for h_2, k_2, and k_3 at a temperature of 20°C and at an ionic strength of 2.6×10^{-2} are 7×10^{-4} mole·l^{-1}, $13.9\pm1.4\times10^4$ l·mole^{-1}·min^{-1}, and $1.5\pm0.2\times10^4$ l·mole^{-1}·min^{-1}, respectively.

We are indebted to the Research Corporation, the Shell Oil Company, and E. I. du Pont de Nemours and Company for grants which supported this research.

[1] J. H. Murib and D. M. Ritter, J. Am. Chem. Soc. **74**, 3394 (1952).
[2] T. H. Siddall, III, and W. C. Vosburgh, J. Am. Chem. Soc. **73**, 4270 (1951).

The Forces between Hydrogen Molecules

ARTHUR A. EVETT AND HENRY MARGENAU
Yale University, New Haven, Connecticut
(Received March 2, 1953)

EARLIER calculations of the H_2-H_2 interaction,[1] based on the use of screening-constant functions, seemed to lead to reasonable answers only with the use of a nuclear charge much greater than the correct value for the isolated molecule, $Z_0=1.166$. The present work is a recalculation of the exchange forces for $Z=Z_0$. A small numerical error in the earlier work is eliminated and the exchange energy, instead of being slightly negative as reported previously, is actually positive. This removes all perplexing features from the problem and yields results in substantial agreement with experiments.

The total interaction, consisting of exchange, van der Waals, and quadrupole energies, is plotted for different relative orientations of the molecules in Fig. 1.

These orientations are:

Case (a): Both molecular axes are parallel to R, the line joining the centers.

Case (b): One axis is parallel, the other perpendicular to R.

Case (c): Both axes are perpendicular to R and parallel to each other.

Case (d): Both axes are perpendicular to R and perpendicular to each other. Case (d) was not treated in the earlier paper.

A weighted average over all orientations is shown in Fig. 2 and is compared with the semi-empirical curve of Hirschfelder, Bird, and Spotz,[2] which was derived by fitting viscosity data. The work of De Boer and Michels,[3] based on an evaluation of second virial coefficients, leads to points slightly lower than Hirschfelder's.

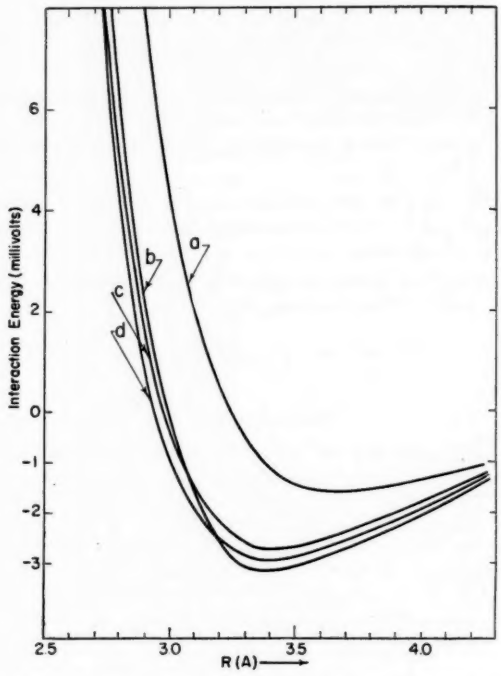

FIG. 1. Total energy of interaction for different molecular orientations as function of intermolecular distance.

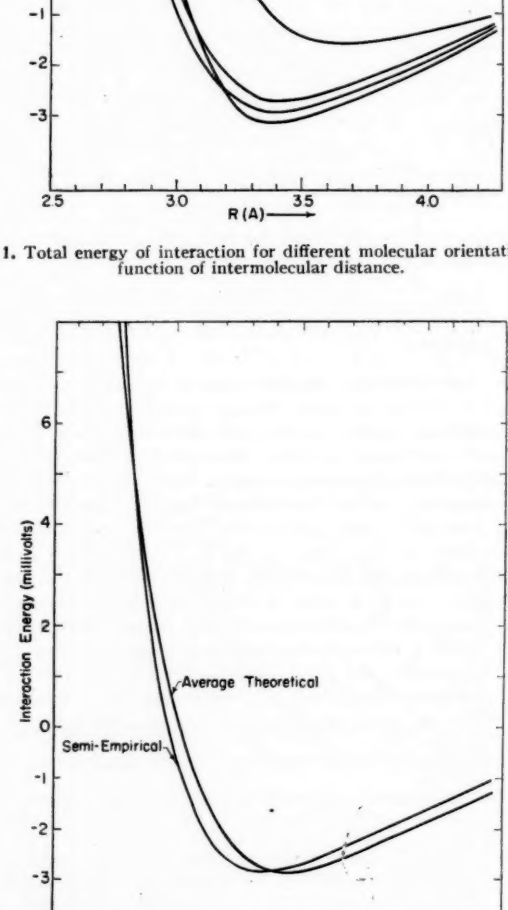

FIG. 2. Comparison of theoretical interaction (averaged over molecular orientations) with empirical curve of Hirschfelder, Bird, and Spotz.

The essential agreement of our interaction, which relies on no empirical parameters, with both of these seems gratifying.

A somewhat fuller account of the present work will be published in *The Physical Review*.

[1] H. Margenau, Phys. Rev. **63**, 131 (1943).
[2] Hirschfelder, Bird, and Spotz, J. Chem. Phys. **16**, 968 (1948).
[3] J. De Boer and A. Michels, Physica **5**, 945 (1938).

Symmetry Assignments for the First Two Excited Singlet Electronic States of the Naphthalene Molecule*

OTTO SCHNEPP† AND DONALD S. MCCLURE
Department of Chemistry and Chemical Engineering, University of California, Berkeley, California
(Received September 2, 1952)

WE report here some data on the electronic spectrum of the naphthalene crystal, which together with our vapor fluorescence work[1] and the absorption studies[2] determine the symmetry of the first two excited singlet electronic states of the naphthalene molecule. The experimental work was an extension and refinement of that of Obreimov[3] and Prikhotjko[4] and will be reported later.

There appear to be four upper electronic states in the near uv spectrum of the crystal. They are described as follows: (1) origin at 29 945 cm^{-1}, appears in absorption and fluorescence as sharp lines (at 20°K), visible in absorption with 2 mm of crystal, 70 percent polarized in b direction (twofold symmetry axis of crystal); (2) origin 31 069 cm^{-1}, absorption and fluorescence as sharp lines, visible in absorption in 20-micron thickness, polarized like (1); (3) origin not present (see following text), 0−1 band at 31 969 cm^{-1}, visible in 0.3 micron crystal as rather broad bands (even at 20°K) polarized like 1 and 2. Two strongly polarized bands, band α 31 485 a polarized and band β 31 635 b polarized are considered to be the two components of the 0−0 band (see below). (4) Origin at 33 820 cm^{-1} appears only in absorption as very diffuse bands in 0.3 micron thickness polarized 100 percent in ac plane. There is continuous absorption on the b axis of about the same intensity as the average of the a axis absorption. We consider that this arises from a different molecular electronic state than the one which produces the ac structure.

The moderately strong absorption system (3) is very similar in its vibrational analysis and intensity distribution to the first absorption region of naphthalene in solid solution (E.P.A.).[5] This correspondence is exhibited starting with the second band of the solution and the 31 969 band of the crystal. The solution spectrum is shifted 240 cm^{-1} to the violet of the crystal spectrum. The center of the weak 0−0 band of the solution spectrum falls between two bands of the crystal (allowing for the 240 cm^{-1} shift); band α and band β. It is believed that α and β are split apart by resonance interactions in the crystal, but that the vibrational additions to the 0−0 band are not so split, because of destruction of the resonance condition by the vibration. At 298°K in the absorption spectrum of a 2-micron crystal, there appears a broad band, 70 percent b polarized and centered at 31 040 cm^{-1}. It is too strong to be the broadened 31 069 band, and it is in the right place to correspond to the 1−0 band of the solution fluorescence. The measured (1−0, 0−1) interval for the vapor is 942 cm^{-1}, and this is very close to the interval 31 969–31 040. We therefore propose that system (3) of the crystal corresponds to the first system of the free molecule.

The strong absorption system (4) is easily analyzed into progressions of 510 and 1400 cm^{-1} in spite of its diffuseness. With this result and its position and intensity, this system certainly corresponds to the second system of the free molecule.

The factor group analysis of the crystal, with C_{2h}^5 and two molecules per unit cell, leads us to expect two active electronic states of the crystal for each one of the free molecule. One will be polarized along b, the other in the ac plane. We now assume that the stronger component will be the one polarized in the crystal direction most nearly coinciding with the direction of the transition moment in the free molecule. The y axis (short axis) of the molecule lies at about 29° from the b axis of the crystal, while the x axis (long axis) lies within a few degrees of the ac plane. Since we have discussed only the strongest crystal transitions, we can say that system (3) is the b component of the first free molecule transition and that the latter is directed along the short molecular axis. Similarly, we can say that system (4) corresponds to the ac component of the second free molecule transition, and the latter lies either along the long molecular axis or perpendicular to the molecular plane. Assuming that all states involved are π-electron states, and that the second free molecule transition is allowed, the second excited singlet state is $^1B_{3u}$.

The work of McConnell and McClure with the substituted naphthalenes[6] has shown that the first free molecule transition is allowed, and this, with our polarization data, which is in agreement with that of Craig and Lyon,[7] determines the symmetry as $^1B_{2u}$. The 0−0 band of the crystal would fall at 31 969–942 +512=31 539 cm^{-1}. This is 21 cm^{-1} below the average of bands α and β. Although this interpretation is contrary to the one we expressed on the basis of our fluorescence data, it is possible to reconcile the latter to fit the new data by assuming that the 512 mode (430) in the upper state acts like a nontotally symmetric mode by inducing a transition moment (as discussed in reference 6). The crystal fluorescence originates almost entirely at the 31 069 band. On our interpretation, the fluorescence has nothing to do with the properties of the first free molecule singlet state, and indeed it has an entirely different vibrational pattern than the vapor fluorescence. We believe that it may be the b component of the second free molecule state, whose ac component begins at 33 820 cm^{-1}. Thus the B_{3u} (b component) would cross both components of B_{2u} in passing from free molecule to crystal.

Further evidence supporting the assignment of the first free molecule transition as allowed is that the 0−0 band appears strongly in the absorption and emission spectrum of a solid solution of naphthalene in durene (the latter does not absorb in this range).

A complete paper is in preparation, including a comparison of the spectrum of naphthalene with those of other molecular crystals that have been studied.

* This work was sponsored by the U. S. Office of Naval Research under Contract N6-ori-211, T.O. III.
† Now at Hebrew Institute of Technology, Haifa, Israel.
[1] O. Schnepp and D. S. McClure, J. Chem. Phys. **20**, 1375 (1952).
[2] H. Sponer and G. Nordheim, Disc. Faraday Soc. **19**, No. 9 (1950).
[3] I. V. Obreimov and C. G. Shabaldas, J. Phys., U.S.S.R. **7**, 168 (1943).
[4] A. F. Prikhotjko, J. Phys., U.S.S.R. **8**, 257 (1944).
[5] M. Kasha and R. V. Naumann, J. Chem. Phys. **17**, 516 (1949). We repeated the work with E.P.A. solutions of naphthalene, paying especial attention to the wavelength measurements. Our results were somewhat different from those of these authors.
[6] H. McConnell and D. S. McClure (to be published).
[7] D. P. Craig and L. E. Lyons, J. Chem. Phys. **20**, 1949 (1952).

The Microwave Spectrum and Structure of Ozone

RICHARD H. HUGHES
Westinghouse Research Laboratories, East Pittsburgh, Pennsylvania
(Received March 9, 1953)

STRUCTURAL studies of the ozone molecule have been made by numerous investigators.[1–7] Microwave spectrum measurements described here permit calculation of the structural parameters to a high degree of accuracy. Two low J lines of O_3^{16}, the $2_{0,2}\rightarrow 1_{1,1}$ at 42 833 mc and the $3_{1,3}\rightarrow 4_{0,4}$ at 11 073 were identified by their Stark components. By using these frequencies and assuming a value of the asymmetry parameter δ between 0.01596 and 0.01600, spectral constants have been obtained which predict almost all observed O_3^{16} lines to within ±200 mc, Table I. The

TABLE I. Microwave spectrum of ozone, O_3^{16}.

$\frac{B+C}{2}=12\,591.7\pm1.0$ mc $A-\frac{B+C}{2}=93\,938\pm3$ mc $\delta=0.015982\pm0.000020$

Identification	Observed frequency	Calculated frequency	Error
$21_{2,20}\rightarrow20_{3,17}$	9201 mc	9228 mc	+ 27
$9_{2,8}\rightarrow10_{1,9}$	10 226	10 209	− 17
$3_{1,3}\rightarrow4_{0,4}$	11 073	11 073	0
$24_{3,21}\rightarrow23_{4,20}$	15 116	14 795	−321
$26_{4,22}\rightarrow27_{3,25}$	16 413	16 219	−194
$19_{2,18}\rightarrow18_{3,15}$	23 861	23 912	+ 51
$46_{6,40}\rightarrow45_{7,39}$	25 300	25 235	− 65
$39_{5,35}\rightarrow28_{6,22}$	25 511	25 790	+279
$17_{1,17}\rightarrow16_{2,14}$	25 649	25 634	− 15
$40_{6,34}\rightarrow41_{5,37}$	27 862	28 246	+384
$25_{1,23}\rightarrow24_{4,20}$	28 960	29 060	+100
$16_{2,14}\rightarrow15_{3,13}$	30 052	30 096	+ 44
$15_{1,15}\rightarrow14_{2,12}$	30 181	30 141	− 40
$19_{1,19}\rightarrow18_{2,16}$	30 525	30 578	+ 53
$23_{3,19}\rightarrow23_{2,22}$	36 023	36 000	− 23
$17_{3,15}\rightarrow18_{2,16}$	37 832	37 962	+130
$2_{0,2}\rightarrow1_{1,1}$	42 833	42 833	0
$13_{1,13}\rightarrow12_{2,10}$	43 654	43 621	− 33

spectrum has been observed and identified between 9000 and 45 000 mc, except for the small region between 12 000 and 15 000 mc for which a source was not available. There were no calculated lines which were not observed. This work was presented in a talk given at the October, 1951, Chicago meeting of the American Physical Society.[8]

The spectra of ozone samples containing 1.5 and 30 percent O^{18} have been measured between 9000 and 45 000 mc. The low J lines of the isotopic molecules were predicted using the structural parameters determined by the O_3^{16} study. After the low J lines (Table II) had been identified by the number of their Stark components and accurately measured, their frequencies were used to determine the spectral constants for the isotopic molecules. Many of the high J lines of these isotopic molecules have been tentatively identified.

TABLE II. Isotopic ozone molecules.

Molecule	Low J lines Identification	Observed frequency	Components
$O^{16}O^{16}O^{18}$	$3_{0,3}\rightarrow2_{1,2}$	19 263[a]	2
	$4_{1,4}\rightarrow5_{0,5}$	32 743[a]	3
	$9_{1,8}\rightarrow8_{2,7}$	33 537[a]	5
$O^{16}O^{18}O^{16}$	$3_{1,3}\rightarrow4_{0,4}$	18 768[a]	3
	$8_{1,7}\rightarrow7_{2,6}$	29 227[a]	6
	$2_{0,2}\rightarrow1_{1,1}$	35 143[a]	2
$O^{16}O^{18}O^{18}$	$2_{0,2}\rightarrow1_{1,1}$	36 688	2
	$8_{1,7}\rightarrow7_{2,6}$	38 859	5
	$4_{1,4}\rightarrow5_{0,5}$	40 476	2
O_3^{18}	$2_{0,2}\rightarrow1_{1,1}$	38 054	2

[a] Seen in 1.5 percent O^{18} sample.

By assuming a planar structure and taking the moments of inertia two at a time, the structural parameters for the molecules as given in Table III were calculated. Because of zero point vibrations, the moments of inertia for a molecule are inconsistent with a planar structure. The existence of a range of parameters for each molecule is caused by this inconsistency of the moments

TABLE III. Structural parameters for ozone.

Molecule	Angle[a] A, B	A, C	B, C	Bond length,[a] A° A, B	A, C	B, C
O_3^{16}	116° 58.6′	117° 2.1′	116° 27.8′	1.2759	1.2771	1.2794
$O^{16}O^{16}O^{18}$	116° 58′	117° 0′	116° 32.6′	1.2761	1.2775	1.2791
$O^{16}O^{18}O^{16}$	116° 58.4′	117° 2.2′	116° 28.5′	1.2758	1.2770	1.2792
$O^{16}O^{18}O^{18}$	116° 59.6′	117° 2.2′	116° 29.5′	1.2759	1.2770	1.2791
O_3^{18}	116° 58.7′	117° 0.8′	116° 25′	1.2747	1.2760	1.2785

[a] Solving using pairs of moments of inertia.

TABLE IV. O_3^{16} Stark effect.

$\Delta\nu=(A+BM^2)E^2$ in mc; E in e.s.u.

Transition	Calculated[a] A	B	Observed A	B
$2_{0,2}\rightarrow1_{1,1}$	48.78	−20.79	48.8	−20.6
$3_{1,3}\rightarrow4_{0,4}$	134	− 9.83	137	−10.8

[a] Assuming dipole moment =0.58 Debye unit.

of inertia with a planar structure, not by experimental inaccuracies. The bond distance agrees well with that given by electron diffraction for ozone[6] but the angle differs by about 10° from the electron diffraction value of 127±3°.

The values of the defect, $\Delta=I_C=I_A-I_B$, have been calculated from the experimental data and are well within the range predicted by the formulas of Darling and Dennison.[9] Apparently the centrifugal distortion at high J's is not very large, as the fit between calculated and observed spectra was good.

The observed Stark effect of O_3^{16} agrees with the calculated within experimental error for an assumed dipole moment of 0.58 Debye unit, Table IV. The dipole moment of O_3^{16} is thus determined to be 0.58±0.03 Debye unit.

The author is particularly indebted to Mr. W. A. Feibelman and to Mr. Leslie A. Johnson of the Research Laboratories. Mr. Feibelman did a considerable portion of the experimental work and Mr. Johnson a large fraction of the calculations.

[1] S. L. Gerhardt, Phys. Rev. **42**, 622 (1932).
[2] Hettner, Pohlmann, and Schumacher, Z. Physik **91**, 372 (1934).
[3] W. G. Penney and G. B. B. M. Sutherland, Proc. Roy. Soc. (London) **A156**, 654, 678 (1936).
[4] D. M. Simpson, Trans. Faraday Soc. **41**, 209 (1945).
[5] A. Adel and D. M. Dennison, J. Chem. Phys. **14**, 379 (1946).
[6] W. Shand and R. A. Spurr, J. Am. Chem. Soc. **65**, 179 (1943).
[7] D. M. Simpson, J. Chem. Phys. **15**, 846 (1947).
[8] R. H. Hughes, Phys. Rev. **85**, 717 (1952).
[9] B. T. Darling and D. M. Dennison, Phys. Rev. **57**, 128 (1940).

Absorption Spectrum of Free HCO Radicals*

D. A. RAMSAY
Division of Physics, National Research Council, Ottawa, Canada
(Received March 16, 1953)

A SYSTEM of bands attributed to the HCO radical was first observed by Vaidya[1] in emission from the inner cone of an ethylene-oxygen flame. These bands which extend from 4100 to 2500A have since been observed by several workers[2,3] in a variety of flames and are now known as the "hydrocarbon flame bands." An isotope shift was observed when the bands were excited in C_2H_2 and C_2D_2 flames with atomic oxygen,[3–5] proving conclusively that the emitter contains one or more H atoms. The main reasons for assigning these bands to HCO are (a) the close similarity of the vibrational structure with that of the β-bands of the isoelectronic molecule NO and (b) the observation by Dyne and Style[6] of these bands in the fluorescence from formaldehyde irradiated with very short ultraviolet radiation.

An attempt was made to obtain the spectrum of the HCO radical in absorption using the method of flash photolysis which has given the absorption spectra of other free radicals.[7–10] Glyoxal, acetaldehyde, and formaldehyde were introduced in separate experiments into an absorption tube and subjected to flash photolysis. Absorption spectra in the region 2000–9000A were taken immediately after the photolysis flash using the high resolving power of a 21-ft concave grating spectrograph. No new absorption bands that could be correlated with the hydrocarbon flame bands were observed, though it must be realized that below 3000A the absorption by the parent molecule prevented detection of new bands.

In each experiment, however, a new band was observed with a head at 6138.2A and a few faint rotational lines degraded to the

red. To obtain more intense spectra (see Fig. 1) a set of multiple reflection mirrors[11,12] was incorporated into the absorption tube. The band at 6138.2A was found to consist of a single P, Q, and R branch. A second band of similar structure was observed at 5624.1A. As these bands do not correspond to any known molecular absorption, it seems very probable from photochemical considerations that they are due to HCO.

At first the simple P, Q, R structure of the bands suggested a $\Pi-\Sigma$ or a $\Sigma-\Pi$ transition of a linear molecule. Analysis of the bands revealed a considerable combination defect between the P and R branches and the Q branches which could be formally explained by Λ-type doubling of the Π-state. Assuming the ground state to be the Π-state, the following molecular constants were obtained from the 6138.2A band:

$$B''=1.450\ \text{cm}^{-1},\quad q''=0.046\ \text{cm}^{-1},\quad B'=1.358\ \text{cm}^{-1},$$

where B'' is the mean of the B'' values obtained from the P and R branches and the Q branch, and q'' is the difference of these two values. There are three reasons which appear to rule out this interpretation, *viz.*, (a) the Λ-doubling constant is excessively large, (b) a linear Π-state of HCO would be expected to show a considerable spin doubling (compare with NO) which is not observed, and (c) the B'' value would require a CO distance equal to or shorter than in the ground state of carbon monoxide (assuming $r_{CH}\geqslant 1.06$A), which appears unlikely. The same arguments apply if the ground state is assumed to be the Σ-state and the excited state the Π-state.

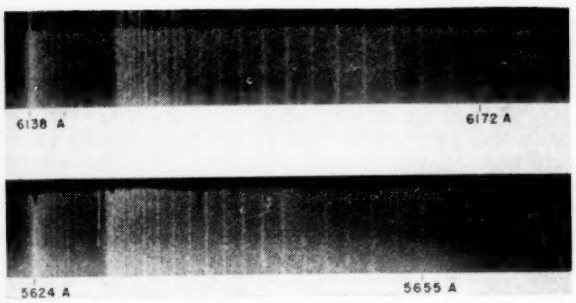

FIG. 1. Two absorption bands of free HCO radicals obtained by flash photolyzing acetaldehyde at 100-mm Hg pressure and using an absorption path of ~20 meters.

On the basis of these considerations it is necessary to assume that the ground state of HCO is nonlinear. An explanation of the simple band structure was suggested by some recent work[13] on the ultraviolet absorption spectrum of HCN which corresponds to a transition between the linear ground state and a nonlinear excited state. If the reverse condition is assumed to hold for HCO, i.e., a nonlinear ground state and a linear excited state, the large combination defect may be accounted for by the slight departure of the ground state from a symmetric top. The simple P, Q, R structure may be explained by assuming that the bands are $\perp$ bands for which only the $K=1$ levels in the ground state can combine with the linear excited state ($K=0$). The absence of a doublet splitting is consistent with the fact that in a nonlinear molecule no orbital angular momentum arises and therefore only a very small splitting due to the magnetic field produced by rotation is to be expected. The rotational constants of the ground state on this basis are $B''=1.496$ cm^{-1} and $C''=1.403$ cm^{-1}. These values are consistent with the molecular parameters $r_{CH}=1.08\pm0.02$A (assumed), $r_{CO}=1.19\pm0.01$A, and $\text{H}-\hat{\text{C}}-\text{O}=120\pm4°$, which appear to be reasonable.

To obtain more accurate data on the structure of the HCO radical, attempts are being made to obtain the new band system in emission and to obtain the absorption spectrum of DCO radicals.

I am greatly indebted to Dr. G. Herzberg for many helpful suggestions and discussions.

* Contribution from the National Research Council of Canada, Ottawa, Canada.

[1] W. M. Vaidya, Proc. Roy. Soc. (London) **A147**, 513 (1934).
[2] A. G. Gaydon, *Spectroscopy and Combustion Theory* (Chapman and Hall, Ltd., London, 1948).
[3] G. A. Hornbeck and R. C. Herman, Ind. Eng. Chem. **43**, 2739 (1951).
[4] G. M. Murphy and L. Schoen, J. Chem. Phys. **19**, 380 (1951).
[5] W. M. Vaidya, Proc. Phys. Soc. (London) **64A**, 428 (1951).
[6] P. J. Dyne and D. W. G. Style, Disc. Faraday Soc. **2**, 159 (1947).
[7] G. Porter, Proc. Roy. Soc. (London) **A200**, 284 (1950).
[8] Norrish, Porter, and Thrush, Nature **169**, 582 (1952).
[9] G. Herzberg and D. A. Ramsay, J. Chem. Phys. **20**, 347 (1952).
[10] D. A. Ramsay, J. Chem. Phys. **20**, 1920 (1952).
[11] J. U. White, J. Opt. Soc. Am. **32**, 285 (1942).
[12] H. J. Bernstein and G. Herzberg, J. Chem. Phys. **16**, 30 (1948).
[13] G. Herzberg and K. K. Innes, unpublished.

Antiferromagnetic Structure in Cr_2O_3

B. N. BROCKHOUSE
Division of Physics, Atomic Energy of Canada Ltd., Chalk River, Ontario, Canada
(Received February 25, 1953)

MAGNETIC susceptibility and specific heat measurements[1] show that chromium sesquioxide is antiferromagnetic with a Néel temperature of about 45°C. In an attempt to determine the magnetic structure, neutron diffraction studies of powdered Cr_2O_3 were made at temperatures of 22°C and −193°C using neutrons of wavelength 1.30$_3$A obtained from a crystal spectrometer. Figure 1 shows a plot of intensity *vs* spectrometer angle for each temperature. All lines can be indexed on the basis of the normal rhombohedral unit cell and no lines which are x-ray extinctions are observed. Marked increases in the intensities of the 110, 211, and 200 lines at the lower temperature are ascribed to magnetic scattering.

Chromium sesquioxide is isomorphous with Al_2O_3 and Fe_2O_3, in which the metal and oxygen atoms are found[2] in special positions (c) and (e) of space group D_{3d}^6.[3] By comparison with Al_2O_3 and Fe_2O_3 the parameter x was taken to be 0.145 for the Cr atoms and 0.55 for the oxygen atoms. The nuclear scattering amplitudes[4] were taken to be 0.35×10^{-12} cm for chromium and 0.58×10^{-12} cm for oxygen. The Debye-Waller factor was neglected. The product of the plane multiplicity j and the nuclear structure factor F_{Nucl}^2 appears in the second column of Table I.

The magnetic structure factor was calculated from the equation[5]

$$jF_{\text{mag}}^2=j\left[\frac{e^2}{mc^2}\gamma S\right]^2 f_{\text{mag}}^2 q^2(I/I_0)^2\left|\sum_1^4 \pm\exp[2^2\pi i(hx+ky+lz)]\right|^2,$$

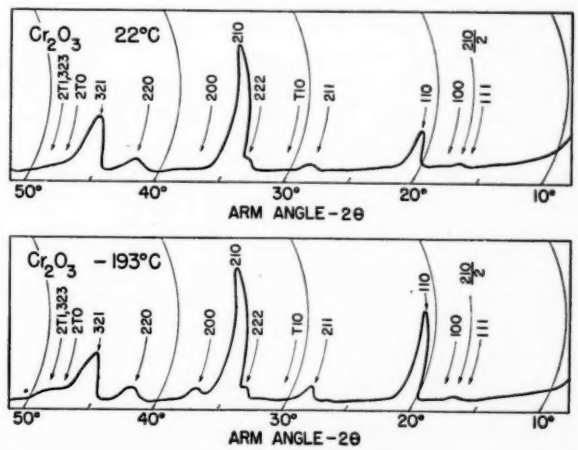

FIG. 1. Trace of intensity *vs* spectrometer angle (2θ) for a powder sample of Cr_2O_3 at two temperatures, recorded by means of a counting rate meter and an Esterline-Angus recorder.

TABLE I. Calculated nuclear and magnetic structure factors for various magnetic structures together with the experimental values.

Planes	jF_{nucl}^2	jF_{mag}^2 (a) ↓↑↓↑	(b) ↑↑↓↓	(c) ↑↓↓↑	jF^2 (Experimental) 22°C	−193°C	$\epsilon=q^2(I/I_0)^2$ 22°C	−193°C
111	0	0	12.9ϵ	2.4ϵ	0(<0.5)	0(<0.5)	—	—
100	0	0	16.5ϵ	27.4ϵ	0(<0.5)	0(<0.5)	—	—
110	3.12	36.8ϵ	0	0	8	22	0.13	0.52
211	3.63	6.3ϵ	0	0	4	7	0.06	0.54
$\bar{1}10$	0.45	0	0	0	0(<1)	0(<1)	—	—
222	12.6	3.2ϵ	0	0	11	10	—	—
210	100	0	26.5ϵ	4.9ϵ	99	100[a]	—	—
$\bar{1}11$	0	0	0.5ϵ	9.0ϵ	{Obscured ((<5)	(<5)	—	—
200	0.79	12.2ϵ	0	0	3	10	0.18	0.75
220	22.7	1.7ϵ	0	0	18	18	—	—

[a] In the low temperature run the 210 peak was used as the standard and arbitrarily taken to have $jF^2=100$ in agreement with the room temperature and the calculated values.

where q is the sine of the angle between the magnetic vectors and the normal to the reflecting plane, I/I_0 is the fraction of the magnetic moments which are aligned, f_{mag} is the magnetic form factor of the Cr ions (for which the form factor given by Shull, Strauser, and Wollan[6] for Mn^{++} was used). S is the spin of the Cr ion and was taken to be $\frac{3}{2}$, i.e., the Cr ions were assumed to be Cr^{+++} and the orbital angular momentum was assumed to give no contribution to the scattering. The + or − sign in the summation is selected according to the orientation of the moment concerned.

The chromium atoms lie on the 111 diagonal of the unit cell as shown in Fig. 2. If the different chromium atoms have the same

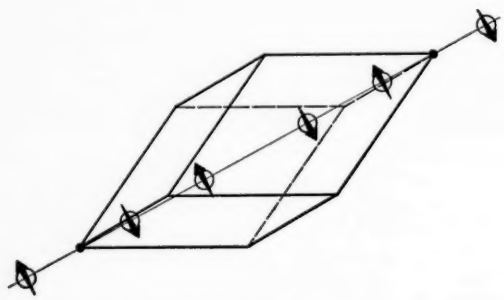

FIG. 2. The unit cell of Cr_2O_3 showing chromium atoms and the relative orientation of their magnetic moments. The orientation of the moment system with respect to the crystal axes is not significant.

moments, oriented parallel and antiparallel, then three magnetic structures are possible. Proceeding along the 111 diagonal the spins of the chromium atoms may be arranged (a) ↑↓↑↓, (b) ↑↑↓↓, or (c) ↑↓↓↑. Values of jF_{mag}^2 for the three structures, computed leaving $\epsilon=q^2(I/I_0)^2$ as a parameter, appear in columns 3 to 5 of Table I.

Experimental values of jF^2 for the two temperatures are listed in columns 6 and 7 of Table I. Because these values are the results of preliminary runs which it has not been possible to repeat, rather large errors, say 20 percent, may exist. The room temperature measurements were standardized on nickel[4] ($f=1.03\times10^{-12}$ cm) and the low temperature measurements were standardized by assuming the 210 reflection to have its calculated value. Comparison of experimental and calculated (nuclear+magnetic) values of jF^2, using the knowledge that ϵ lies between 0 and 1, shows that the correct structure is type (a), displayed in Fig. 2. In columns 8 and 9 the deduced value of ϵ is given. This quantity is expected to be small at 22°C, as observed. At −193°C $(I/I_0)^2$ is expected to be slightly less than unity and the average of q^2 over a number of systems of planes should be about $\frac{2}{3}$. The agreement with observation indicates that the chromium atoms have about the magnetic moment assumed.

The results of these experiments show that the magnetic structure is almost certainly as given in Fig. 2 and that the magnetic moments have roughly the value expected for ions with spin $\frac{3}{2}$ and no effective orbital contribution. Nothing can be said about the orientation of the system of moments with respect to the crystal axes. More complicated structures, in which the Cr atoms are divided into antiparallel pairs having different moments or orientations are considered unlikely, on physical grounds. However it can readily be shown that such structures yield 100 and 111 reflections and hence are, to a considerable extent, excluded by this work.

[1] J. Volger, Nature **170**, 1027 (1952); G. Foex and M. Graff, Compt. rend. **209**, 160 (1939).
[2] R. W. G. Wyckoff, *Crystal Structures* (Interscience Publishers, Inc., New York, 1948), Chapter V.
[3] *Internationale Tabellen zur Bestimmung von Kristallstrukturen* (Gebrüder Borntraeger, Berlin, 1935).
[4] C. G. Shull and E. O. Wollan, Phys. Rev. **81**, 527 (1951). (The Cr amplitude is from unpublished work.)
[5] This formula is based on the work of O. Halpern and M. H. Johnson, Phys. Rev. **55**, 898 (1939).
[6] Shull, Strauser, and Wollan, Phys. Rev. **83**, 333 (1951).